

MARINE PHYSICAL
LABORATORY

FILE COPY
4

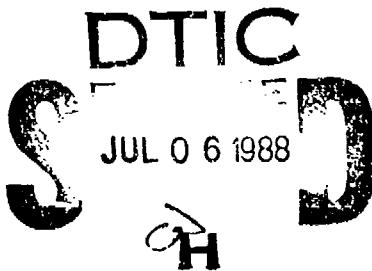
SCRIPPS INSTITUTION OF OCEANOGRAPHY

San Diego, California 92152

AD-A195 019

FREELY DRIFTING SWALLOW FLOAT ARRAY:
MAY 1987 TRIP REPORT

G. L. D'Spain, R. L. Culver, W. S. Hodgkiss, and G. L. Edmonds



MPL TECHNICAL MEMORANDUM 402

MPL-U-15/88

Approved for public release; distribution unlimited.

May 1988

87 01 1104

Table of Contents

- I. Introduction
- I. Deployment Geometry
 - a) Swallow Float Deployment and Retrieval
 - b) OBS Deployment
 - c) Deployment Depths
- II. Scorpius Ship Tracks
- III. Swallow Float Log Summary
- IV. Environmental Data
 - a) Anemometer Readings
 - b) Hydrographic Cast Data from CalCOFI Cruise 8705
 - c) Additional Environmental Data
- V. Swallow Float Data - General Indication of Data Integrity
- VI. The 8 kHz Surface and Bottom Bounce Data
- VII. The 8 kHz Interelement Range Data
- VIII. Battery Voltage, Float Heading, and AGC Level
 - a) Battery Voltage
 - b) Float Heading
 - c) AGC Level
- IX. RMS Velocity and Pressure
 - a) Swallow Float Data
 - i) Midwater Floats
 - ii) Bottom-Mounted Floats
 - b) Ocean Bottom Seismometer Data
- X. Geophone and Hydrophone Time Series
 - a) Swallow Float Data
 - i) 8 kHz Acoustic Localization Ping
 - ii) Tape Recorder Contamination
 - iii) Ambient Ocean Noise
 - b) Ocean Bottom Seismometer Data
- XI. Velocity and Pressure Power Spectra
 - a) Swallow Float Data
 - i) Background Ambient Noise
 - ii) Tether and Ship Generated Signals
 - b) Ocean Bottom Seismometer Data
- Acknowledgements
- References
- Appendix 1 - Swallow Float Geophone Data Acquisition System
- Appendix 2 - Loran-C Position Fixes
- Appendix 3 - Calibration Curves for the OBS Instruments
- Figures



Accession For	
NTIS	GRA&I
DTIC TAB	<input type="checkbox"/>
Unannounced	<input type="checkbox"/>
Justification _____	
By _____	
Distribution _____	
Availability Codes _____	
Dist	Avail and/or Special

1

Freely Drifting Swallow Float Array: May 1987 Trip Report

G. L. D'Spain, R. L. Culver, W. S. Hodgkiss, and G. L. Edmonds

Marine Physical Laboratory
Scripps Institution of Oceanography
San Diego, CA 92152

ABSTRACT

Representative data collected by the Marine Physical Laboratory's Swallow floats during the 5-6 May, 1987 deployment near 32.5° N, 120.5° W are presented herein. The results include the 8 kHz acoustic localization ping arrival data, the battery voltage, compass heading, and AGC level measurements, and the three-component, VLF particle velocity data. The data set is of extremely high quality and it appears to provide a rich source of information on ambient ocean noise in the 1-20 Hz band.

Data from the concurrent deployment of 13 ocean bottom seismometers operated by Dr. L. Dorman's group at Scripps Institution of Oceanography are also presented. These data include the three-component geophone data from the nine properly functioning instruments (instruments 1, 2, 4, 5, 6, 8, 12, 13, and 14), regular OBS hydrophone (OAS model E-2PD) data from instruments 2, 4, 8, 12, 13, and 14, and data from ultra-low frequency hydrophones of the Cox-type design on instruments 1, 5, and 6. A preliminary comparison between the OBS data and the Swallow float geophone data show some common spectral peaks and that calibrated spectral levels are comparable.

Finally, to help interpret the acoustic/seismic data collected by the instruments, plots of the position of the research vessel, the *Scorpius*, are given. Wind speed measurements taken on the *Scorpius* during the experiment and sound velocity profiles derived from CalCOFI Cruise 8705 hydrographic cast data are presented as well.

Introduction

The purpose of this trip report is to present representative data collected during the 5-6 May, 1987 deployment of the Swallow floats and to compare these data with those collected by concurrently deployed ocean bottom seismometers. The 12 Swallow floats, which have been under development for the last six years at the Marine Physical Laboratory, are neutrally buoyant, independently drifting, very low frequency (1-20 Hz) sensors. They each contain within a 0.432 m diameter glass shell a three-component geophone (to measure the VLF sound), a magnetic compass, and the necessary hardware to record up to 25 hours of data. They also contain an 8 kHz acoustic localization system [1,2]. Figure 1 is a schematic drawing of a float.

This deployment was part of a month-long multi-sensor experiment, from 21 April to 23 May 1987, conducted near DSDP hole # 469 (32.5° N, 120.5° W). The duration of the experiment was determined by the recording capacity of the 13 ocean bottom seismometers (OBS) operated by Dr. LeRoy Dorman's group at Scripps Institution of Oceanography. Selected data from the nine operational ocean bottom seismometers are presented for comparison with the Swallow float data. The experiment also involved an initial deployment of the Swallow floats and the deployment of 8 ship-launched and 12 air-launched expendable sonobuoys by Jim McEachern's group at the Naval Air Development Center (NADC) on 22-23 April, 1987. A discussion of the results of this first Swallow float deployment and the NADC sonobuoys are contained in a companion trip report [3].

Note that all times listed in this report are in local Pacific Daylight Time. To obtain Greenwich Mean Time, add 7 hours to the local time.

I. Deployment Geometry

a) Swallow Float Deployment and Retrieval

Swallow float deployment began at 10:21 local time on 5 May, with the deployment of the midwater-column floats, and lasted until 12:32. that same day. Float retrieval started the following morning with the recall of float 0 at 09:53. Refer to Section III, the Log Summary, for the corresponding times for the other floats. Figure I.1 shows the Swallow float deployment and retrieval positions. Only 11 of the 12 floats were deployed; float 6 quit its program execution after a count of 46. Also, float 5 never returned to the surface and was lost. The deployment positions of the three bottom-mounted buoys, floats 9, 10 (indicated by the hexadecimal "A"), and 11 (hexadecimal "B"), formed a triangular array so that stable absolute position fixes could be obtained for the midwater-column buoys. The midwater-column floats were ballasted for about 1800 m depth and were deployed in the approximate center of the triangular array. Also indicated on the figure is the site of DSDP 469 [4] and the locations of the four successful expendable bathythermograph (XBT, model T-4) measurements taken from the *Scorpius*.

The midwater buoys drifted northwest of their initial position during the 26-to-32 hour period they were in the water. The float drift pattern is in striking contrast to the pattern observed in the April deployment, shown in Figure I.2. The obvious explanation for the difference in drift pattern is the difference in deployment depths; during the May deployment, the midwater buoys were ballasted to about 1800 m depth, whereas in April they stabilized at 425 m. However, changes in the current structure probably also took place over the two-week period between deployments. Evidence for changes in current is provided by examination of the retrieval locations of the bottom-mounted buoys with respect to their deployment positions (which form the aforementioned triangle shown in these and subsequent figures). The deployment-retrieval geometry of the bottom-mounted buoys is consistent with the drift direction of the midwater buoys.

A final point is that the dispersal of the floats was greater in this deployment than in April. This may have been partially due to the larger variation in deployment depth in May than in April (Section VI). However, the differences in retrieval position may partially result from positioning errors (re Appendix 2).

b) OBS Deployment

The deployment positions of the 13 ocean bottom seismometers, referenced to the triangular array of bottom-mounted Swallow floats, are shown in Figure I.3. The interelement spacing of the OBS array was quite small (a few tens of meters) compared to the Swallow float array due to the short wavelengths of the Scholte waves being studied in that experiment [5]. Figure I.4 is an enlarged picture of the OBS array and Figure I.5 plots the nine sensors which provided useable data. Each OBS is indicated by its capsule number in hexadecimal, except for the Oregon State University seismograph, which is plotted using an "O". Table I.6 gives the OBS name, its corresponding number, and its deployment location. The deployment locations in minutes are with respect to 32° N, 120° W.

Using the Scripps Institution of Oceanography's thruster, presently under development by Dr. Fred Spiess and his research group, the OBSs were positioned on the ocean bottom in 3800 m deep water within a couple of meters of their desired position, a truly remarkable achievement. They recorded 3 minutes of data either every 15 min, every 3 hours, or every 6 hours, enabling up to 31 days of data to be obtained. The data sampling interval and the total period over which data were recorded for each OBS is shown in Figure I.7, courtesy of Dr. Dorman's research team. (Julian day 115 corresponds to 25 April, Julian day 120 is 30 April, 125 is 5 May, etc.) Note that the "L" after Juan, Lynn, and Karen signifies that a deep sea differential pres-

sure gauge developed by C. S. Cox, T. Deaton, and S. C. Webb at Scripps [6] was attached to the OBS.

An extensive list of the beginning sample times for all OBS events recorded while the Swallow floats were in the water in April as well as in May is given in Tables I.8 and I.9. Table I.8 provides the information for all nine properly functioning instruments and Table I.9 provides the information for Lynn (OBS 5) and Karen (OBS 6), which recorded data every three hours instead of every six hours (re Figure I.7). The following table lists the starting time for each OBS event and the corresponding Swallow float record number for the May sea trip. Note that only instruments 5 and 6 recorded the even-numbered events.

Time (local)	OBS Event	Swallow Float Record
May 5		
11:01	309	87
14:01	310	327
17:01	311	567
20:01	312	807
23:01	313	1047
May 6		
02:01	314	1287
05:01	315	1527
08:01	316	1767
11:01	317	2007

During each 3-minute data-collection period (actually 179 sec), the OBSs sample at a 128-Hz rate, compared to a 50-Hz sampling rate for the Swallow floats. Their effective bandwidth is from 0.1-30 Hz, although analysis by Dr. Dorman's group indicates significant correlation between the various instruments' signals at 0.05 Hz. This compares to an effective bandwidth for the Swallow floats of around 0.5 Hz to 20 Hz, where the lower frequency limit will probably be extended once accurate float calibration is done. For additional information on the OBSs, see [7].

c) Deployment Depths

The simultaneous deployment of the midwater Swallow floats at 1800 m and the ocean bottom seismometers and bottom-mounted Swallow floats at 3800 m provide the opportunity to correlate midwater ambient ocean noise with ocean bottom noise. An initial comparison between the two sets of data is given in this report. Figure I.10 illustrates the coverage with respect to depth of these two sensor systems. Symbols representing the Swallow floats (circles) and the OBSs (triangles) are superimposed on an average sound speed profile for the area of the experiment, obtained from historical temperature and salinity measurements archived by the National Oceanographic Data Center [8] and an equation relating temperature, salinity, and depth to the sound speed [28]. The dashed lines at 140 m and 400 m indicate the deployment depth of the NADC sonobuoys and the Swallow floats, respectively, in the April trip. The closely spaced dashed line at 3800 m represents the ocean bottom depth at our study site. Table IV.5 in Section IV lists the calculated sound velocities at specific depths for this profile.

II. Scorpius Ship Tracks

To correctly interpret the received signals on the Swallow floats and the ocean bottom seismometers, the position of the Scorpius, as determined by Loran-C position fixes, were written intermittently into the Swallow floats' log book. The positions of the ship during the recording period of the floats (10:00, 5 May to 11:00, 6 May) are shown in Figure II.1. (A listing of all of the logged ship fixes is contained in Table II.4). Each "+" in the figure indicates a log book entry; the entries were made at irregular time intervals and therefore ship speed information cannot be obtained directly from this plot. The track begins at the deployment position for float 0, near the center of the triangular array, and follows a rather tortuous path thereafter. However, it can be easily unraveled by plotting the positions for shorter time intervals.

After deploying the midwater floats (they were deployed before the bottom-mounted floats since they required 8 to 10 hours to stabilize at 1800 m, whereas the bottom floats sank in about 2 hours), the ship moved to deploy floats 9, 10, and 11, in that order. It then traveled north to deploy the second XBT just north of the triangular array, and then northwest about 12.5 km while waiting for the midwater floats to sink. The Scorpius then returned to the west of the array to begin surveying the floats' positions. While conducting the surveys, the ship followed a clockwise path, finishing near the southern tip of the array, where the third XBT was taken. It then headed west to begin the northeast-trending run across the array.

A plot of the ship track during the run across the float array is shown separately in Figure II.2. Fifteen ship position fixes are plotted, from 21:20, 5 May, to 06:00, 6 May. Also shown on this figure, as two northwest-southeast trending lines, are the approximate locations of the base, the 1800 fathom contour line (3292 meters), and top, the 600 fathom contour line (1097 meters), of the Patton escarpment. This topographic feature may have caused ship noise to be effectively coupled into the deep sound channel, resulting in clipping of the float geophone signals. This point will be discussed further in Section IX.

Figure II.1 then shows the return of the ship to the array, where a float survey and subsequent float recall was started.

Figure II.3 plots the logged position of the Scorpius closest in time to when the nine events, events 309 to 317, were recorded by the ocean bottom seismometers. The plotted point labeled "1" corresponds to the ship's position during event 309, "2" corresponds to event 310, etc. The ship was closest to the OBS array during the recording of event 309, probably resulting in increased signal levels. The rms levels presented in Section IXb show evidence of this.

III. Swallow Float Log Summary

Note: All times are in local Pacific Daylight Time. To obtain standard Greenwich Mean Time, add 7 hours.

5 May 1987

- 09:30 About 400 m from the proposed center of the Swallow float array, begin initial check of floats. All floats checked out normally.
- 09:56 Synchronize floats by Greg Edmond's watch.
- 10:05 Ship's position is 32° 36.76' N, 120° 33.02' W.
- 10:21 Deploy float 0. Ship location is 32° 36.99' N, 120° 32.95' W.
- 10:27 Deploy float 1. Ship location is 32° 36.87' N, 120° 32.86' W.
- 10:30 Deploy float 2. Ship location is 32° 36.80' N, 120° 32.79' W.
- 10:33 Deploy float 3. Ship location is 32° 36.74' N, 120° 32.79' W.
- 10:36 Deploy float 4. Ship location is 32° 36.69' N, 120° 32.75' W.
- 10:40 Deploy float 5. Ship location is 32° 36.59' N, 120° 32.69' W.
- 10:45 Deploy float 7. Ship location is 32° 36.45' N, 120° 32.58' W. Float 6's program found to be stopped at a count of 46; it will not be deployed.
- 10:59 Resynchronize float 8.
- 11:04 Deploy float 8. Ship location is 32° 36.38' N, 120° 32.46' W.
- 11:07 Resynchronize float 9. Float 8 and 9 are the two floats whose internal identity inexplicably changed during the deployment in April [3].
- 11:19 Took first XBT reading. The resulting temperature profile is nonsensical and is discarded.
- 11:30 Deploy float 9. Ship location is 32° 37.30' N, 120° 30.36' W.
- 12:02 Deploy float 10. Ship location is 32° 38.38' N, 120° 34.37' W.
- 12:32 Deploy float 11. Ship location is 32° 34.34' N, 120° 33.31' W.
- 12:37 Resynchronize float 6 and make way for center of the array.
- 13:14 Float 6 program stopped again. The float will not be launched.
- 13:28 Ship's position is 32° 36.06' N, 120° 32.32' W.

Float	Slant Range (m)
0	2272
1	2898
2	3100
3	-
10	4363

Float survey is stopped.

- 13:49 The 2nd XBT is taken. Ship location is 32° 38.75' N, 120° 32.79' W.
- 15:21 Ship's position is 32° 43.37' N, 120° 37.40' W.
- 17:20 Location is 32° 36.57' N, 120° 35.12' W. Begin second float survey.

Float	Time	Slant Range (m)	Horizontal Range (m)
0	17:19	3420	3073
1	17:19	3468	3127
2	17:20	3459	3117
3	17:21	3458	3116
4	-	3568	3237
5	-	3640	3317
7	17:24	3875	3573
8	-	4034	3745
9	-	-	-
10	-	5185	3632
11	17:28	-	-

The horizontal range assumes a float depth of 500 m.

17:37 Begin another float survey. Ship location is 32° 36.89' N, 120° 34.99' W.

18:08 Begin another float survey. Ship location is 32° 37.87' N, 120° 33.31' W.

Float	Slant Range (m)	Horizontal Range (m)
0	2368	1832
1	2483	1979
2	2550	2062
3	2582	2102
4	2655	2191
5	2888	2468
7	3100	2713
8	3274	2910
9	5520	4096
10	4530	2614
11	7762	6823

The time is 18:18 and the ship location is 32° 38.04' N, 120° 32.88' W.

18:37 Another float survey is conducted.

19:12 The last float survey of the day is conducted. Ship location is 32° 35.39' N, 120° 31.93' W.

19:45 The 3rd XBT is taken. Ship location is 32° 34.65' N, 120° 33.18' W.

21:20 Ship's position is 32° 34.00' N, 120° 37.00' W. Change ship course to begin run across the float array. The ship heading is 026° magnetic and the engine is turning at 1200 rpm.

22:30 Ship's position is 32° 38.98' N, 120° 31.80' W. The starboard diesel engine is turning at 985 rpm and the port engine is turning at 1110 rpm. The engines are V-8 engines, 4 blades are on the shaft, and the reduction gear ratio is 3.8 : 1.

6 May 1987

01:00 Ship's position is 32° 45.75' N, 120° 25.17' W. The run across the array is completed and the ship will continue same heading to depart the area. The scientific party retires until about 08:00, 7 May. The ship personnel on the bridge will continue to record wind speed and direction and sea height observations.

02:30 Ship's position is 32° 55.60' N, 120° 14.80' W.

02:44 Secure port main engine to add lube oil.

03:00 Restart port main engine; engine turning at 900 rpm. Secure starboard main engine.
03:15 Restart starboard main engine; engine turning at about 1000 rpm.
04:30 Ship's position is 32° 48.87' N, 120° 20.07' W.
06:00 Ship's position is 32° 52.31' N, 120° 15.70' W.
06:40 Change ship course to heading 209° magnetic and increase speed. Both shafts are running at 1500 rpm.
07:00 Ship's position is 32° 49.18' N, 120° 19.73' W.
07:30 Ship's position is 32° 46.40' N, 120° 22.82' W.
08:00 Ship's position is 32° 43.45' N, 120° 26.19' W.
08:30 Ship's position is 32° 40.73' N, 120° 29.29' W.
09:01 Ship is dead in the water, taking 4th KBT. Ship location is 32° 38.03' N, 120° 32.05' W. Begin float survey.

Float	Time	Slant Range (m)	Horizontal Range (m)
0	09:02	3134	2566
1	09:03	3210	2658
2	09:04	3270	2730
3	09:04	3125	2555
4	09:07	3040	2553
5	09:08	2869	2234
7	09:08	2996	2395
8	09:09	2656	1953
9	09:09	4833	3100
10	09:10	5301	3796
11	09:10	7892	6971

09:24 Underway for the next survey position, due east. Port engine turning at 1600 rpm and the starboard at 1710 rpm.
09:33 Begin another survey.
09:43 Attempt three times to recall float 0.
09:53 Try to release float 0 again. The float returns a long ping, signifying that it has released.
10:35 Range to float 0 is 1695 m. Ship's position is 32° 37.61' N, 120° 33.81' W.
10:41 Release float 1. Range to float 1 is 2424 m.
11:35 Ship location is 32° 37.78' N, 120° 33.37' W. Range to float 0 is 1090 m; range to float 1 is 1988 m.
11:40 Recall float 2. Range to float 2 is 2305 m.
11:45 Float 0 is on the surface.
12:10 Recover float 0. Ship's position is 32° 37.36' N, 120° 33.81' W.
12:45 Recall float 3.
12:57 Recover float 1. Program LED display is "00". Ship location is 32° 37.98' N, 120° 33.88' W.
13:46 Recall float 4.
13:58 Recover float 2. Program display is "HH". Ship location is 32° 37.43' N, 120° 34.32' W.
14:42 Recover float 3. Ship location is 32° 38.42' N, 120° 34.11' W.

14:49 Release float 5.
15:20 Deploy 5th XBT. Ship location is 32° 38.01' N, 120° 34.89' W.
15:28 Release float 7.
15:38 Recover float 4. Ship location is 32° 37.79' N, 120° 34.31' W.
16:34 Recall floats 8 and 10.
17:34 Recover float 7. Ship location is 32° 38.46' N, 120° 34.00' W.
19:00 Recover float 8. Ship location is 32° 38.79' N, 120° 34.09' W.
19:07 Recall float 11.
19:00 Recover float 10. Ship location is 32° 38.31' N, 120° 34.82' W.
21:07 Release float 9.
23:15 Recover float 11. Ship location is 32° 34.62' N, 120° 33.69' W.

7 May 1987

01:53 Recover float 9. Ship location is 32° 37.41' N, 120° 30.48' W.
02:48 Attempt to release float 5 again; no luck. Range to float 5 is 3268 m. The ship will move into a position over float 5 to determine if it is ascending. Ship location is 32° 38.41' N, 120° 33.54' W.
04:05 Ship's position is 32° 39.56' N, 120° 34.58' W. Range to float 5 is 1988 m. Float-ship range is increasing.
04:18 Float 5 is not ascending. Underway for San Diego.

Post recovery observations:

Float 0 data tape appears to only have 359 records on it although it was at end of tape mark and its program was running when it was recovered.
Float 1 data tape not at end of tape mark; 357 records are on tape.
Float 2 has an impaired release mechanism. The resistance across the pins is 2.5 kΩ, rather than the proper 100 Ω.

IV. Environmental Data

a) Anemometer Readings

Wind speed and direction, measured by the anemometer on board the *Scorpius*, were recorded approximately every two hours in the Swallow float log. Figure IV.1 plot these data. Note that the wind vectors, starting at the dashed line in the plots, points in the direction the wind is blowing *from*. The vertical axis provides the scale to determine the wind velocity magnitude in m/sec.

These wind data show the same gross features as those taken during the April deployment [3]. The wind was blowing steadily, mainly from the west-northwest, with a gradual shift north-easterly over the duration of the experiment. As in April, a slight decrease in wind speed occurred in a 4-hour interval just before midnight. However, the average wind velocity magnitude in May, just less than 9 knots (4.6 m/sec), is less than the average in April of almost 12 knots (6.2 m/sec).

b) Hydrographic Cast Data from CalCOFI Cruise 8705

A set of temperature and salinity measurements, made at station 90.70 on CalCOFI cruise 8705 [29], and the equation for sound speed from reference [28] were used to calculate the sound velocity profile in Figure IV.2. The CalCOFI measurements were taken the evening before our arrival at the study site, at 19:22, 4 May, local time. The location of station 90.70, $32^{\circ} 5.1' N$, $120^{\circ} 38.3' W$, was about 60 km from Deep Sea Drilling Project hole 469.

The method of measuring temperature was to use paired protected reversing thermometers which record the temperature to $0.01^{\circ} C$. Salinity was determined to three decimal places from the 20-bottle samples collected at each depth using inductive-type salinometers [29].

Figure IV.3 shows a comparison of the CalCOFI-data-derived sound velocity profile with the profile calculated from National Oceanographic Data Center historical data [8]. Also shown on the plot are the sound velocity profiles derived from data taken at three other stations surrounding hole 469; station 87.60 ($32^{\circ} 59.4' N$, $120^{\circ} 21.0' W$, taken at 10:47, 7 May), station 87.70 ($32^{\circ} 39.4' N$, $121^{\circ} 02.0' W$, taken at 16:26, 7 May), and station 90.60 ($32^{\circ} 25.1' N$, $119^{\circ} 57.6' W$, taken at 01:14, 5 May). What is notable about this plot is that the hydrographic cast data encompass the historical profile and that the only possibly significant deviations are the few meters/sec higher velocity at the surface and at 500 m depth. Tables IV.4 and IV.5 provide numerical values for the sound speed profiles derived from the CalCOFI data at station 90.70 and the historical data, respectively.

c) Additional Environmental Data

Environmental information gathered by other organizations will be used to supplement the preceeding data set. These include:

- a) Basic weather observations taken by California Cooperative Oceanic Fisheries Investigation (CalCOFI) cruise 8705;
- b) basic weather information including wind speed and direction, collected at San Miguel, San Nicolas, and Santa Cruz islands from 20 April through 22 May, by the Pacific Missile Test Center;
- c) basic weather information taken at San Clemente island, from 20 April through 22 May, by the Naval Oceanography Command Facility;

d) wave height measurements from a Datawell waverider buoy located at Begg Rock, about 125 km northeast of our site, from 20 April through 22 May (excluding 9-17 May); data provided by the Coastal Data Information Program;

e) wave hindcasts every 12 hours, from 20 April through 22 May, at 7 spherical grid points (separated by 2.5°) surrounding our study site, provided by the Fleet Numerical Oceanography Center in Monterey; and,

f) wave hindcasts provided by Pacific Weather Analysis, a private consulting firm in Santa Barbara.

Finally, the locations of commercial ships, within the area 27.5° N to 37.5° N and 115.5° W to 125.5° W, during the month-long duration of the experiment has been provided by the Fleet Numerical Oceanography Center.

V. Swallow Float Data - General Indication of Data Integrity

The remainder of this report will be devoted to a discussion of the data collected by the Swallow floats and a comparison of these data to those collected by the ocean bottom seismometers.

During deployment, each Swallow float accumulates one record of data in a buffer. Each record is composed of 7644 bytes representing 44 sec of data. The record is then written to cassette tape during a one-second period in which no data is accumulated. This 45-sec cycle is then repeated until the cassette tape is completely filled; typically, 1800 to 2000 records, or 22.5 to 25 hours, of data are written. The first step in the data analysis is to scan all the floats' cassette tapes with a general screening program. This program checks each record for the proper location of resynchronization characters and the proper sum of byte values in a group prior to a checksum. The results of the screening are given in Figure V.1.

Note that at the end of every data tape (except for float 0), a record with zero bytes was recorded. Therefore, all internal data records of those floats which have only one entry in the table (floats 2, 10, and 11) passed the screening test. Since the internal record count starts at 0, the last entry under each float in the second column gives the total number of records.

Eight floats, including the three bottom-mounted floats, wrote full data tapes. Floats 0 and 1 stopped writing data prematurely. The data cassette for float 0 had a tape defect which allowed only about 75 % of the tape to be usable. Most of the errors listed in the table for this float occur in records adjacent to this defect. It did write a total of 1443 records. Float 1's tape apparently lost synchronization after record 276 (3.75 hours after synchronization) and every record after that until it stopped writing was defective. As mentioned previously, float 5 was lost and float 6 was never deployed. This implies that over 70 % of the total possible amount of data that could have been recorded by 12 normally functioning Swallow floats was actually recorded. Useable data were obtained from six midwater-column buoys (floats 0, 2, 3, 4, 7, and 8) and all 3 bottom-mounted buoys (floats 9, 10, and 11). In comparison, about 60 % of the possible data in the April deployment was recorded, by five midwater-column buoys (floats 0, 1, 2, 3, and 5) and 2 bottom-mounted buoys (floats 8 and 9).

Of the data that was written to tape, the types of errors that can occur have been described elsewhere [11]. However, Figure V.1 shows that only a very small percentage of records, about 0.12 %, contained errors. The comparable figure for April was 0.14 %.

VI. The 8 kHz Surface and Bottom Bounce Data

The acoustic localization system on the Swallow floats is composed of a hydrophone hanging from the underside of the floats' glass sphere by a 1.83 meter cable (re Figure 1) and an 8 kHz narrow-band energy detection circuit. The source strength of the hydrophone is 192 dB re 1 μ Pa at 1 meter. The 12 floats take turns generating an 8 kHz ping with a 45-sec (one record) delay between pings. The arrivals of the pings are then recorded by all the floats. These data have been used to successfully localize (an rms error of less than 2 m) the Swallow floats during the September, 1986 experiment. This section presents the data for the self-generated ping arrivals and the next section discusses the inter-buoy ping data.

Figures VI.1 through VI.10 plot the surface and bottom bounce data for floats 0, 1, 2, 3, 4, 7, 8, 9, 10, and 11, respectively. These data are plotted on the same depth scale as that used in the April deployment [3]. The abscissa is in units of internal record number. It can be easily converted into time after initial float synchronization (at 09:56, 5 May) by multiplying the record number by 3/4 minute per record. The sampling interval in the plots is 12 records, or 9 minutes.

For the first 50 records of data for the midwater floats and the first 150-200 records of data for the bottom-mounted floats, the floats were still on the ship's deck. (Note that both floats 8 and 9 were resynchronized and, therefore, their data is offset in time with respect to the other floats. Float 8 was resynchronized at 10:59, 5 May, representing an 84-record offset, and float 9 was resynched at 11:07, a 94.7 record offset). The records written after deployment show the surface reflection diverging from the arrival at 0 depth (which is due to the reception of the range ping simultaneous with its transmission) as the buoys descended. The midwater buoys took somewhat over 8 hours to stabilize at depth. The depths to which they sank were approximately:

float 0	1800 m
float 2	1800 m
float 3	1680 m
float 4	1580 m
float 7	1960 m
float 8	1900 m

The bottom buoys spent just over 2 hours in sinking to the 3800 m deep ocean bottom.

Both the arrival at 0 depth, which is the recording of the transmitted pulse itself, and the surface reflection are followed by a string of later arrivals. The duration of the later arrivals following the surface reflection are much longer, indicating that scattering from the rough sea surface is the dominant mechanism. However, in April, the duration of the two sets of later arrivals is almost identical to each other, and the duration of both is longer than in May. The source of this additional reverberation is possibly due to the ringing of the Swallow float glass spheres [16]. Float ringing may not have been as prevalent in May since the 4 °C decrease in temperature going from 425 m to 1800 m effectively "detuned" the floats' glass spheres to the 8 kHz ping. Numerical studies have shown that a temperature decrease of 4 °C causes over a 50 Hz decrease in the resonant frequency for a given mode since the speed of sound in the air inside the spheres is temperature dependent. Note that the later returns after the transmitted pulse are quite prominent while the floats are in the upper 600 m or so of the water column in the May data set. Volume reverberation from organisms, bubbles, and particulate matter in the water column does not appear to be significant; recordings of the 8 kHz ping by the NADC sonobuoys in April (which were at 140 m depth [3]) show a symmetric, 80 cycle arrival of almost exactly 10 msec duration and no scattered arrivals.

The 200 m thick band of reverberation arrivals after the surface reflection in the May data, representing about 1/4 second, are also much less variable over the period of the experiment than in April. (The thickness of the band of reverberation arrivals varies somewhat from

one float to the next. This is probably a result of a difference in sensitivity between the floats' 8 kHz detection system). In April, the reverberations varied from 300 m thick (0.4 sec) to 50 m (1/30 sec). The variation is thought to be caused by variations in ship noise [3].

For the bottom buoys, the arrivals after 0 depth probably represent multiple reflections between the float and the ocean floor. The bottom-mounted floats are suspended above the bottom by a distance determined by their tethers to the ballast weights. In the May deployment, these tethers were 4.57 m in length; in April, they were 3.05 m.

The reflection of the pulse from the bottom can be seen in all midwater float plots (except for float 1). It is the arrival which is symmetric to the surface bounce phase about a line at 1900 m (half the water depth). The bottom-bounce pulse is apparently weaker than the surface return since it can only be clearly seen once the float is less than about 3000 m above the bottom. It also is not followed by detectable scattered arrivals.

The bottom-to-surface-to-float return, which is reinforced by the surface-to-bottom-to-float pulse, is distinguishable on most of the midwater buoys. Careful measurement of the arrival of this phase indicates a total water depth of 3813 m (assuming a constant speed of sound of 1500 m/sec). The water depth indicated by the surface bounce return on the bottom-mounted floats is 3808 m. The difference in the two measurements is mainly due to the distance between the bottom floats' hydrophones and the ocean bottom. In addition, the surface-to-bottom-to-surface-to-float multiple can be picked out on float 4's plot, and to a lesser extent on floats 0, 3, and 7's plots. Assuming a loss in intensity due to a) spherical spreading (-78 dB), b) attenuation in the water (-5 dB) [12], and c) imperfect reflection at the ocean bottom (-6 dB) [12], this latter pulse is more than 89 dB lower in intensity than it is at one meter. The acoustic location circuit is thus a sensitive indicator of energy at 8 kHz.

If one looks closely at the plot for float 0 (Figure VI.1), an apparent pulse return occurs at a depth of about 175 m and is independent of the float's depth. Careful measurement of this arrival at record 1000 indicates a depth of 168 m. It is apparently a reflection off float 2 since the inter-element range plots in the next section (Figures VII.1b and VII.2a) show a float 0-to-float 2 distance of 171 m. Float 2's surface-and-bottom-bounce plot does not show a corresponding reflection off float 0 probably because float 2's 8 kHz detection system is less sensitive than that of float 0. Evidence for a difference in sensitivity can be seen by comparing the detectability of the surface-to-bottom-to-float phase in Figure VI.1 vs VI.3.

The presence of internal waves is indicated by the variation in float depth once the floats come to equilibrium. (The possibility of apparent variations in float depth caused by changes in the density of scatterers near the ocean surface has recently been ruled out. Refer to the discussion in the next section). Recently completed work [13] has determined the theoretical Swallow float response to forcing by an internal wave pressure gradient. This, in combination with the edge detection algorithm (for optimally determining the float-surface distance from the data [14]) and the recently-developed capability of algorithmically co-locating the floats, will allow the Swallow floats to be used as an array for the study of internal wave propagation. The experiment location is an ideal place to investigate the possible generation of internal waves by ocean swell passing over topographic features [15] since the Patton escarpment is only 25 km northeast of the study site.

The seemingly random vertical lines appearing on the plots between records 200 to 800 and 1800 to 2000 represent times when the floats were being acoustically requested from the ship to issue an 8 kHz location ping. This is done to survey the floats' positions.

VII. The 8 kHz Interelement Range Data

Figures VII.1 through VII.9 plot the 8 kHz ping arrivals recorded on a given float and generated by a different float. These plots have the same sampling rate and abscissa scale as those in Section VI, but the range scale on the ordinate is doubled. Note that the direct path arrival between two floats is followed by the surface bounce phase. And just as in the previous section, the other less prominent phases also appear. Of these, the bottom bounce phase is the most prominent. Again, the initial set of records were written while the floats were still on board.

In order to determine the range between two floats, the two distances indicated by the direct arrivals recorded by the two floats must be averaged. For example, consider the range between floats 0 and 2 near record 1000 (i.e. 12 hours, 30 min after float synchronization, or at 22:26, 5 May). This time was chosen because float 0's surface-and-bottom-bounce data (Figure VI.1) show an arrival at 168 m depth at this time which is apparently a reflection off float 2. Float 2's recording of the direct arrival pulse from float 0 (Figure VII.2a) indicates an inter-float range of 611 meters. However, float 0's recording of float 2's ping indicates a range of -270 meters (Figure VII.1b), an unrealistic measurement. The problem arises due to the difference in the drift rates of the floats' internal clocks. A unit of time measured by float 0's clock is longer than one measured by float 2's clock; float 0 detects the arrival of float 2's location ping before its clock has reached the time of float 2's ping generation. The average of the two distances is 171 m, which corresponds to the 168 m distance determined by float 0's detection of a reflection off float 2.

Averaging does not completely eliminate the error introduced by differences in clock drift rate. This is due to the drift which occurs in the time interval between the two floats' ping generation. Therefore, interpolation is performed in order that both floats' estimates of their interelement range are made at approximately the same time. This reduces the error from clock drift differences to an order of magnitude smaller than the nominal error of 1.5 m due to the 1 kHz acoustic localization circuit sampling rate. Other, more dominant, errors in the 8 kHz localization data are discussed in reference [26].

Another way of determining the interelement float range is from one buoy's interelement range data, by measuring the gap between the direct arrival and the surface reflected arrival [3]. Preliminary work on another data set using this approach has shown that the resulting inter-float range estimates not well constrained. However, the estimates become better constrained as the depth of deployment increases in relation to the inter-float separation. Therefore, the data from this deployment may be ideally suited to the use of this "gap" method. The method assumes that the first *reflection* arrival is the phase which reflects off the ocean air-water interface. The fact that this is indeed the case has been verified, at least in the April experiment, by studying the waveforms of the direct and surface-reflected pings as recorded by the NADC sonobuoys. Therefore, the possibility of a near surface layer scattering the 8 kHz signal back to the floats [9,12,19] and contaminating the surface reflection arrival appears to be eliminated.

The interelement range data for a midwater float receiving a bottom-mounted buoy ping, e.g. Figure VII.1g for float 0's reception of float 9's ping, shows an interesting set of triple arrivals for a short period between about records 250 and 300. This triplet is composed of the direct arrival and the surface bounce phase (with its attendant scattered arrivals), and the bottom-bounce phase, which decreases in range with time to ultimately merge with the direct arrival as the bottom float reaches the ocean bottom. The direct arrival in this figure after record 300 has a slightly longer duration than the direct arrival from another midwater float due to the distance above the bottom of float 9.

Likewise, the interelement range data for two bottom floats, e.g. Figure VII.8i for float 10 from float 11, also shows an interesting "hourglass" pattern of arrivals just after the floats were deployed. The direct and surface-bounce paths are easily identifiable, as well as the bottom-bounce phase which ultimately merges with the direct arrival. The base of the "hourglass" is formed by the surface-to-bottom-to-float 10 phase which merges with the surface-bounce phase

as float 10 (which was deployed before float 11) reaches the bottom. Also merging with the surface-bounce phase is the bottom-to-surface-to-float 10 phase, seen at about 11600 m range. Following this phase is the surface-to-bottom-to-surface-to-float 10 arrival, which has the same appearance as the surface-bounce phase.

Figure VII.8i also shows that once float 11 came within 300 to 400 m of the ocean bottom (float 10 had already sunk to the bottom), the direct path phase can no longer be heard. The bottom-mounted buoys do not rest directly on the ocean bottom. Rather, they float a distance above the bottom determined by the length of the tether to the ballast weight, which was 4.57 m long in this deployment. The inability of the bottom-mounted floats to hear each other's direct-path ping arrival is a result of the shadow zone created by the upward refracting sound velocity profile in addition to any possible interfering topography.

The plots showing the range from float 0 (Figures VII.2a, VII.3a, VII.4a, VII.5a, VII.6a, VII.7a, VII.8a, and VII.9a) indicate that float 0 began ascending towards the surface before floats 2, 4, 8, 9, and 10 had finished recording data. The float was acoustically recalled at 09:53, 6 May, almost 24 hours after synchronization at 09:56, 5 May (Section III).

VIII. Battery Voltage, Float Heading, and AGC Level

Figures VIII.1 through VIII.10 show the battery voltage, compass reading, and automatic gain control (AGC) level for all ten recovered floats. The measured value of each of these quantities for every 45 sec record is plotted. As mentioned in Section V, float 0 wrote only 1443 records because of a tape defect and float 1 failed prematurely; the cause of the failure is as yet undetermined.

a) Battery Voltage

The battery level for all floats remains fixed at 6.0 volts throughout the full duration of the data recording. Therefore, the length of float deployment is not determined by limitations in power supply, but rather by the size of data storage.

b) Float Heading

A close examination of the compass heading plot for buoy 1 reveals that a fixed value of 0 occurs just after record 200 and remains there, even though other problems did not start until after record 276. This problem is as yet unexplained. Float 2's compass appears to have begun malfunctioning around record 950 and the heading ultimately stuck at zero shortly before record 1600. This is believed to be caused by lack of proper balance of the float. Before previous deployments, the floats were accurately trimmed in the laboratory since the float compasses can only tolerate a maximum tilt of 3°. However, this was not done before the May experiment due to lack of time between the April and May deployments. Any future plans to quickly redeploy the floats must take this potential problem into account.

The compass readings for the midwater floats typically depict complete float rotations as the float descends in the water; the rotation appears to slow as the floats approach their equilibrium depth. After stabilizing at depth (after record 600) the floats continued to oscillate with a characteristic 25-to-45-minute period. The restoring force responsible for the oscillations is possibly the prevailing ocean current. Relative motion between the floats and the water can occur even after the floats come to their equilibrium depth since they respond differently in the vertical direction than the water [13]. That is, the floats can move from one water layer to another, in which the current may be different, in the presence of an internal wave field. A second force, which is thought to be due to the interaction of the earth's magnetic field with a weak magnetic dipole in the floats (possibly due to the permanent magnets in the geophones), appears to align the midwater floats at about a 300° heading [11].

The characteristic rotation period does not appear in the buoy heading data for the bottom-mounted buoys, Figures VIII.8, VIII.9, and VIII.10. The time of descent to the bottom is dominated by very rapid rotations due to the relatively large vertical descent rate. Upon reaching the bottom, the heading remains approximately fixed for both floats 9 and 10. Float 11, however, turned slowly counter-clockwise, as seen from above, throughout the full duration of the deployment. These differences in the compass heading data for the bottom-mounted floats are thought to be caused by differences in the ocean currents at the float locations.

The compass heading can be used to rotate the horizontal components of the geophone particle velocity time series so that all the floats' geophone axes point in approximately the same direction. This was not done for the data presented in Sections IX, X, and XI.

c) AGC Level

The AGC is a variable gain amplifier which adjusts the output from the three components of the geophone before input to the A/D converter. This allows the full dynamic range of the A/D converter to be used. A gain change always occurs once every record, in 1/2 dB increments. The gain decreases by 0.5 dB if more than 1 % of the points sampled after 5 seconds into the record on all three components are clipped; otherwise it increases by 1/2 dB. The maximum rate of change is therefore 2/3 dB per minute, given the 45 sec duration of a record. This implies that arrivals of sufficient amplitude to cause signal clipping must last long enough for the AGC level to adjust. Otherwise, only time of arrival information can be obtained.

The AGC level is quite similar for all the midwater floats. (Recall that float 8's data is offset by 84 records and float 9's data is offset by almost 95 records due to resynchronization). After the 12 dB decrease over the first 24 records (the AGC level is automatically set at 12 dB gain upon float synchronization; this initial decrease represents the maximum possible slope in these plots), the gain remains at zero during the noisy, 8-hour descent to depth. It then rises to a level between 15 and 20 dB, about 5 dB greater than in the April experiment [3]. The passage of the research vessel Scorpius over the top of the float array (see Figure II.2) caused the main dip in the AGC gain, beginning at about record 655 (21:52, 5 May) and lasting for about an hour. It is curious that a double-trough structure appears in the data. It suggests that perhaps the ship radiated sound in preferential directions or that propagation effects in an inhomogeneous waveguide are important. Note that a series of smaller troughs appear in the AGC gain after the ship passed over the array. These may be evidence of a range-dependent, constructive interference pattern between normal modes propagating in the deep sound channel. Troughs which appear later in the data, e.g. just after record 1700, may be due to the coupling of ship noise into the deep sound channel by bottom topography. The Patton escarpment, with up to a 20' slope, was located about 20 to 30 km northeast of the float array, the same direction in which the Scorpius left the study site. Note finally that the overall level in the AGC gain was 1 to 2 dB lower after the passage of the Scorpius than before.

The AGC gain for both bottom floats 9 and 10 remained at 0 dB for almost the full duration of the deployment. However, bottom float 11's AGC gain was greater than zero for two time intervals, between approximately records 400-700 and 1525-1700. In fact, for a 3-hour period after record 400, float 11's AGC gain was 3 to 4 dB higher than the highest gain attained by the midwater buoys. These two intervals are thought to represent times when the float, because of changes in the prevailing ocean current, was temporarily unrestrained by its tether to the bottom and was drifting freely. Therefore, the contamination from tether strumming, float rocking, flow noise, etc, was not present. Floats 9 and 10 presumably remained at the end of their tethers for the full duration of the deployment. This is consistent with the compass heading data for these two floats; their tethers prevented them from rotating.

IX. RMS Velocity and Pressure

The root mean squared signal level on the three components of the geophones in Swallow floats 0, 1, 2, 3, 4, 7, 8, 9, 10, and 11 are plotted to provide an indication of potentially interesting events in the data set. These plots are presented in Figures IX.1 through IX.10. The averaging period is 5 sec, or 250 points (since the geophone sampling rate is 50 Hz), yielding eight rms velocity values per component per record. Information on the geophone recording system is contained in Appendix 1.

For comparison, the rms velocity level on the three geophone components and the rms pressure level on the hydrophone for ocean bottom seismometers 1, 2, 4, 5, 6, 8, 12, 13, and 14 are also presented. These data are plotted in Figures IX.11 through IX.19. Refer to Tables I.8 and I.9 for the time of the first sample point for each event. Also refer to the table in Section Ib, which gives the correspondence between the recording times for the OBS events and the Swallow float records. The averaging period for Figures IX.11 through IX.19 is also 5 sec, or 640 sampled points because of the 128 Hz OBS sampling rate. Refer to reference [7] for a discussion of the OBS data acquisition system.

a) Swallow Float Data

i) Midwater Floats

Since the rms plots for the midwater buoys show similar features, the following discussion will use float 2's plots (Figures IX.3a through IX.3j) as reference.

The upward curving appearance of the rms levels for the first 24 records is caused by the decrease in the AGC setting as it steps in 0.5 dB increments from 12 dB to 0 dB gain. The geophone signal is clipped throughout this time and the apparent increase in signal level is due to the decrease in the AGC gain. Therefore, whenever clipping occurs, signal amplitude information cannot be obtained.

Around record 45, the float was deployed. The level on the z component decreases more quickly after deployment than on the horizontal components due to the rocking motion of the float as it descends. The large spikes appearing on the z component every 12 records (e.g. Figure IX.3c) is caused by the acoustic localization ping issued by the float. The pings cause the signal to be clipped; therefore, the fact that the spike amplitudes decrease as the float descends is due to the increase in the AGC gain, not a change in float-ping coupling. Small inter-ping spikes, clearly seen on the rms plots after the float has come to its equilibrium depth, are the impulses imparted to the float by the cassette tape recorder at the beginning of each record. The tape recorder impulses appear more clearly in float 3's vertical rms velocity plots and are especially strong in float 7 and 8's data. More will be said about tape recorder contamination in the next section.

The sources of the "large" arrival at record 365 (14:30, 5-5) in Figure IX.3b and the spikes around record 500 (16:11, 5-5) in Figure IX.3c on the z component are at present unknown. Many of the other midwater floats' rms velocity plots show similar spikes between records 300 and 500 (especially notable is the double arrival at float 3 at record 375; Figure IX.4b). The spike arrival times at the various floats differ enough so that a single acoustic source cannot account for the arrivals. The depth to which the floats have sunk when these spikes occur is between 1100 and 1600 m. One conjecture is that the signals are generated by pressure-induced "pops" and "creaks".

The rms velocity on the horizontal components begins to decay between records 475 and 500 (around 16:00, 5 May) and stops decreasing near record 600. As observed in previous deployments, the rms level remains higher on the horizontal components than on the vertical.

Also, the levels observed in this deployment are less than those in April [3]. This is probably due to differences in ship generated noise (both the United States Naval Service tug, the Narragansett, and the Scripps research vessel, the Melville, were on site in April; only the Scorpius was present in May) and with differences in the depth of float deployment (425 m in April vs 1800 m in May). Wind speeds were slightly higher in April than in May, but only marginally so.

A small arrival at record 781 (19:42, 5 May) appears on the horizontal components of all midwater floats. (Recall that since float 8 was resynchronized 63 minutes after the other floats, its data is offset by 84 records. Therefore, the arrival occurs at record 697 in float 8's data). This arrival may be ship related; the Scorpius was near bottom float 11's position ("B" in Figure I.1) finishing the deployment of XBT #3.

The dominant arrival on all three components just before record 975 is definitely ship related; it is caused by the aforementioned passage of the Scorpius across the float array. The arrival shape is due to clipping which commences at about record 969 to 970. As the AGC gain steps down to correct for the clipping, the gain-corrected rms velocity rises. The closest point of approach occurs at about record 972 when the rms velocity peaks, especially on the z component. Thereafter, the rms level decreases on the z component. However, the horizontal components show an interesting and complicated pattern. The clipped arrival around record 1010 is the cause of the second trough in the AGC gain plots mentioned in the previous section. A number of later arrivals occur on the horizontal components as the ship steams away from the array, resulting in the small troughs in the AGC gain plots in Section VIII. The following table provides a list of the arrival times of the more predominant signals and the float components on which the signals are easily visible:

Signal Arrival Times in RMS Velocity Data

Record Number	Local Time	Float Components Detecting Arrivals
1065	23:15	0(x,z), 2(x,y,z), 3(x,y,z) 4(x,y,z), 7(x,y), 8(x)
1068	23:17	0(x,y,z), 2(x,y,z), 3(x,y,z) 4(x,y,z), 7(x,y), 8(x)
1157	00:24	0(x,y,z), 2(x,y,z), 3(x,y) 4(x,y,z), 7(x,y), 8(x,y,z)
1160	00:26	0(y), 2(x,y), 3(y) 4(x,y), 7(x,y), 8(y)
1201	00:57	0(x,y,z), 2(x,y,z), 3(y) 4(x,y,z), 7(x,y), 8(x,y,z)
1268	01:47	0(x,y,z), 2(x,y,z), 3(x,y,z) 4(x,y,z), 7(x,y), 8(x,y,z)
1274	01:51	0(x,y,z), 2(x,y,z), 3(x,y,z) 4(x,y,z), 7(x,y,z), 8(x,y,z)
1282	01:57	0(x), 2(y), 3(y) 4(x,y), 7(x,y), 8(x)
1290	02:03	0(x,y,z), 2(x,y), 3(x,y) 4(x,y,z), 7(x,y), 8(y)
1412	03:35	0(x,y), 2(x,y), 3(y) 4(x,y), 7(x,y), 8(x,y)
1449	04:03	2(x,y,z), 3(x,y,z) 4(x,y,z), 7(x,y,z), 8(x,y,z)
1548	05:17	2(x,z), 3(y,z) 4(x,y,z), 7(y,z), 8(z)
1729	07:33	2(x,y,z), 3(x,y,z) 4(x,y,z), 7(x,y,z), 8(x,y,z)
1782	08:13	2(y), 3(x) 4(x), 7(x), 8(y)
1911	09:49	2(x,z), 4(x,y,z), 8(x,y)

Some of the arrivals above caused clipping of the geophone signals. The most prominent of the later arrivals, at record 1729, occurred when the Scorpius was 25 km northeast of the array and returning to the study site. Again, these arrivals may result from the constructive interference of normal modes propagating in the deep sound channel (or the result of convergence zones from a ray theory point of view) and/or from coupling of the ship noise into the sound channel by bottom topography (specifically, the Patton escarpment). A triple-peak arrival at record 1503 (04:45, 6 May) in float 2's rms velocity data was not detected by any of the other floats and so was not included in the above table.

ii) Bottom-Mounted Floats

The rms velocity levels for the bottom-mounted floats are shown in Figures IX.8, IX.9, and IX.10. Unlike the midwater floats, the vertical component remains completely clipped throughout the rapid descent to the bottom giving the maximum possible rms levels. The levels then quickly change once the floats have reached the bottom (just after record 210 for float 9, around record 330 for float 10, and record 375 for float 11). Note that the rms levels for floats 9 and 11 decrease once the bottom is reached, whereas float 10's levels increase.

The geophone signals are dominated by the effects of the tether to the bottom. However, as mentioned in the last section, there are short time intervals in which the tether-induced noise is reduced. Float 9's rms levels are relatively low between records 205 and 725, and between records 1450 and 1800. (Recall that since float 9 was resynchronized 71 minutes after the other floats, its data are offset by almost 95 records). For float 10, almost the entire geophone data set was tether-contaminated. A couple of short record sections between records 1200 and 1400 (Figure IX.9g) may contain useable data. Note that float 10's rms velocity on the y component between records 1325 and 1400 clearly show the spikes caused by the tape recorder.

Float 11's rms velocity data are less than maximum during much of the deployment, with an especially quiet period occurring between records 375 and 700. (Note that a 12-record sequence of the time series in this quiet period are plotted in the next section; Figures X.9c). The recording of the float's self ping every 12 records during this period shows a broad, low-level peak on the horizontal components, rather than the characteristic sharp spike seen in the mid-water float's data. This indicates that clipping took place throughout most of the record in which the self ping occurred. The apparent increase in the tape recorder contamination around record 700 in Figure IX.10d is due to the AGC gain reduction caused by the increasing tether contamination on the horizontal components. This increasing tether contamination masks the presence of the Scorpius which was just north of float 11 involved in the deployment of XBT #3 during record 785.

b) Ocean Bottom Seismometer Data

The three-component rms velocity level recorded by the geophone and the rms pressure recorded by the hydrophone on the nine operating OBSs are shown in Figures IX.11 through IX.19. As mentioned in Section Ib, the OBS instruments were programmed to record almost three minutes (179 sec) of data every three hours (OBS 5 and 6) or every six hours (OBS 1, 2, 4, 8, 12, 13, 14). Each three-minute piece of data comprises an event. Those events which were recorded while the Swallow floats were in the water during the May trip are shown. For event recording times, refer to Section Ib. Note, though, that event 311 for OBS 2 was recorded about 42 minutes earlier than for the other instruments, and events 313 and 315 were recorded about 12 minutes and 31 minutes earlier on OBS 8. The cause of this premature event recording, which happens in about 5 % of the cases, is thought to be due to misinterpretation of the obs clock signal. Also note that the horizontal geophone components are nonrotated, so that the individual geophone axes do not necessarily point in the same direction. The ocean bottom seismometers do not contain compasses, but, hopefully, the distribution of noise sources will be sufficiently azimuthally anisotropic to allow the horizontal axes to be properly aligned.

The maximum gain-corrected rms level is set to 1.0 counts on all plots. For some components, specifically the Cox-type hydrophones on OBS 1 and 5 (both instruments malfunctioned; re the next section) and the x-axis geophone component on OBS 14, the maximum level was greater than 1.0 for all May events. The maximum rms level was also sporadically greater than 1.0 for other OBS horizontal geophone components.

Spurious spikes occur throughout the data, e.g. in events 313 and 315 recorded by instrument 4's hydrophone channel and in events 315 and 317 recorded on OBS 12's vertical geophone axis. These spikes are not due to propagating energy in the medium since their occurrence is not coherent across the channels of an OBS, nor between one OBS and another. Also, some of the rms levels for an event appear to be suspiciously smooth. For example, the hydrophone channel for OBS 2 shows little variability, except during event 313.

A couple of generalizations can be made about the data. First, it appears that the highest rms levels were recorded during event 309. This event was recorded when the Scorpius was close to the array involved in the initial deployment of the Swallow floats (re Figure II.3). The increased level is especially prominent on the x axis of OBS 4.

Another feature of the geophone data is that the rms levels on the x axis are greater than on both the vertical axis and the y axis for most of the instruments; OBS 6 is the notable exception. The dominance of the x axis versus the y axis levels may indicate that the horizontal axes of most of the geophones were approximately aligned, and that the spatial distribution of the seismic energy sources was anisotropic. However, since seismic energy is composed of both shear and compressional wave components, the dominant mechanism of propagation must be known, or the signals from more than one instrument must be coherently combined, before information on the spatial distribution of the sources can be obtained. Another possibility is that the gimbal mechanism used for in situ leveling of the seismometer [7] did not completely compensate for seismometer tilts, thus degrading the sensitivity of one (or both) of the horizontal components.

The fact that the horizontal axis levels are consistently greater than on the vertical axis is an aspect that has been seen in the Swallow float geophone data for all deployments. However, the mechanisms of propagation in the two cases are different. The OBS geophones record the motion of the sediment, where the propagation of seismic energy in the sediment is probably dominated by low-order-mode, Stonely wave propagation in the 1-20 Hz frequency band [20]. The Swallow float geophones measure water particle velocity due to compressional sound propagation. In the water column, the ambient noise field in the very-low-frequency band is known to be anisotropic under calm weather conditions, with energy arriving mainly in the horizontal direction.

X. Geophone and Hydrophone Time Series

A sample of the time series recorded by the Swallow float geophones, the ocean bottom seismometer geophones, and the OBS hydrophones is shown in the next set of plots, Figures X.1 through X.18.

a) Swallow Float Data

Two blocks of records, records 957 through 968, and records 1300 through 1311, are plotted for each of the geophones' three orthogonal components of all recording Swallow floats. (Because of the time offsets due to resynchronization, records 873-884 and 1216-1227 are plotted for float 8, and those plotted for float 9 are 862-873 and 1205-1216). In addition, records 563 through 574 are plotted for bottom-mounted float 11 (Figures X.9c). The sampling rate for the Swallow float data in Figures X.1 through X.9 is 50 Hz for the 44 sec that the floats are accumulating data. The one second gap during the 45th second when the data is being written to cassette tape is shown as a straight line. The maximum amplitude is ± 1.0 volt. The vertical axis scale is only approximate in the plots in that the time series doesn't always attain full scale in a record; thus, the actual scale, since it isn't annotated, is not evident. Refer to Appendix 1 for more information on the geophone data acquisition system.

The times corresponding to the three blocks of records are 21:54 to 22:03 on 5 May for records 957-968, 02:11 to 02:20 on 6 May for records 1300-1311, and 16:58-17:07, 5 May for float 11's records 563-574. The first block of records was chosen since records 957-968 were written when the Scorpius was beginning to be heard by the floats as it steamed towards the array. Records 1300 through 1311 were written in the early morning hours of 6 May, while the Scorpius was about at its furthest point from the array (i.e. at the furthermost northeast point in Figure II.1). Float 11's block of 12 records from 563 to 574 were written when tether contamination was not present and when event 311 was recorded by the ocean bottom seismometers.

i) 8 kHz Acoustic Localization Ping

One very prominent arrival, especially on the z component, is due to the 8 kHz self-generated acoustic localization ping which occurs 10 seconds into the record in which the float is pinging. As mentioned before, the floats take turns issuing an 8 kHz ping; one float pings every 45 seconds. The order in which the floats ping is determined by their number. For example, float 0 pings in records 960 and 1308; float 2 pings in records 962 and 1310; float 3 pings in records 963 and 1311, etc. It is rather surprising that the localization ping is so well recorded on the geophones. The center frequency of the ping is 8 kHz, whereas the geophone sensitivity decreases sharply above 20 Hz (the sensitivity is down 19.5 dB at 25 Hz, re Appendix 1). In addition, the duration of the generated pulse is only 10 msec, yet the z component is clipped for up to a second after the ping arrival. Recently completed work has shown that an idealized model of the Swallow floats' glass sphere is resonant at 8 kHz [16, 25]. A nonlinear coupling mechanism between resonant modes may result in the creation of the very low frequency signal recorded on the geophones. Alternatively, since the localization hydrophone source level is so high (192 dB re 1 μ Pa at 1 meter) and the geophone circuit is so sensitive (a fixed gain of 95 dB occurs in addition to the AGC gain presented in section VIII, re Appendix 1), then the hydrophone need generate just a small amount of 1-20 Hz energy in order for it to be heard on the geophones. The short duration of the localization ping insures that, at least theoretically, some low frequency power is generated (about 45 dB lower than the power at 8 kHz). The ringing that is observed could then be caused by the smearing effect of the geophone response on the time series [16]. A third possibility is that 8 kHz energy is aliased into the 1-20 Hz frequency band. The anti-aliasing filter response (re Appendix 1) near 8 kHz is 86 db below the passband level; the locali-

zation ping may, however, be sufficiently loud to overcome the filter attenuation.

The duration of clipping on the z component caused by the float's self ping *may* be greater in April than in May. This is especially notable since the AGC gain in April was lower than in May. The implication is that the 8 kHz ping was more effectively coupled into motion at the geophones in April than in May. The reason, as stated in Section VI with regard to the later arrivals in the 8 kHz data, may be due to the difference in temperatures, 6.1° C in April vs 2.3° C in May, at the two deployment depths. The resonant frequency of the floats' glass sphere is sensitive to the speed of sound in the enclosed air, which is temperature-dependent. Note that the localization ping has a marked effect on the bottom-mounted float 11's data (Figures X.9c); the z component in Figure X.9c.k is clipped for over 2.5 seconds. The temperature of 1.5° at the bottom may have caused the glass sphere to again become tuned to the 8 kHz ping.

ii) Tape Recorder Contamination

A troublesome contaminating effect that appears at the beginning of most of the records is caused by the action of the cassette tape recorder. Much effort has been expended in filtering out this contamination [17]. Also, modifications were made to the supports for the RF antennae on the floats prior to the April deployment, since laboratory studies had shown a correlation between the signal induced on the geophones by motion of the antennae and the observed contamination. The following table lists the various reinforcements that were added to the RF antennae supports:

Float	Addition to Radio Beacon Antenna Support
0	metal clamp and rubber pads
2	PVC staves
3	nylon guy wires
4	Stainless steel clamp with rubber pads
7	Vinyl tube with conduit
8	PVC staves
9	PVC staves
10	PVC staves with nylon guy wires
11	Stainless steel clamp with rubber pads

The second set of floats constructed at MPL (floats 3, 7, 8, 9, 10, and 11) were outfitted with a "noisier" type of tape recorder than the first six floats (floats 0, 1, 2, 4, 5, and 6). Floats 3, 7, 8, and 11 (in records 563-574) are obviously more contaminated by tape recorder effects than the other midwater floats. The nylon guy wires attached to float 3's radio beacon support appear to have shortened the period of the contamination compared to floats 7 and 8. However, the reduction may have also been a result of the placement of the float 3's resident ballast, in the form of an epoxy, lead shot mixture, inside the glass sphere, as well as the additional support provided by the nylon guy wires. The tape recorder may impart an impulse to the float's glass sphere, which then rings. The placement of the epoxy, lead shot mixture on the inside bottom of the glass shell may have damped the ringing.

The other midwater floats typically show a second or so of contamination on the y axis, little contamination on the vertical axis, and some amount of 3 second oscillations on the x axis. A calculation, assuming no viscous dissipation and an ideal float model for the analytical computation of the floats' moment of inertia, predicts a float rocking period of 2 sec. The restoring force is provided by the float's ballast weights. The tape recorder may therefore excite float

rocking in a way such that it is preferentially recorded on the x axis. Float rocking may limit the interpretation of the Swallow float data at frequencies near the microseism peak.

iii) Ambient Ocean Noise

The data recorded during the early morning hours of 6 May (records 1300 to 1311) are much quieter than those recorded in the early morning hours of the April trip. One contributing factor is the difference in deployment depths; the data in the April experiment were collected much nearer the sound channel axis and the surface than in this deployment. However, the close proximity of the Melville to the array in the April deployment certainly increased the observed levels.

An aspect of the geophone data that has been observed in all Swallow float deployments is that the noise levels on the z component are lower than on the x and y components. This suggests that most of the ambient noise is propagating in the horizontal direction. The calm weather conditions at the study site during the experiment, the distance of shipping traffic from the float array, and the deployment of the floats above the critical depth would be plausible arguments for such an observation in this experiment. Once the floats are localized, and the differences in float clock drifts/offsets are accounted for, the coherence between the floats' time series will hopefully be sufficiently large to allow beamforming to determine the azimuthal dependence of the ambient noise level.

The time series recorded by bottom-mounted float 11 while it was uncontaminated by tether strumming (records 563-574 in Figures X.9c.i through X.9c.k) shows lower noise levels, especially on the horizontal components, than the midwater floats. During the writing of this interval of records, the Scorpius was over 9 km to the northwest. The lower levels are probably due to the float being significantly below the critical depth.

b) Ocean Bottom Seismometer Data

The time series for events 311, 313, 314, and 315 for all recording components during the May trip are plotted in Figures X.10 to X.18. These events were chosen for plotting because: event 311 was recorded at the same time as records 566-571, when bottom-mounted Swallow float 11 was free of tether effects, event 313 was recorded as the Scorpius was leaving the array area after having passed overhead, event 314 was recorded just 10 minutes before Swallow float record 1300, during a time presumably devoid of Scorpius ship noise, and event 315 was plotted since only two OBS instruments recorded event 314 and environmental conditions were about the same during event 314 and 315. Refer to Section Ib for the exact time that each event was recorded and the correspondence between OBS event number and Swallow float record number.

Two events are shown on each plot; the events are separated by a dashed line. Each 179-second event is divided into four 45-second time series; the last time series is nonzero for only the first 44 seconds. This time scale was chosen to correspond to the Swallow float time scale in Figures X.1 through X.9. The vertical scale is determined by the largest deviation from zero over both events and is given at the top of the plots. The data sampling rate was 128 Hz.

The quality of the recorded data for both the regular OBS hydrophones and the Cox-type hydrophones is not very good. Of the three hydrophones of the Cox-type design, only the hydrophone on OBS 6 recorded useable data; the hydrophone on OBS 1 appears to be contaminated by some electrical signal and the one on OBS 5 stopped recording data some time between the April and May Swallow float deployments. The regular OBS hydrophone time series are, in many cases, contaminated by down-going spikes spaced a half-second apart (e.g. OBS 8, Figures X.15a.l and X.15b.l; OBS 12, Figures X.16a.l and X.16b.l; OBS 13, Figures X.17a.l and X.17b.l; and OBS 14, Figures X.18a.l and X.18b.l). This Dirac-delta-comb-like contamination is believed by Dr. Dorman's group to be due to the hydrophone software. Filtering out this contamination

would probably result in useable data, especially for OBS 8. In addition, sporadic spikes of large amplitude occur in many of the data. For example, the hydrophone data for OBS 4 (Figures X.12a.l and X.12b.l) shows little structure due to normalization by the large amplitude of infrequently occurring spikes and OBS 14's data (Figures X.18a.l and X.18b.l) contains a large number of both up-going and down-going spikes.

The OBS geophone data, on the other hand, appears to be of consistently good quality. (Only the *y* and *z* axes of OBS 5 and the *x* axis of OBS 6 appear to be at all contaminated. This is thought to be due to a problem with the tape recorder software which sometimes allowed a sample from the wrong channel to be recorded. The missing component data for OBS 12 was due to the difficulty in transcribing its data cassette tape). A somewhat surprising observation is that for some of the instruments, a difference in frequency content between the geophone components exists. The *y* axis of OBS 1 has higher frequency content than its other two components and the time series for the three components of instruments 2 and 4 look different. This aspect of the data will be discussed further in Section XI.

A coherent arrival was recorded 10 to 15 seconds into event 313 on many of the OBS geophones' vertical axis, re Figure X.11a.k for OBS 2, Figure X.12a.k for OBS 4, Figure X.13a.k for OBS 5, Figure X.14a.k for OBS 6, and Figure X.17a.k for OBS 13. This arrival can also be seen on some of the rms velocity plots of the midwater-column Swallow floats (Figure IX.1f for float 0, IX.3f for float 2, IX.4f for float 3, and IX.5f for float 4). The signal was however recorded well on the *horizontal* Swallow float geophone components rather than the *vertical* axis as in the OBS geophone data. Again, the difference may be due to the difference in the mode of signal propagation in the water column and in the sediment. The signal was probably ship-generated since the Scorpius had sailed over the top of the array about an hour ago, and was still about 9 km to the northeast (Figure II.2).

XI. Velocity and Acoustic Pressure Power Spectra

The power spectral estimates for each Swallow float geophone component (in Figures XI.1 through XI.9) and each OBS geophone component and hydrophone (in Figures XI.10 through XI.18) for selected time periods are now presented. The time periods chosen for further analysis were Swallow float records 968 (collected at 22:02, 5 May) and 1311 (02:20, 6 May) for all floats, records 566 through 571 (17:01 to 17:04, 5 May) for bottom-mounted float 11, and OBS events 311 (17:01, 5 May), 313 (23:01, 5 May), 314 (02:01, 6 May), and 315 (05:01, 6 May). Swallow float record 968 was recorded while the *Scorpius* was almost over the Swallow float array and record 1311 was written while the ambient noise levels were supposedly uncontaminated by ship noise, as were OBS events 314 and 315. OBS event 313 was recorded as the *Scorpius* steamed away from the array to the northeast. Event 311 was recorded at the same time as records 566 through 571, corresponding to a time when Swallow float 11 was uncontaminated by tether effects.

The Swallow float geophone power spectral estimates were made by dividing a 40.96-sec portion of each 44-sec-long record into seven 512-point segments (10.24 sec long), with a 50 % overlap between segments. The 40.96-sec piece was gotten after skipping over the first three seconds of each record to avoid contamination from the tape recorder impulse. Each 10.24-sec segment was then Fourier transformed after being windowed with a Kaiser-Bessel window with $\alpha = 2.5$. (A 4π prolate spheroidal window of order 0 was also used because it provides superior protection against broadband bias [31] and the dynamic range of the underlying spectrum is quite large below 5 Hz. The resulting spectral estimates were indistinguishable from those gotten using the Kaiser-Bessel window. This is due to the pre-whitening effect of the Swallow float geophone response, shown in Appendix 1). The seven estimates were then averaged incoherently to reduce the variance of the estimates. The OBS geophone and hydrophone estimates were gotten by taking the first 32 sec of each event and partitioning it into seven 8-sec long portions which were also overlapped by 50 %. The segments were then windowed and transformed just as with the Swallow float data. Again, the seven estimates were incoherently averaged, giving a 90 % confidence interval for the estimates of about +3.3 dB to -2.3 dB.

All geophone-component power spectral estimates were calibrated to give units of dB re $(1m/sec)^2$ per Hz. Refer to Appendix 1 for information on the Swallow float geophone system, reference [7] for information on the OBS geophones and regular hydrophones, and reference [6] for information on the Cox-type hydrophones installed on OBS 1, 5, and 6. For the Swallow float geophone data, the factor of 243.5 dB re $(1\mu Pa)^2/(m/sec)^2$ (explained in the next paragraph) was then added to convert the units of the Swallow float particle velocity power spectrum from dB re $(1m/sec)^2$ per Hz to equivalent pressure power units of dB re $(1\mu Pa)^2$ per Hz. The Swallow float pressure power spectral estimates at the top of the figures were derived by summing together the three geophone components' power spectra [2]. This procedure allows comparison of the Swallow float spectrum levels with those reported in the underwater acoustics literature. The OBS pressure power spectral estimates were obtained directly from the hydrophone data. Future enhancements to the Swallow floats include the installation of a very low frequency, sensitive hydrophone to eliminate the need to derive the pressure power spectrum.

The conversion factor of 243.5 dB re $(1\mu Pa)^2/(m/sec)^2$ comes from the fact that acoustic pressure is related to particle velocity in a dense fluid by $\rho_0 c$, where ρ_0 is the ambient water density and c is the speed of sound. Assuming plane wave propagation in a homogeneous medium of density 1000 kg/m^3 and speed of sound 1500 m/sec , then this factor is equal to 243.5 dB re $(1\mu Pa)^2/(m/sec)^2$ [2]. Accounting for the true density and speed of propagation in the ocean could increase this factor by up to a half dB or so. However, the unknown degree of curvature of the received wave field reduces this factor by an amount dependent upon kr , k being the propagation vector and r the range [30]. Therefore, the relationship is only approximate.

Note that the conversion discussed above was not applied to the OBS geophone data. In an elastic medium which can support shear stress, the principle components of stress are not equal, and the above procedure is not valid. However, one boundary condition at the ocean-

sediment interface is the continuity of vertical particle velocity. (The horizontal particle velocity components of the sediment do not couple into the water because of the water's inability to support shear. This may be one way of explaining the larger levels on the horizontal components of the OBS geophones compared to the vertical component; the horizontal components experience a free surface at the ocean-sediment interface whereas the vertical component does not). Therefore, under the plane-wave approximation to the particle velocity-pressure relationship, the OBS vertical geophone component's spectrum can be converted into an equivalent pressure spectrum in the water just above the interface by adding 243.5 dB re $(1\mu Pa)^2/(m/sec)^2$.

a) Swallow Float Data

The power spectral estimates from the Swallow float geophone data are shown in Figures XI.1 through XI.9. Those spectra recorded while the noise field was relatively free of Scorpius ship noise, i.e. record 1311 for all recording floats (corresponding to record 1227 for float 8 and record 1216 for float 9) and records 568-571 for float 11, will be discussed first. The effects of the close proximity of the ship during record 968 will then be presented in part ii).

i) Background Ambient Noise

The dominant feature in the spectra is the rise in noise levels to the microseismic peak as frequency is decreased below 5 Hz. The derived pressure spectral levels in record 1311 for the midwater floats, Figures XI.1b, 2b, 3b, 4b, 5b, and 6b, change from about 75 db re $(1\mu Pa)^2$ per Hz at 5 Hz to almost 110 dB at 1 Hz. It should be noted that uncertainties in the calibration curve of the geophone and lack of knowledge of the system electronic noise below a few Hertz makes interpretation of the spectra in this frequency range difficult. Above 5 Hz, the spectra are relatively flat, remaining at a pressure power level of about 75 db re $(1\mu Pa)^2$ per Hz. Note that the derived pressure power spectrum is dominated by the power on the horizontal components; the spectral levels on the z axis are 10 to 15 dB lower than the horizontal components.

The spectral levels above 5 Hz for float 11 in records 568 through 571 (Figure XI.9c through Figure XI.9h) are about 10 dB lower than those for the midwater floats. Since the ocean bottom is significantly below the critical depth, the bottom-mounted floats are shielded at the higher frequencies from noise propagating in the deep sound channel. At lower frequencies, below a few hertz, the deep sound channel can no longer trap acoustic energy. Note that the spectral levels at 1 Hz recorded by float 11 are about the same as those recorded by the midwater floats. (See also a plot of spectral differences in Figure XI.10e presented in the next section). However, some tether-generated noise may still be present in float 11's geophone data which is not present in the midwater column float data; re part ii of this section.

A broad spectral peak at 12.6 Hz appears on all three geophone components for the midwater column floats during record 1311 as well as for float 1' in records 568 through 571. Although this peak is up to 10 dB above the background noise on all three components, it is predominantly arriving from a nearly horizontal direction since the background levels on the horizontal components are much greater than on the vertical component. An accompanying spectral peak occurs at 18.2 Hz. The source, or sources, of these peaks is unknown.

ii) Tether and Ship Generated Signals

A predominant feature of the bottom-mounted Swallow float geophone data is the contaminating effect of the float tether to the bottom. The large spectral peaks in Figures XI.7 through XI.9b are due to the tether. These peaks occur mostly below 5 Hz; peaks at higher fre-

quencies occur only when the time series are clipped. The presence of the tether generates a geophone signal probably by causing the float to rock in a bottom current about the pivot point at which the tether is attached to the float. Variations in the tension on the tether may also cause the glass sphere to vibrate. In addition, the tether itself may also strum, although if this was a significant contributing factor, the strumming frequency could be moved to frequencies outside the range of interest by redesigning the float tether.

The spectra for the midwater column floats equipped with noisy cassette tape recorders, floats 3, 7, and 8 (re Section X), show low frequency spectral peaks due to excitation of float rocking by the tape recorder. These spectral peaks, recorded most predominantly on the horizontal components, would have been of greater magnitude if not for the three-second delay introduced at the beginning of each record.

The presence of the Scorpius in record 968 is most clearly indicated by the spectral peak on the z axis at 20.8 Hz. Its amplitude on the midwater column floats' spectra is between 65 and 70 dB re $(1\mu Pa)^2$ per Hz, or -179 to -173 dB re $(1m/sec)^2$ per Hz. While the ship was passing over the top of the array, a tachometer readout on the bridge indicated that the engines' rotation rate was 1200 rpm. (Direct measurements of the engines' rotation rate were made about 30 minutes after record 968 was recorded, at the same ship speed as in record 968. These measurements indicated that the port engine was turning at 1110 rpm and the starboard engine was rotating at 985 rpm. However, the measurements were very difficult to make). Using a reduction gear ratio of 3.8-to-1, and the fact that the Scorpius prop has four blades, the predicted blade rate frequency is 21.1 Hz, which is quite close to the location of the spectral peak. The blade rate frequency line is buried in the background noise on the horizontal components.

The presence of the Scorpius also causes a broadband increase of up to almost 20 dB in the spectral levels between about 4 and 10 Hz. This effect can most easily be seen by plotting the difference in spectra recorded while the Scorpius was near the array and when it was far from it. Figure XI.10a presents the result of subtracting the spectrum recorded by float 0 during record 968 from that recorded during 1311. This plot is representative of the differences measured by the other midwater column floats. The difference is greatest around 5 Hz. Note also the upgoing peak at 12.6 Hz on all three components discussed in part i) above and the down-going peak at 20.8 Hz on the z axis corresponding to the blade rate frequency of the Scorpius.

Four additional spectral differences plots are given. Note that the spectrum from the float and record listed first in the figure title is subtracted from the spectrum recorded by the second float and record. In Figure XI.10b, a comparison is made between the spectra measured by float 0 and by float 2 during record 968. Taking into account the (+3.3 dB)-to(-2.2 dB) 90 % confidence interval for the spectral estimates, the spectra measured by the two floats differ by an insignificant amount, especially in the derived pressure spectra. Figure XI.10c presents the comparison for record 968 between float 0 and float 7. The spectral peaks due to float rocking caused by the noisy cassette tape recorder in float 7 are clearly evident. The lower levels recorded by float 7's y axis compared to float 0's y axis, which are not completely compensated by a reciprocal relationship between the two floats' x axes, may be partially explained by the Scorpius being closer to float 0 than to float 7 during record 968. The difference in the spectra during record 968 for floats 0 and bottom-mounted float 11 is shown in Figure XI.10d. Only float 11's x axis was partially clipped during this time (re Figures X.9a). Except for the tether-contaminating effects below 5 Hz, the spectral levels recorded by float 0 are greater by about 5 dB than those recorded by float 11.

Finally, the last spectral difference plot, Figure XI.10e, illustrates the difference in ambient noise levels recorded by the midwater column floats and the tether-uncontaminated bottom-mounted floats. (Refer to the discussion in part i of this section regarding this point). The surface environmental conditions during the recording of records 968 and 1311 were quite similar. The spectral levels above 5 Hz recorded by bottom float 11 are 5 to 10 dB less than those recorded by midwater float 0. The difference is especially marked on the horizontal components. This may be indicative of the difference in the two floats' ability to hear distant sources. Below 5 Hz, the two floats' spectral levels become approximately equal, due either to the inability of

the sound channel to trap very low frequency sound or to possible contamination by float 11's tether. Note the tape-recorder-induced peak at about 0.5 Hz on float 11 spectra.

b) Ocean Bottom Seismometer Data

Figures XI.11 through XI.19 plot the power spectral estimates obtained from the ocean bottom seismometer data. Only the first half of the frequencies, up to 32 Hz, are plotted so that the frequency range of the horizontal axes approximates that of the Swallow float power spectral plots. The power spectra are in units of dB re $(1\mu Pa)^2$ per Hz for the hydrophone data and dB re $(1m/sec)^2$ per Hz for the geophone data.

As mentioned in the previous section, the hydrophone data in the top panel of the figures is not of very good quality. Of the three Cox-type hydrophones, only the one on OBS 6 functioned properly during the May Swallow float deployment and it provided useable data only up to about 1 Hz. (See also [6]). The regular OBS hydrophones spectra are contaminated in most cases by spectral peaks spaced every 2 Hz due to the hydrophone software spikes discussed in Section X. The exception is the data for OBS 4. Background levels are about 75 to 80 dB re $(1\mu Pa)^2$ per Hz above 10 Hz, but the levels vary by up to 15 dB between instruments. Compare the levels reported by OBS 14 (Figure XI.19a) to those reported by OBS 4 (Figure XI.13a). Also, a jump of about 5 dB in the spectrum level above 10 Hz occurs between events 313 and 315 for OBS 4 (Figures XI.13b and XI.13c) without a corresponding jump in levels between these events for the other instruments. This variability in background levels is probably due to the sporadic spikes in the hydrophone data discussed in Section X. These spikes must be filtered out of the time series before reliable spectra can be calculated. In any case, the background levels reported by some of the hydrophones during event 311 approximate those derived from bottom-mounted float 11's geophone data during records 566 through 571 (compare Figure XI.17a for OBS 12 and Figure XI.18a for OBS 13 with Figures XI.9c through XI.9h).

The OBS geophone data in the bottom three panels of the figures have the same overall appearance as the Swallow float geophone data; a relatively flat spectrum above a transition frequency of about 5 to 10 Hz and the rise towards the microseismic peak below this frequency. However, it appears that the frequency at which this transition occurs is much more variable in the OBS data than in the Swallow float data. For example, the y component of OBS 1 in event 313 (Figure XI.11b) has a transition frequency of about 1 Hz, whereas the x axis does not reach its asymptotic level until about 9 Hz. This is reflective of the difference in the appearance of the various components' time series, as mentioned in Section X. The various time series also appear differently because of the puzzling occurrence of spectral "lumps". The y axis of OBS 1, 2, and 4 above 26 Hz and the x axis of OBS 4 centered around 19.2 Hz contain high spectral values.

The spectral levels above the transition frequency, excluding the aforementioned spectral "lumps", are generally between -175 and -190 dB re $(1m/sec)^2$ per Hz. This is exactly the range of geophone levels measured by Swallow float 11 during records 566 to 571. (To convert the Swallow float data from units of dB re $(1\mu Pa)^2$ per Hz to dB re $(1m/sec)^2$ per Hz, subtract 243.5 dB, as discussed at the beginning of this section). The horizontal components are generally 5 to 10 dB higher than the vertical component, similar to the Swallow float data. However, the mechanisms of noise propagation are different in the two cases, as discussed in Section IX, part b.

A few spectral peaks appear to be consistently recorded by the ocean bottom seismometers. A 25.0 Hz peak occurs during event 311 on the z axis of all instruments and on some of the horizontal components. This peak is unfortunately outside the frequency range that is plotted for Swallow float 11 spectra. (There is a possibly related, 24.1 Hz peak on float 11's vertical axis in records 566, 568, and 569). It may have been caused by the Scorpius, which was about 8 km from the OBS array (but over 9 km from Swallow float 11). The ship possibly also caused the peak at 23.7 Hz on the horizontal components during event 313, as it steamed away from

the array. How this ship-generated energy in the water column becomes coupled into horizontal, ocean-sediment interface motion is a question yet to be answered. The frequency of this 26.7 Hz peak is not too different from the blade rate frequency of 20.8 Hz recorded by the Swallow floats an hour earlier. Another peak during this event at 19.9 Hz, which only appears on the z axis spectra recorded by instruments 1, 2, 4, and 12, may also be associated with the blade rate frequency peak. However, this 19.9 Hz peak seems to also be present during event 315, when the ship was over 30 km from the array.

An additional set of spectral peaks which appear in both events 313 and 315 are at 12.8 Hz and 13.5 Hz. Recall that the Swallow float data recorded during record 1311 (almost three hours earlier than event 315) also showed a peak at 12.6 Hz. All of these peaks occur predominantly on the x and y axes. This is also true of a 7.8 Hz peak, which is present mostly during event 315. A consistent, 18.2 Hz peak recorded by all instruments on the horizontal components during event 315 also corresponds to a spectral peak previously recorded by the Swallow float data (refer to part a) of this section). As mentioned previously, the source of these spectral peaks is unknown.

Acknowledgements

We would like to thank Marvin Darling at the Marine Physical Laboratory for his many contributions to the Swallow float project. We appreciate the ocean bottom seismometer data provided to us by Dr. Dorman and his research team and the many helpful discussions we had with them. The crew of the Scorpius was very patient and helpful.

We want to also thank the following people who provided us with necessary supplemental data:

Jim Charters at Scripps Institution of Oceanography,
Jay Morford at the Fleet Numerical Oceanography Center,
Rich Dixon at the Pacific Missile Test Center,
Mr. Mikoly at the Naval Oceanography Command Facility,
Dr. R. Seymour and Julie Thomas with the Coastal Data Information Program.

This work was supported by the Office of Naval Research, Code 1125, under contract N00014-87-K-0010.

References

- [1] W. S. Hodgkiss and V. C. Anderson, "Acoustic positioning for an array of freely drifting sensors" IEEE J. Oceanic Eng. 8(3), (1983).
- [2] Richard L. Culver, "Infrasonic ambient ocean noise spectra from freely drifting sensors" SIO Ref 85-22, Marine Physical Laboratory, Scripps Institution of Oceanography, San Diego, CA (1985).
- [3] G. L. D'Spain, R. L. Culver, W. S. Hodgkiss, and G. L. Edmonds, "Trip report - April, 1987 Swallow float deployment" Marine Physical Laboratory, Scripps Institution of Oceanography, San Diego, CA (1987).
- [4] R. S. Yeats, B. U. Haq, et al, "Site 469: base of the Patton escarpment" in Initial Reports of the Deep Sea Drilling Project 63, (1981).
- [5] A. W. Sauter, L. M. Dorman, and A. E. Schreiner, "A study of the sea floor structure using ocean bottom shots and receivers" in Ocean Seismo-Acoustics, ed. T. Akal and J. M. Berkson, Plenum Press, (1986).
- [6] C. S. Cox, T. Deaton, and S. C. Webb, "A deep sea differential pressure gauge" J. Atmos. Oceanic Technol. 1, (1984).
- [7] R. D. Moore, L. M. Dorman, C. Y. Huang, and D. L. Berliner, "An ocean bottom, microprocessor based seismometer" Marine Geophys. Res. 4, (1981).
- [8] J. Churgin and S. J. Halimski, Temperature, Salinity, Oxygen, and Phosphate in Waters off the United States, Eastern North Pacific, National Oceanographic Data Center, 3, (1974).
- [9] C. S. Clay and H. Medwin, Acoustical Oceanography, J. Wiley and Sons, (1977).
- [10] R. Urick, Principles of Underwater Sound, 3rd ed., McGraw-Hill, (1983).
- [11] R. L. Culver, W. S. Hodgkiss, G. L. Edmonds, and V. C. Anderson, "Freely drifting Swallow float array: September, 1986 trip report" MPL Tech. Mem. 391, Marine Physical Laboratory, Scripps Institution of Oceanography, San Diego, CA (1987).
- [12] L. Brekhovskikh and Yu. Lysanov, Fundamentals of Ocean Acoustics, Springer-Verlag, (1982).
- [13] R. L. Culver, G. L. D'Spain, and W. S. Hodgkiss, "Vertical oscillation in freely drifting Swallow floats" Marine Physical Laboratory, Scripps Institution of Oceanography, San Diego, CA (1987).
- [14] R. L. Culver, W. S. Hodgkiss, V. C. Anderson, J. C. Nickles, and G. L. Edmonds, "Freely drifting Swallow float array: initial estimates of interelement range" MPL Tech. Mem 380, Marine Physical Laboratory, Scripps Institution of Oceanography, San Diego, CA (1985).

- [15] R. G. Williams, "The internal tide off Southern California" SIO Ref. 86-1, Marine Physical Laboratory, Scripps Institution of Oceanography, San Diego, CA (1986).
- [16] G. L. D'Spain, "The resonant response of the Swallow floats' glass sphere" Marine Physical Laboratory, Scripps Institution of Oceanography, San Diego, CA (unpublished notes).
- [17] R. L. Culver, W. S. Hodgkiss, G. L. Edmonds and V. C. Anderson, "Removing resonant oscillation signals from Swallow float data" MPL Tech. Mem. 395, Marine Physical Laboratory, Scripps Institution of Oceanography, San Diego, CA (1987).
- [18] P. M. Morse, *Vibration and Sound*, American Institute of Physics, (1976).
- [19] V. C. Anderson, "Sound scattering from a fluid sphere" J. Acoust. Soc. Am., 22 (4), (1950).
- [20] A. E. Schreiner, L. M. Dorman, J. A. Hildebrand, D. Lahav, and D. Bibee, "Observations of deep-ocean ambient noise using a seismometer array" J. Acoust. Soc. Am. Suppl. 1, 82, DD7, (1987).
- [21] E. S. Maloney, *Dutton's Navigation and Piloting*, Naval Institute Press, 13th ed., (1978).
- [22] M. Pieuchot, *Seismic Instrumentation*, vol. 2, from *Handbook of Geophysical Exploration*, Section I - Seismic Exploration, ed. K. Helbig and S. Treitel, Geophysical Press, (1982).
- [23] A. B. Williams, *Electronic Filter Design Handbook*, McGraw-Hill, (1981).
- [24] A. Antoniou, *Digital Filters: Analysis and Design*, McGraw-Hill, (1979).
- [25] G. C. Gaunaudi and A. Kalnins, "Resonances in the sonar cross sections of coated spherical shells", Int. J. Solids Structures, 18 (12), (1982).
- [26] R. L. Culver, G. L. D'Spain, W. S. Hodgkiss, and G. L. Edmonds, "Timing errors in the Swallow float data" Marine Physical Laboratory, Scripps Institution of Oceanography, San Diego, CA (in press).
- [27] G. L. D'Spain, W. S. Hodgkiss, and G. L. Edmonds, "Trip report - August, 1987 Swallow float deployment with RUM" MPL Tech. Mem. 400, Marine Physical Laboratory, Scripps Institution of Oceanography, San Diego, CA (1987).
- [28] K. V. Mackenzie, "Nine-term equation for sound speed in the oceans" J. Acoust. Soc. Am., 70 (3), (1981).
- [29] Scripps Institution of Oceanography, "Data Report - Physical, Chemical, and Biological Data, CalCOFI Cruise 8703 and 8705, SIO Ref. 87-19, (1987).
- [30] G. L. D'Spain, "The calculation of acoustic pressure from particle velocity revisited" Marine Physical Laboratory, Scripps Institution of Oceanography, San Diego, CA (unpublished notes).
- [31] D. J. Thomson, "Spectrum estimation techniques for characterization and development of WT4 waveguide-I" Bell Syst. Tech. J., 56, (1977).

Appendix 1 - Swallow Float Geophone Data Acquisition System

A block diagram of the Swallow float geophone system appears in Figure A1.1. (Note that the figures for this appendix appear immediately following the text, before Appendix 2). The water particle motion is first coupled into motion at the geophone. The particle velocity at the geophone is then converted into voltages representing the three orthogonal components of particle velocity. The geophones are electromagnetic transducers in which a voltage is produced across a moving, conducting coil by its motion through the magnetic field lines produced by a permanent magnet. The resulting voltage is proportional to the velocity of the coil with respect to the magnet. Constraining the coil to move in only one direction are elastic springs connecting the coil to the instrument casing. (Laboratory tests have determined that the geophones can withstand a maximum tilt from vertical of about 15°). Using the theoretical equation of motion for this system [22], the transducer frequency response was derived and is shown in Figure A1.2. (The amplitude response curve is identical to the manufacturer's calibration curve provided with the geophones). The near-critical damping of the coil is achieved using a $60\text{ k}\Omega$ shunt resistor. Note that the f^2 roll-off of the geophone amplitude response below the natural frequency of 8 Hz aids in "pre-whitening" the ocean ambient noise, which appears to increase as f^{-4} below about 5 Hz. The geophone in each Swallow float is composed of three such transducers oriented to measure in three orthogonal directions.

The three signals next undergo a fixed gain of 95 dB and an additional gain determined by the AGC (see Section VIII) so that the full dynamic range of the A/D converter can be used.

Before digitizing, the signals are passed through a five-pole, four-zero, elliptic, anti-aliasing filter. Elliptic filters theoretically have the sharpest transition region for a given number of poles and circuit complexity. The filter frequency response and the pole, zero locations in the s plane are shown in Figure A1.3 [23,24]. Incoming signals are amplified by a maximum of 4.6 dB in the passband, which has a 0.28 dB equal ripple. The cut-off frequency (the highest frequency at which the amplitude gain is equal to the passband gain) is 20 Hz, and the attenuation is 19.5 dB at the Nyquist frequency of 25 Hz. The maximum equal ripple level in the stop band is 50.1 dB below the level in the pass band and is first reached at 31 Hz. Before installation in the floats, all filters were adjusted so that broadband noise input to the filters yielded the same amplitude response and same null location at the filters' output.

The three signals are then digitized at a 50 Hz sampling rate and then put into a temporary buffer. After 44 seconds of data (equal to one data record) have accumulated in the buffer, a one second period of writing the data to cassette tape takes place. During this time, no data is accumulated. The 45 second cycle then repeats until the cassette tape is full. The cassette tape can store up to 17 Mbytes of unformatted data, which is sufficient space for up to 2000 data records.

Both the RMS velocity plots discussed in Section IX and the geophone time series plots of Section X have been corrected for the variable AGC level. No other adjustments have been made in these plots. The power spectral plots of Section XI, however, have been corrected for all electronic system gains (including the geophone and the anti-aliasing filter responses) and therefore report estimates of the actual signal power level at the input to the geophones.

In the summer of 1988, the entire geophone data acquisition system will be calibrated in the Navy calibration facility in Hotham Sound in southeastern Canada.

BLOCK DIAGRAM OF THE GEOPHONE DATA ACQUISITION SYSTEM

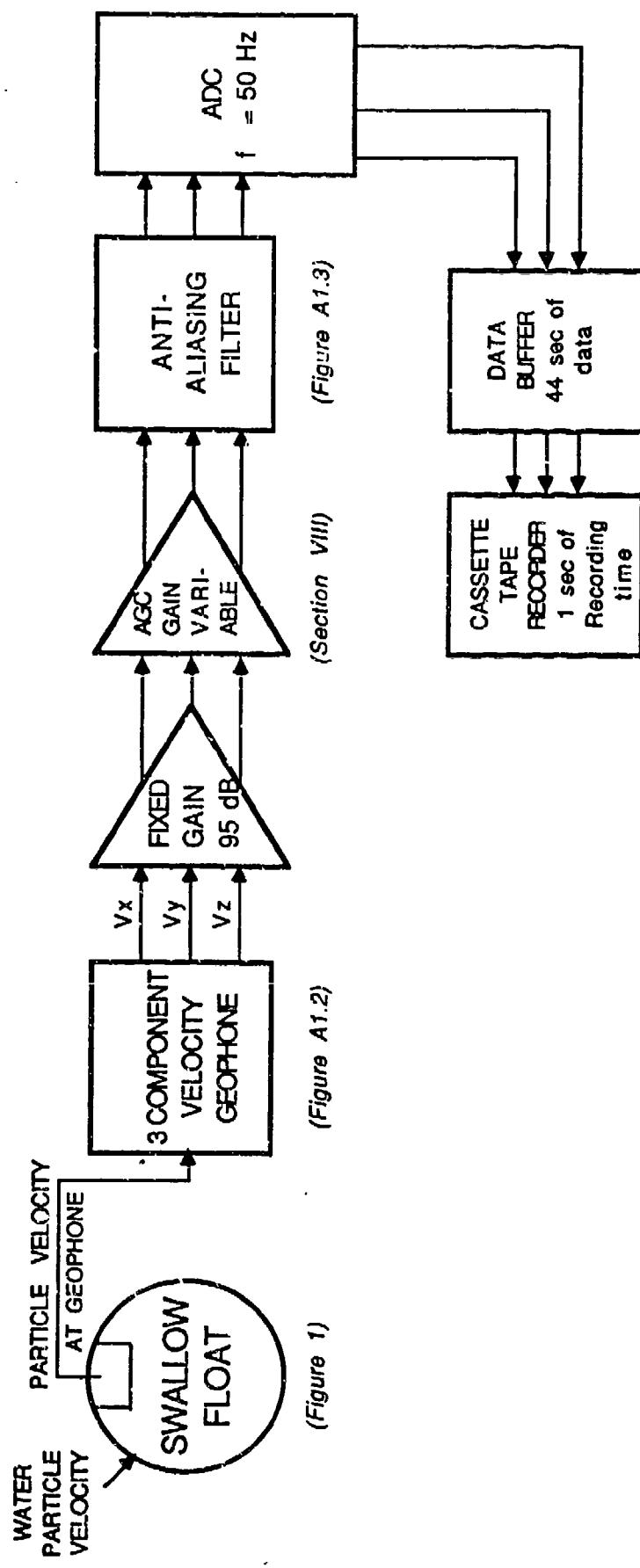


Figure A1.1

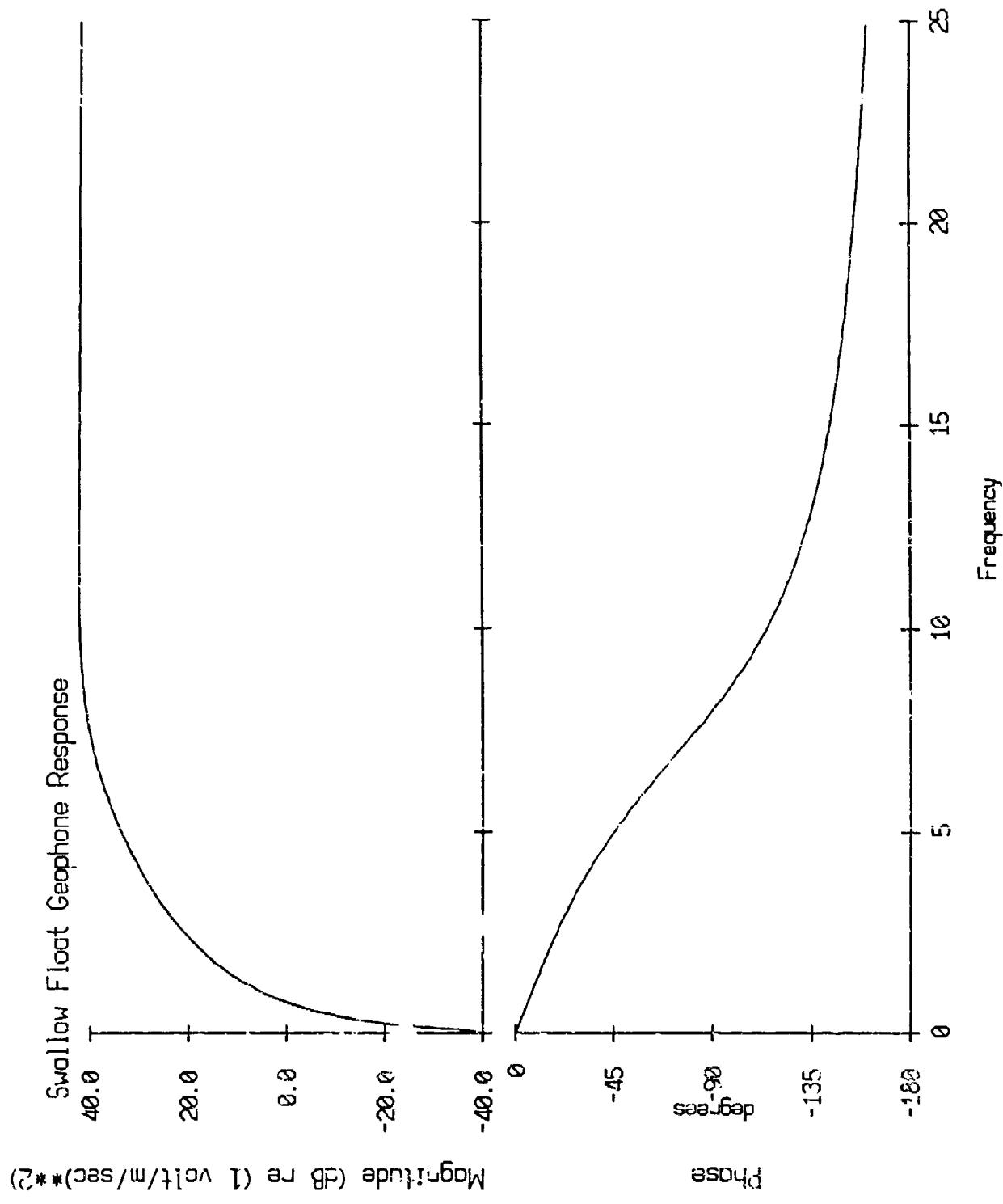


Figure A1.2

Low Pass Filter Transfer Function

Normalized S-Plane Representation
Poles and Zeros of Low-Pass Filter

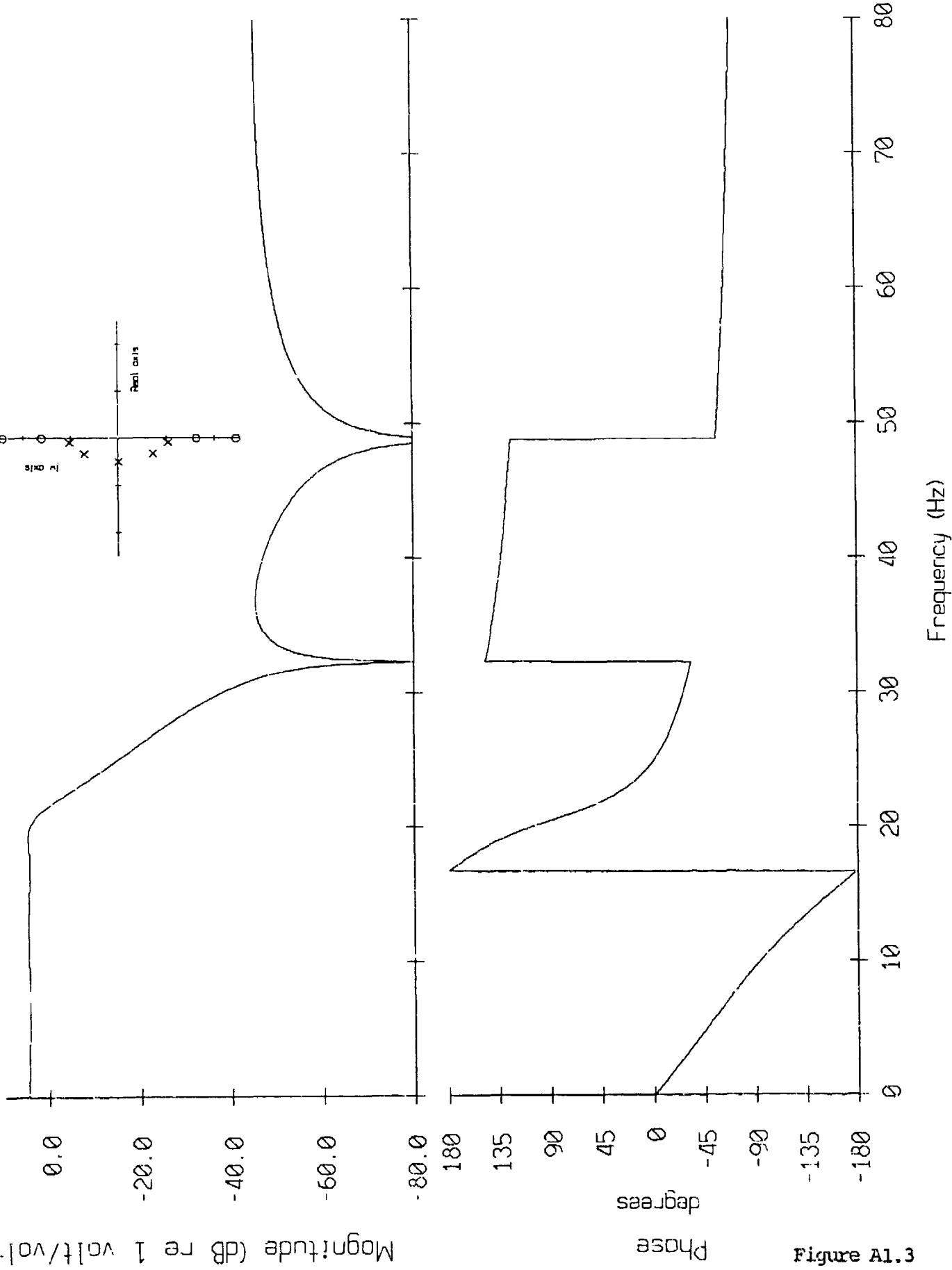


Figure A1.3

Appendix 2 - Loran-C Position Fixes

This short discussion is based upon the material on pp. 708-725 of [21].

Loran, or Long Range Navigation, is based upon the measurement of time differences between pulse radio emissions, with a carrier frequency of 100 kHz, issued from two or more transmitting stations. Loran-C is characterized by the use of multiple pulses, allowing a higher signal-to-noise ratio with the same power output at a transmitting station, and by the use of a phase matching procedure to refine the time-of-arrival estimates.

Position accuracy depends upon the variation in propagation conditions along the signal path and on the position of the ship with respect to the transmitting stations, as well as on the distance from the chain of stations. Therefore, an interval of accuracies, rather than a single value, is given. Our study site was about 400 km from the nearest station; this results in an accuracy interval of about 25-100 meters, or 0.01-0.06 minute.

Loran-C position fixes, however, can be expected to much more precise than accurate. The relative distances between a number of fixes made in the same general area are much more reliable than the absolute position of any one fix. This is because all the fixes are affected by the same propagation effects and station-receiver geometry.

Appendix 3 - Calibration Curves for the OBS Instruments

The calibration curves for the three types of instruments installed on the ocean bottom seismometers are given in Figures A3.1, A3.2, and A3.3. Each of the three plots represents the frequency response of the whole instrument-amplifier-filter system. The curve for the OBS geophone was provided by Allan Sauter and Tony Schreiner, Allan Sauter also provided us with the regular OBS hydrophone system curve, and the Cox-type hydrophone curve was given to us by Dalia Lahav.

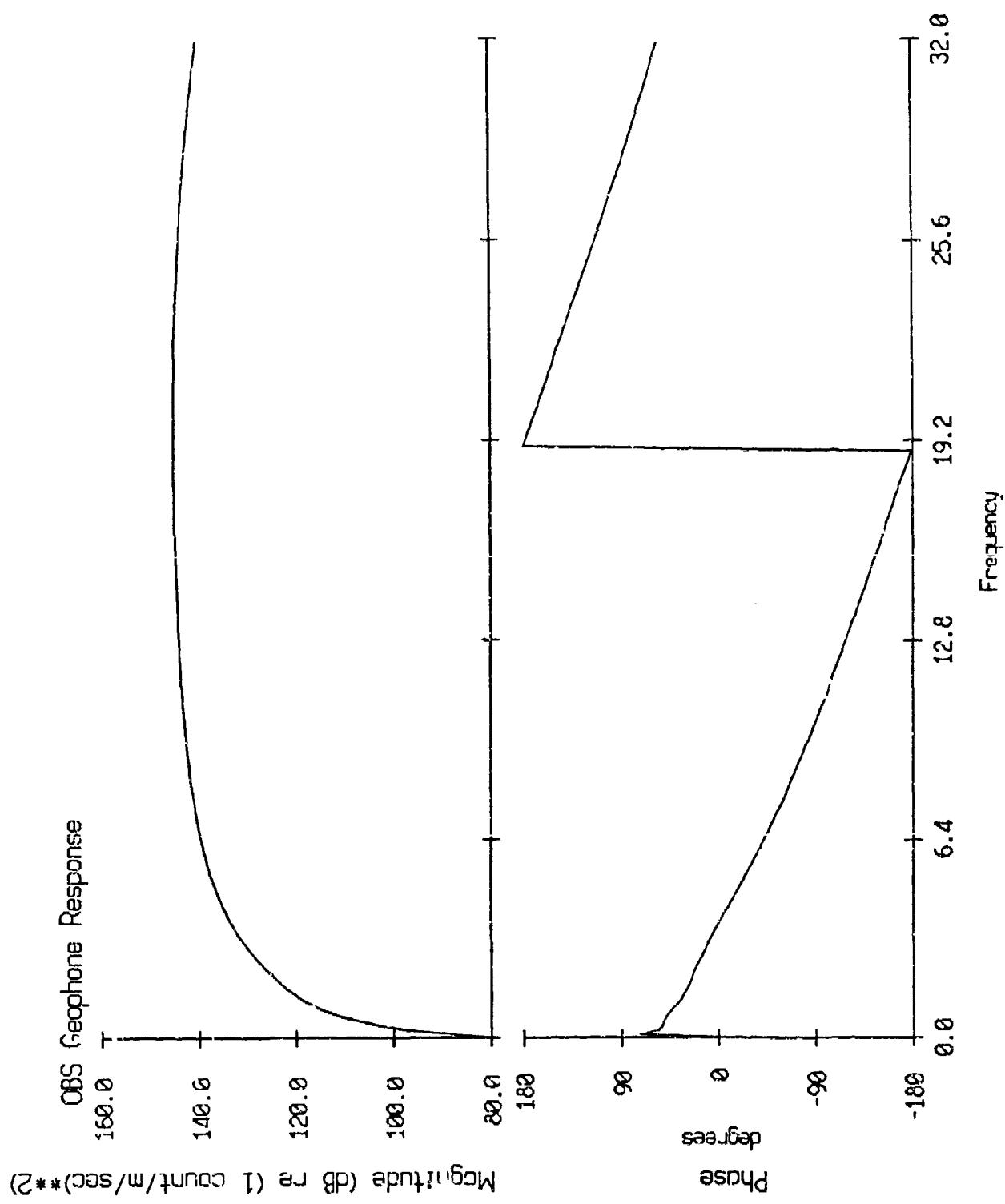


Figure A3.1

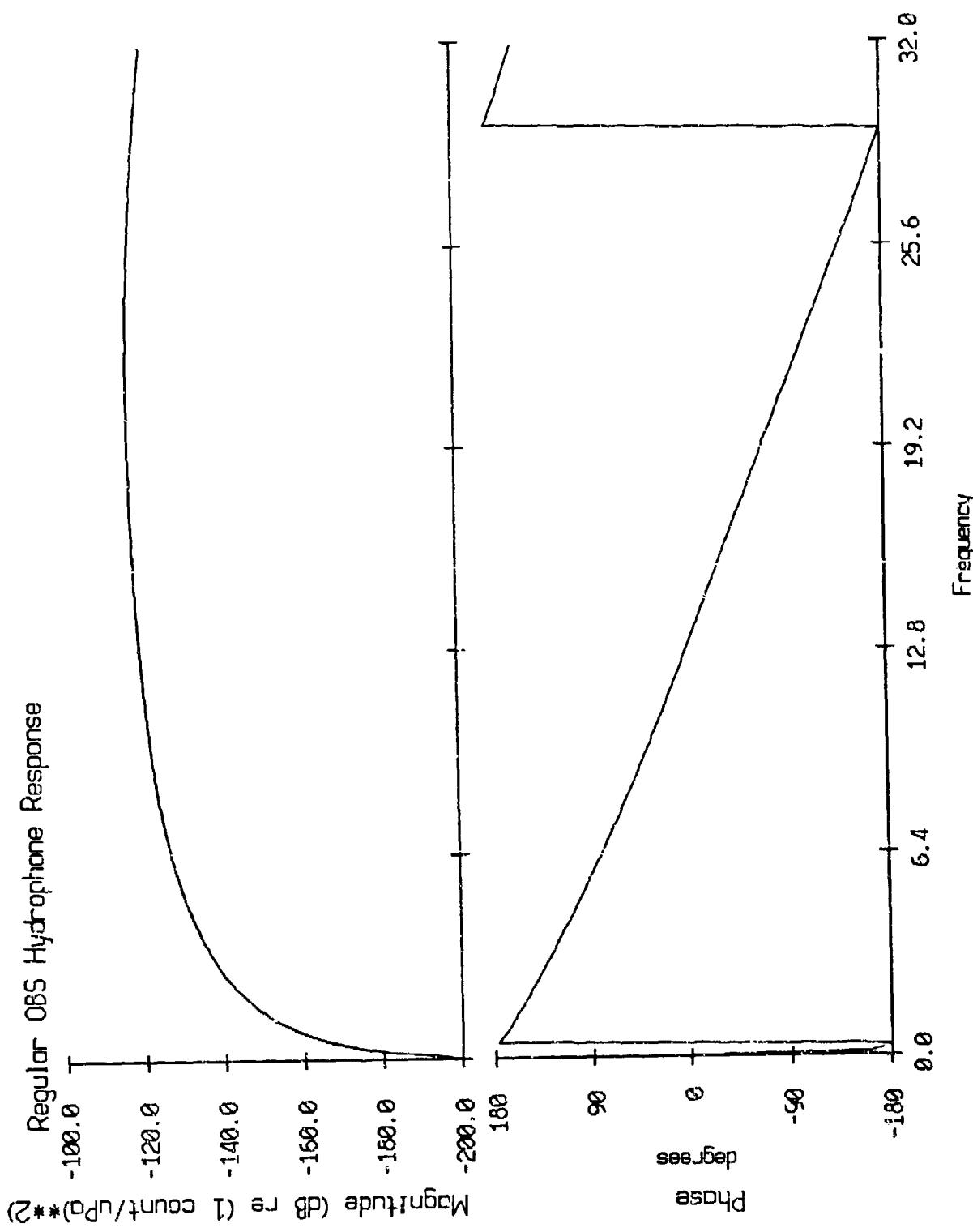


Figure A3.2

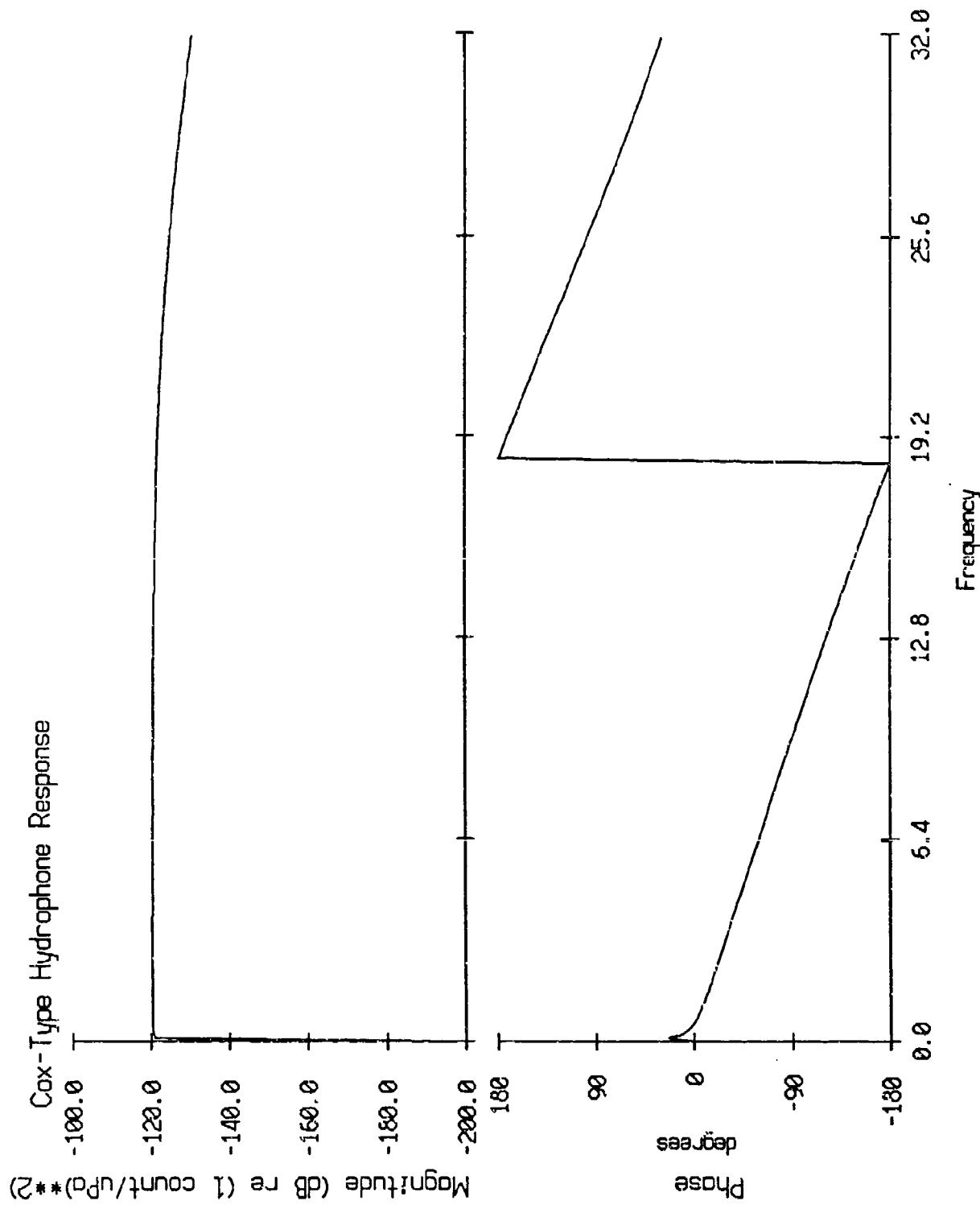


Figure A3.3

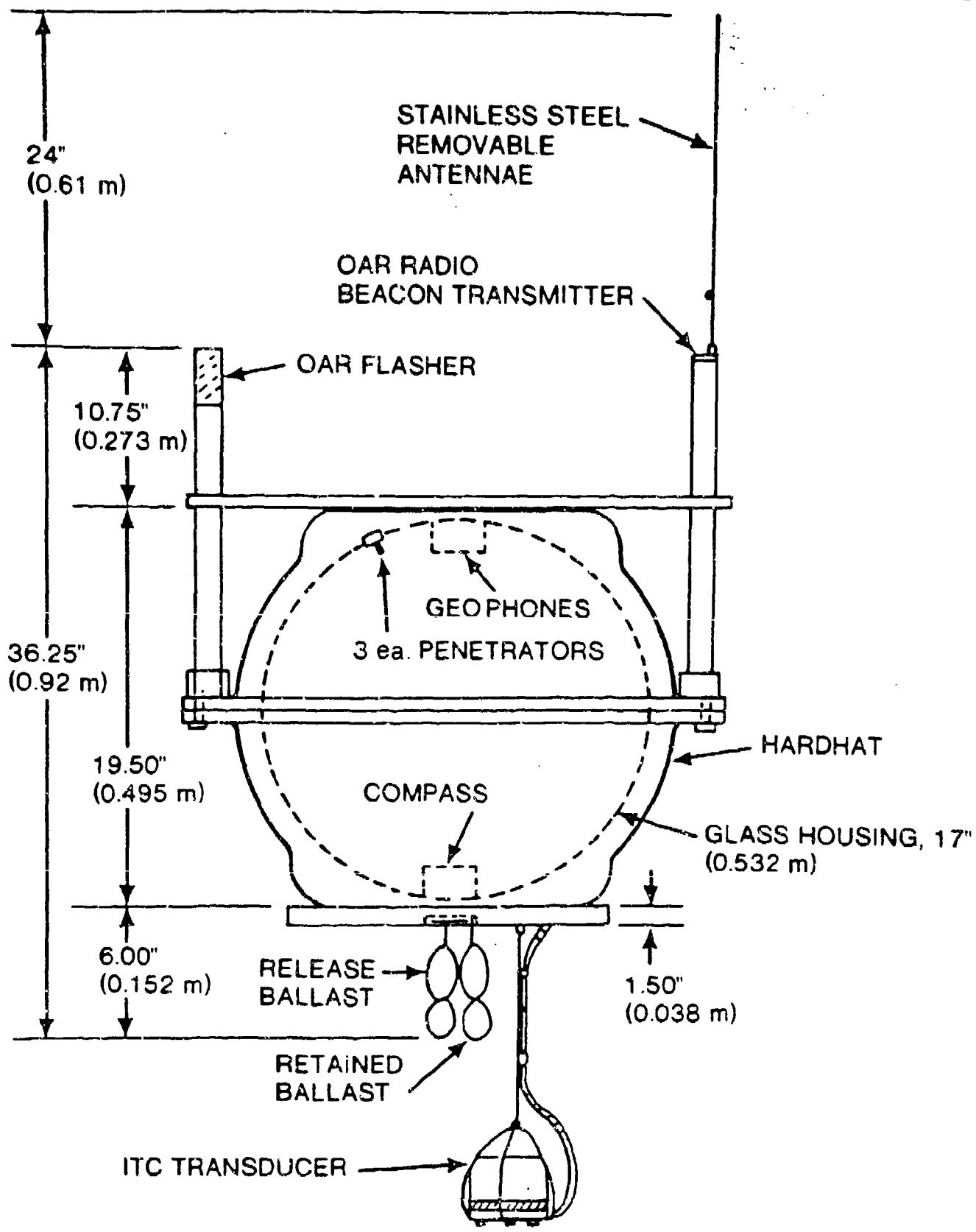


Figure 1

Figure 1

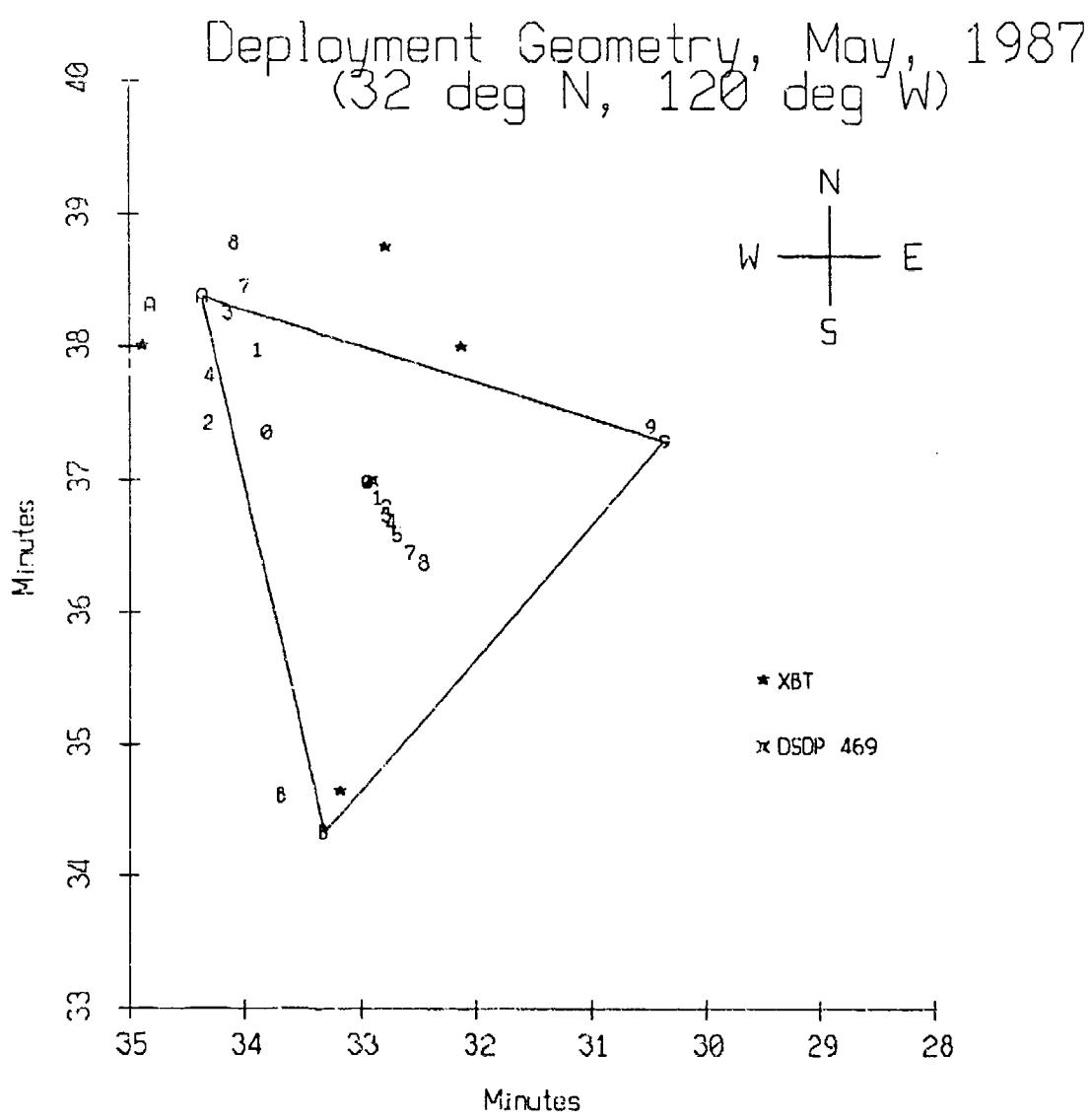


Figure I.1

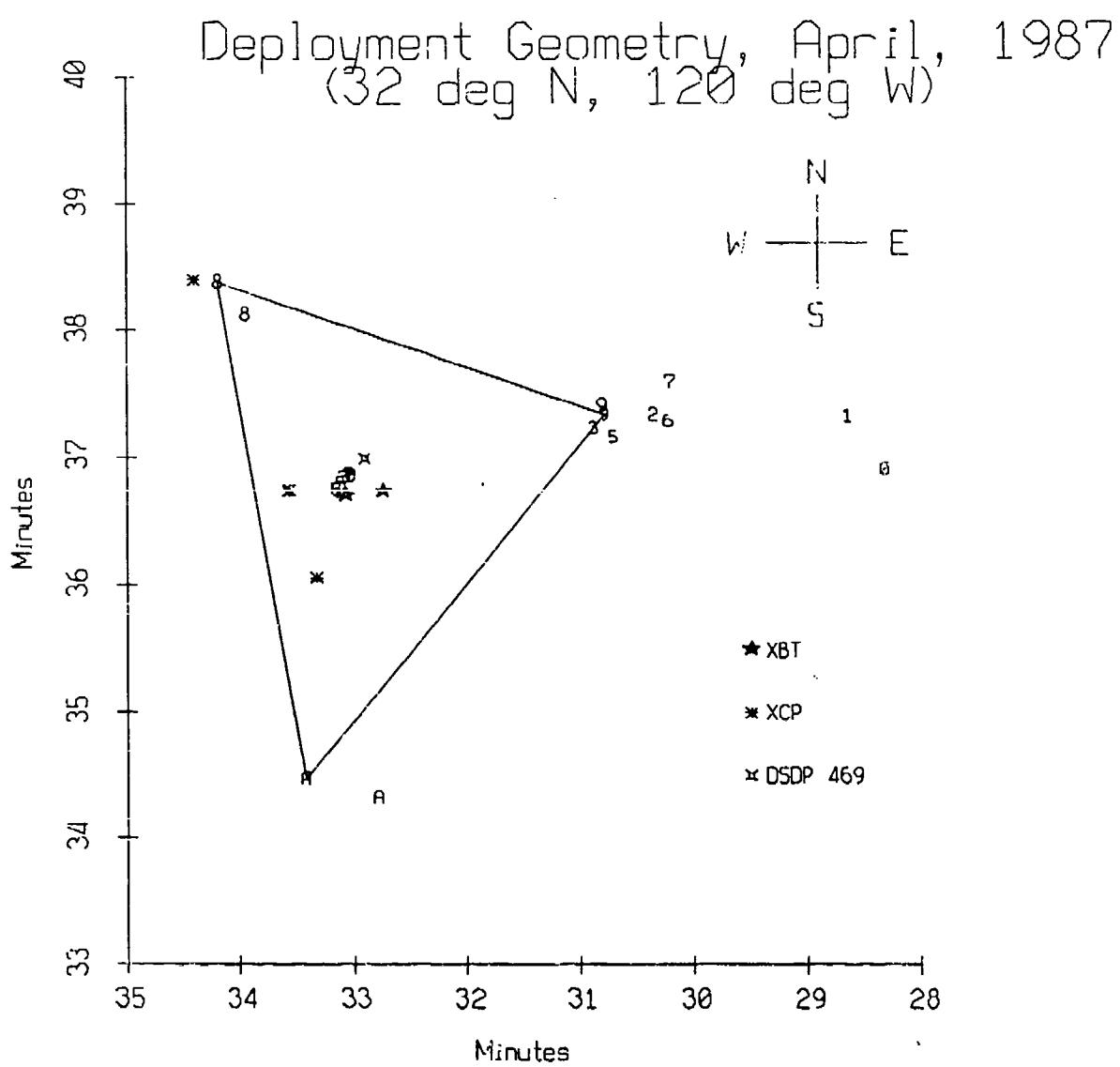


Figure I.2

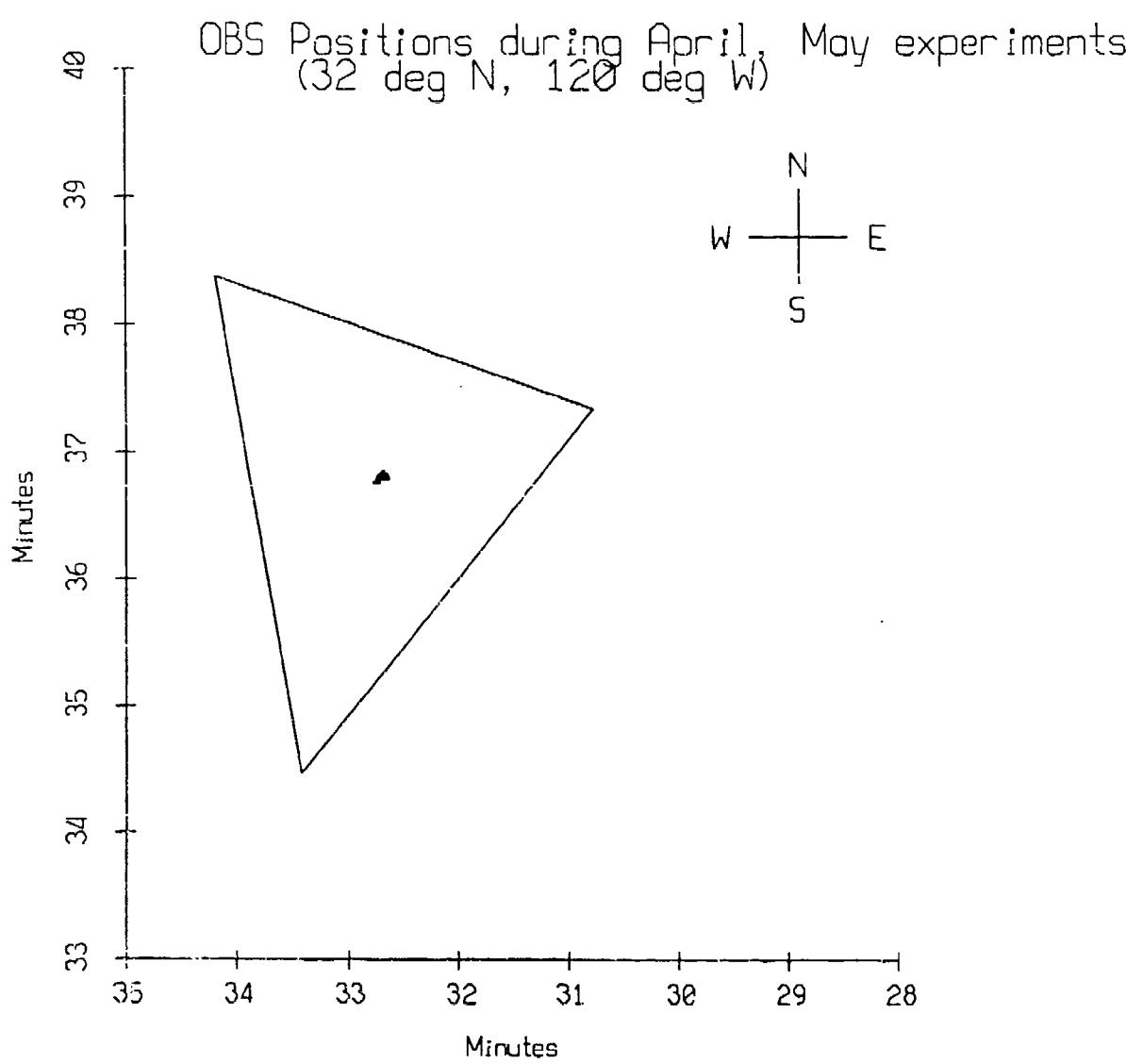


Figure I.3

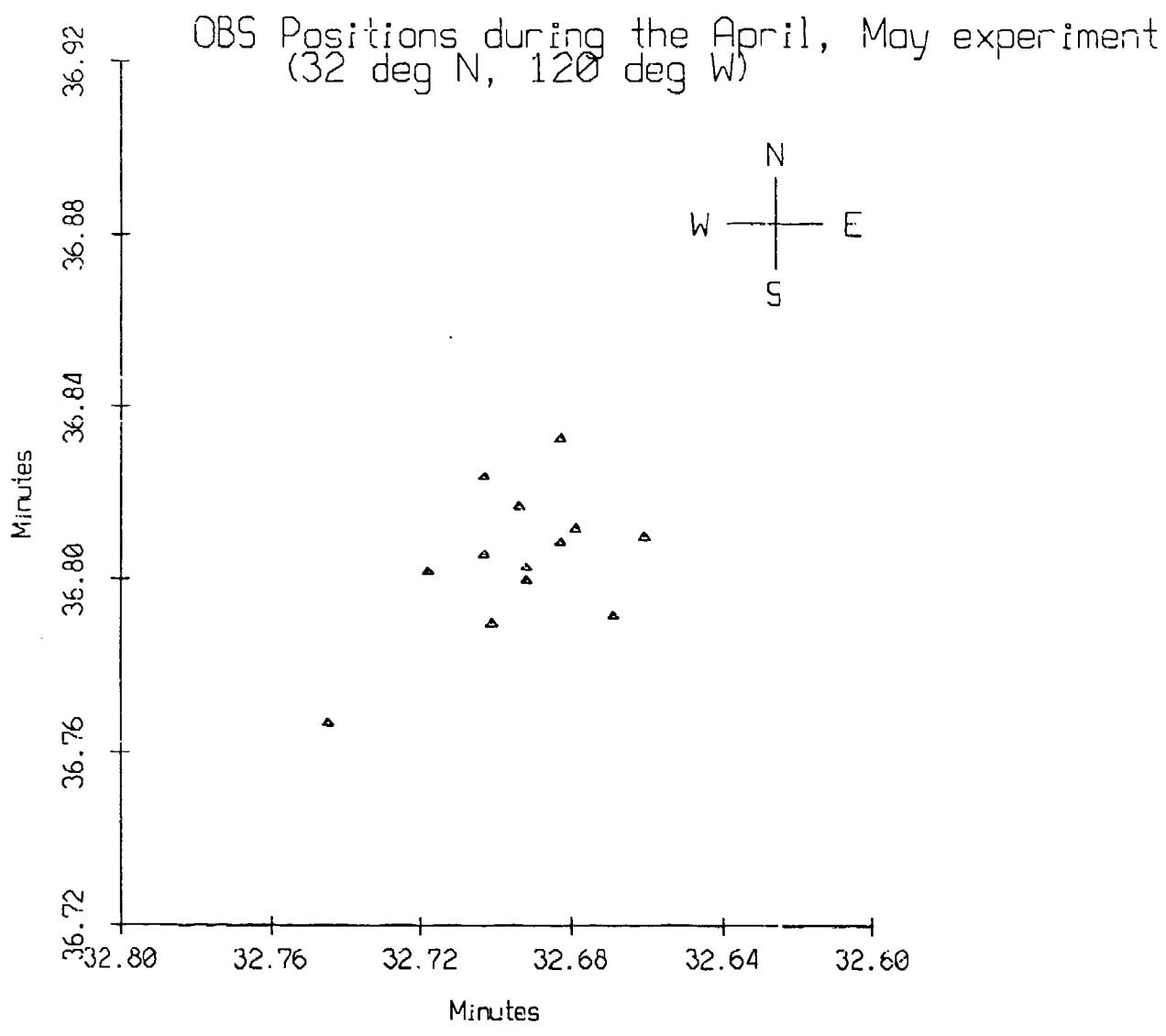


Figure I.4

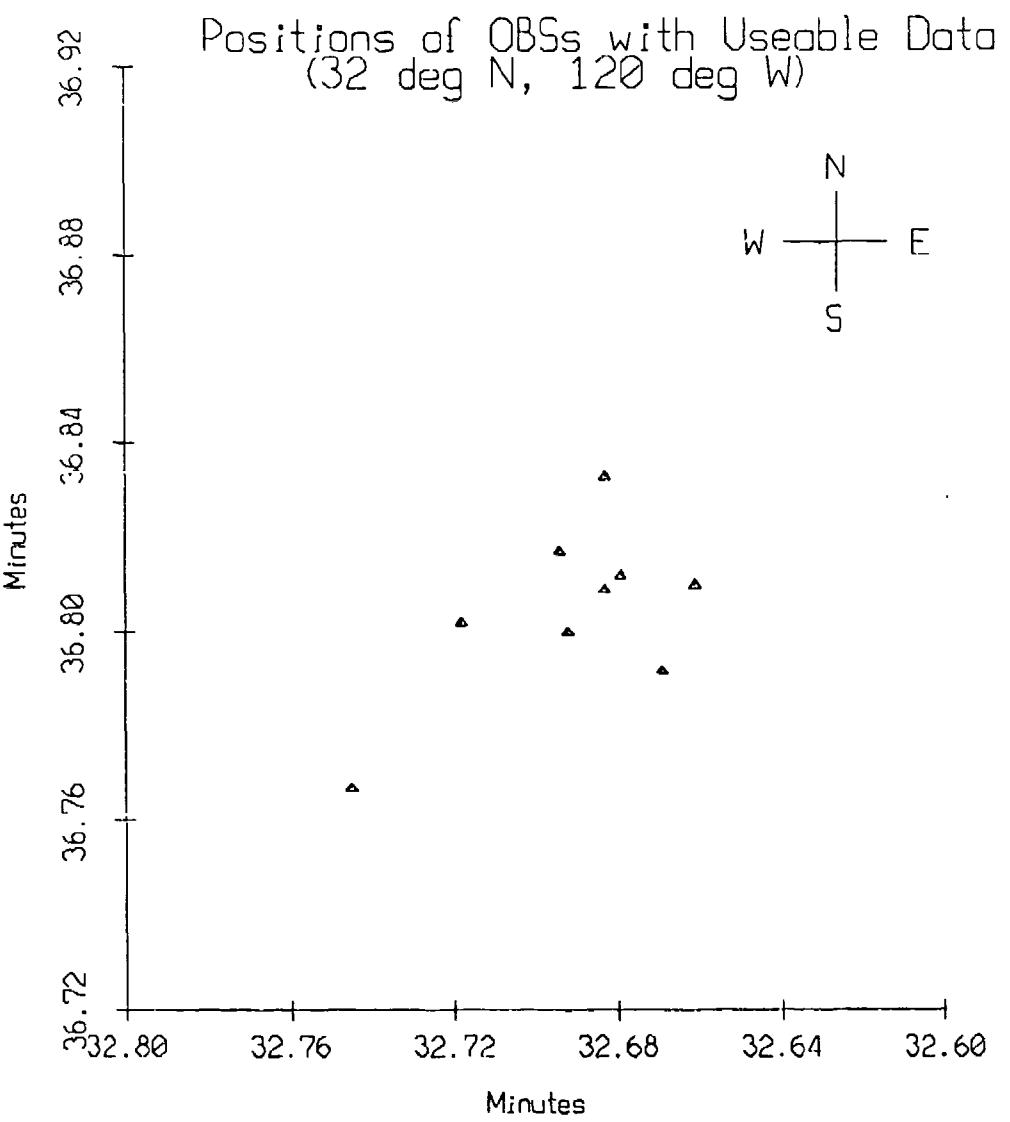


Figure I.5

OBS Deployment April, 1987		
OBS Name	OBS Capsule Number	Deployment Position (32° N, 120° W)
Suzie	10 (plotted as "A")	36.803' N 32.692' W
McKisic	4	36.800' N 32.692' W
Fitz	13 (plotted as "D")	36.817' N 32.694' W
Judy	8	36.812' N 32.679' W
Karen	6	36.802' N 32.718' W
Jean	12 (plotted as "C")	36.810' N 32.661' W
Morris	14 (plotted as "E")	36.833' N 32.683' W
Phred	2	36.792' N 32.669' W
Hazel	7	36.824' N 32.703' W
Janice	9	36.790' N 32.701' W
Lynn	5	36.809' N 32.683' W
Juan	1	36.767' N 32.745' W
O.S.U.	-- (plotted as "O")	36.806' N 32.703' W

Notes:

All positions in minutes are with respect to 32° N, 120° W. Suzie, Hazel, Janice, and O.S.U. did not provide useable data.

O.S.U. and Juan were deployed by free-fall from the Melville; all others were deployed using the Scripps thruster.

OBS Recording Times (in local Pacific Daylight Time):

All instruments, except Juan, began recording at 23:01, 21 April (06:01, 22 April in Greenwich Mean Time). Juan began recording at 19:01, 22 April. All instruments, except Lynn and Karen, recorded 3 minutes of data every 6 hours, starting at 1 minute after the hour. Lynn and Karen sampled 3 minutes of data, starting at 23:01, 21 April, every 15 minutes, until 23:01, 23 April. After a 6 hour interval, until 05:01, April 24, these two OBSs began recording 3 minutes of data, starting at 1 minute after the hour, every 3 hours. All instruments recorded data every 15 minutes during a 4 hour period beginning at 19:01, 22 April.

* Information courtesy of Dr. Dorman's research group

OBS Coverage

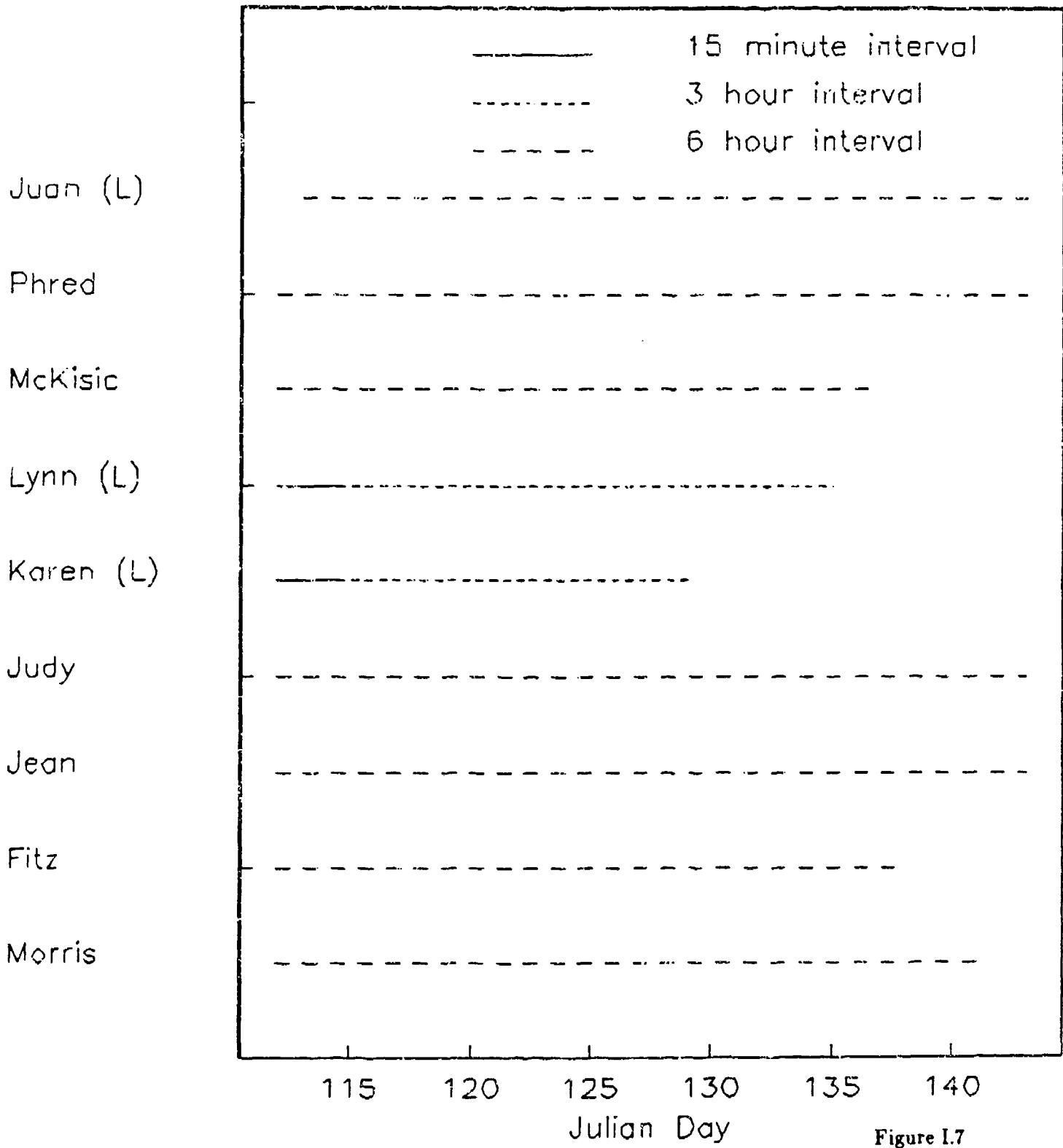


Figure I.7

OBS Data Recording Times April, May 1987

(Times are in local Pacific Daylight Time; add 7 hours to get GMT).

Event	Date	Time (hr:min) of First Sample	Duration of Event (sec)
073	4-22	11:00	179
097	4-22	17:00	179
105	4-22	19:00	29
106	4-22	19:15	29
107	4-22	19:30	29
108	4-22	19:45	29
109	4-22	20:00	29
110	4-22	20:15	29
111	4-22	20:30	29
112	4-22	20:45	29
113	4-22	21:00	29
114	4-22	21:15	29
115	4-22	21:30	29
116	4-22	21:45	29
117	4-22	22:00	29
118	4-22	22:15	29
119	4-22	22:30	29
120	4-22	22:45	29
121	4-22	23:00	179
145	4-23	05:00	179
309	5-5	11:00	179
311	5-5	17:00	179
313	5-5	23:00	179
315	5-6	05:00	179
317	5-6	11:00	179

Table I.8a

Individual OBS Data Recording Times April, May 1987

Time (sec) of First Sample for Each OBS

Event	1	2	4	5	6	8	12	13	14
073	----	57.057	57.488	56.559	56.825	58.441	57.310	57.695	57.452
097	----	57.054	57.488	56.572	56.826	58.470	57.313	57.698	57.461
105	57.504	57.053	57.488	56.576	56.827	58.480	57.314	57.699	57.464
106	57.504	57.053	57.488	56.577	56.827	58.481	57.314	57.699	57.465
107	57.504	57.053	57.488	56.577	56.827	58.483	57.314	57.699	57.465
108	57.504	57.053	57.488	56.578	56.827	58.484	57.314	57.699	57.466
109	57.504	57.053	57.488	56.579	56.827	58.485	57.314	57.699	57.466
110	57.504	57.053	57.488	56.579	56.827	58.486	57.315	57.700	57.466
111	57.504	57.053	57.488	56.580	56.827	58.487	57.315	57.700	57.467
112	57.504	57.052	57.488	56.580	56.827	58.489	57.315	57.700	57.467
113	57.504	57.052	57.488	56.581	56.827	58.490	57.315	57.700	57.468
114	57.504	57.052	57.488	56.581	56.827	58.491	57.315	57.700	57.468
115	57.505	57.052	57.488	56.582	56.827	58.492	—	57.700	57.468
116	57.505	57.052	57.488	56.582	56.827	58.494	57.315	57.700	57.469
117	57.505	57.052	57.488	56.583	56.827	58.495	—	57.700	57.469
118	57.505	57.052	57.488	56.583	56.827	58.496	57.316	57.701	57.470
119	57.505	57.052	57.488	56.584	56.828	58.497	57.316	57.701	57.470
120	57.505	57.052	57.488	56.585	56.828	58.498	57.316	57.701	57.470
121	57.505	57.051	57.488	56.585	56.828	58.500	57.316	57.701	57.471
145	57.507	57.049	57.488	56.598	56.829	58.529	57.319	57.704	57.481
309	60.609	59.913	60.485	60.235	59.887	62.964	60.474	60.864	60.955
311	60.611	*	60.485	60.248	59.888	62.994	60.477	60.867	60.965
313	60.613	59.907	60.485	60.261	59.889	*	—	60.870	60.975
315	60.615	59.905	60.485	60.274	59.891	*	60.484	60.873	60.984
317	60.617	59.902	60.485	60.287	59.892	63.082	60.487	60.877	60.994

* For obs 2, event 311 was recorded about 42 minutes earlier, at 16:18 32.910, than for the other instruments; for obs 8, event 313 was recorded about 12 minutes earlier, at 22:48 44.022, and event 315 was recorded 31 minutes early, at 04:30 04.050. The cause of these premature recordings of an event is thought to be due to misinterpretation of the clock signal.

OBS Data Recording Times, April, May 1987
for Lynn (#5) and Karen (#6)

(Times are in local Pacific Daylight Time; add 7 hours to get GMT).

Event	Date	Time (hr:min) of First Sample	OBS 5 Time (sec)	OBS 6 Time (sec)	Duration of Event (sec)
063	4-22	08:30	56.554	56.825	179
064	4-22	08:45	56.554	56.825	179
065	4-22	09:00	56.555	56.825	179
066	4-22	09:15	56.555	56.825	179
067	4-22	09:30	56.556	56.825	179
068	4-22	09:45	56.556	56.825	179
069	4-22	10:00	56.557	56.825	179
070	4-22	10:15	56.557	56.825	179
071	4-22	10:30	56.558	56.825	179
072	4-22	10:45	56.559	56.825	179
073	4-22	11:00	56.559	56.825	179
074	4-22	11:15	56.560	56.825	179
075	4-22	11:30	56.560	56.825	179
076	4-22	11:45	56.561	56.825	179
077	4-22	12:00	56.561	56.825	179
078	4-22	12:15	56.562	56.825	179
079	4-22	12:30	56.562	56.826	179
080	4-22	12:45	56.563	56.826	179
081	4-22	13:00	56.563	56.826	179
082	4-22	13:15	56.564	56.826	179
083	4-22	13:30	56.564	56.826	179
084	4-22	13:45	56.565	56.826	179
085	4-22	14:00	56.566	56.826	179
086	4-22	14:15	56.566	56.826	179
087	4-22	14:30	56.567	56.826	179
088	4-22	14:45	56.567	56.826	179
089	4-22	15:00	56.568	56.826	179
090	4-22	15:15	56.568	56.826	179
091	4-22	15:30	56.569	56.826	179
092	4-22	15:45	56.569	56.826	179
093	4-22	16:00	56.570	56.826	179
094	4-22	16:15	56.570	56.826	179
095	4-22	16:30	56.571	56.826	179
096	4-22	16:45	56.572	56.826	179
097	4-22	17:00	56.572	56.826	179
098	4-22	17:15	---	56.826	179
099	4-22	17:30	---	56.827	179

(continued on the next page)

OBS Data Recording Times, April, May 1987
for Lynn (#5) and Karen (#8)

(continued from the previous page)

Event	Date	Time (hr:min) of First Sample	OBS 5 Time (sec)	OBS 5 Time (sec)	Duration of Event (sec)
100	4-22	17:45	---	56.827	179
101	4-22	18:00	---	56.827	179
102	4-22	18:15	---	56.827	179
103	4-22	18:30	---	56.827	179
104	4-22	18:45	---	56.827	179
105	4-22	19:00	56.576	56.827	29
106	4-22	19:15	56.577	56.827	29
107	4-22	19:30	56.577	56.827	29
108	4-22	19:45	56.578	56.827	29
109	4-22	20:00	56.579	56.827	29
110	4-22	20:15	56.579	56.827	29
111	4-22	20:30	56.580	56.827	29
112	4-22	20:45	56.580	56.827	29
113	4-22	21:00	56.581	56.827	29
114	4-22	21:15	56.581	56.827	29
115	4-22	21:30	56.582	56.827	29
116	4-22	21:45	56.582	56.827	29
117	4-22	22:00	56.583	56.827	29
118	4-22	22:15	56.583	56.827	29
119	4-22	22:30	56.584	56.828	29
120	4-22	22:45	56.585	56.828	29
121	4-22	23:00	56.585	56.828	179
122	4-22	23:15	56.586	56.828	179
123	4-22	23:30	56.586	56.828	179
124	4-22	23:45	56.587	56.828	179
125	4-23	00:00	56.587	56.828	179
126	4-23	00:15	56.588	56.828	179
127	4-23	00:30	56.588	56.828	179
128	4-23	00:45	56.589	56.828	179
129	4-23	01:00	56.589	56.828	179
130	4-23	01:15	56.590	56.828	179
131	4-23	01:30	56.590	56.828	179
132	4-23	01:45	56.591	56.828	179
133	4-23	02:00	56.592	56.828	179
134	4-23	02:15	56.592	56.828	179
135	4-23	02:30	56.593	56.828	179
136	4-23	02:45	56.593	56.828	179
137	4-23	03:00	56.594	56.828	179
138	4-23	03:15	56.594	56.828	179
139	4-23	03:30	56.595	56.829	179

(continued on the next page)

**OBS Data Recording Times, April, May 1987
for Lynn (#5) and Karen (#8)**

(continued from the previous page)

Event	Date	Time (hr:min) of First Sample	OBS 5 Time (sec)	OBS 6 Time (sec)	Duration of Event (sec)
140	4-23	03:45	56.595	56.829	179
141	4-23	04:00	56.596	56.829	179
142	4-23	04:15	56.596	56.829	179
143	4-23	04:30	56.597	56.829	179
144	4-23	04:45	56.598	56.829	179
145	4-23	05:00	56.598	56.829	179
146	4-23	05:15	56.599	56.829	179
147	4-23	05:30	56.599	56.828	179
148	4-23	05:45	56.600	56.829	179
149	4-23	06:00	56.600	56.829	179
150	4-23	06:15	56.601	56.829	179
151	4-23	06:30	56.601	56.829	179
152	4-23	06:45	56.602	56.829	179
153	4-23	07:00	56.602	56.829	179
154	4-23	07:15	56.603	56.829	179
155	4-23	07:30	56.603	56.829	179
156	4-23	07:45	56.604	56.829	179
157	4-23	08:00	56.605	56.829	179
158	4-23	08:15	56.605	56.829	179
159	4-23	08:30	56.606	56.830	179
160	4-23	08:45	56.606	56.830	179
161	4-23	09:00	56.807	56.830	179
162	4-23	09:15	56.807	56.830	179
163	4-23	09:30	56.808	56.830	179
309	5-5	11:00	59.235	59.887	179
310	5-5	14:00	59.242	59.888	179
311	5-5	17:00	59.243	59.888	179
312	5-5	20:00	59.255	59.889	179
313	5-5	23:00	59.261	59.889	179
314	5-6	02:00	59.268	59.890	179
315	5-6	05:00	59.274	59.891	179
316	5-6	08:00	59.281	59.891	179
317	5-6	11:00	59.287	59.892	179

Table I.9c

Sound Speed Profile : Area 23
(31-34 deg N, 120-125 deg W)
with Instruments' Deployment Depths

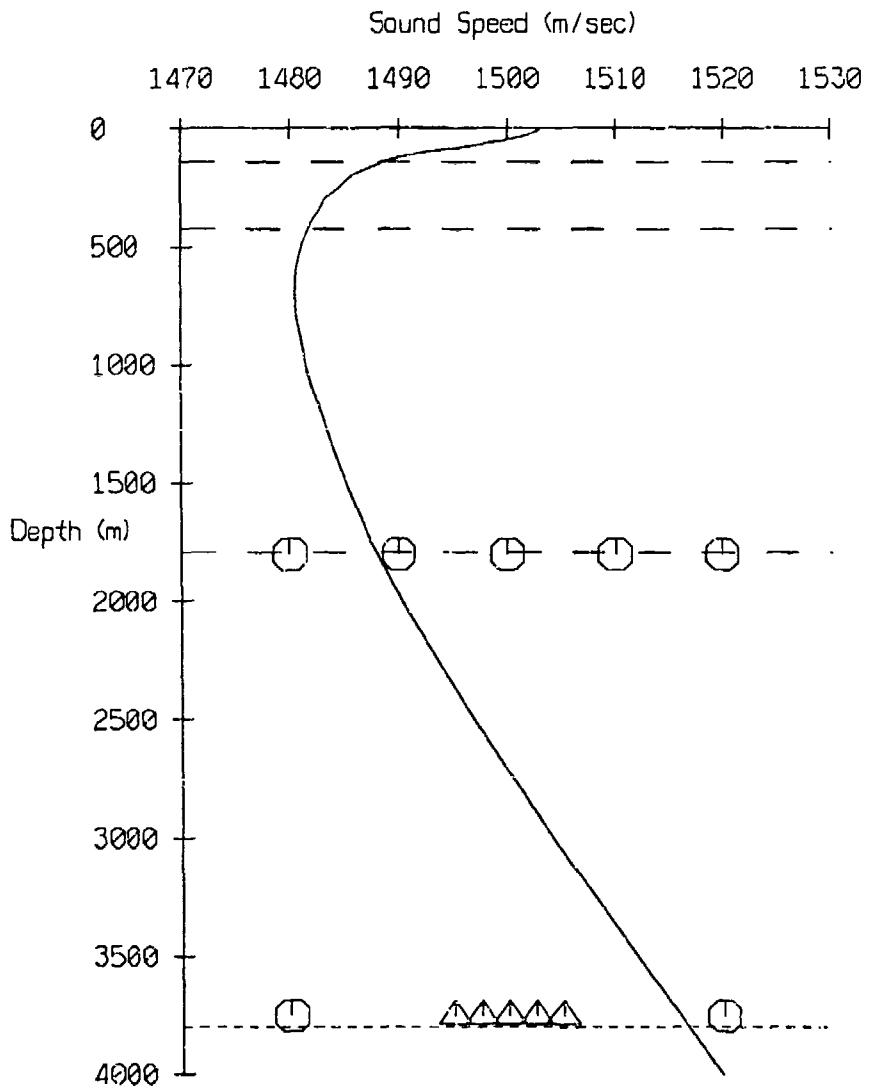


Figure I.10

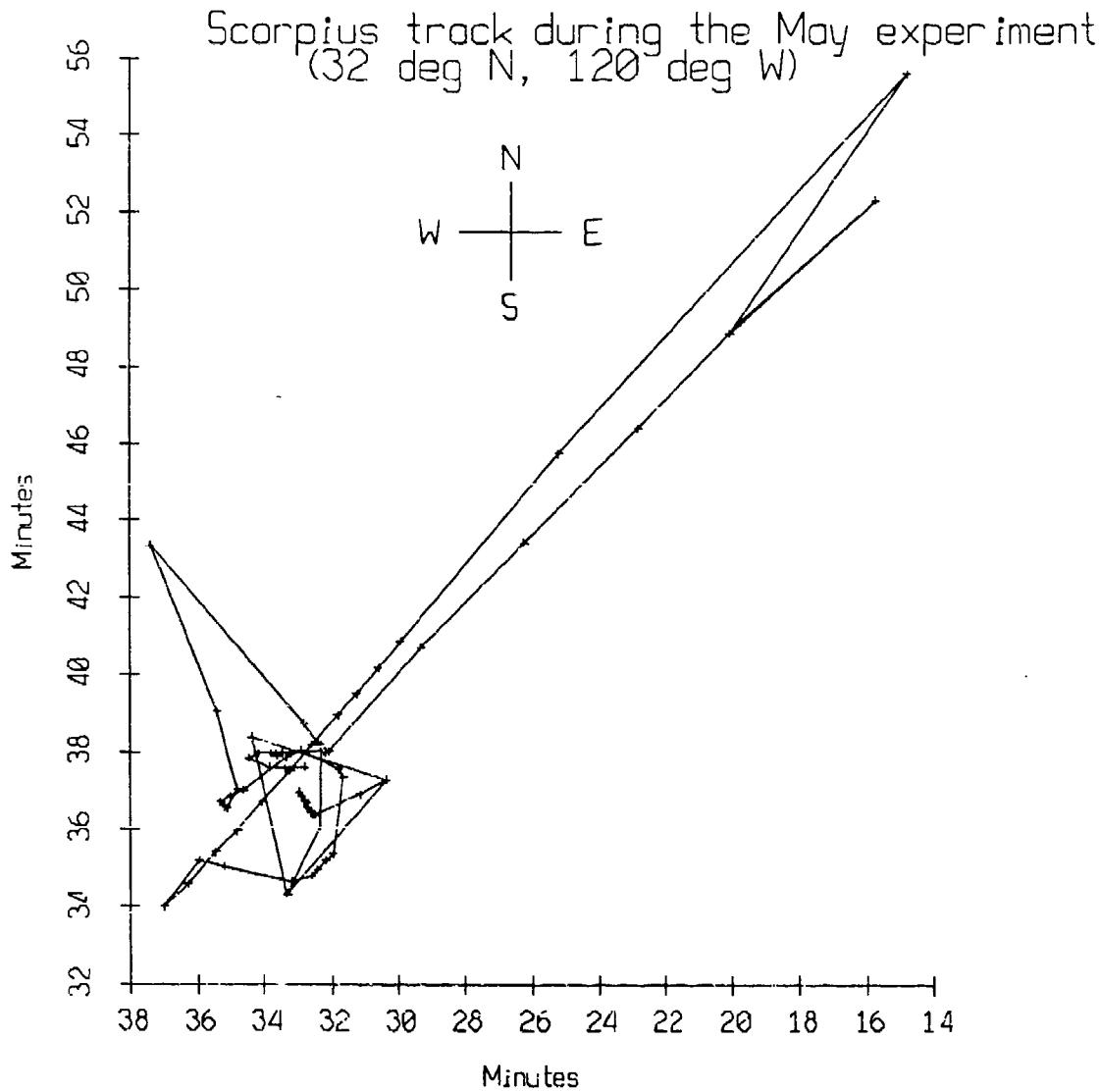


Figure II.1

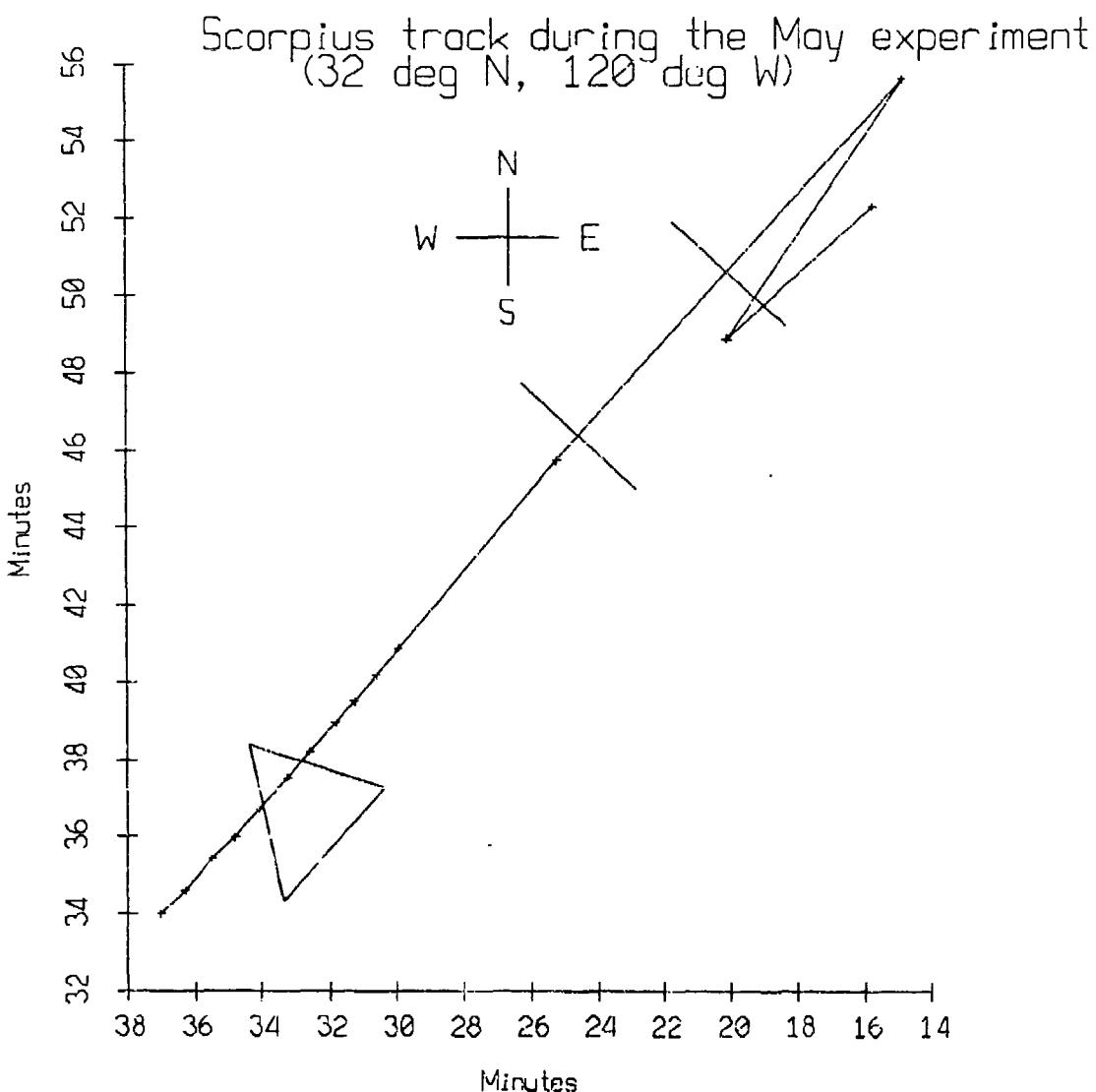


Figure II.2

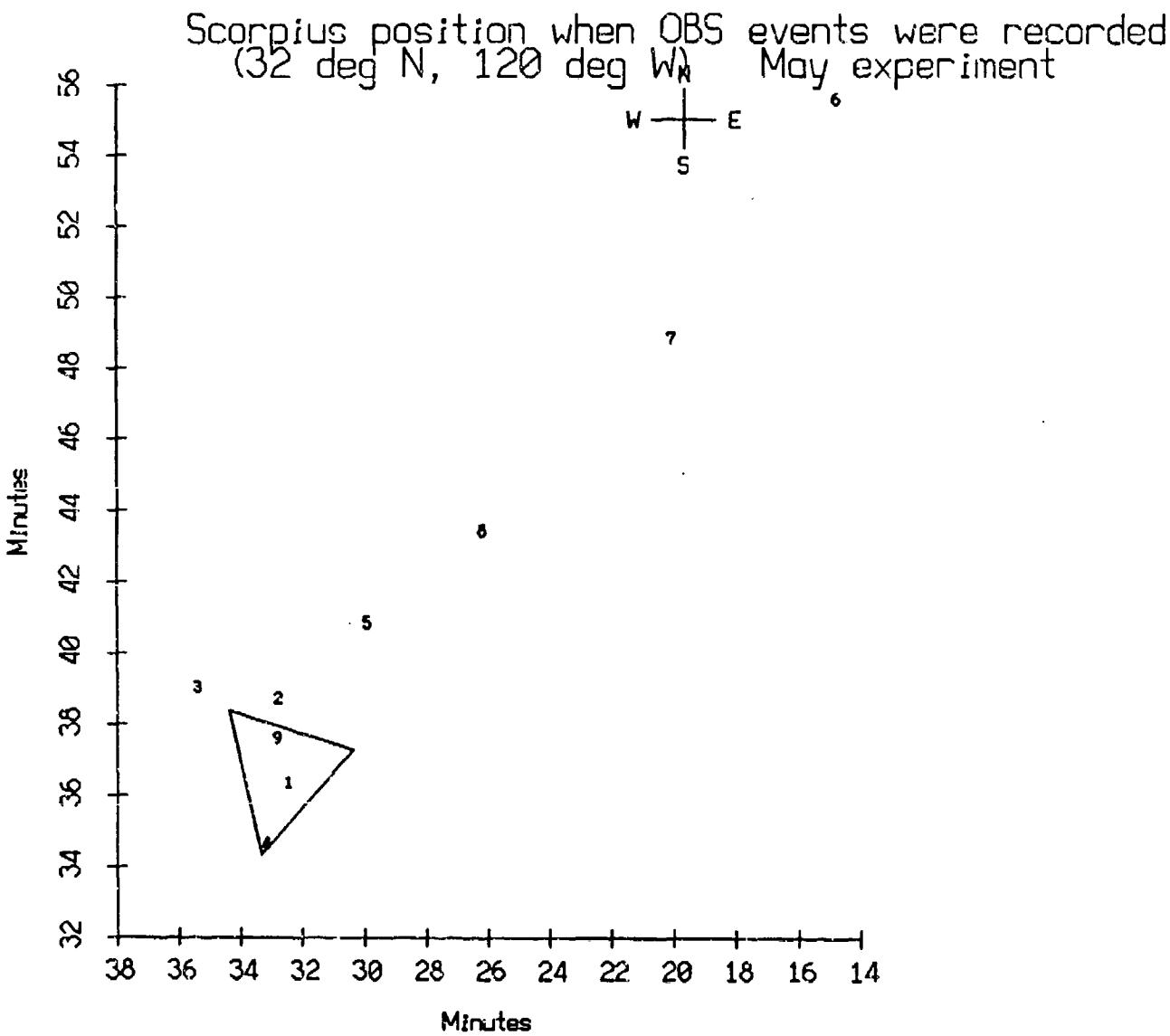


Figure II.3

All Loran-C Position Fixes of the Scorpius
 (referenced to 32° N, 120° W)

5 May

Latit (min)	Long (min)	Time (local)	Latit (min)	Long (min)	Time (local)	Latit (min)	Long (min)	Time (local)
36.76	33.02	10:05	36.99	32.95	10:21	36.87	32.86	10:27
36.80	32.79	10:30	36.74	32.79	10:33	36.69	32.75	10:36
36.59	32.69	10:40	36.45	32.58	10:45	36.39	32.52	10:54
36.38	32.46	11:04	36.94	31.13	11:19	37.30	30.36	11:30
38.38	34.37	12:02	34.34	33.31	12:32	36.06	32.32	13:28
38.18	32.29	13:36	38.26	32.40	13:38	38.75	32.79	13:49
43.37	37.40	15:21	39.05	35.41	16:53	37.05	34.81	17:12
36.57	35.12	17:20	36.62	35.16	17:24	36.73	35.30	17:28
36.89	34.99	17:37	37.02	34.63	17:47	37.87	33.31	18:08
38.04	32.88	18:18	37.54	31.78	18:37	37.35	31.64	18:43
35.39	31.93	19:12	35.21	32.16	19:18	34.98	32.42	19:26
34.82	32.58	19:31	34.65	33.18	19:45	35.05	35.18	20:35
35.20	35.96	21:00	34.00	37.00	21:20	34.58	36.28	21:30
35.43	35.45	21:41	35.98	34.81	21:50	36.73	34.06	22:00
37.52	33.23	22:10	38.20	32.56	22:20	38.98	31.80	22:30
39.53	31.24	22:40	40.18	30.59	22:50	40.88	29.92	23:00

6 May

45.75	25.17	1:00	55.60	14.80	2:30	48.87	20.07	4:30
52.31	15.70	6:00	49.18	19.73	7:00	46.40	22.82	7:30
43.45	26.19	8:00	40.73	29.29	8:30	38.03	32.05	9:01
38.00	32.13	9:07	38.02	32.17	9:10	38.00	33.48	9:34
37.91	33.59	9:40	37.99	33.66	9:50	37.99	33.76	10:00
37.99	34.18	10:15	37.85	34.46	10:25	37.61	33.81	10:35
37.59	33.37	10:45	37.61	32.77	10:55	37.64	32.83	11:05
37.67	33.04	11:15	37.75	33.21	11:25	37.78	33.37	11:35
37.91	33.33	11:45	37.36	33.81	12:10	37.52	33.66	12:23
38.14	33.85	12:45	37.98	33.88	12:57	37.68	34.57	13:25
37.70	34.47	13:46	37.43	34.32	13:58	38.02	34.63	14:26
38.42	34.11	14:42	38.26	34.15	14:49	38.01	34.89	15:20
37.86	34.57	15:28	37.79	34.31	15:38	37.78	34.04	16:00
38.48	33.79	16:17	38.99	33.97	16:34	38.91	33.96	16:44
38.46	34.00	17:34	38.12	33.73	17:49	39.00	34.02	18:30
38.81	34.08	18:55	38.79	34.09	19:00	38.31	34.82	20:29
37.22	31.51	21:07	36.23	31.99	21:30	34.98	32.75	21:50
34.37	33.35	22:05	34.49	34.15	22:33	34.35	33.70	22:40
34.62	33.69	23:15						

(continued on the next page)

Figure II.4a

Scorpius Loran-C Position Fixes (continued)

7 May

Latit (min)	Long (min)	Time (local)	Latit (min)	Long (min)	Time (local)	Latit (min)	Long (min)	Time (local)
			37.68	31.18	0:29	37.43	30.44	0:53
37.50	30.02	1:32	37.58	30.33	1:40	37.41	30.48	1:53
38.41	33.54	2:48	38.45	34.42	3:06	38.78	34.65	3:20
39.08	34.51	3:30	39.39	34.36	3:40	39.59	34.24	3:45
39.62	34.50	3:55	39.56	34.58	4:05			

Position fixes are with respect to 32° N, 120° W and the times that the fixes were taken are local Pacific Daylight Time. To obtain Greenwich Mean Time, add 7 hours.

Figure II.4b

Anemometer Readings after 00:00 a.m., 5-5-87
Measurements on the Scorpius

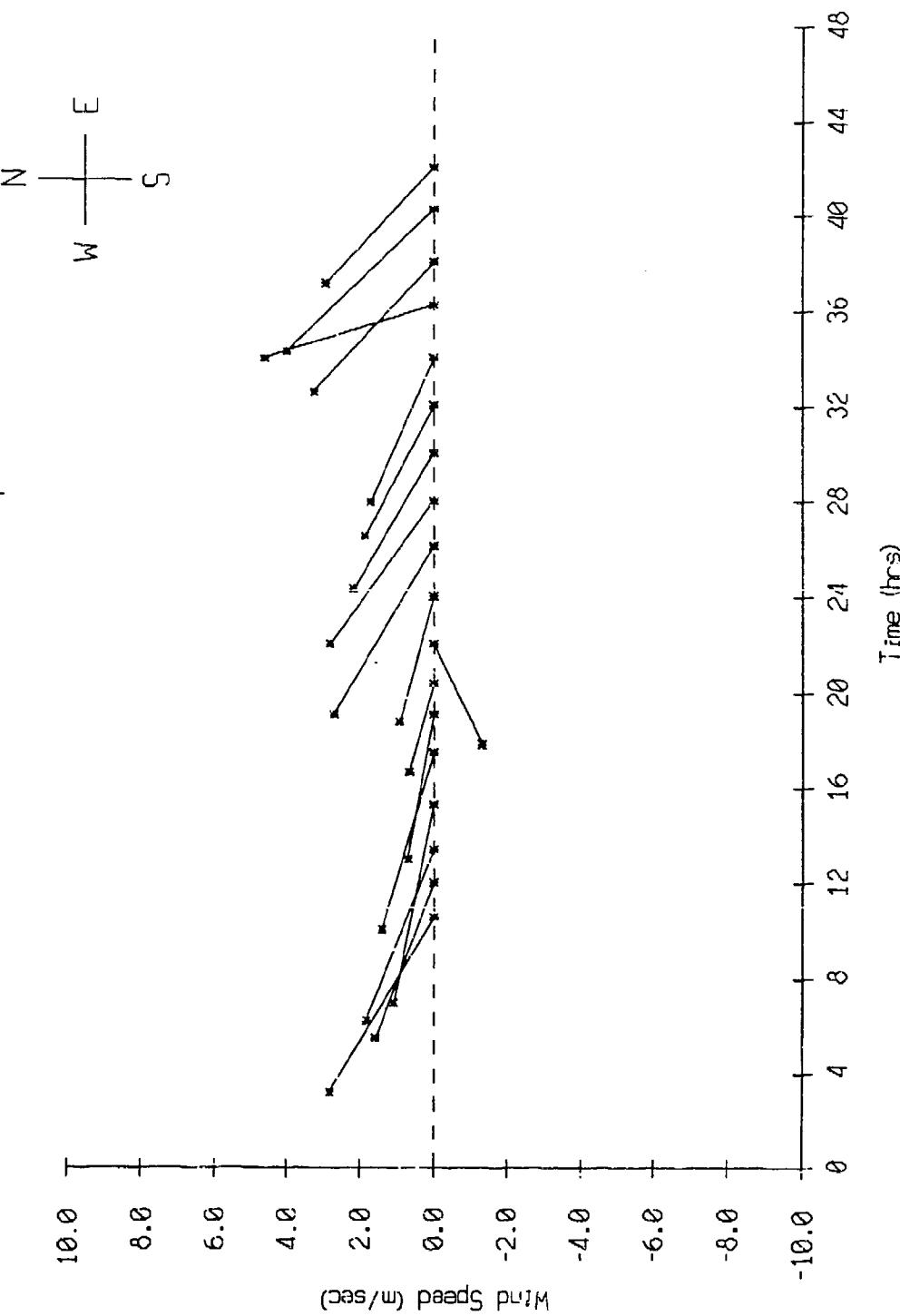


Figure IV.1

Sound Speed Profile
CalCOFI cruise 8705, sta. 90.70, 5-5-87

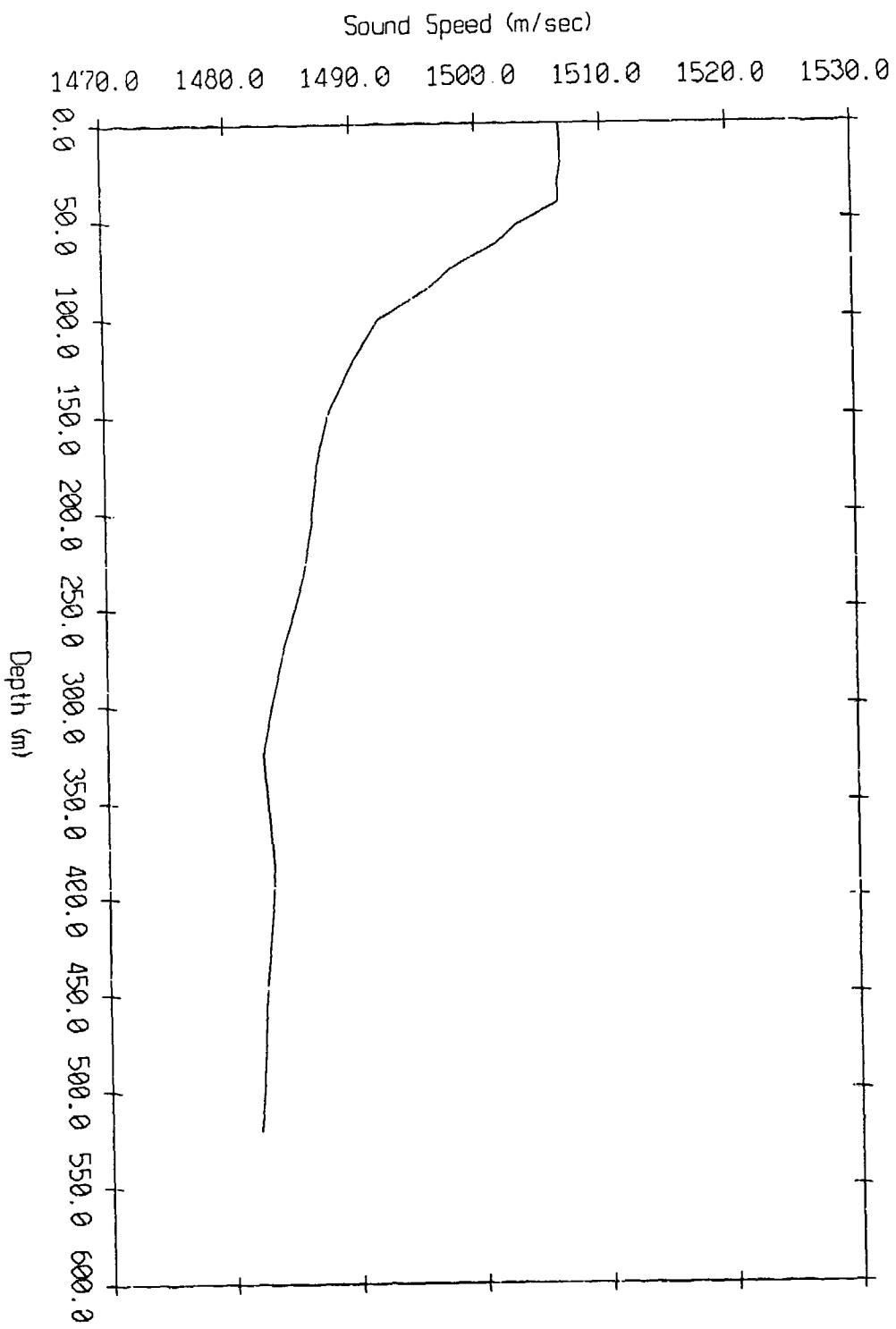


Figure IV.2

Sound Speed Profiles from CalCOFI and NODC Data

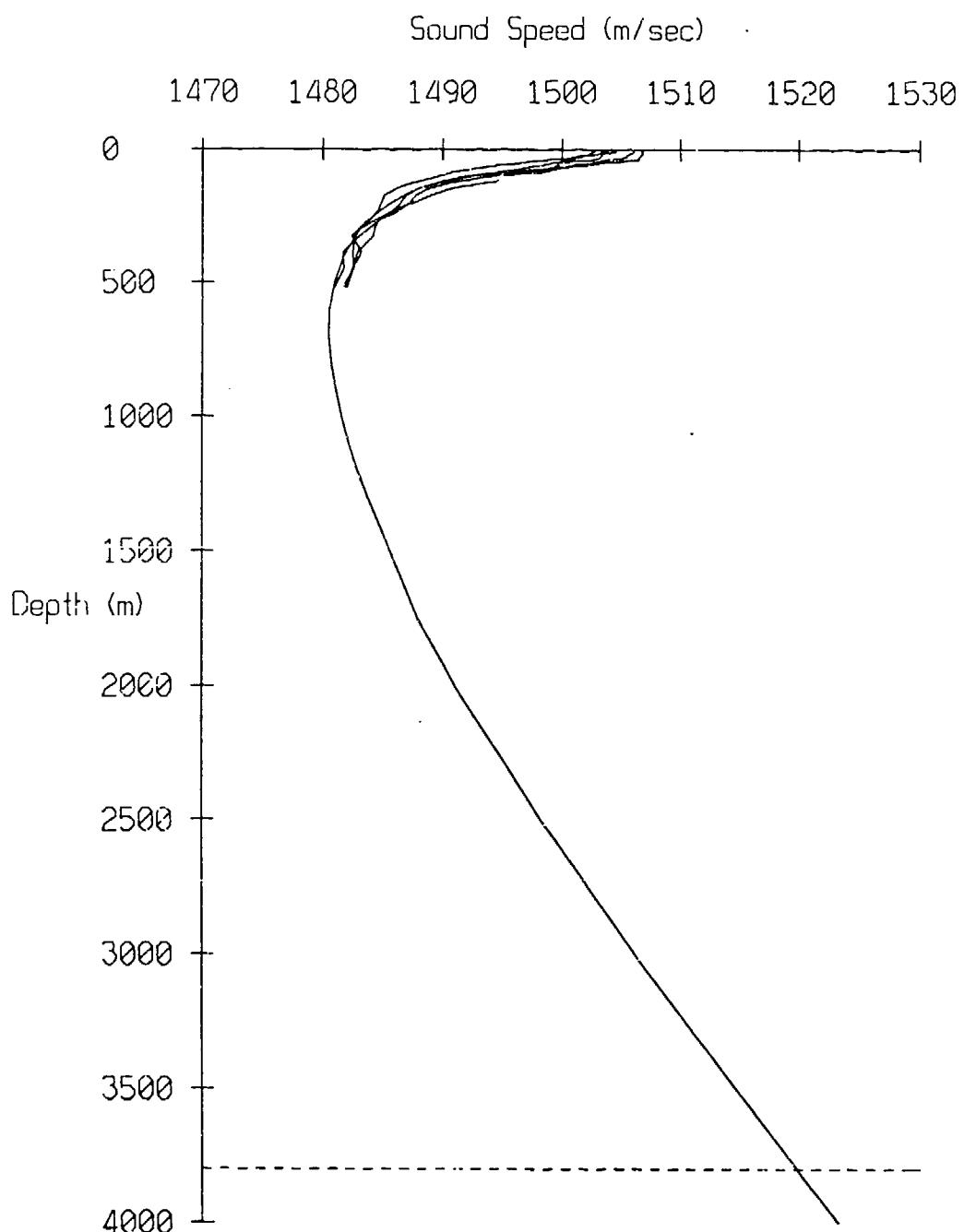


Figure IV.3

Sound Velocity Profile from CalCOFI Cruise 8705 Data
 (32° 05.1' N, 120° 38.3' W)

Depth (m)	Speed of Sound (m/sec)
0.0	1506.641
10.0	1506.834
20.0	1506.774
30.0	1506.526
31.0	1506.511
41.0	1506.547
50.0	1503.951
52.0	1503.267
62.0	1501.466
71.0	1498.734
75.0	1497.899
85.0	1496.013
100.0	1492.262
101.0	1492.042
121.0	1490.144
125.0	1489.779
145.0	1488.214
150.0	1487.926
175.0	1486.986
200.0	1486.558
204.0	1486.516
232.0	1485.819
250.0	1485.107
271.0	1484.210
300.0	1483.107
325.0	1482.478
383.0	1483.285
400.0	1483.156
451.0	1482.491
500.0	1482.153
521.0	1481.984

Table IV.4

Average Sound Velocity Profile from Historical NODC Data
Area 23 (31° - 34° N, 120° - 125° W)

Depth (m)	Speed of Sound (m/sec)
0.0	1502.939
10.0	1502.605
20.0	1502.196
30.0	1501.609
50.0	1499.648
75.0	1496.214
100.0	1492.466
125.0	1489.750
150.0	1487.870
200.0	1485.772
250.0	1484.276
300.0	1483.158
400.0	1481.773
500.0	1481.041
600.0	1480.587
700.0	1480.507
800.0	1480.742
900.0	1481.110
1000.0	1481.638
1100.0	1482.289
1200.0	1483.038
1300.0	1483.871
1400.0	1484.759
1500.0	1485.690
1750.0	1488.079
2000.0	1491.128
2500.0	1498.310
3000.0	1506.229
4000.0	1523.247

Table IV.5

May, 1987 Deployment Data Screening Results

record number	internal record number	#of bytes written	first missing resync	pass header checksum?	pass range checksum?	#of failed acoustic checksums?
Float 0						
359	358	268	0	yes	no	0
360	****	7676	1	no	no	88
1069	1067	310	0	yes	no	0
1070	****	6632	1	no	no	77
1080	1077	3878	0	yes	yes	1
1081	****	3076	1	no	no	33
1082	1078	634	8	yes	yes	28
1083	****	5266	1	no	no	60
1113	1108	132	0	yes	no	0
1114	0	6820	1	no	no	79
Float 1						
204	203	926	0	yes	yes	0
205	0	5994	1	no	no	69
269	****	7644	1	no	no	88
276	274	7646	78	yes	yes	13
277	275	3498	39	yes	yes	15
278	****	156	1	no	no	15
279	****	198	1	no	no	15
280	0	370	1	no	no	15
281	-65	512	1	no	no	15
282	278	1298	11	yes	yes	17
283	10	128	1	no	no	17
284	****	484	1	no	no	17
285	****	378	1	no	no	17
286	230	146	1	no	no	17
287	****	26	1	no	no	17
288	****	0	1	no	no	17
289	0	256	1	no	no	17
290	****	1370	1	no	no	26
291	****	200	1	no	no	26
292	****	10	1	no	no	26
293	0	46	1	no	no	26
294	****	28	1	no	no	26
295	****	0	1	no	no	26
296	-509	276	1	no	no	26
297	225	176	1	no	no	26
298	278	724	2	yes	no	26
299	278	0	2	yes	no	26
300	278	-2	2	yes	no	26

Figure V.1a

May, 1987 Deployment Data Screening Results

record number	internal record number	# of bytes written	first missing resync	pass header checksum?	pass range checksum?	# of failed acoustic checksums?
301	****	36	1	no	no	26
302	2402	250	1	no	no	26
303	****	236	1	no	no	26
304	50	134	1	no	no	26
305	7168	0	1	no	no	26
306	7168	0	1	no	no	26
307	7168	0	1	no	no	26
308	****	34	1	no	no	26
309	****	0	1	no	no	26
310	0	2	1	no	no	26
311	****	234	1	no	no	26
312	****	0	1	no	no	26
313	****	0	1	no	no	26
314	****	0	1	no	no	26
315	408	2	1	no	no	26
316	****	20	1	no	no	26
317	****	0	1	no	no	26
318	0	22	1	no	no	26
319	0	0	1	no	no	26
320	0	0	1	no	no	26
321	0	0	1	no	no	26
322	0	0	1	no	no	26
323	****	8	1	no	no	26
324	****	20	1	no	no	26
325	****	0	1	no	no	26
326	512	6	1	no	no	26
327	512	0	1	no	no	26
328	512	-2	1	no	no	26
329	512	0	1	no	no	26
330	0	2	1	no	no	26
331	0	2	1	no	no	26
332	7936	0	1	no	no	26
333	7936	0	1	no	no	26
334	7936	-2	1	no	no	26
335	7936	0	1	no	no	26
336	7936	0	1	no	no	26
337	7936	0	1	no	no	26
338	7936	0	1	no	no	26
339	7936	0	1	no	no	26
340	7936	0	1	no	no	26
341	7936	0	1	no	no	26
342	7936	0	1	no	no	26
343	7936	0	1	no	no	26
344	7936	0	1	no	no	26

Figure V.1b

May, 1987 Deployment Data Screening Results

record number	internal record number	# of bytes written	first missing resync	pass header checksum?	pass range checksum?	# of failed acoustic checksums?
345	7936	0	1	no	no	26
346	7936	0	1	no	no	26
347	7936	0	1	no	no	26
348	7936	0	1	no	no	26
349	7936	0	1	no	no	26
350	7936	0	1	no	no	26
351	7936	0	1	no	no	26
352	7936	0	1	no	no	26
353	7936	0	1	no	no	26
354	7936	0	1	no	no	26
355	7936	0	1	no	no	26
356	7936	0	1	no	no	26
357	7936	0	1	no	no	26
358	0	0	1	no	no	51

Float 2

1980	1978	0	0	yes	yes	0
------	------	---	---	-----	-----	---

Float 3

429	428	7642	67	yes	yes	24
430	429	7642	29	yes	yes	62
1263	1262	7642	0	yes	yes	1
1868	1867	534	0	yes	yes	1
1869	****	6348	1	no	no	73
1879	1876	0	0	yes	yes	0

Float 4

977	976	1648	0	yes	yes	1
985	985	7642	6	yes	yes	1
1419	1419	5680	0	yes	yes	1
1420	****	1696	1	no	no	16
1964	1062	0	0	yes	yes	0

Float 7

1571	1570	3434	0	yes	yes	1
------	------	------	---	-----	-----	---

Figure V.1c

May, 1987 Deployment Data Screening Results							
record number	internal record number	# of bytes written	first missing resync	pass header checksum?	pass range checksum?	# of failed acoustic checksums?	
1572	****	5156	1	no	no	58	
1908	1905	0	0	yes	yes	0	
Float 8							
1104	1104	7642	0	yes	yes	1	
1894	1893	0	0	yes	yes	0	
Float 9							
28	27	7642	0	yes	yes	1	
55	54	6406	0	yes	yes	1	
56	****	7396	1	no	no	86	
186	129	4370	0	yes	yes	1	
187	-257	2540	1	no	no	27	
1945	1886	0	0	yes	yes	0	
Float 10							
1953	1951	0	0	yes	yes	0	
Float 11							
1911	1910	0	0	yes	yes	0	

Figure V.1d

Float 0, May, 1987 Sea Trip: surface & bottom bounces

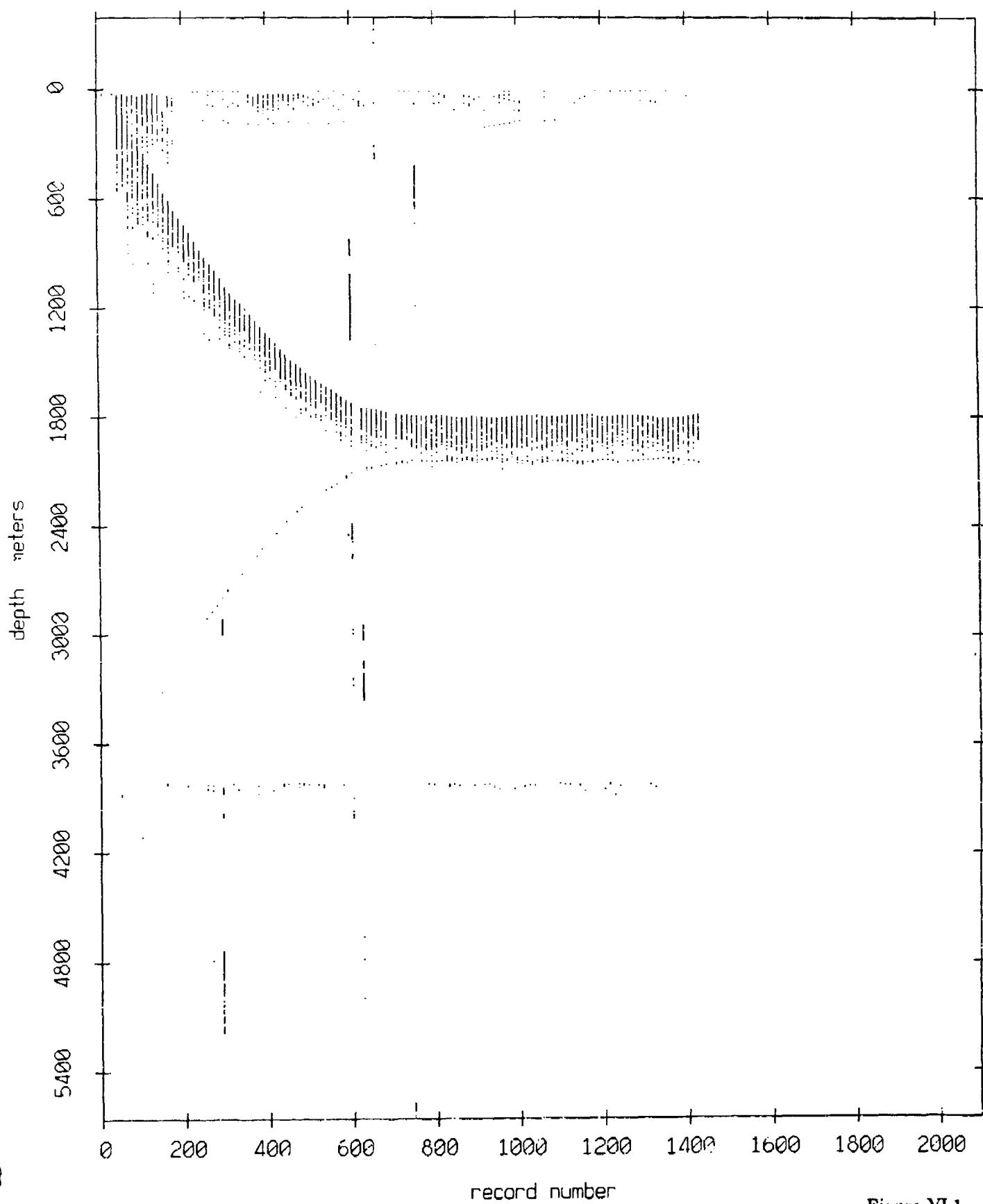


Figure VI.1

Float 1, May, 1987 Sea Trip: surface & bottom bounces

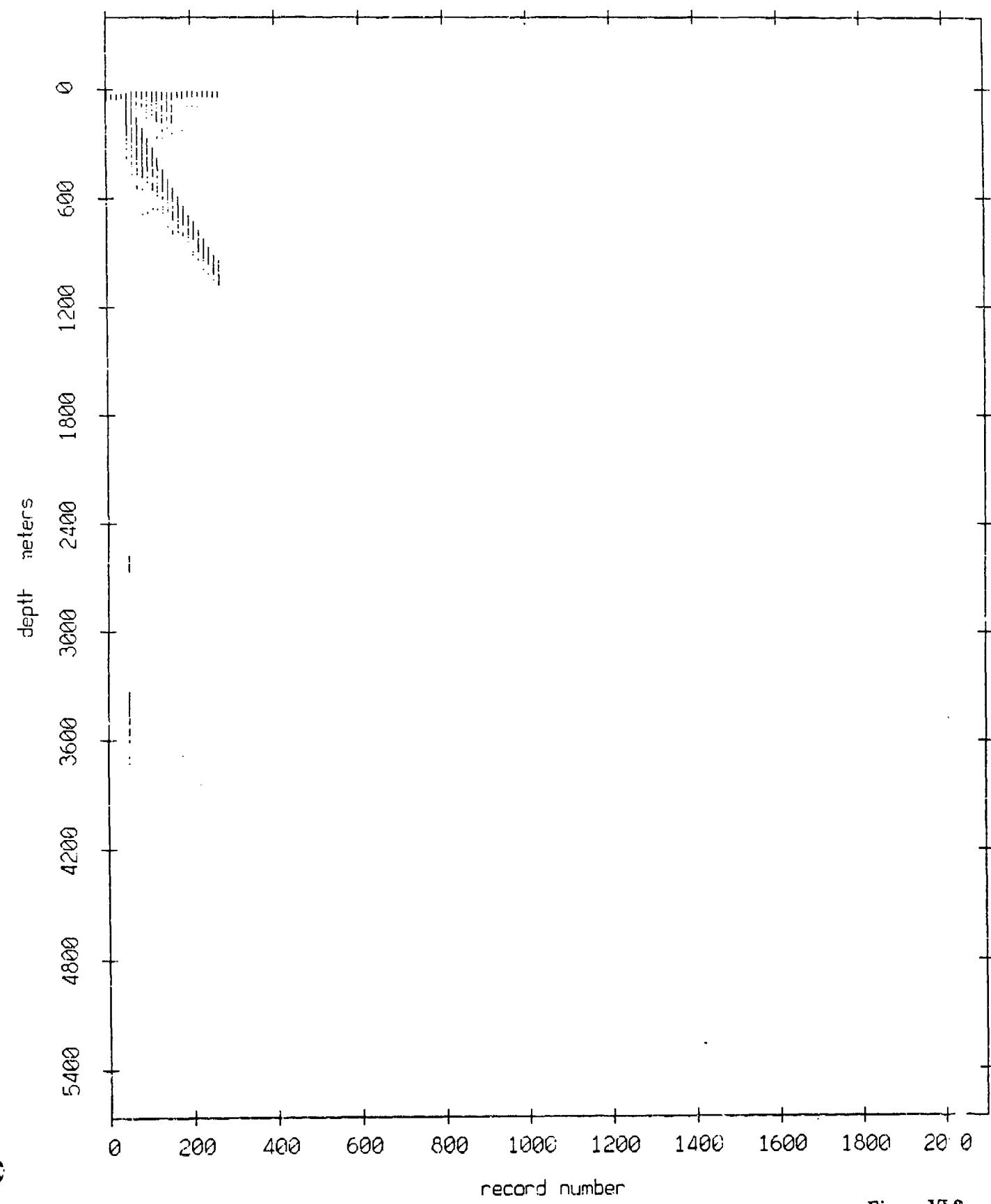


Figure VI.2

Fleet 2, May, 1987 Sea Trip: surface & bottom bounces

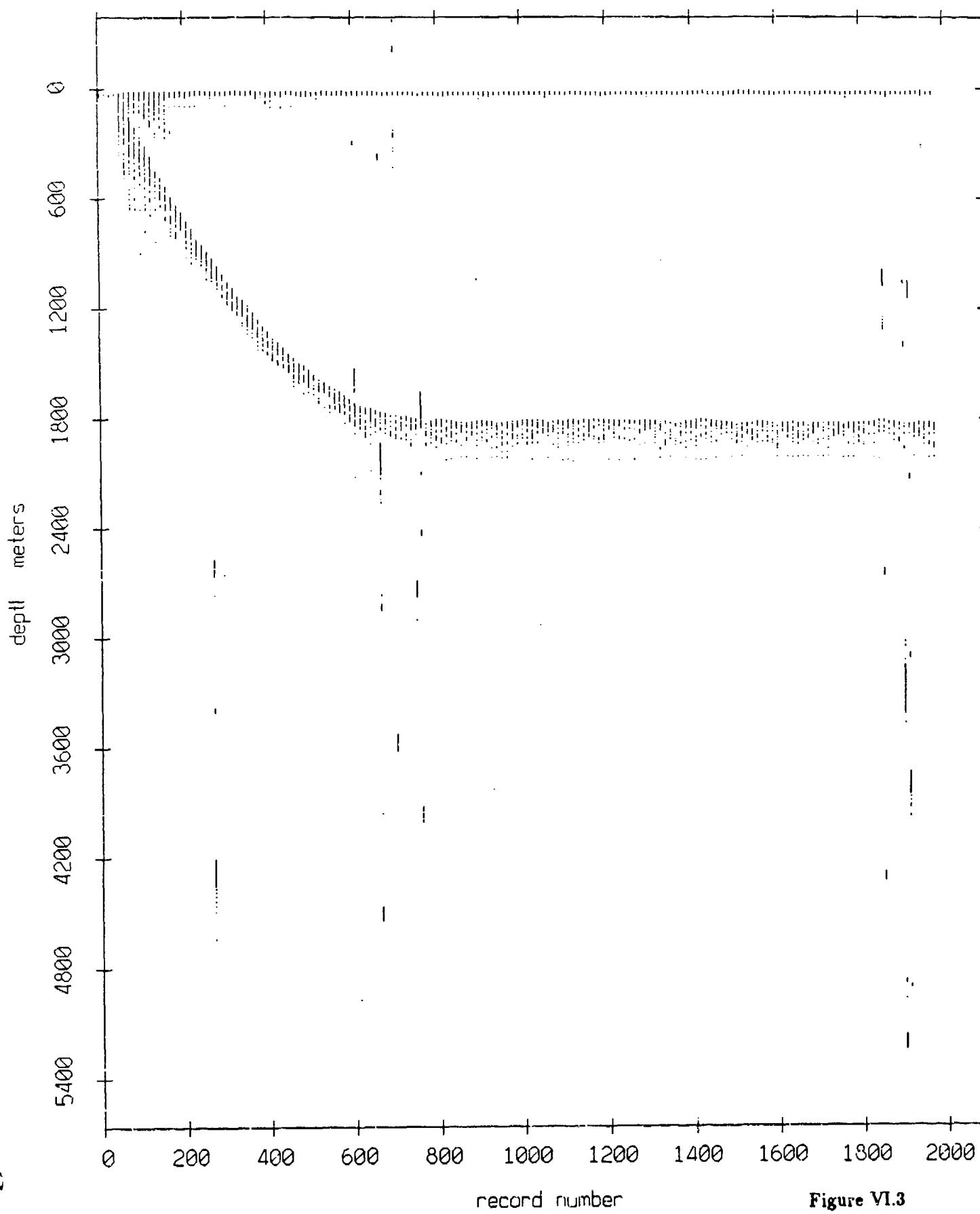


Figure VI.3

Float 3, May, 1987 Sea Trip: surface & bottom bounces

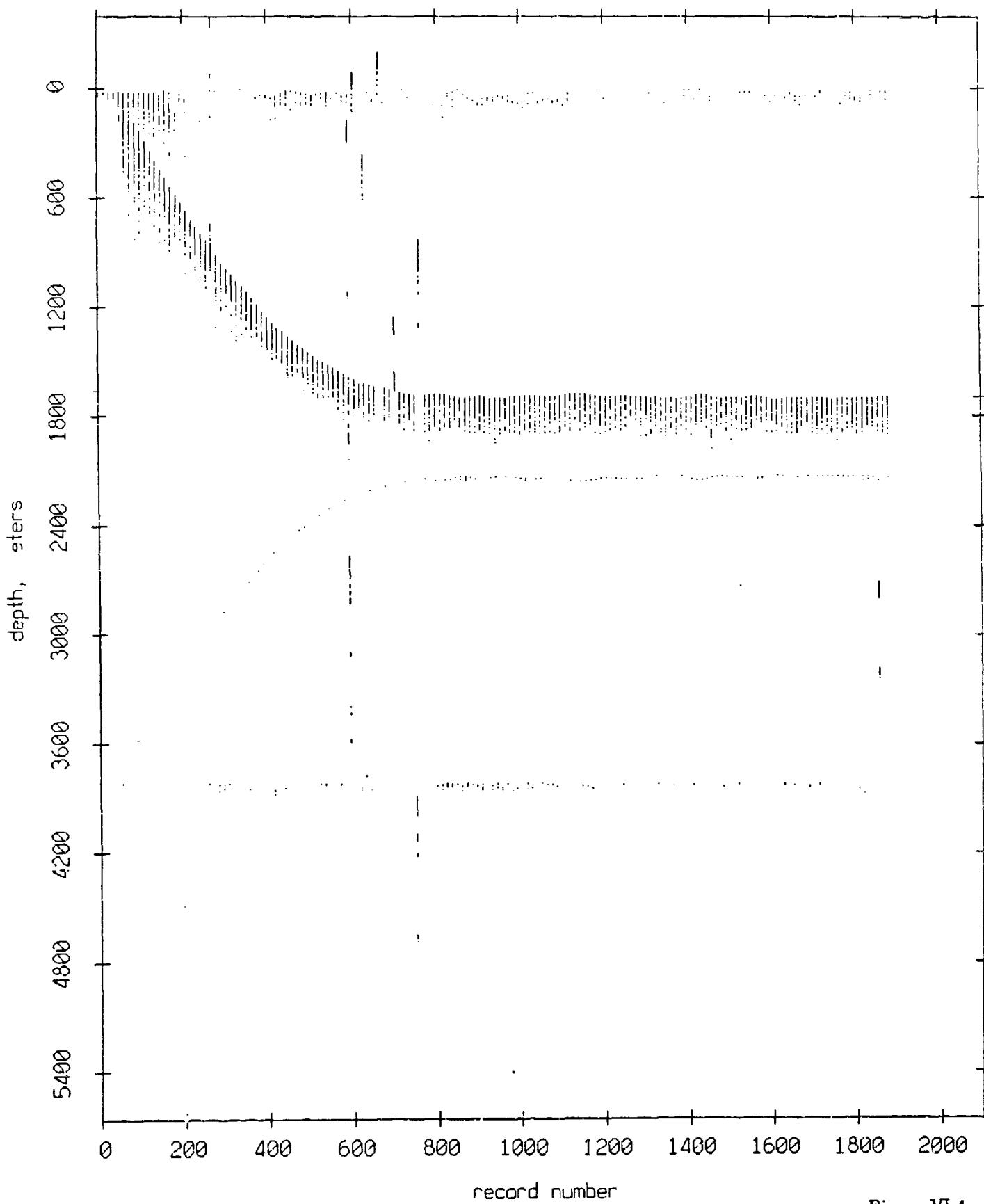


Figure VI.4

Fleet 4, May, 1987 Sea Trip: surface & bottom bounces

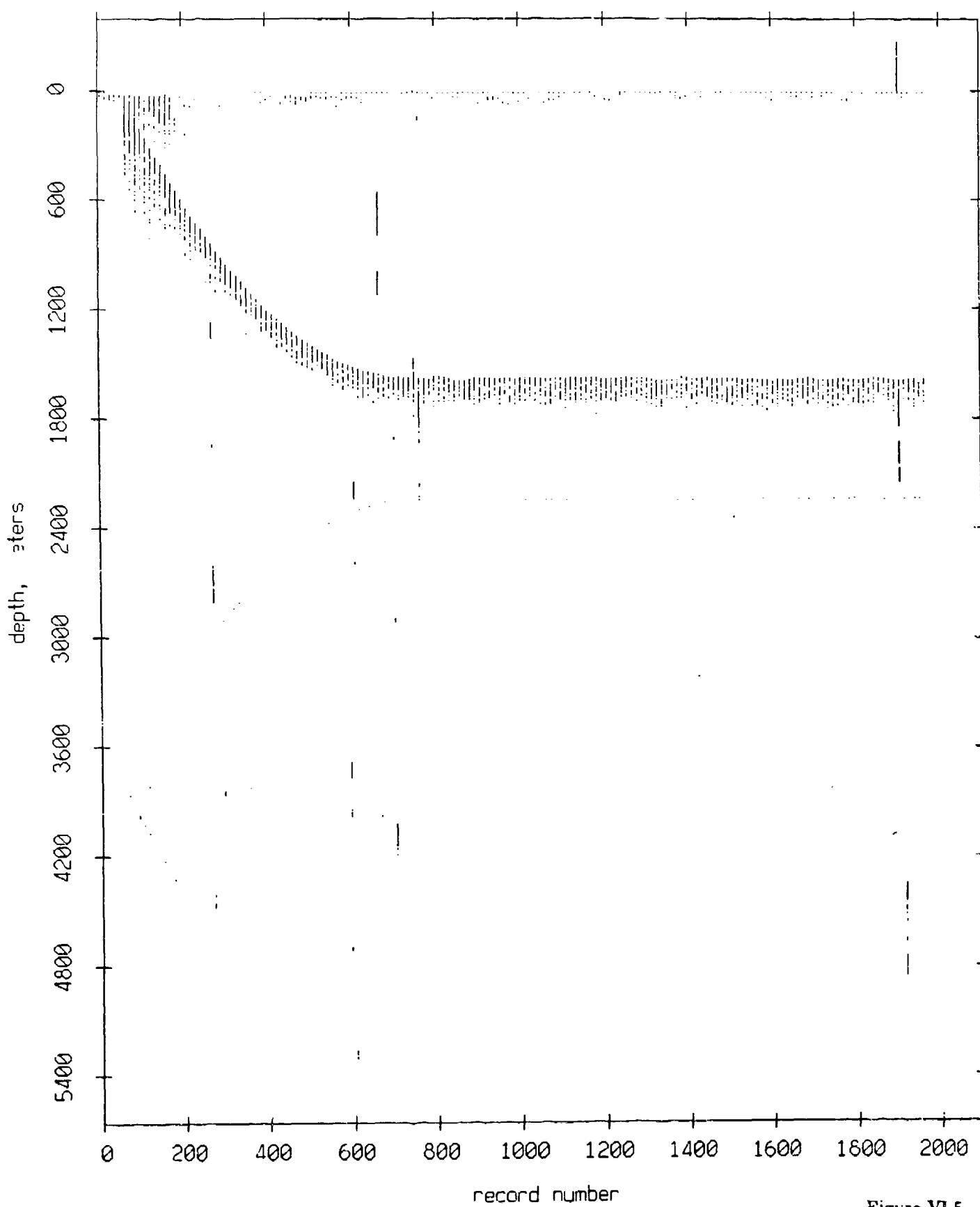


Figure VI.5

Float 7, May, 1987 Sea Trip: surface & bottom bounces

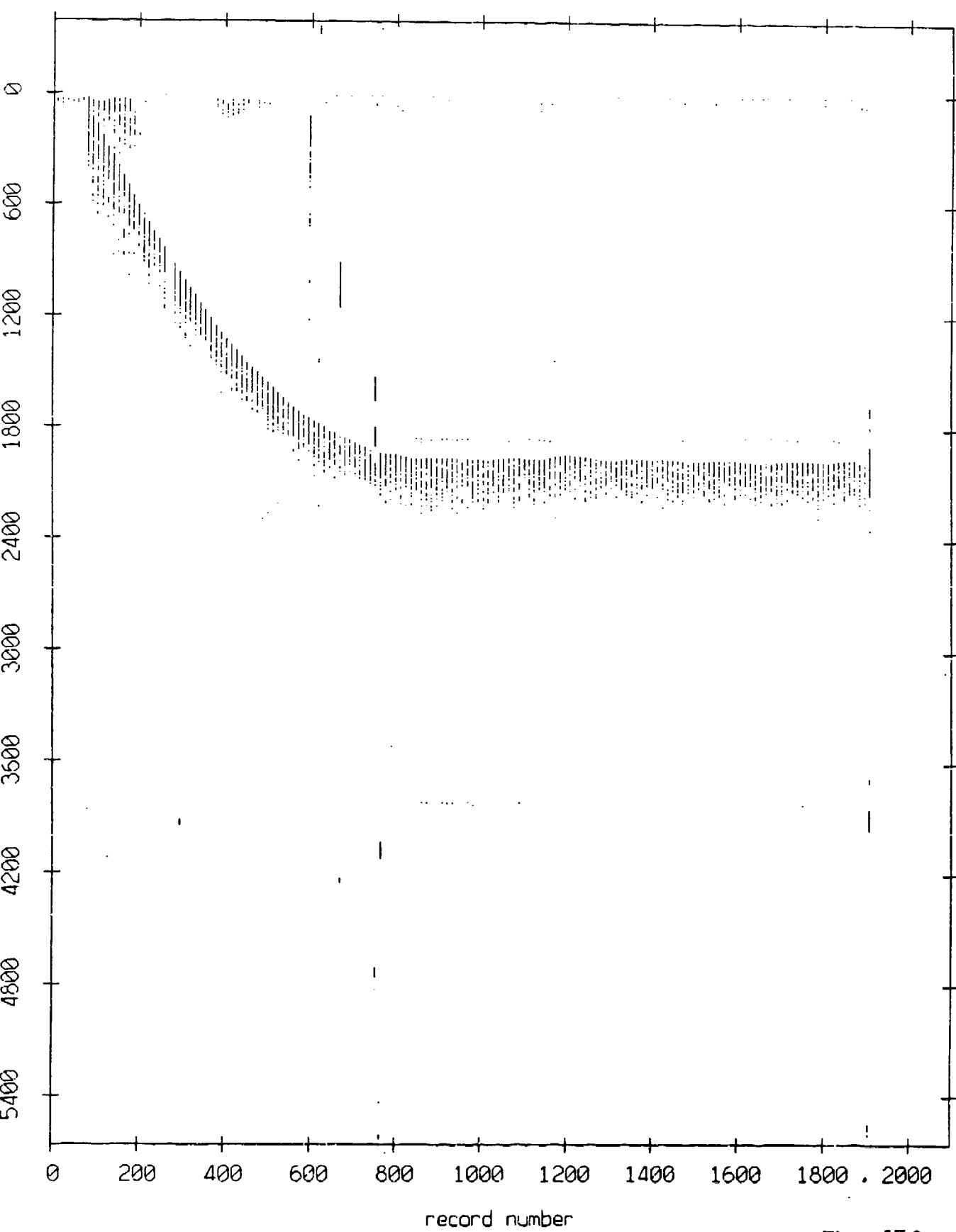


Figure VI.6

Float 8, May, 1987 Sea Trip: surface & bottom bounces

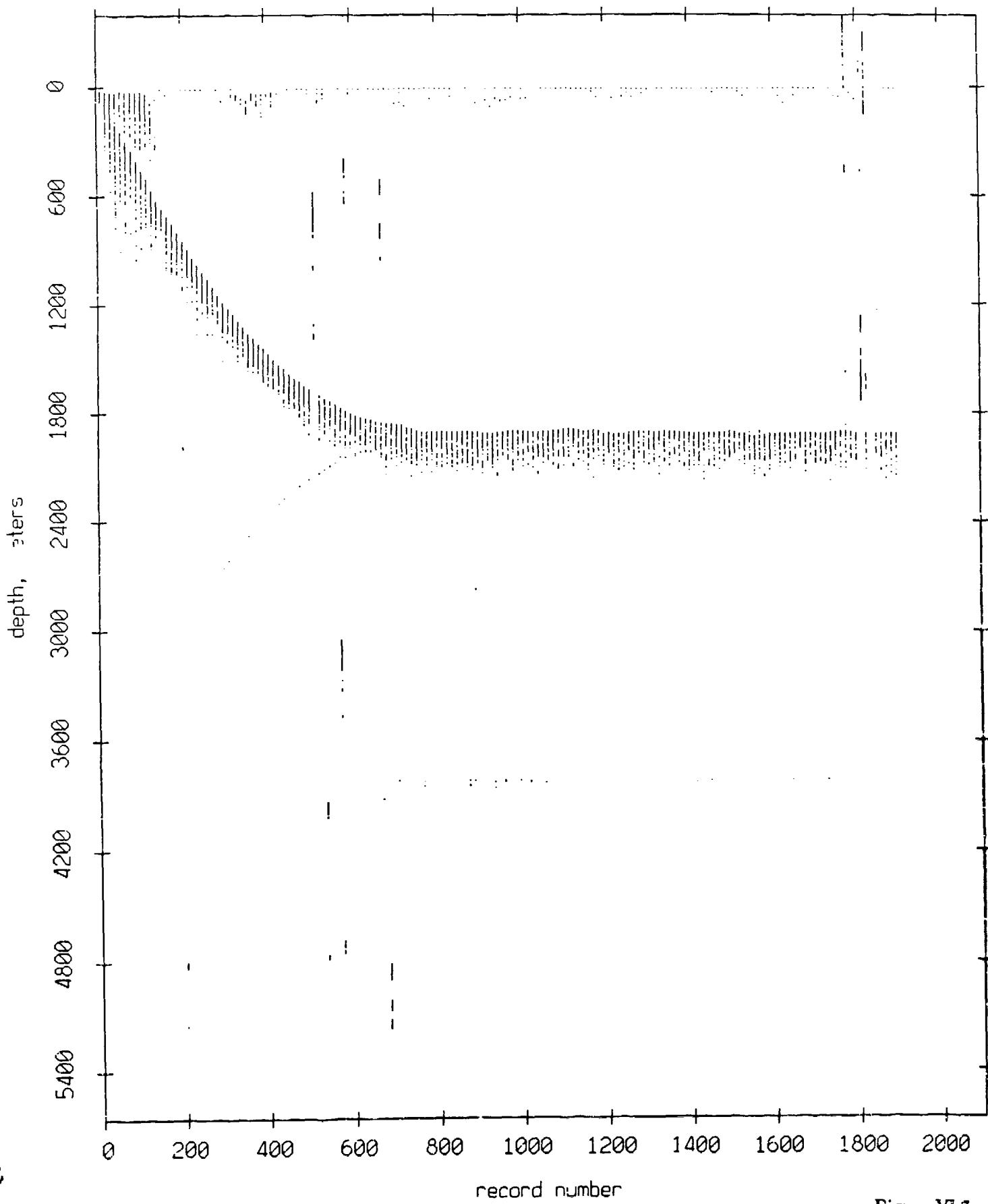


Figure VI.7

Fleet 9, May, 1987 Sea Trip: surface & bottom bounces

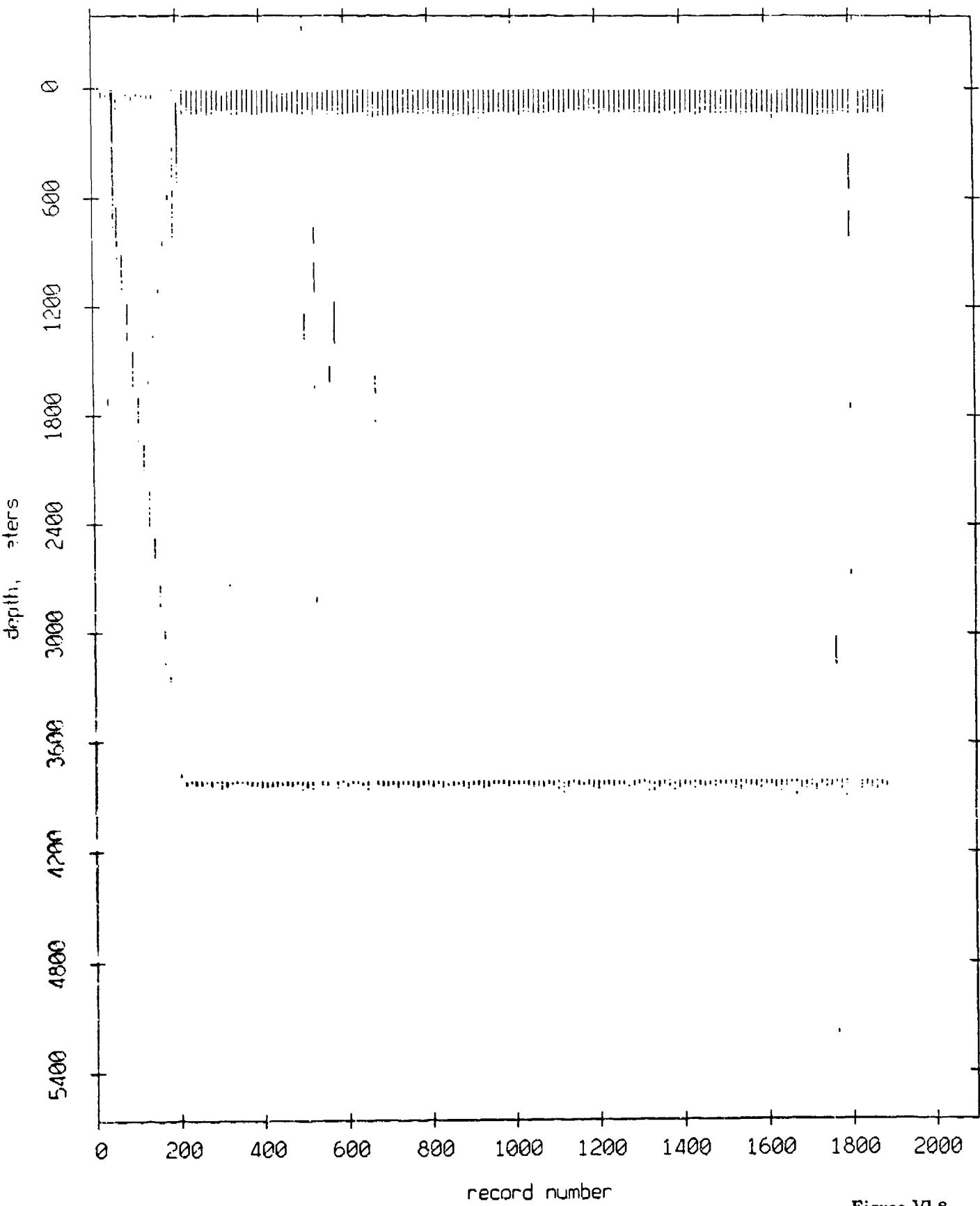


Figure VI.8

Fleet 10, May, 1987 Sea Trip: surface & bottom bounces

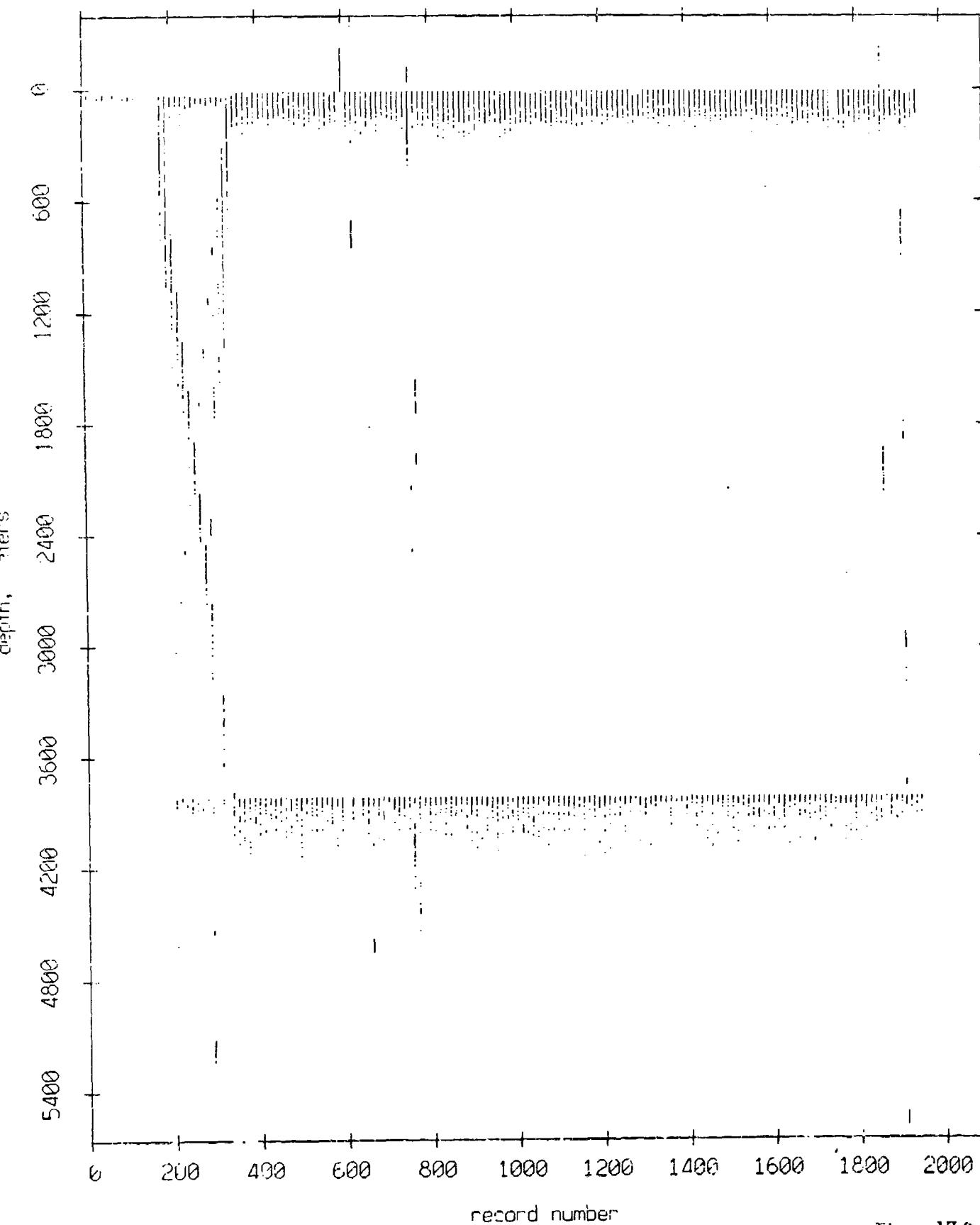


Figure VI.9

Float 11, May, 1987 Sea Trip: surface & bottom bounces

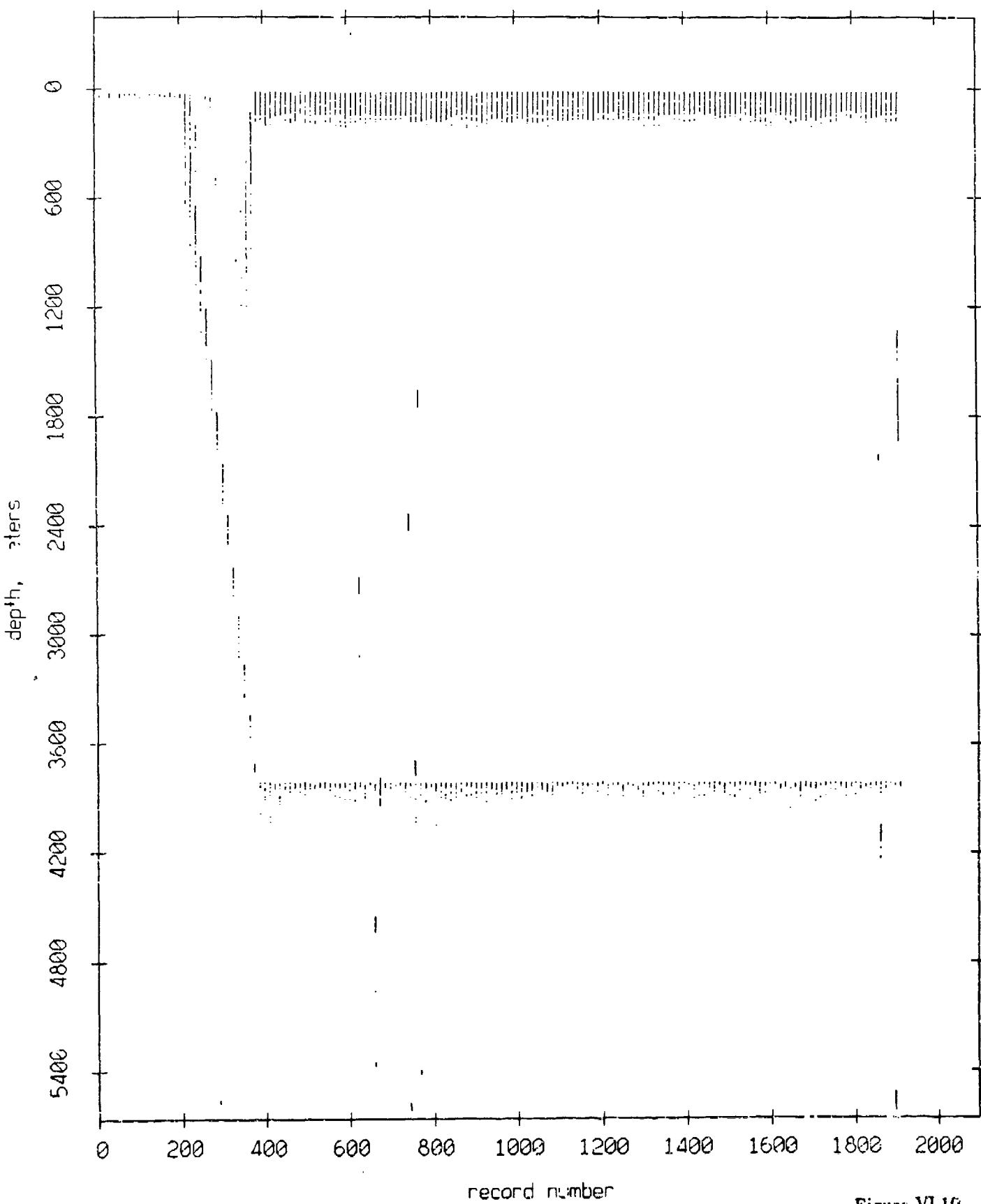


Figure VI.10

Float 0, May, 1987 Sea Trip: range from float 1

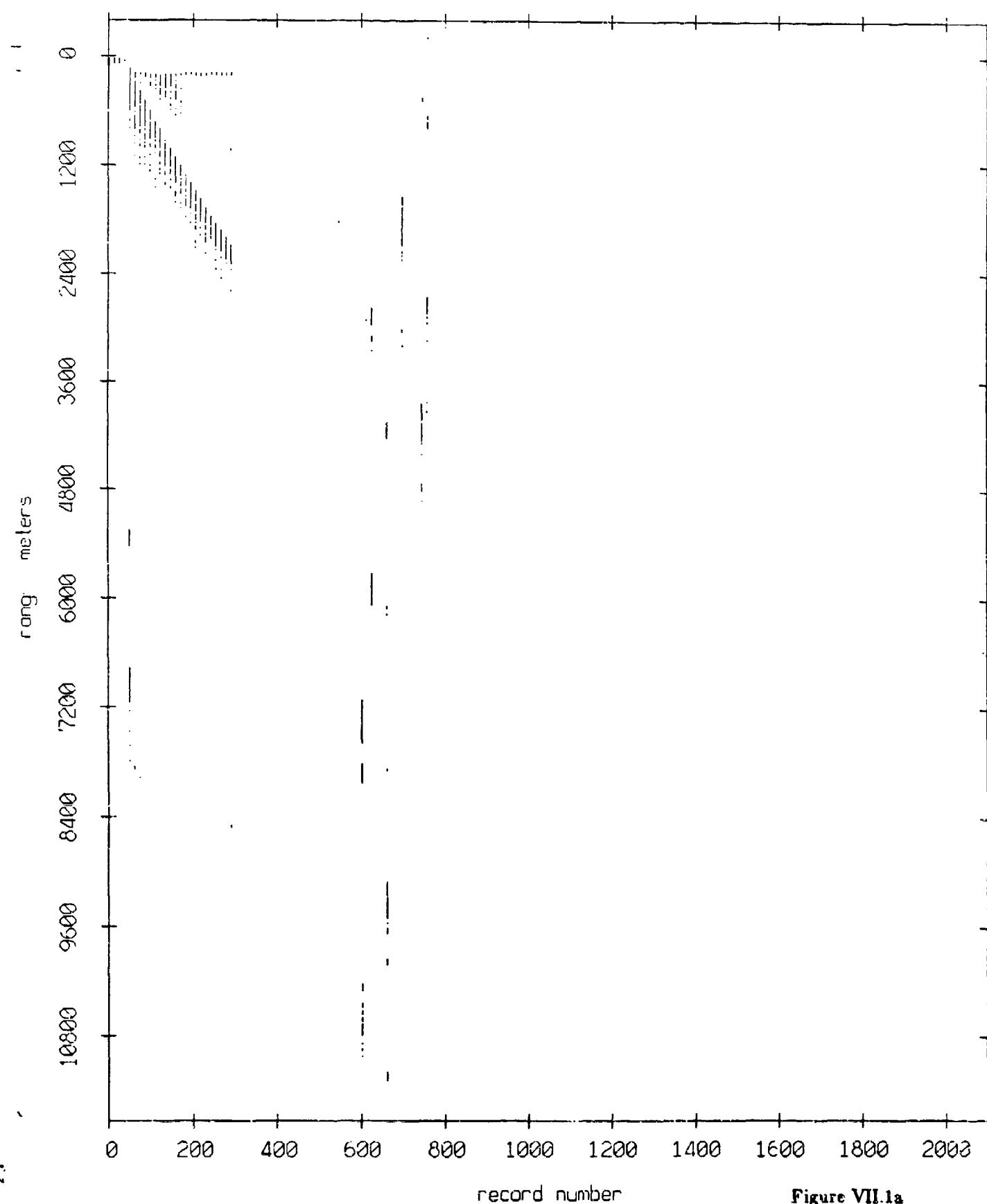


Figure VII.1a

Float 0, May, 1987 Sea Trip: range from float 2

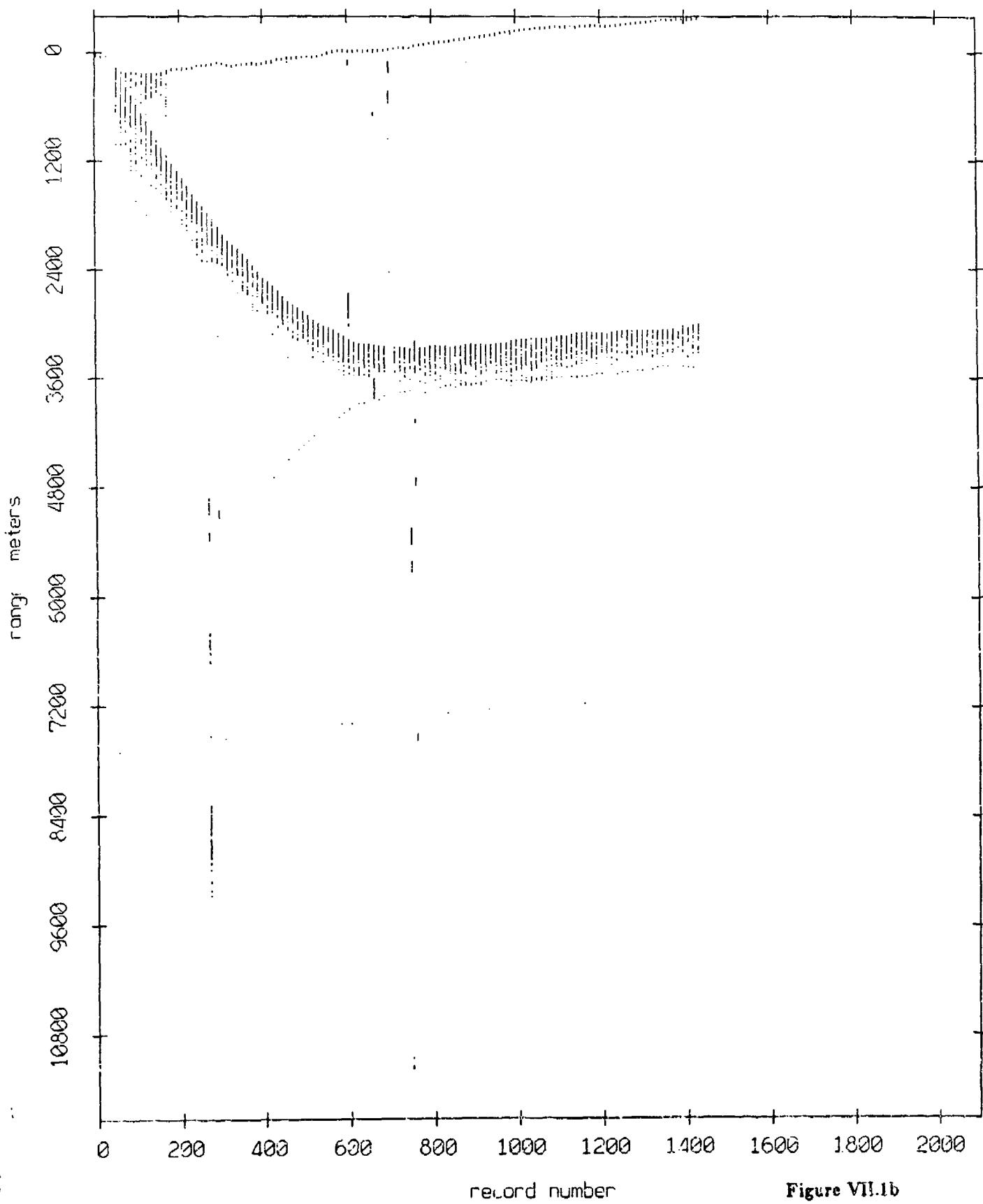


Figure VII.1b

Float 0, May, 1987 Sea Trip: range from float 3

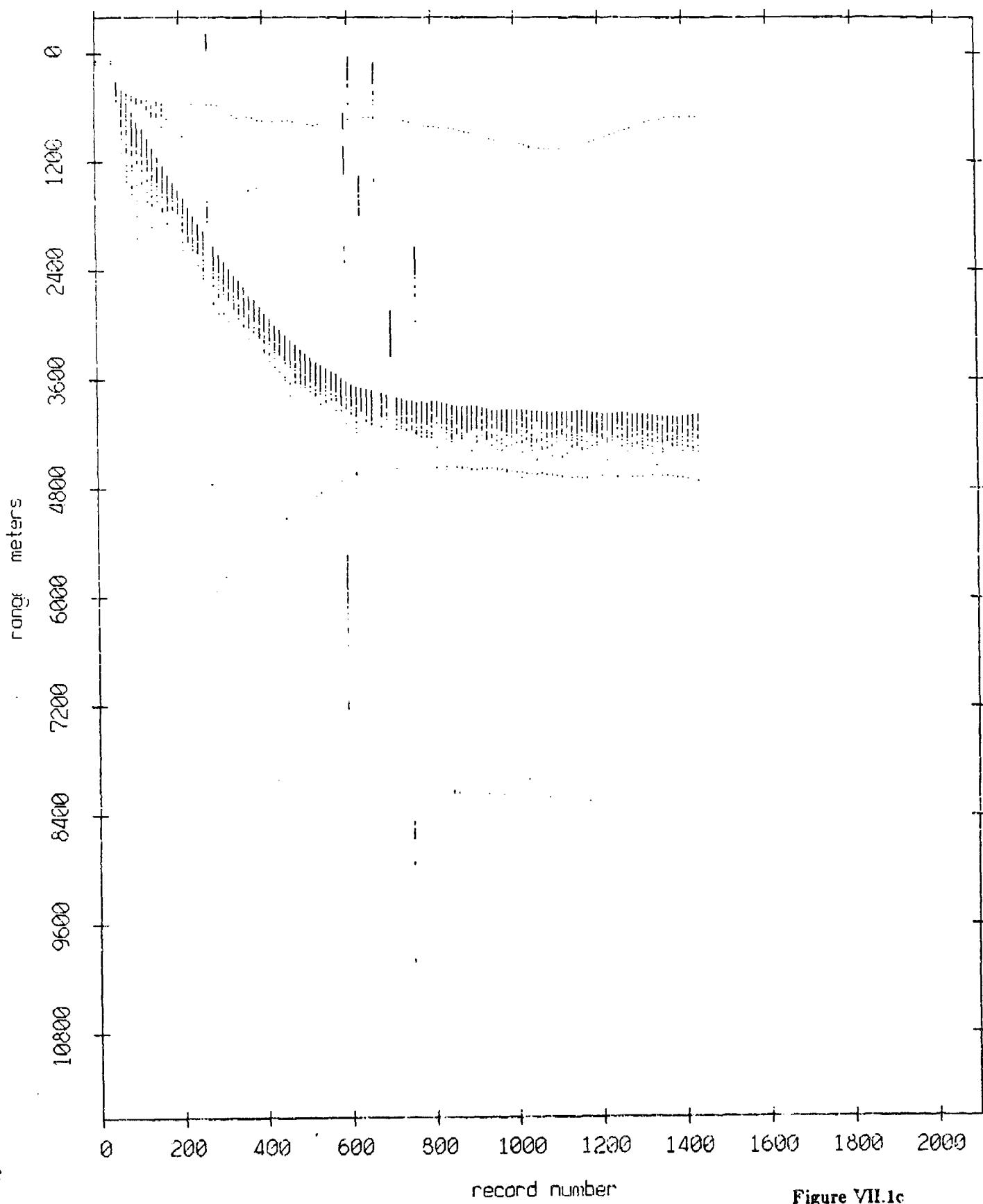


Figure VII.1c

Float 0, May, 1987 Sea Trip: range from float 4

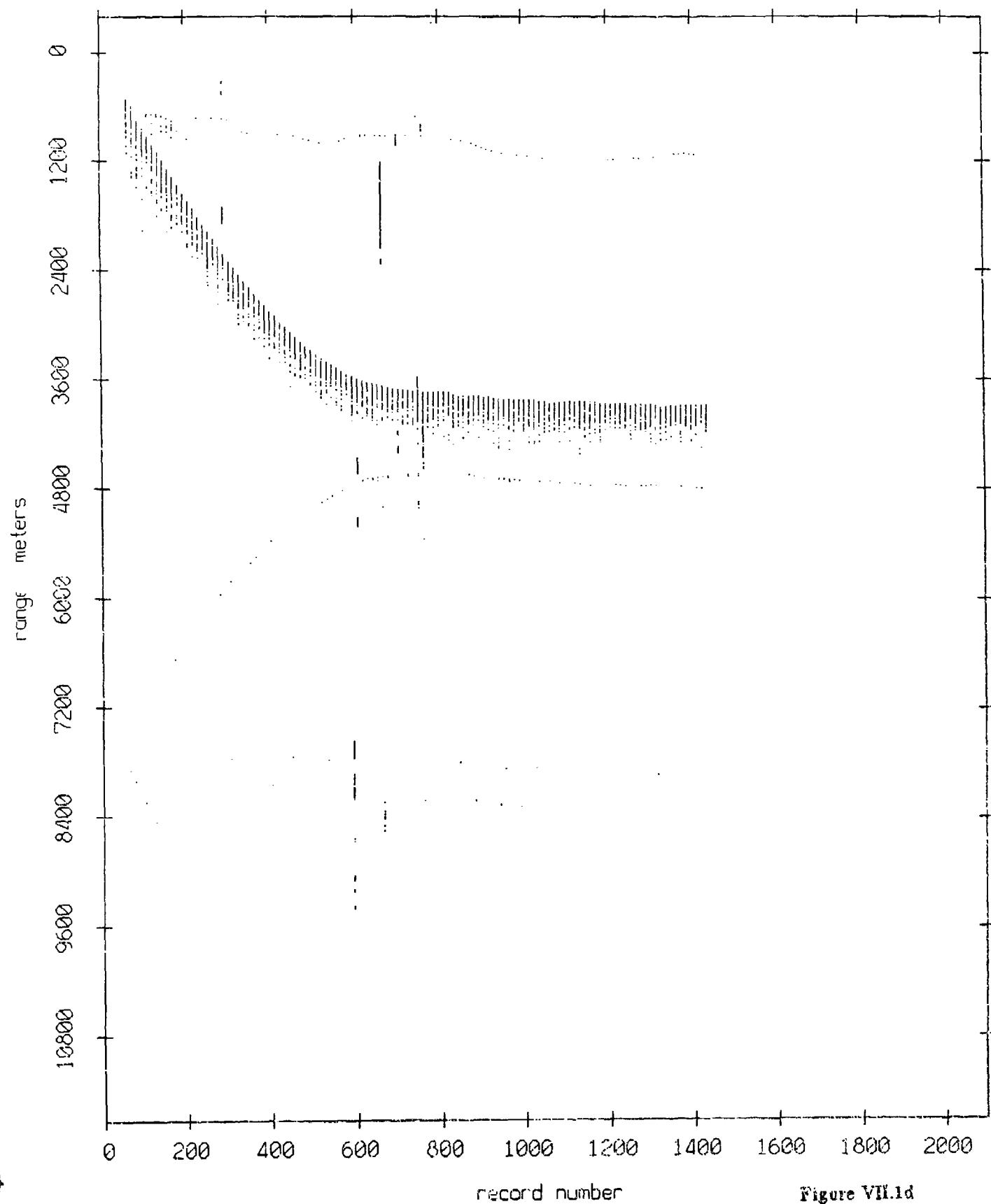


Figure VII.1d

Float 0, May, 1987 Sea Trip: range from float 7

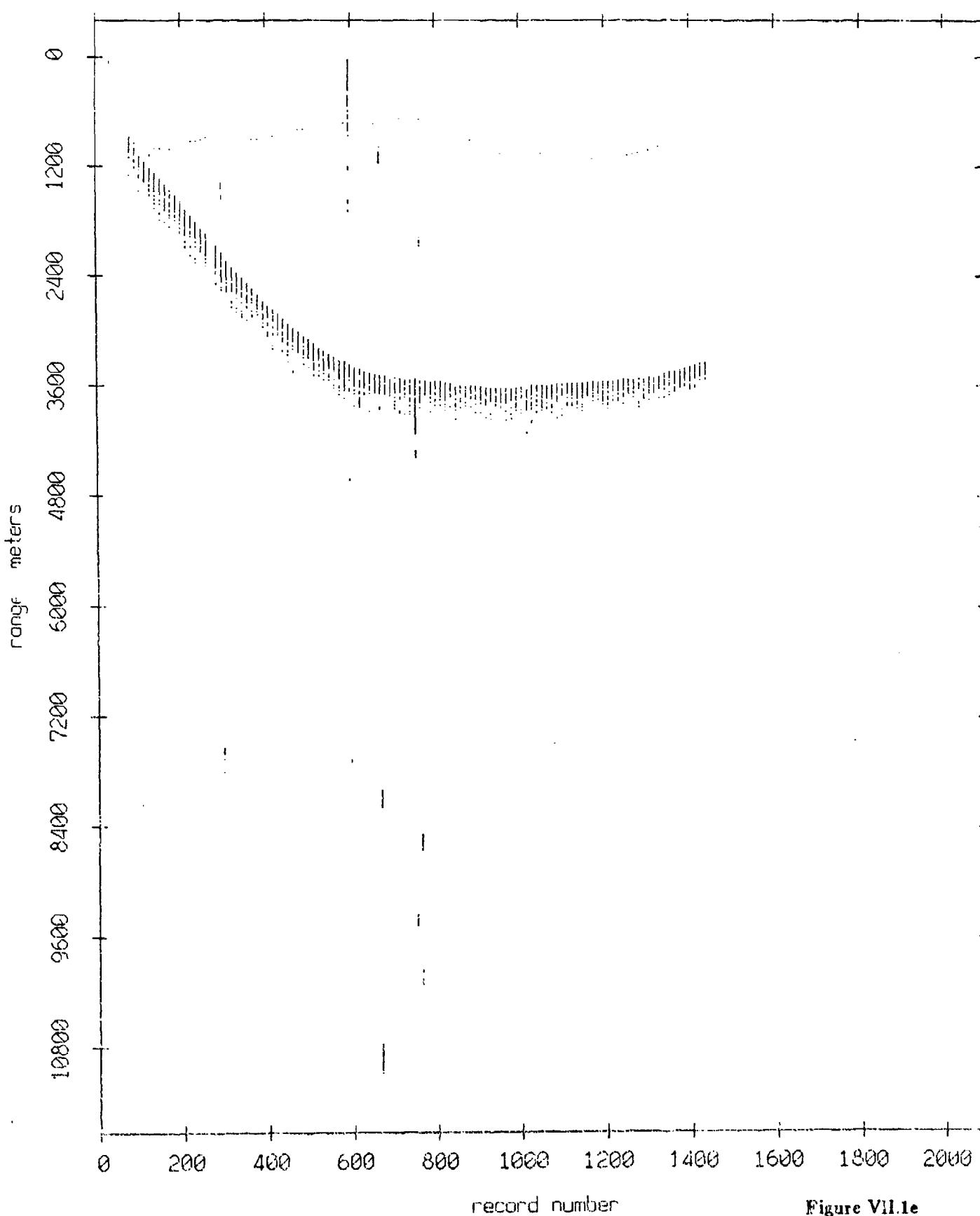


Figure VII.1e

Float 0, May, 1987 Sea Trip: range from float 8

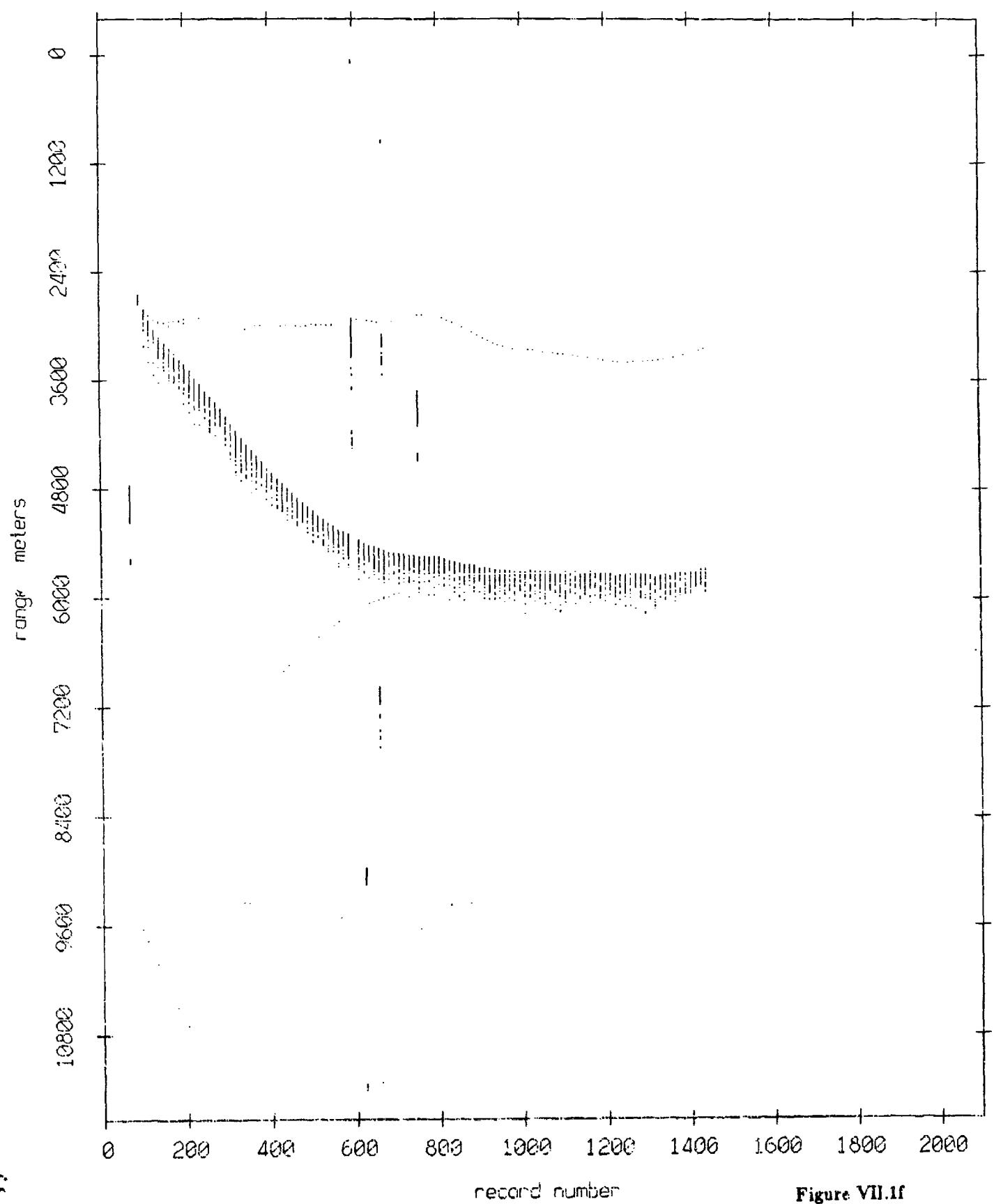


Figure VII.1f

Float 0, May, 1987 Sea Trip: range from float 9

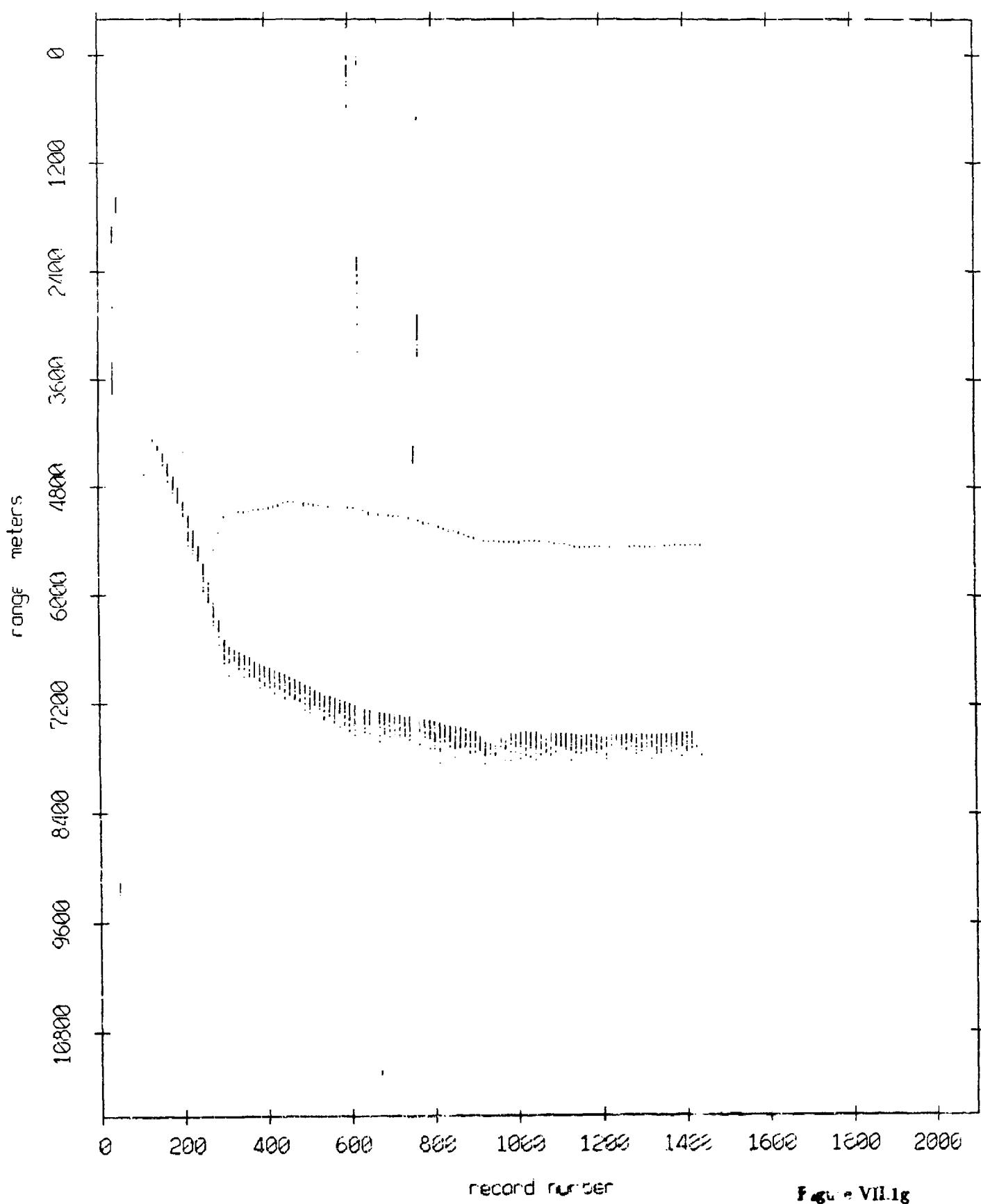


Figure VII.1g

Fleet 0, May, 1987 Sea Trip: range from float 10

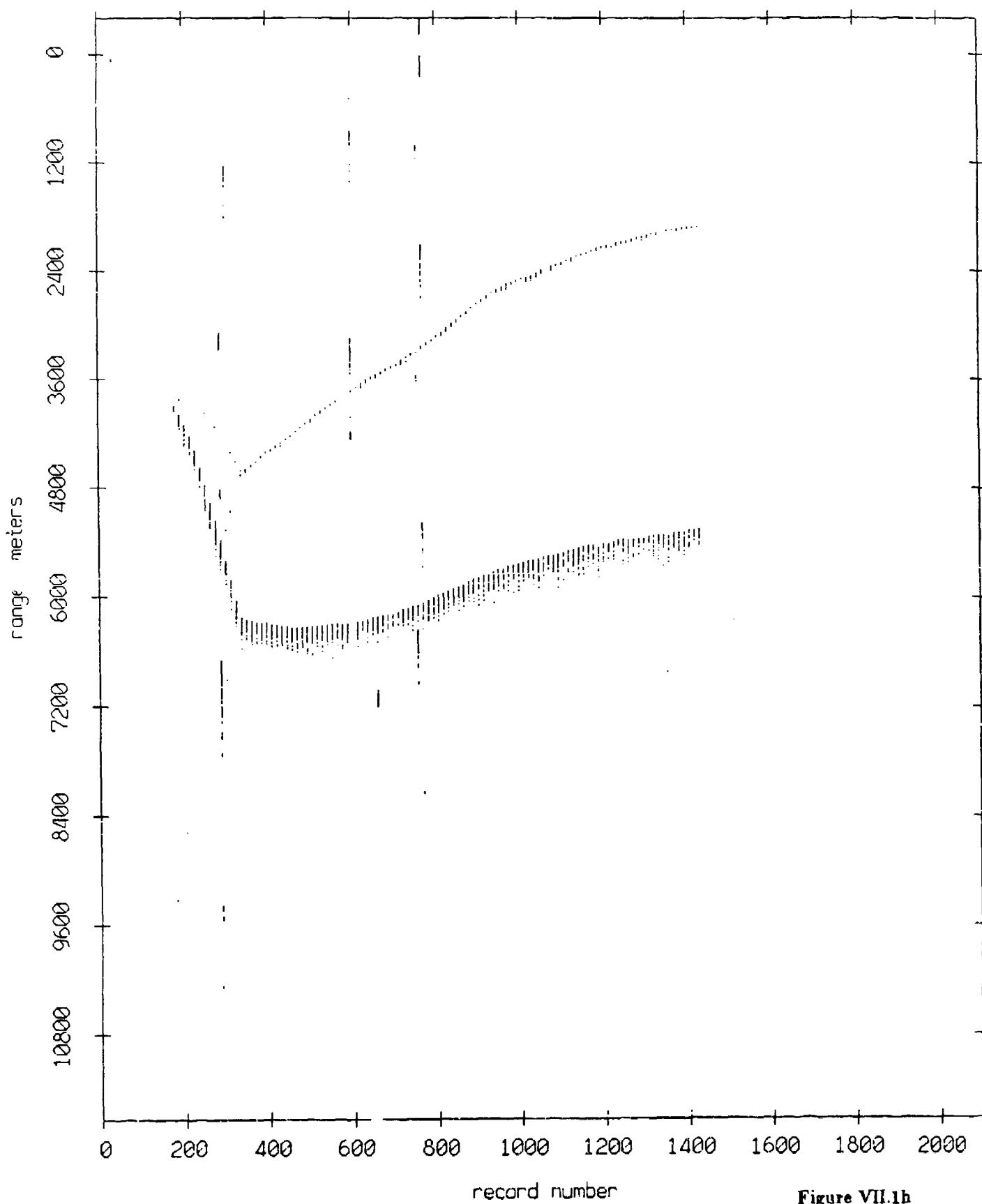


Figure VII.1h

Float 0, May, 1987 Sea Trip: range from float 11

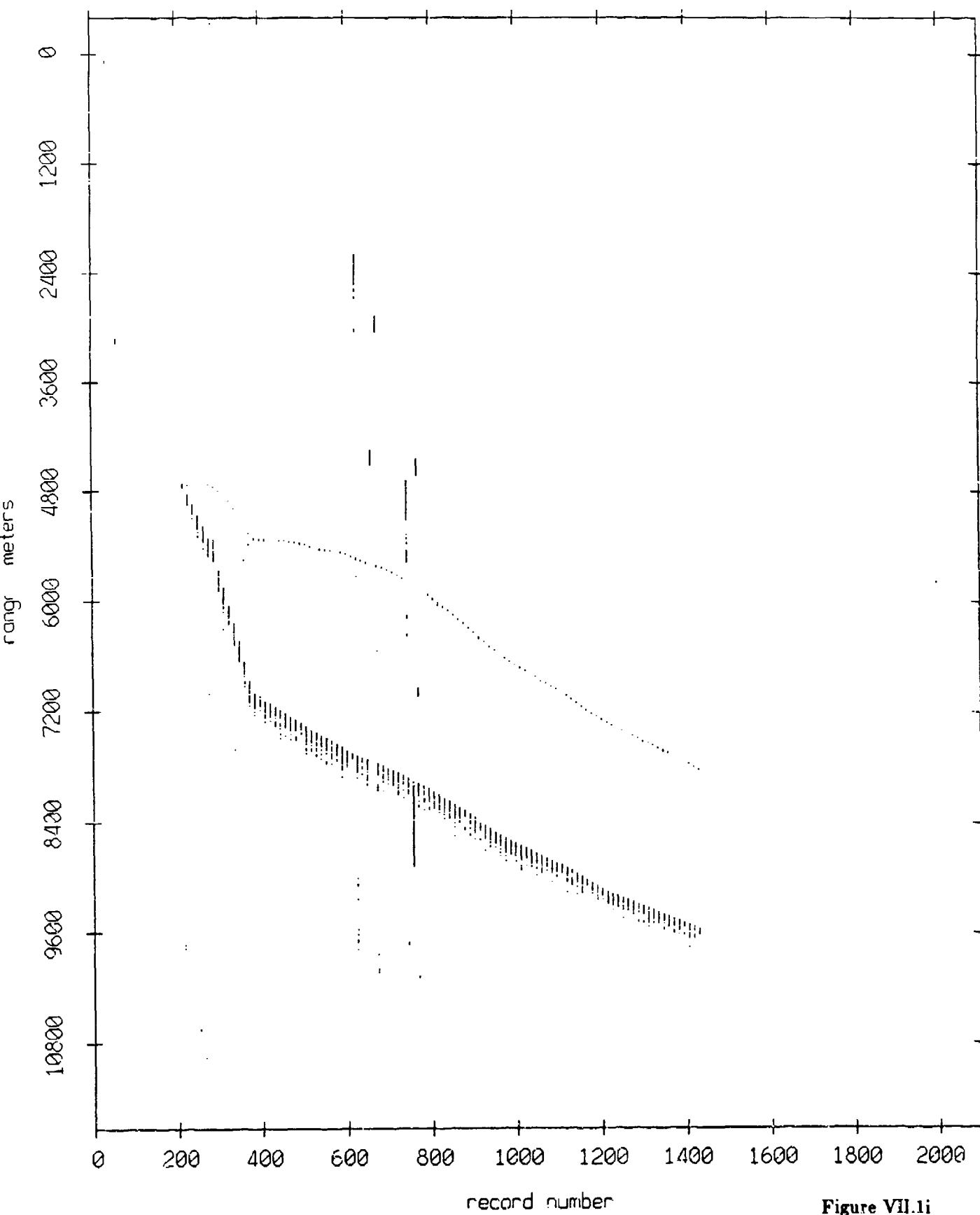


Figure VII.1i

Float 2, May, 1987 Sea Trip: range from float 0

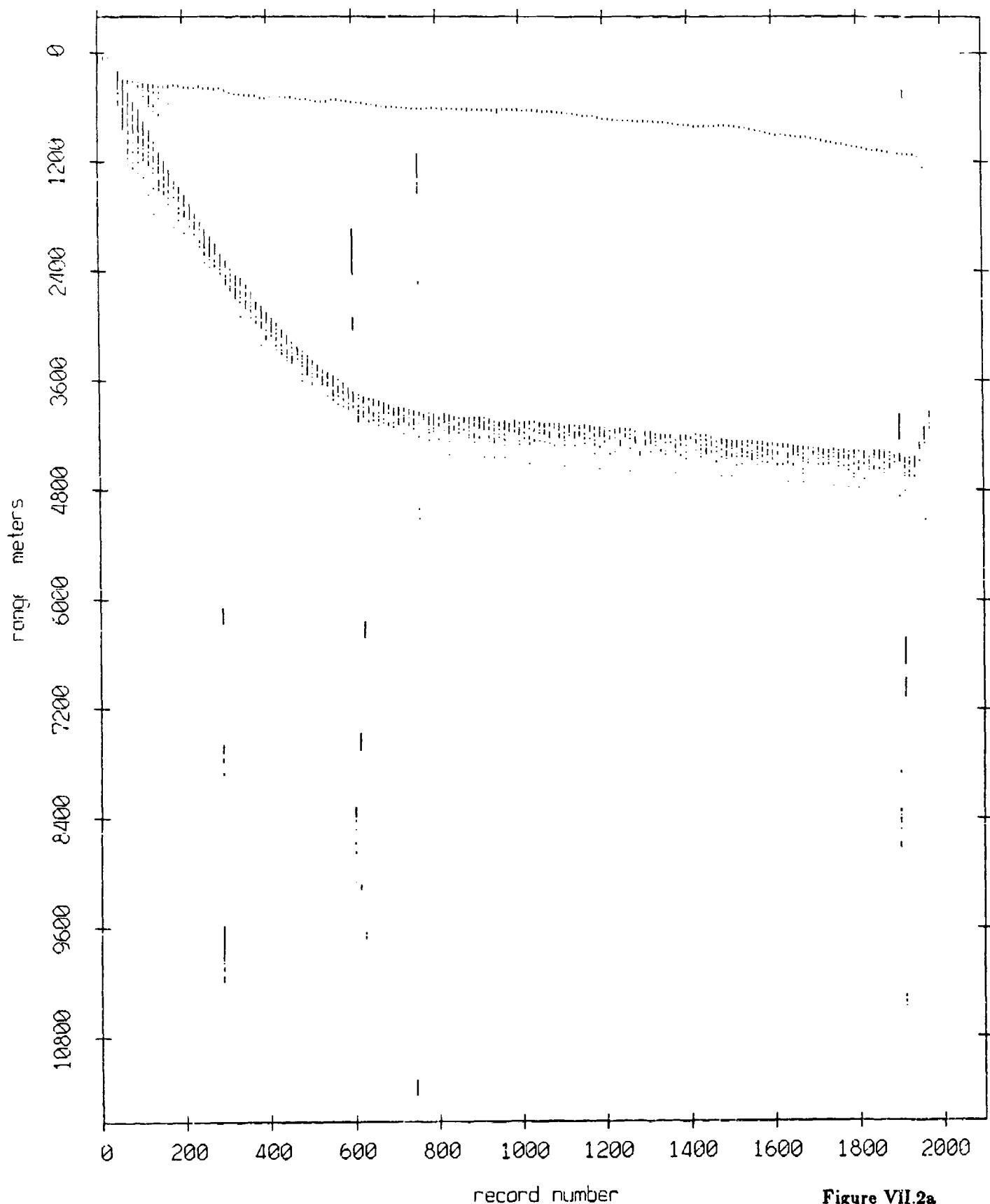


Figure VII.2a

Float 2, May, 1987 Sea Trip: range from float 1

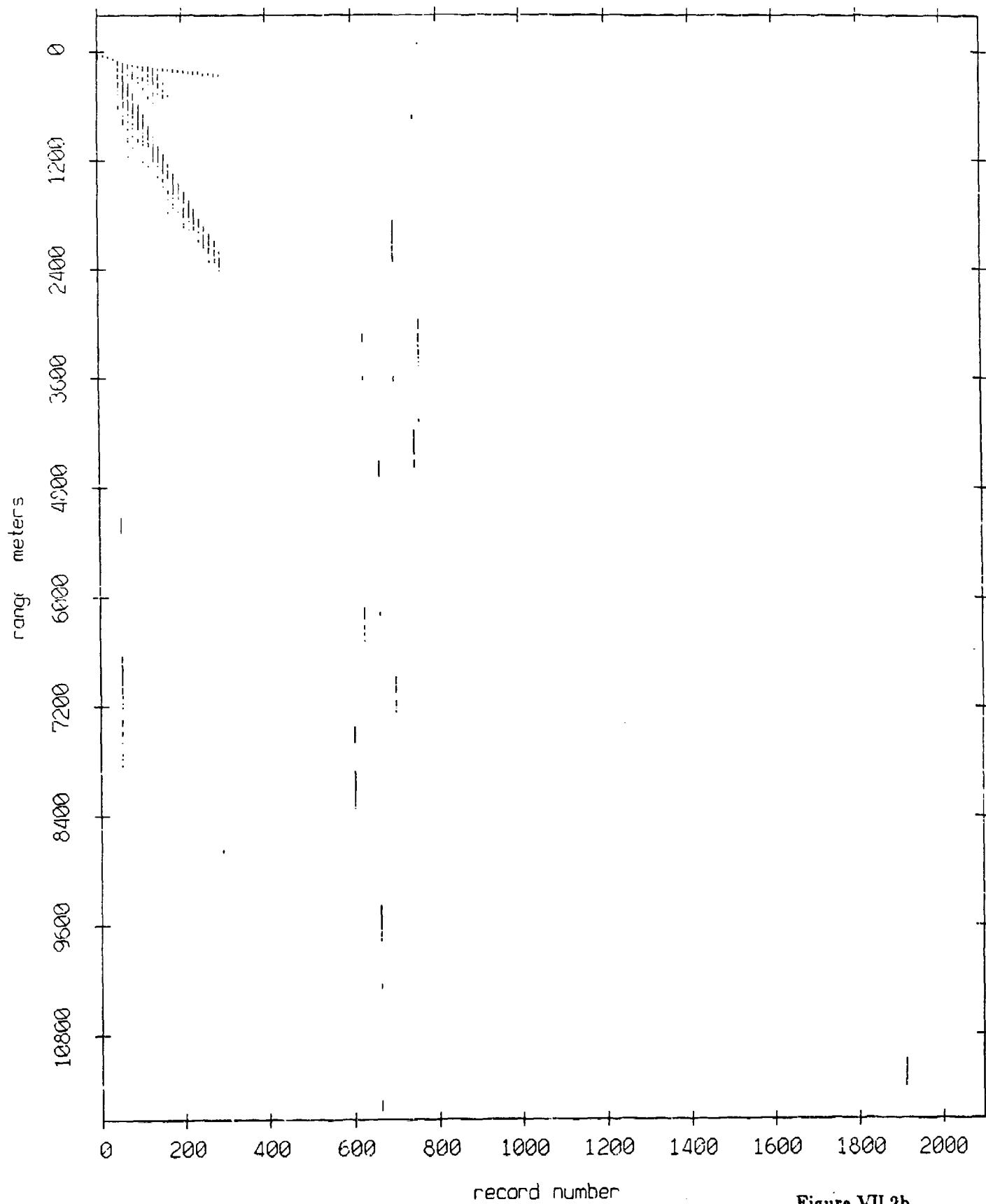


Figure VII.2b

Float 2, May, 1987 Sea Trip: range from float 3

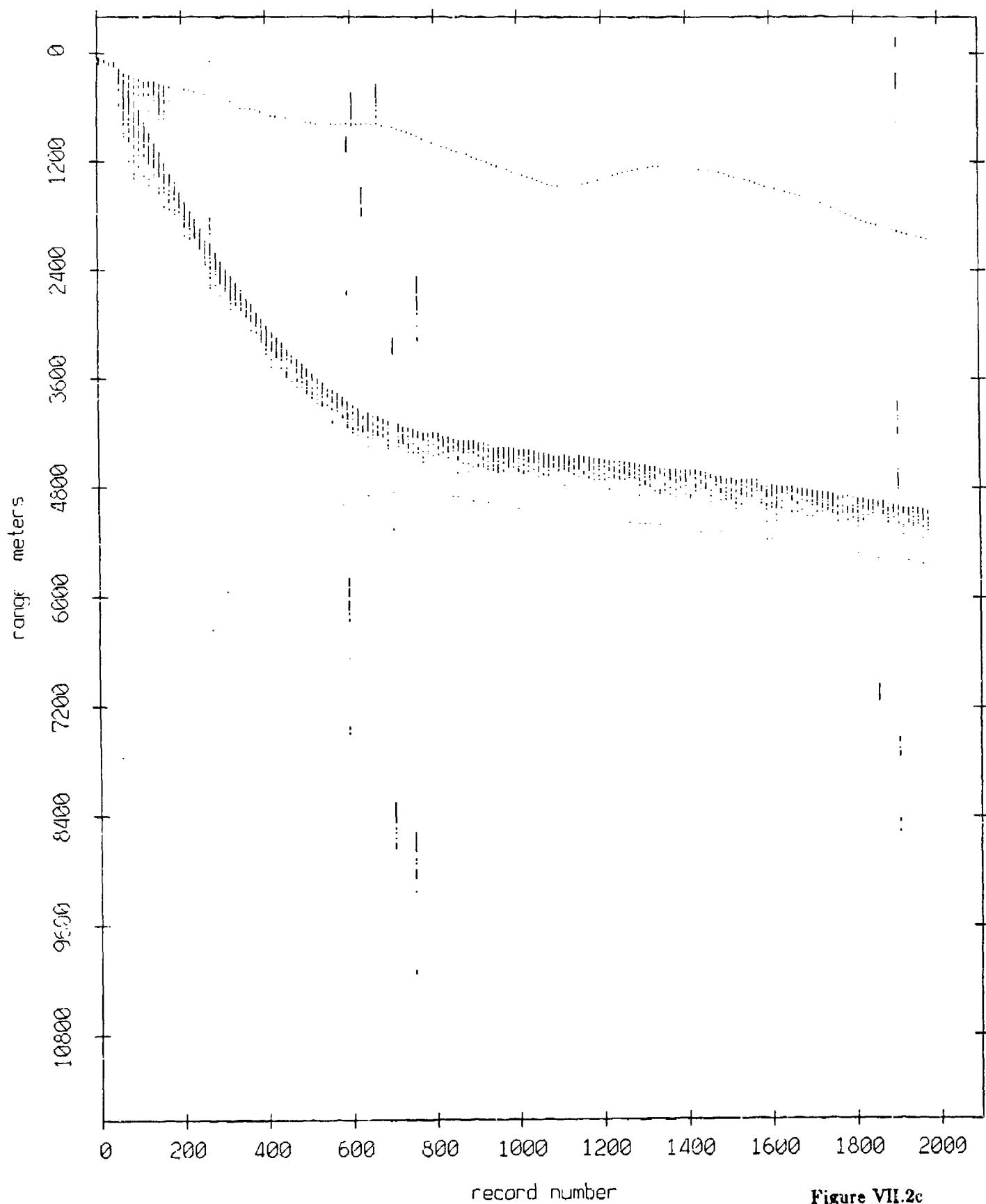


Figure VII.2c

Float 2, May, 1987 Sea Trip: range from float 4

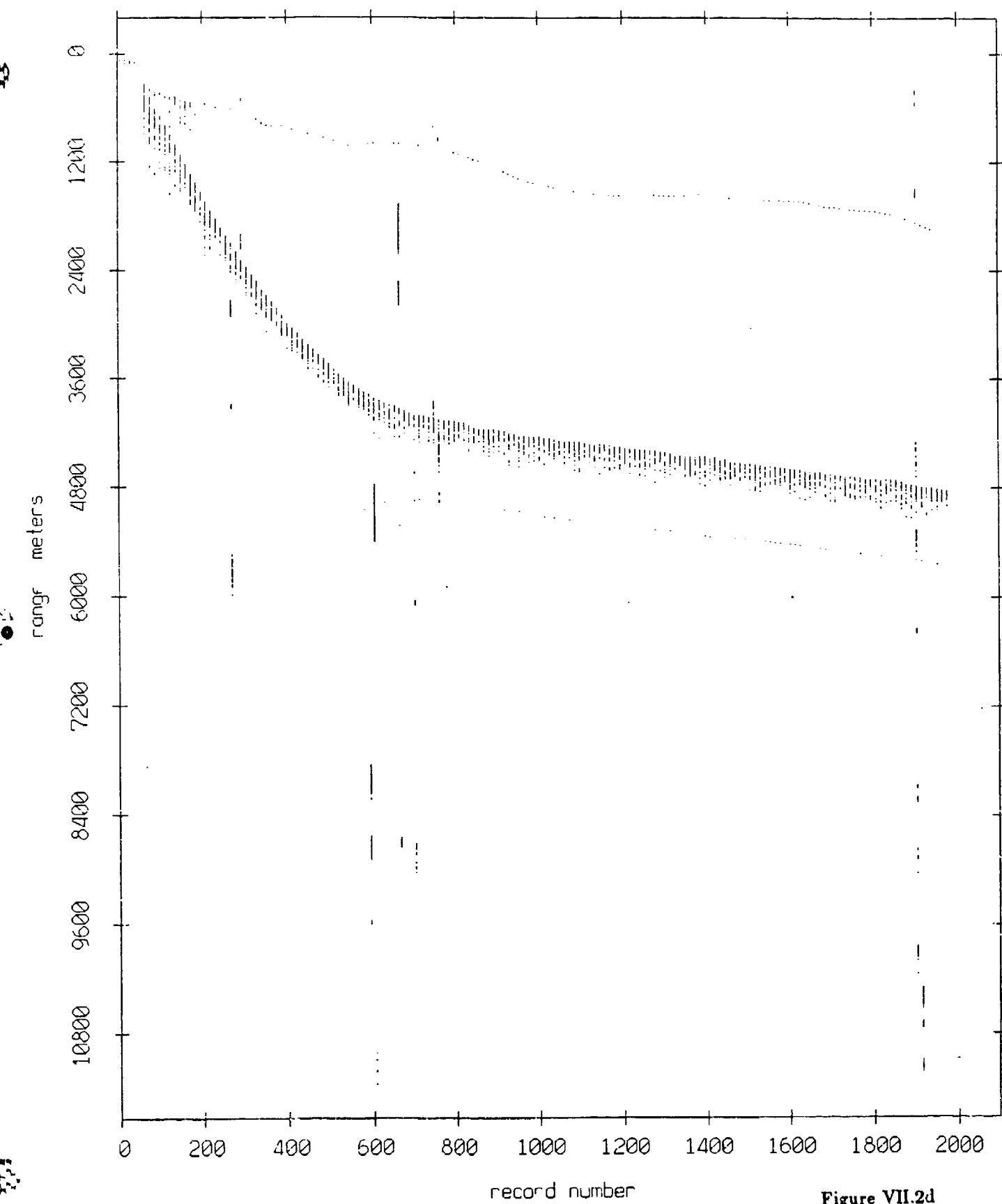


Figure VII.2d

Float 2, May, 1987 Sea Trip: range from float 7

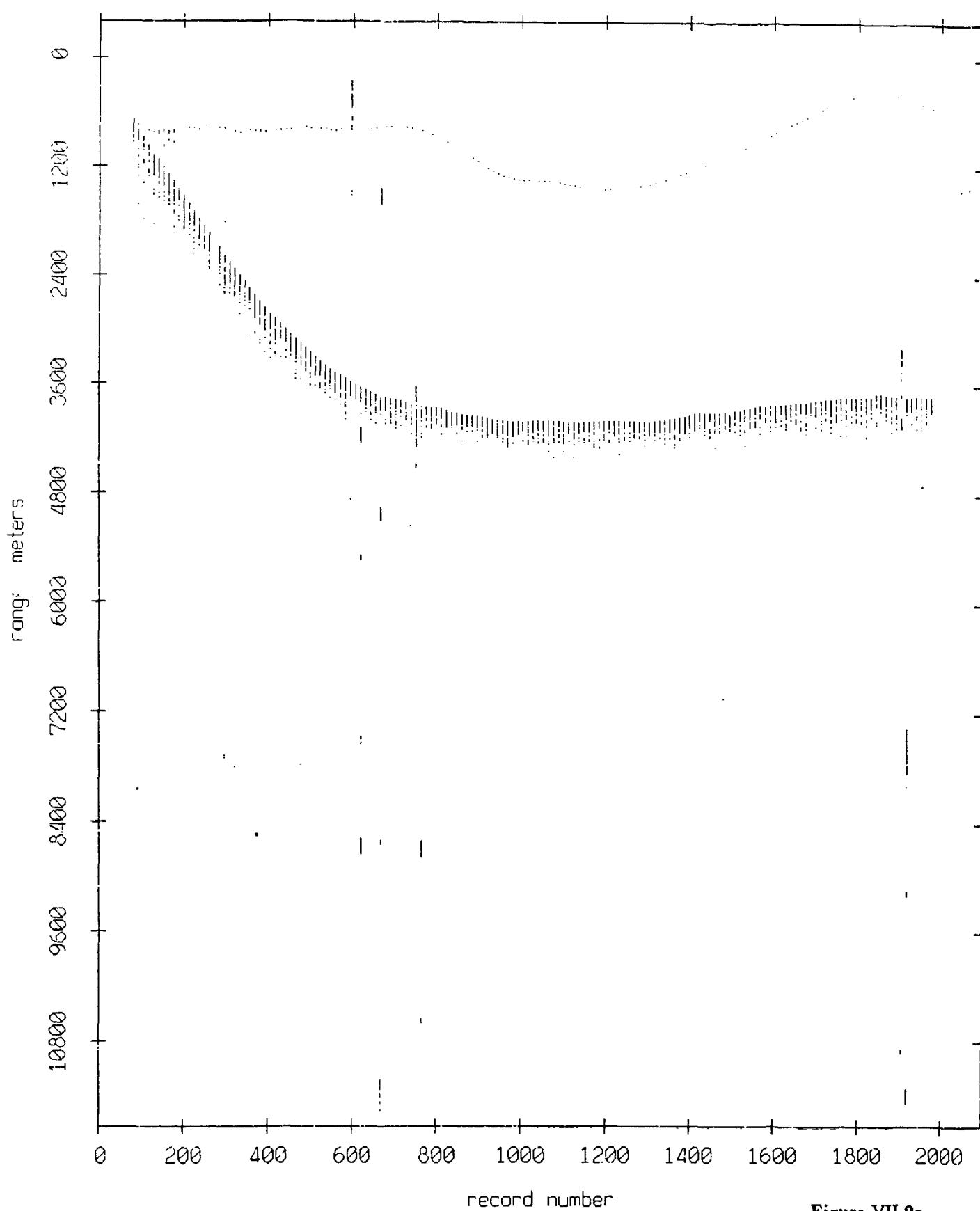


Figure VII.2e

Float 2, May, 1987 Sea Trip: range from float 3

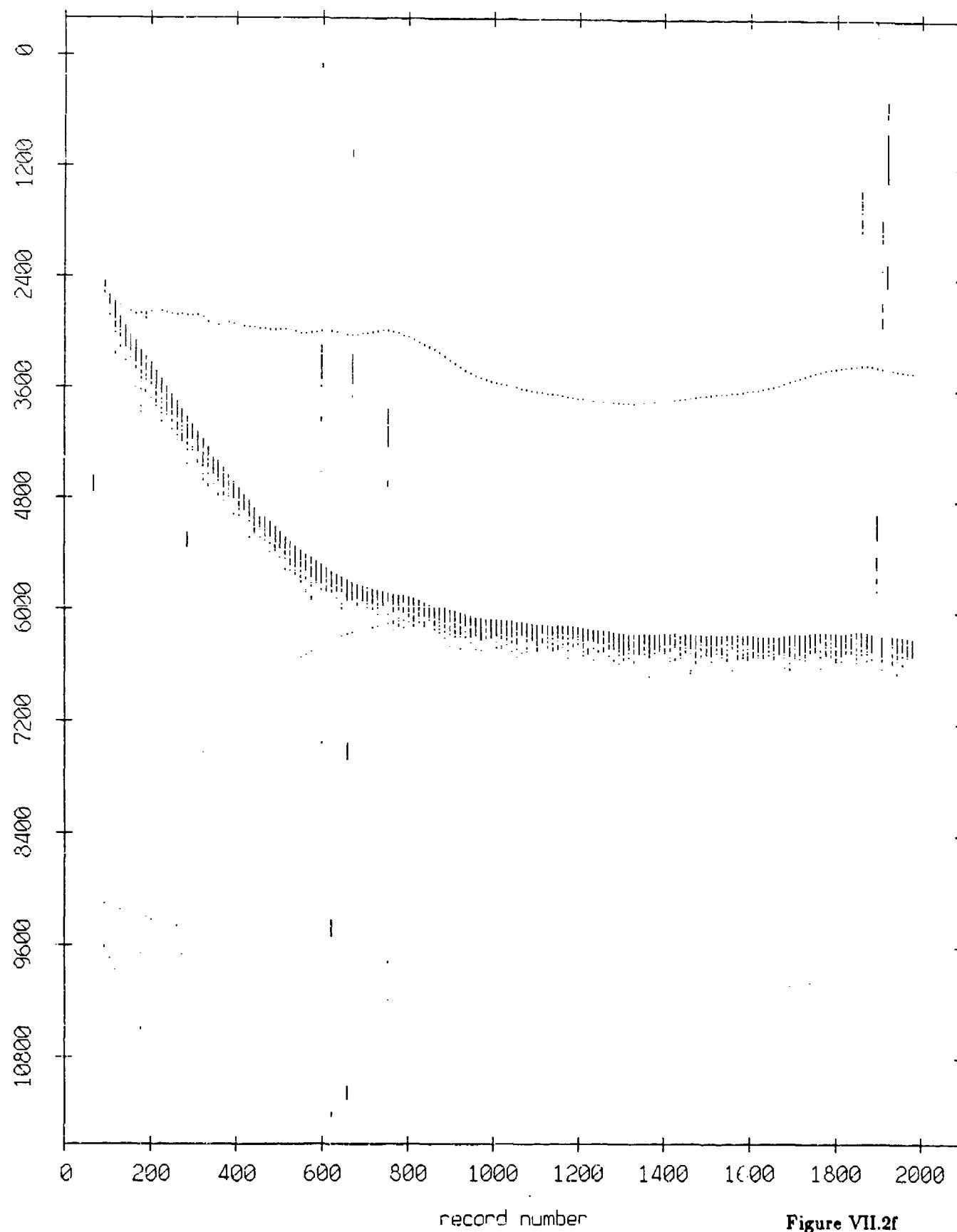


Figure VII.2f

Fleet 2, May, 1987 Sea Trip: range from float 9

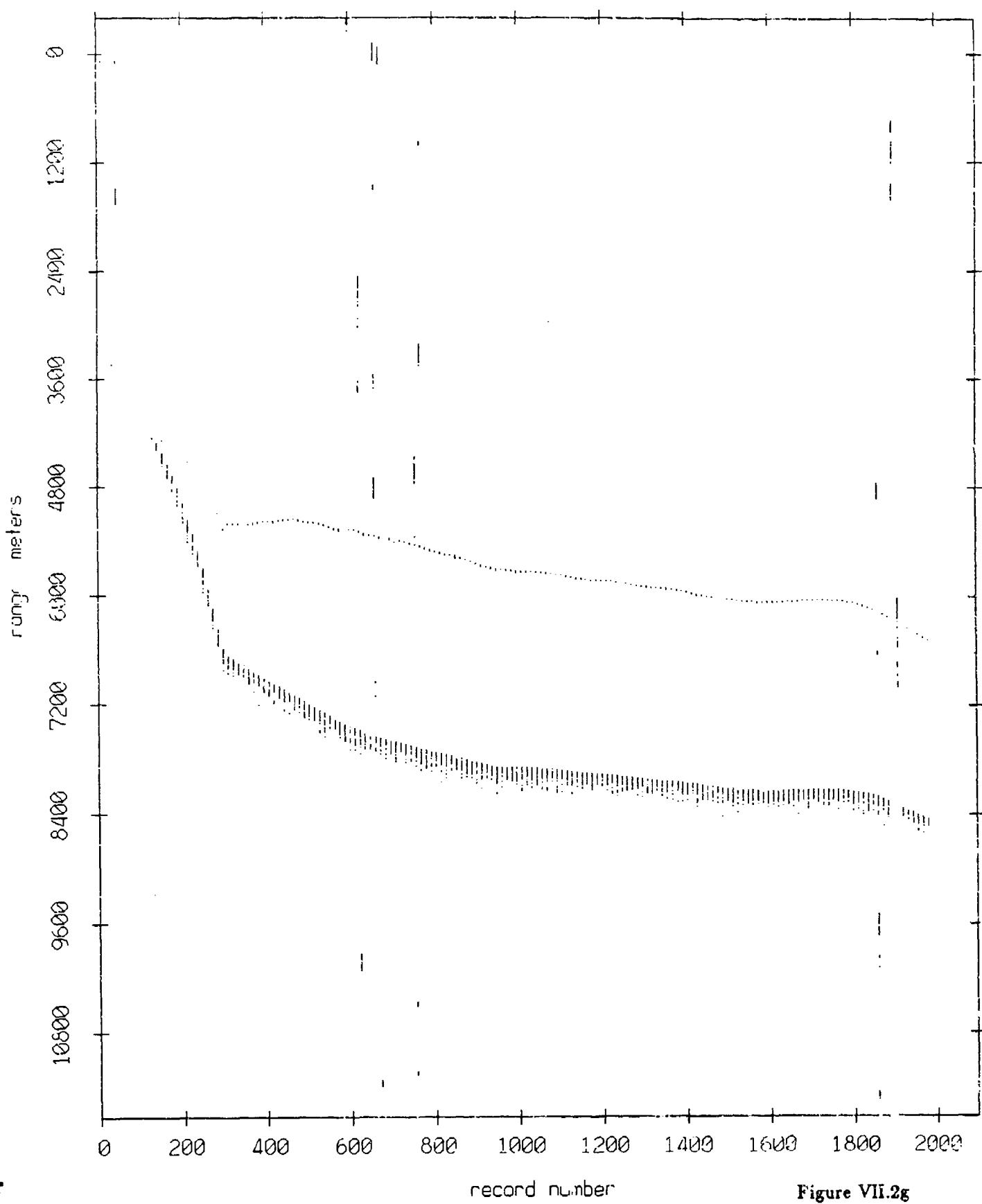


Figure VII.2g

Fleet 2, May, 1987 Sea Trip: range from fleet 10

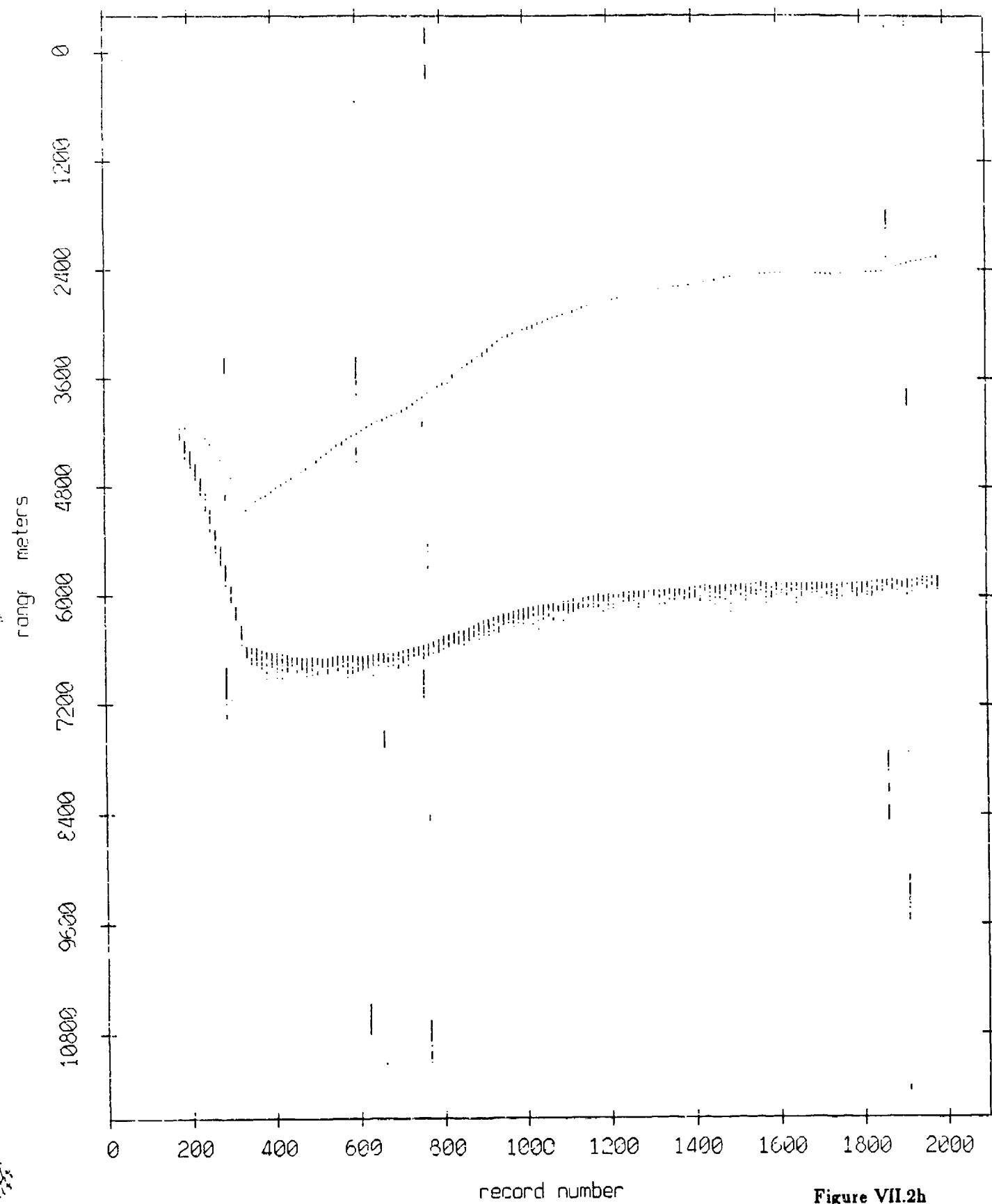


Figure VII.2h

Fleet 2, May, 1987 Sea Trip: range from float 11

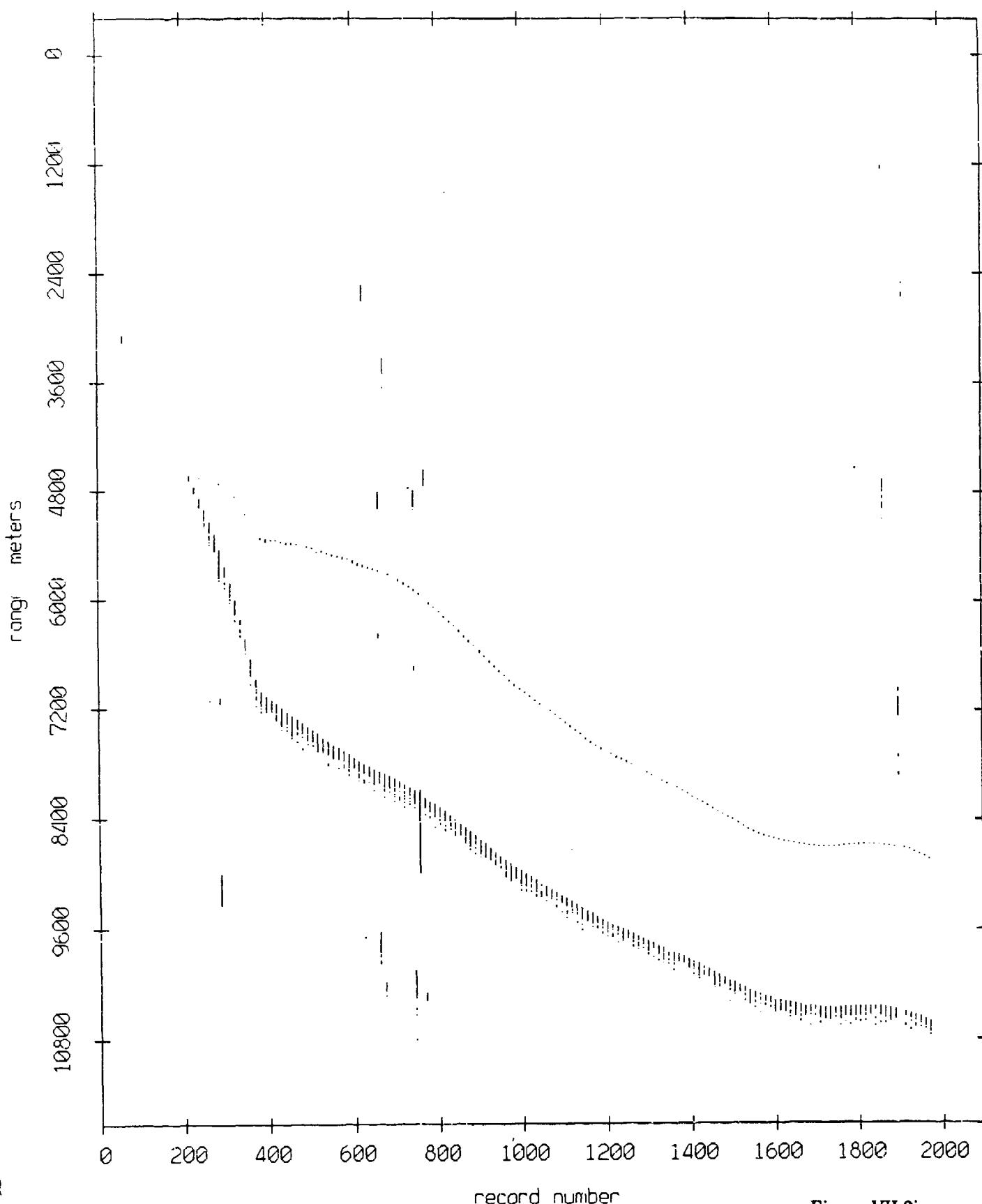


Figure VII.2i

Fleet 3, May, 1987 Sea Trip: range from float 0

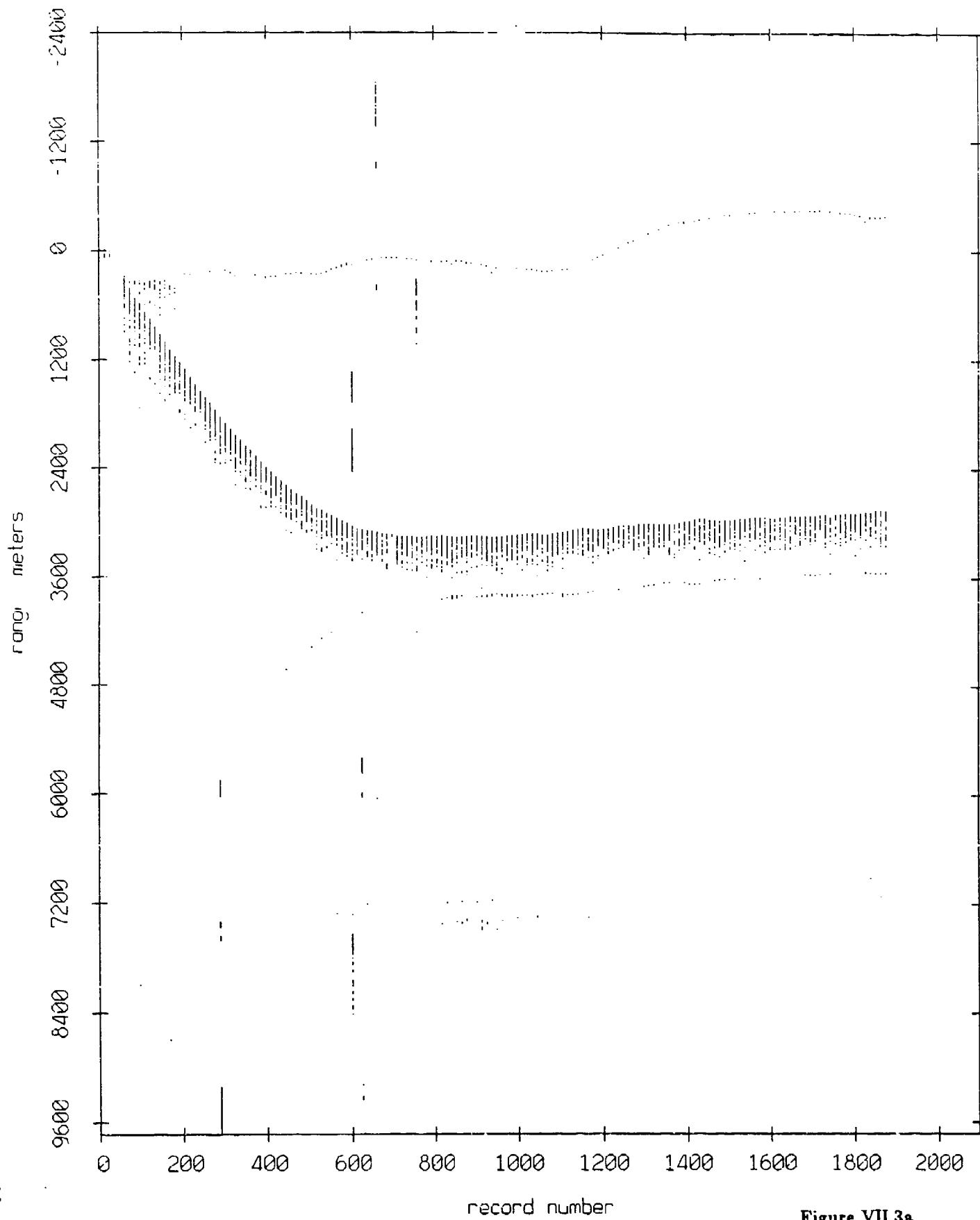


Figure VII.3a

Fleet 3, May, 1987 Sea Trip: range from float 1

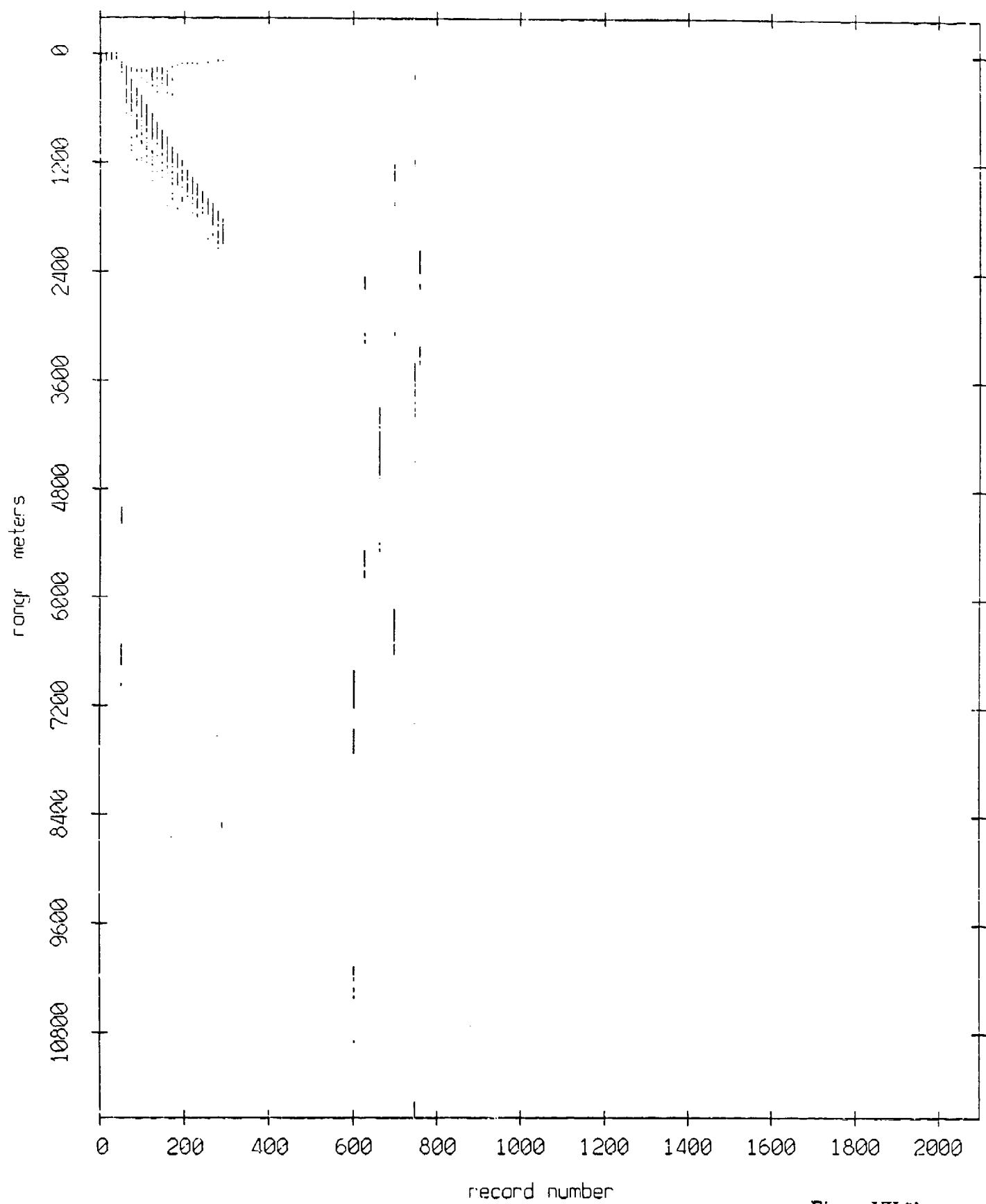


Figure VII.3b

Fleet 3, May, 1987 Sea Trip: range from float 2

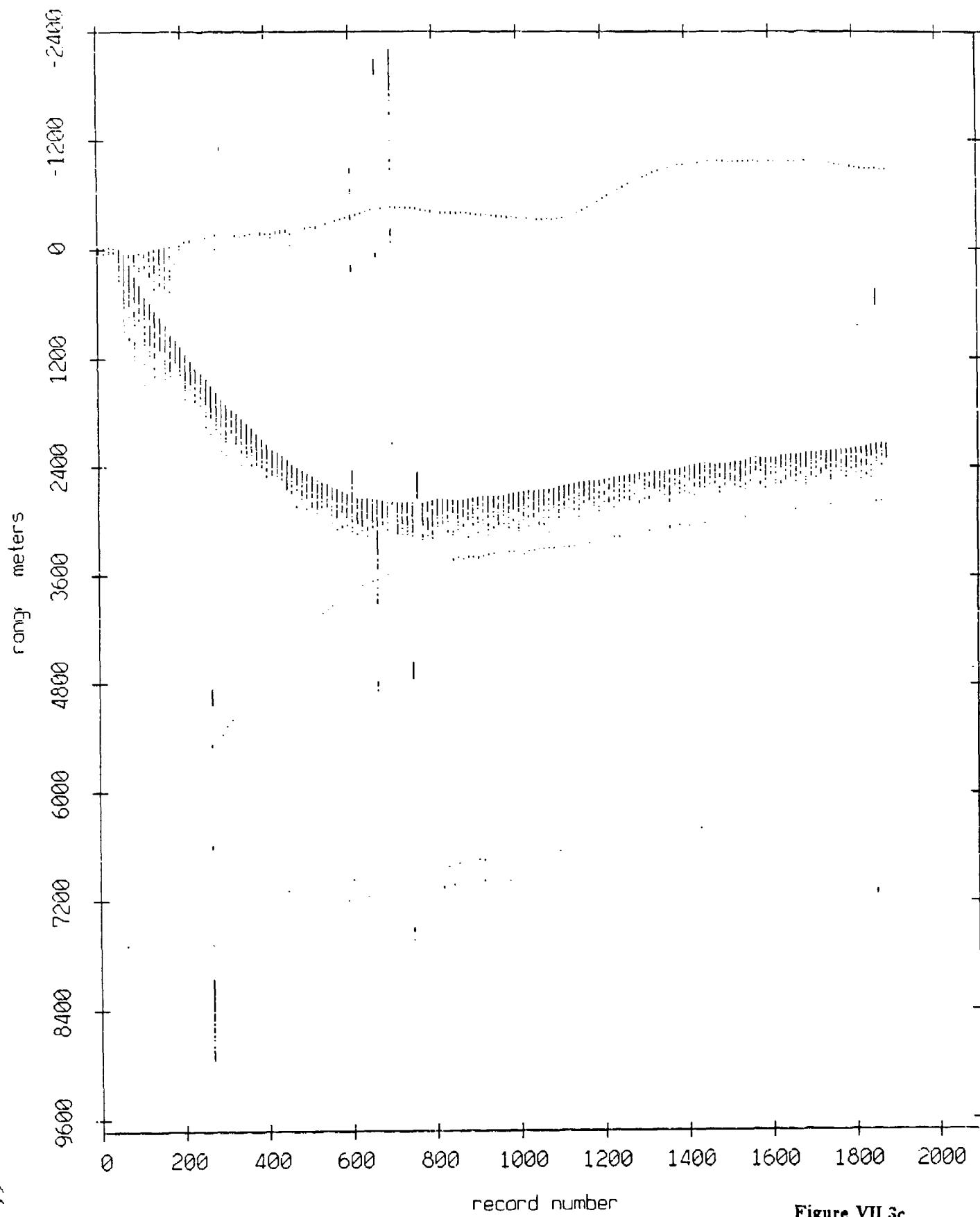


Figure VII.3c

Fleet 3, May, 1987 Sea Trip: range from float 4

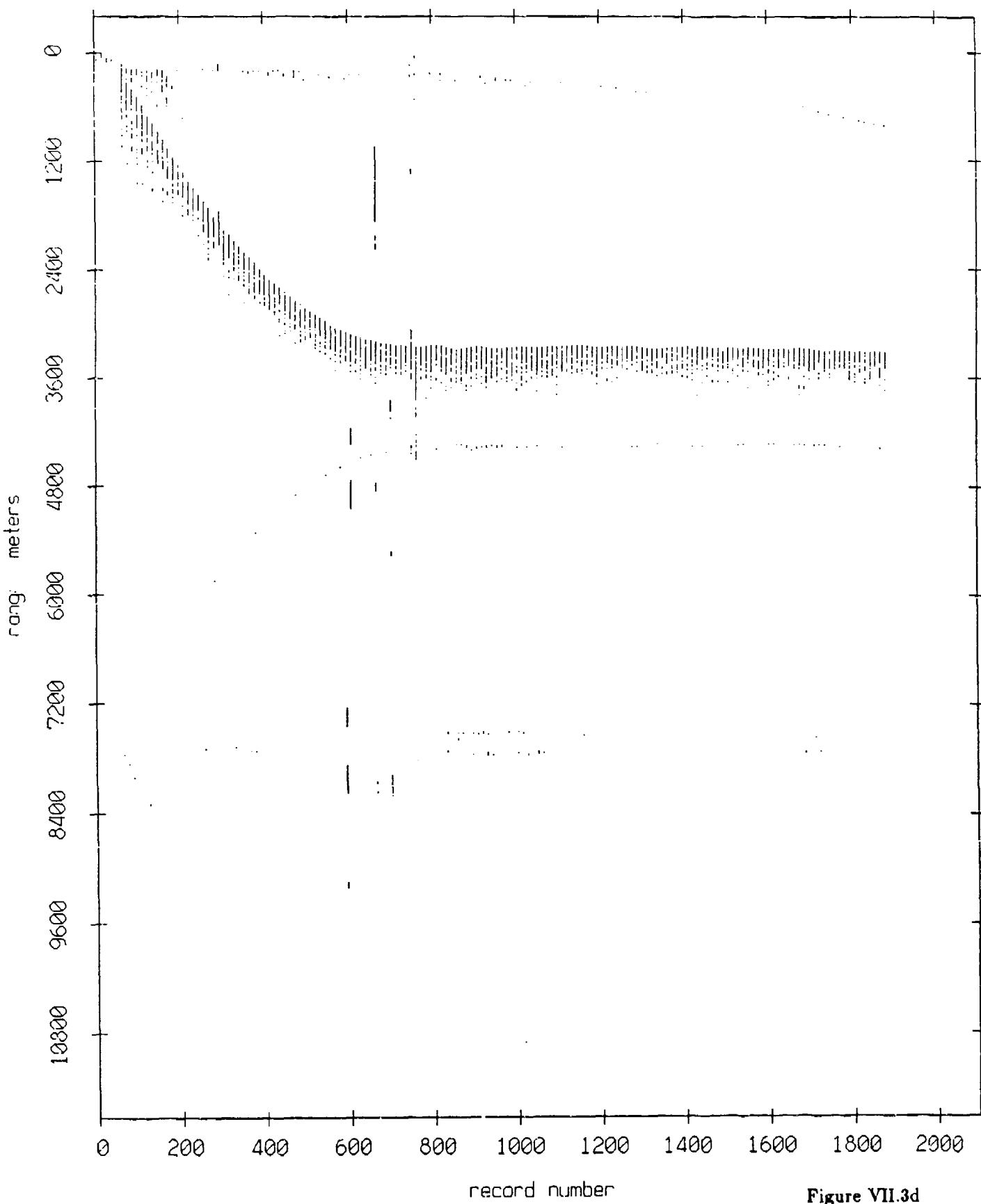


Figure VII.3d

Fleet 3, May, 1987 Sea Trip: range from float 7

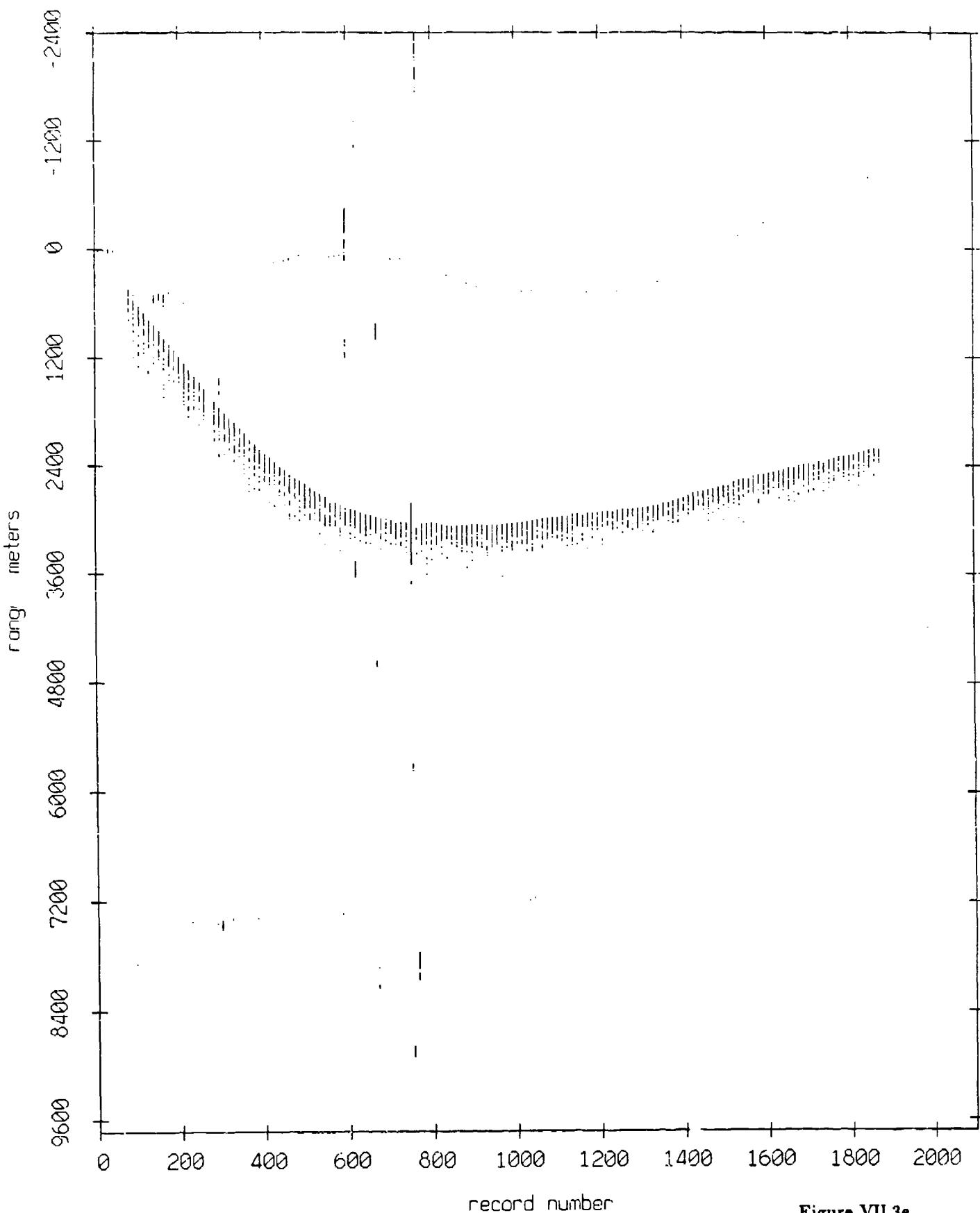


Figure VII.3e

Fleet 3, May, 1987 Sea Trip: range from float 8

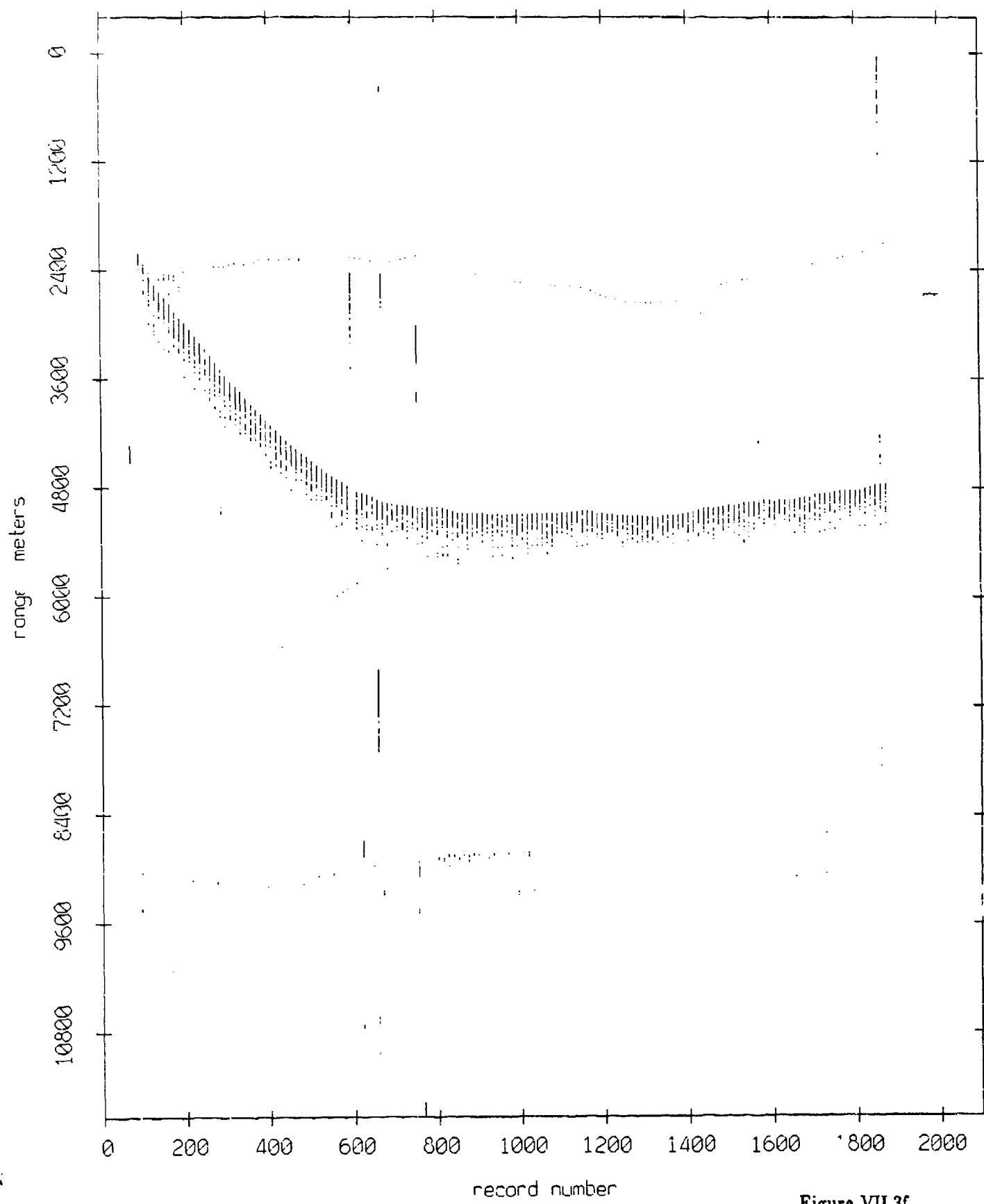


Figure VII.3f

Fleet 3, Mo., 1987 Sec Trip: range from float 9

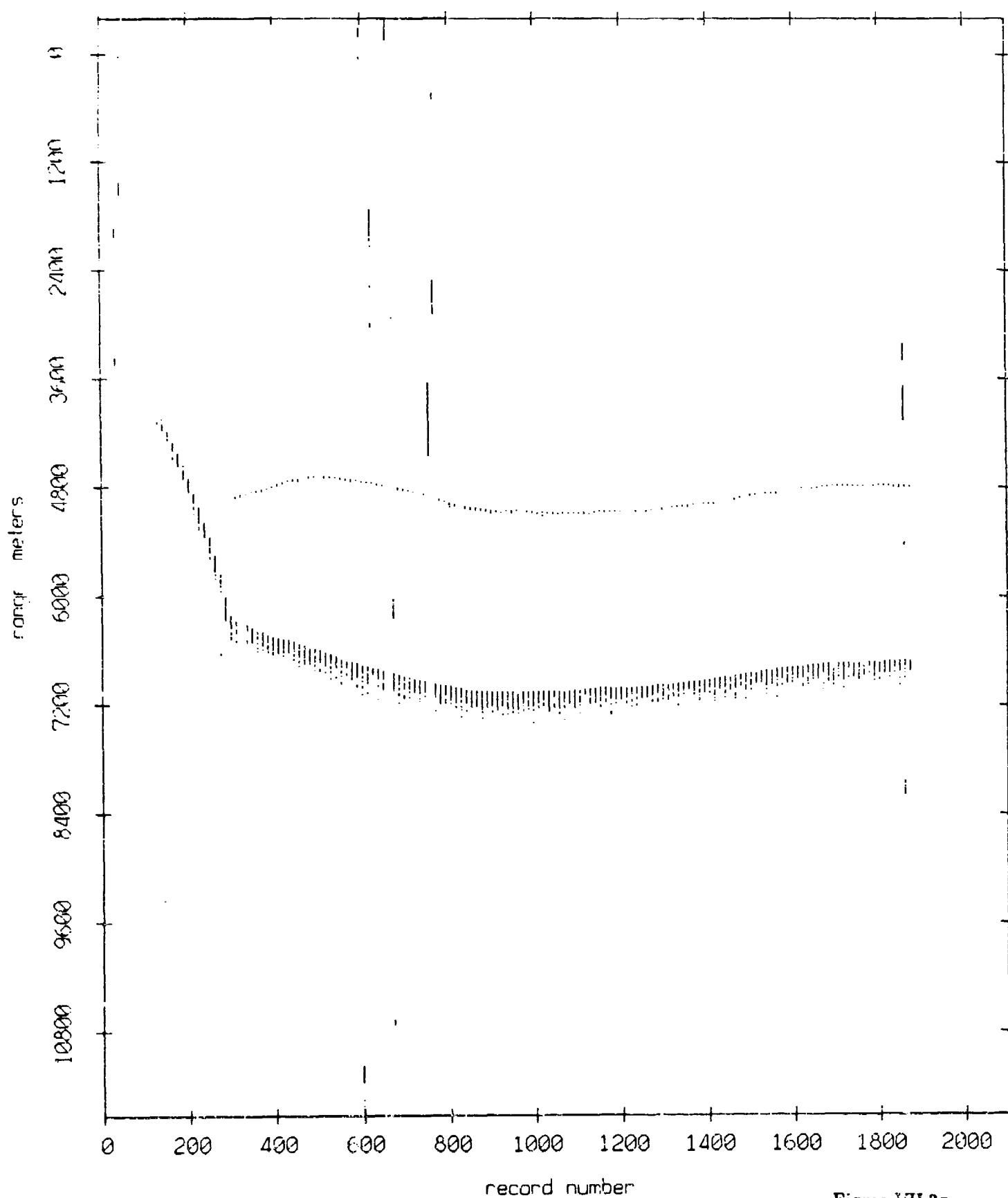


Figure VII.3g

Fleet 3, May, 1987 Sea Trip: range from float 10

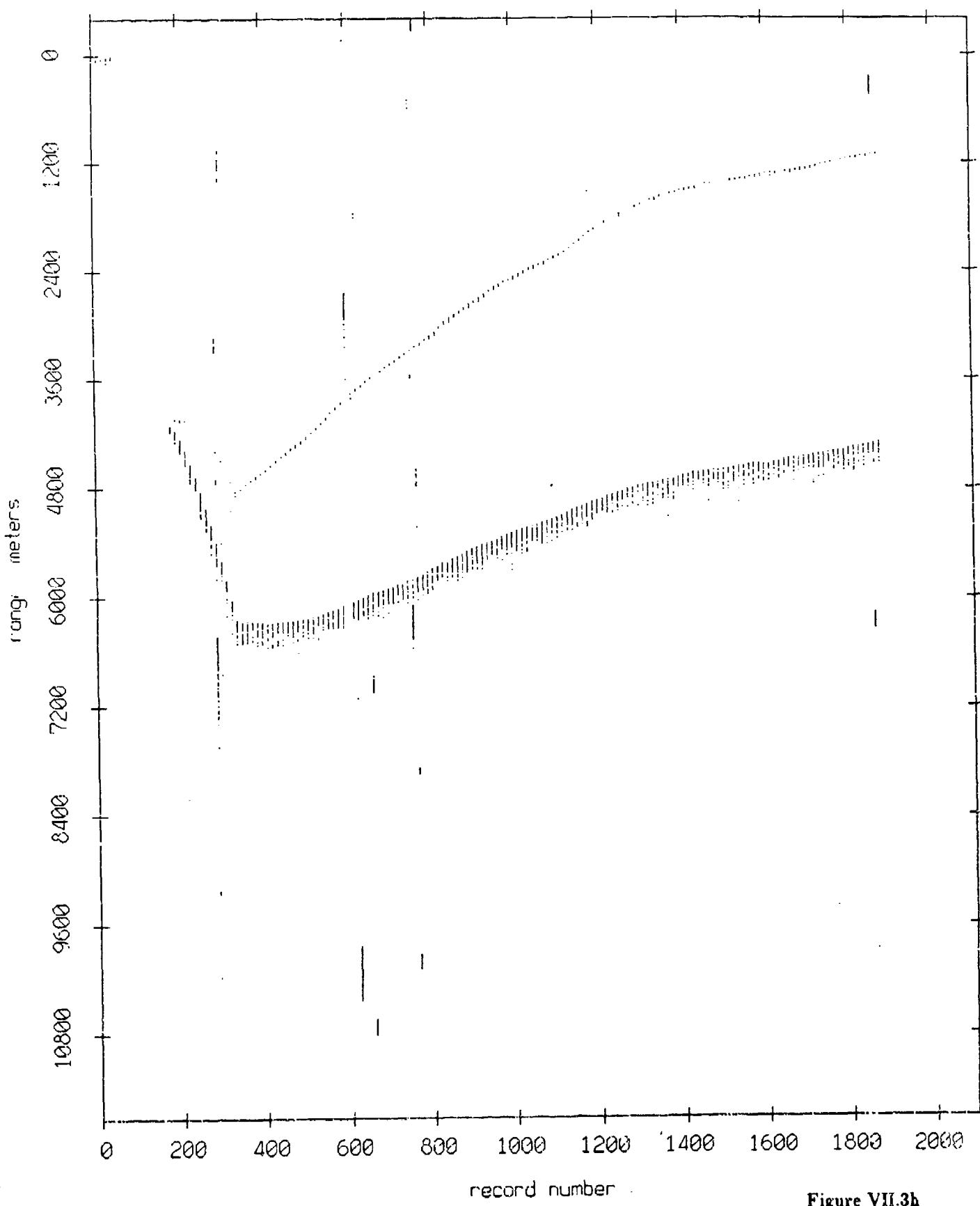


Figure VII.3h

Fleet 3, May, 1987 Sea Trip: range from float 11

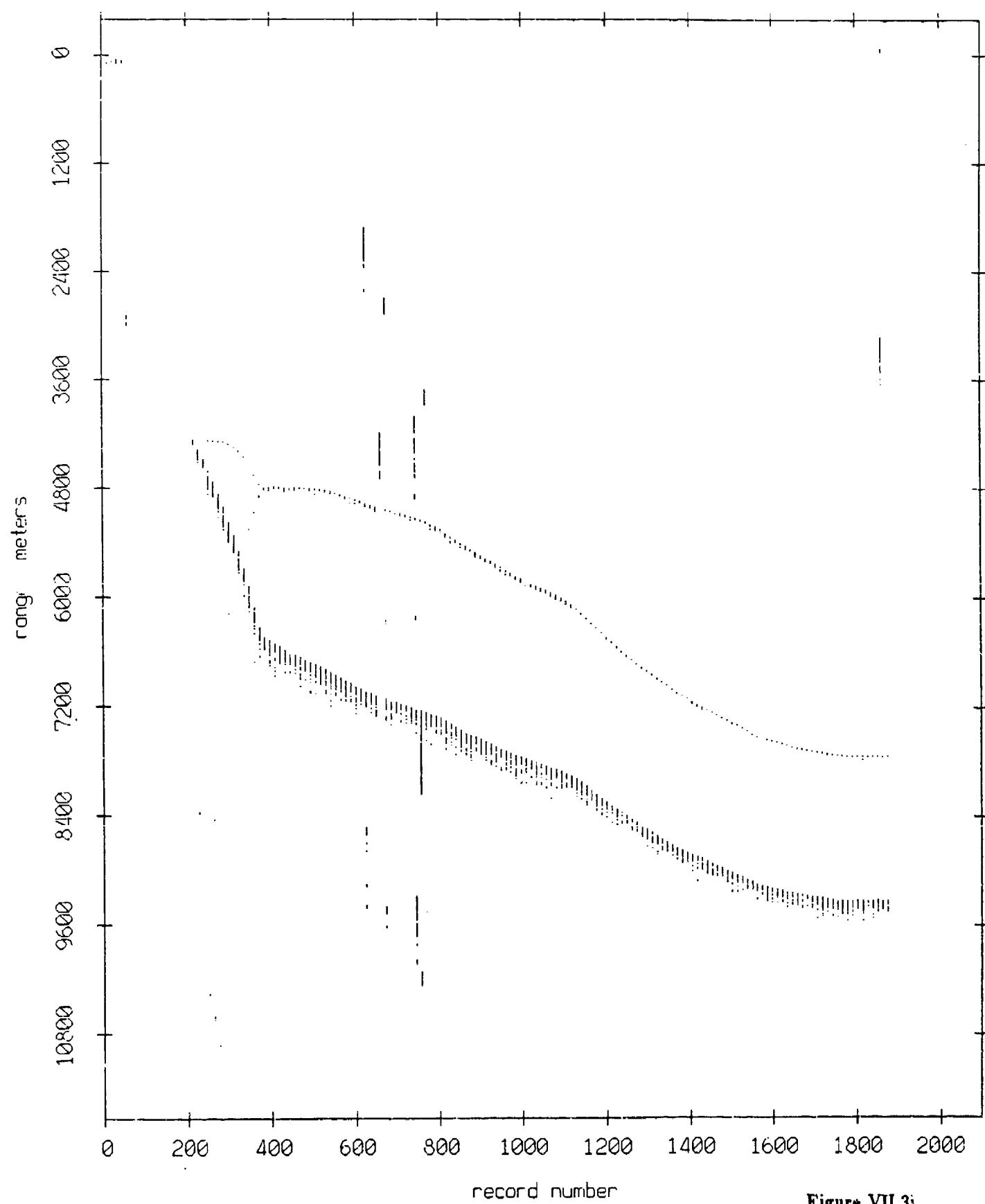


Figure VII.3i

Fleet 4, May, 1987 Sea Trip: range from float 0

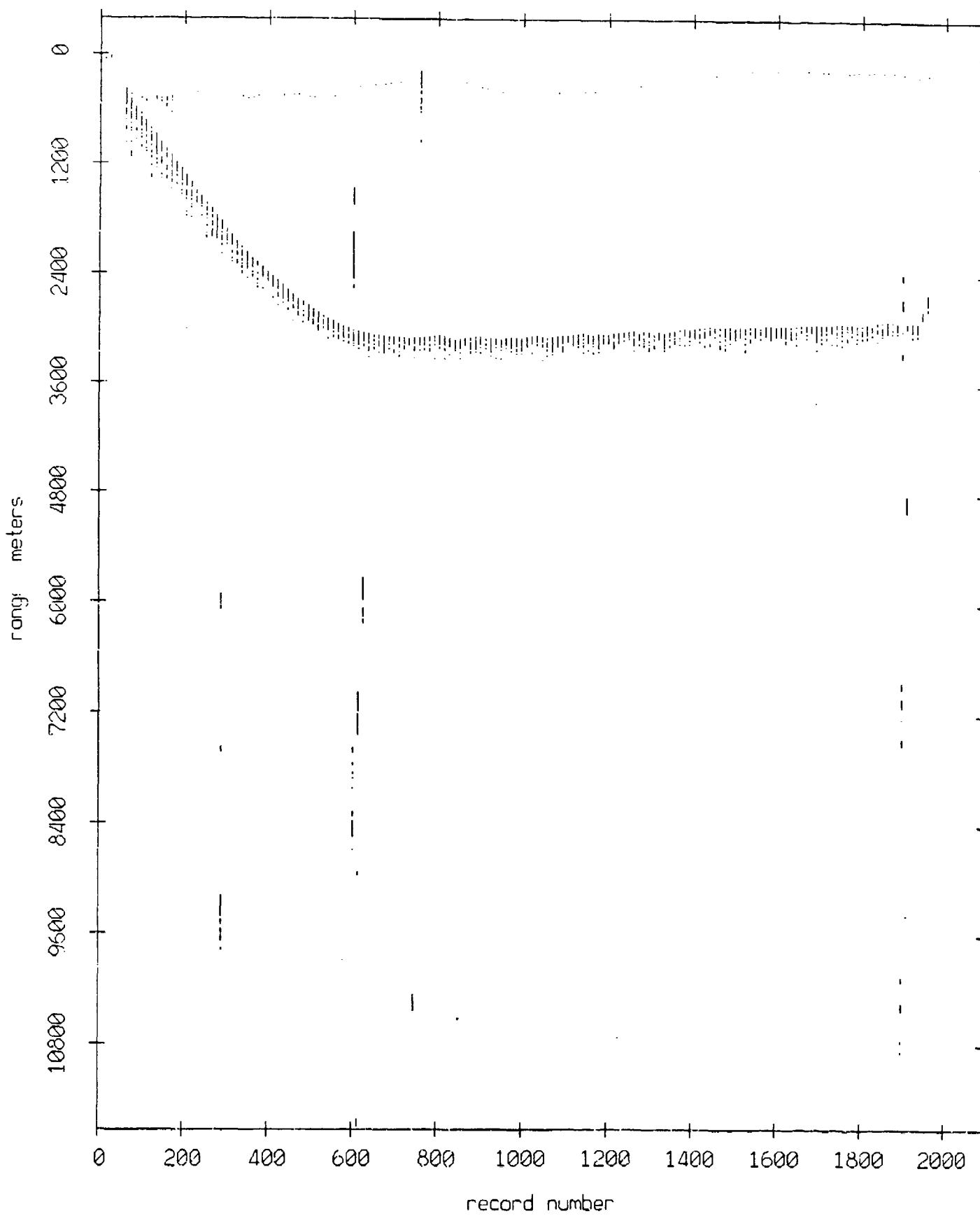


Figure VII.4a

Float 4, May, 1987 Sea Trip: range from float 1

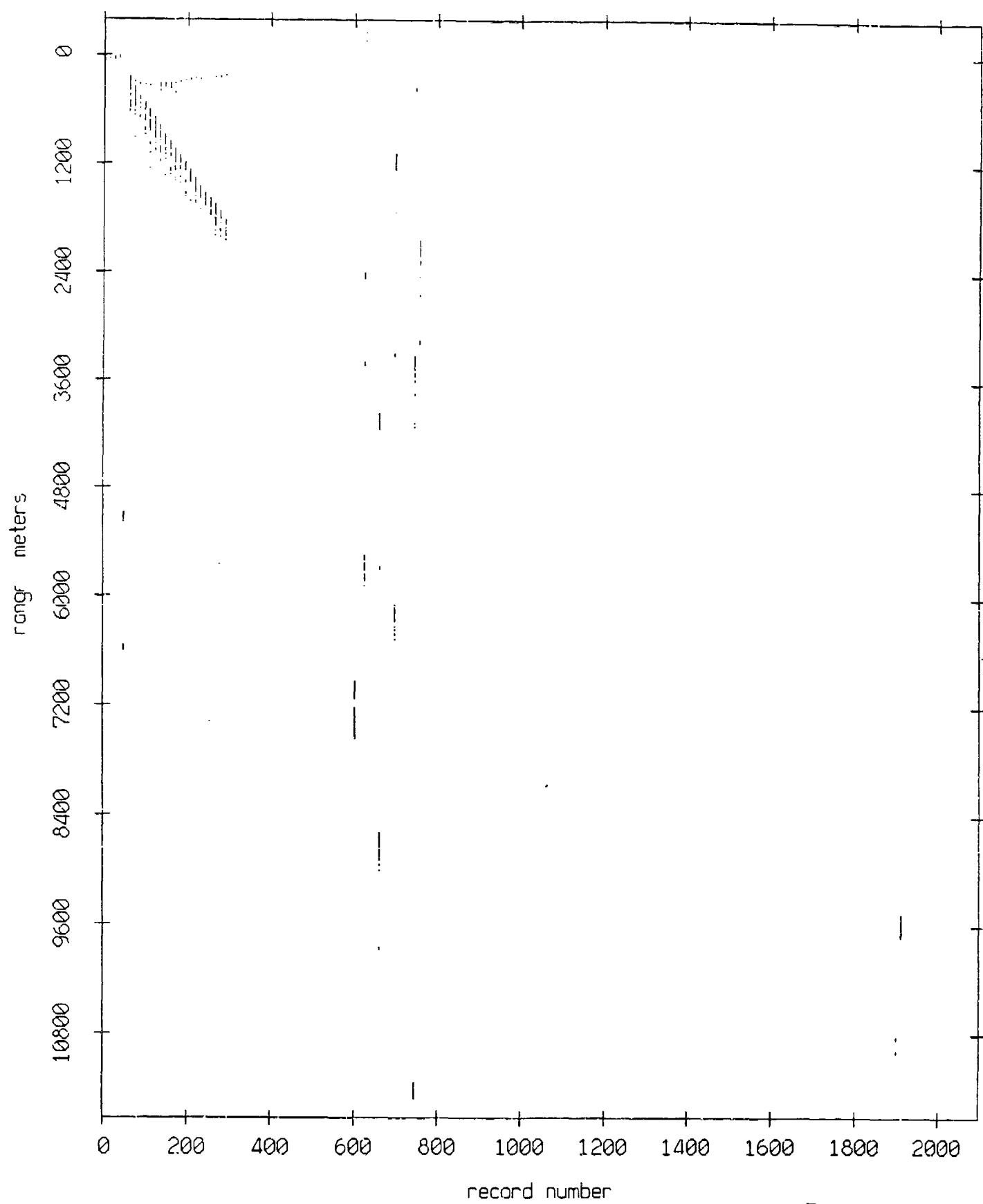


Figure VII.4b

Fleet 4, May, 1987 Sea T-rip: range from float 2

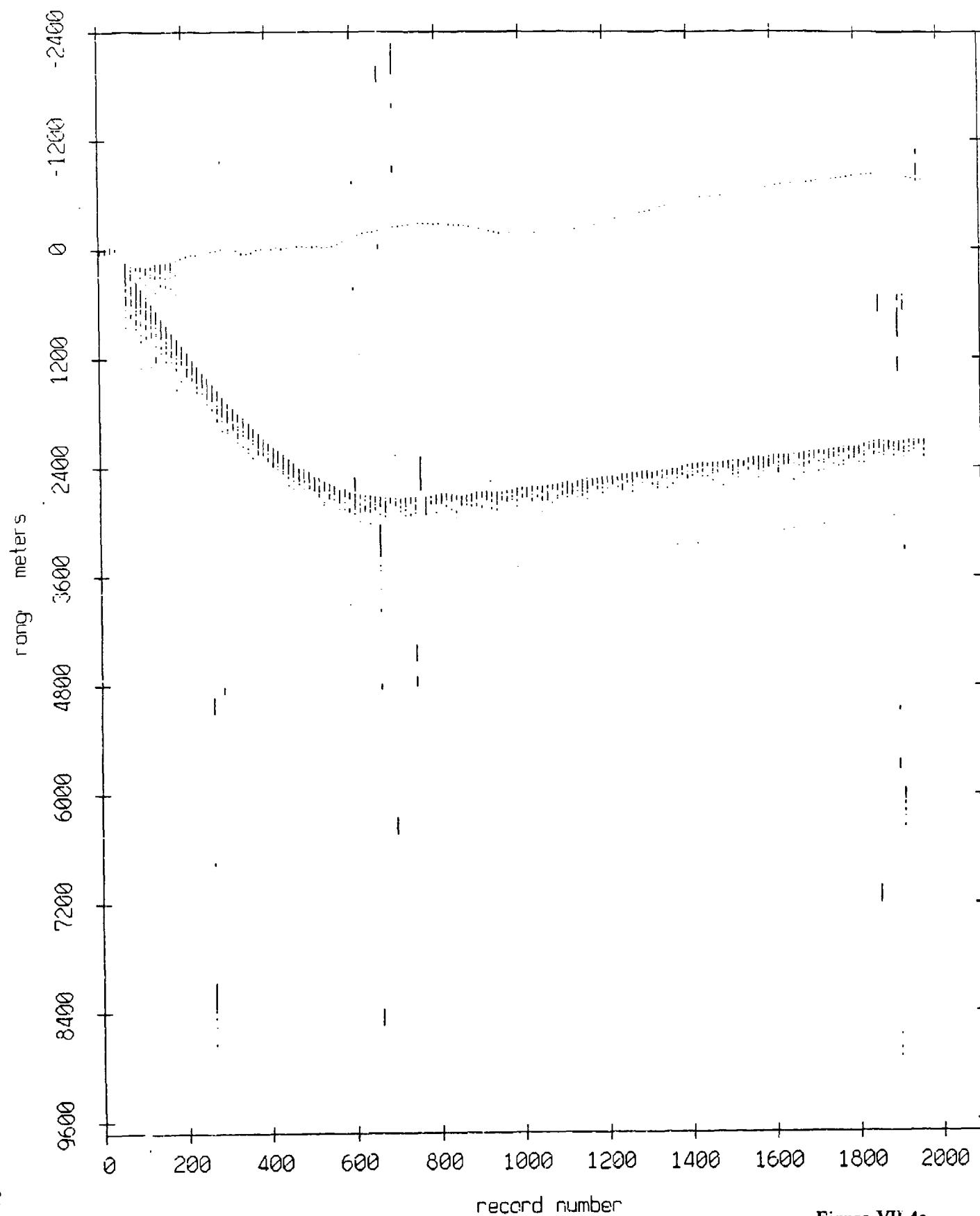


Figure VII.4c

Fleet 4, May, 1987 Sea Trip: range from float 3

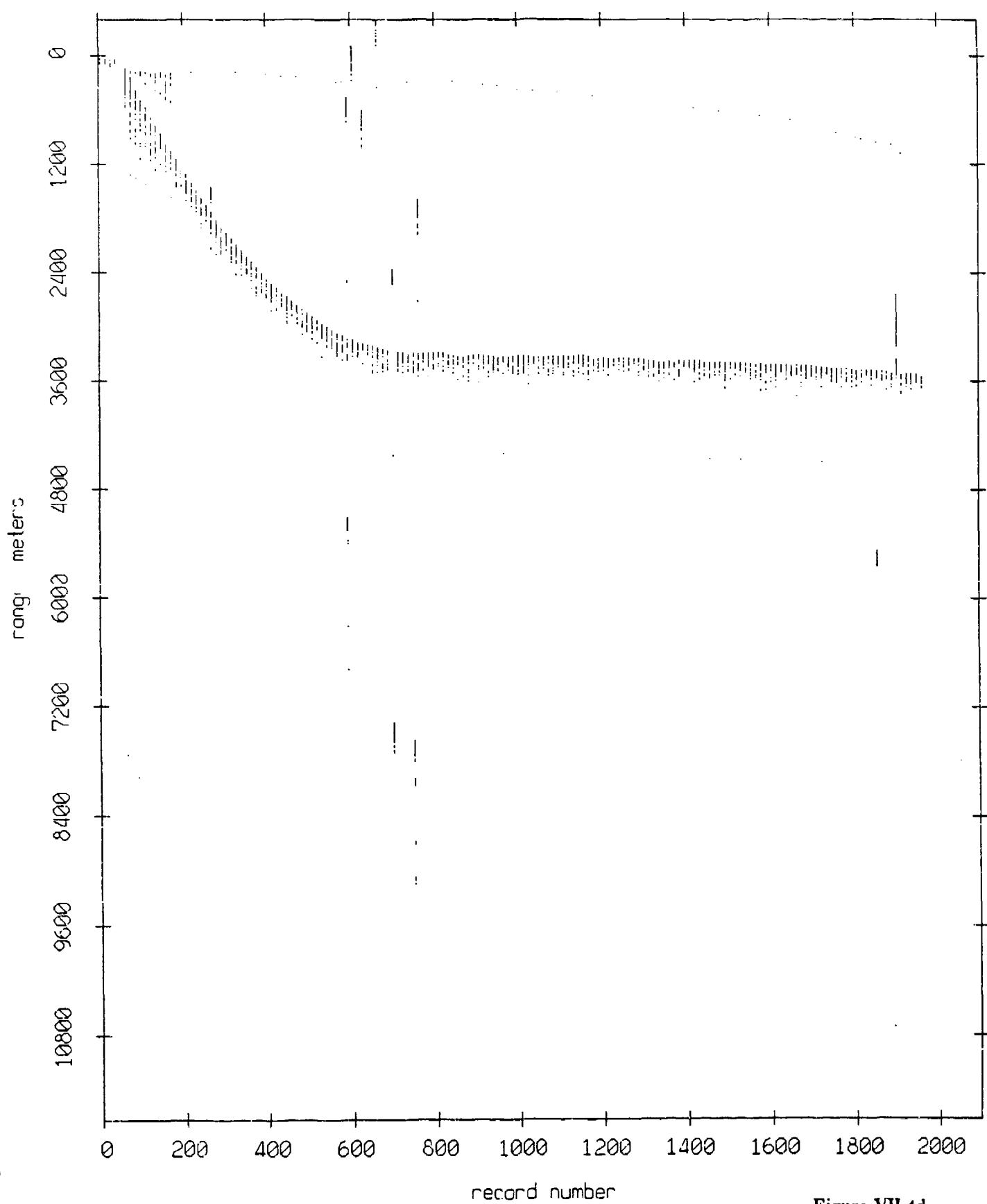


Figure VII.4d

Fleet 4, May, 1987 Sea Trip: range from float 7

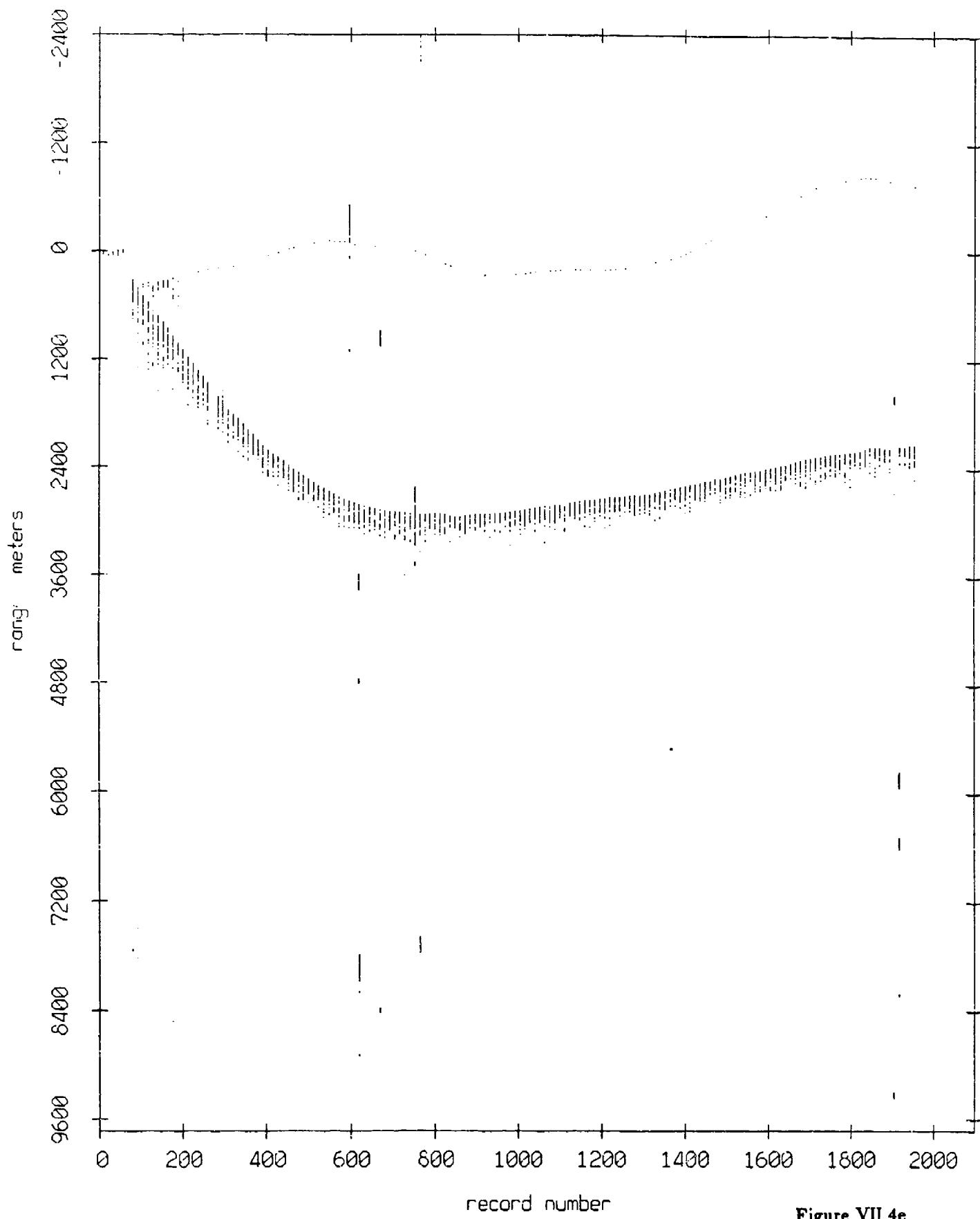


Figure VII.4e

Fleet 4, May, 1987 Sea Trip: range from Fleet 3

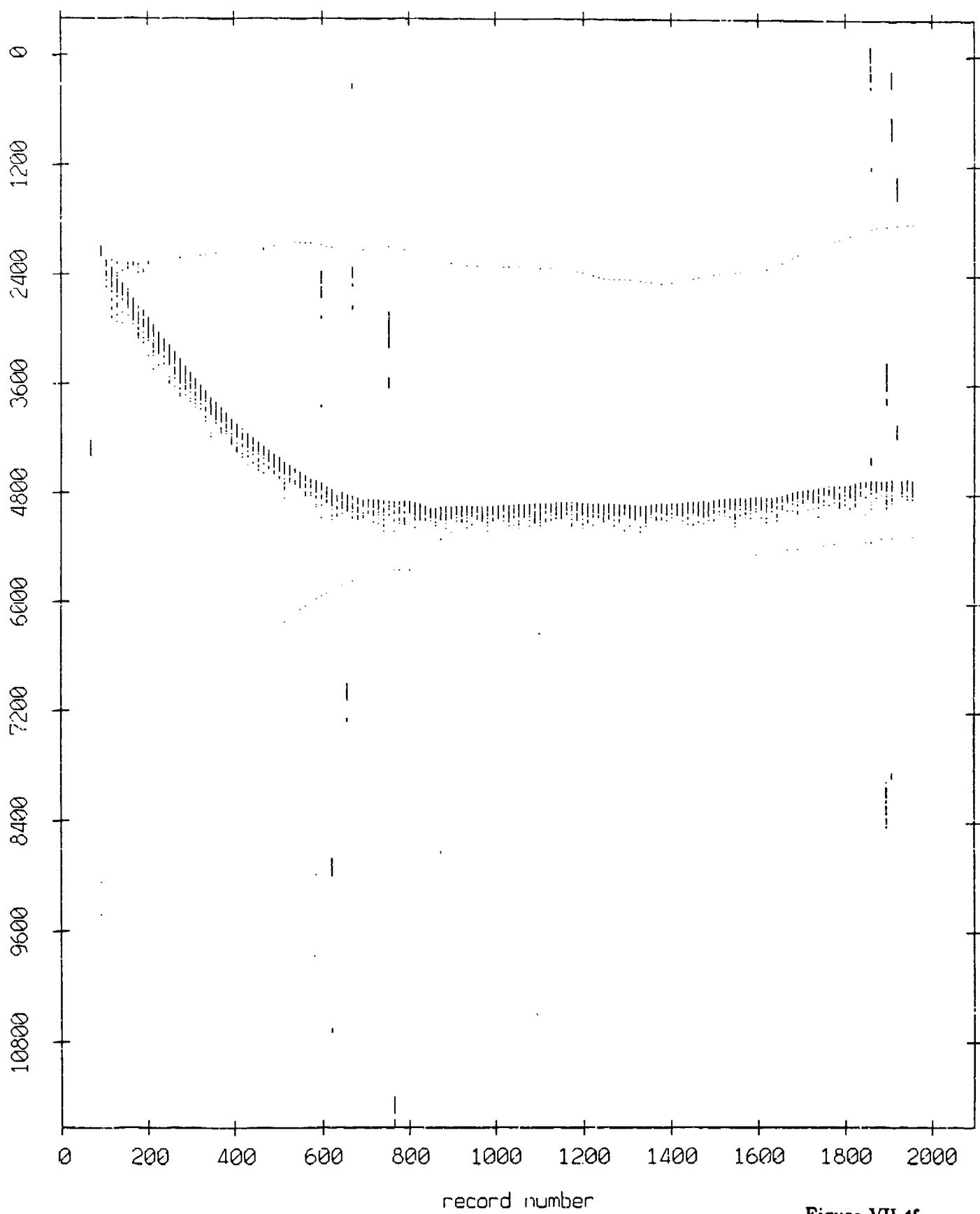


Figure VII.4f

Fleet 4, May, 1987 Sea Trip: range from float 9

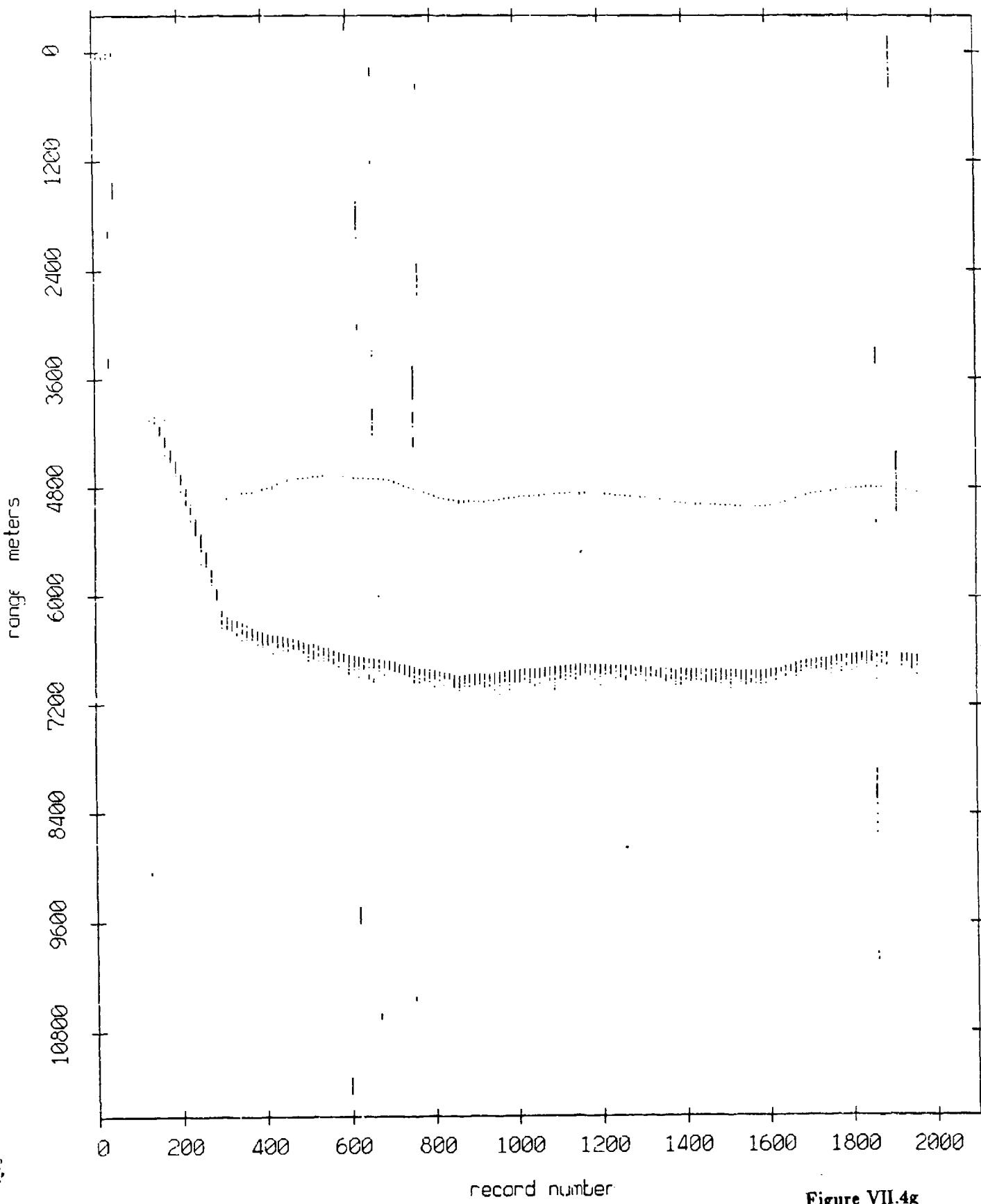


Figure VII.4g

Float 4, May, 1987 Sea Trip: range from float 10

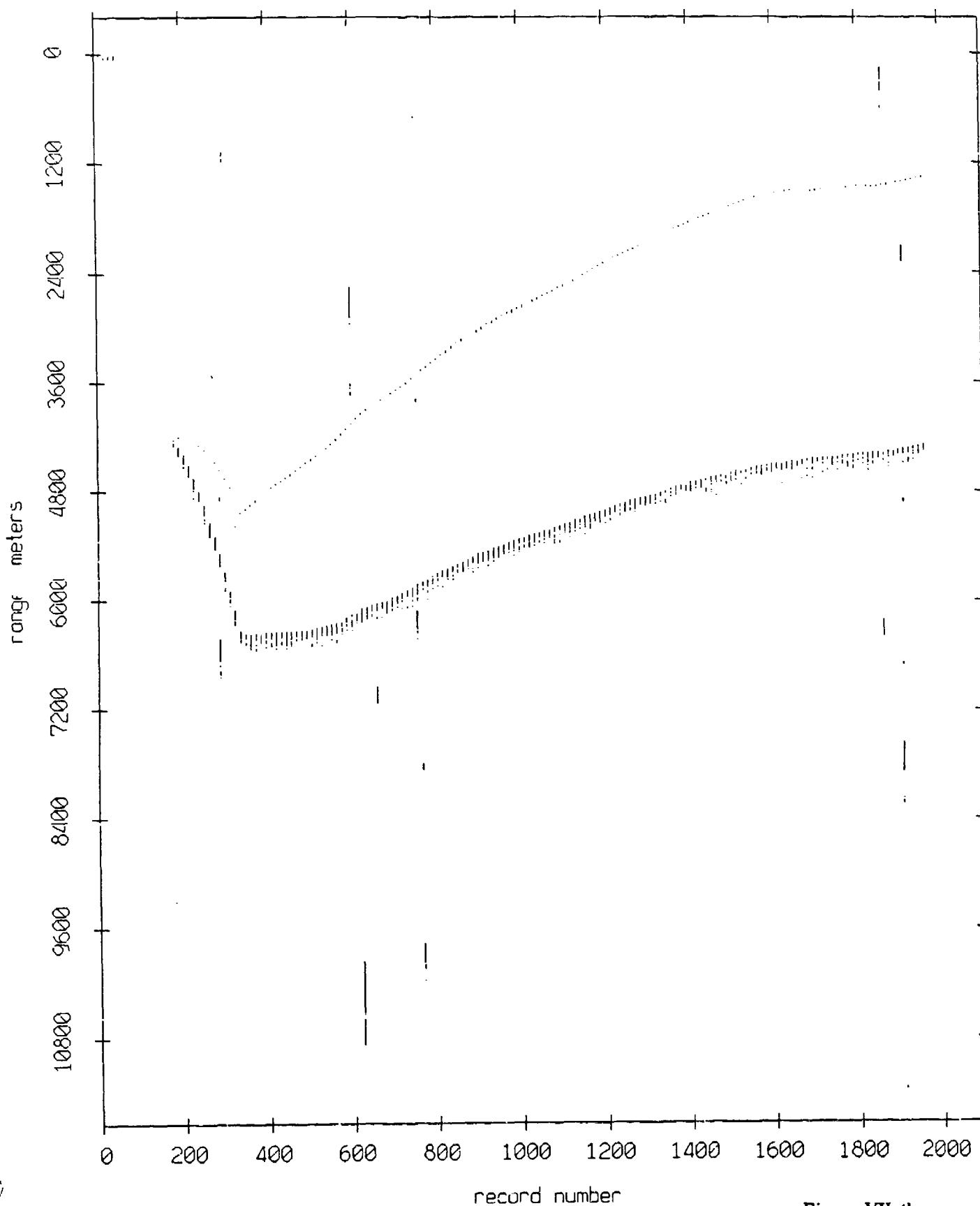


Figure VII.4h

Fleet 4, May, 1987 Sea Trip: range from float 11

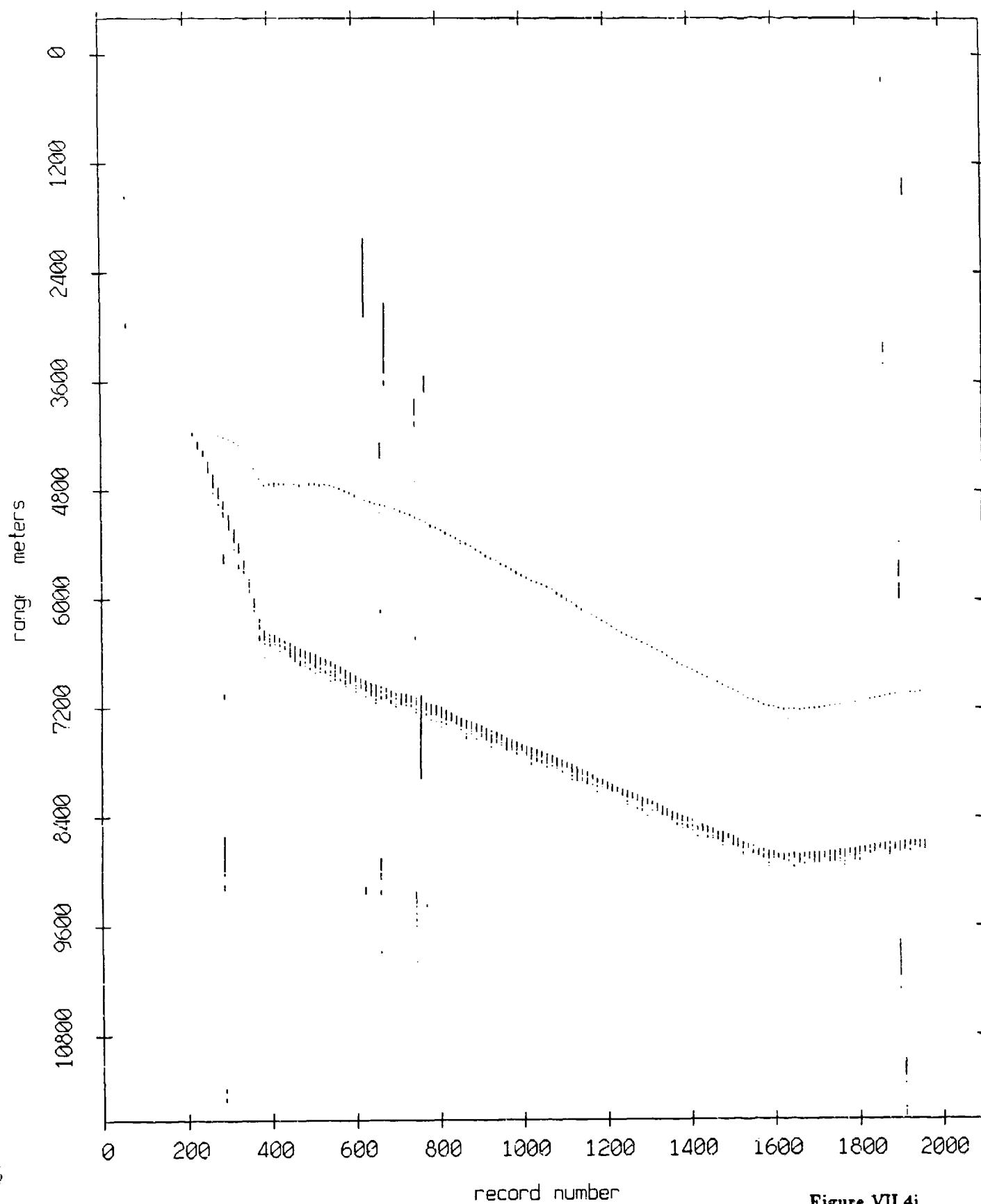


Figure VII.4i

Fleet 7, May, 1957 Sea Trip: range from fleet 6

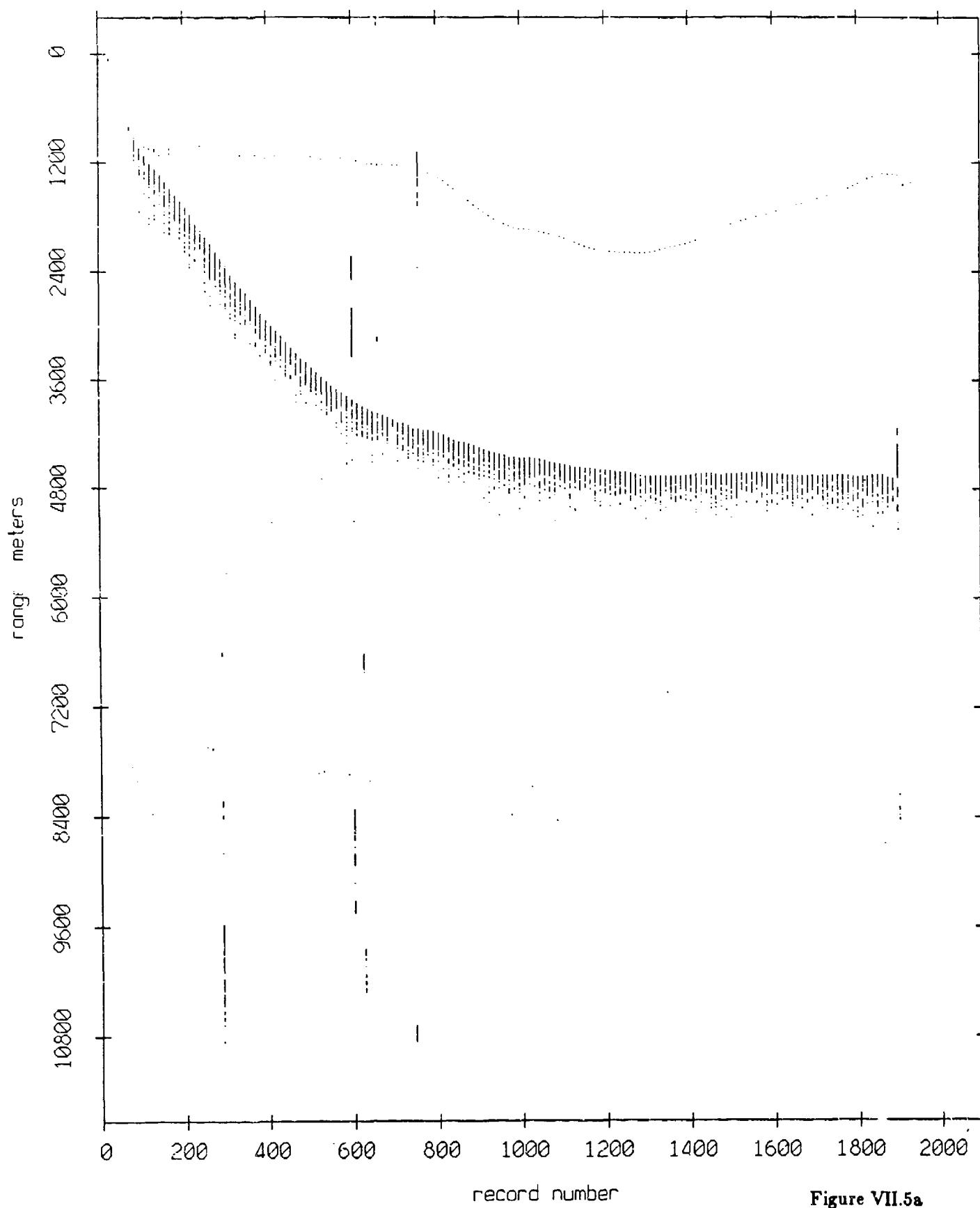


Figure VII.5a

Fleet 7, May, 1987 Sea Trip: range from float 1

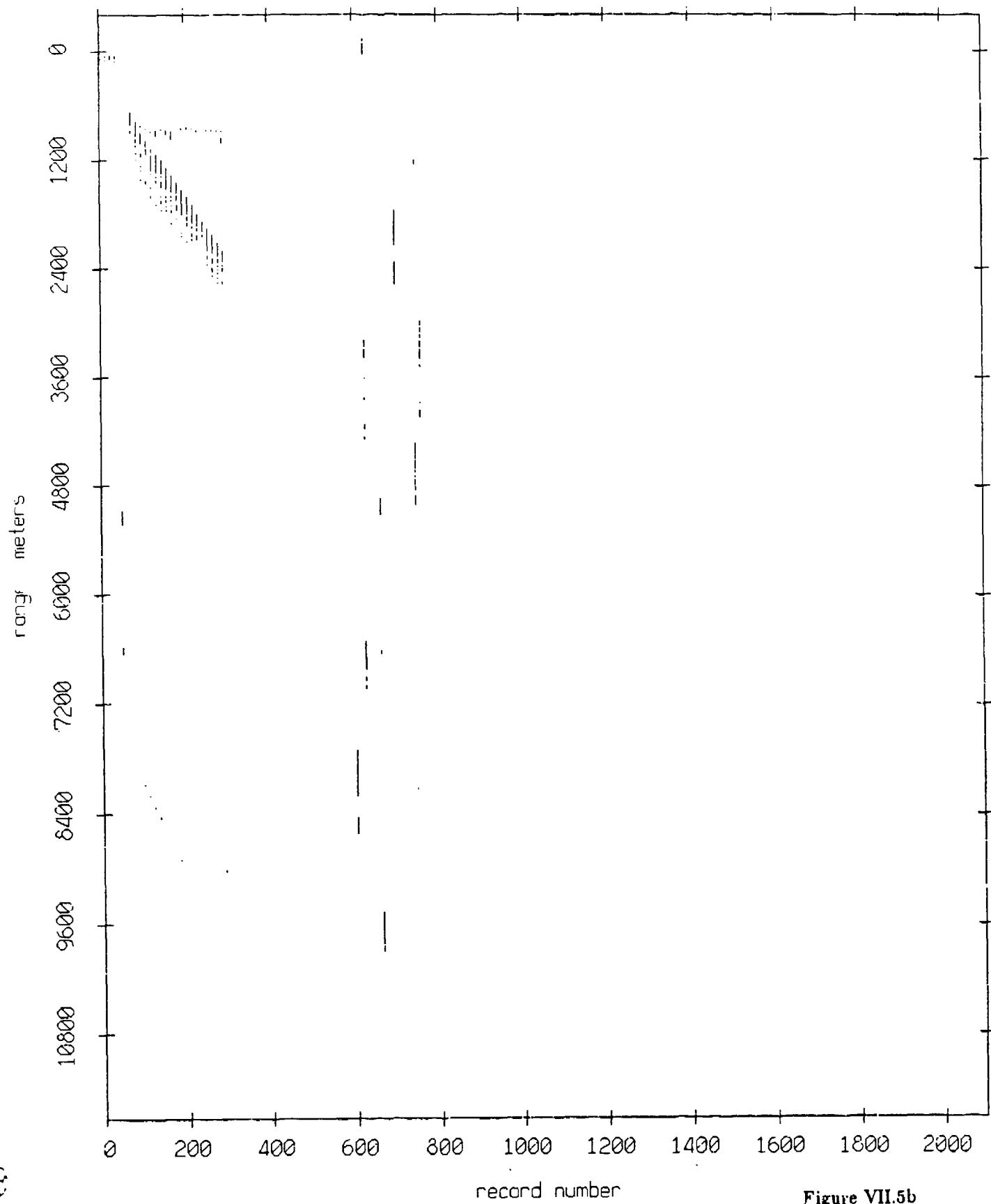


Figure VII.5b

Fleet 7, May, 1987 Sea Trip: range from fleet 2

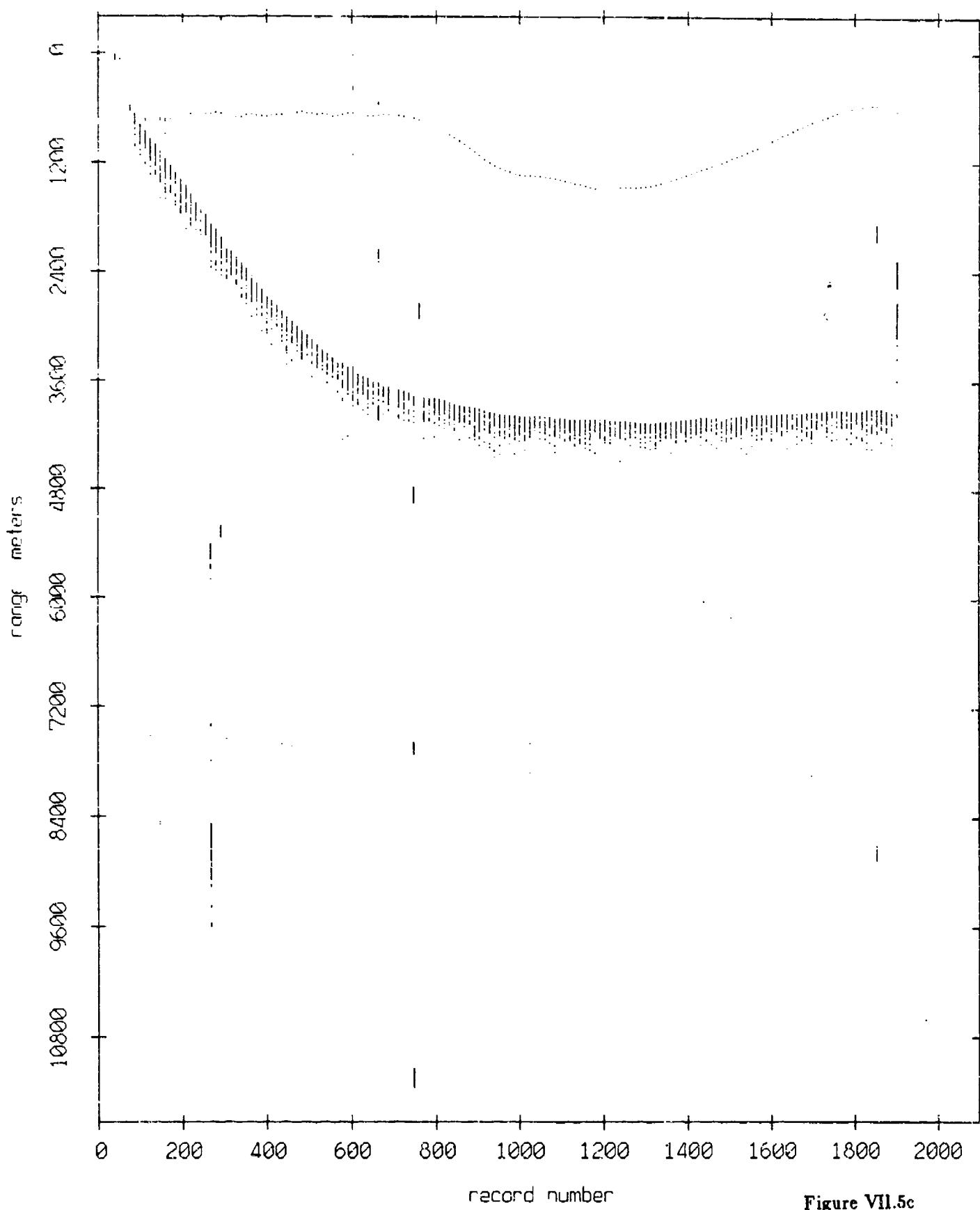


Figure VII.5c

Float 7, May, 1987 Sea Trip: range from float 3

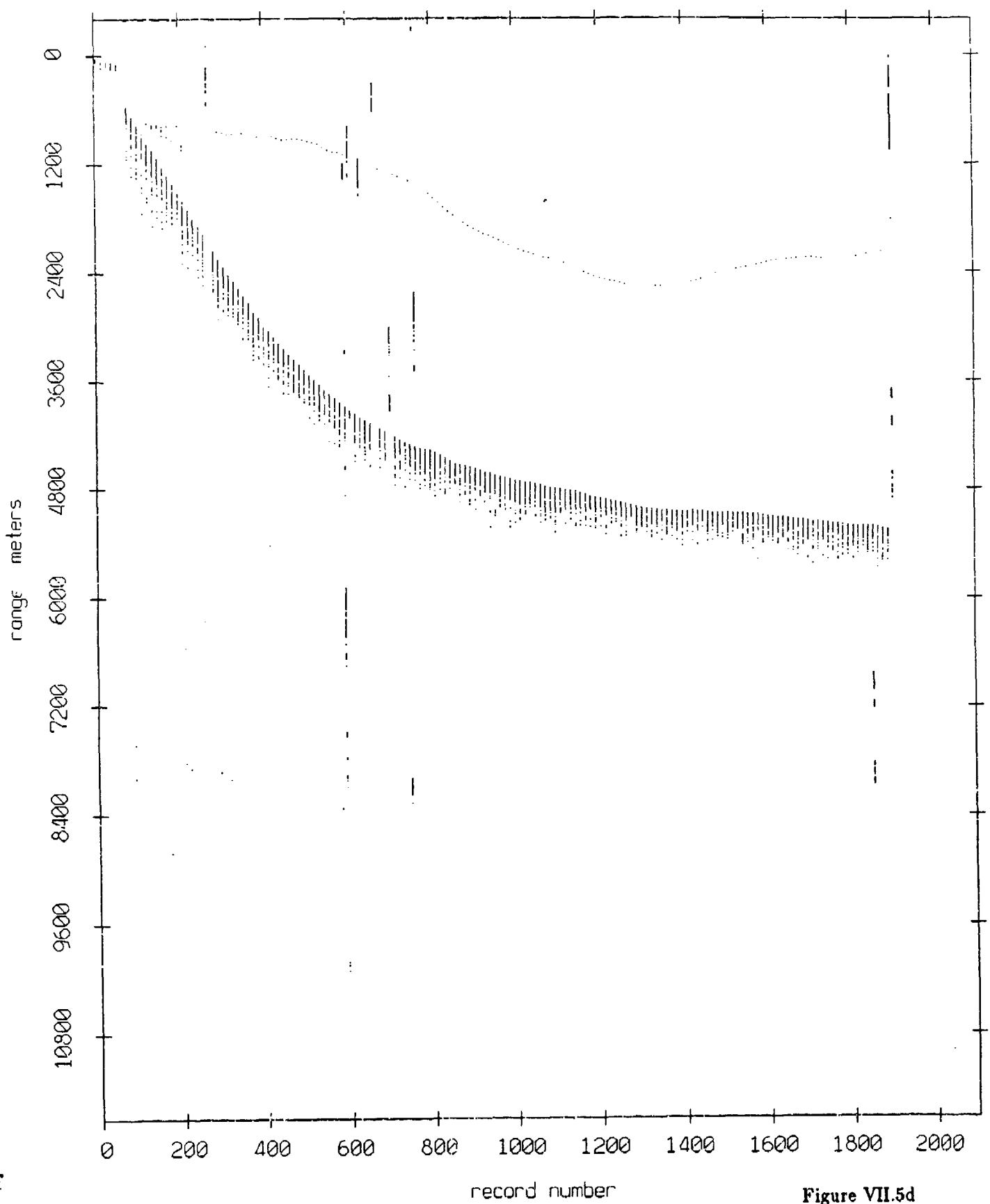


Figure VII.5d

Fleet 7, May, 1987 Sea Trip: range from float 4

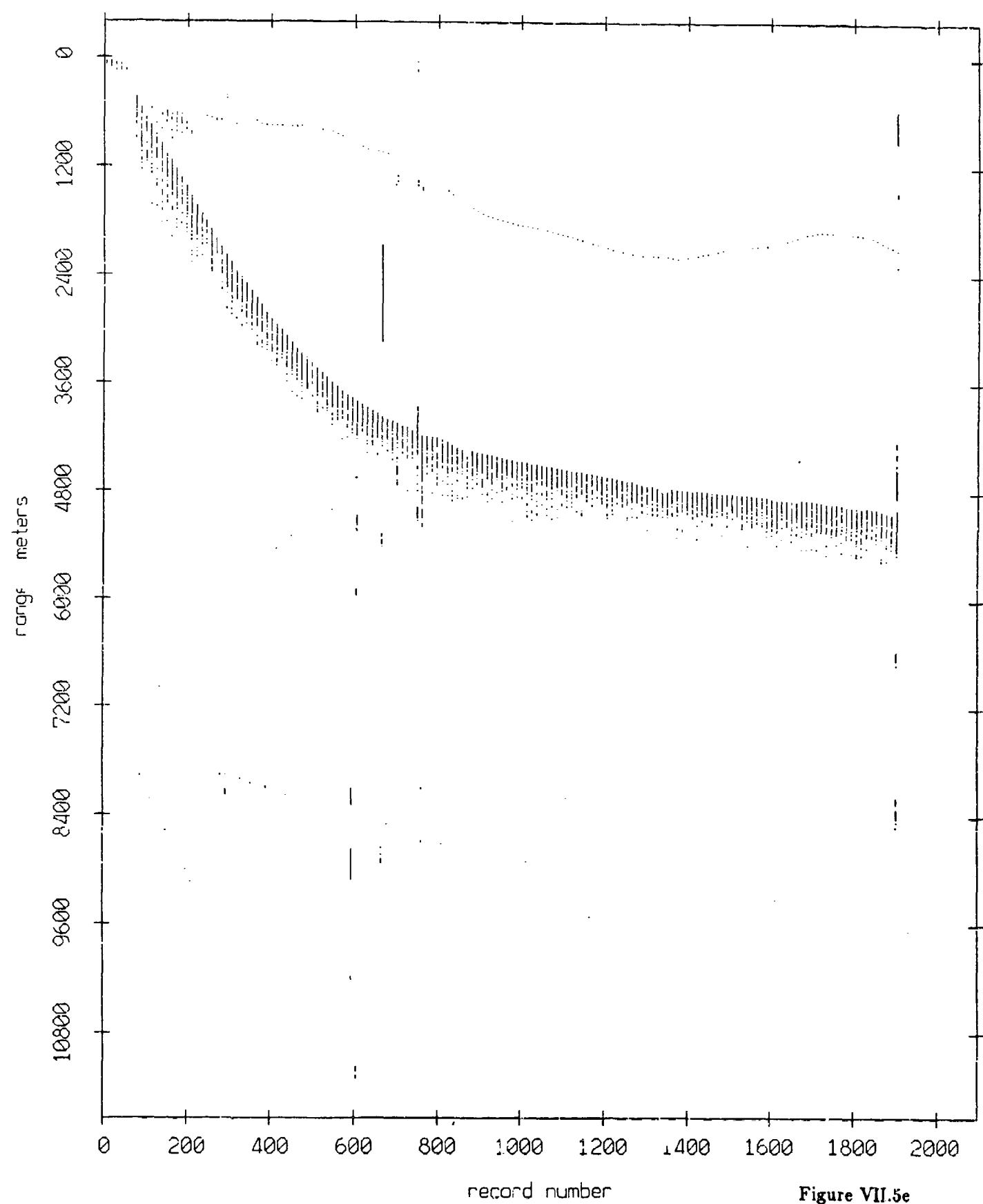


Figure VII.5e

Float 7, May, 1987 Sea Trip: range from float 5

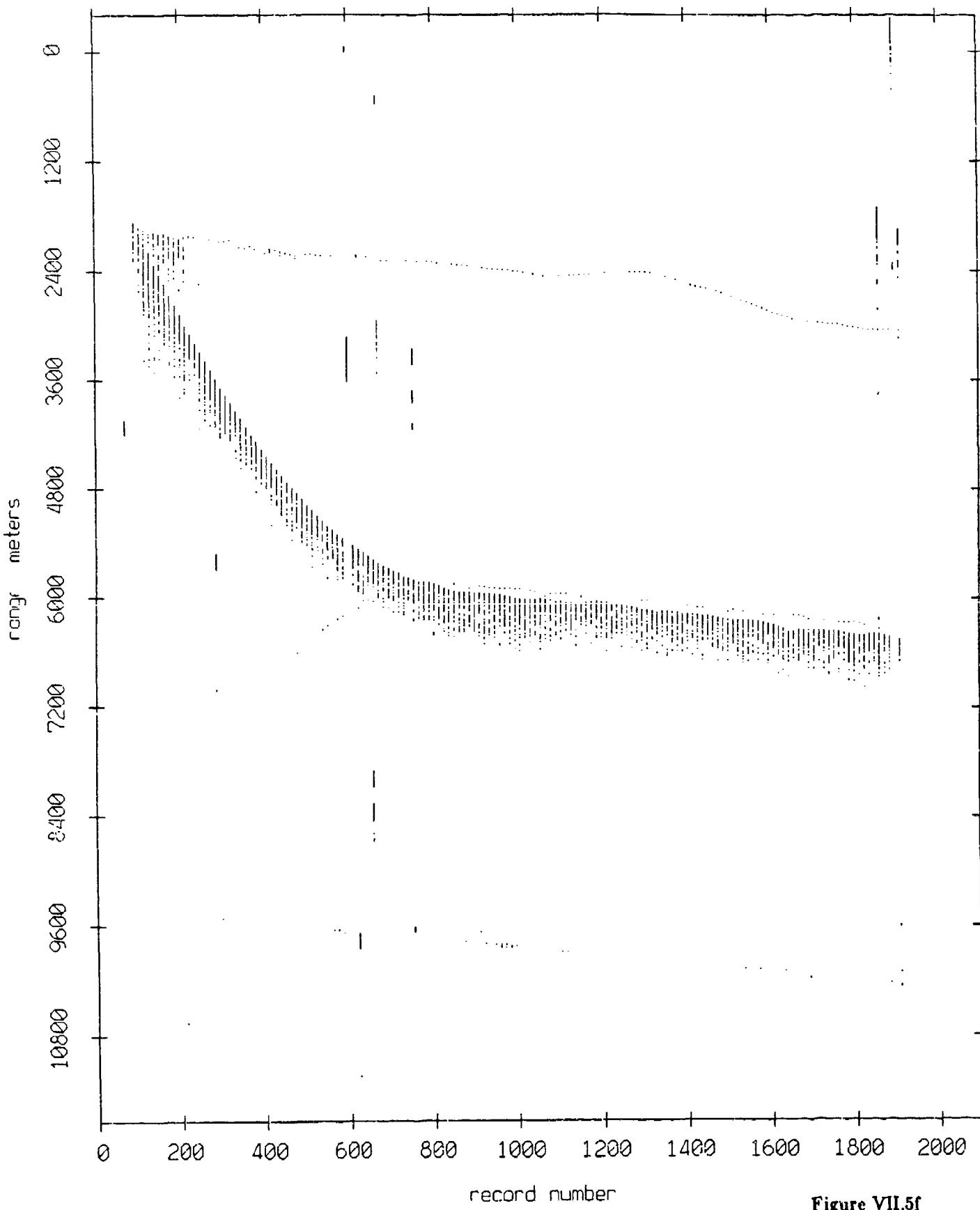


Figure VII.5f

Float 7, May, 1987 Sec Trip: range from float 9

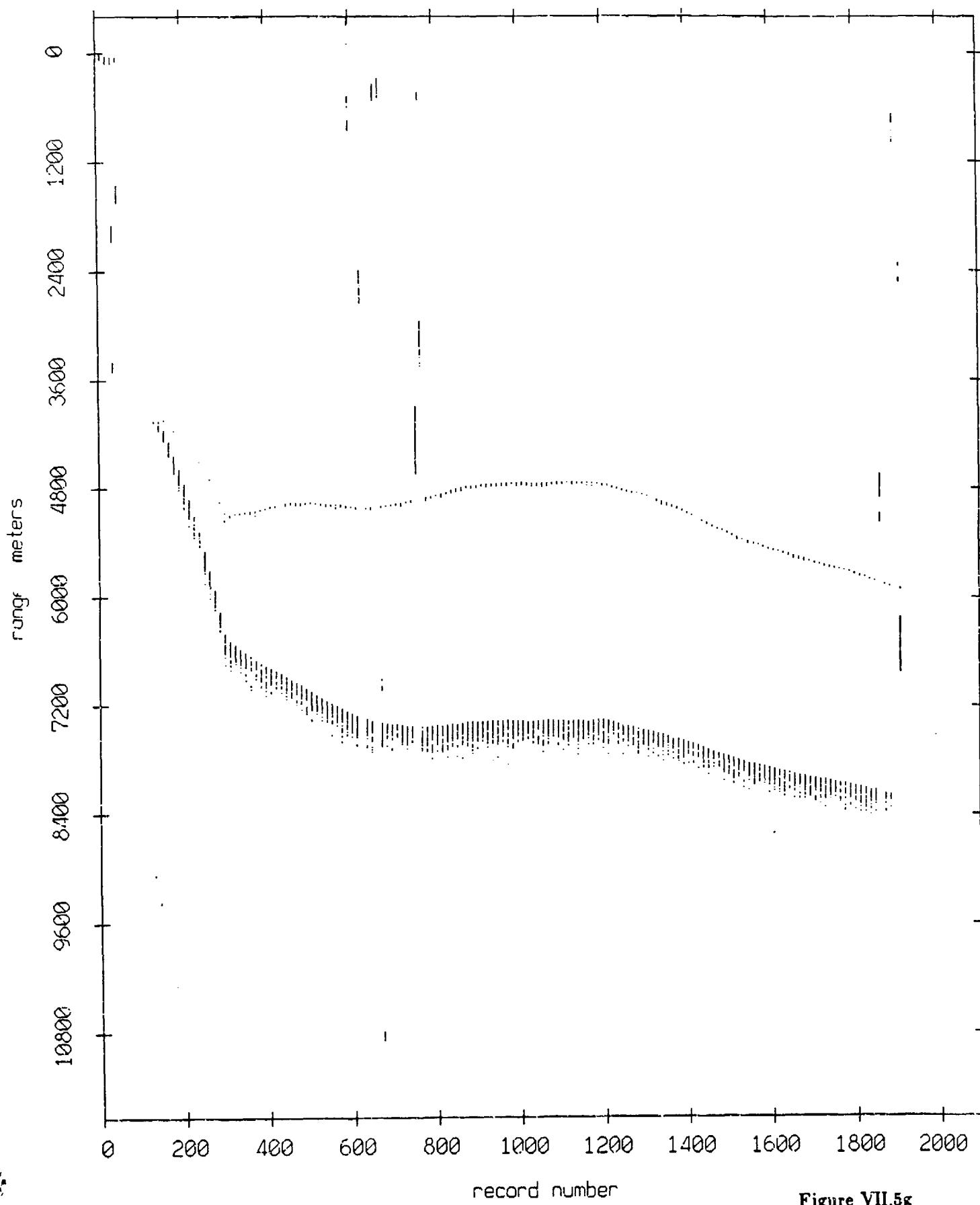


Figure VII.5g

Float 7, May, 1987 Sea Trip: range from float 10

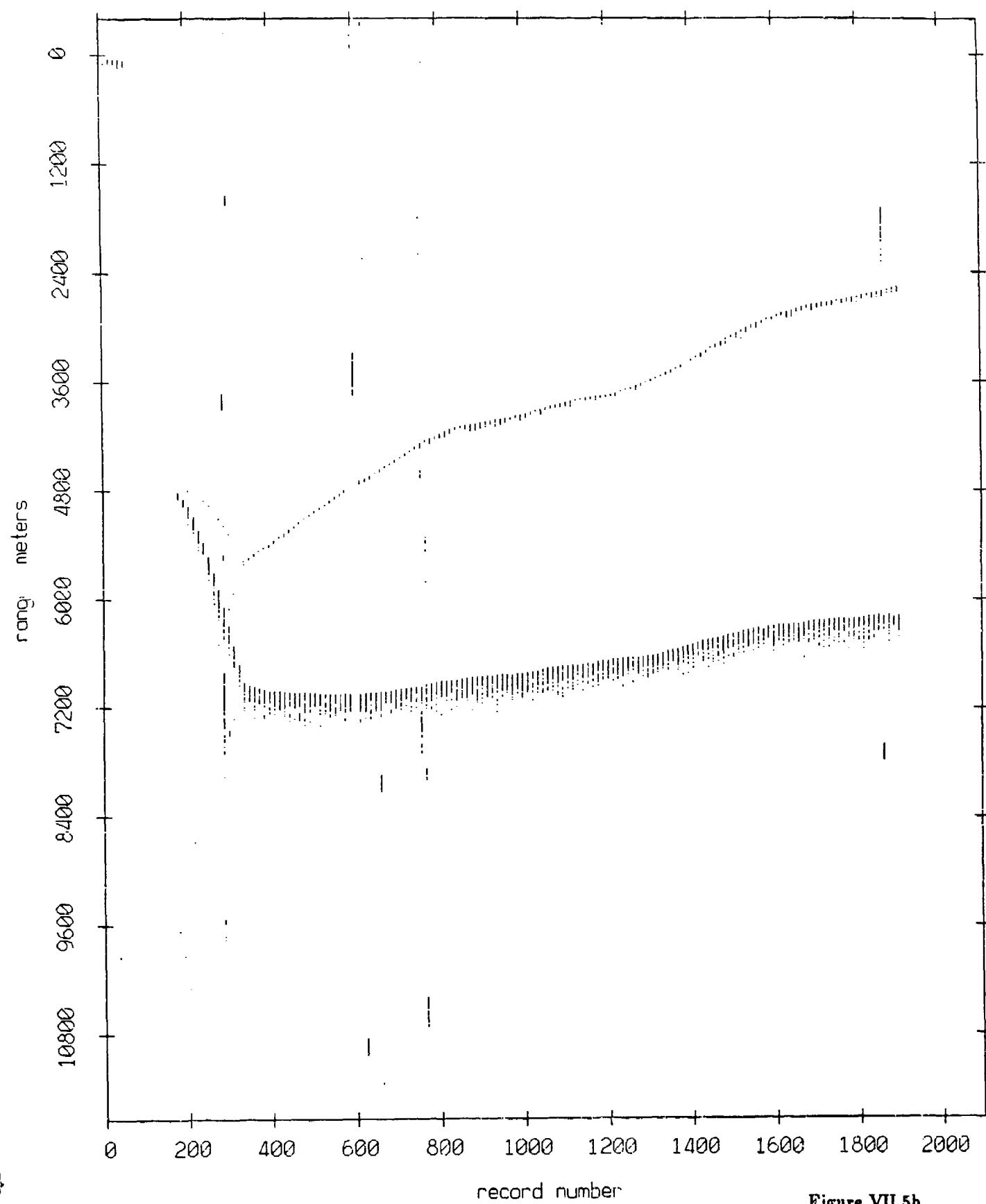


Figure VII.5h

Fleet 7, May, 1987 Sea Trip: range from float 11

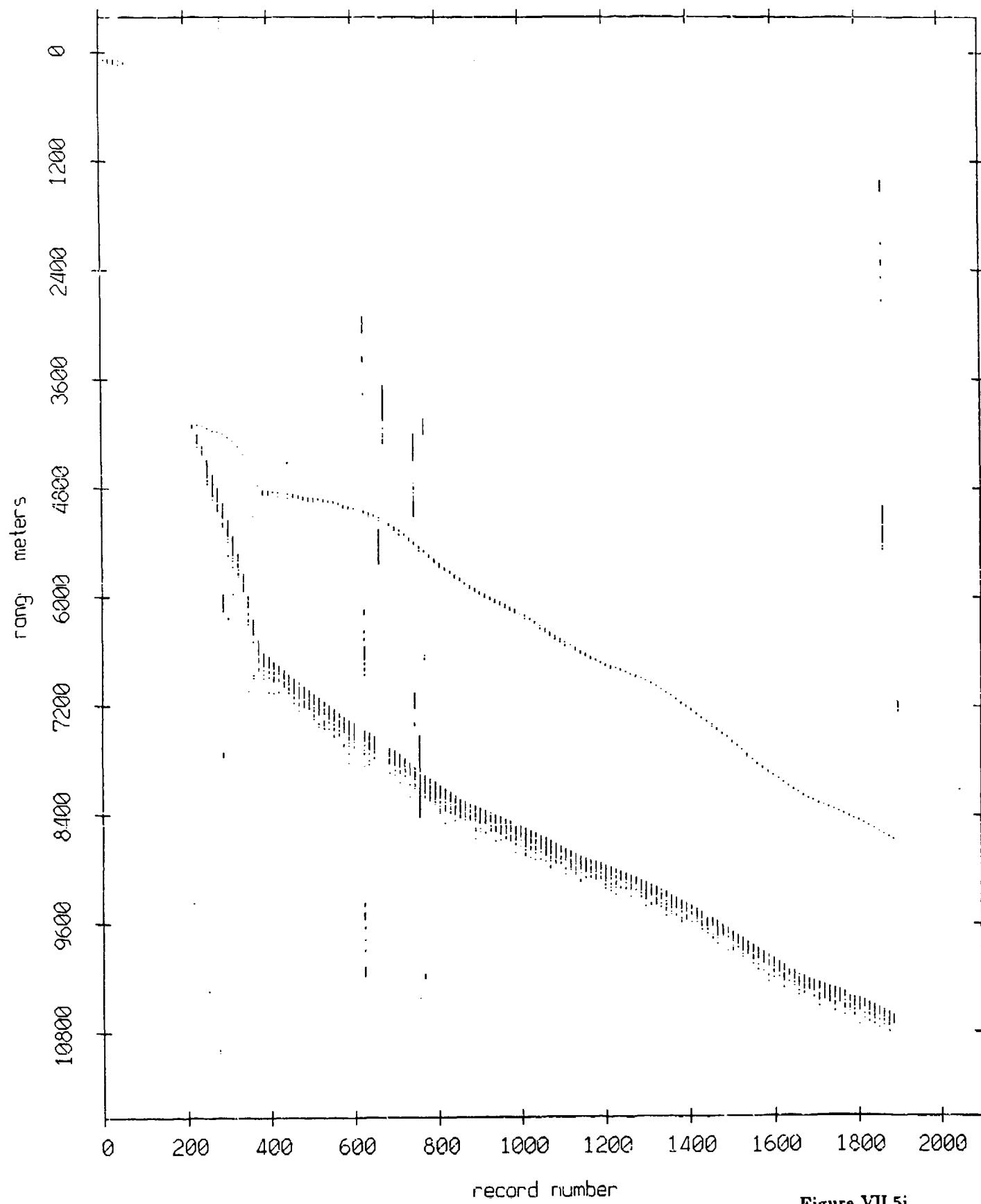


Figure VII.5i

Float 8, May, 1987 Sea Trip: range from float 0

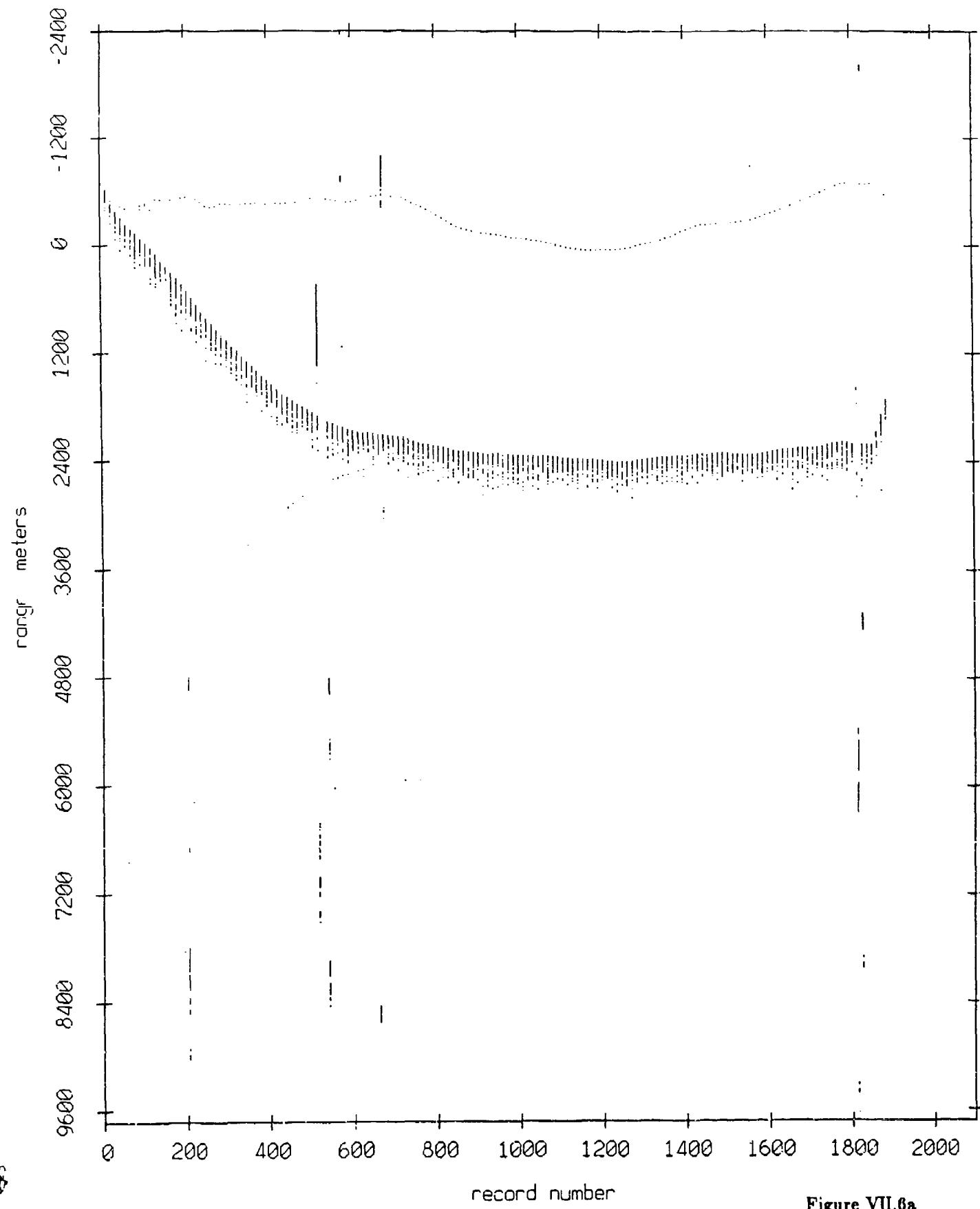


Figure VII.6a

Float 8, May, 1987 Sea Trip: range from float 1

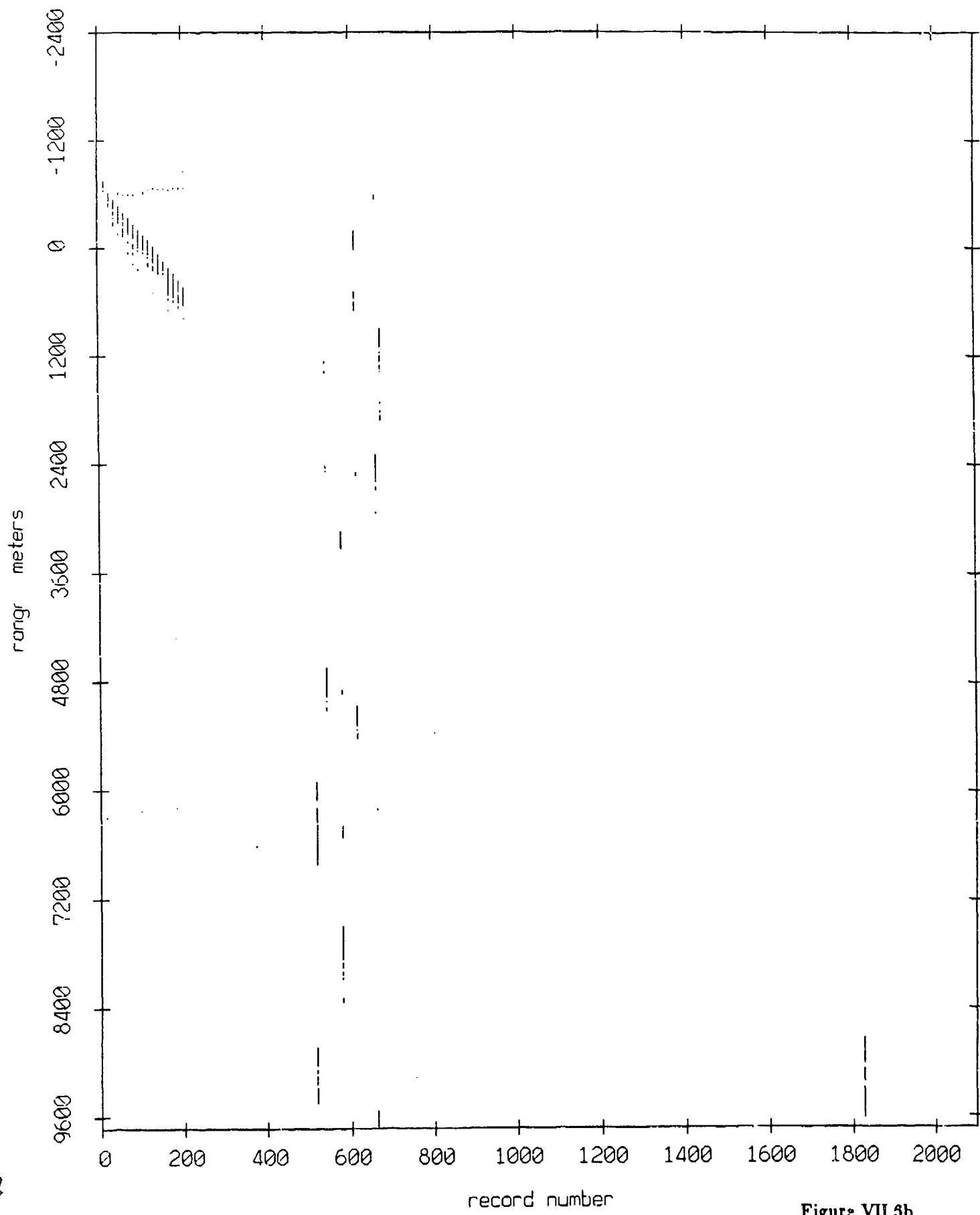


Figure VII.3b

Float 8, May, 1987 Sea Trip: range from float 2

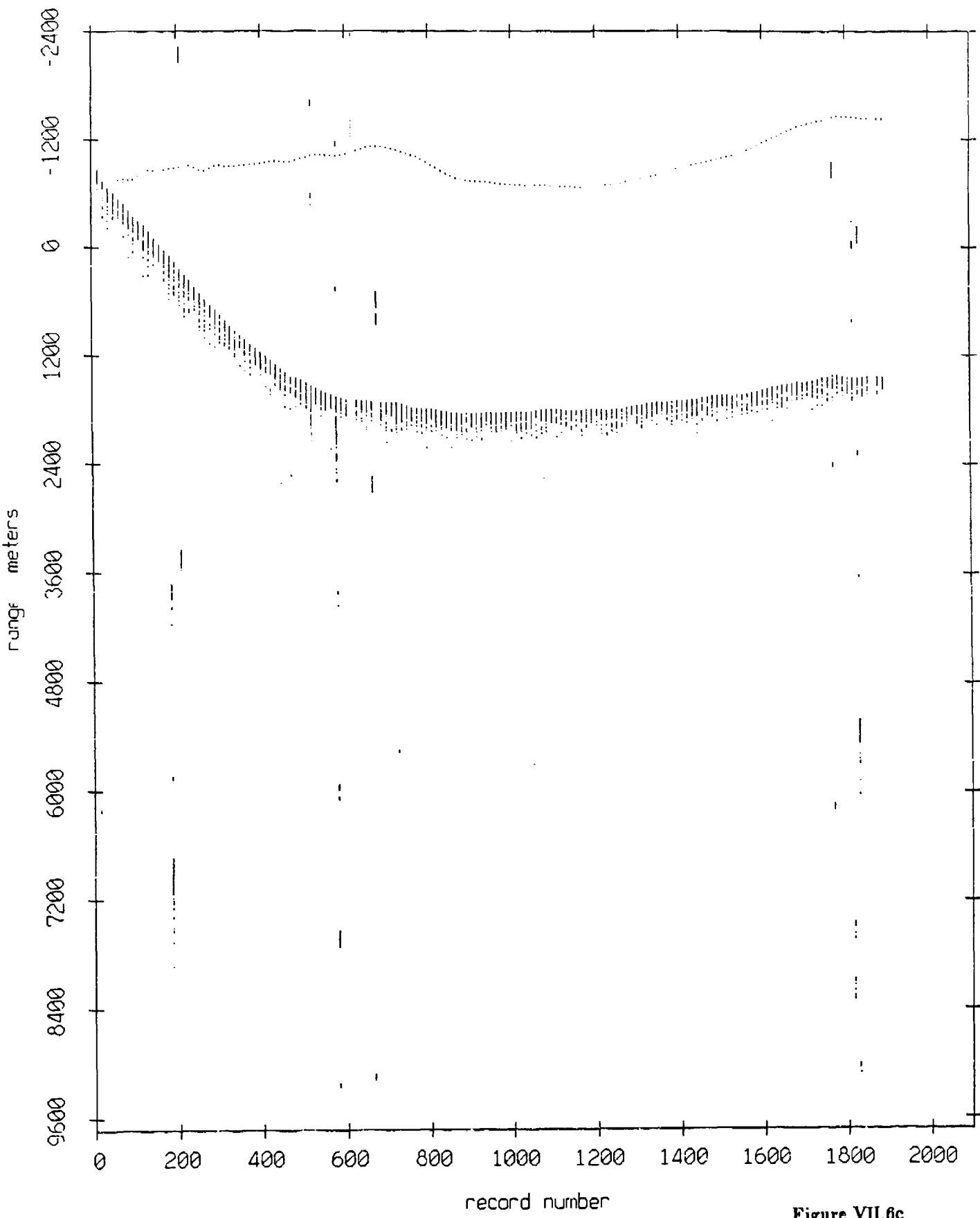


Figure VII.6c

Fleet 3, May, 1987 Sea Trip: range from float 3

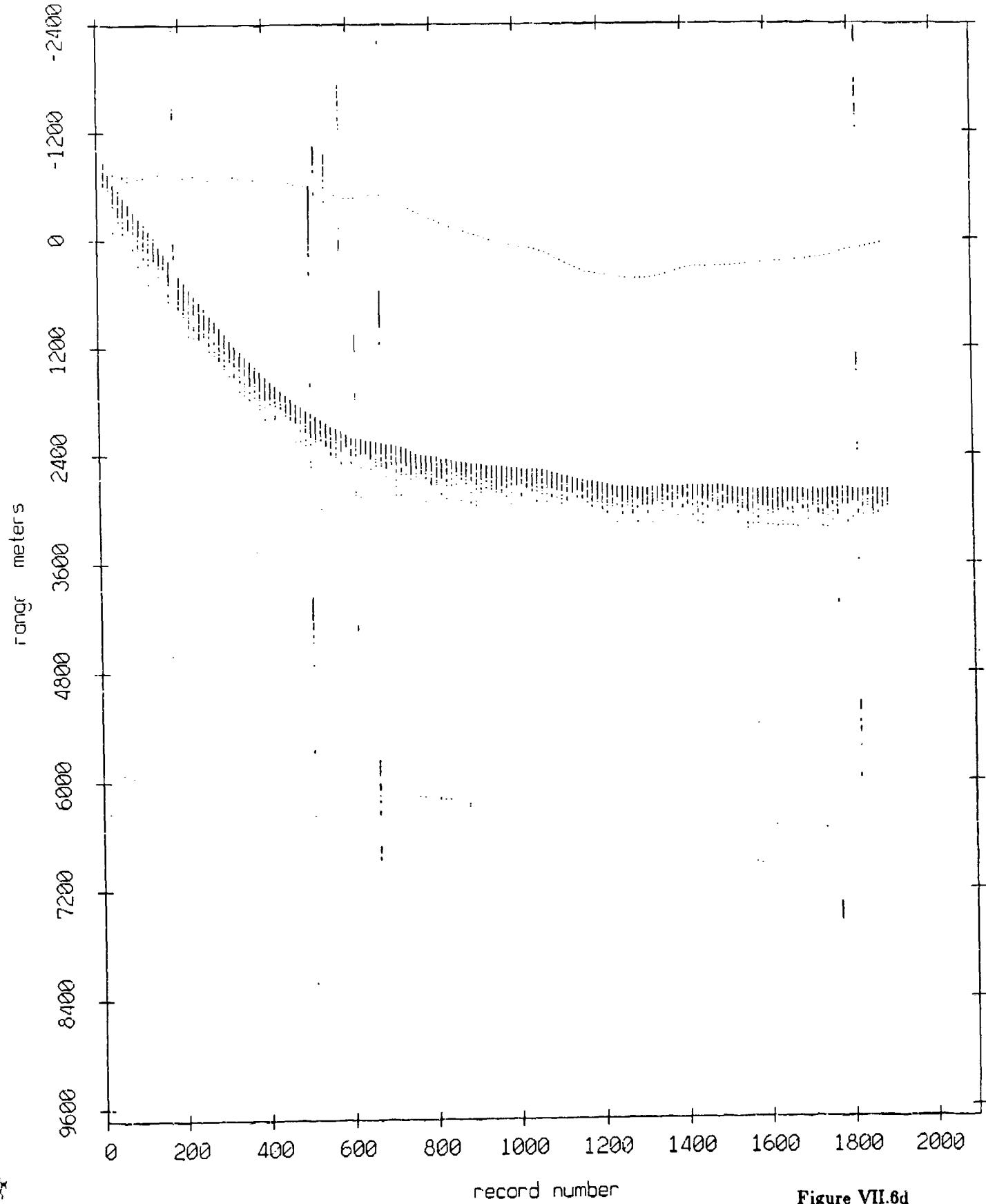


Figure VII.6d

FRIULI, MAY, 1957 SHEET 11 OF 16: RANGE FROM 1000' 4

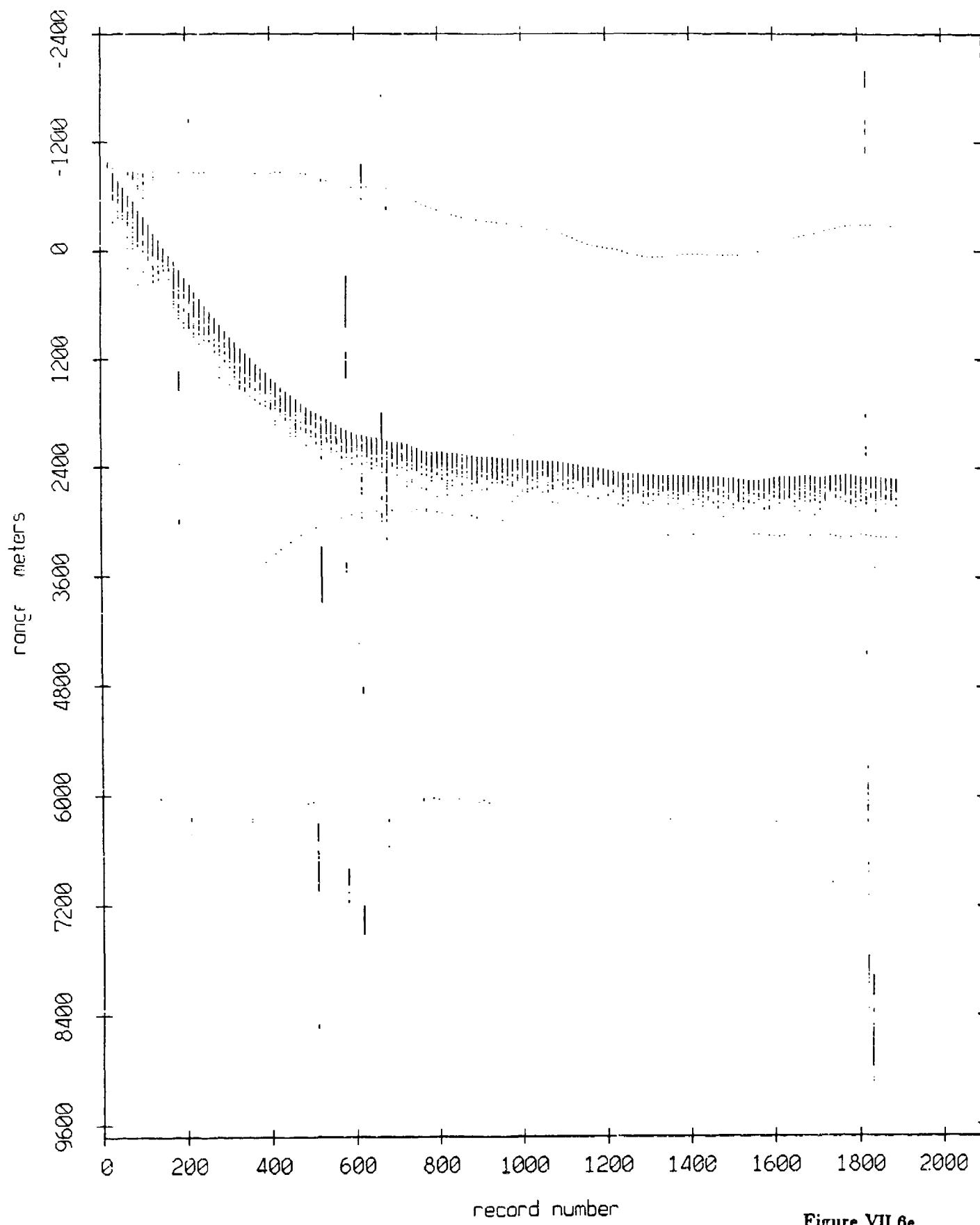


Figure VII.6e

Fleet 8, May, 1987 Sea Trip: range from float 7

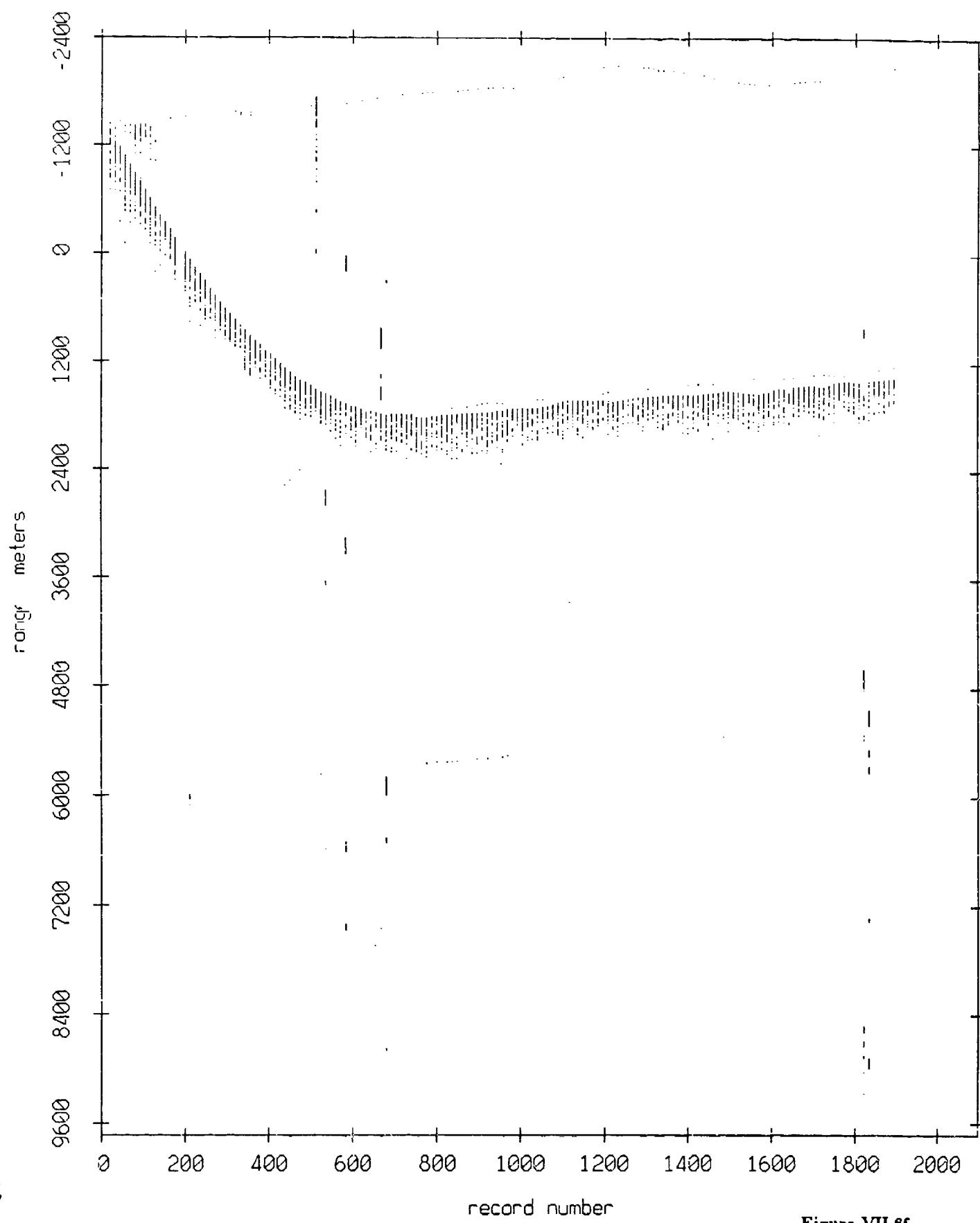


Figure VII.6f

Float 3, May, 1987 Sea Trip: range from float 9

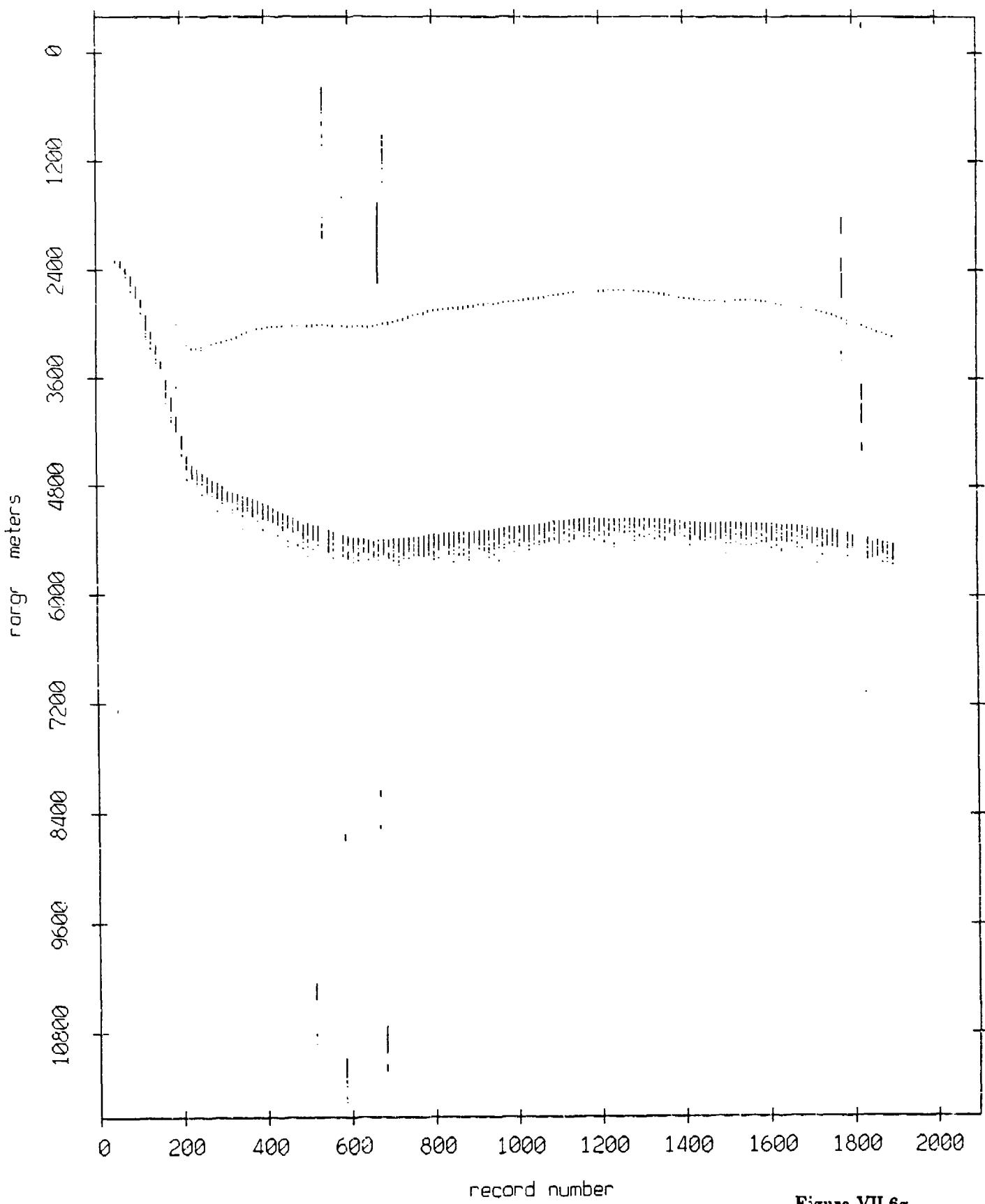


Figure VII.6g

Fleet 8, May, 1987 Sea Trip: range from float 10

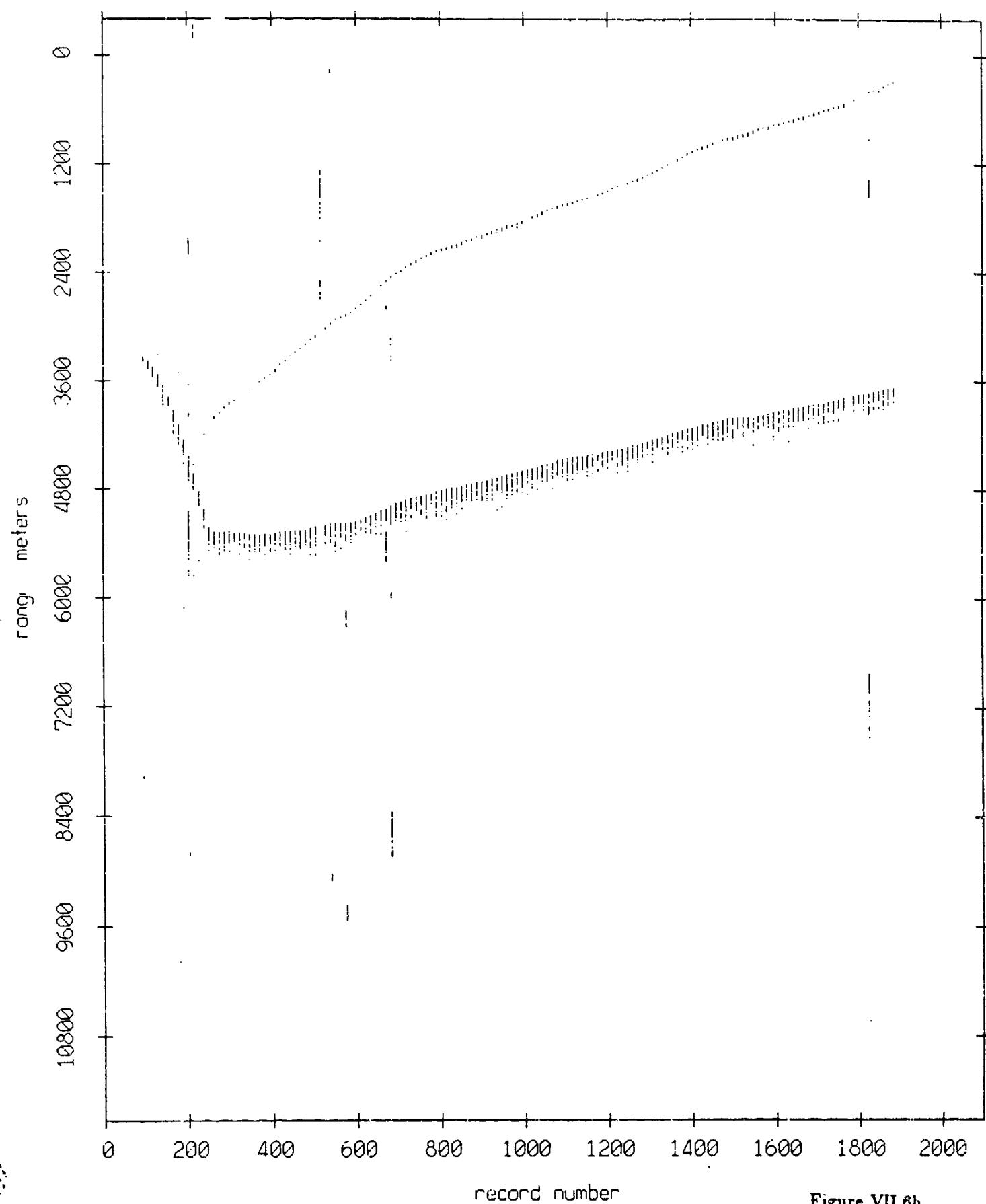


Figure VII.6h

Float 6, May, 1957 Sea Trip: range from float 11

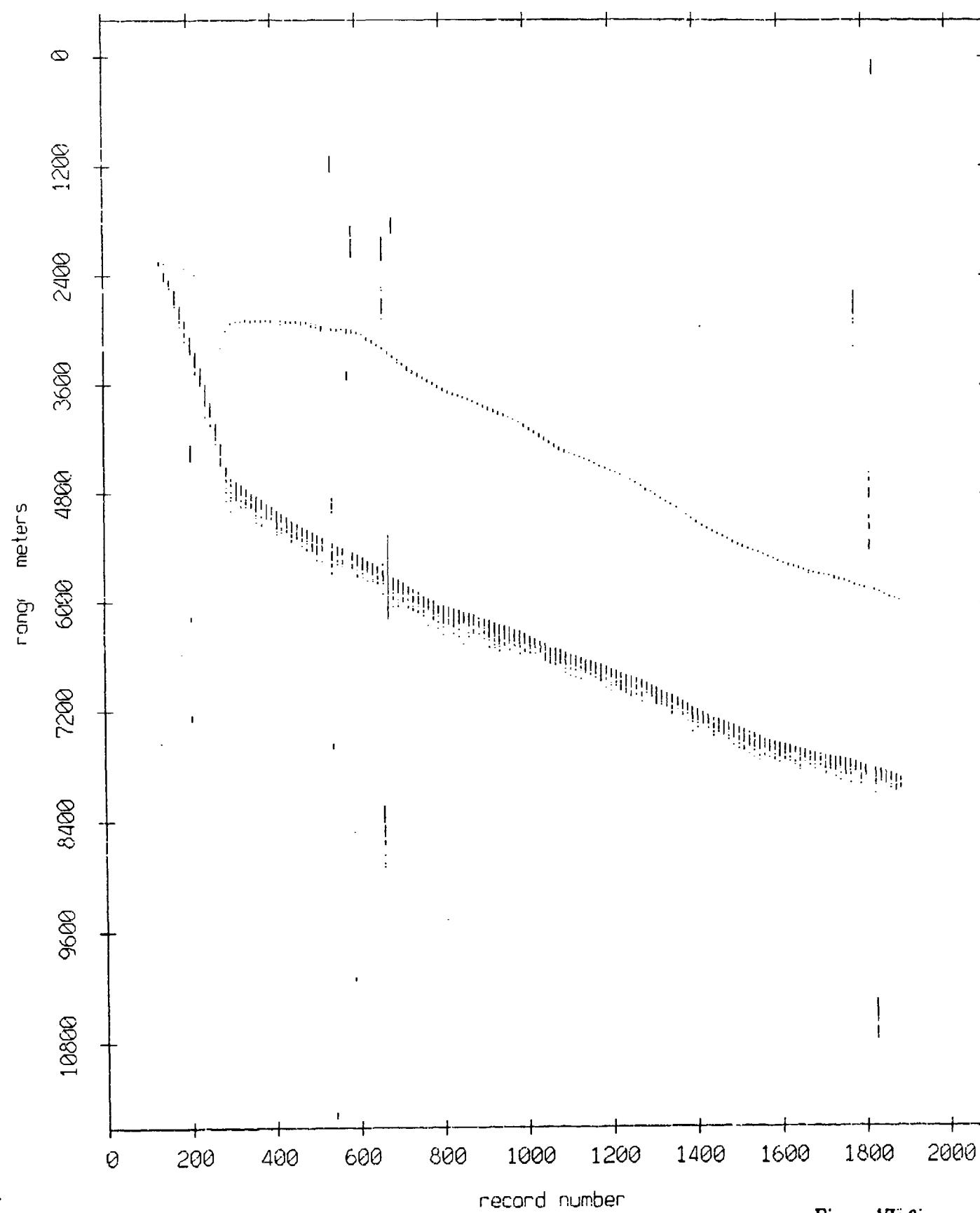


Figure VII.6i

Float 9, May, 1987 Sea Trip; range from float 0

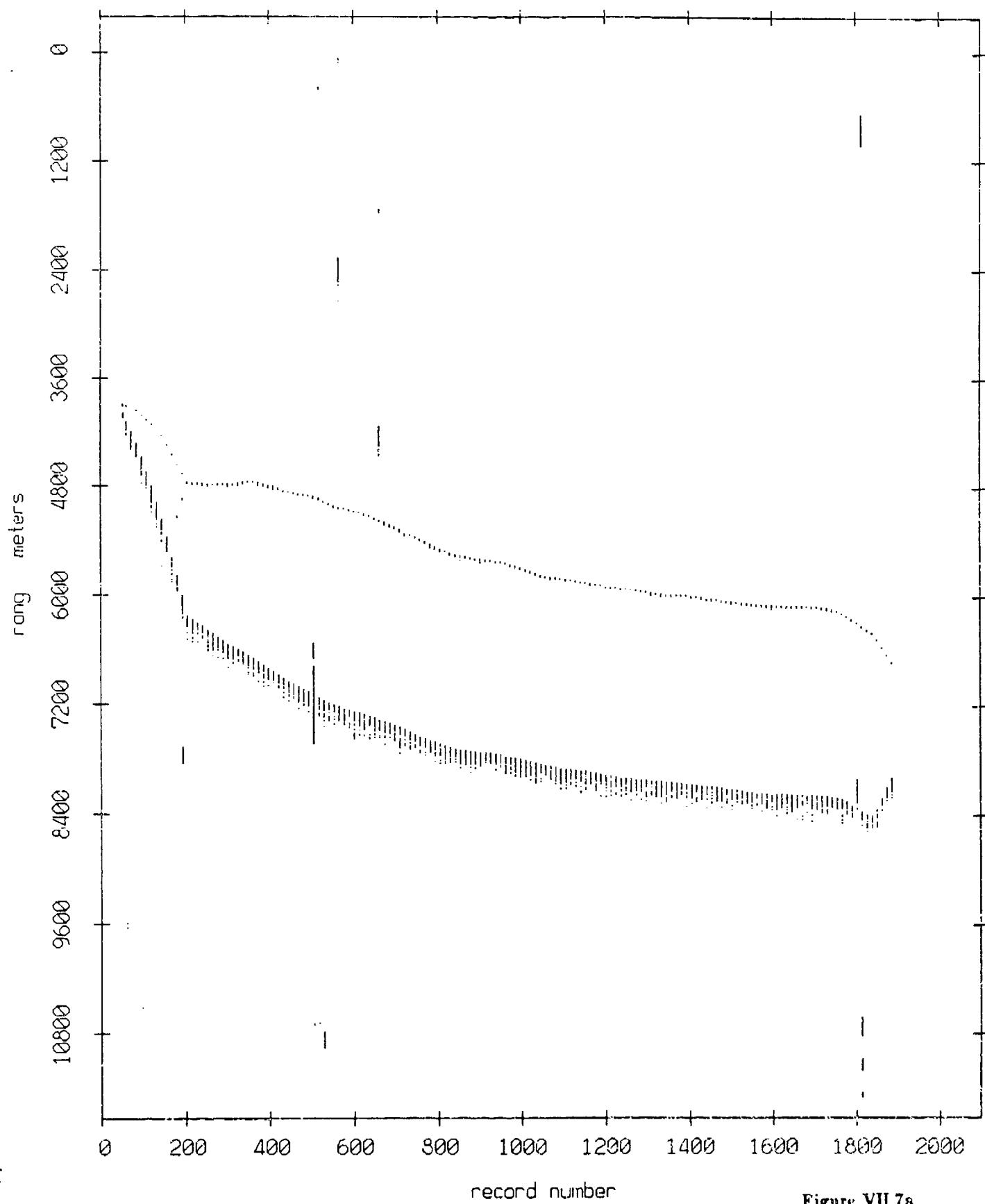


Figure VII.7a

Float 9, May, 1987 Sea Trip: range from float 1

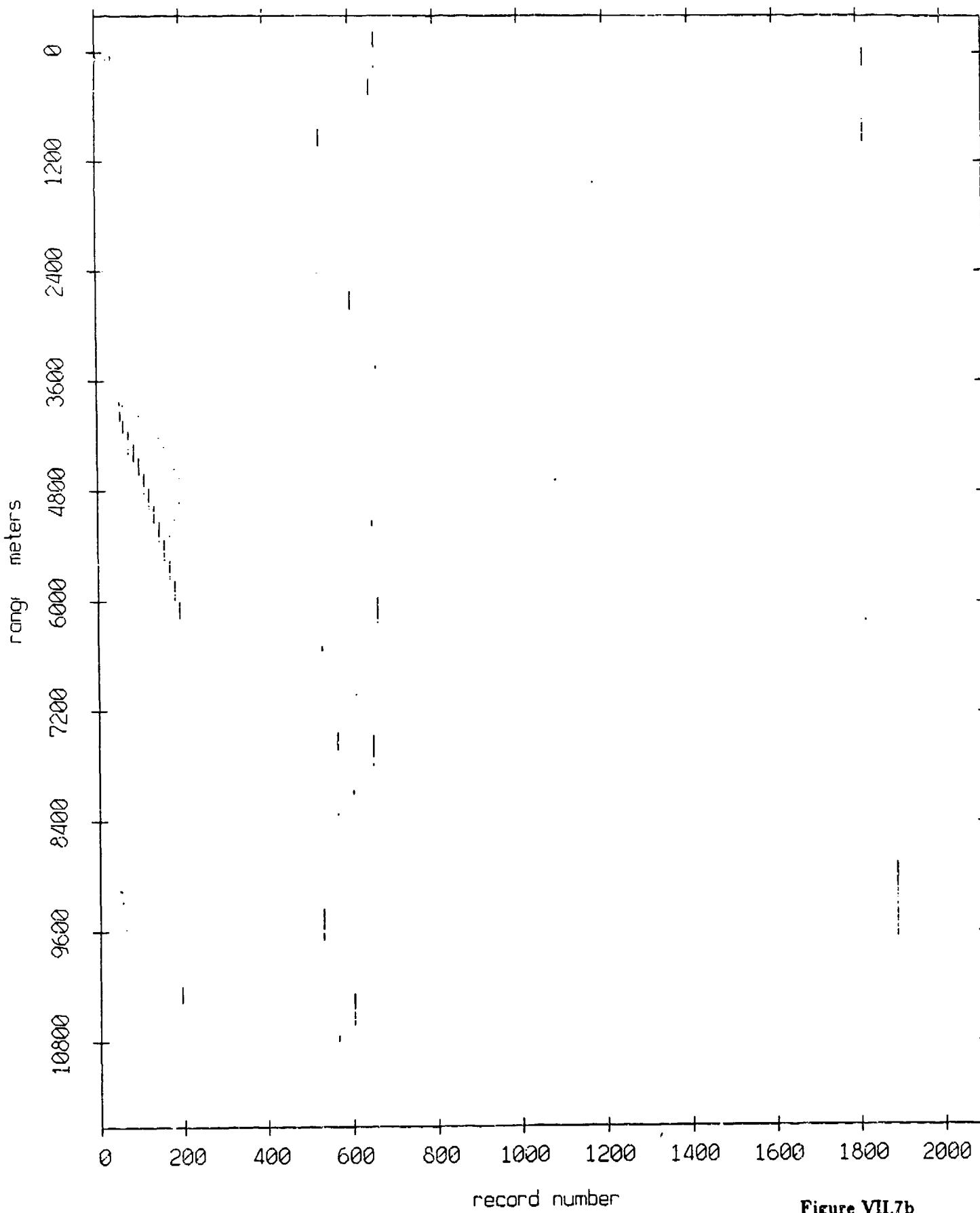


Figure VII.7b

Fleet 9, May, 1987 Sea Trip: range from float 2

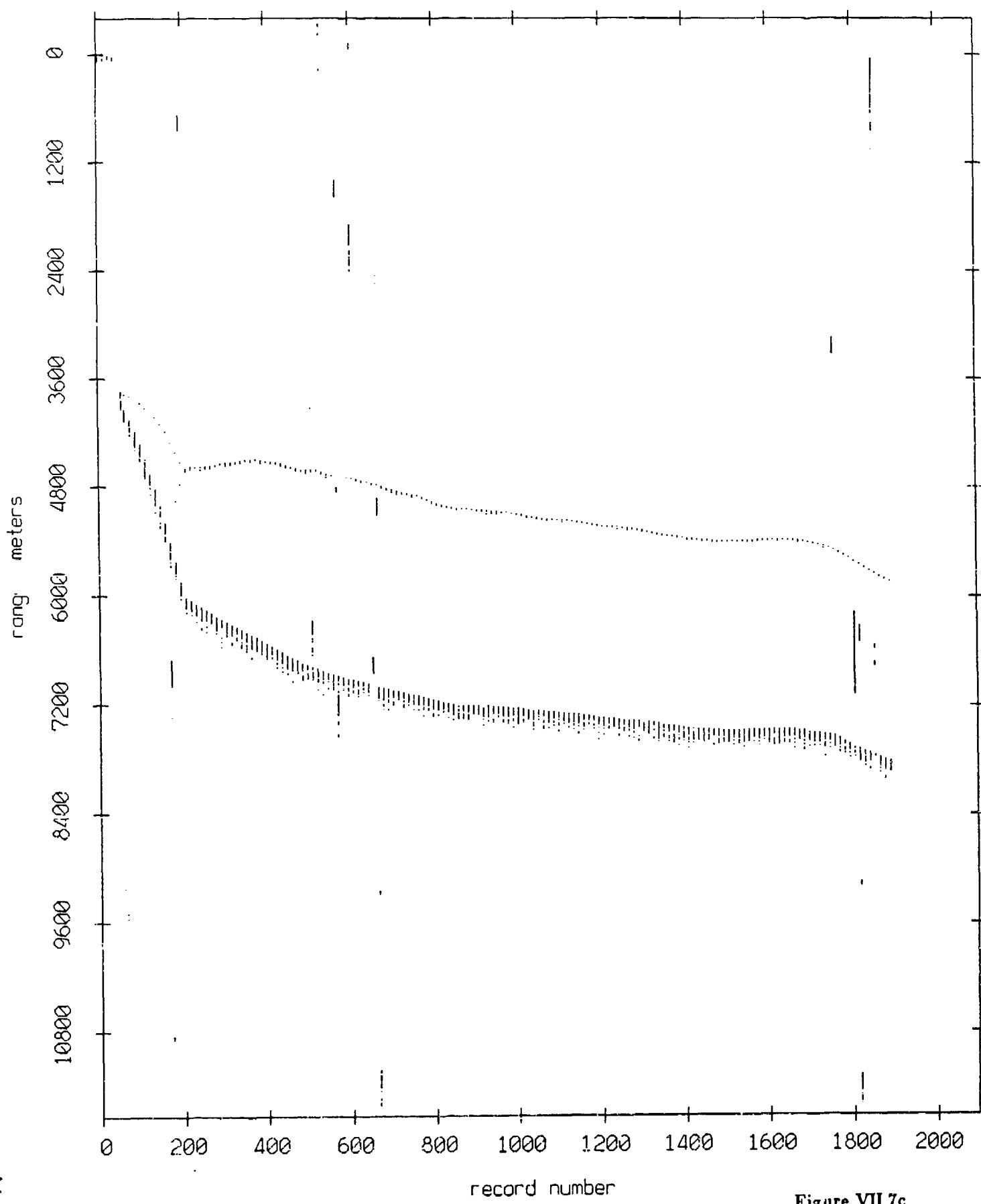


Figure VII.7c

Fleet 9, May, 1987 Sea Trip: range from float 3

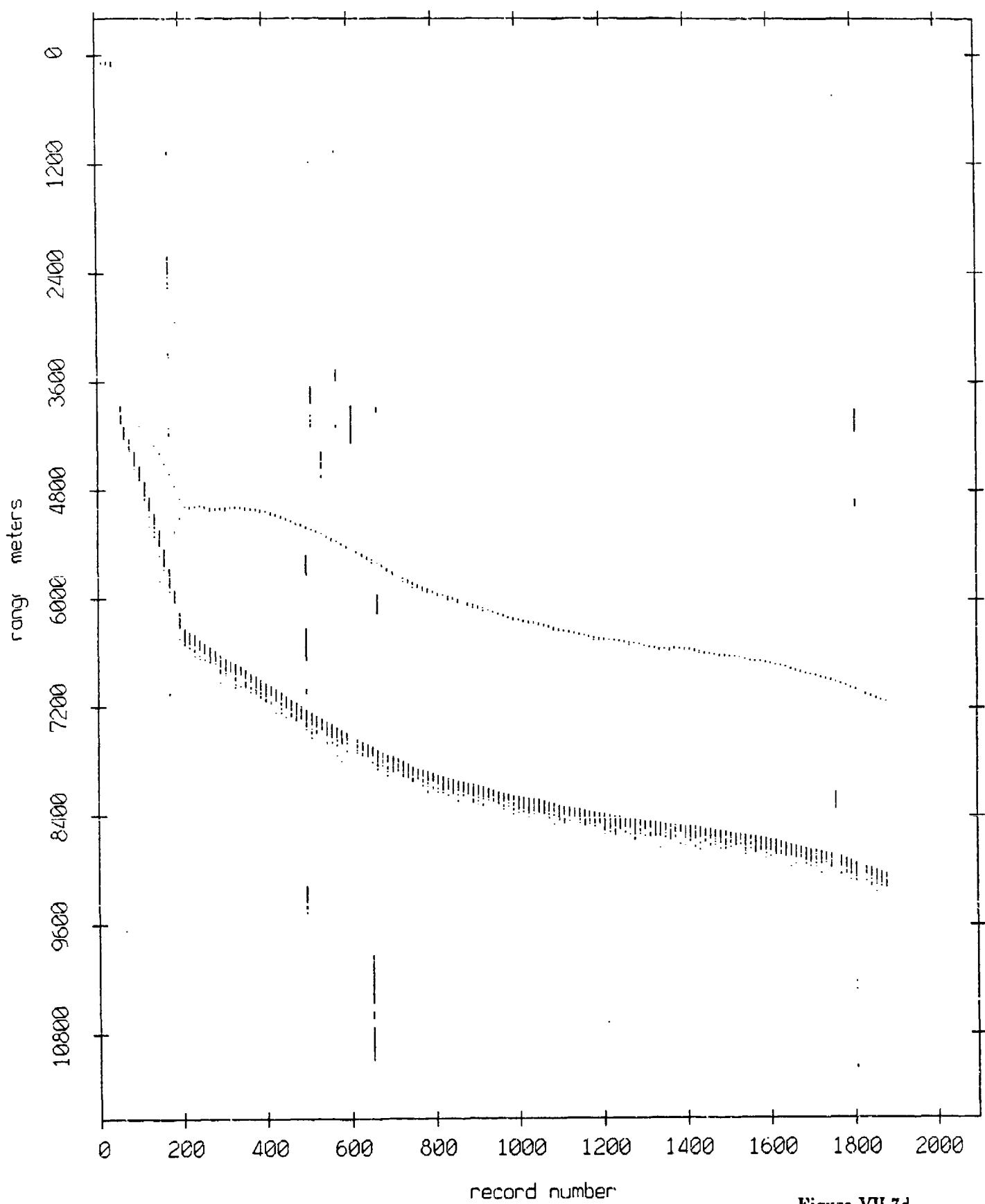


Figure VII.7d

Fleet 9, May, 1987 Sea Trip: range from float 4

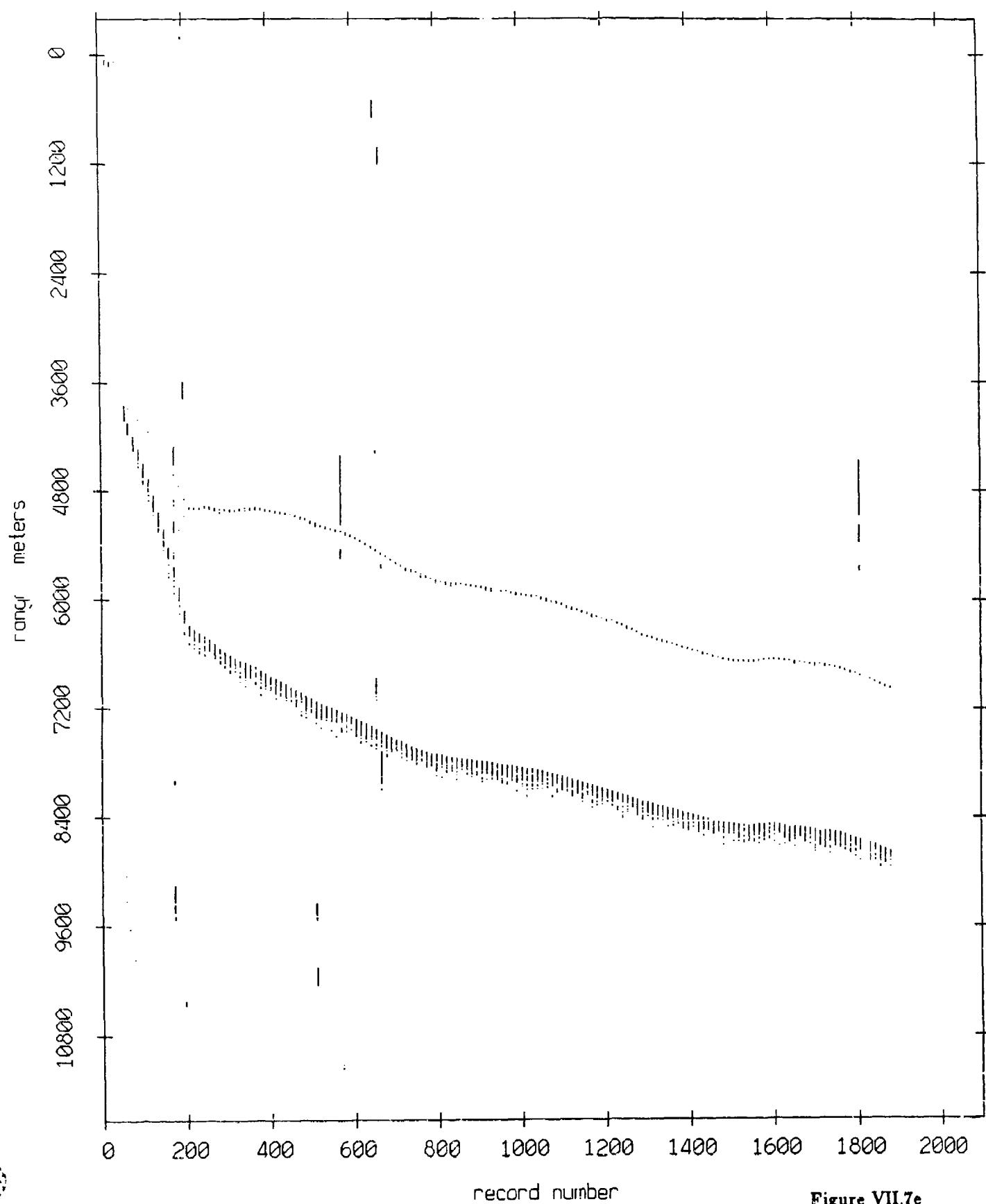


Figure VII.7e

Fleet Y, May, 1987 Sea Trip: range from fleet Y

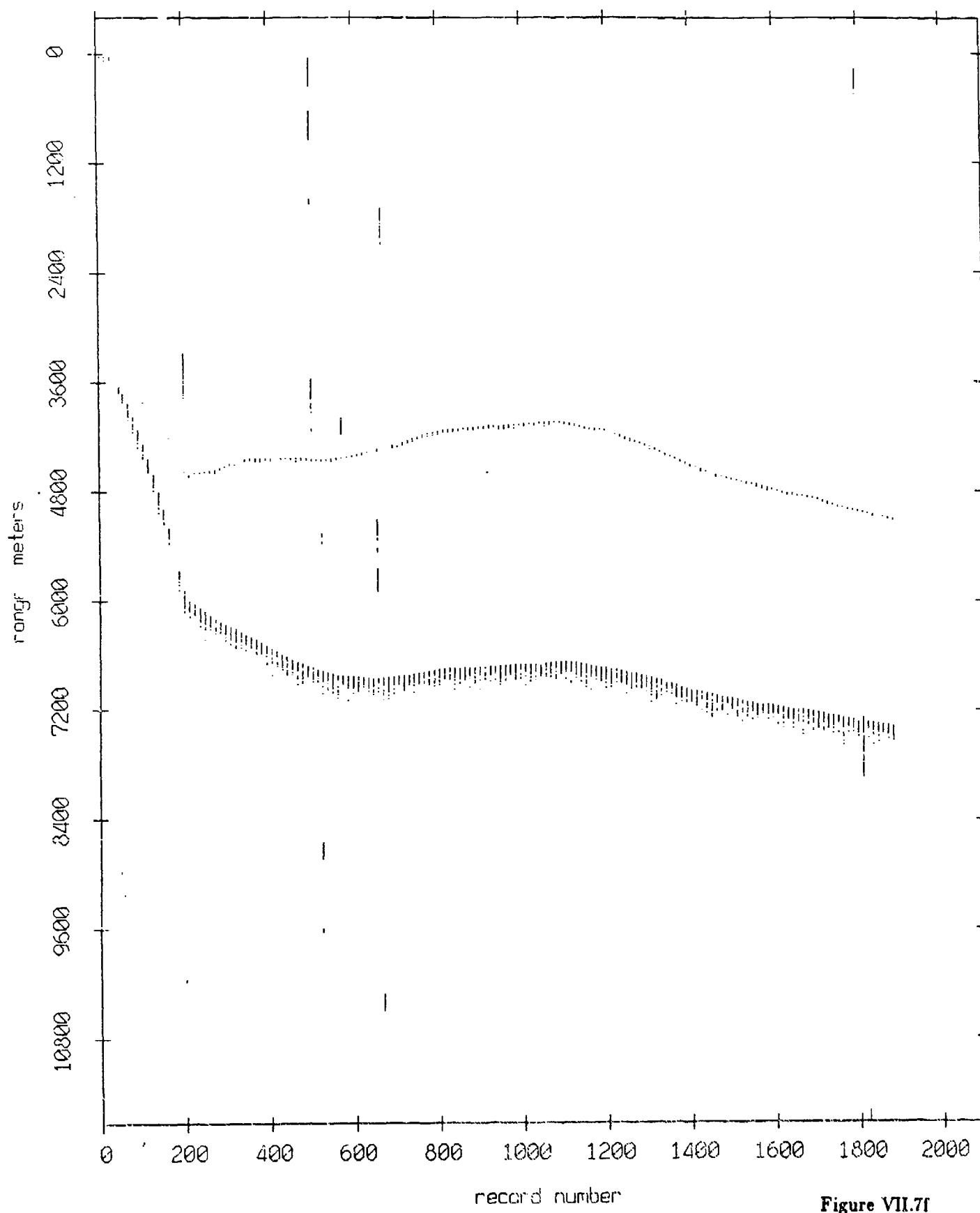


Figure VII.7f

Float 9, May, 1987 Sea Trip: range from float 8

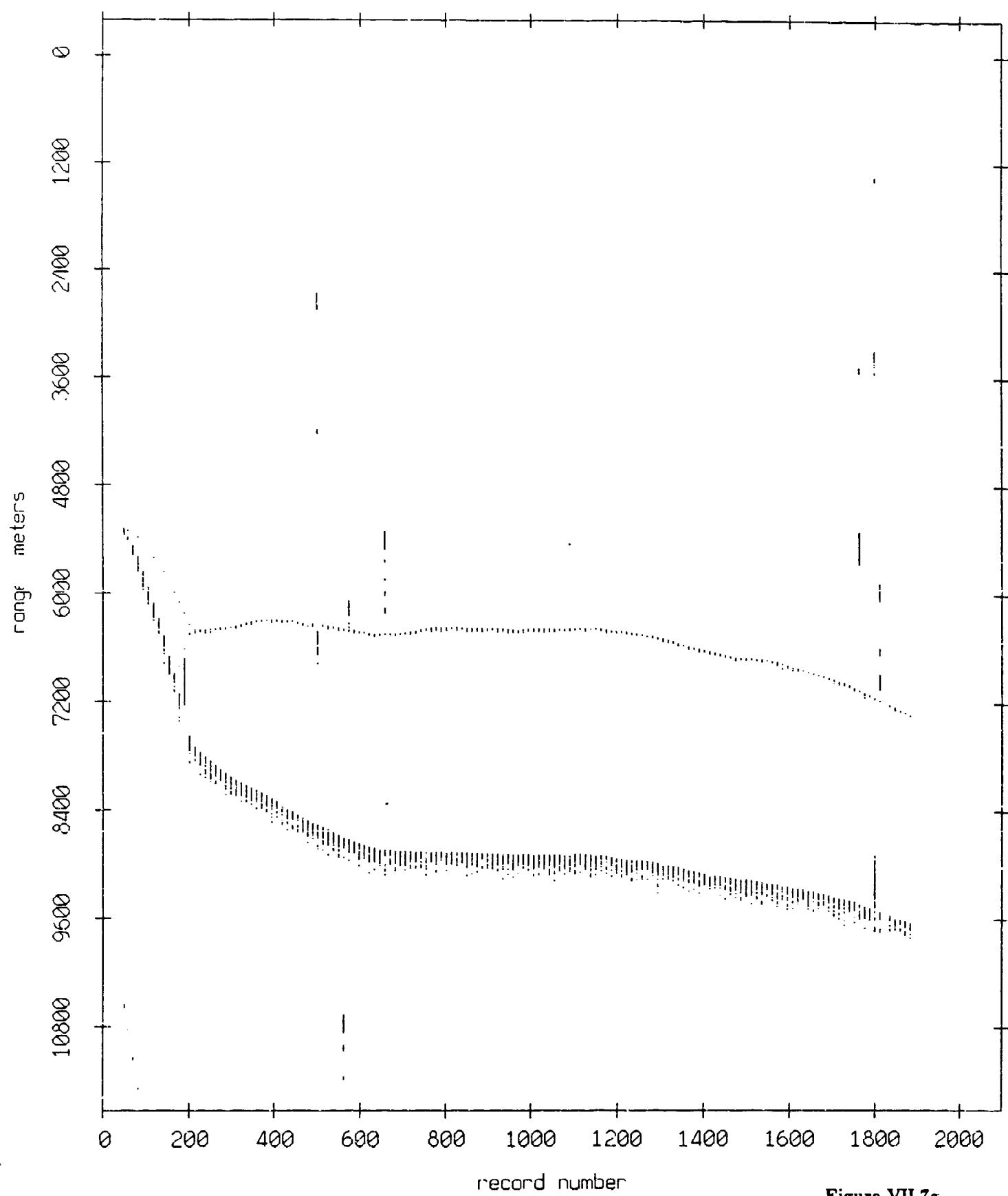


Figure VII.7g

Float 9, May, 1987 Sea Trip: range from float 10

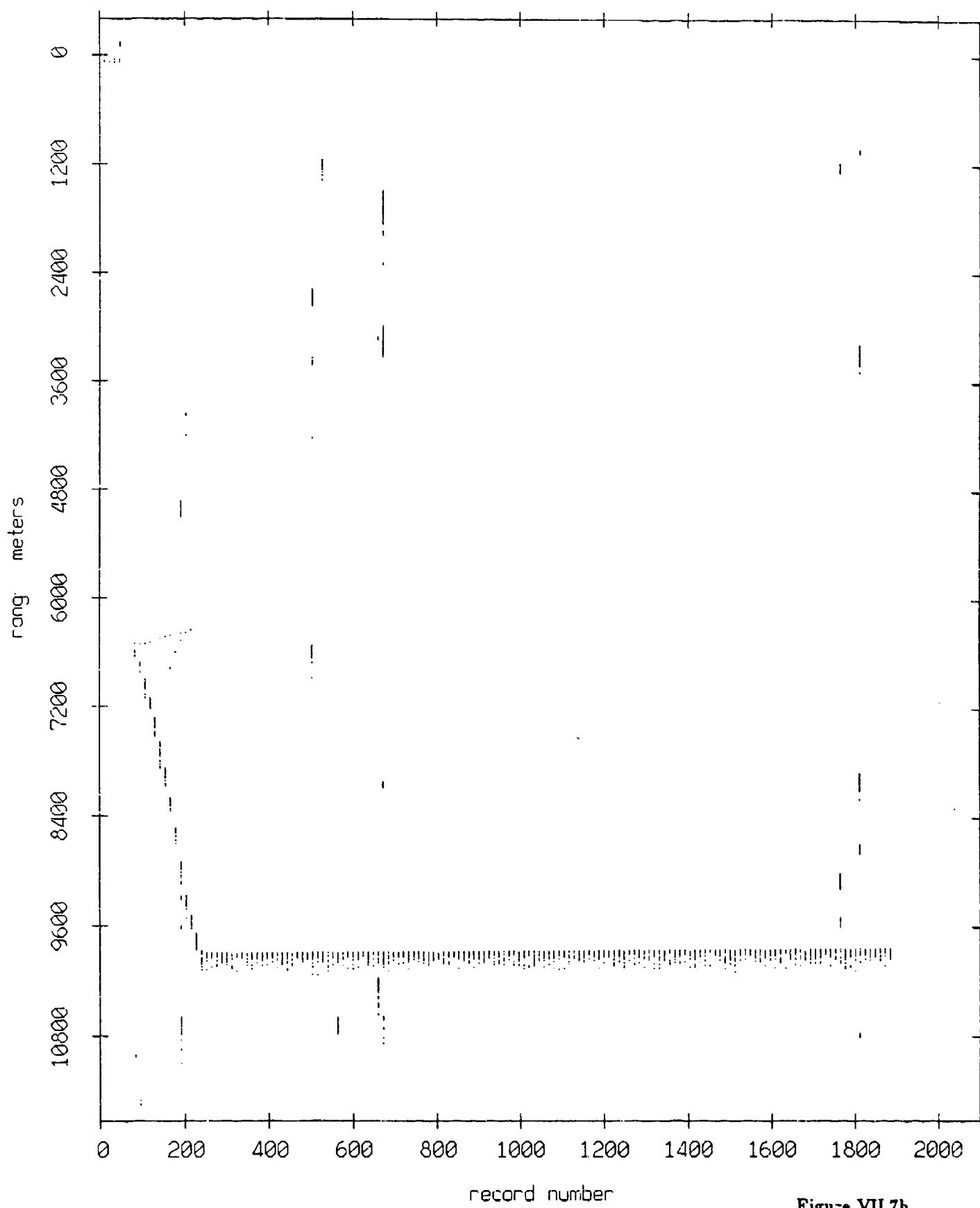


Figure VII.7h

Float 9, May, 1987 Sea Trip: range from float 11

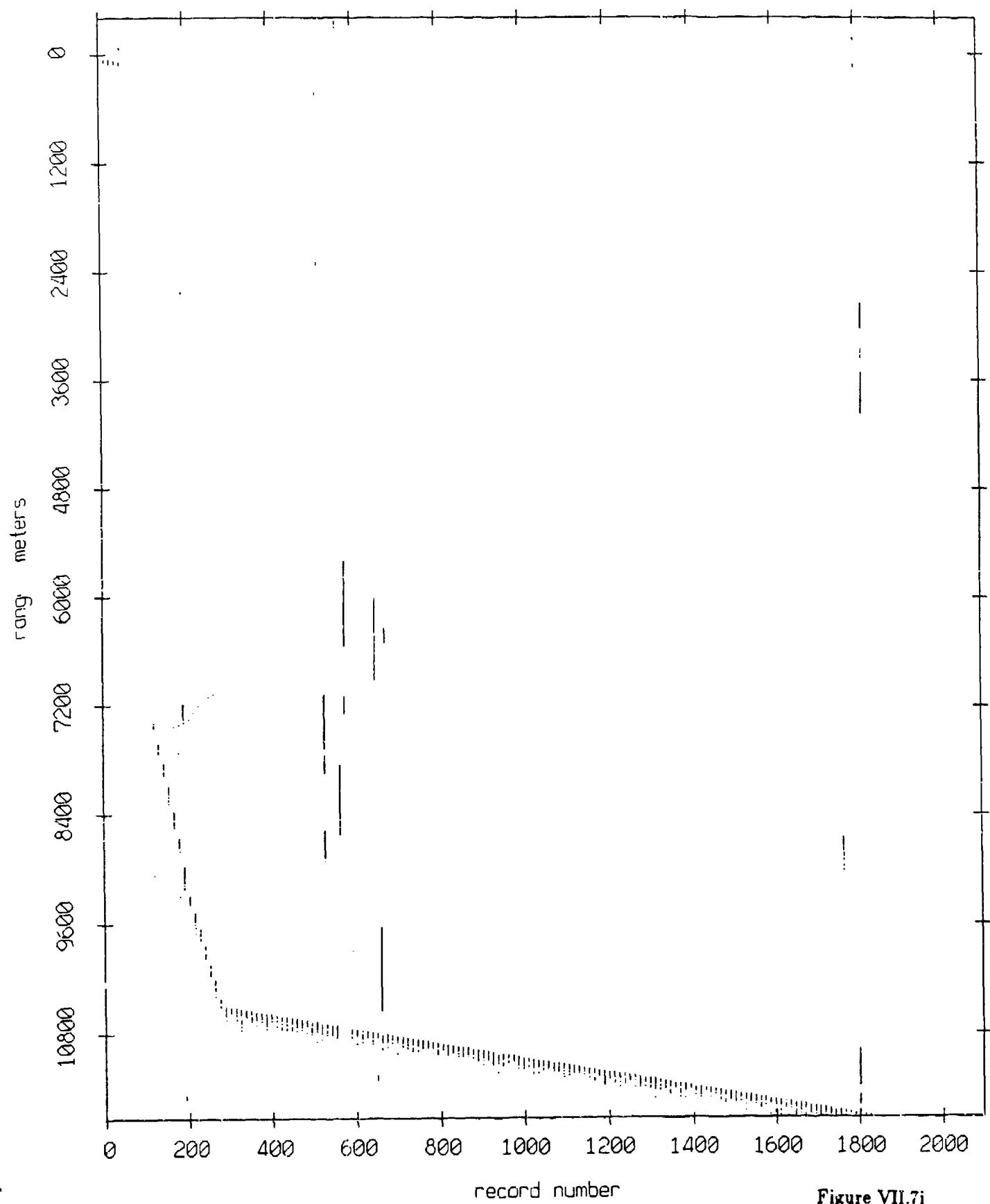


Figure VII.7i

Float 10, May, 1987 Sea Trip: range from float 0

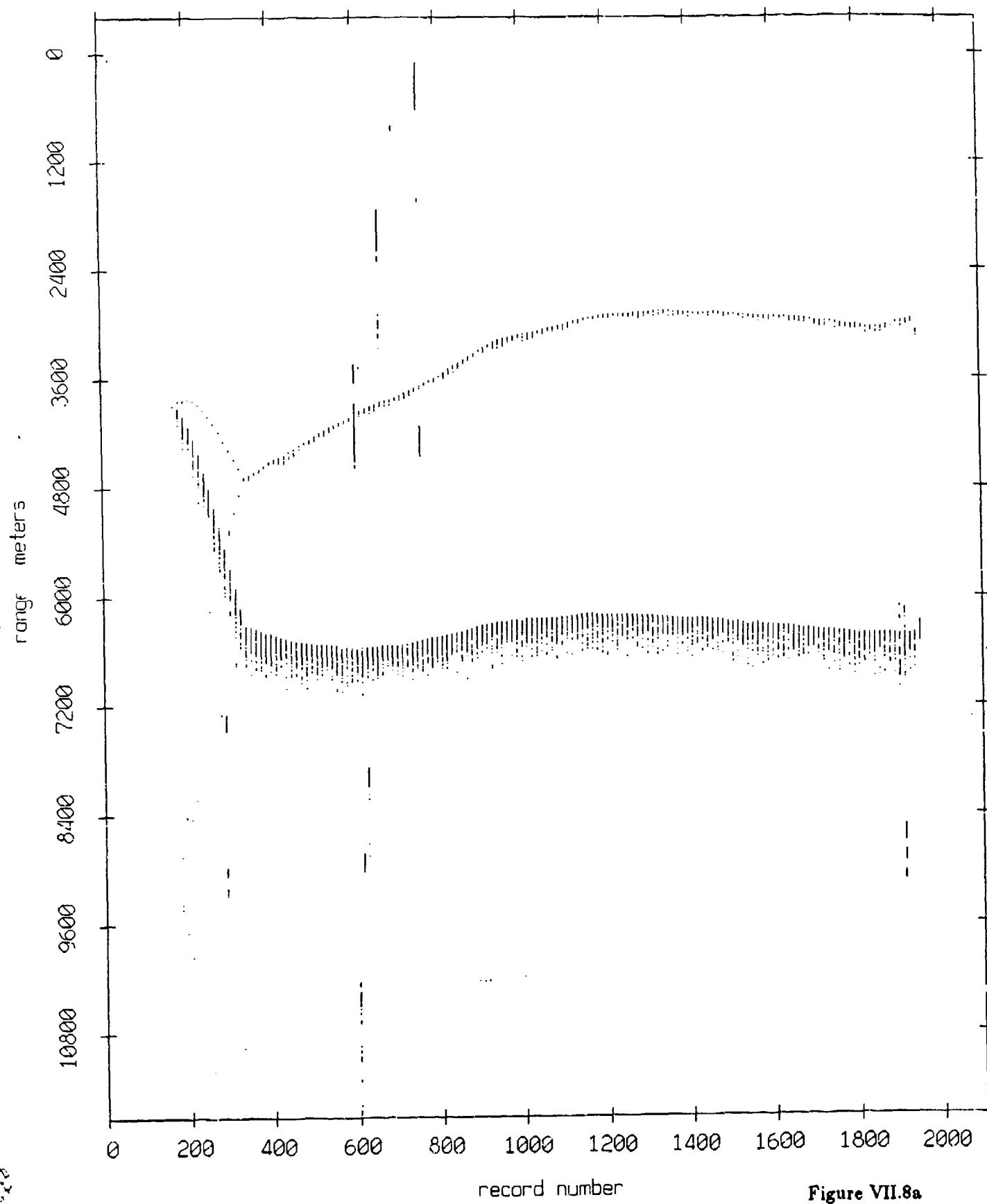


Figure VII.8a

Fleet 10, May, 1987 Sea Trip: range from float 1

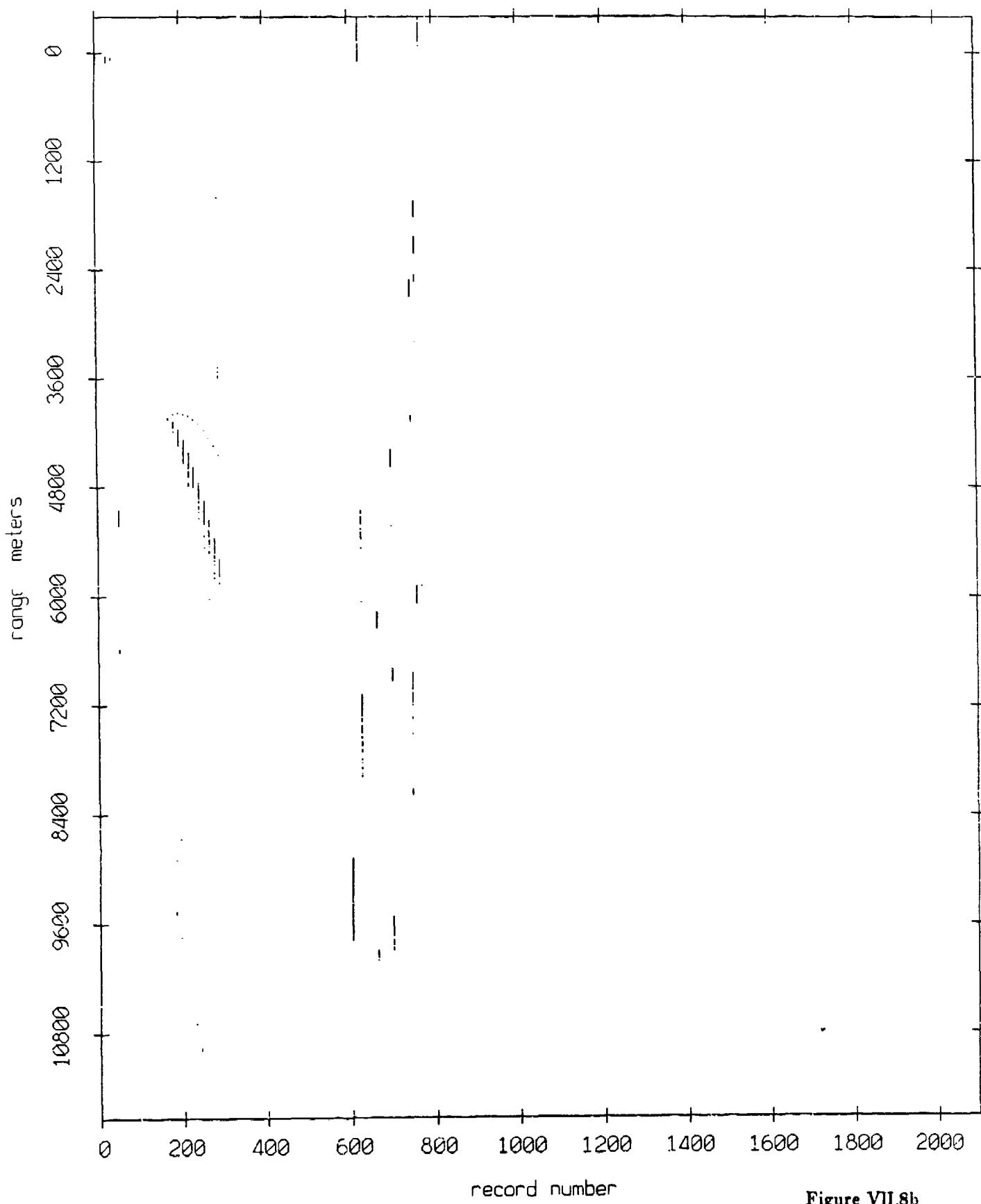


Figure VII.8b

Float 10, May, 1987 Sea Trip: range from float 2

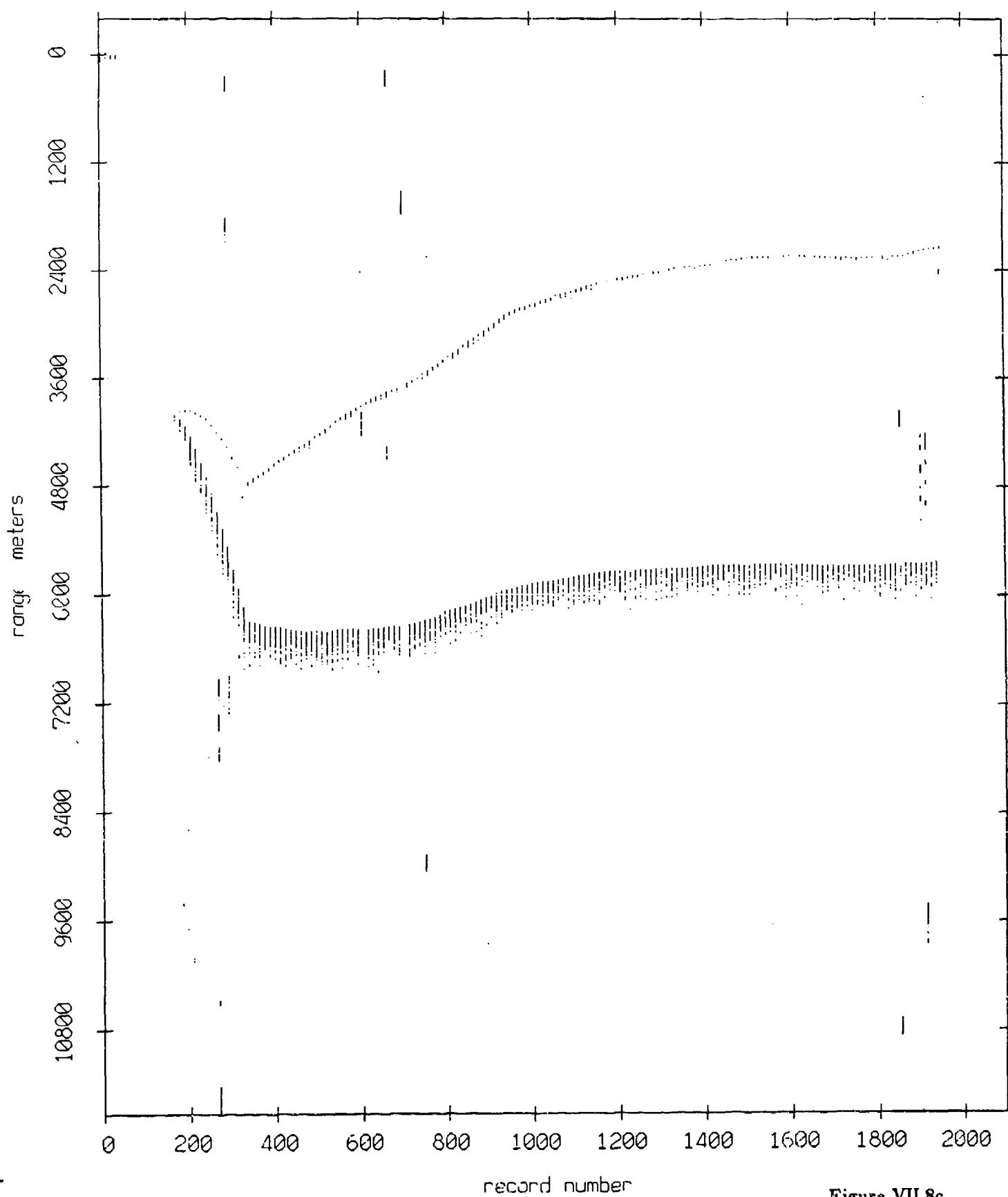


Figure VII.8c

Fleet 10, May, 1987 Sea Trip: range from float 3

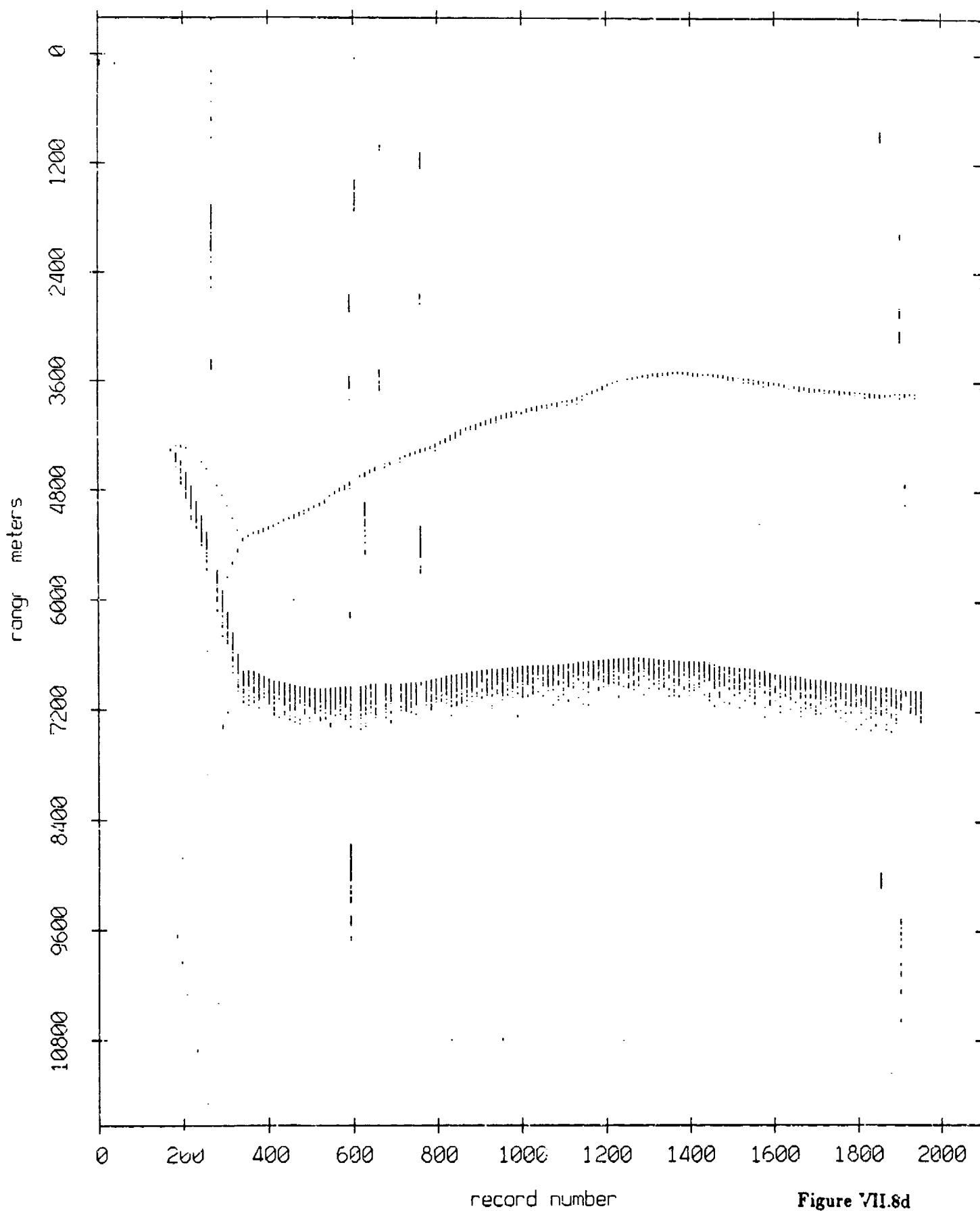


Figure VII.8d

Float 10, May, 1987 Sea Trip: range from float 4

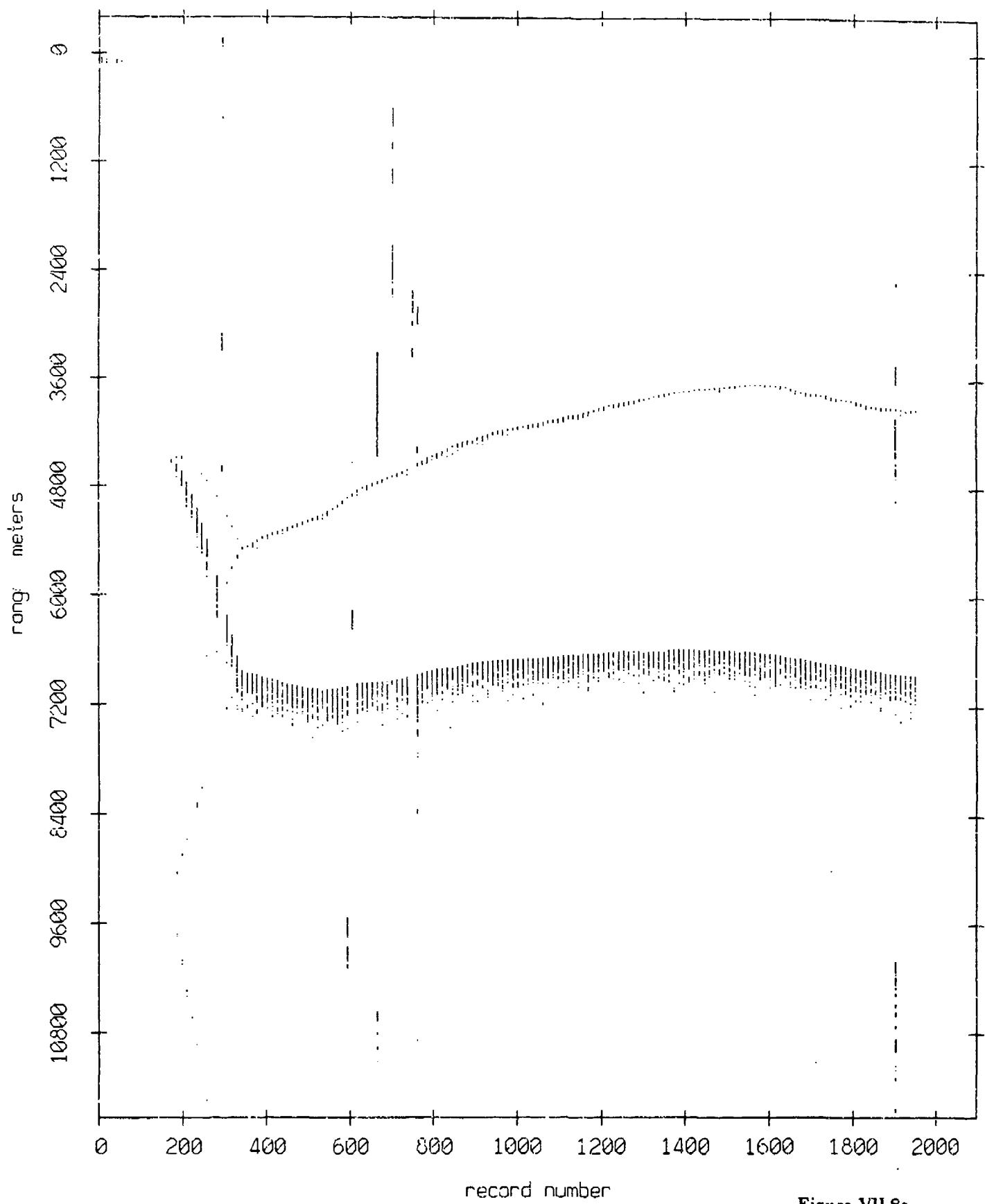


Figure VII.8e

Float 10, May, 1987 Sea Trip: range from float 7

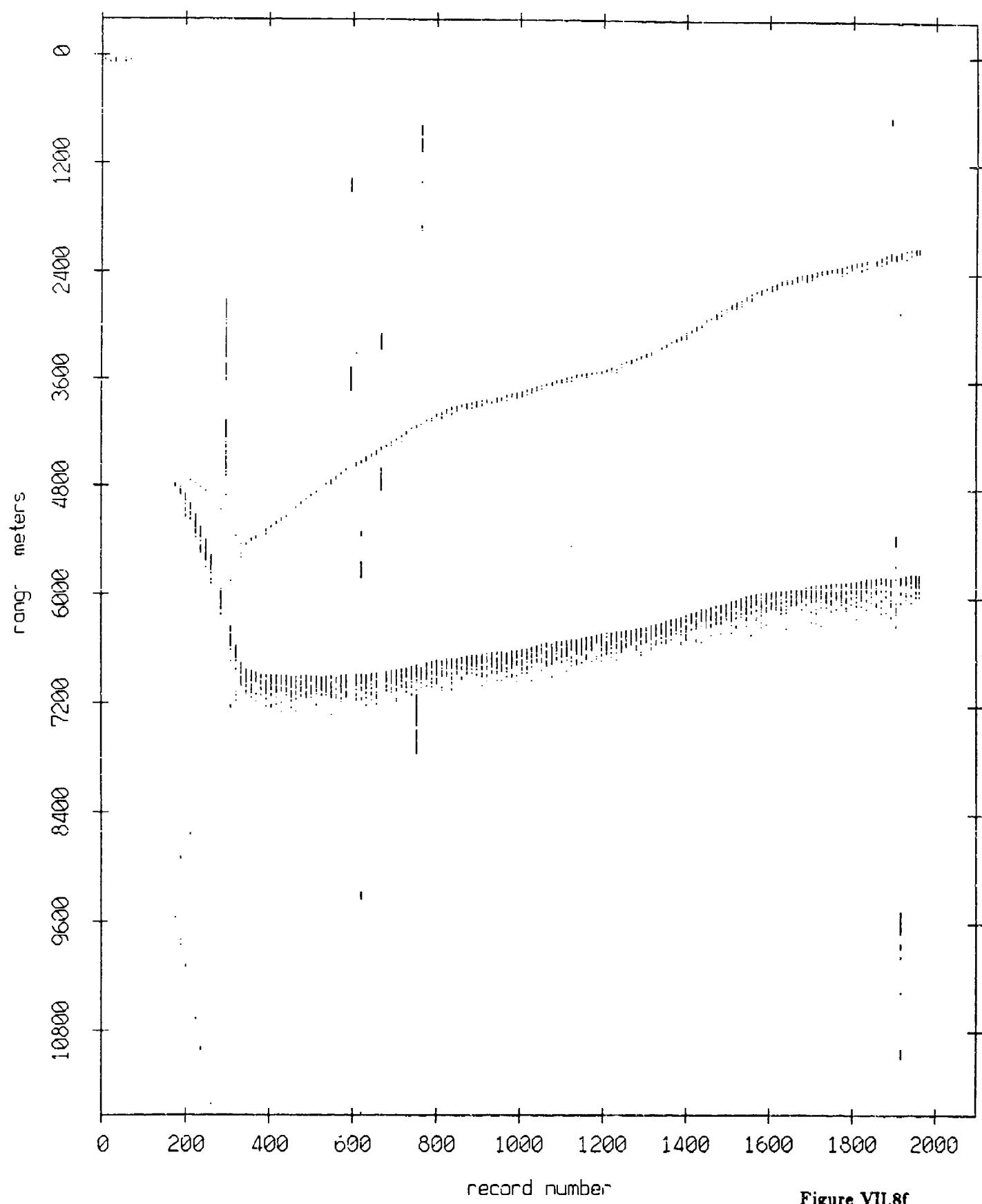


Figure VII.8f

Float 10, May, 1987 Sea Trip: range from float 8



Figure VII.8g

Float 10, May, 1987 Sea Trip: range from float 9

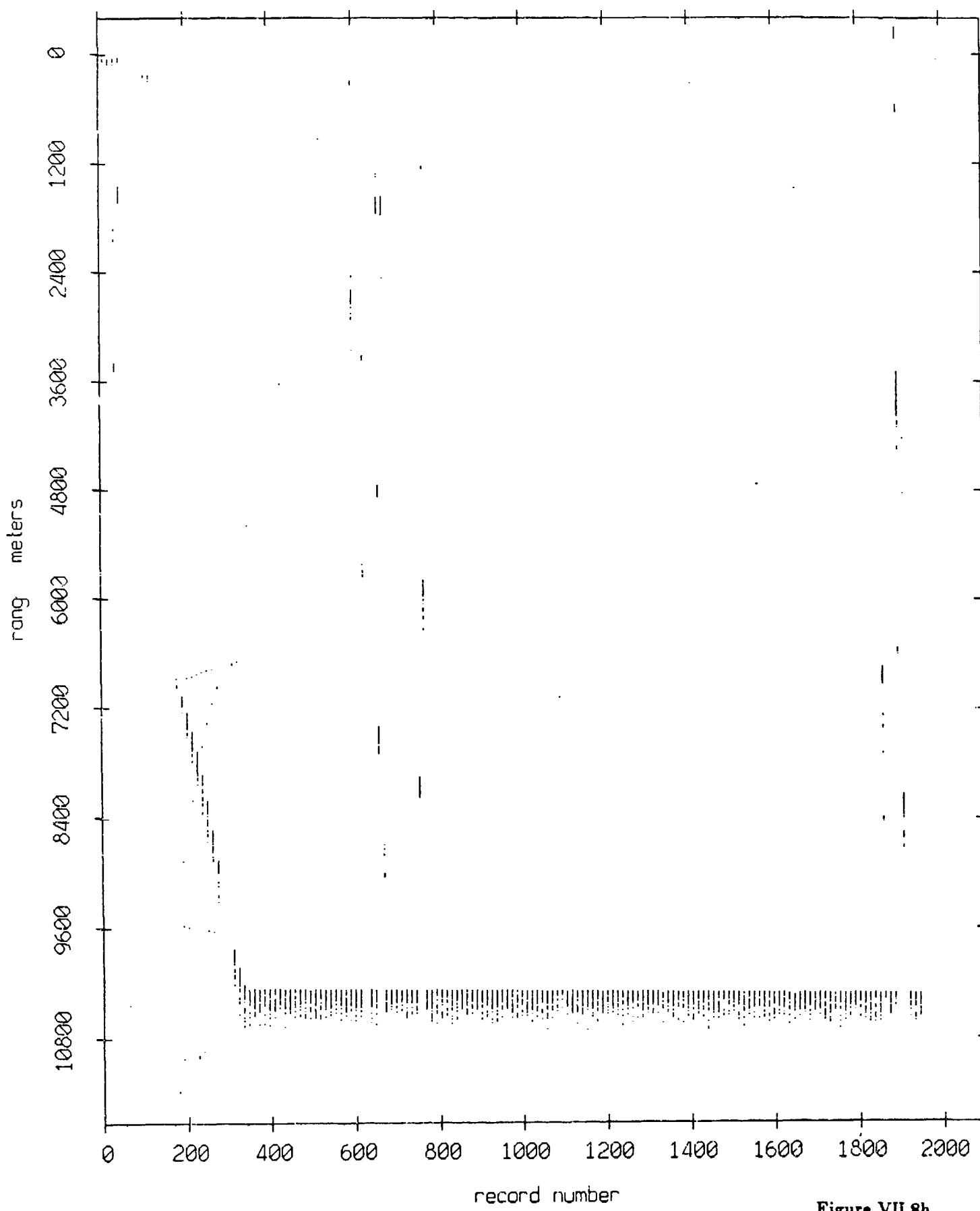


Figure VII.8h

Float 10, May, 1987 Sea Trip: range from float 11

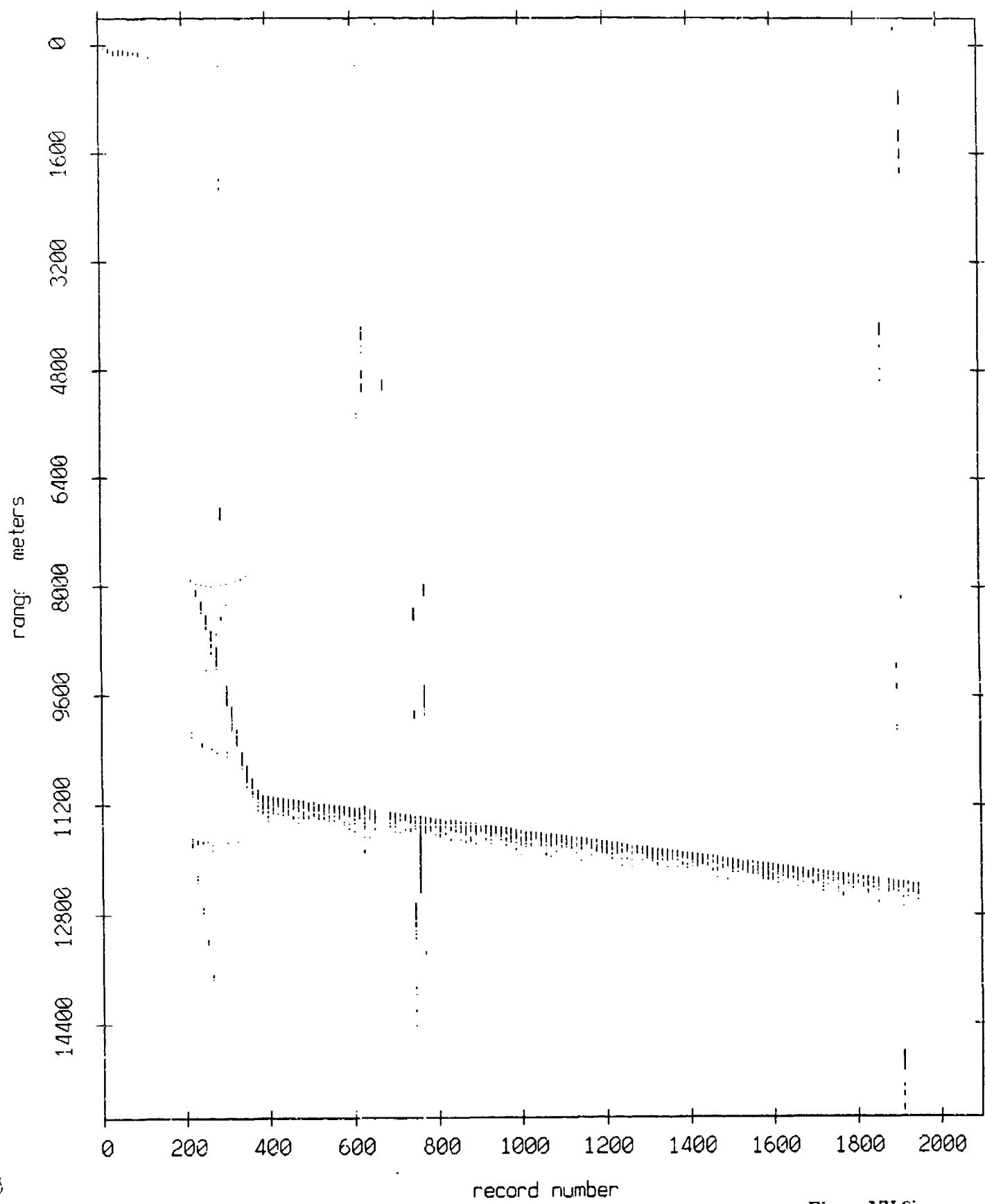


Figure VII.8i

Fleet 11, May, 1987 Sea Trip: range from float 8

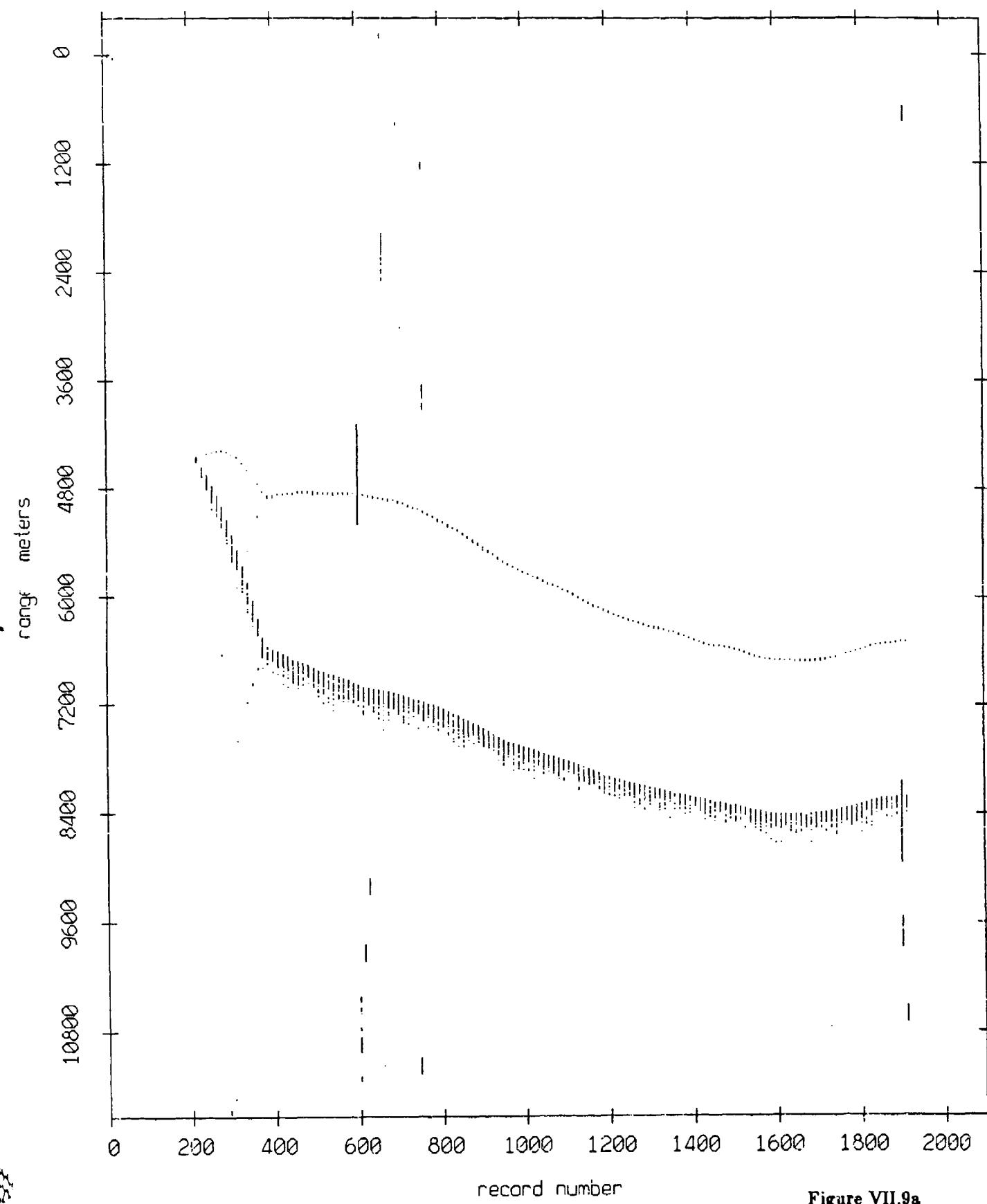


Figure VII.9a

Float 11, May, 1987 Sea Trip: range from float 1

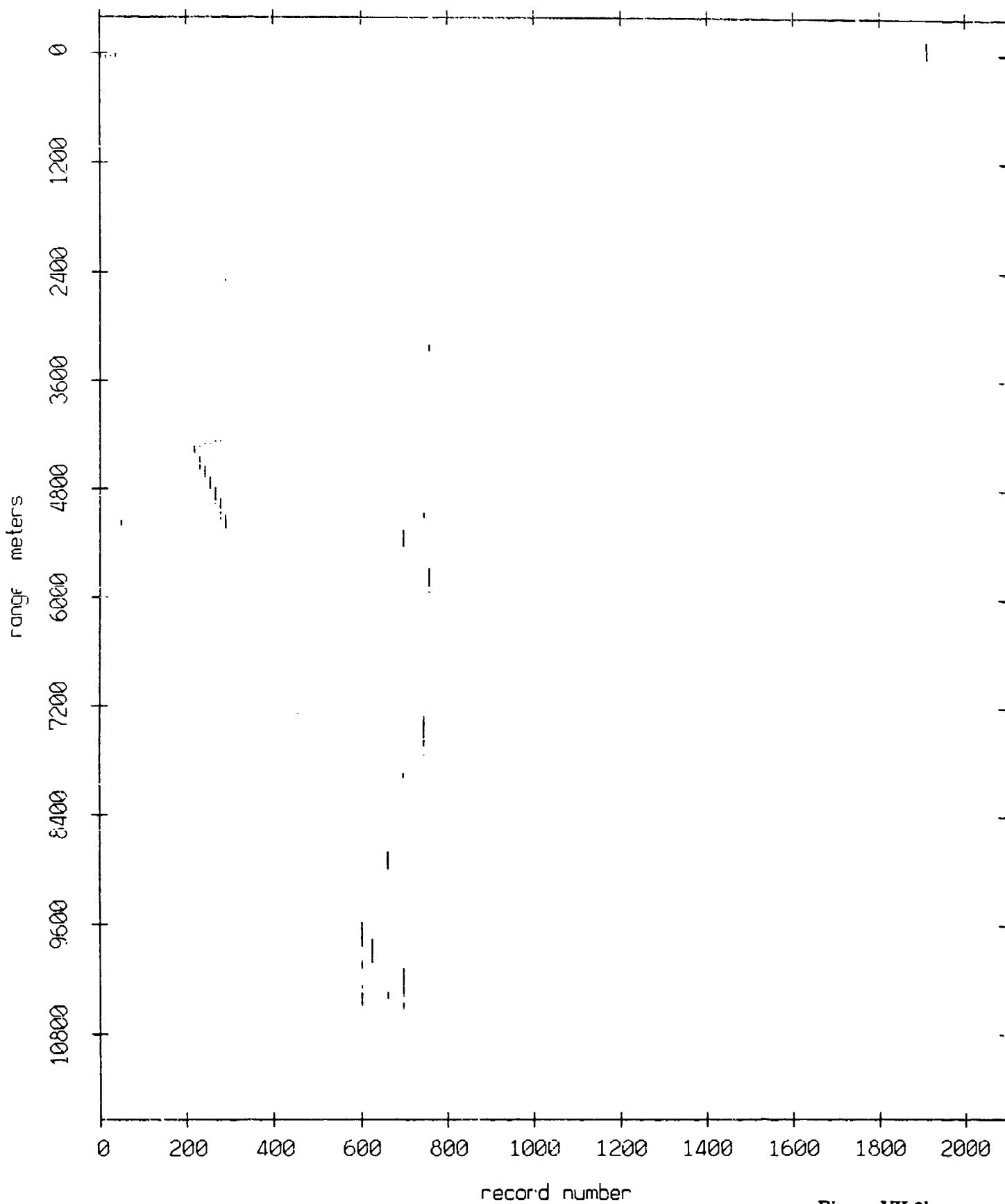


Figure VII.9b

Float 11, May, 1987 Sea Trip: range from float 2

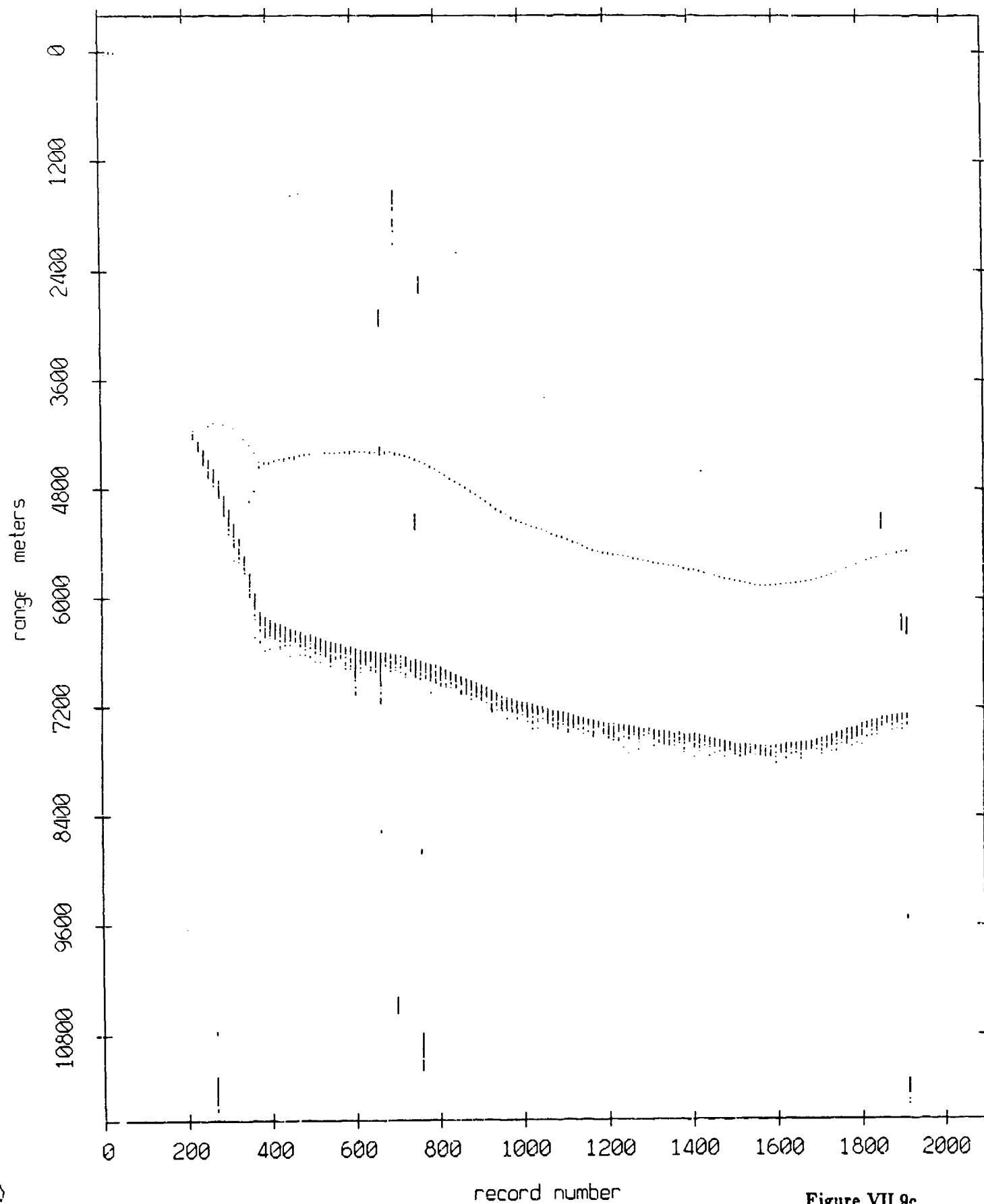


Figure VII.9c

Fleet 11, May, 1987 Sea Trip: range from float 3

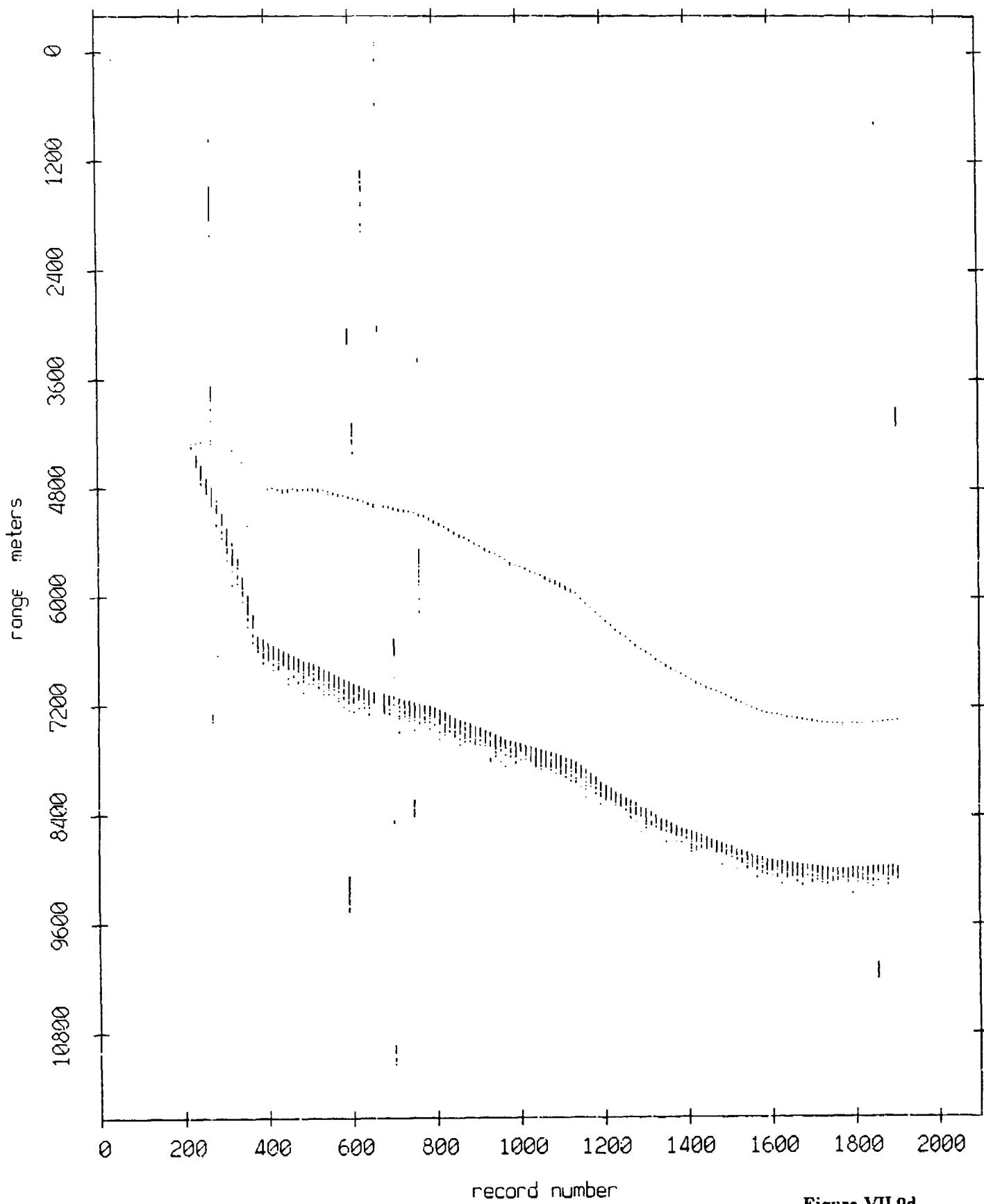


Figure VII.9d

Float 11, May, 1987 Sea Trip: range from float 4

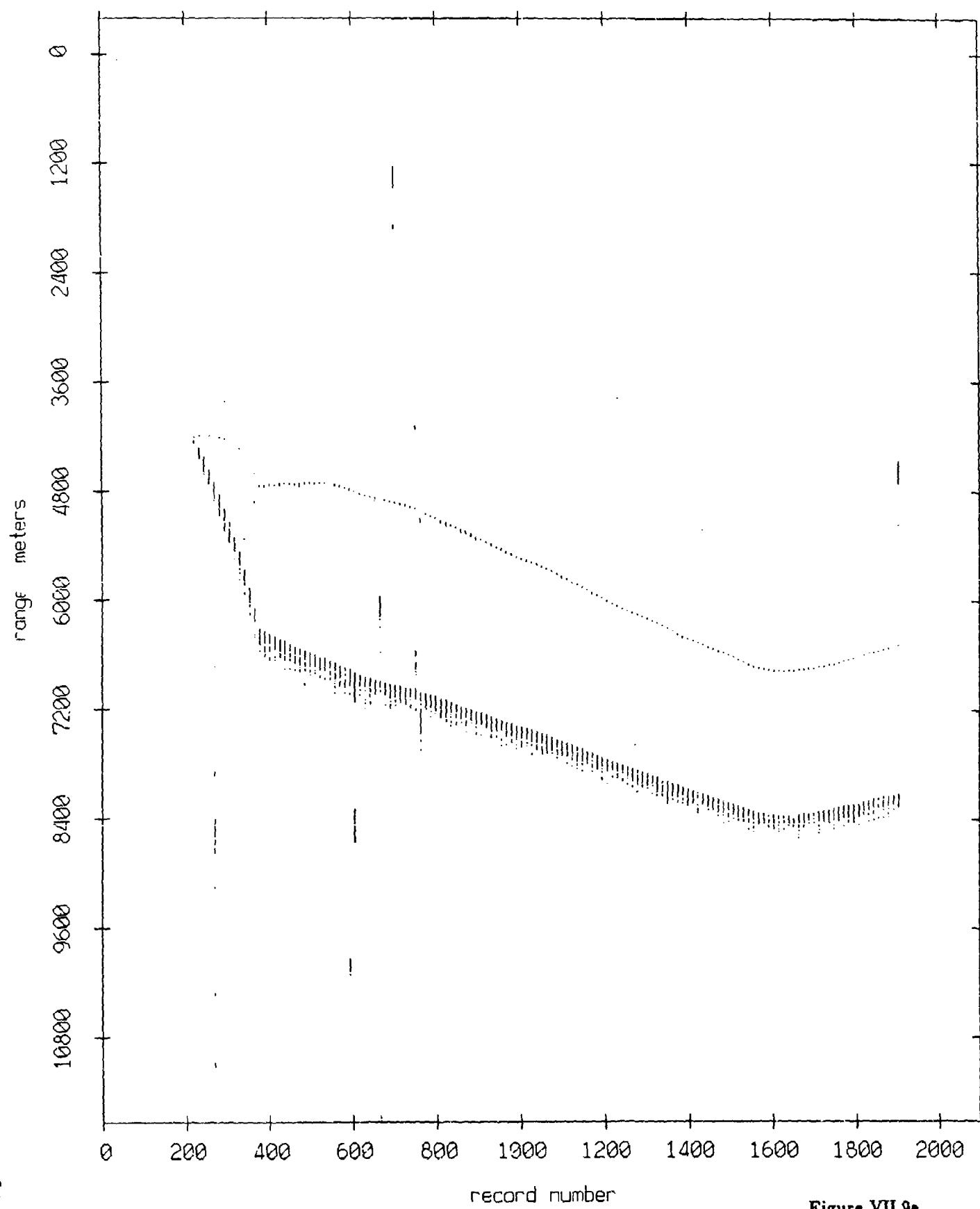


Figure VII.9e

Fleet 11, May, 1987 Sea Trip: range from float 7

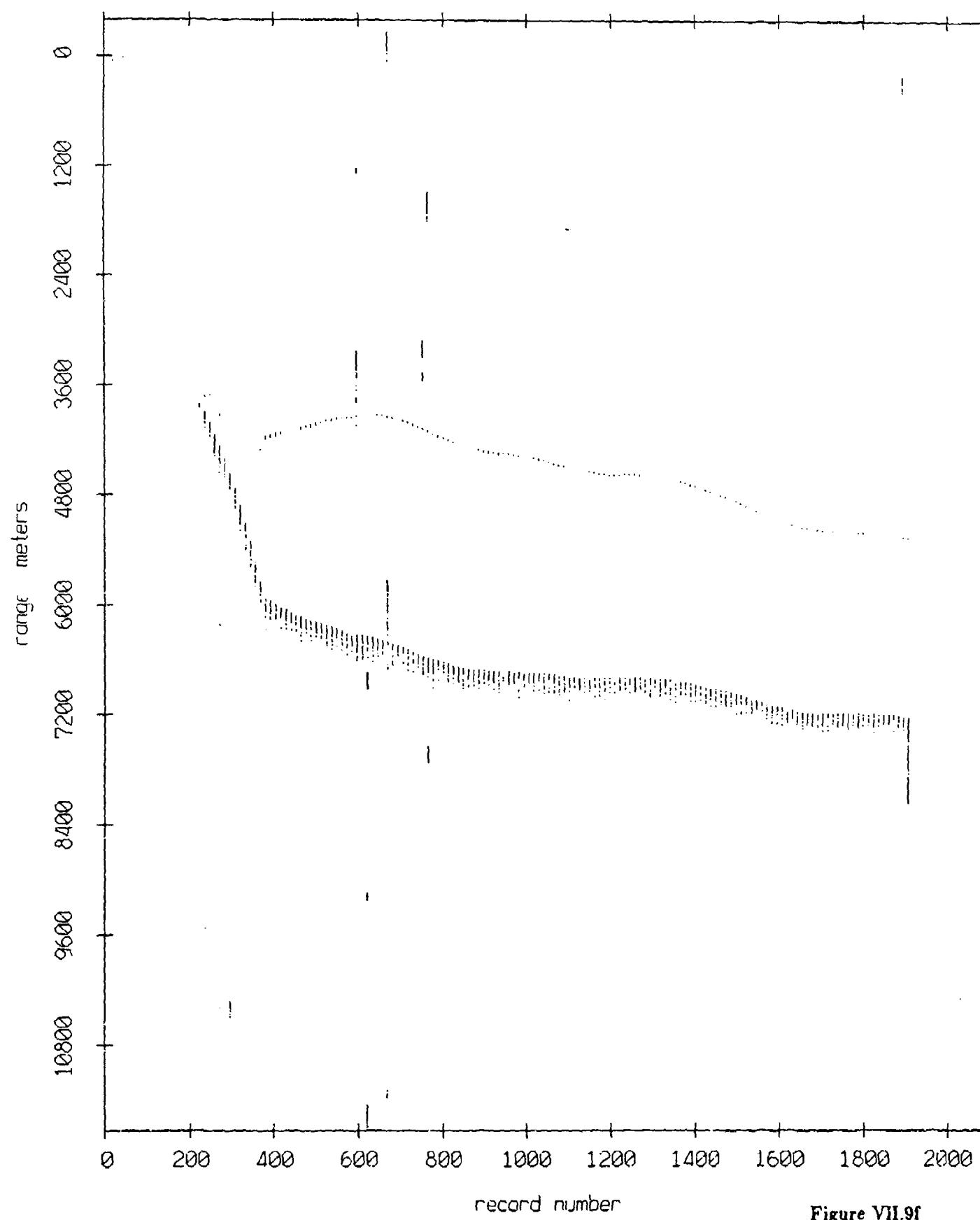


Figure VII.9f

Float 11, May, 1987 Sea Trip: range from float 8

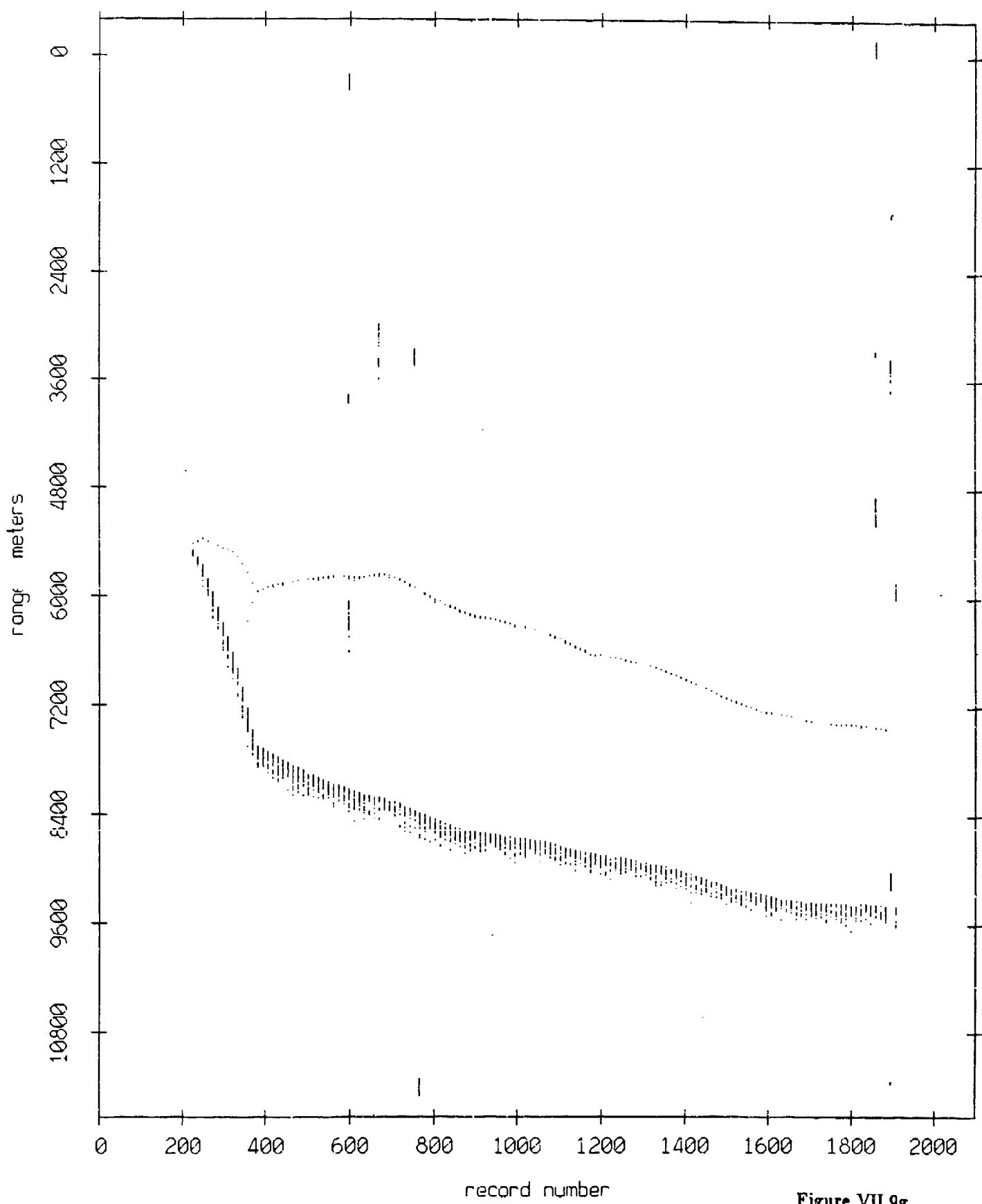


Figure VII.9g

Fleet 11, May, 1987 Sea Trip: range from float 9

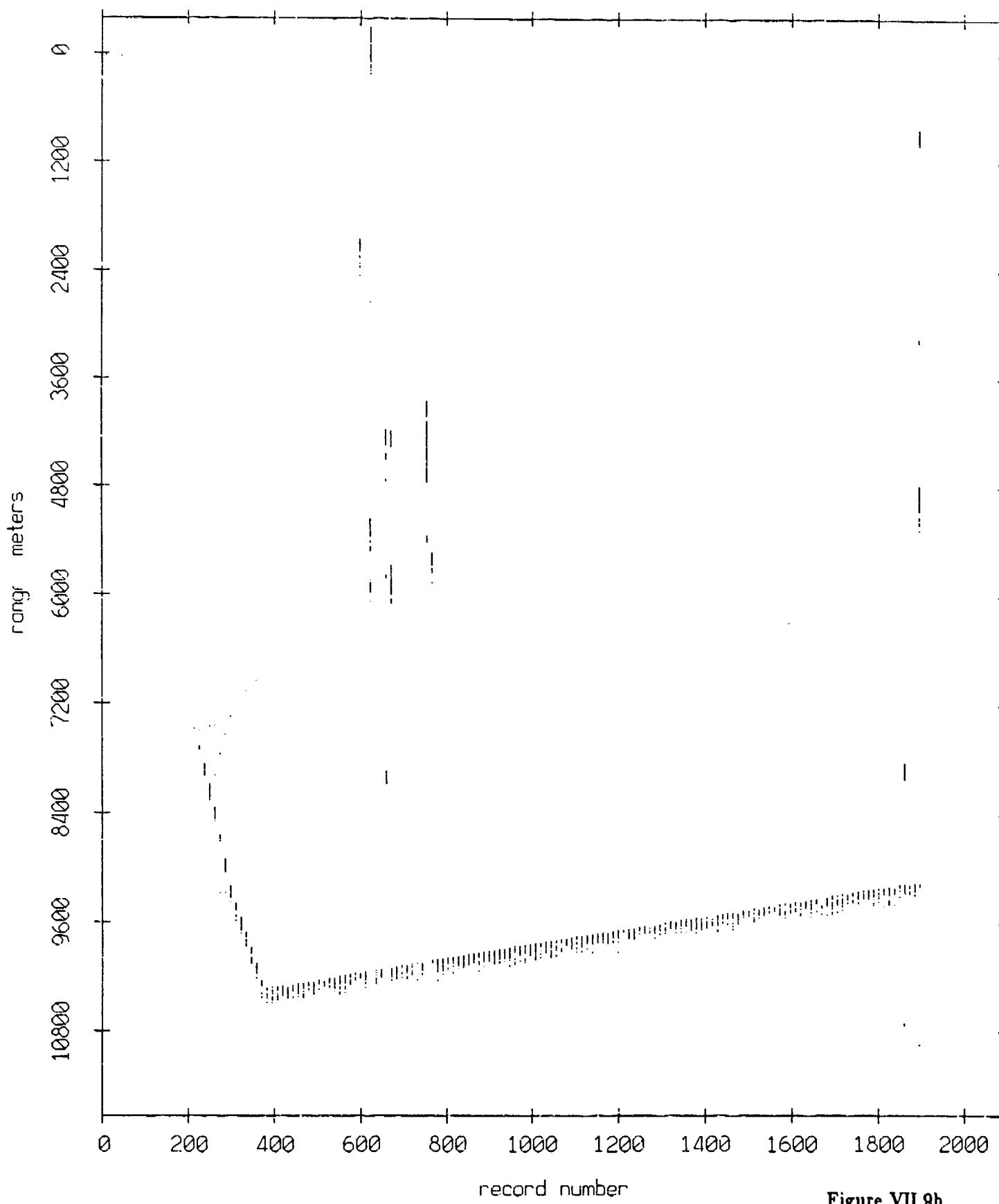


Figure VII.9h

Float 11, May, 1987 Sea Trip: range from float 10

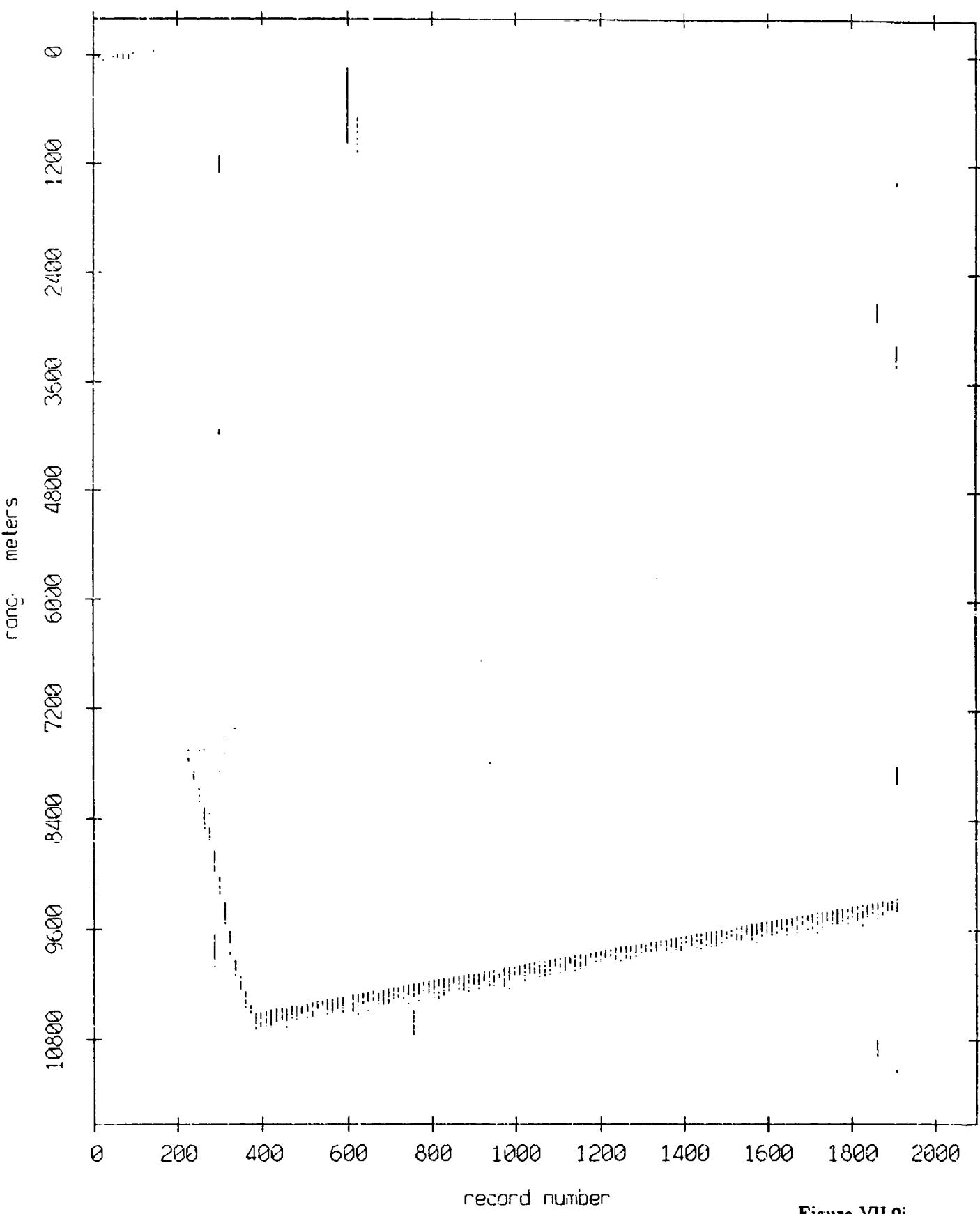


Figure VII.9i

AGC Level and Buoy Heading, Float 0, May 1987 Sea Trip

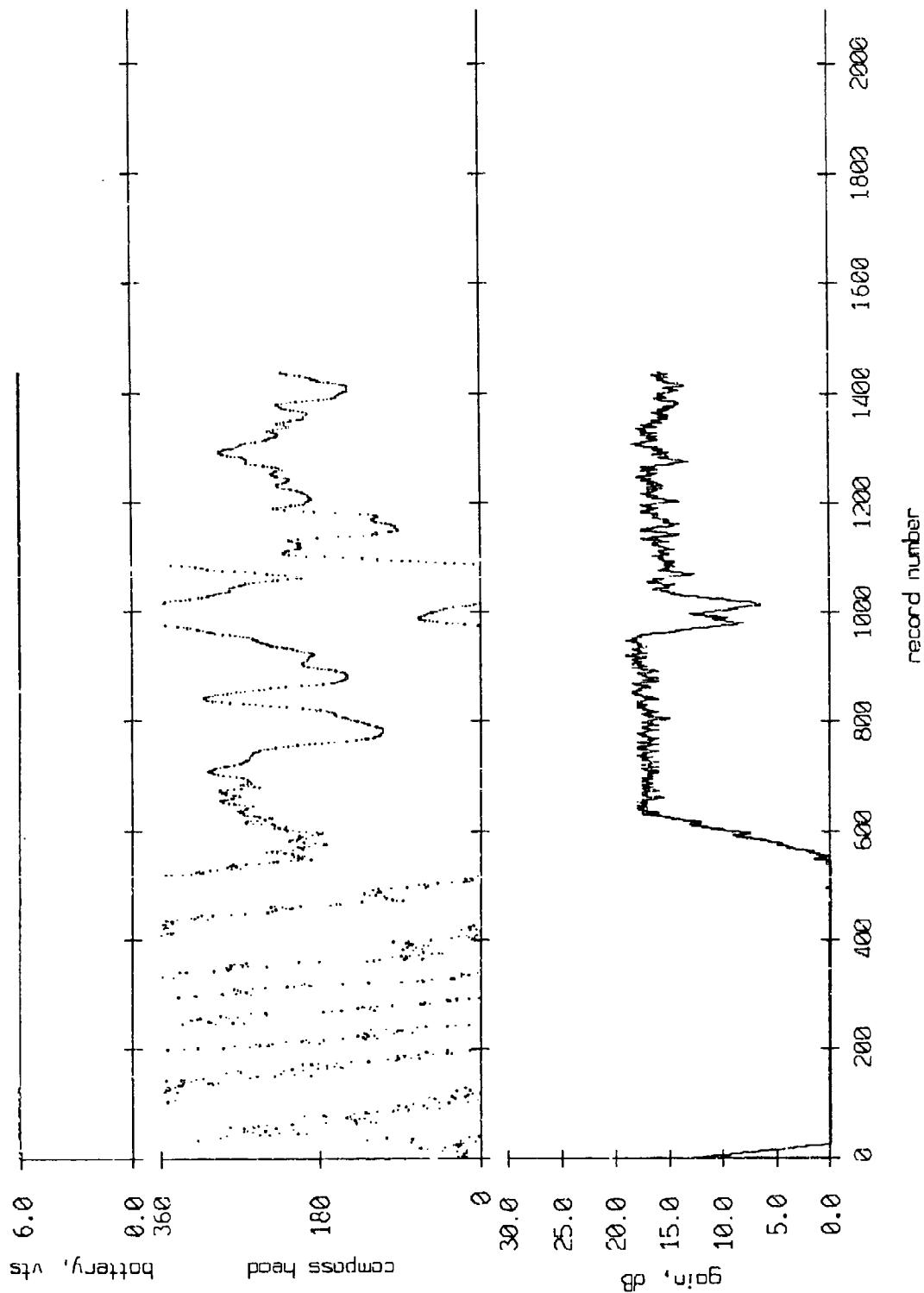


Figure VIII.1

AGC Level and Buoy Heading, Float 1, May 1987 Sea Trip

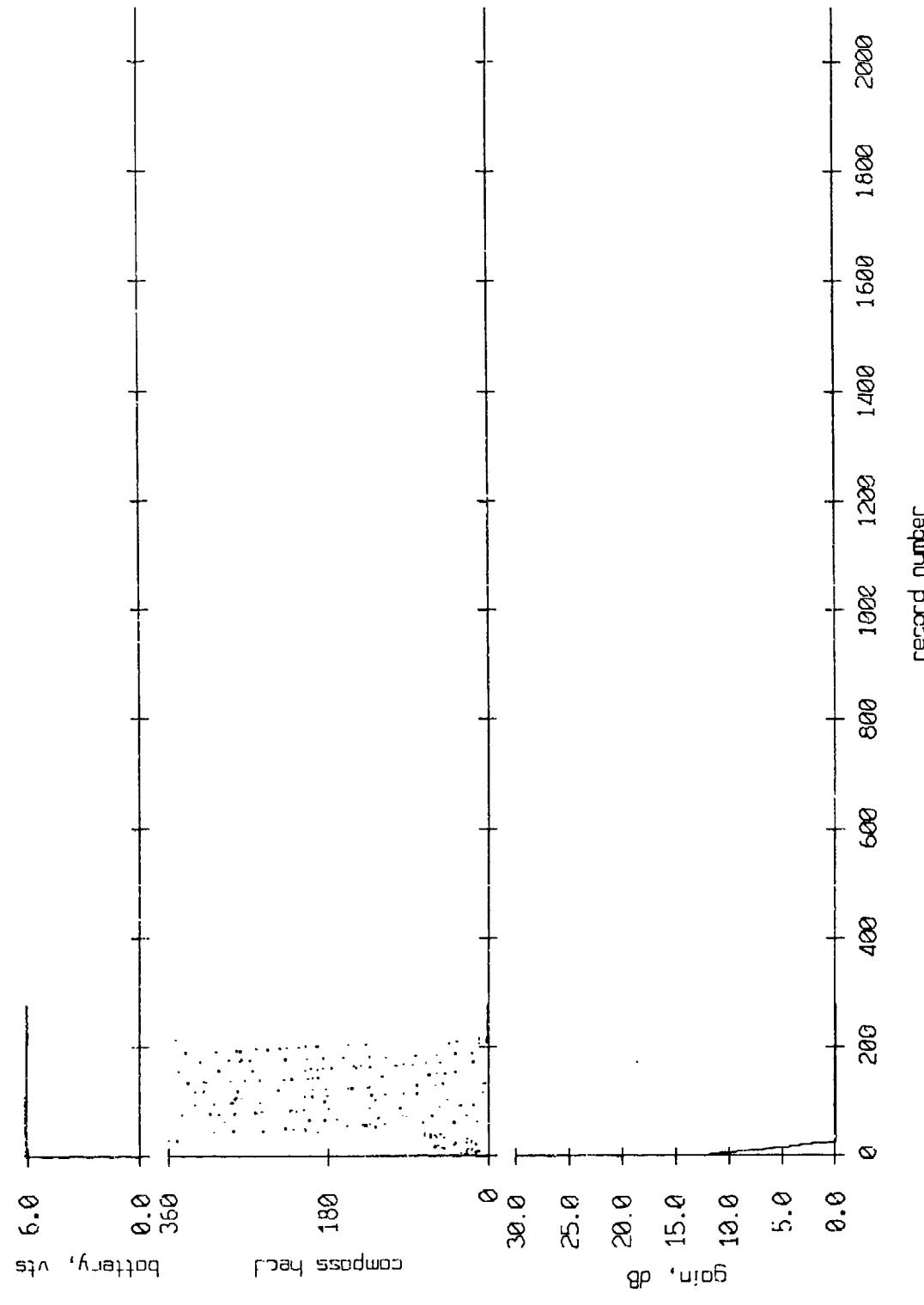


Figure VIII.2

AGC Level and Buoy Heading, Float 2, May 1987 Sea Trip

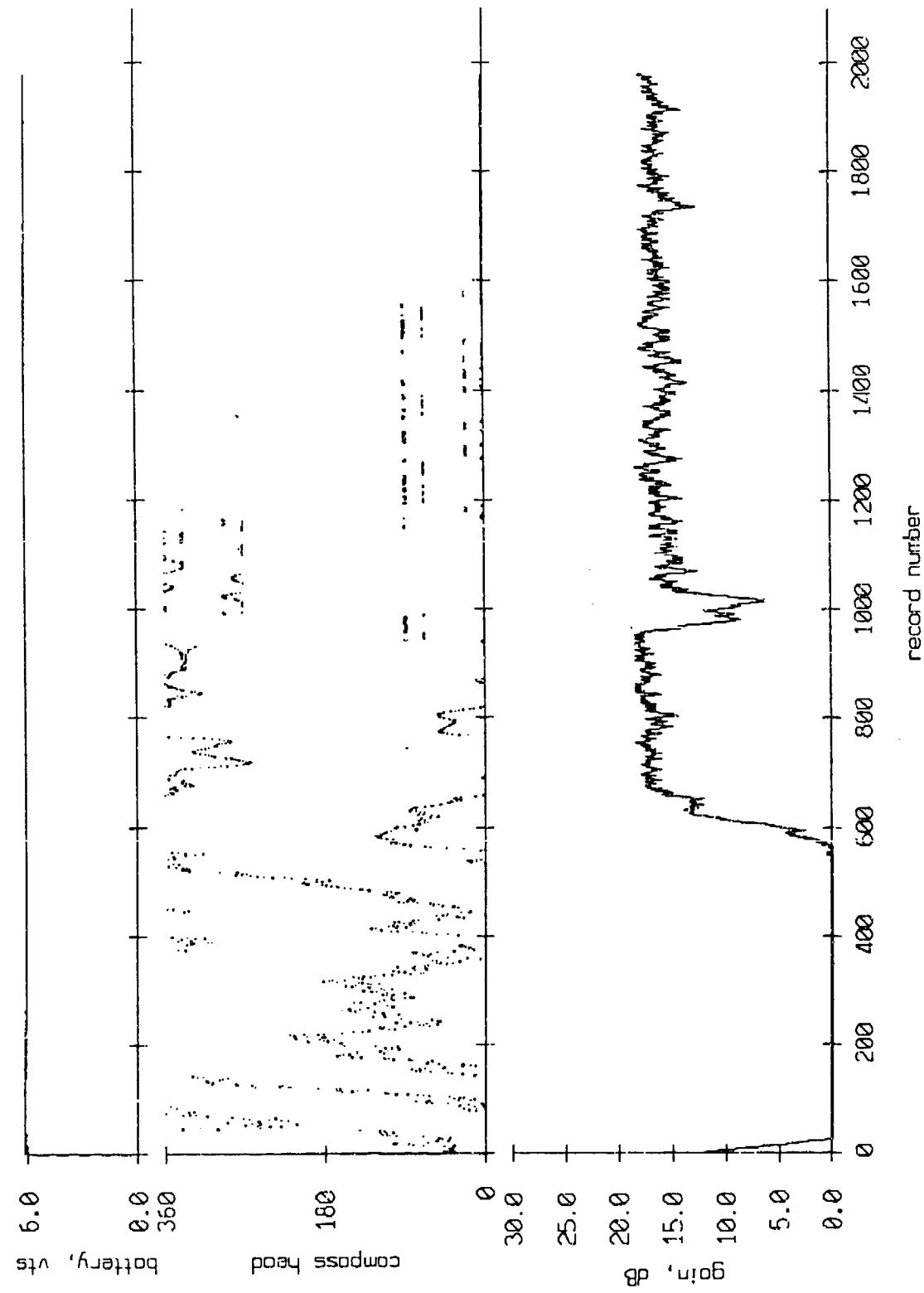


Figure VIII.3

AGC Level and Buoy Heading, Float 3, May 1987 Sea Trip

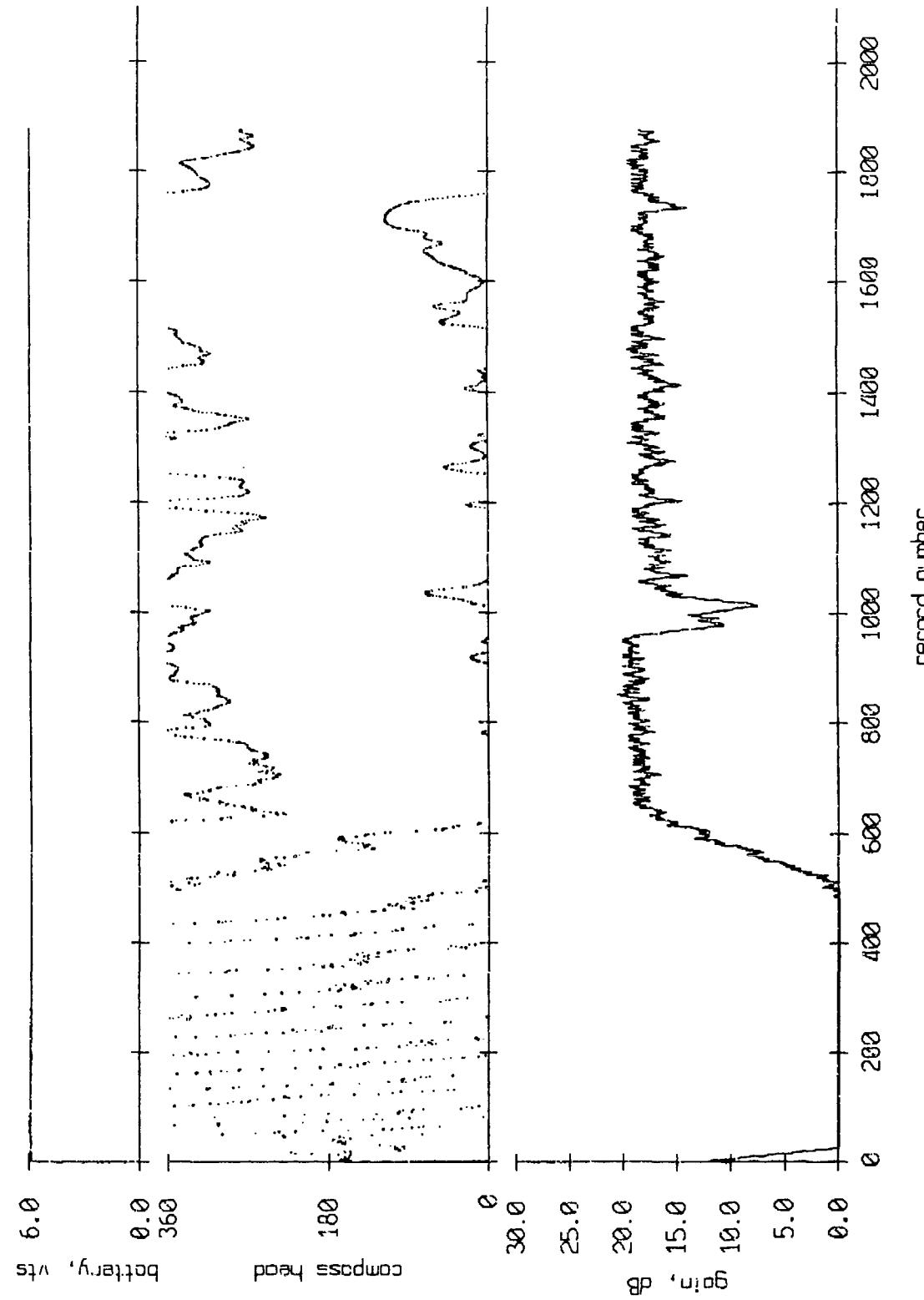


Figure VIII.4

AGC Level and Buoy Heading, Float 4, May 1987 Sea Trip

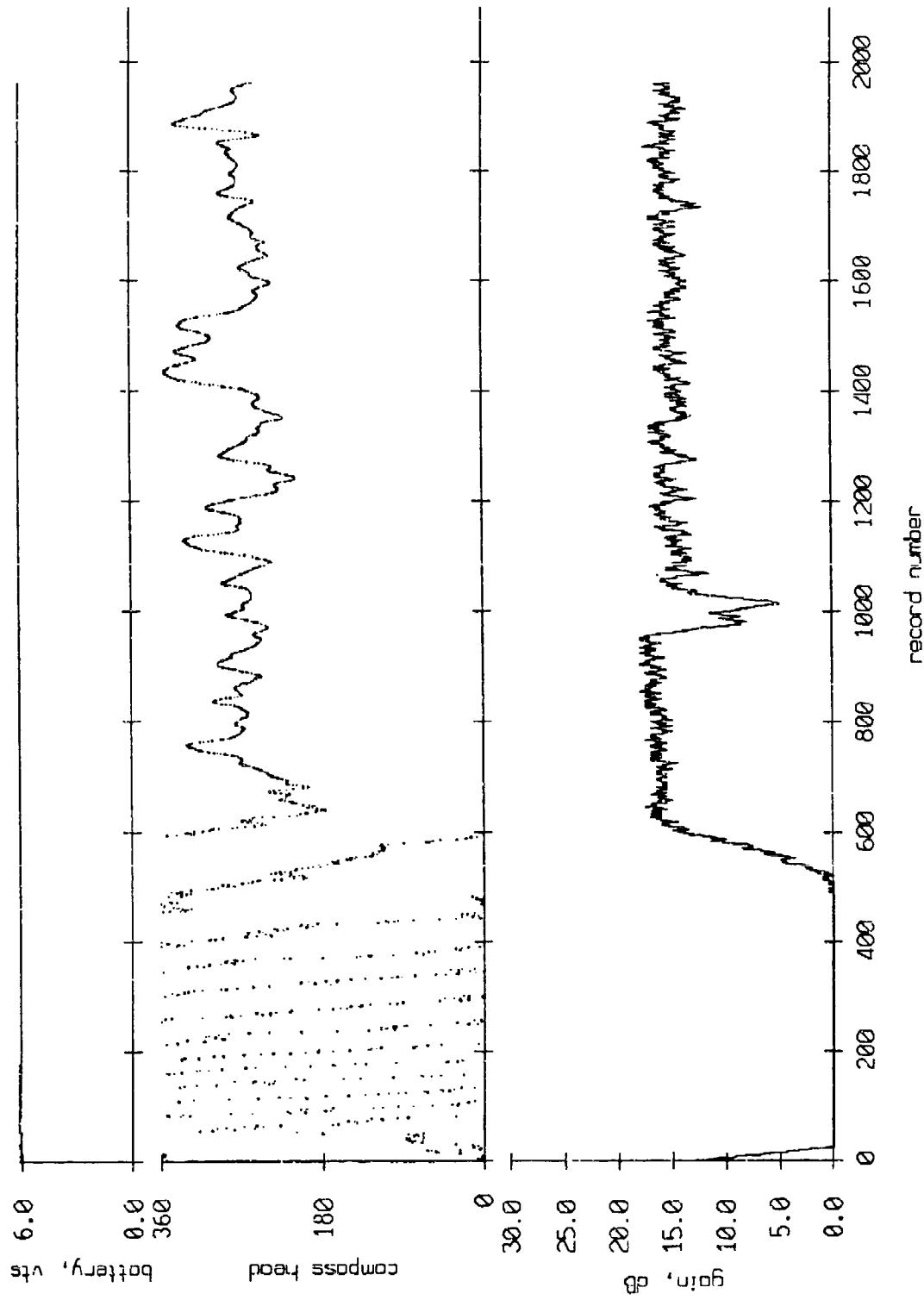


Figure VIII.5

AGC Level and Buoy Heading, Float 7, May 1987 Sea Trip

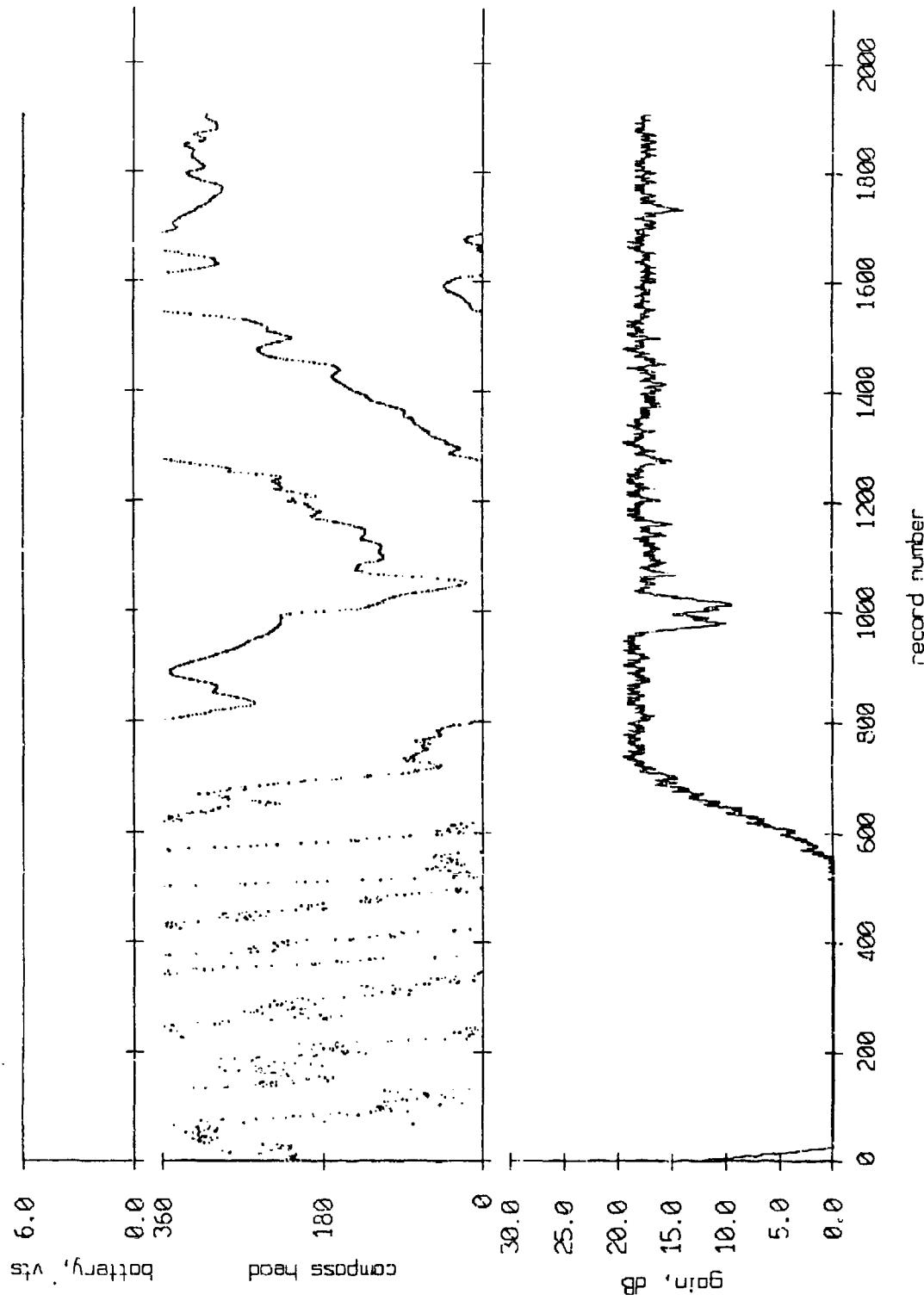


Figure VIII.6

AGC Level and Buoy Heading, Float 8, May 1987 Sea Trip

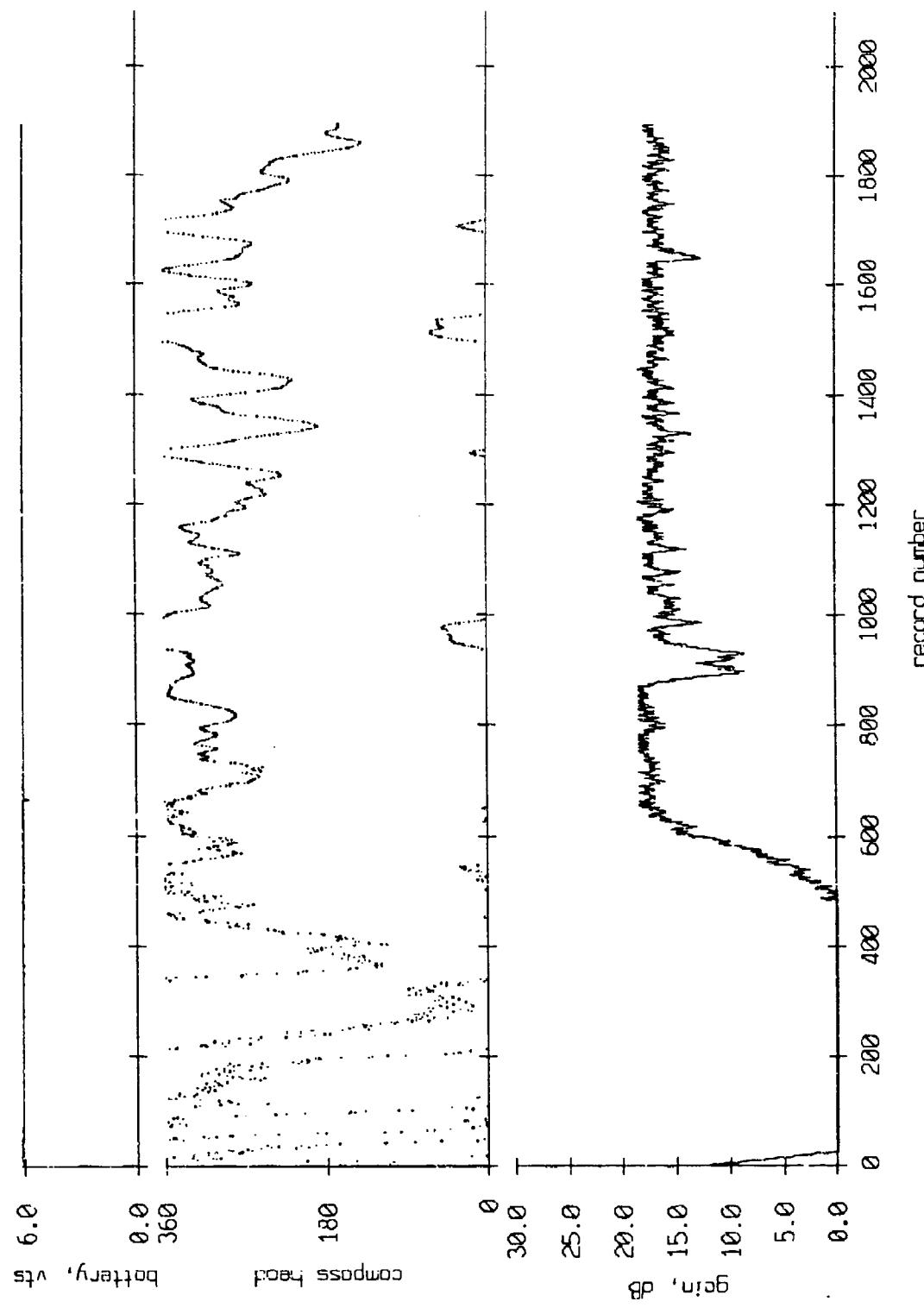


Figure VIII.7

ACC Level and Buoy Heading, Float 9, May 1987 Sea Trip

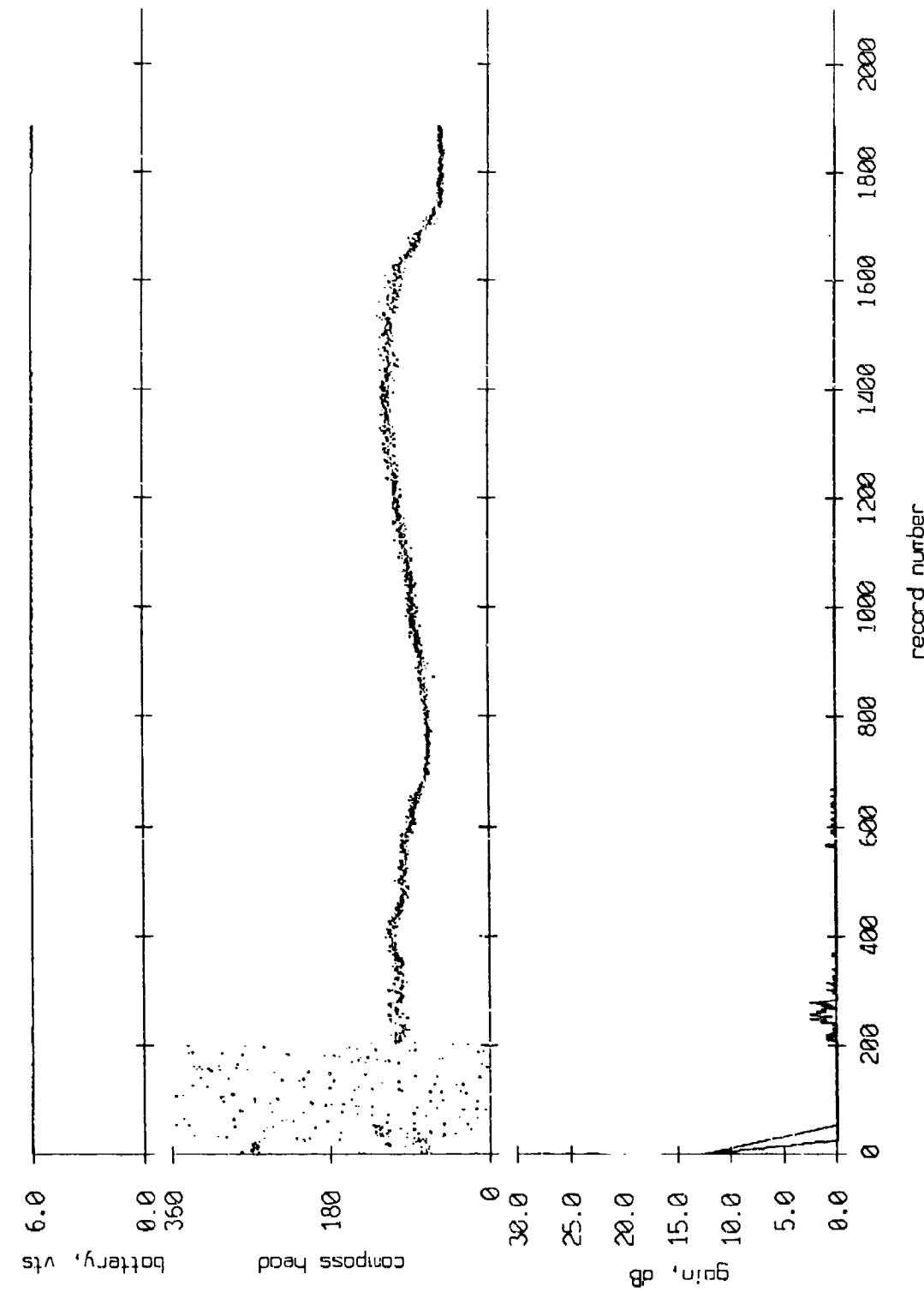


Figure VIII.8

AGC Level and Buoy Heading, Float 10, May 1987 Sea Trip

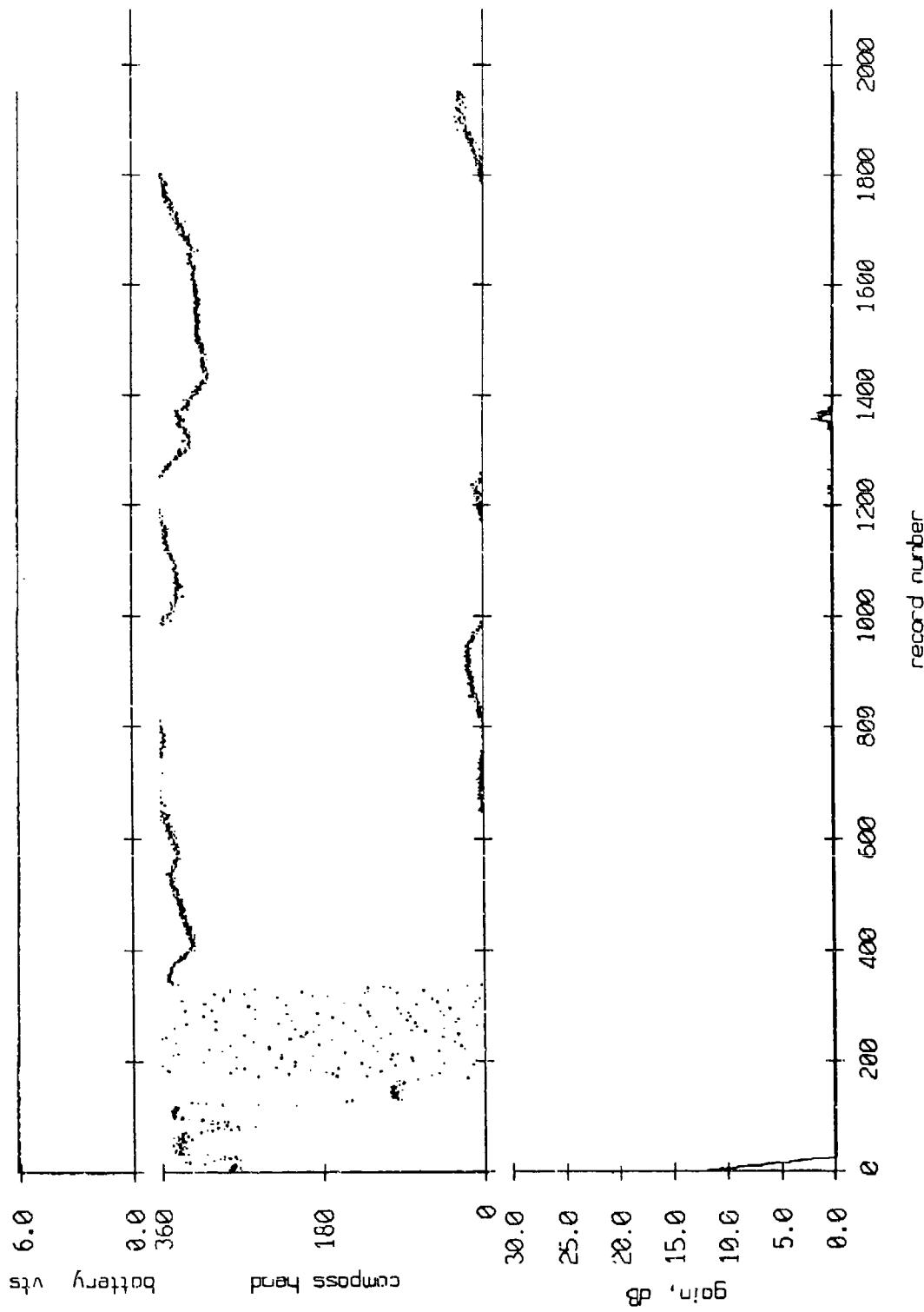


Figure VIII.9

AGC Level and Buoy Heading, Float 11, May 1987 Sea Trip

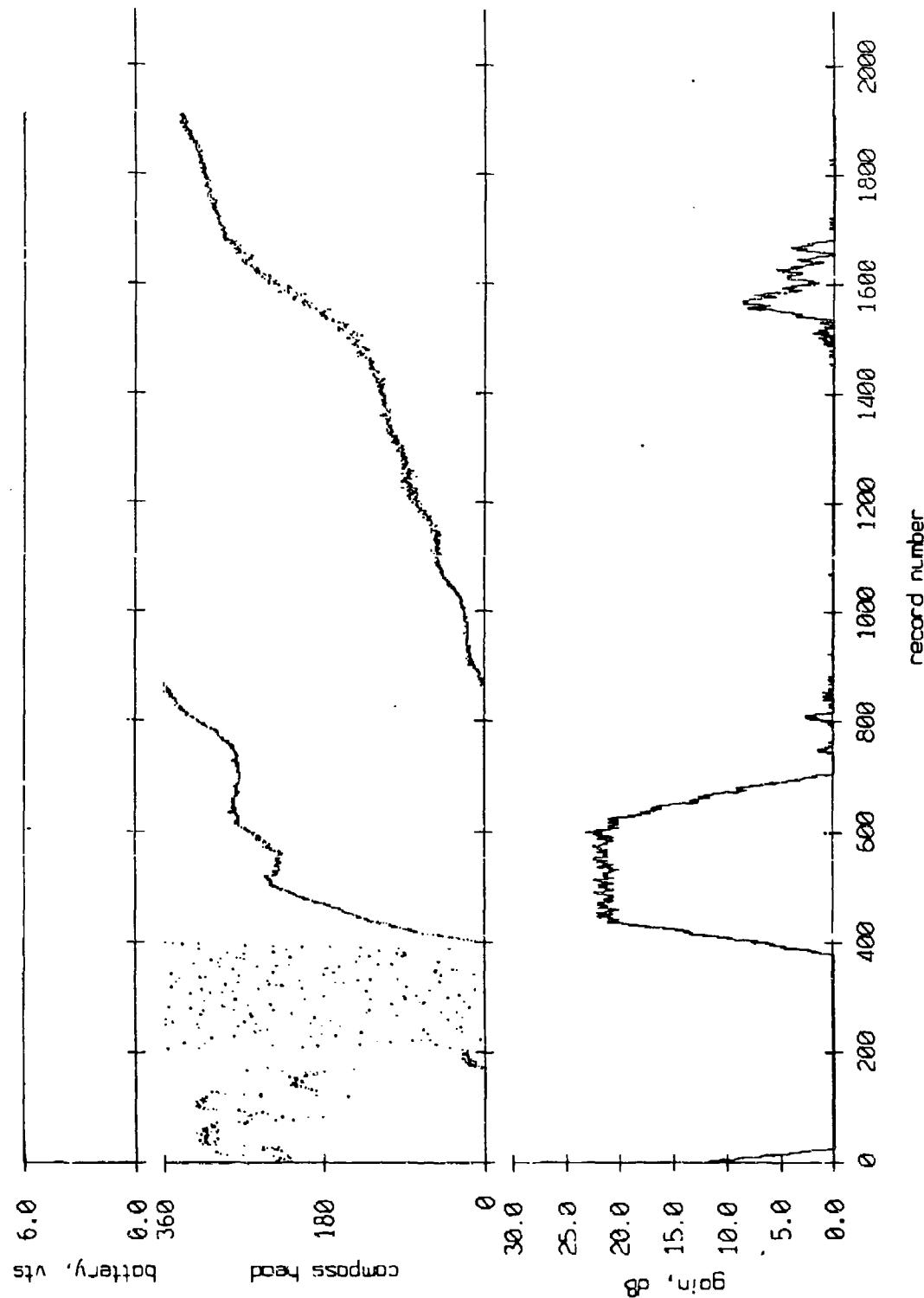


Figure VIII.10

Float 0, May, 1987 Deployment
averaging period = 5.00 sec.

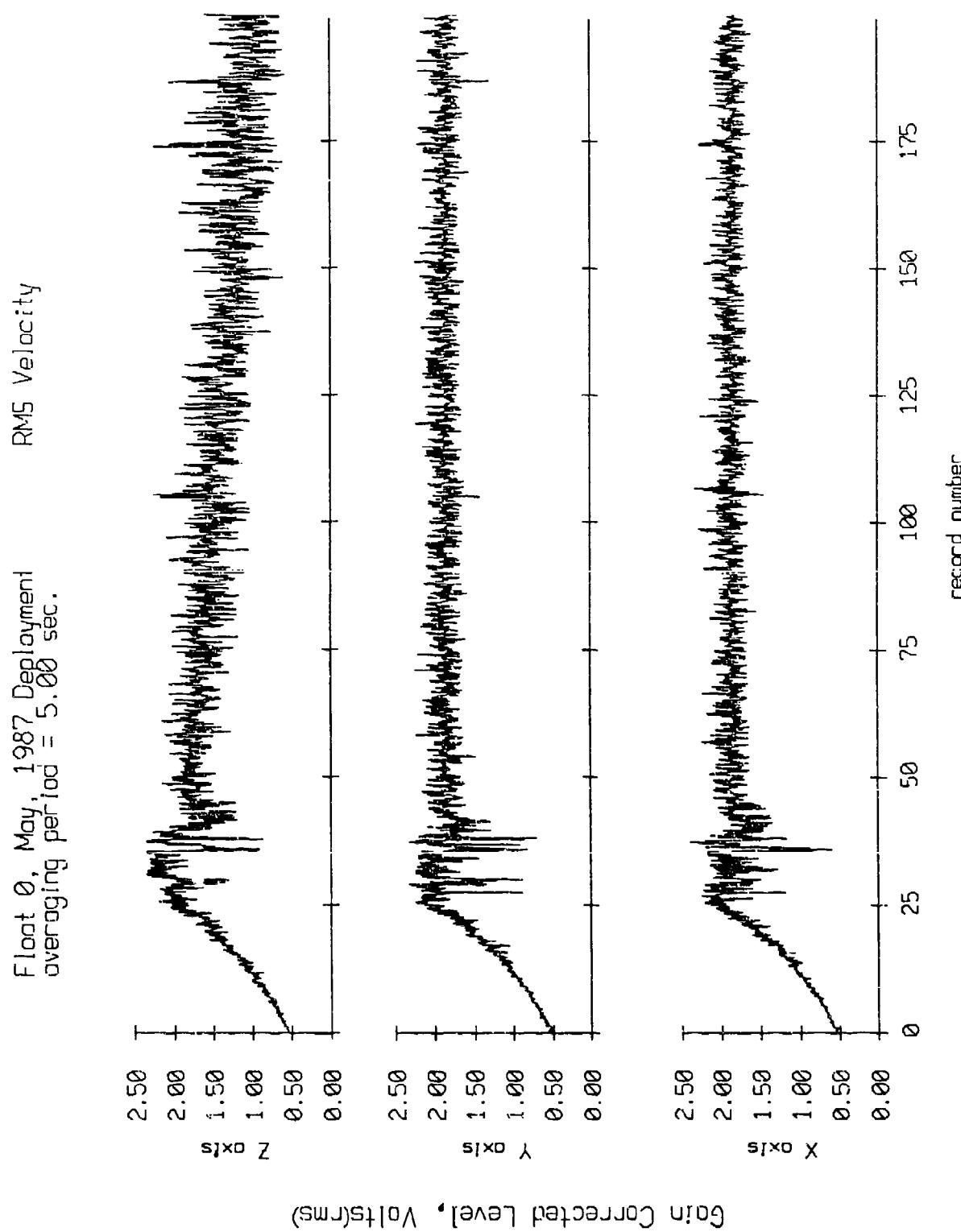


Figure IX.1a

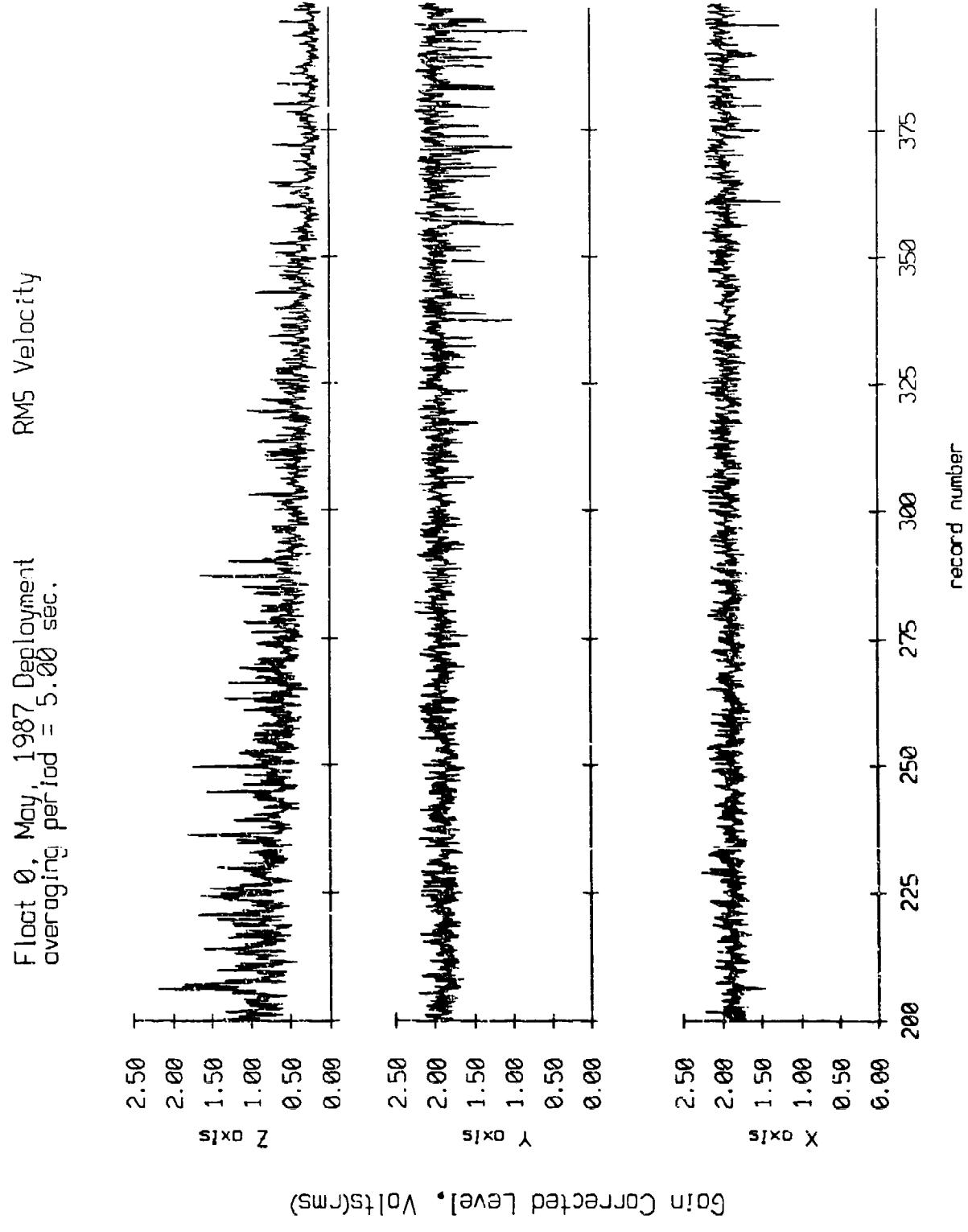


Figure IX.1b

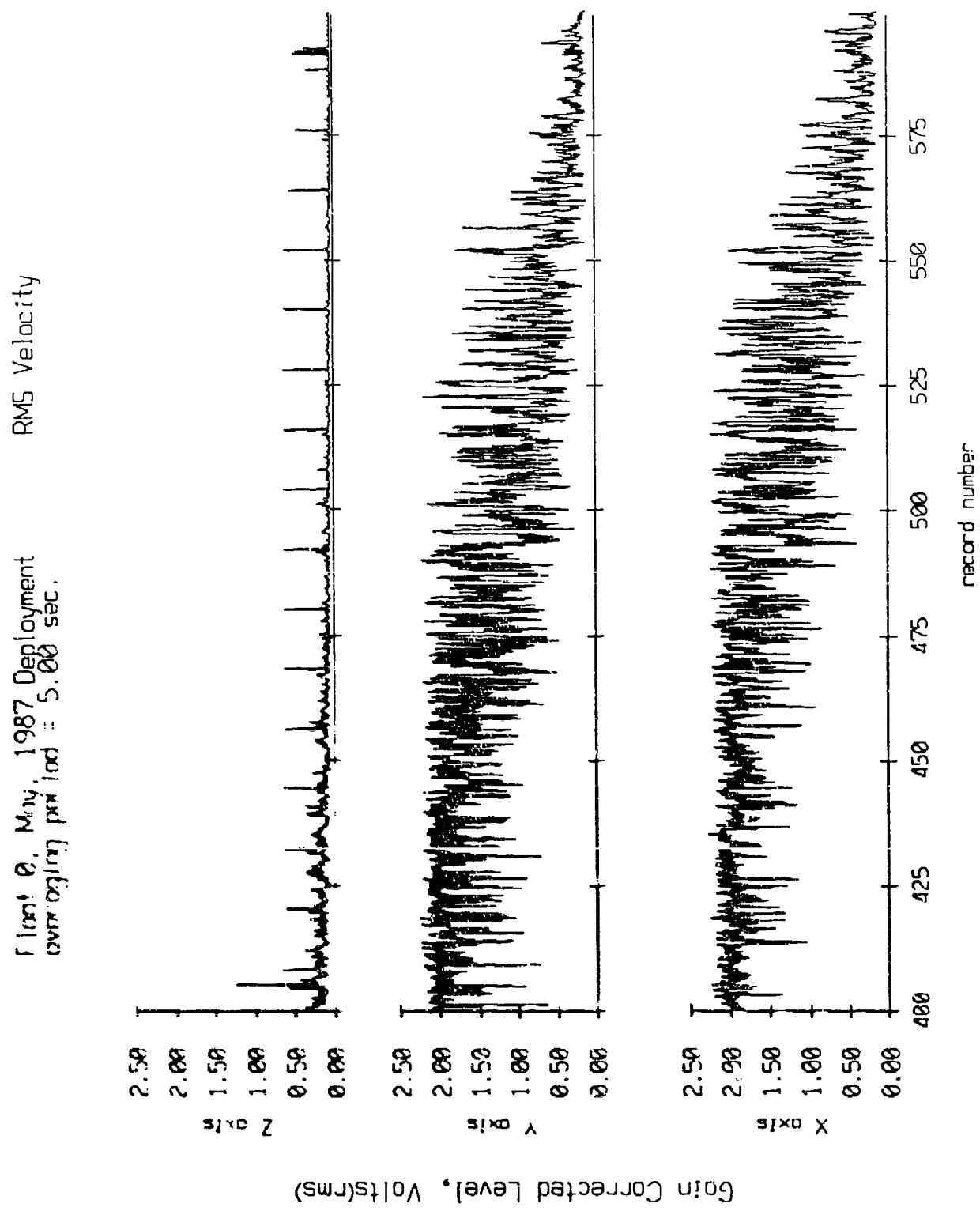
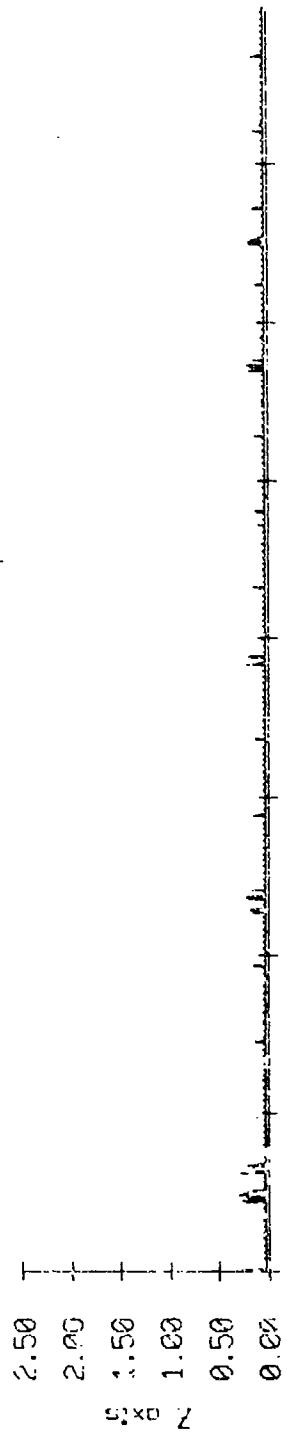


Figure IX.1c

Flight 0, May, 1987 Deployment
averaging period = 5.00 sec.

RMS Velocity



Gain Corrected Level, Volts(rms)

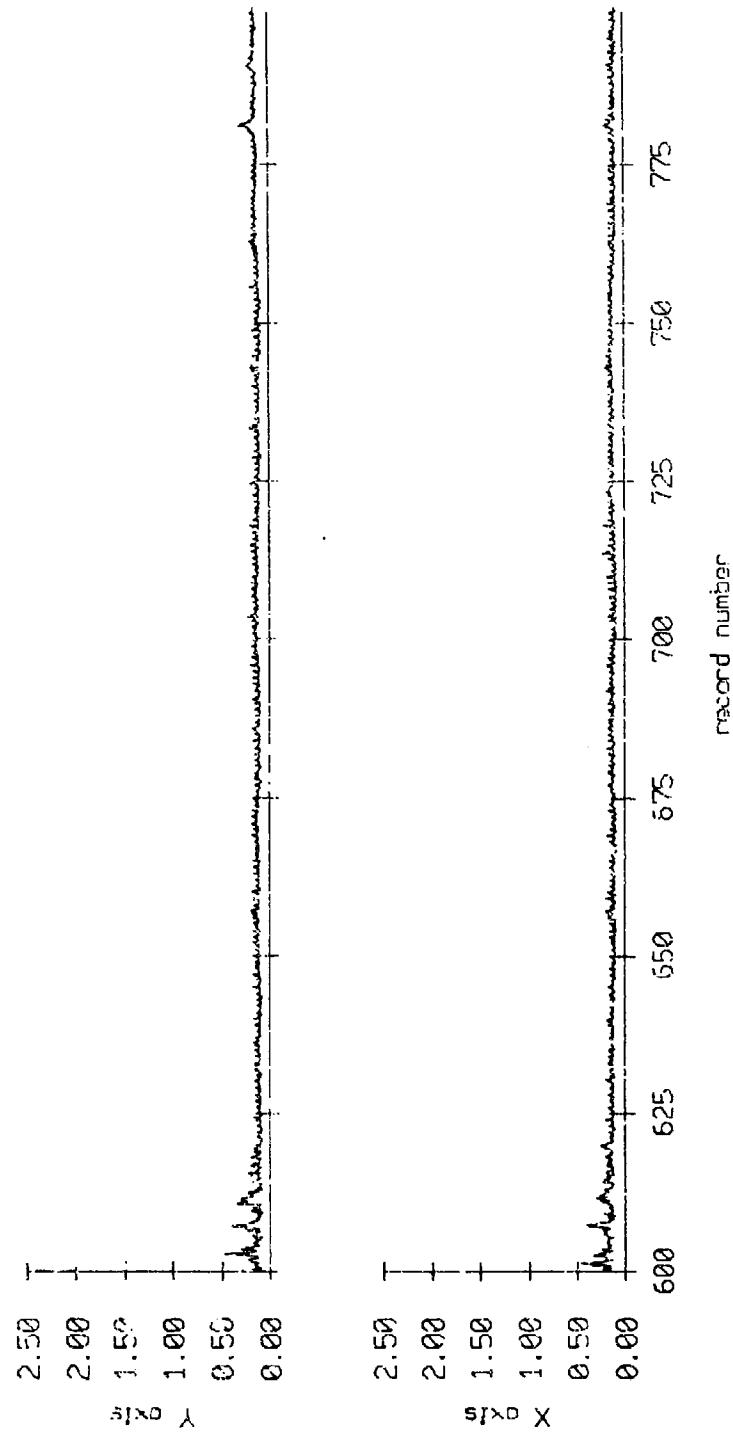


Figure IX.1d

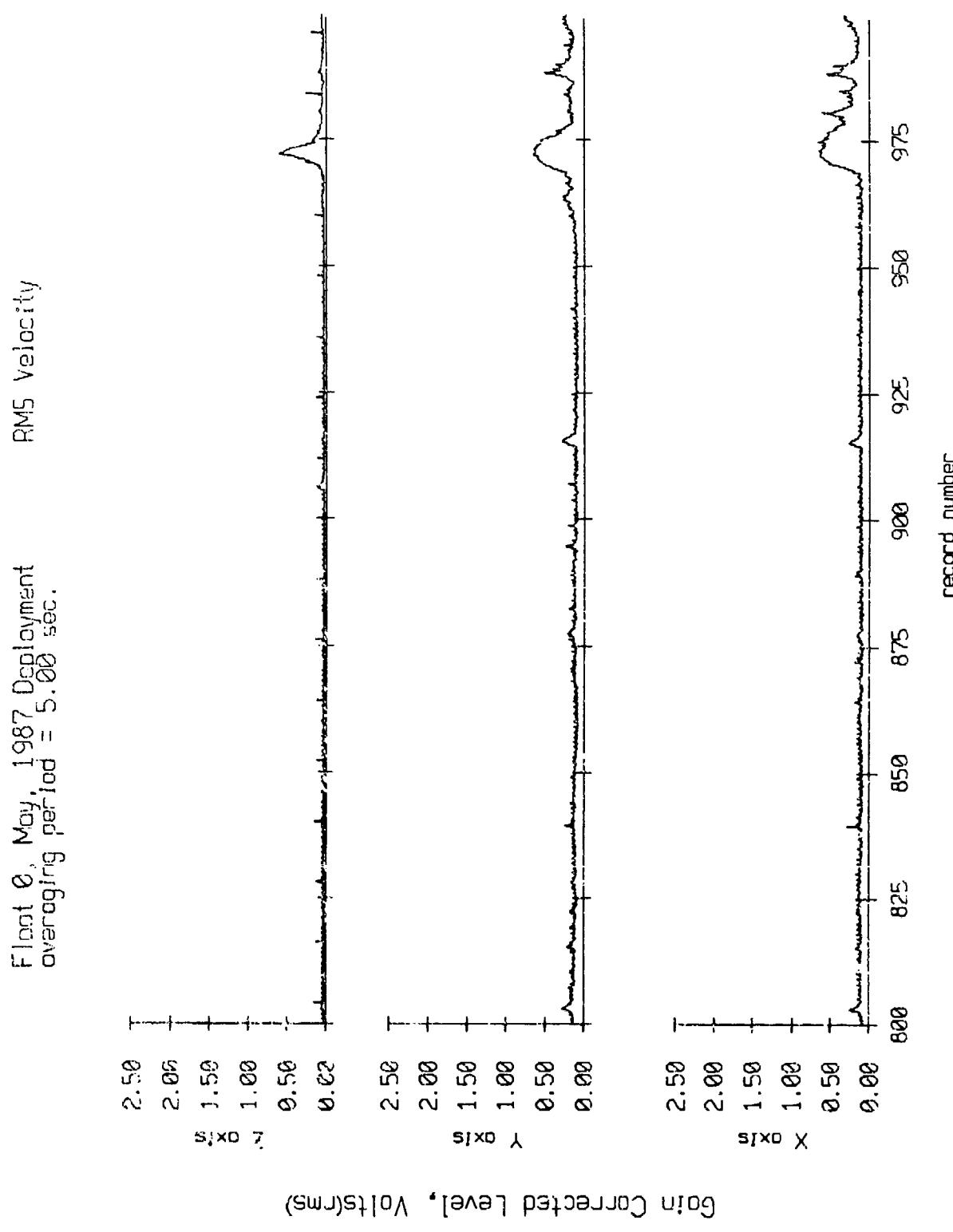
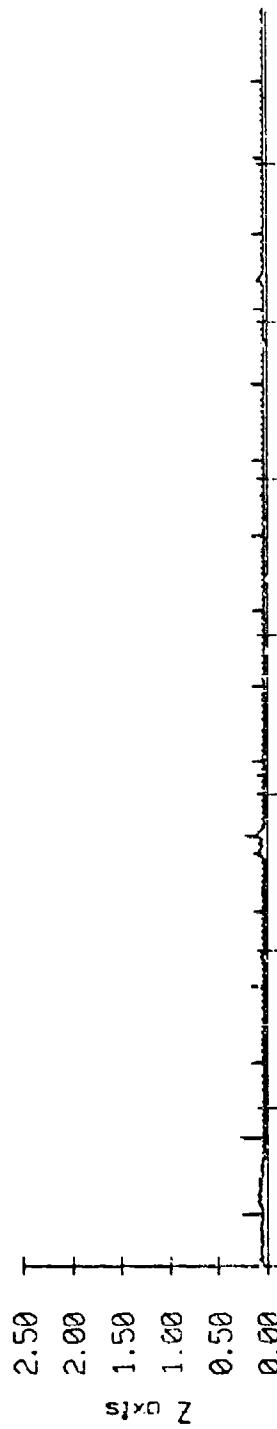


Figure IX.1e

Float 0, May 1987 Sec Trip.
overgoing period = 5.00 sec.



Gain Corrected Level, Volts(RMS)

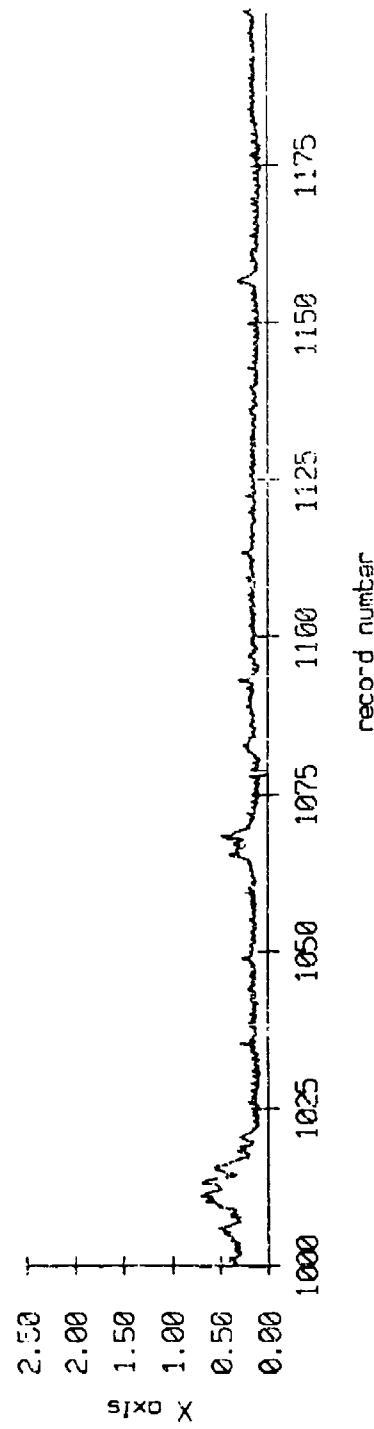
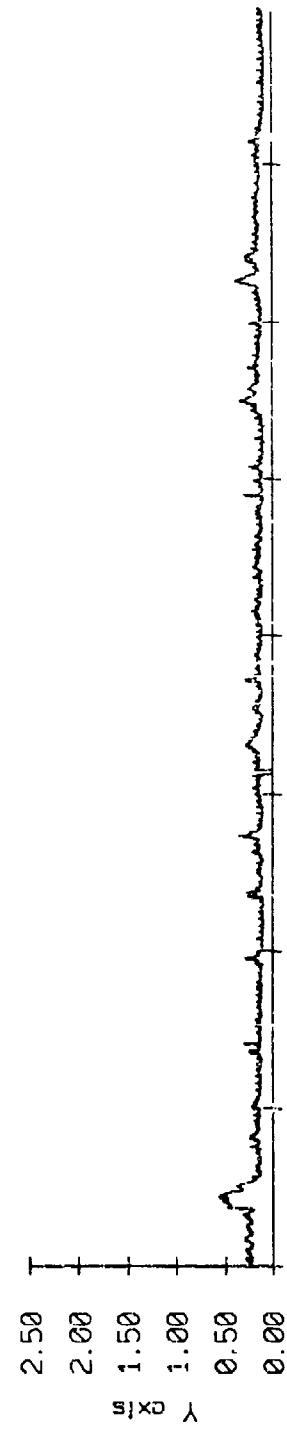


Figure IX.1f

Fleet 0, May 1987 Sea Trip
overaging period = 5.00 sec.

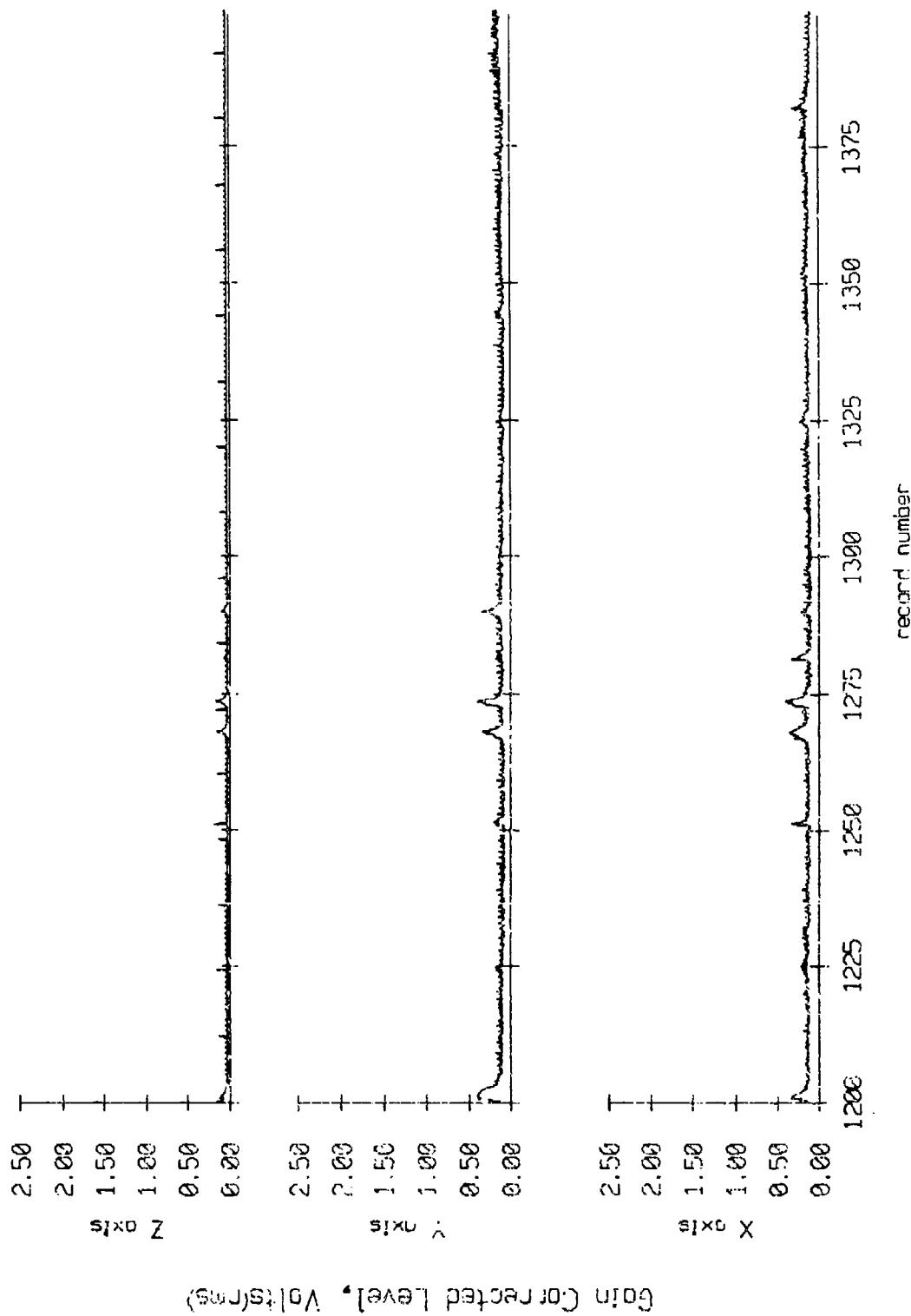


Figure IX.18

Float 0, May 1987 Seg Trip
averaging period = 5.00 sec.

RMS Velocity

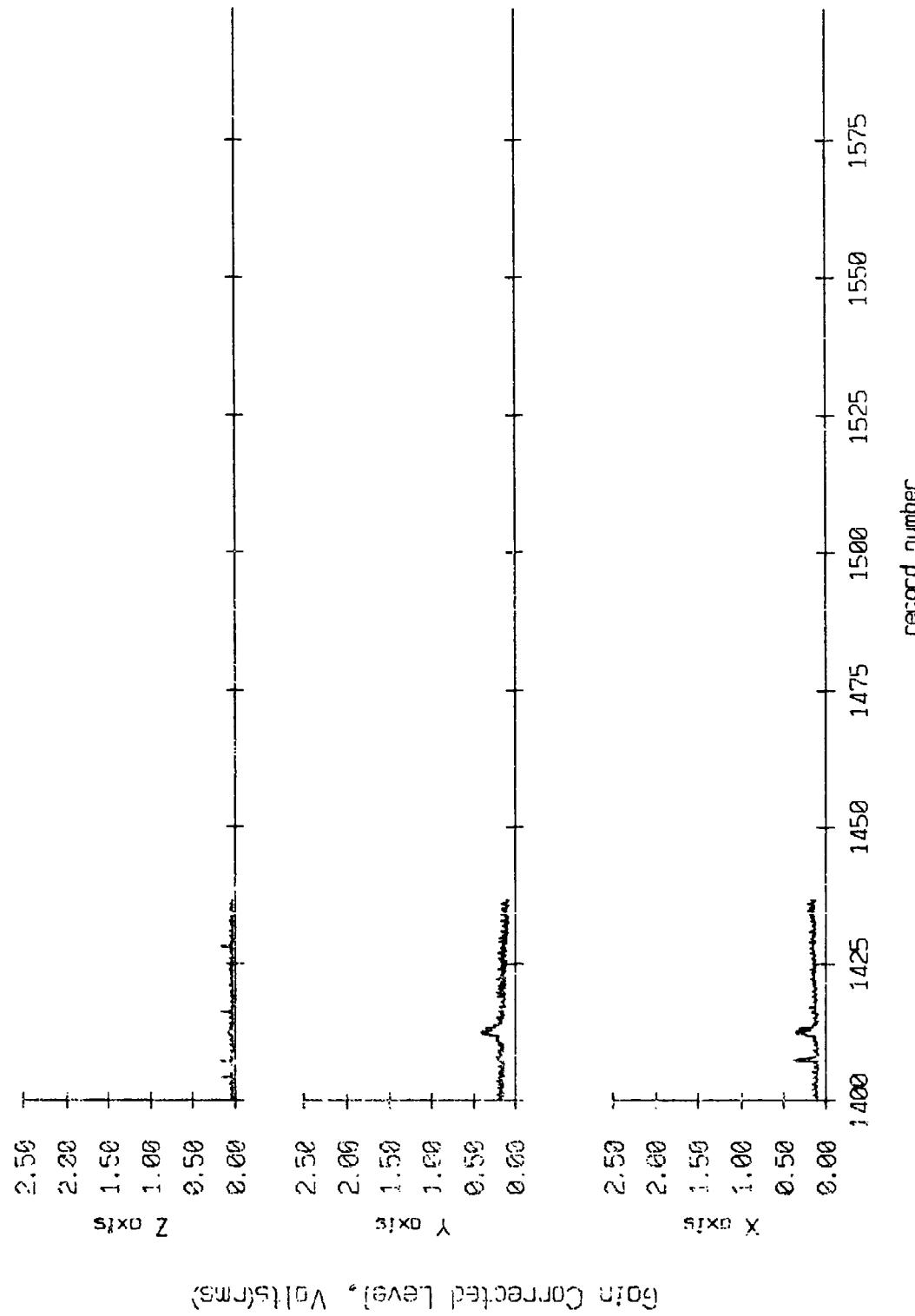
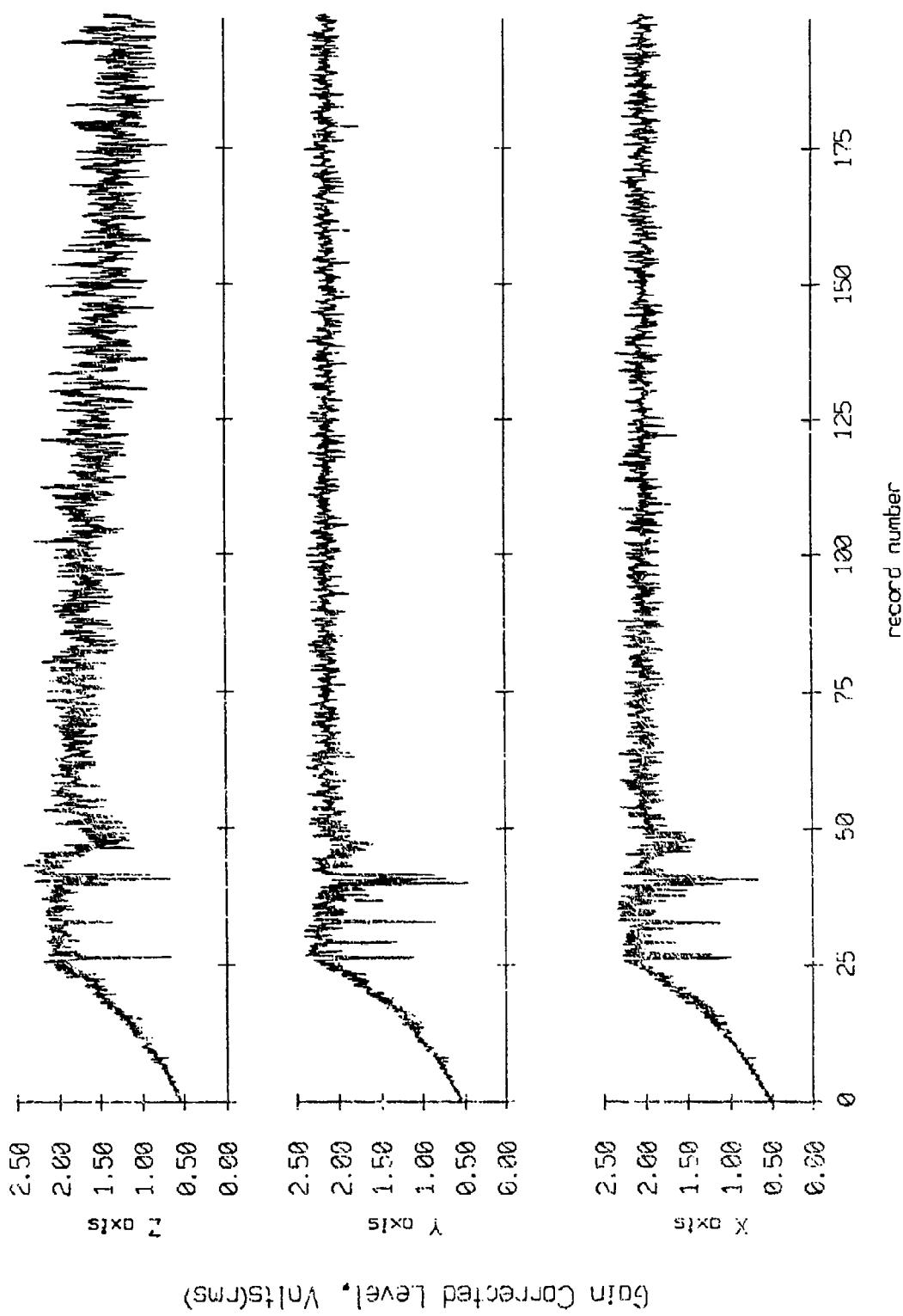


Figure IX.Jh

Float 1, May, 1987 Deployment
overaging period = 5.00 sec.

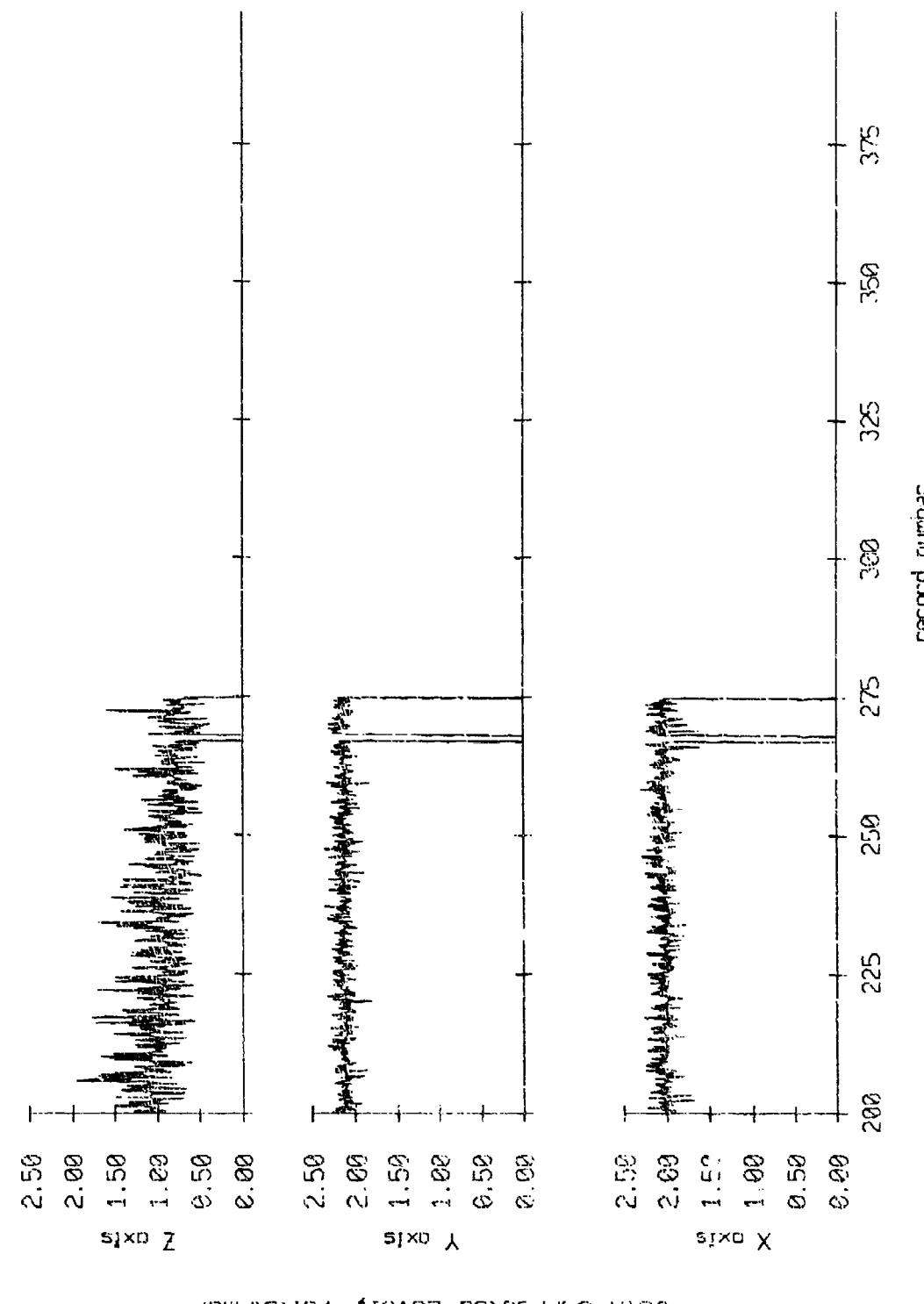
RMS Velocity



Gain Corrected Level, Volts(RMS)

Figure IX.2a

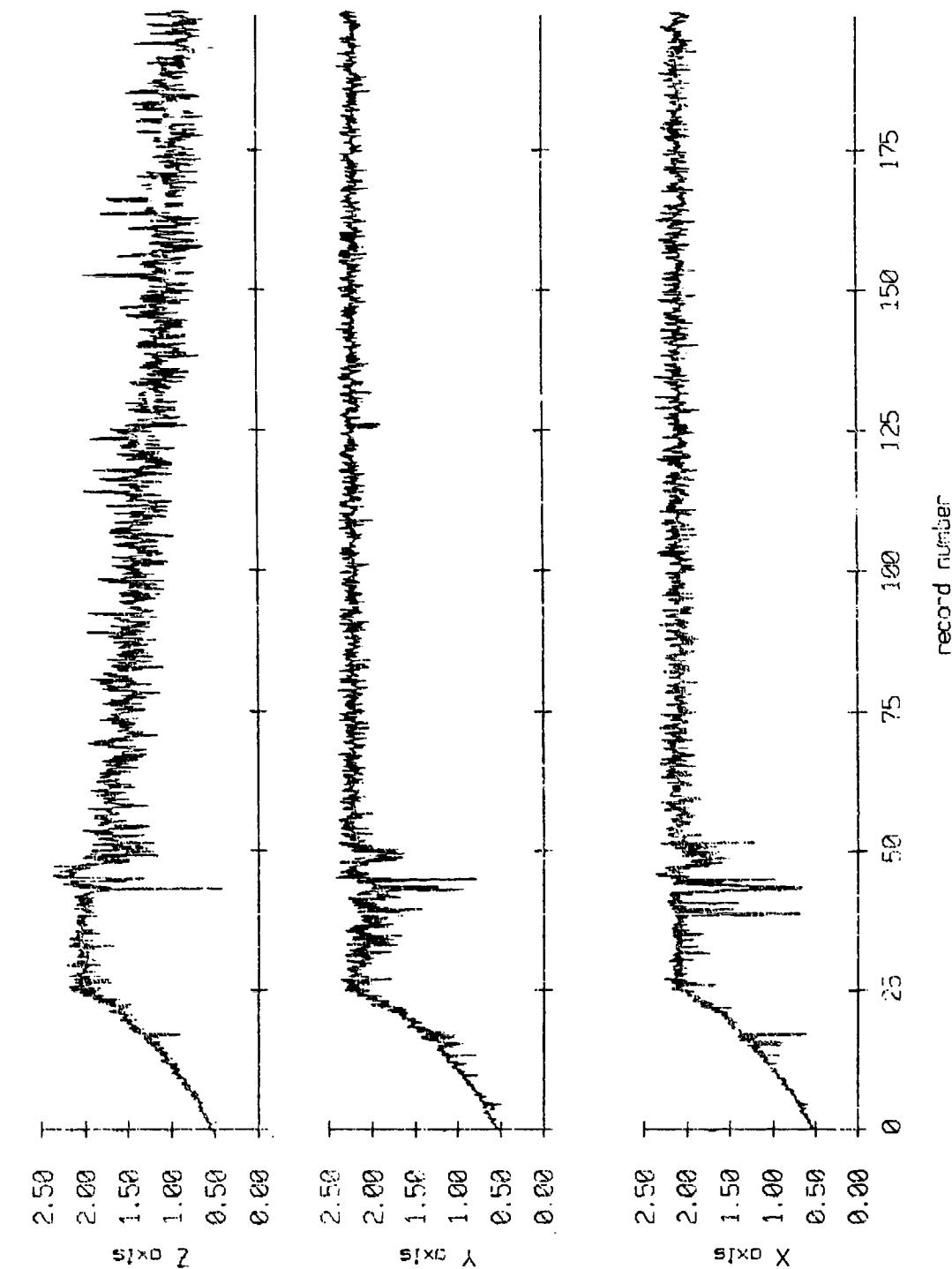
Floot 1, May 1987 Deployment
averaging period = 5.00 sec.



Gain Corrected Level, Volts(rms)

Figure IX.2b

Figure 2, May, 1987 Deployment
overranging period = 5.00 sec.



Gain Corrected Level, Volts(rms)

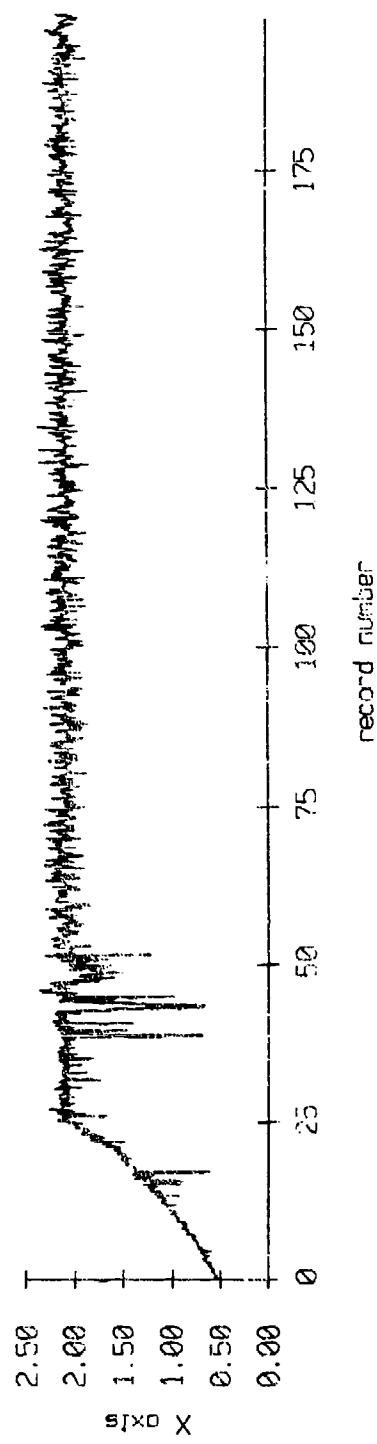
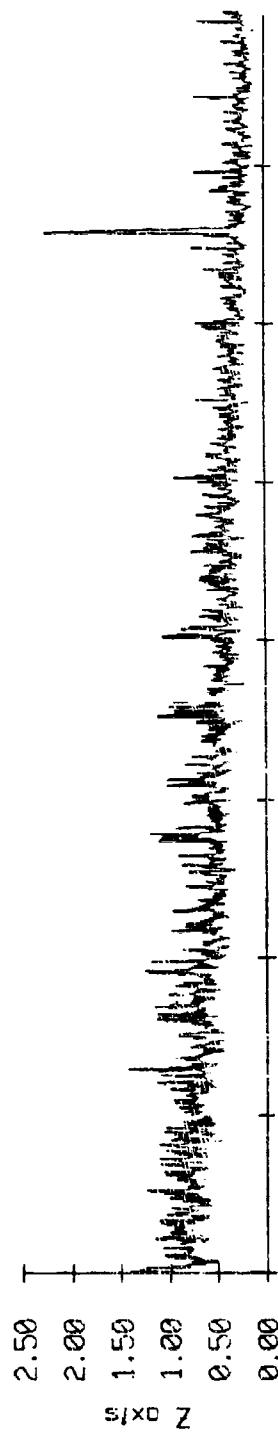


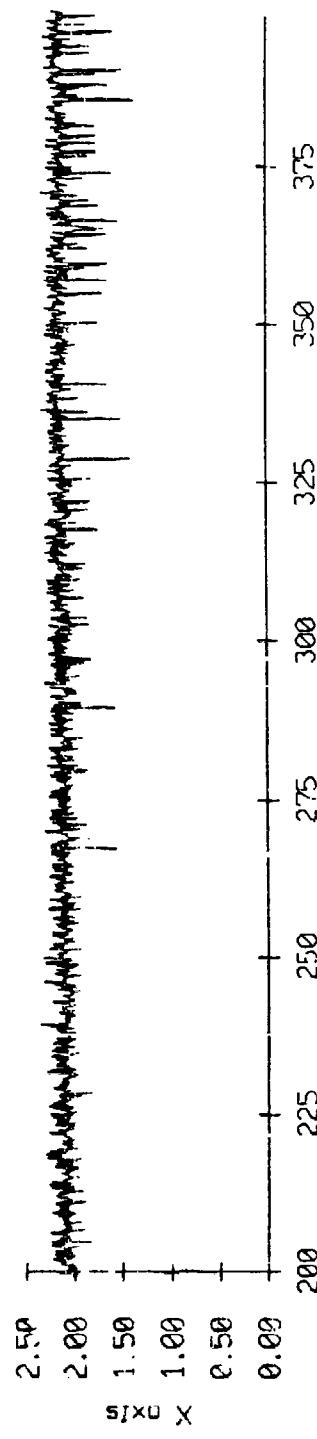
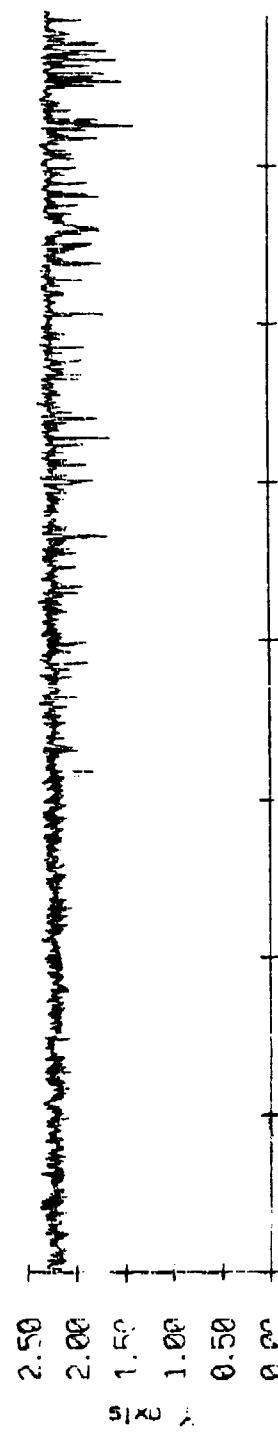
Figure IX.3a

Fleet 2, May, 1987 Deployment
overaging period = 5.00 sec.

RMS Velocity



Z in [corrected level], Volts(rms)

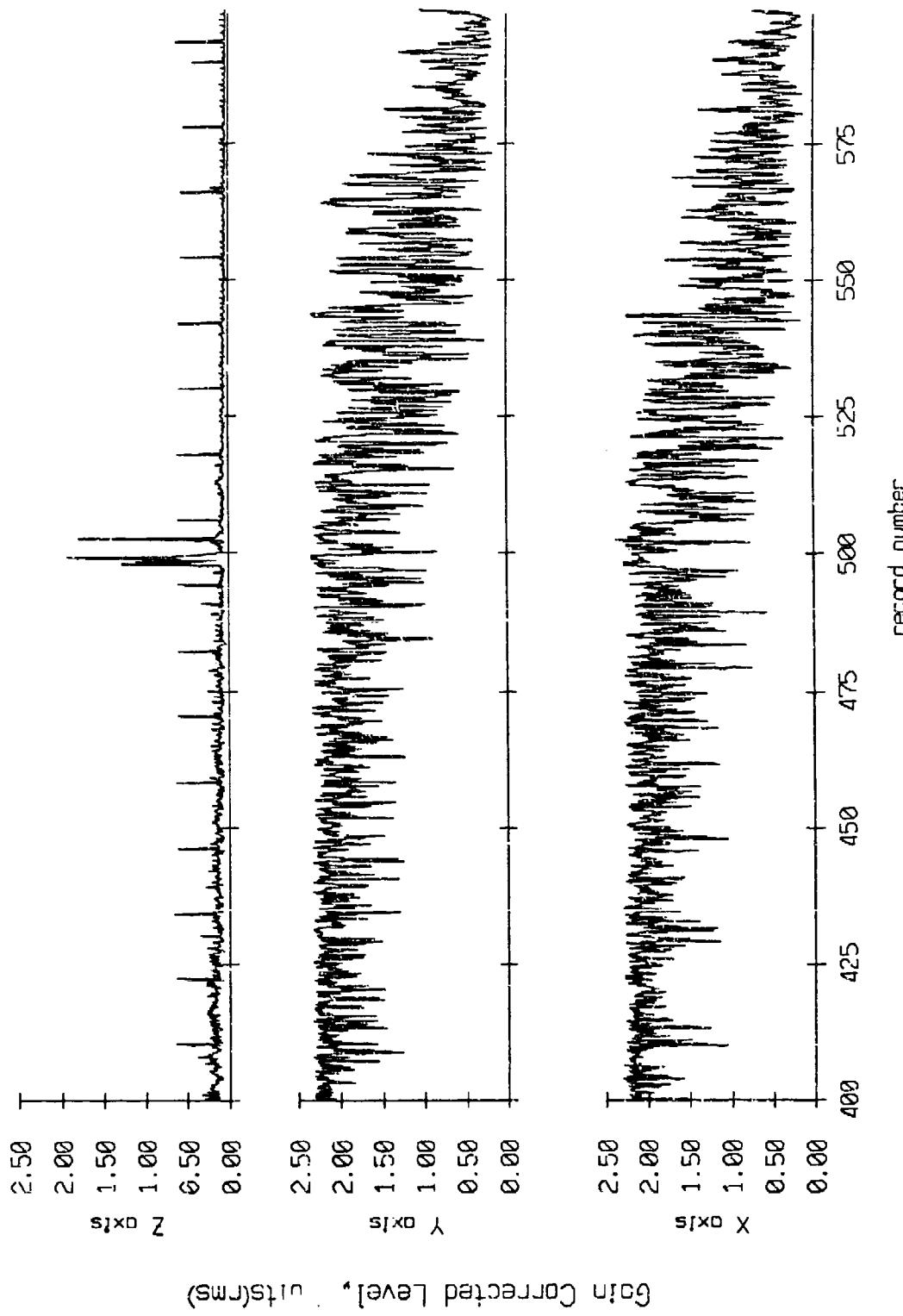


record number

Figure IX.3b

Fleet 2, May, 1987 Deployment
overranging period = 5.00 sec.

RMS Velocity



Gain Corrected Level, units (rms)

Figure IX.3c

Float 2, May, 1987 Deployment
averaging period = 5.00 sec.

RMS Velocity

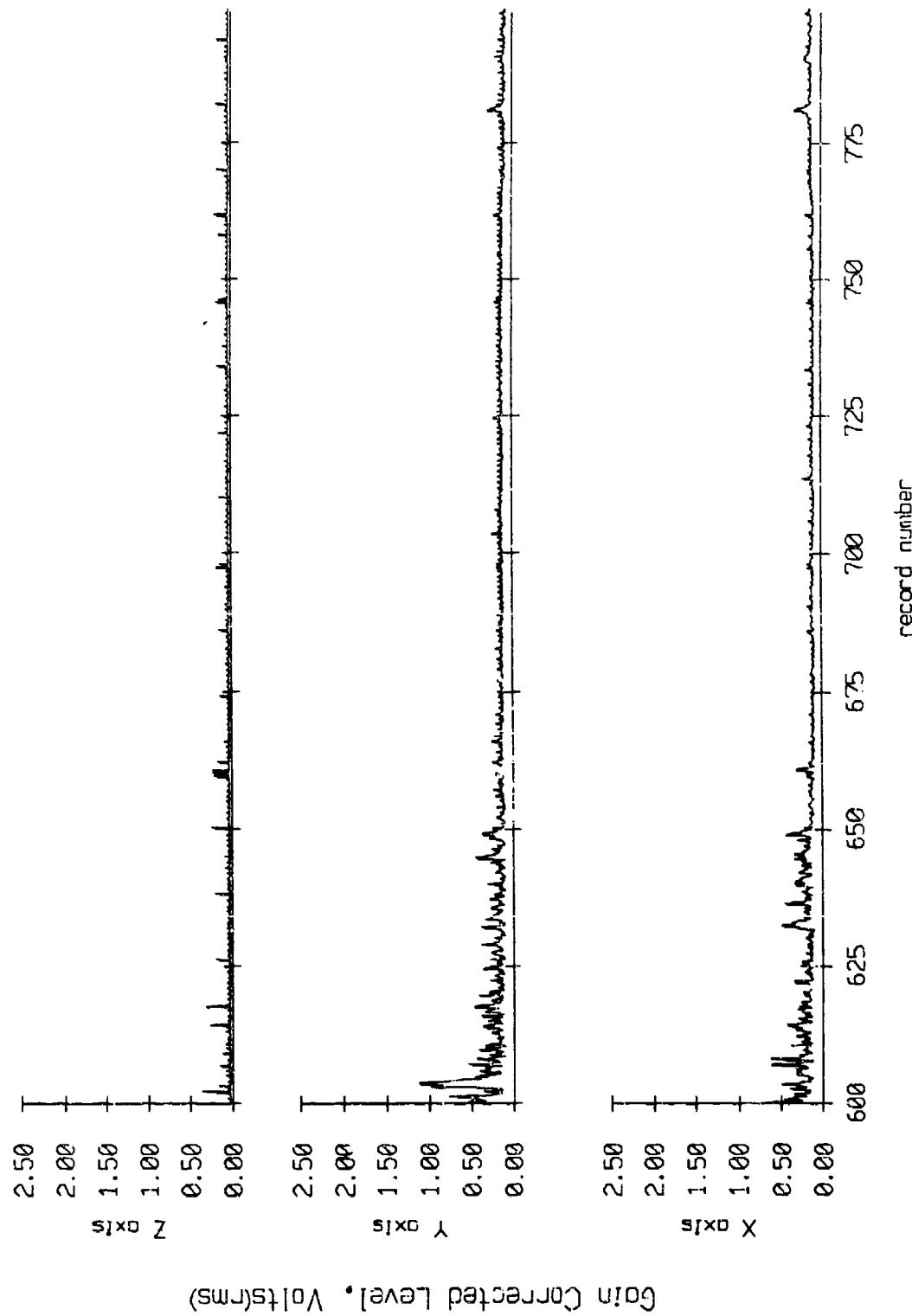


Figure IX.3d

Fleet 2, May, 1987 Deployment
averaging period = 5.00 sec.

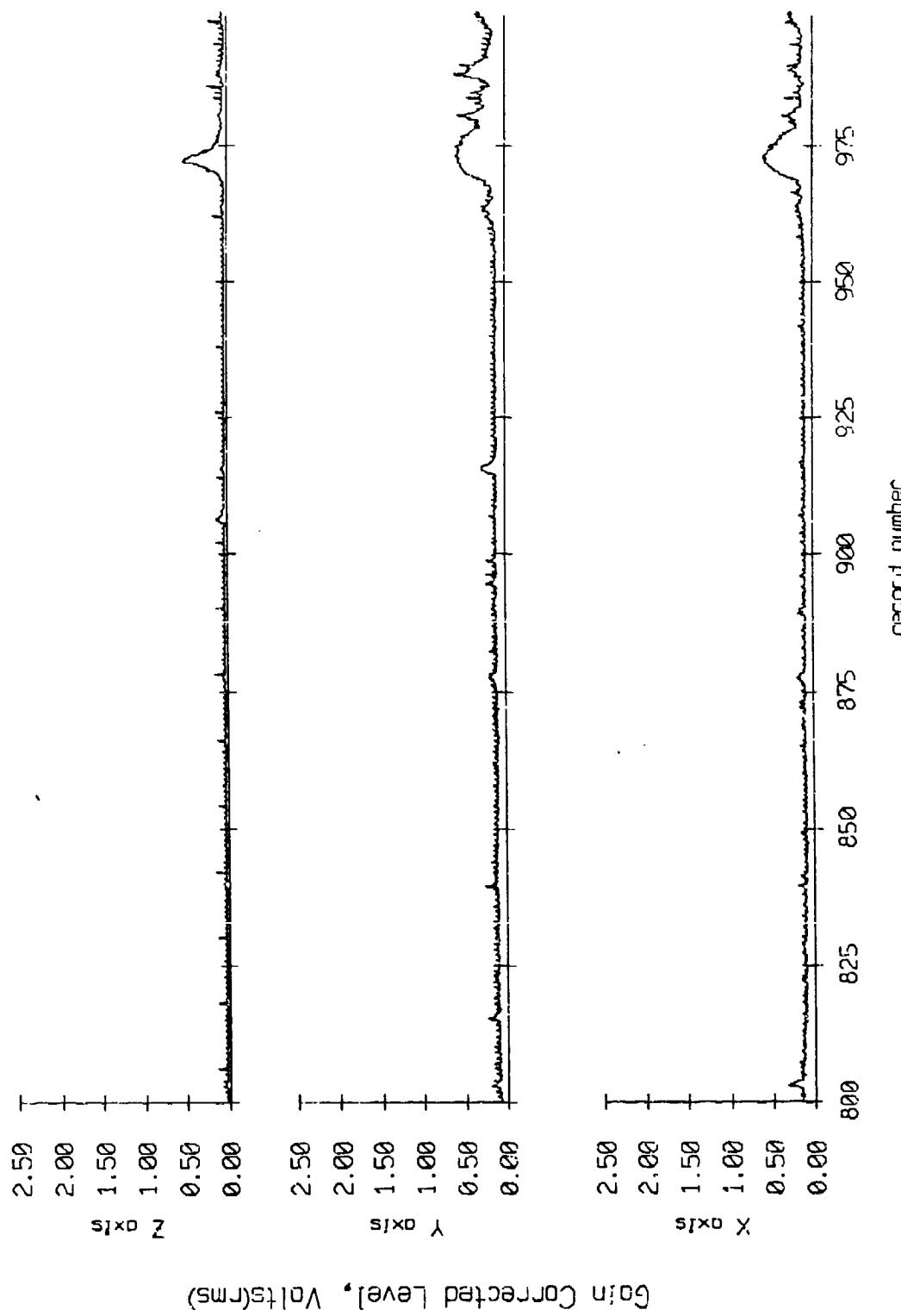
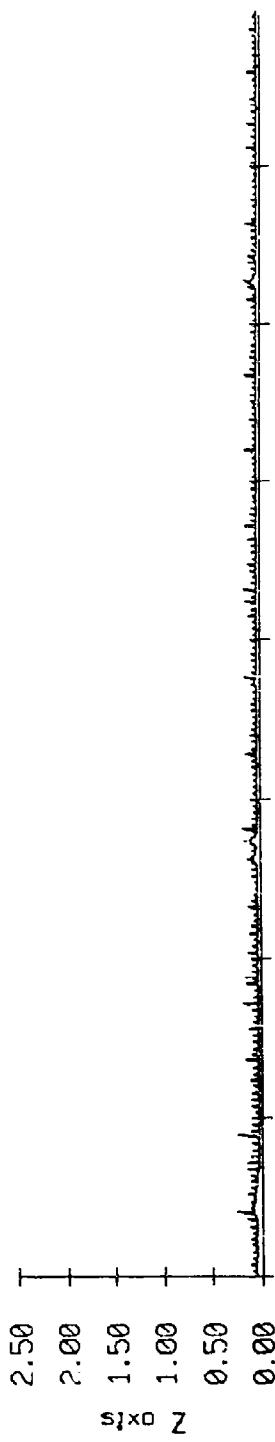


Figure IX.3e

Fleet 2, May, 1987 Deployment
overaging period = 5.00 sec.

RMS Velocity



Gain Corrected Level, Volts(rms)

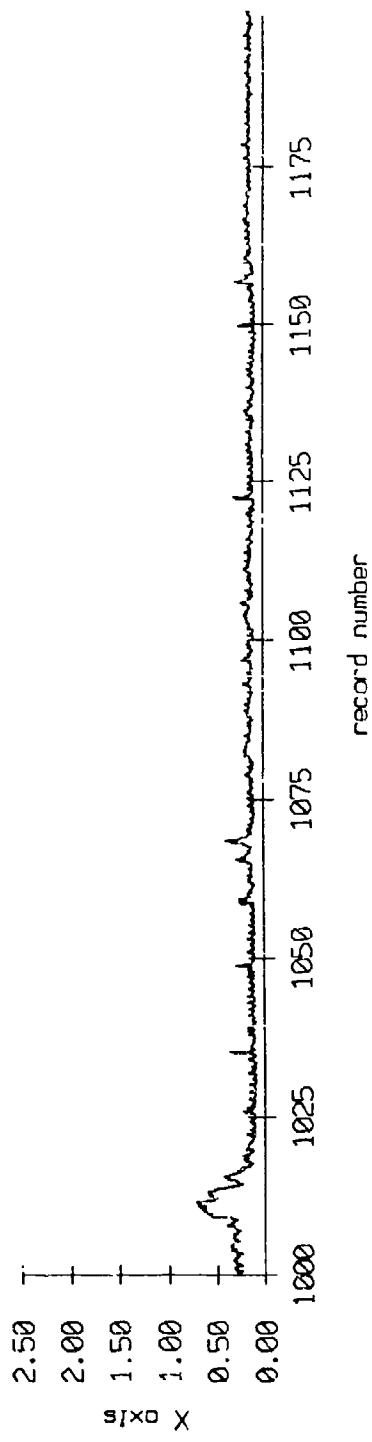


Figure IX.3f

Float 2, May, 1987 Deployment
overgong period = 5.00 sec.

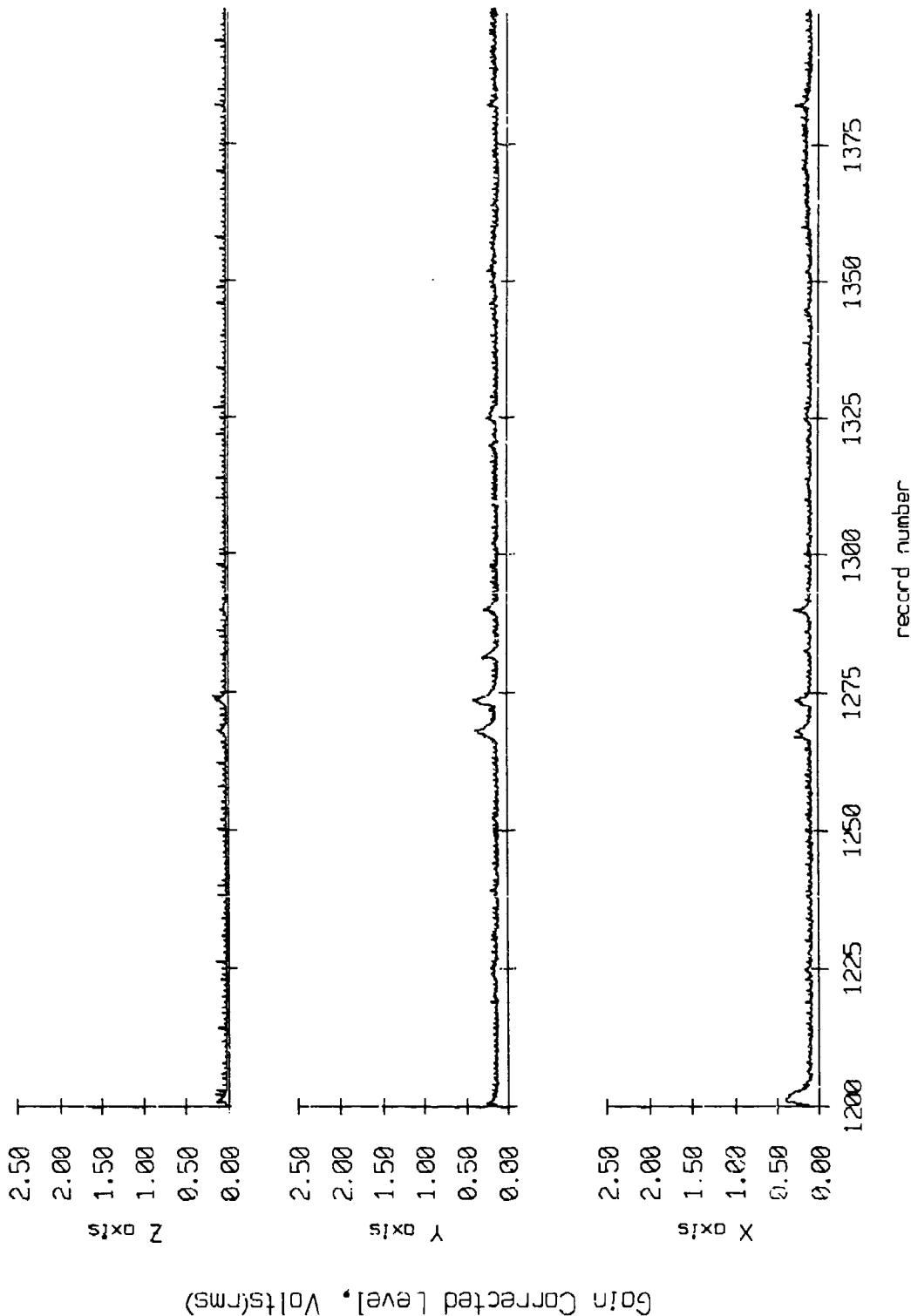


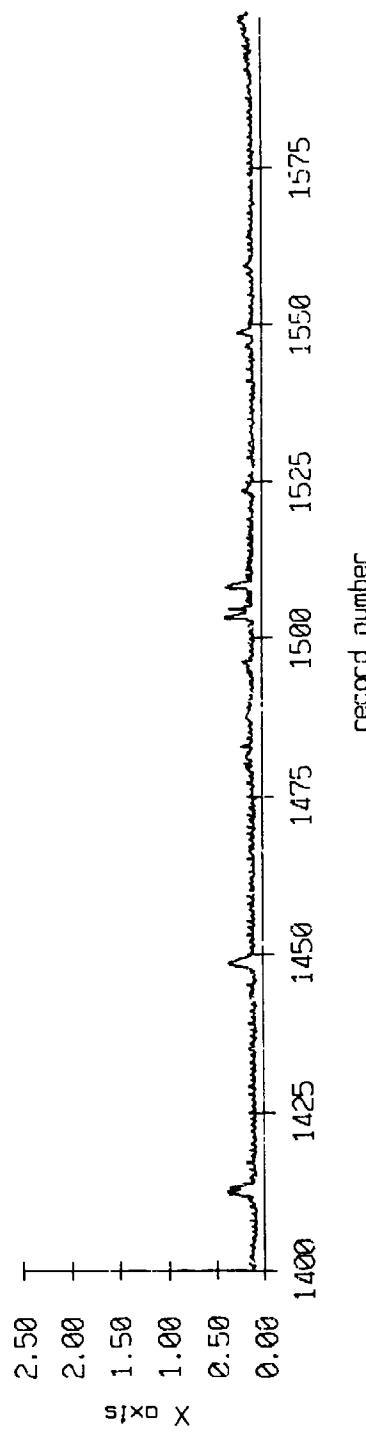
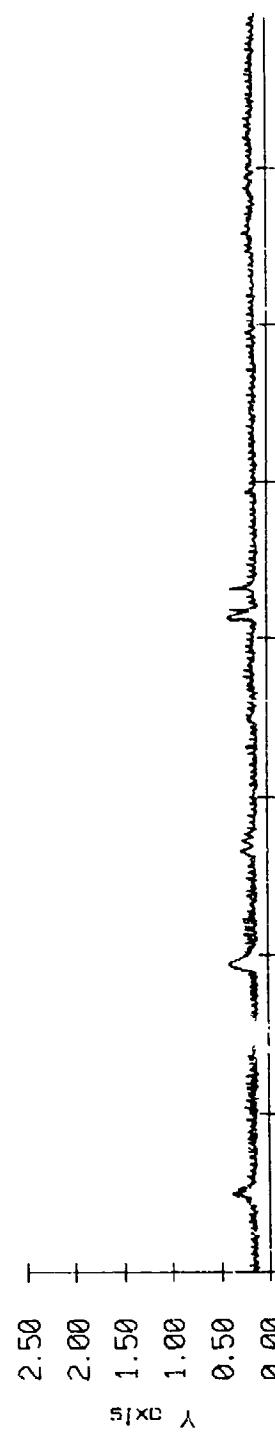
Figure IX.3g

Fleet 2, May, 1987 Deployment
overaging period = 5.00 sec.

RMS Velocity



Gain Corrected Level, Volts(cms)



record number

Figure IX.3h

Float 2, May, 1987 Deployment
Oscillating period = 5.00 sec.

RMS Velocity

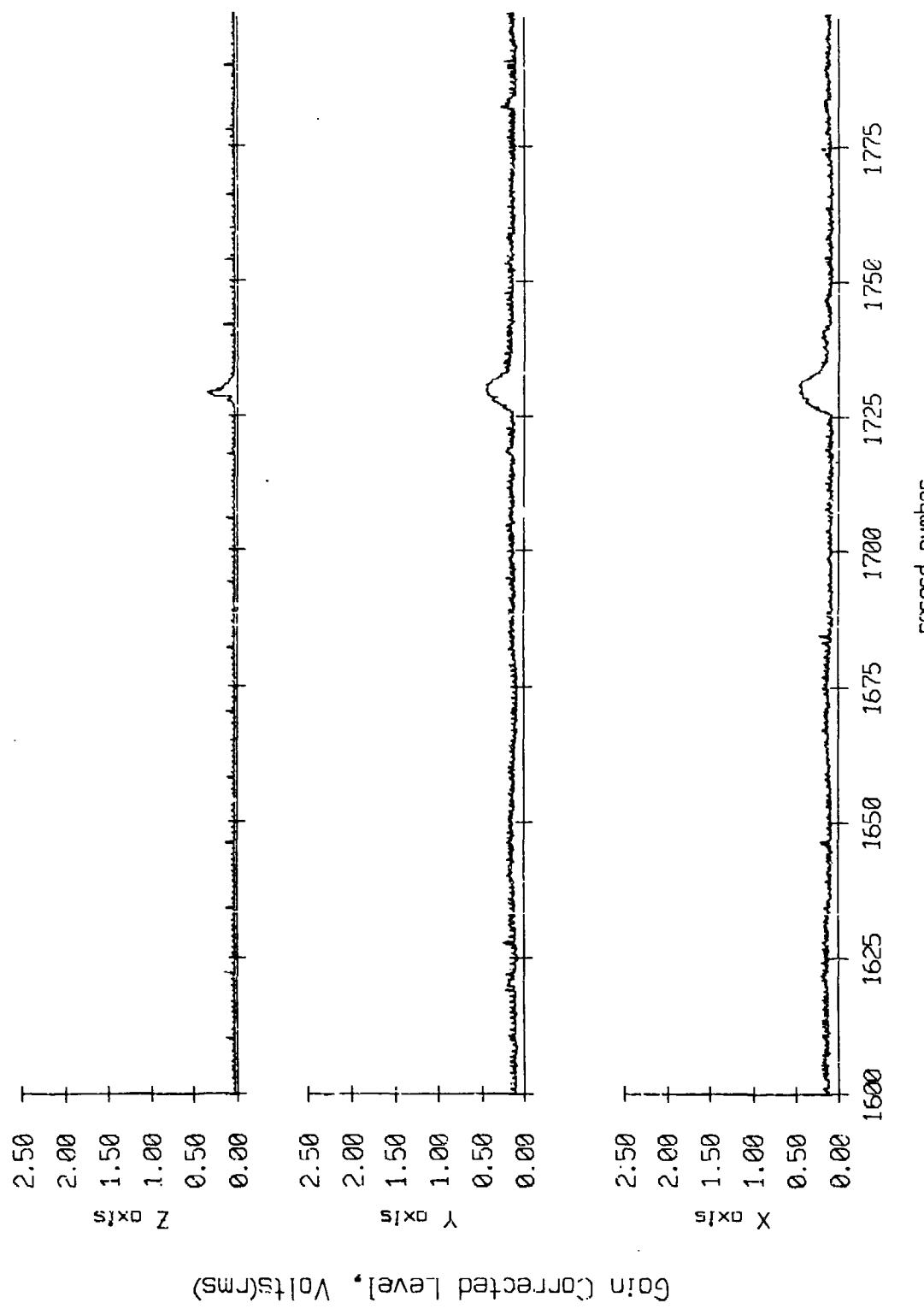


Figure IX.3i

Float 2, May, 1987 Deployment
overaging period = 5.00 sec.

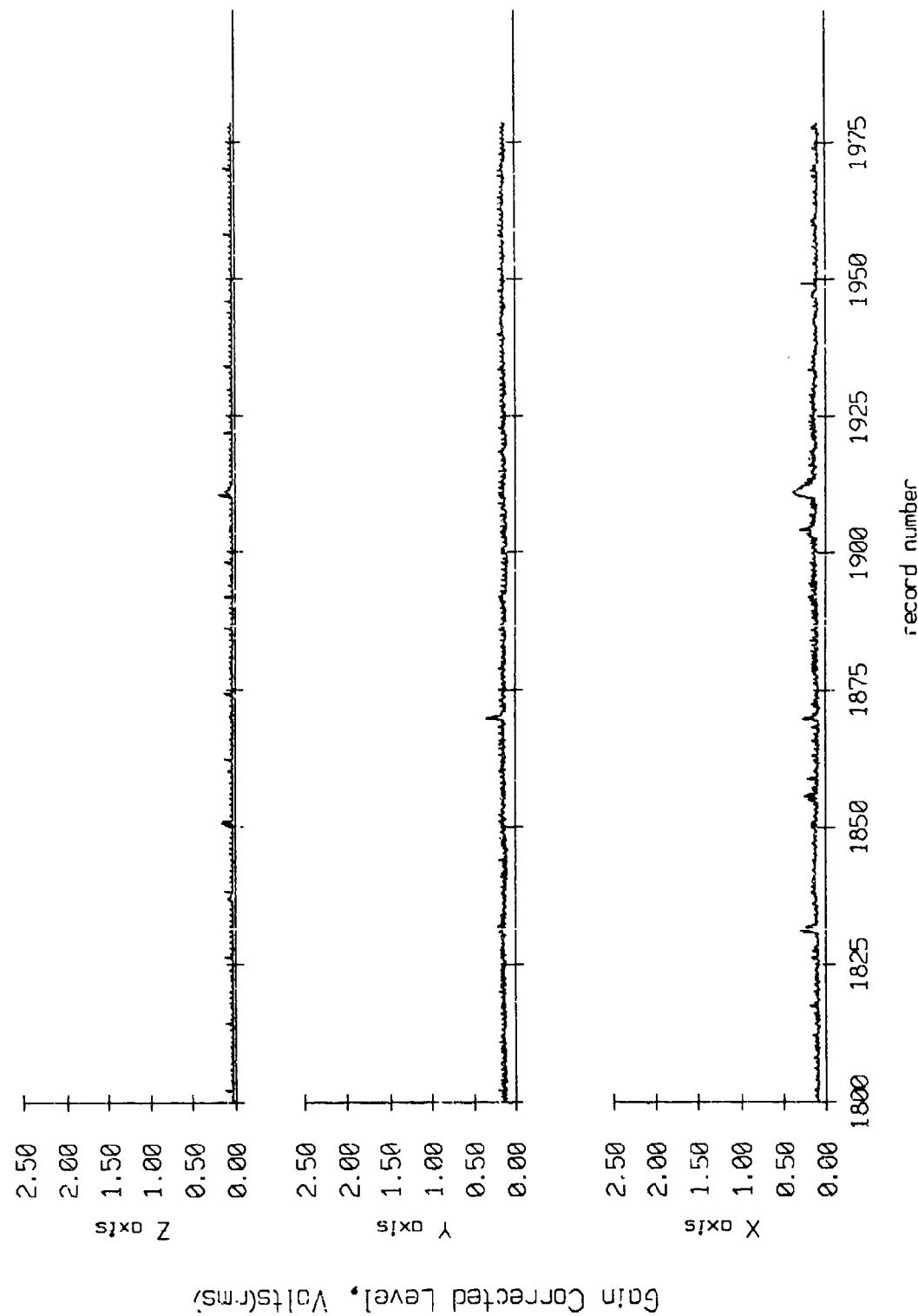
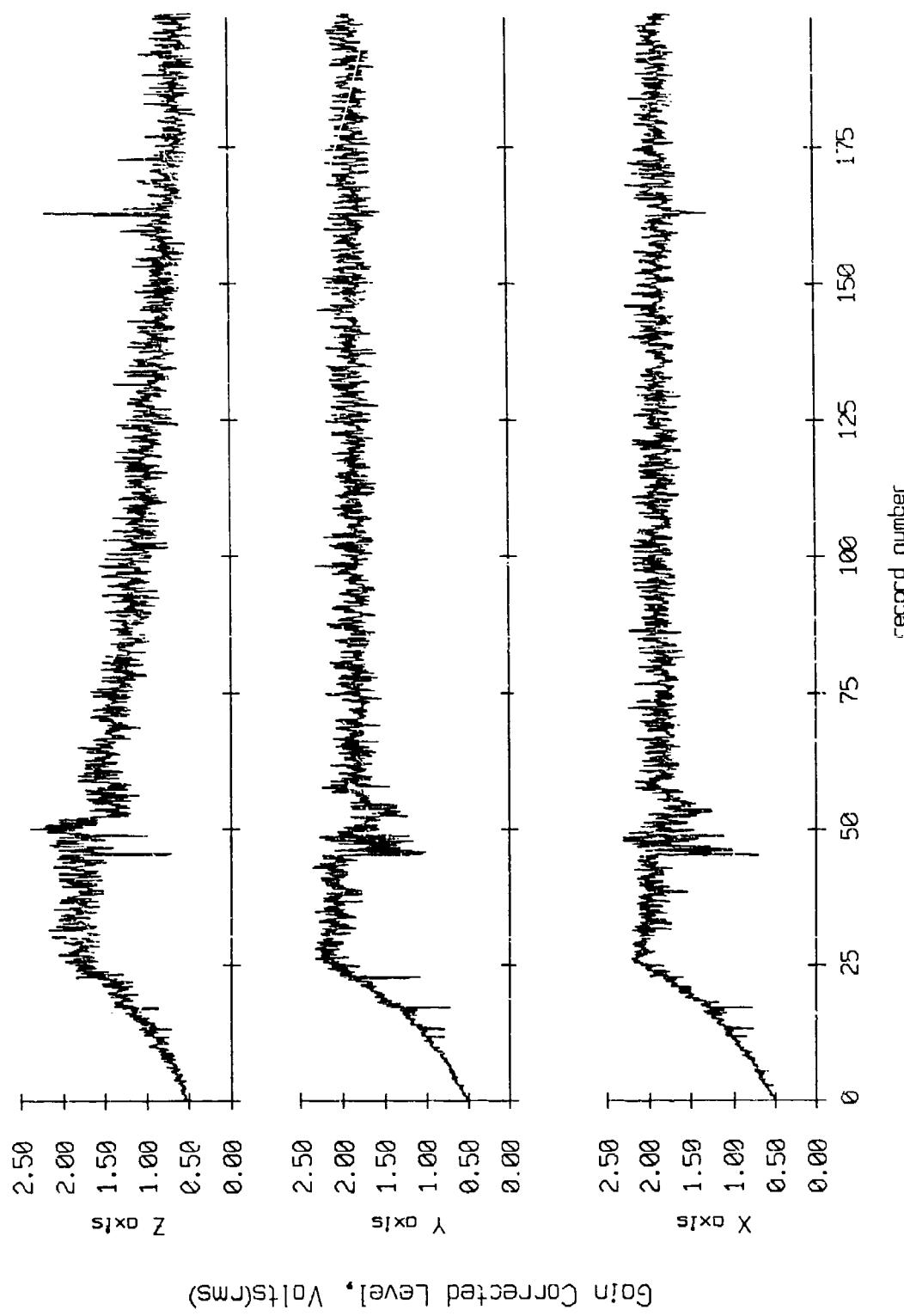


Figure IX.3j

Float 3, May 1987 Deployment
averaging period = 5.00 sec.

RMS Velocity



Gain Corrected Level, Volts(RMS)

Figure IX.4a

Float 3, May, 1987 Deployment
overaging period = 5.00 sec.

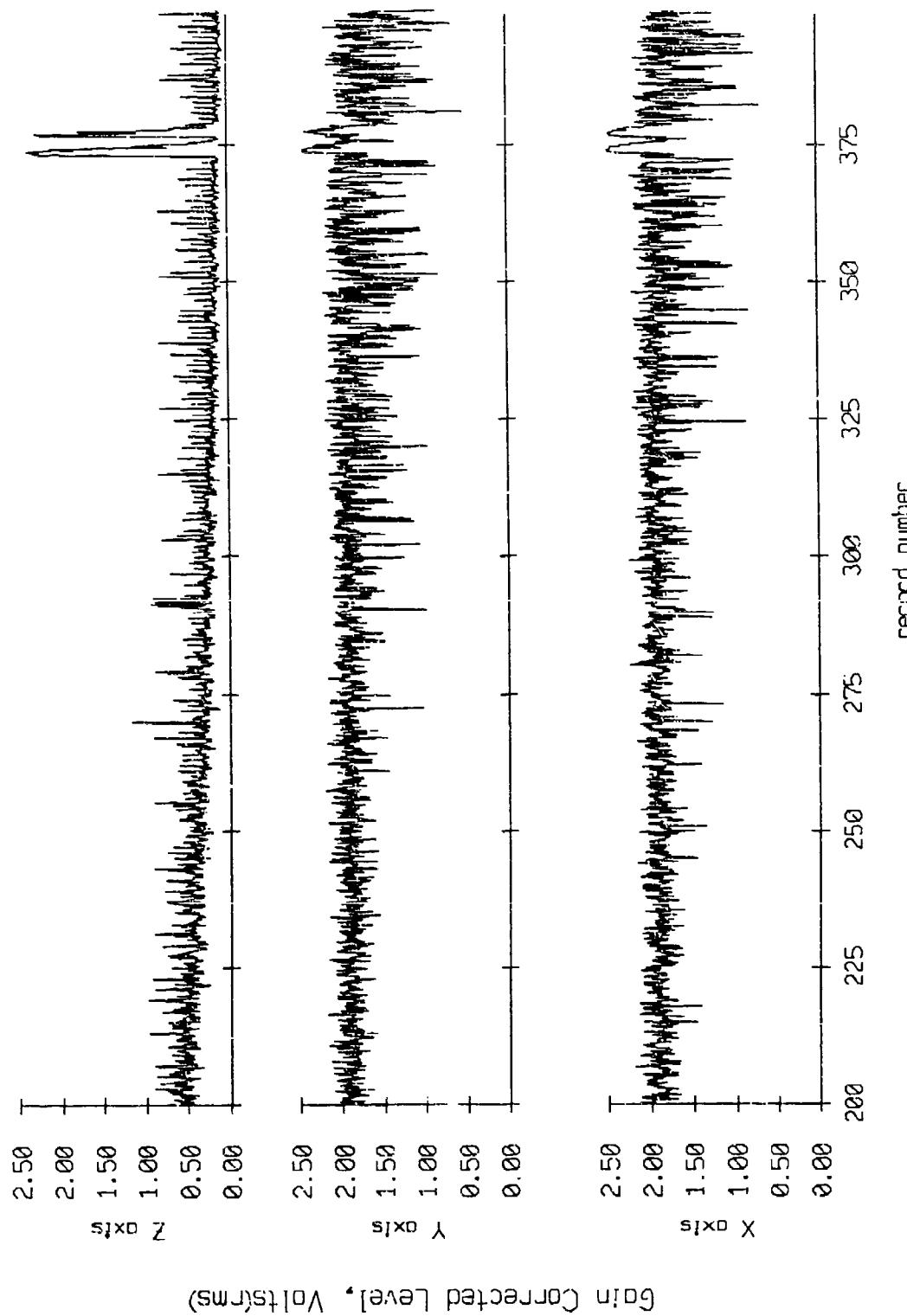
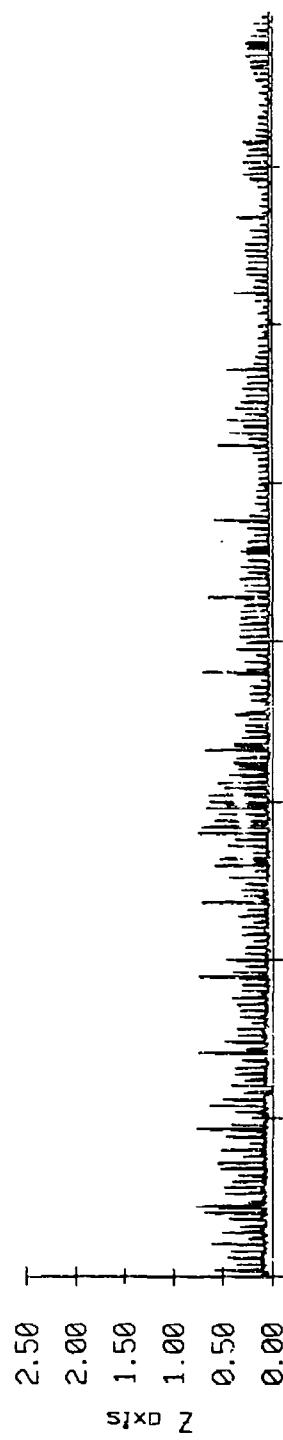


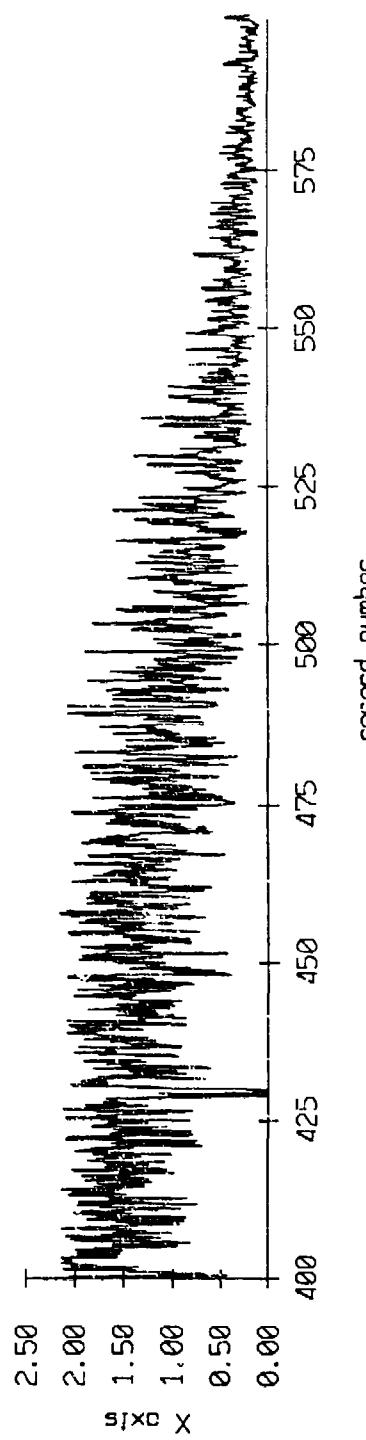
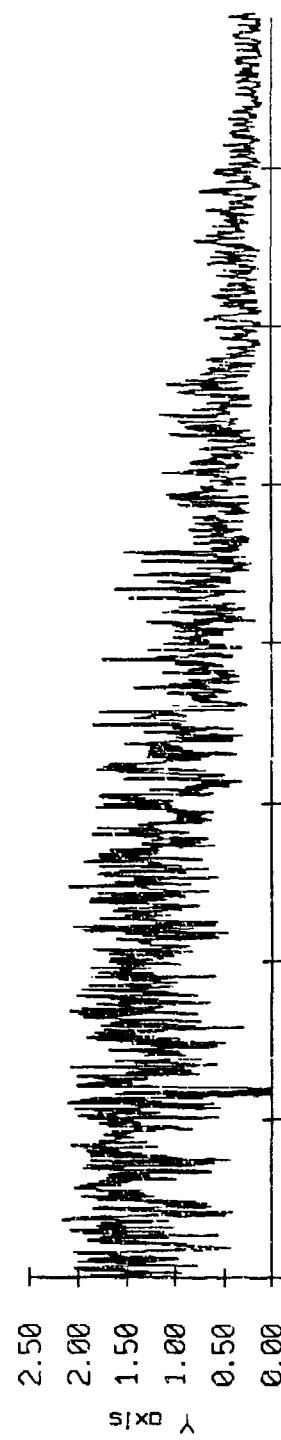
Figure IX.4b

Float 3, May, 1987 Deployment:
overaging period = 5.00 sec.

RMS Velocity



Gain Corrected Level, Volts(rms)



record number

Figure IX.4c

Float 3, May 1987 Deployment
averaging period = 5.00 sec.

RMS Velocity

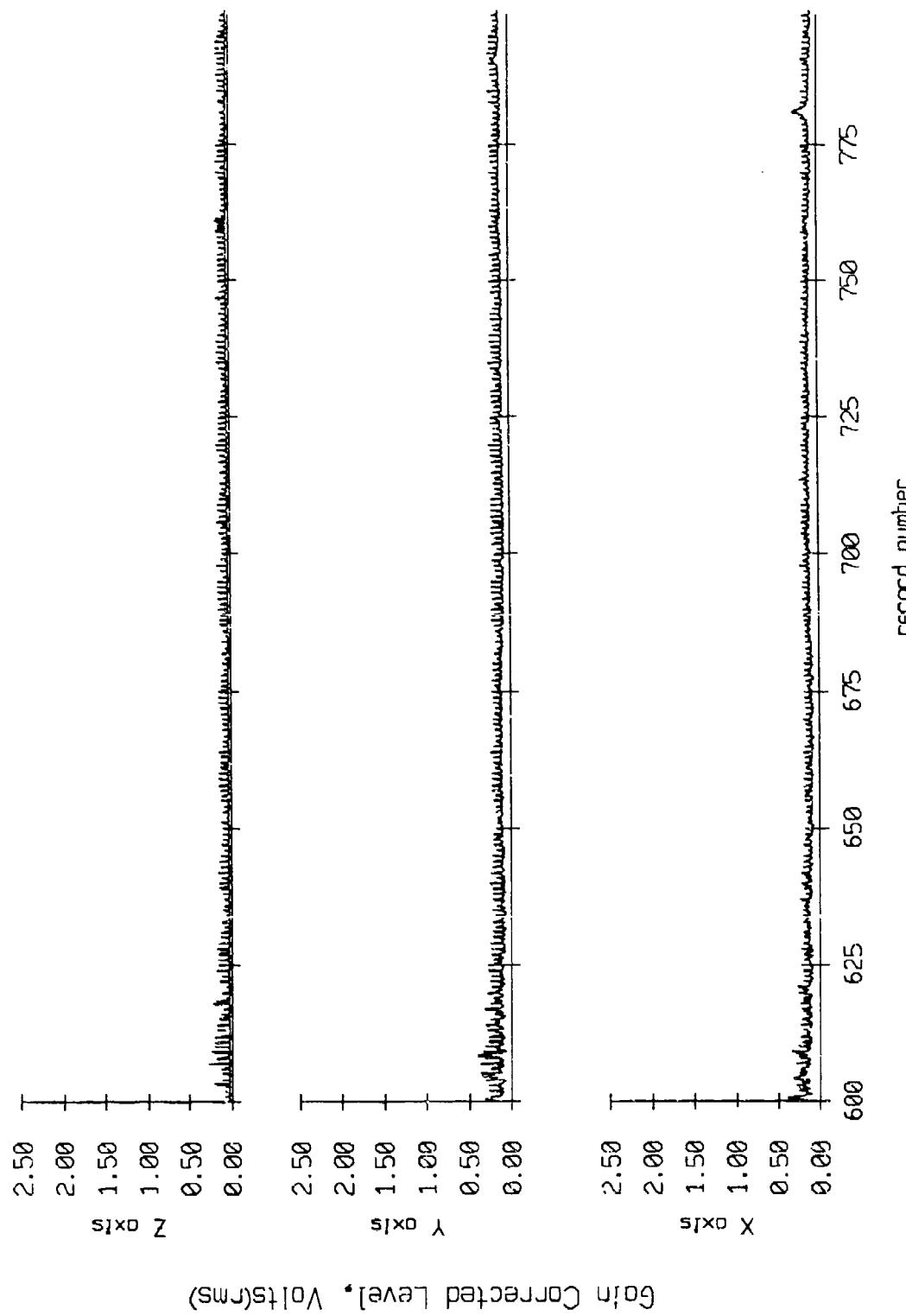


Figure IX.4d

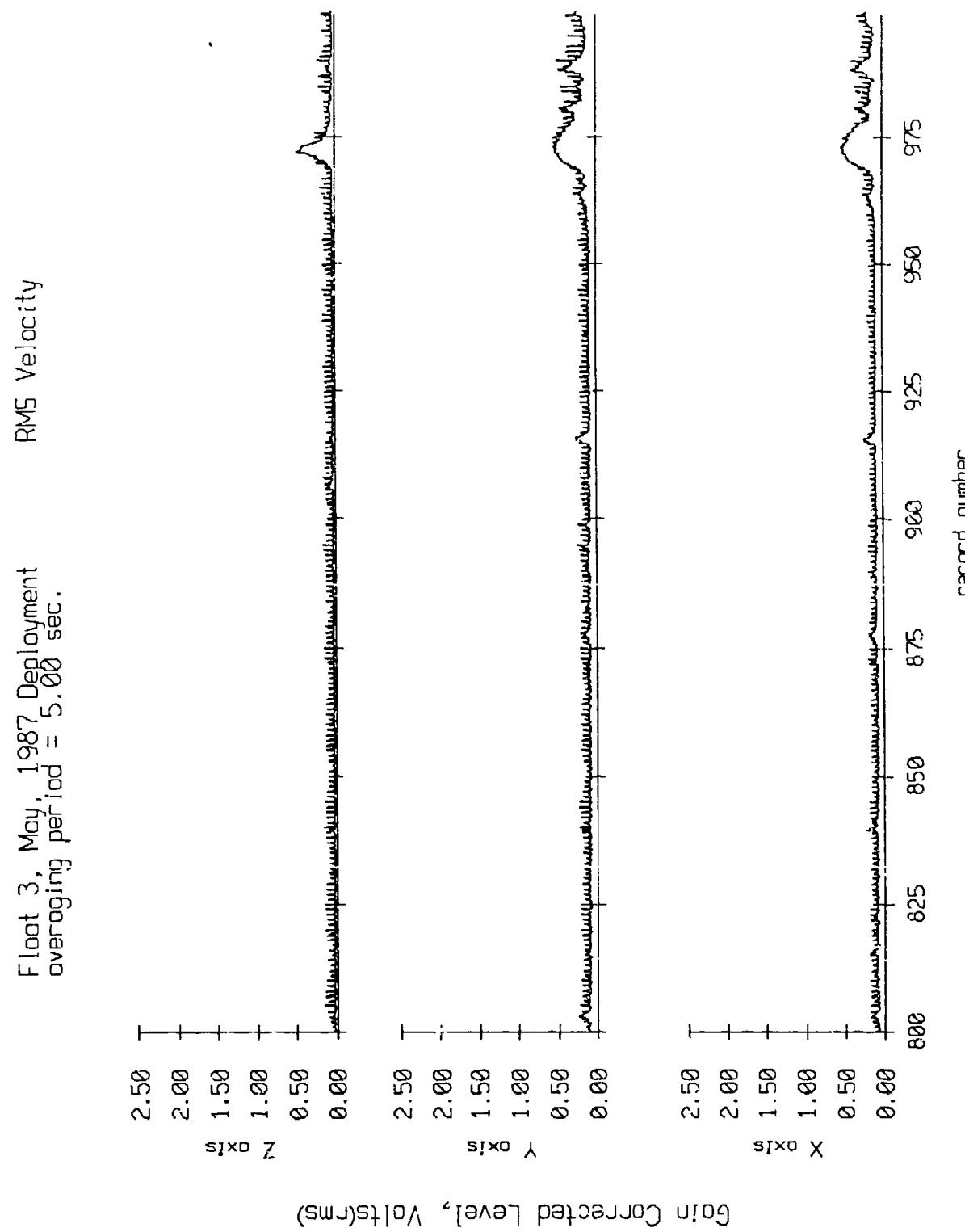


Figure IX.4e

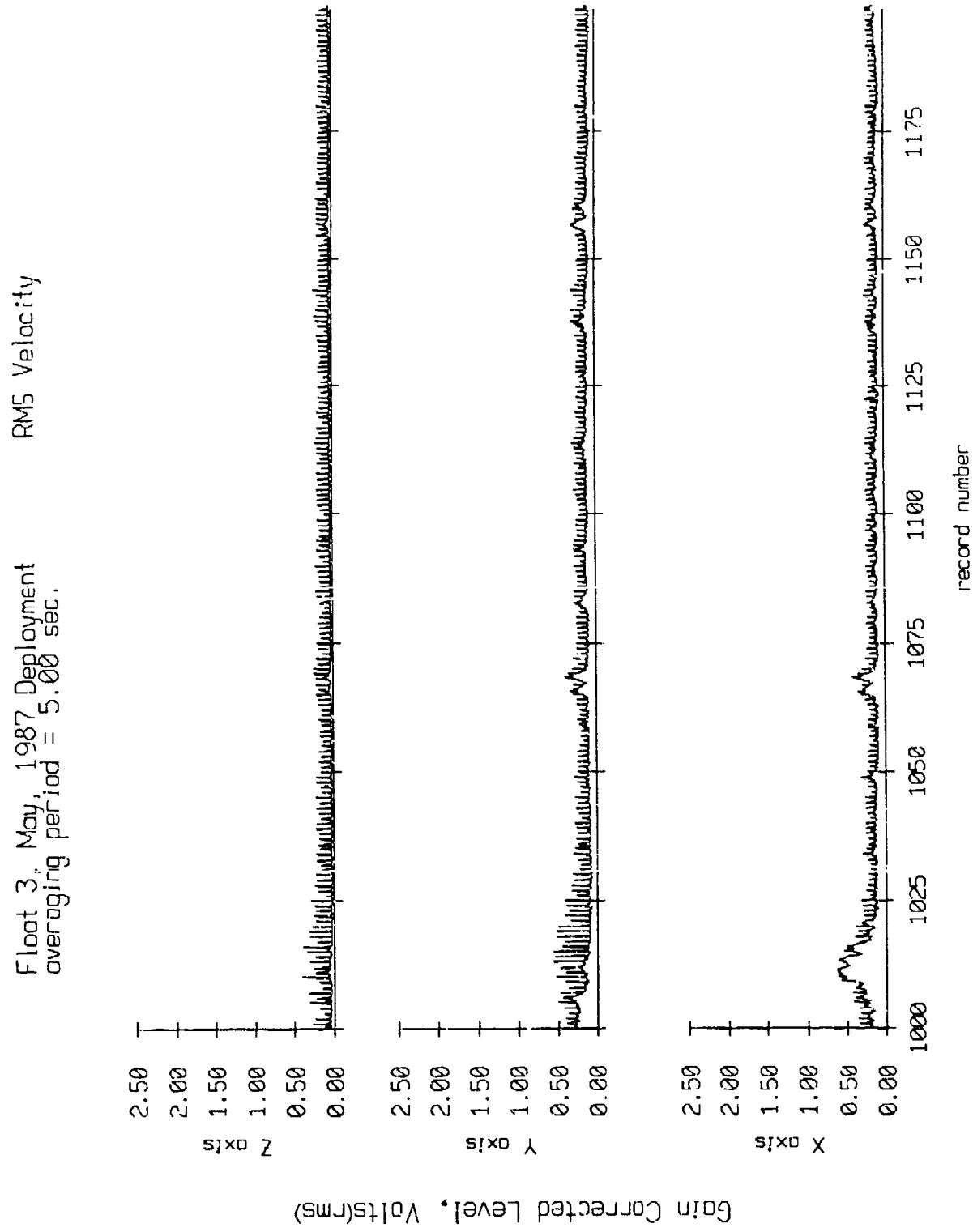


Figure IX.4f

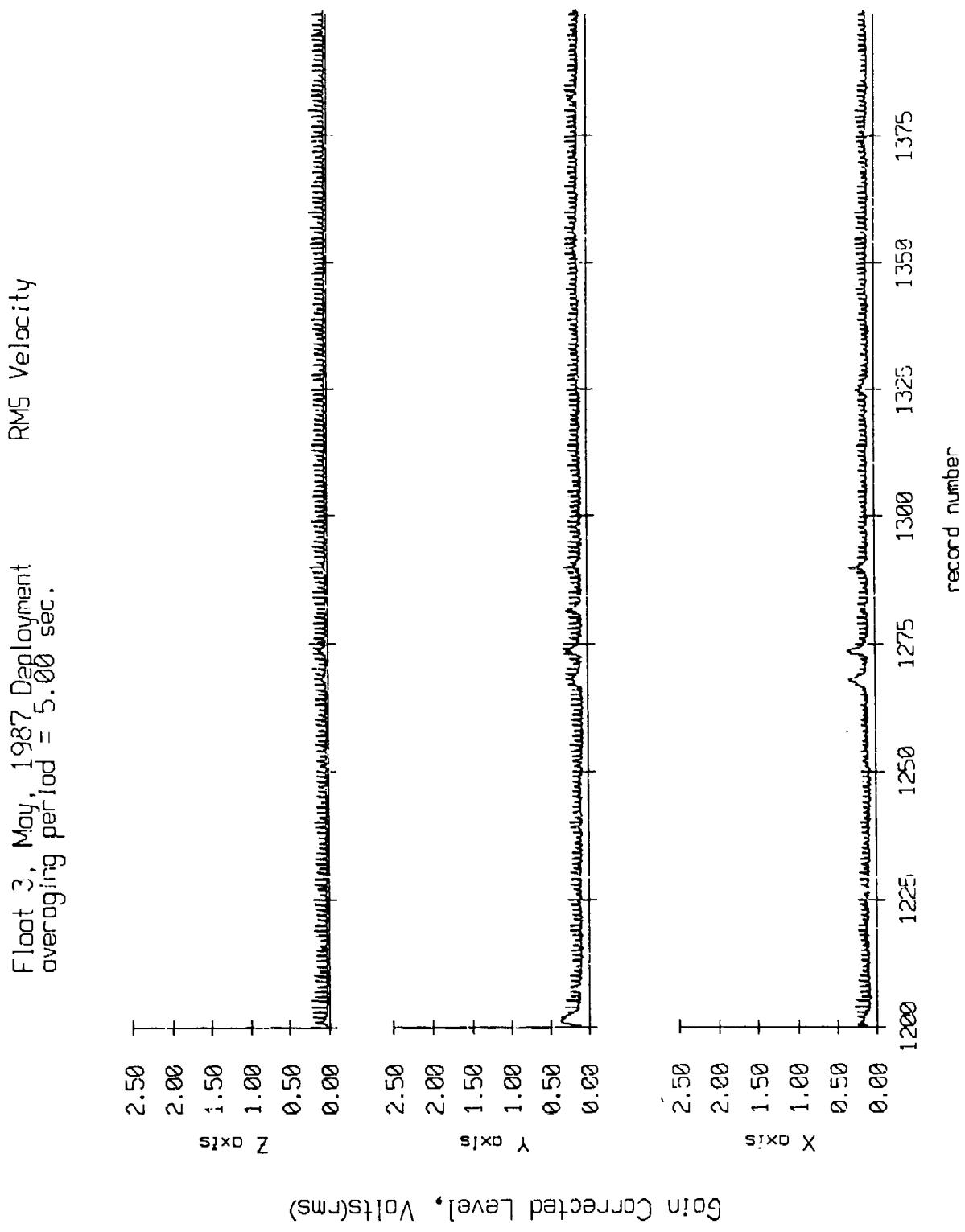


Figure IX.4g

Flight 3, May, 1987 Deployment
overaging period = 5.00 sec.

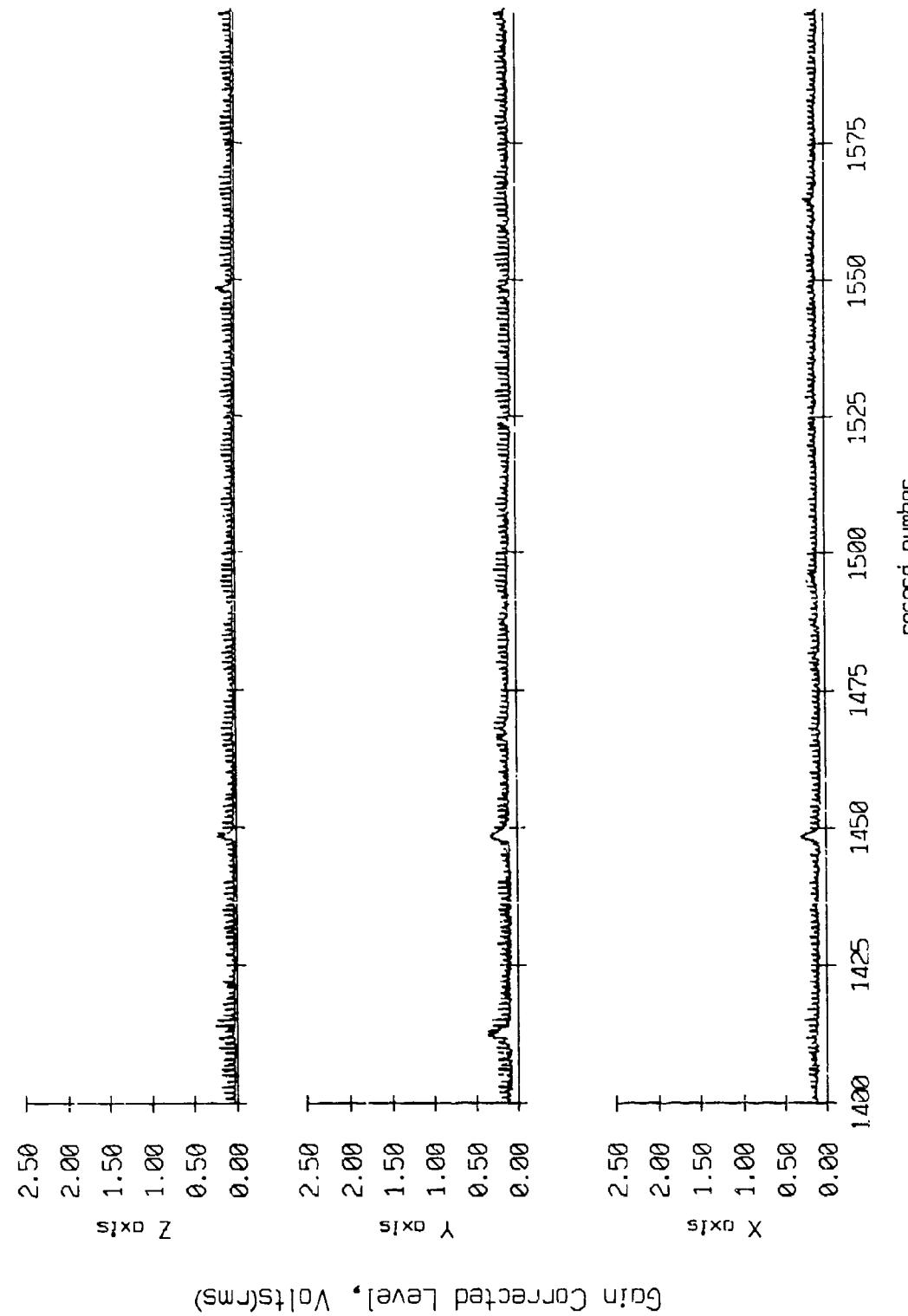


Figure IX.4h

Float 3, May, 1987 Deployment
averaging period = 5.00 sec.

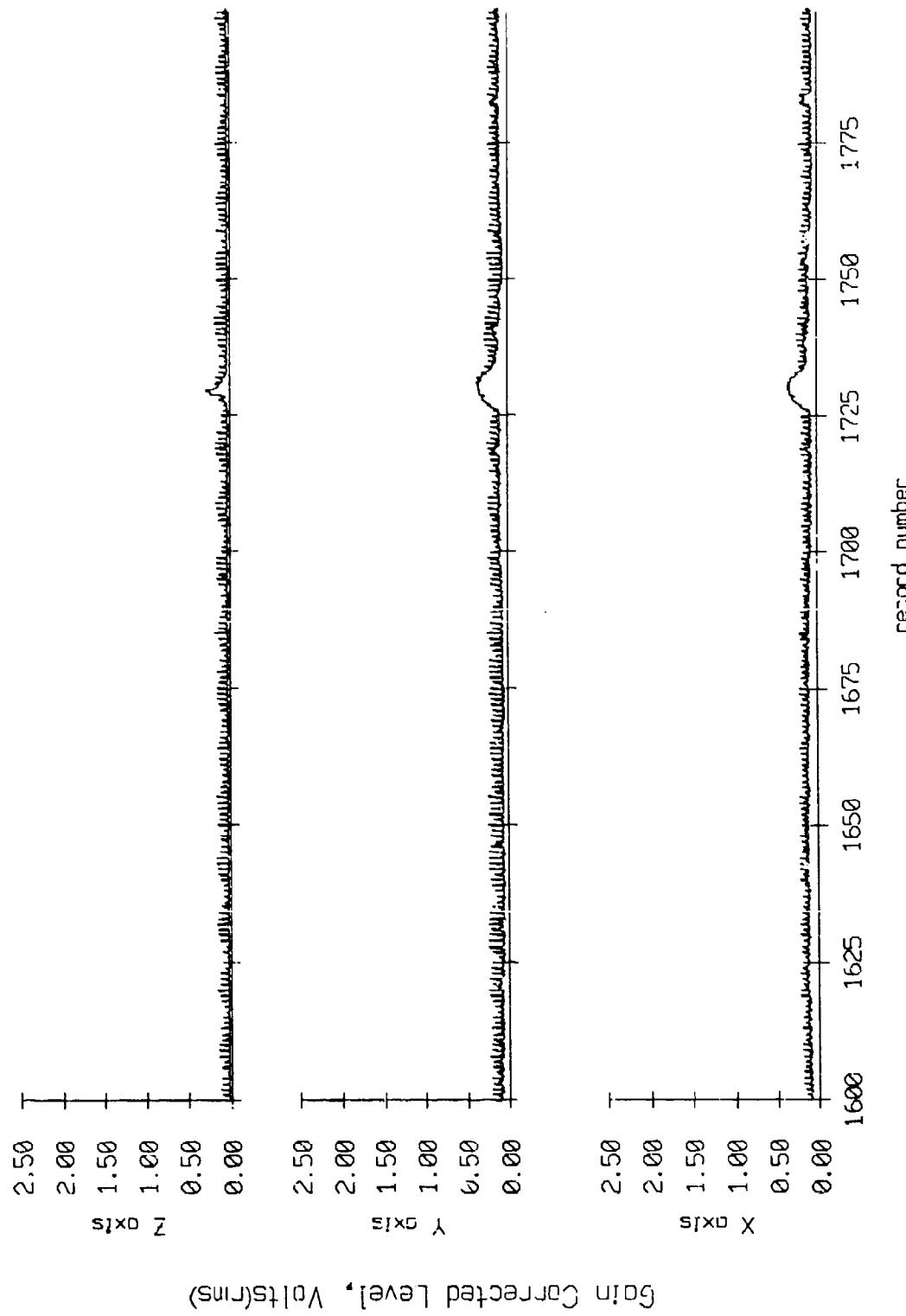


Figure IX.4i

Fleet 3, May, 1987 Deployment
overgoing period = 5.00 sec.

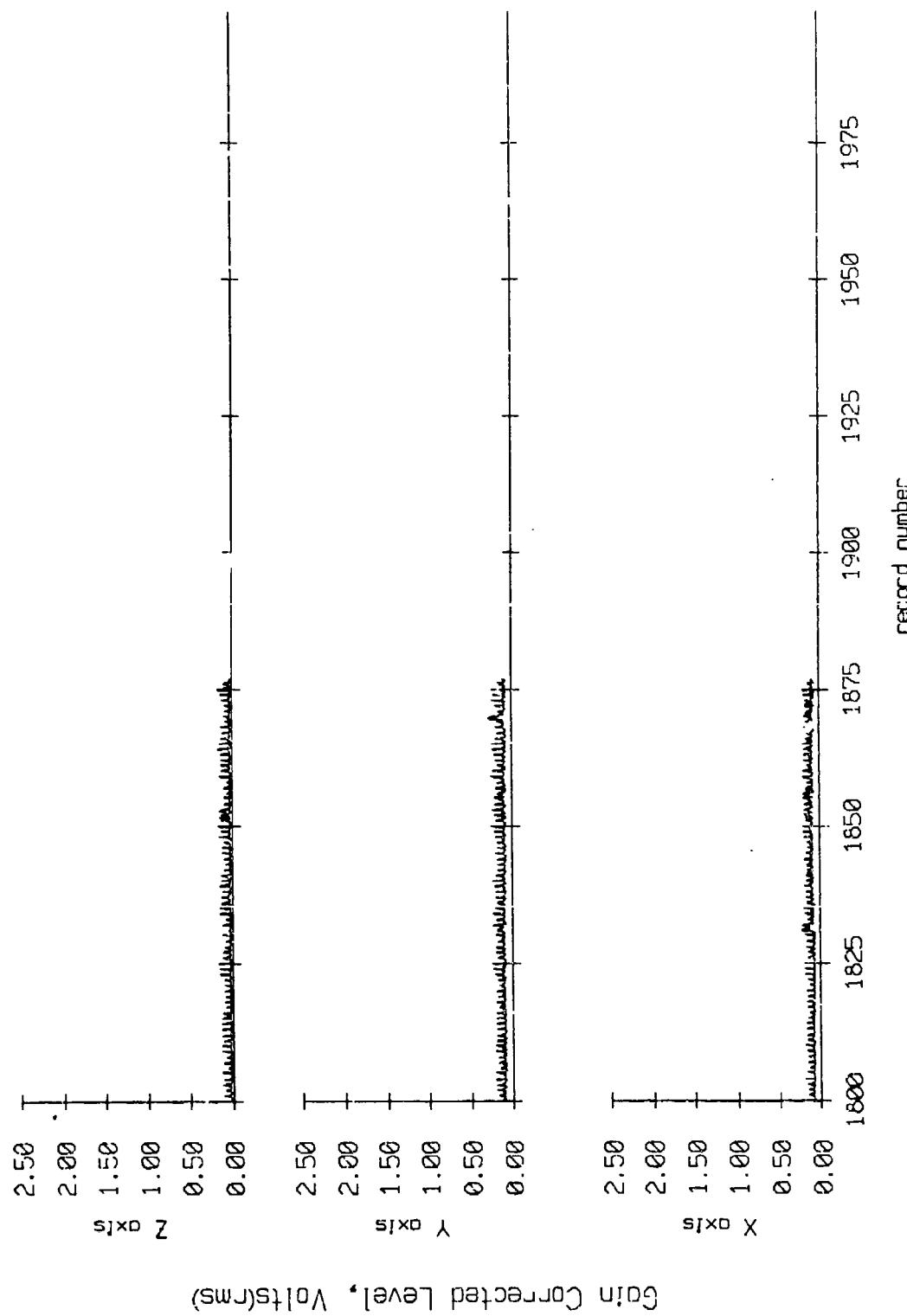


Figure IX.4j

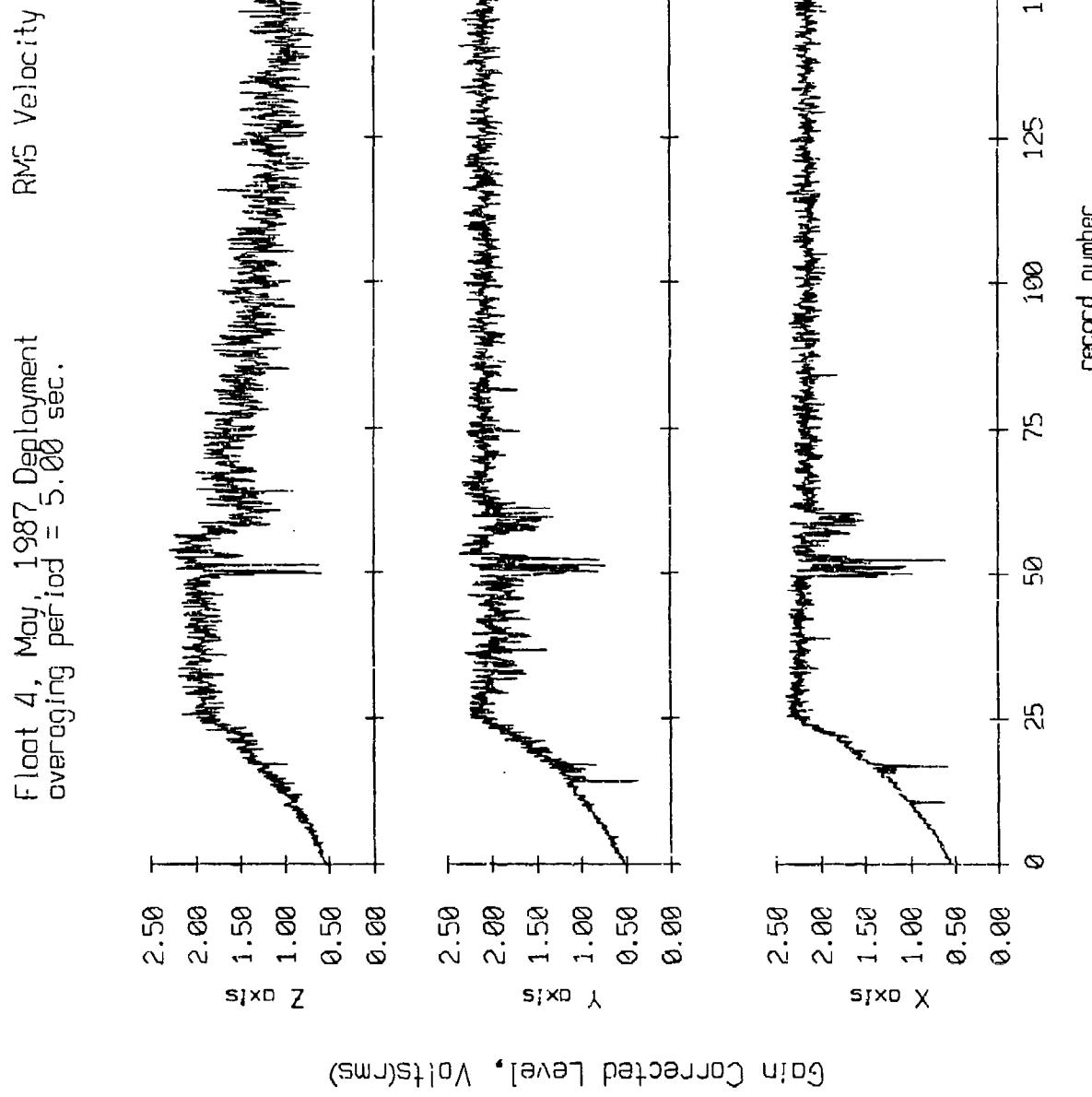


Figure IX.5a

Float 4, May, 1987 Deployment
overaging period = 5.00 sec.

RMS Velocity

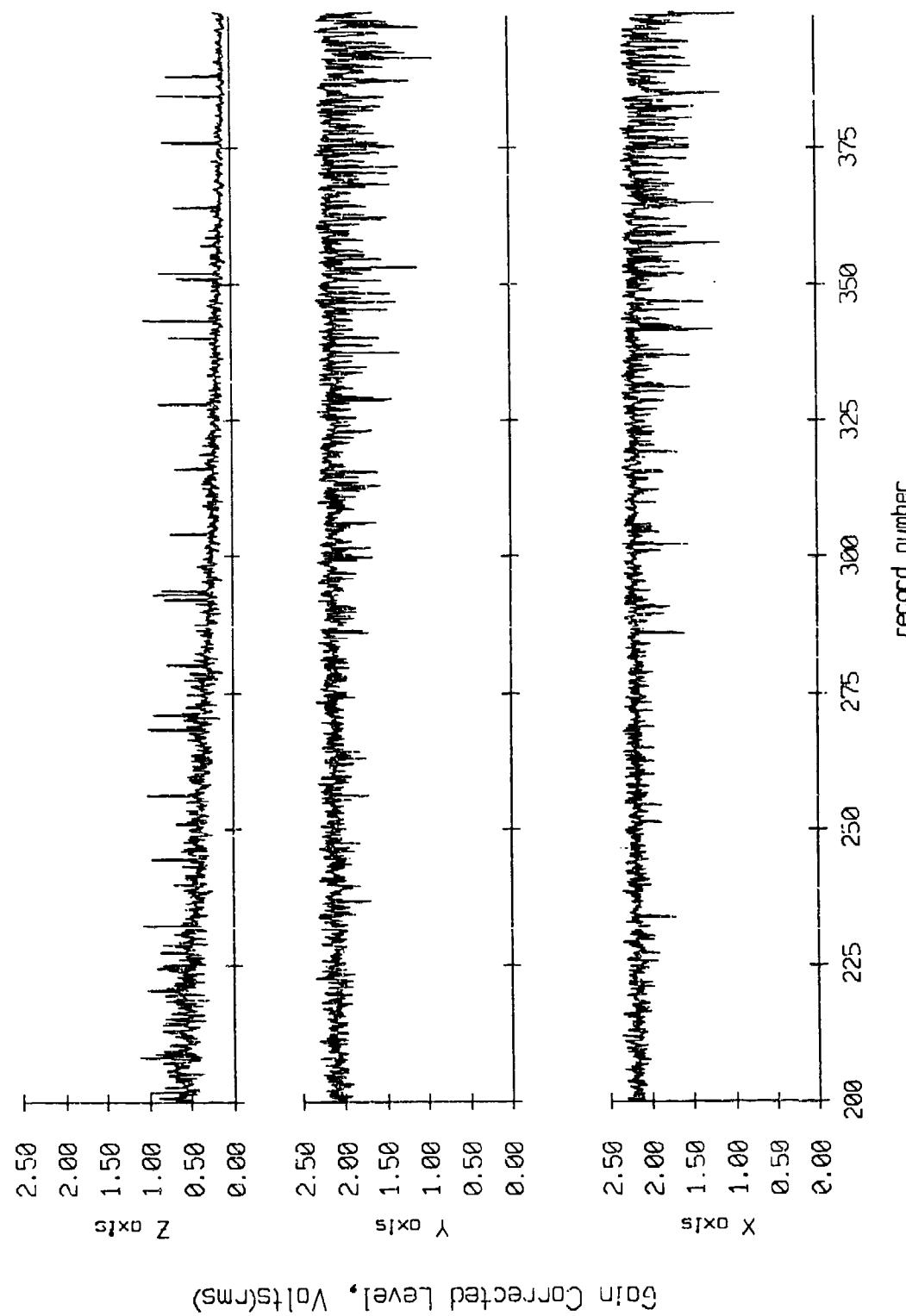


Figure IX.5b

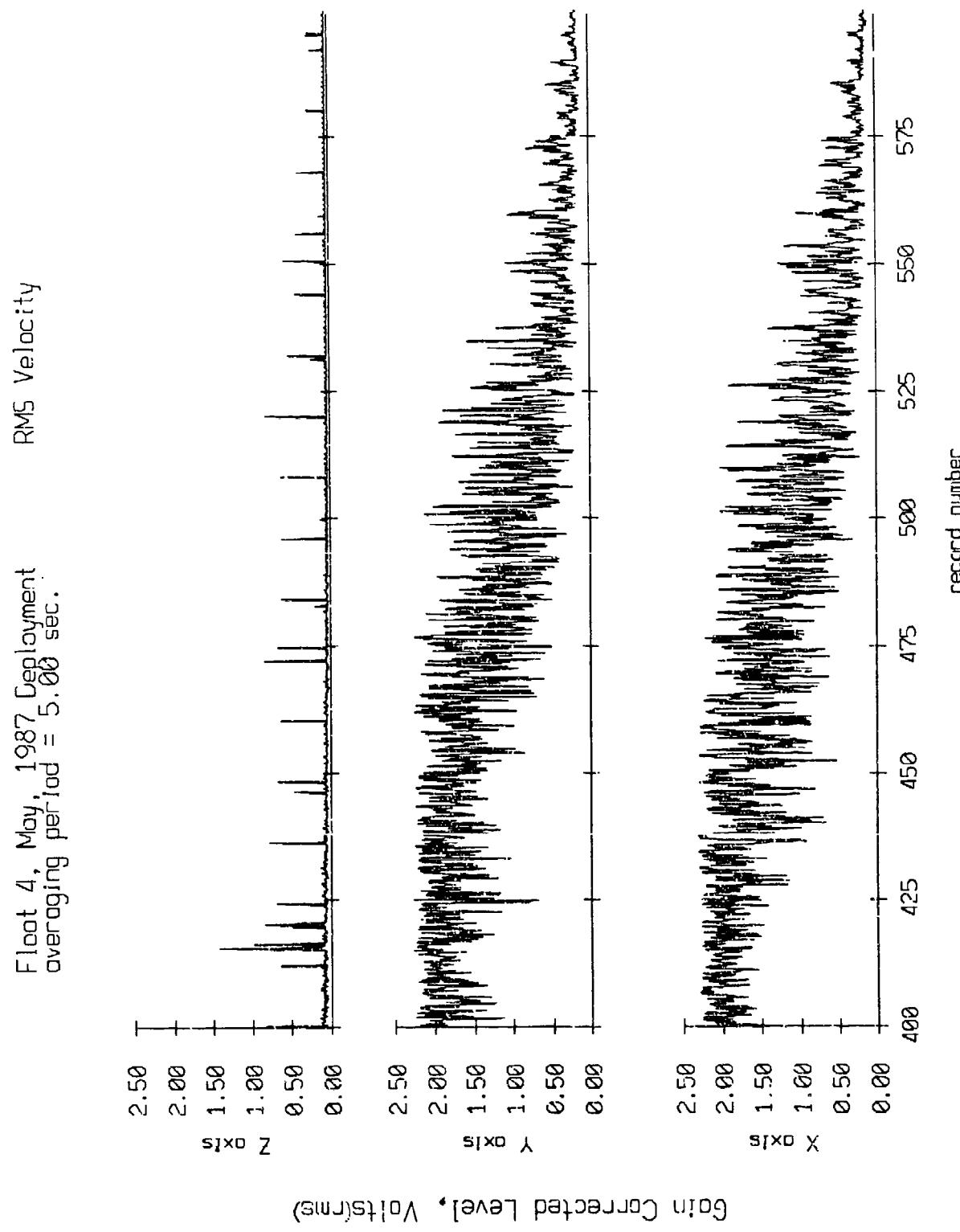


Figure IX.5c

Fleet 4, May 1987 Deployment
overaging period = 5.00 sec.

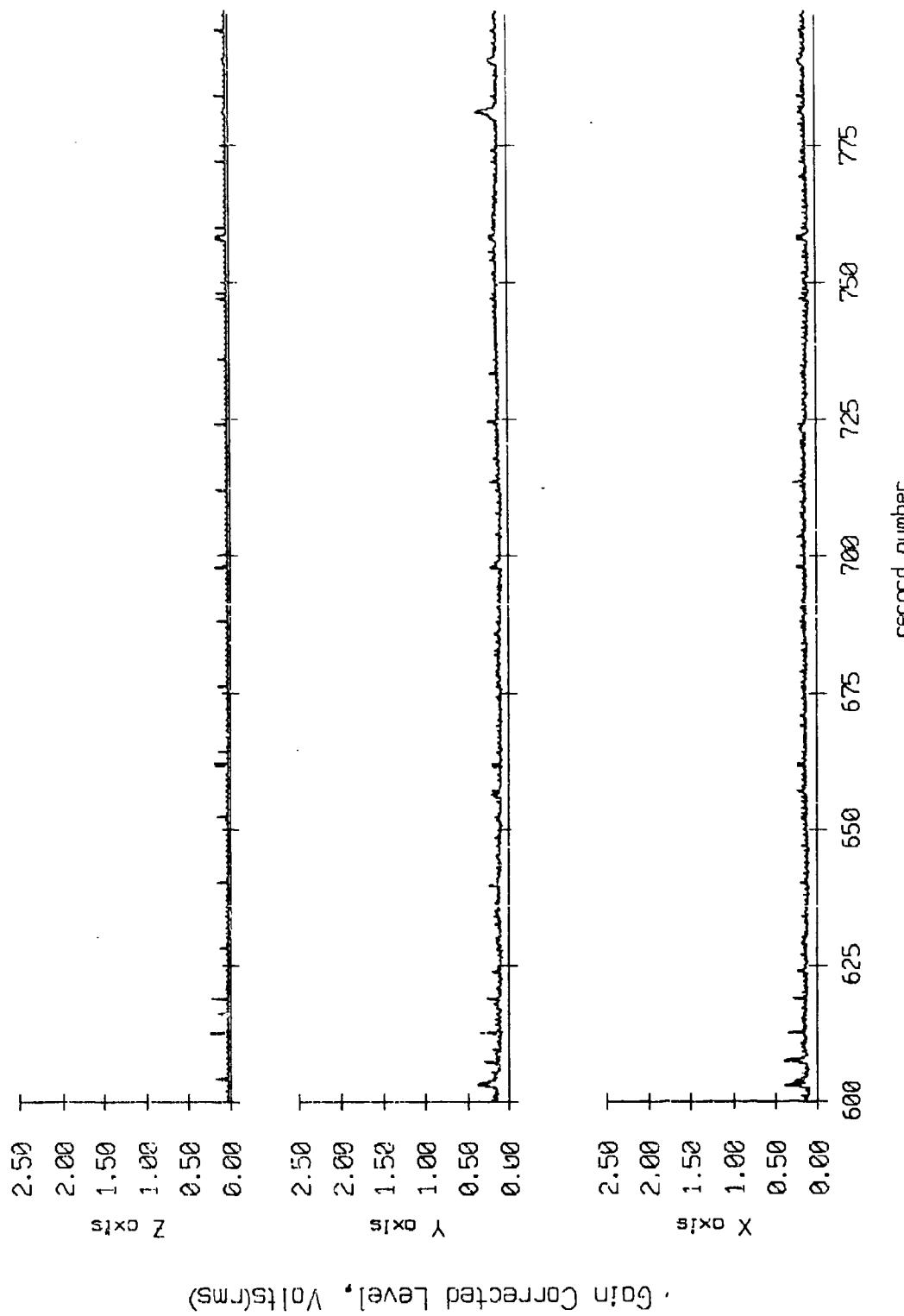


Figure IX.5d

Fleet 4, May, 1987 Deployment
overgaging period = 5.00 sec.

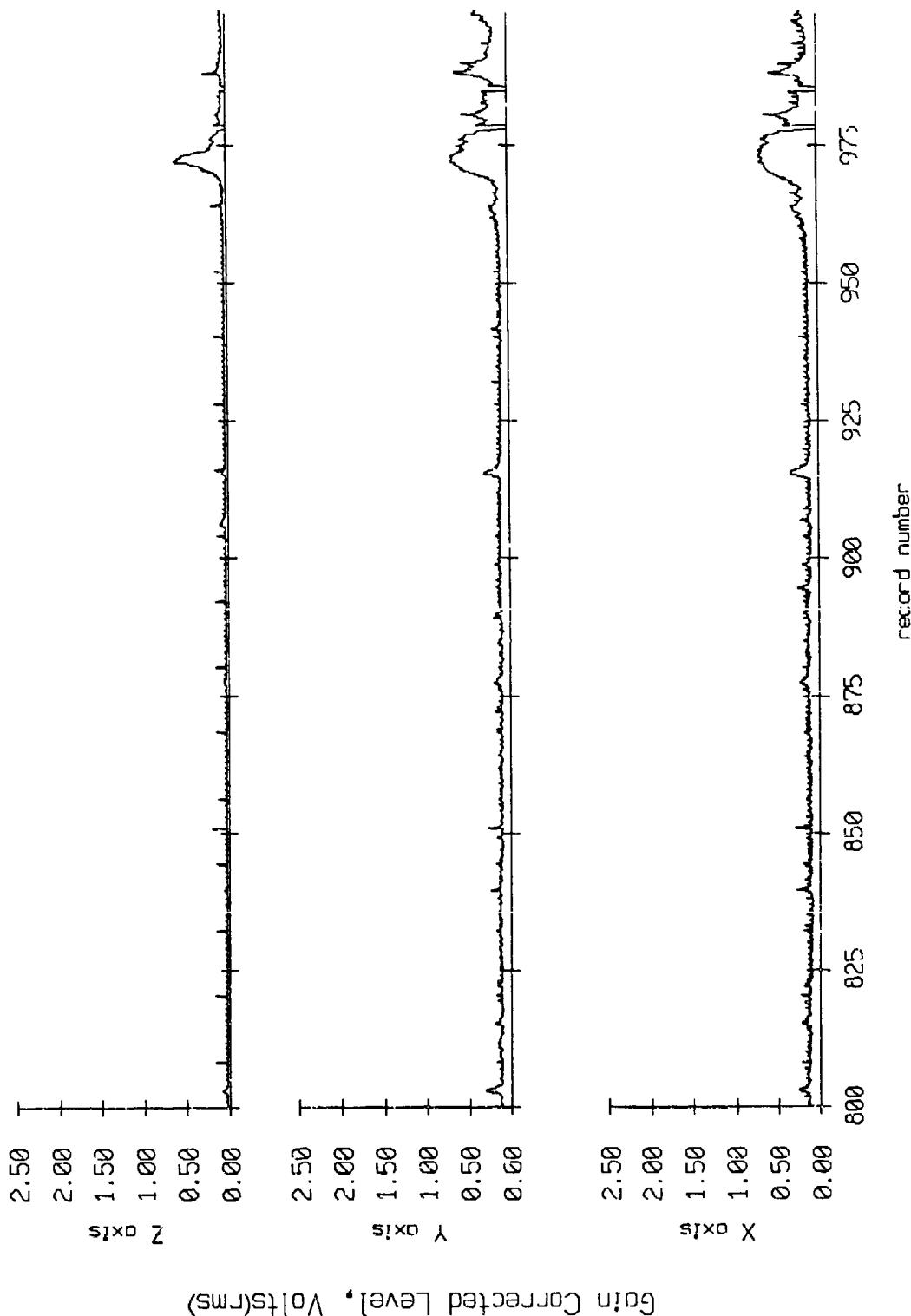


Figure IX.5e

Fleet 4, May 1987 Deployment
overaging period = 5.00 sec.

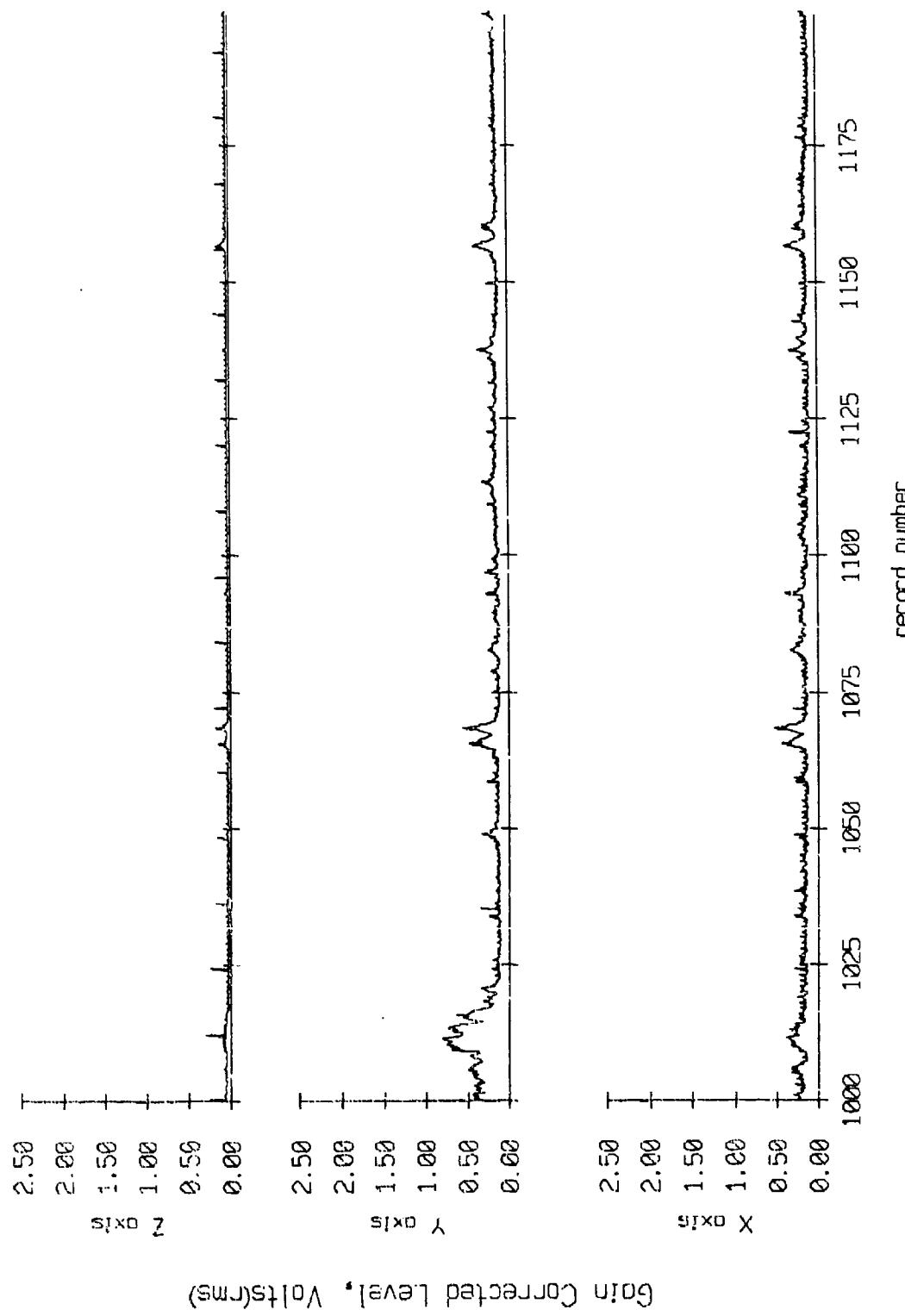
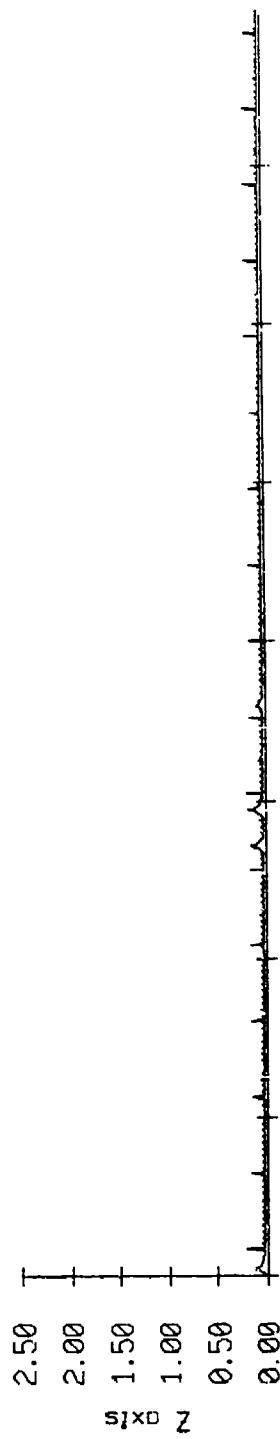


Figure IX.5f

Float 4, May 1987 Deployment
overdging period = 5.00 sec.

RMS Velocity



Gain Corrected Level, Volts(rms)

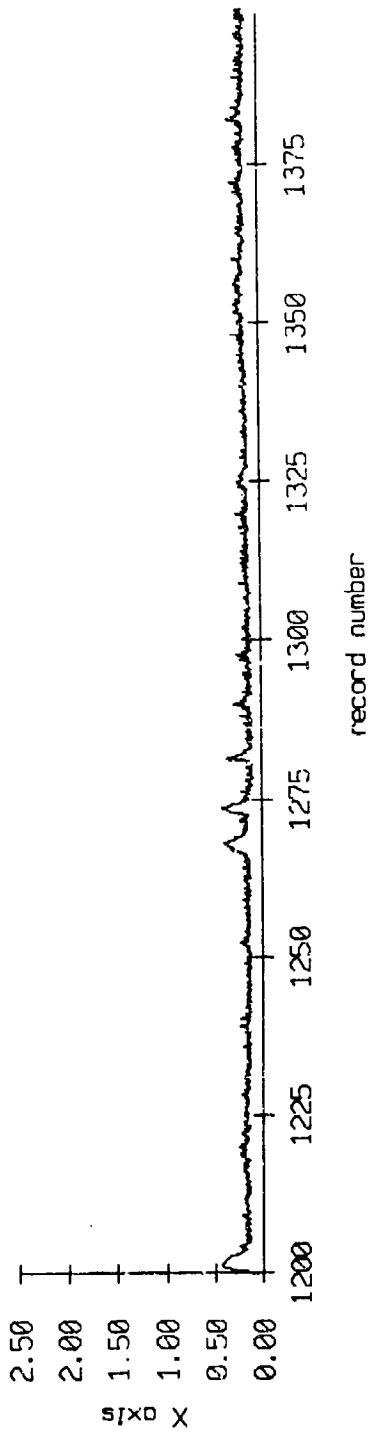


Figure IX.5g

Float 4, May, 1987 Deployment
averaging period = 5.00 sec.

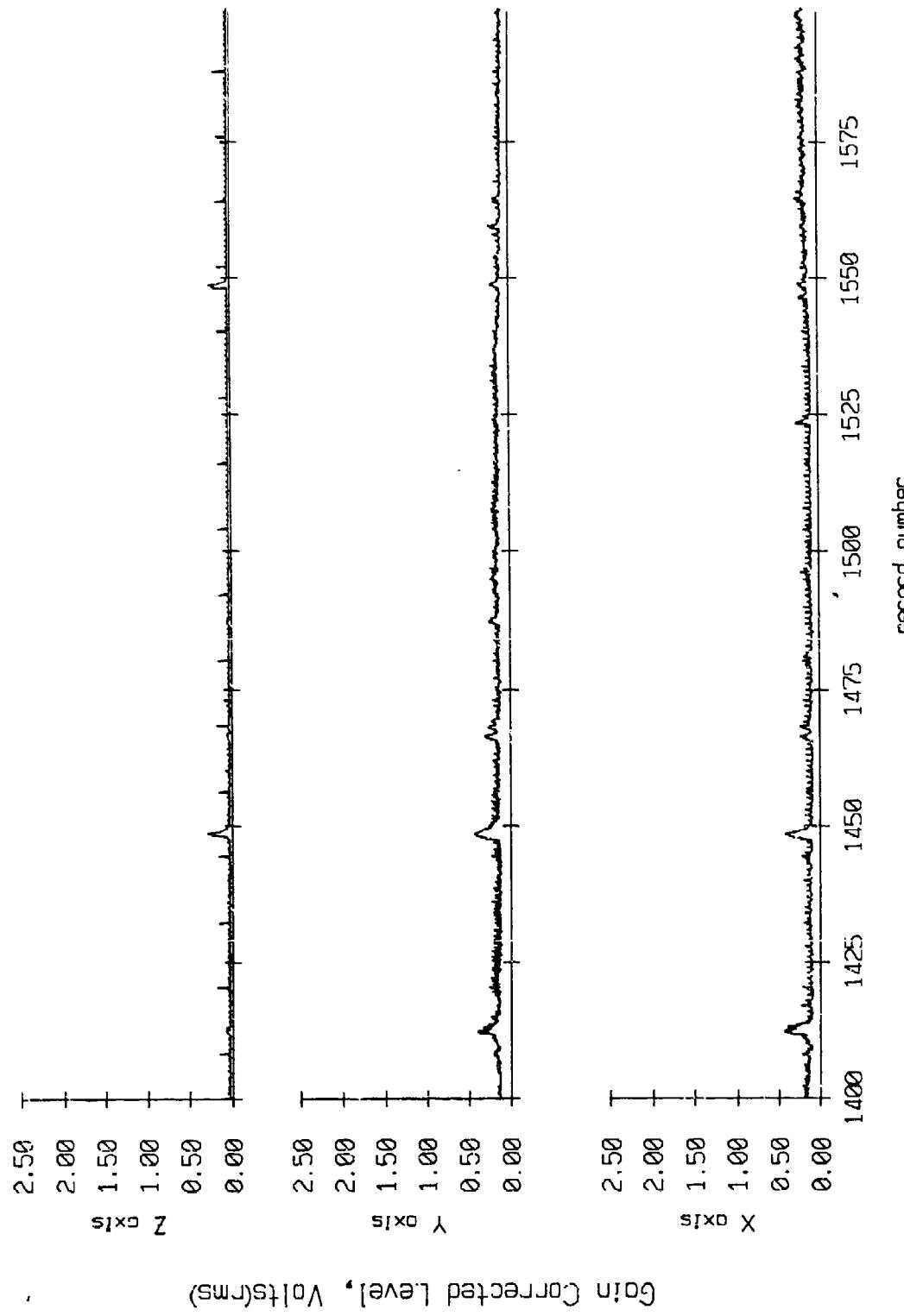


Figure IX.5h

Float 4, May, 1987 Deployment
averaging period = 5.00 sec.

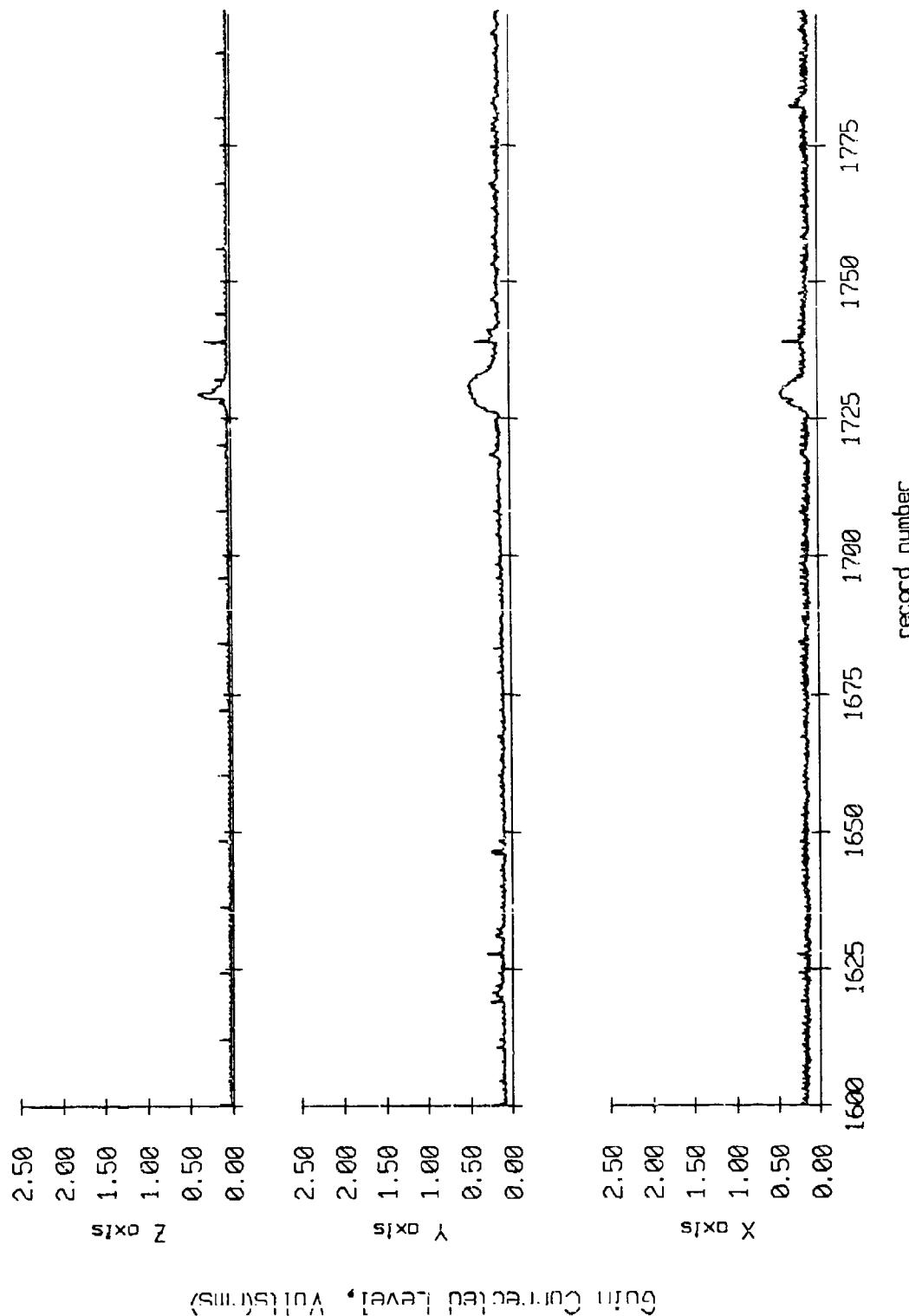


Figure IX.5i

Float 4, May, 1987 Deployment
overaging period = 5.00 sec.

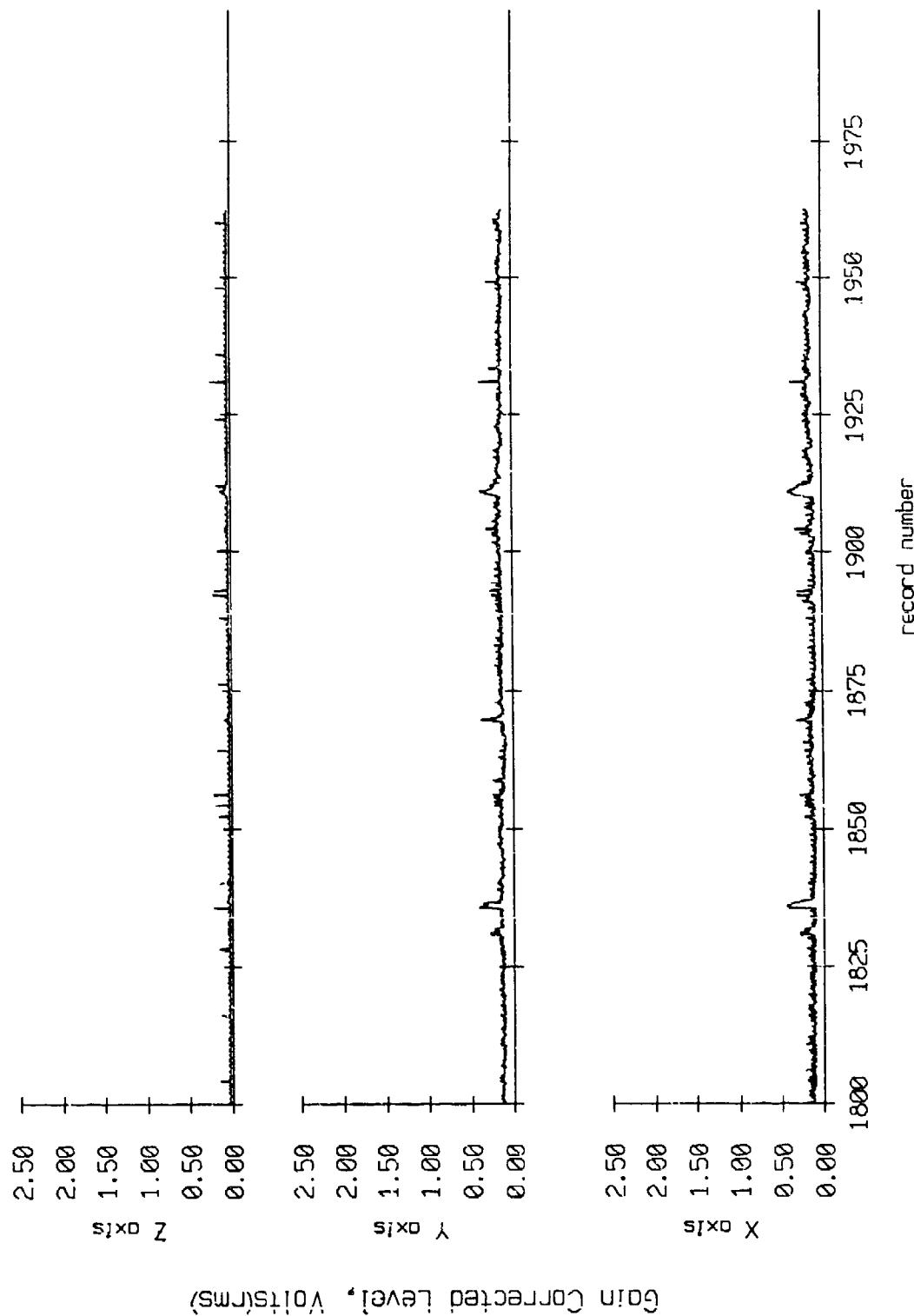


Figure IX.5j

Float 7, May, 1987 Deployment
averaging period = 5.00 sec.

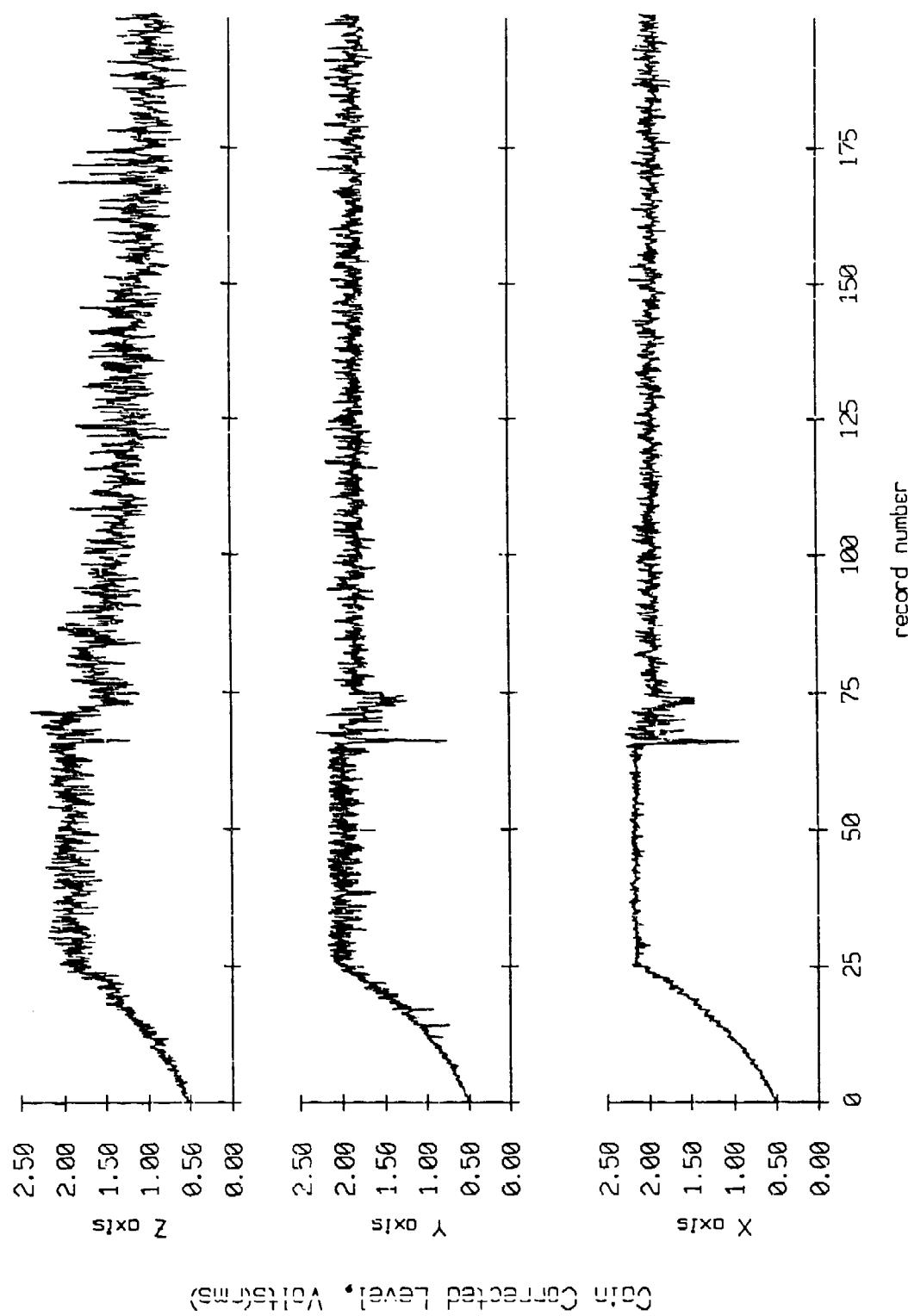


Figure IX.6a

Fleet 7, May, 1987 Deployment
averaging period = 5.00 sec.

RMS Velocity

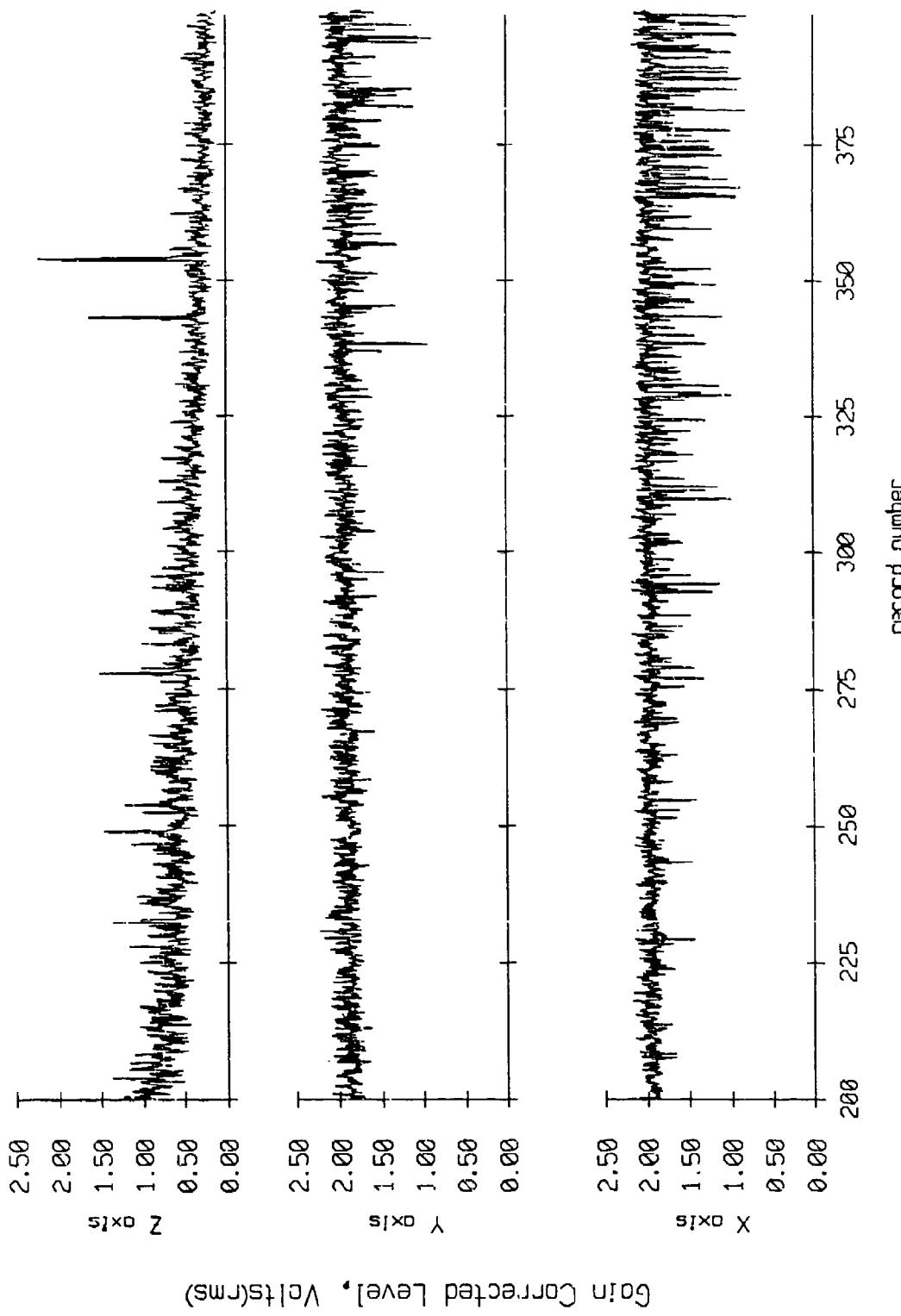
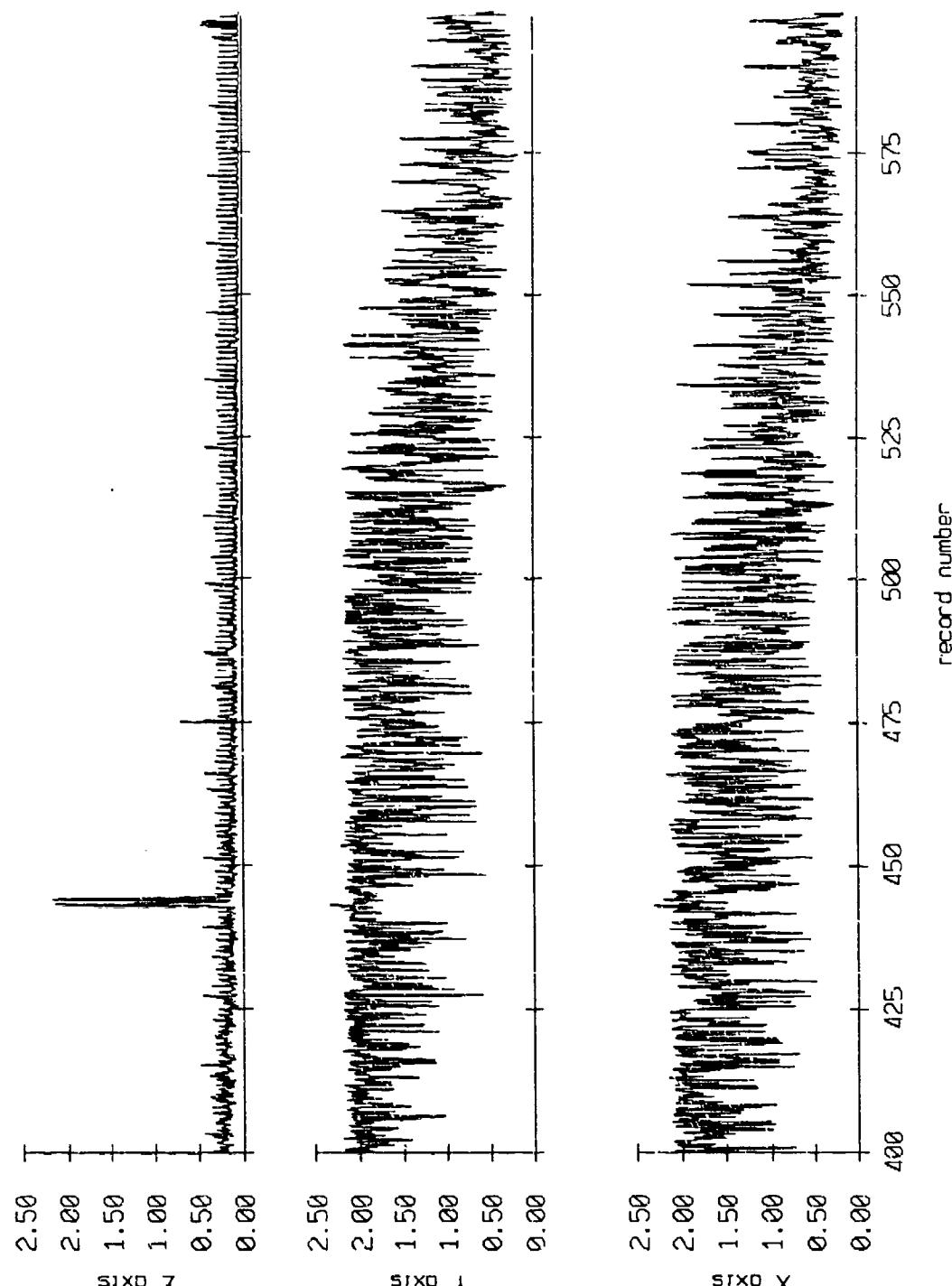


Figure IX.6b

Float 7, May, 1987 Deployment
overgaging period = 5.00 sec.

RMS Velocity



Gain Corrected Level, Volts(RMS)

Figure IX.6c

Float 7, May 1987 Deployment
overgoing period = 5.00 sec.

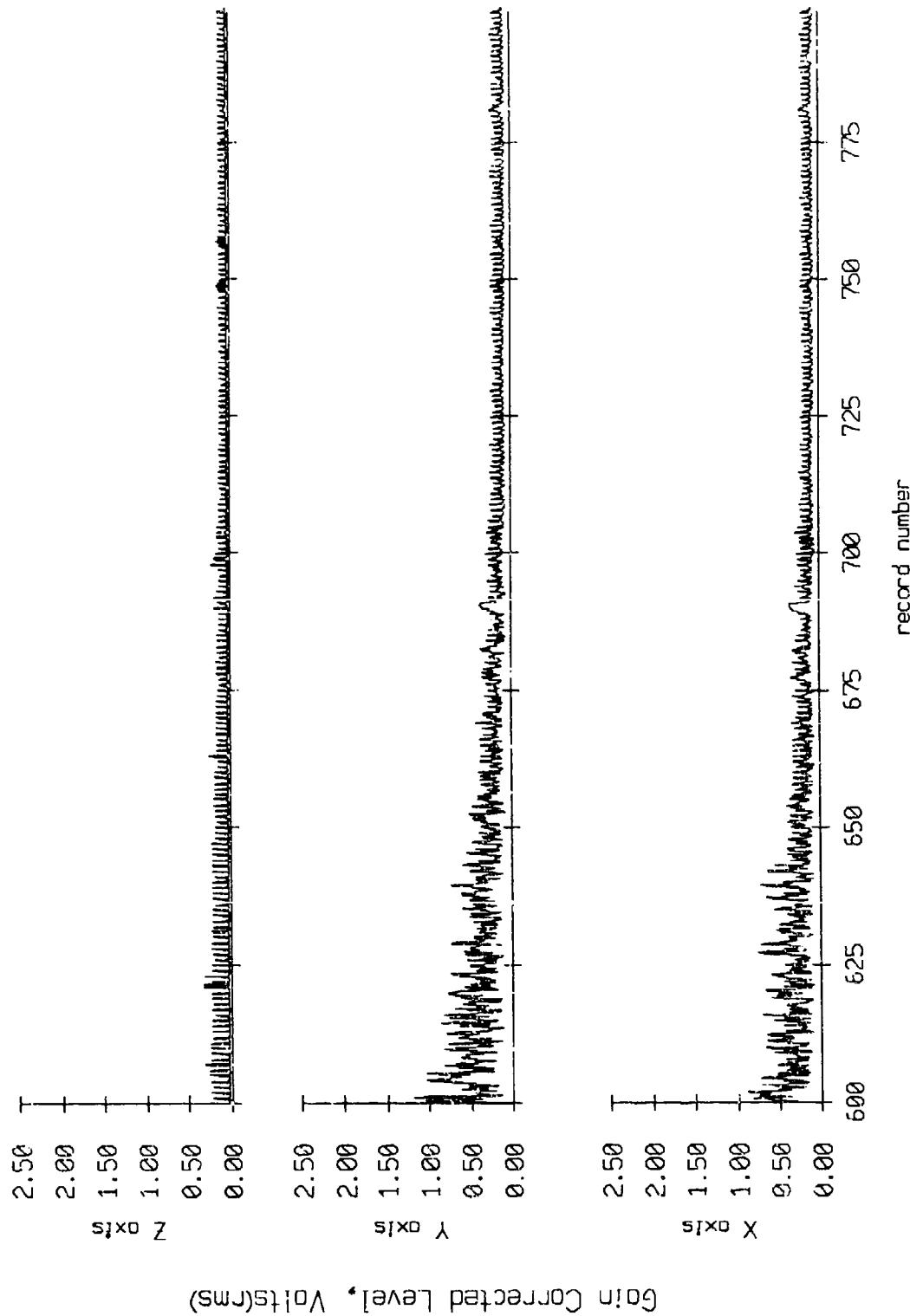


Figure IX.6d

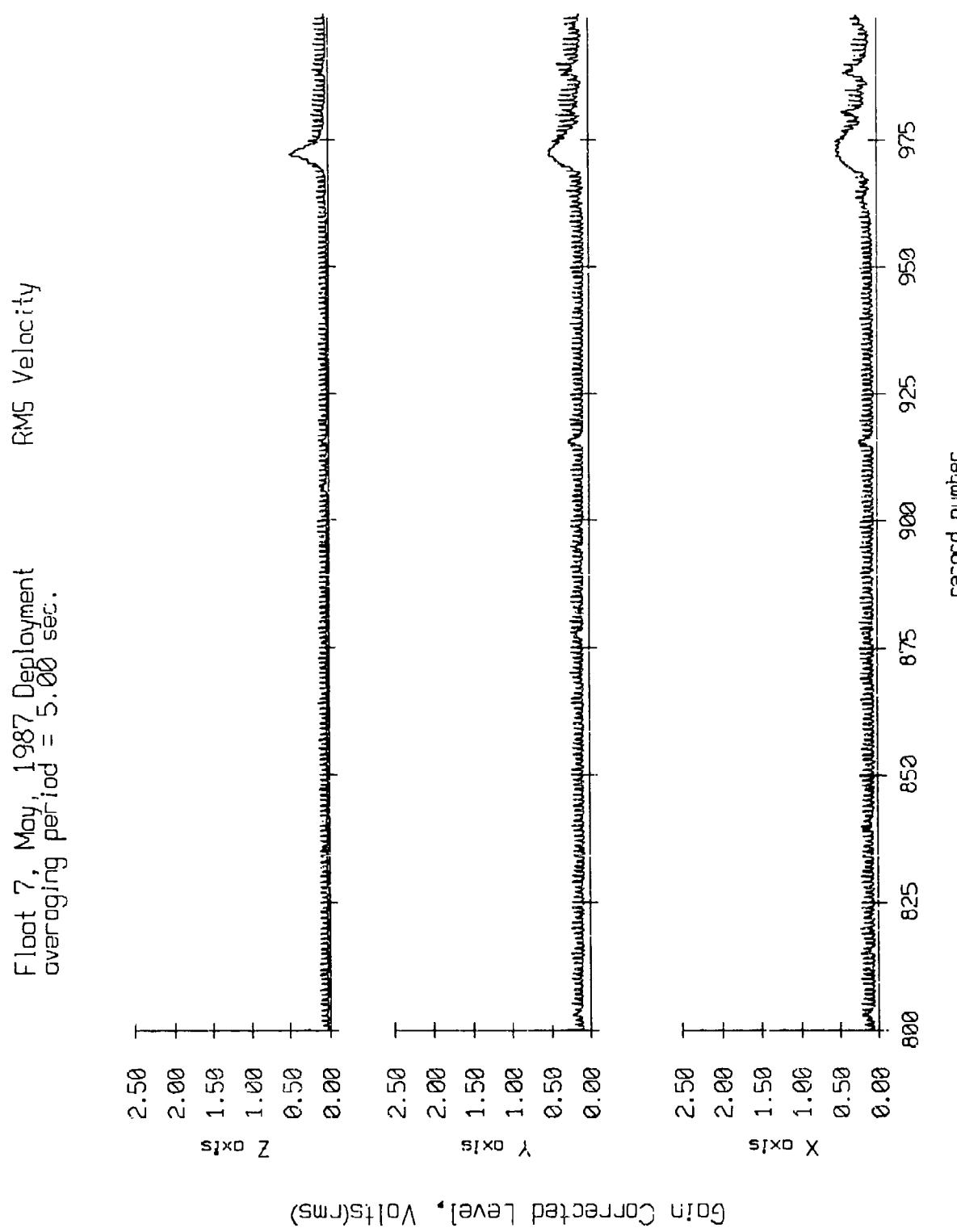
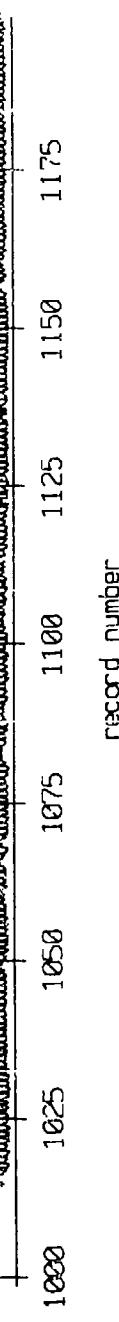


Figure IX.6e



Floot 7, May, 1987 Deployment = 5.00 sec.
Averaging Period = 5.00 sec.

Gain Corrected Level, Volts(RMS)

Figure IX.6f

Float 7, May, 1987 Deployment
averaging period = 5.00 sec.

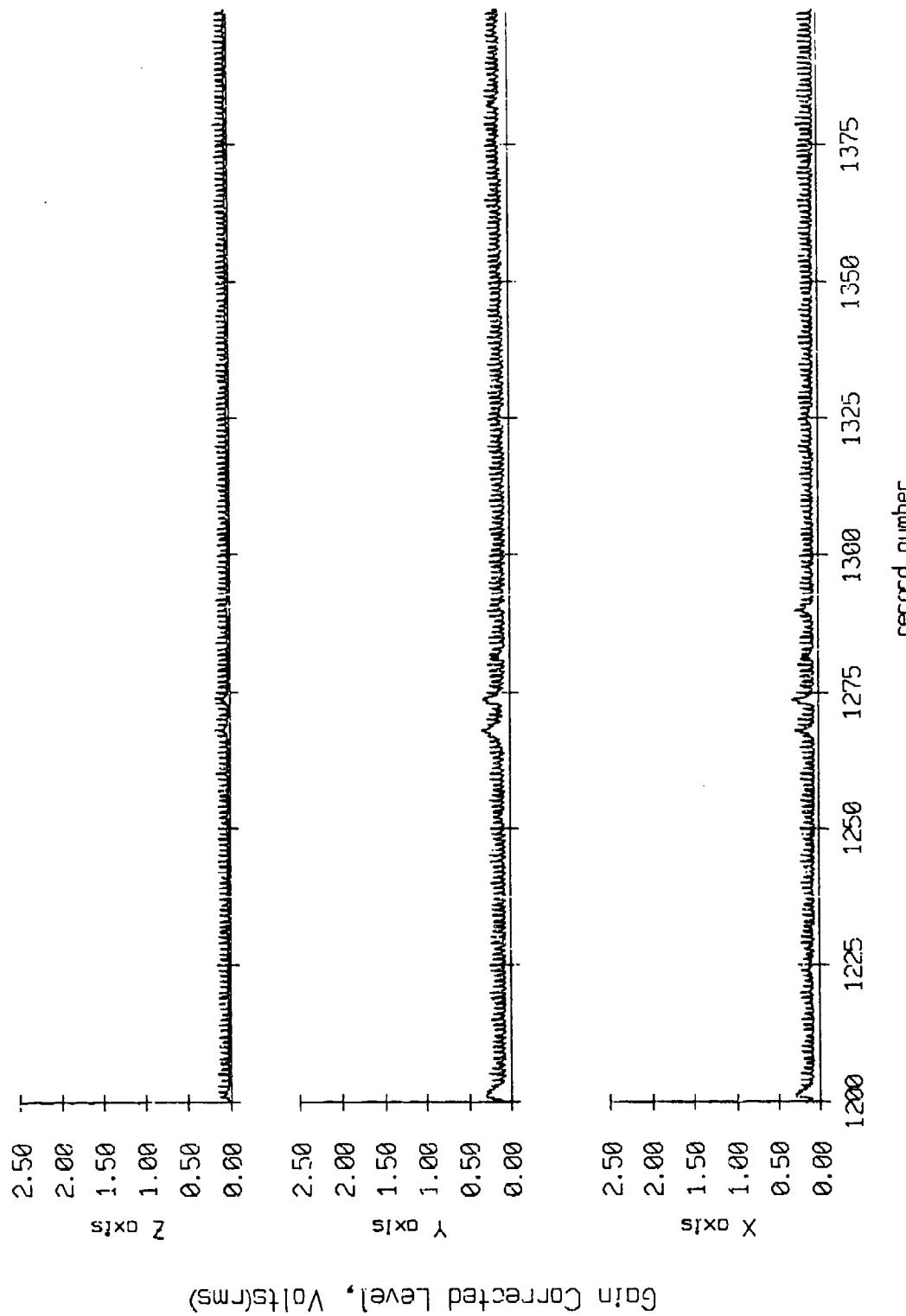


Figure IX.6g

Float 7, May, 1987 Deployment
averaging period = 5.00 sec.

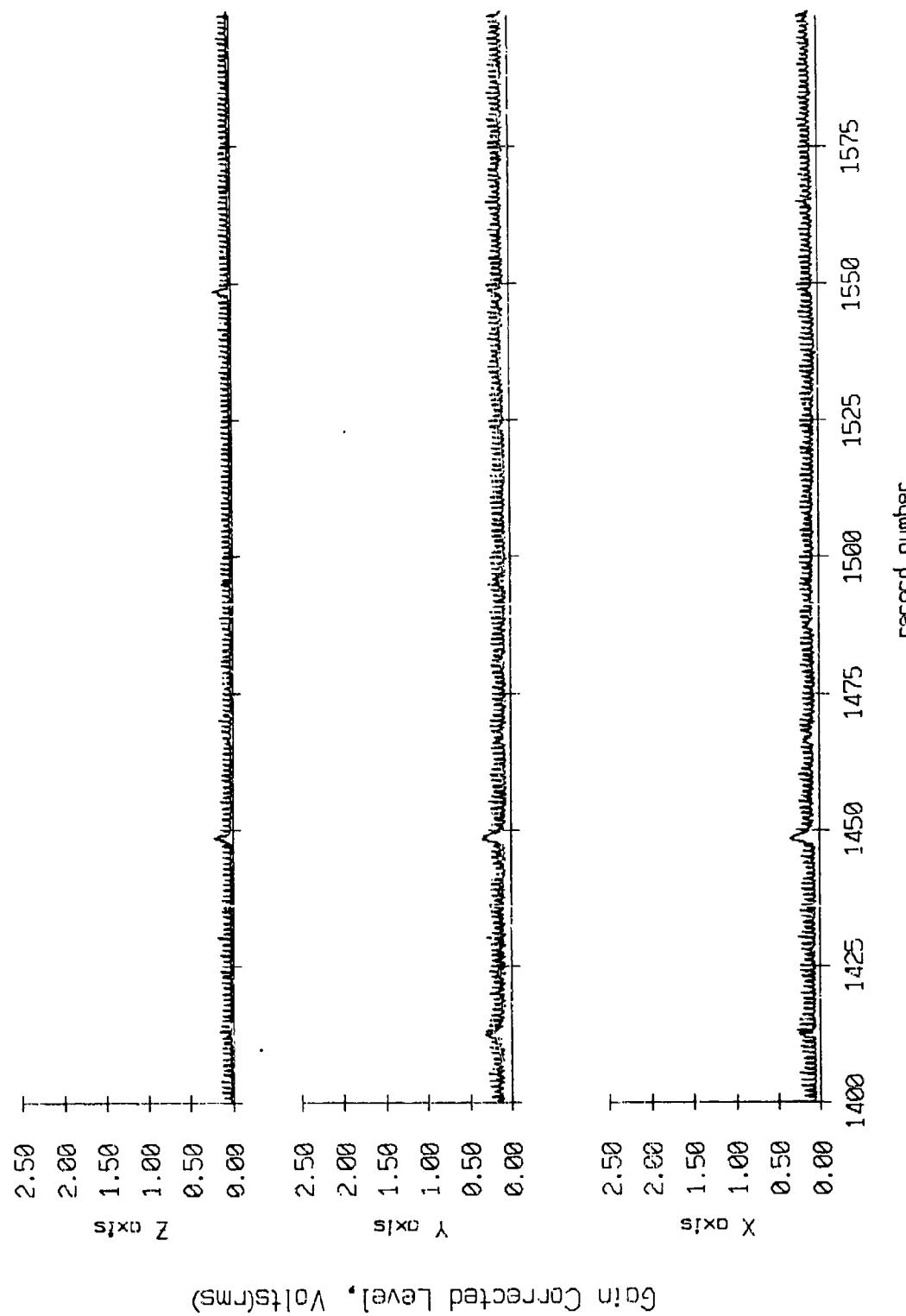


Figure IX.6h

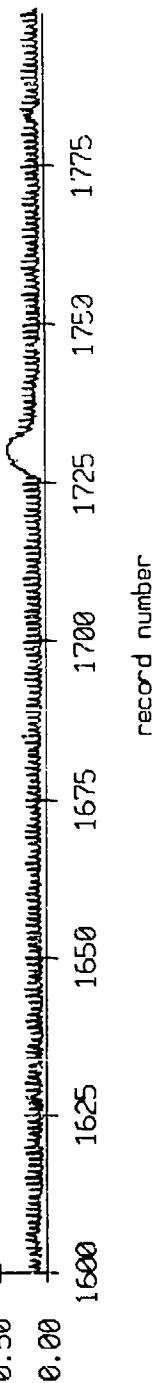


Figure IX.6i

Floct 7, May, 1987 Deployment
overgning period = 5.00 sec.

RMS Velocity

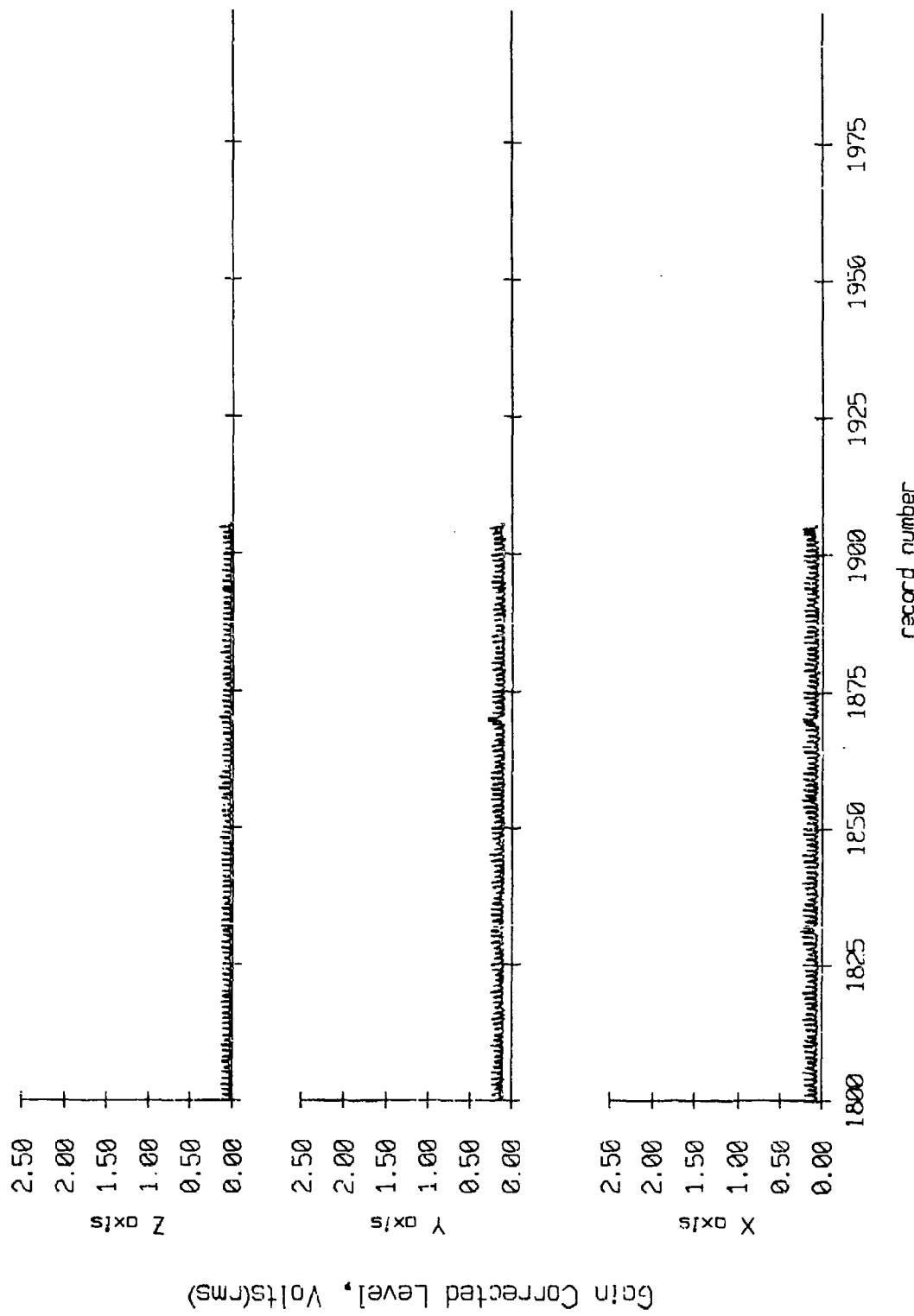


Figure IX.6j

Float 8, May, 1987 Deployment
overriding period = 5.00 sec.

RMS Velocity

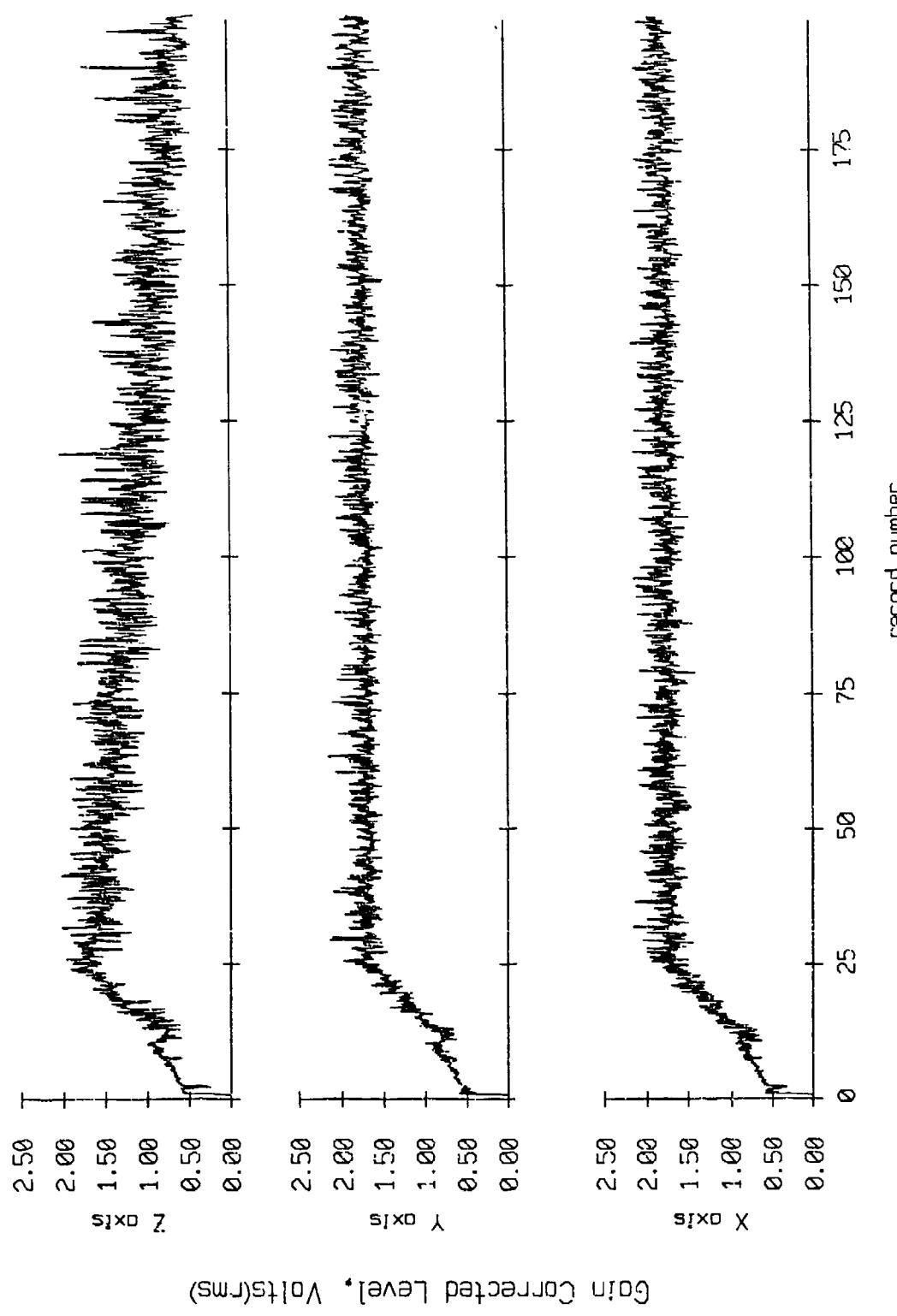


Figure IX.7a

Float 8, May 1987 Deployment
averaging period = 5.00 sec.

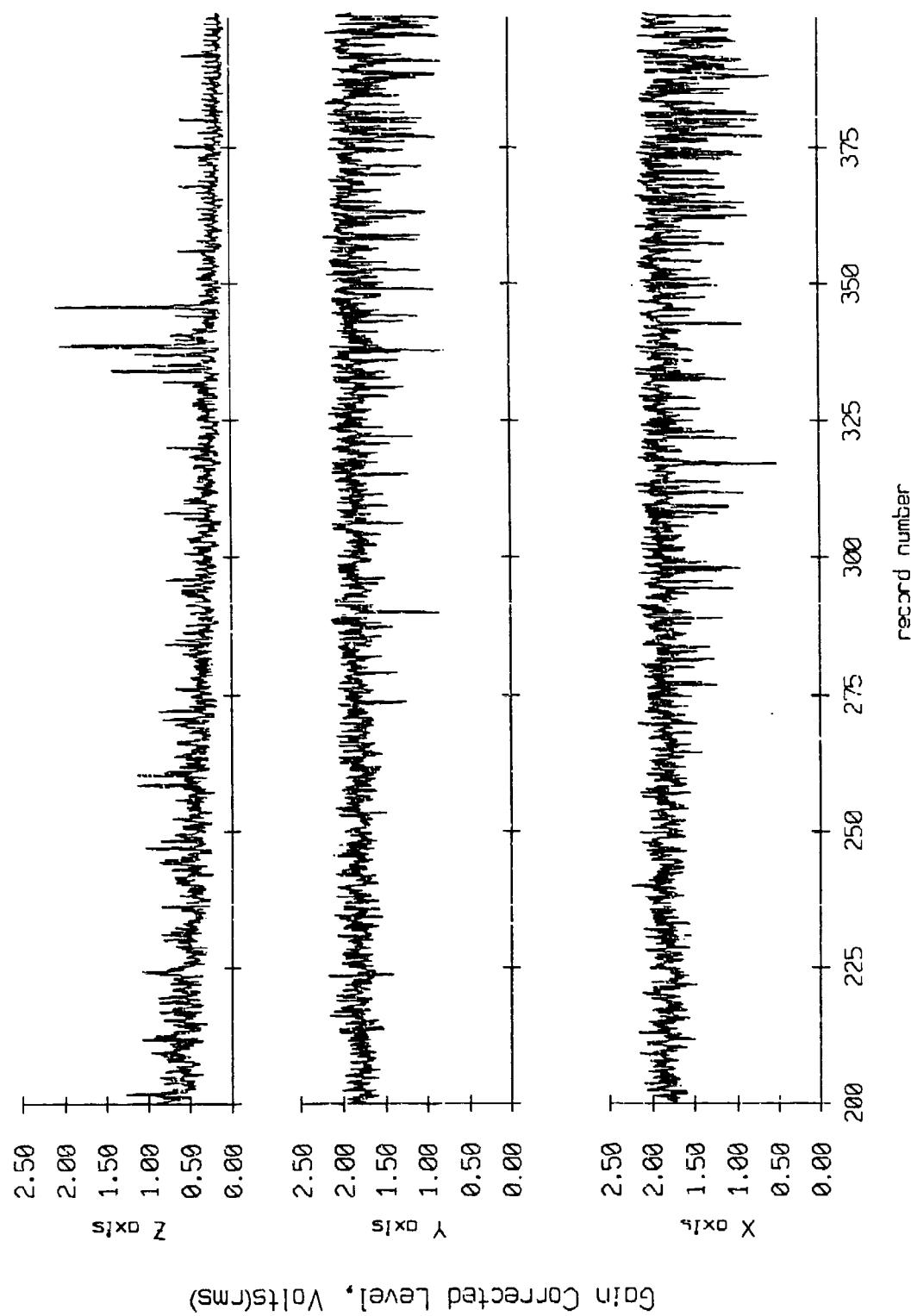


Figure IX.7b

Float 8, May, 1987 Deployment
overaging period = 5.00 sec.

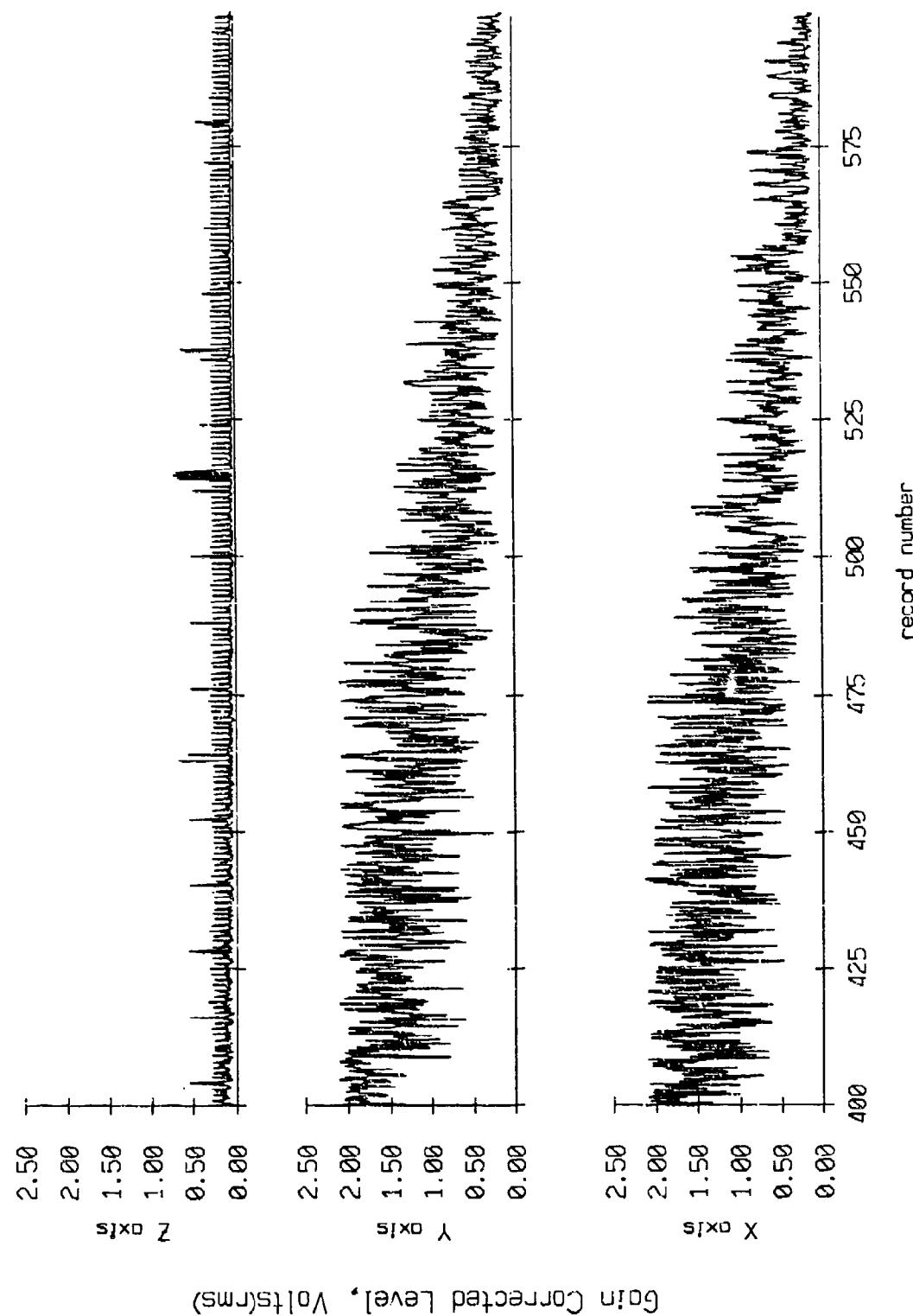


Figure IX.7c

Float 8, May, 1987 Deployment
overgaging period = 5.00 sec.

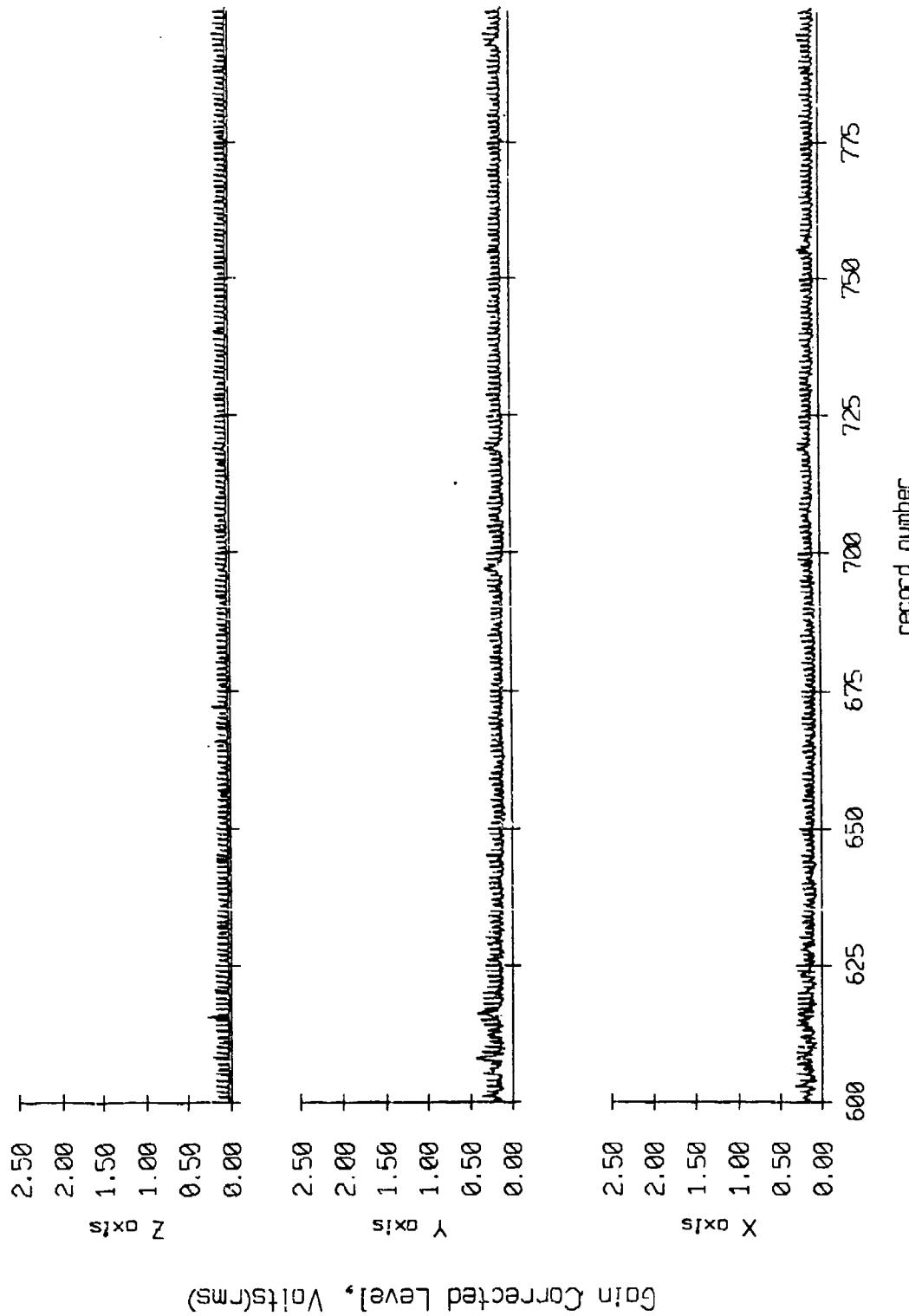


Figure IX.7d

Float 8, May 1987 Deployment
overaging period = 5.00 sec.

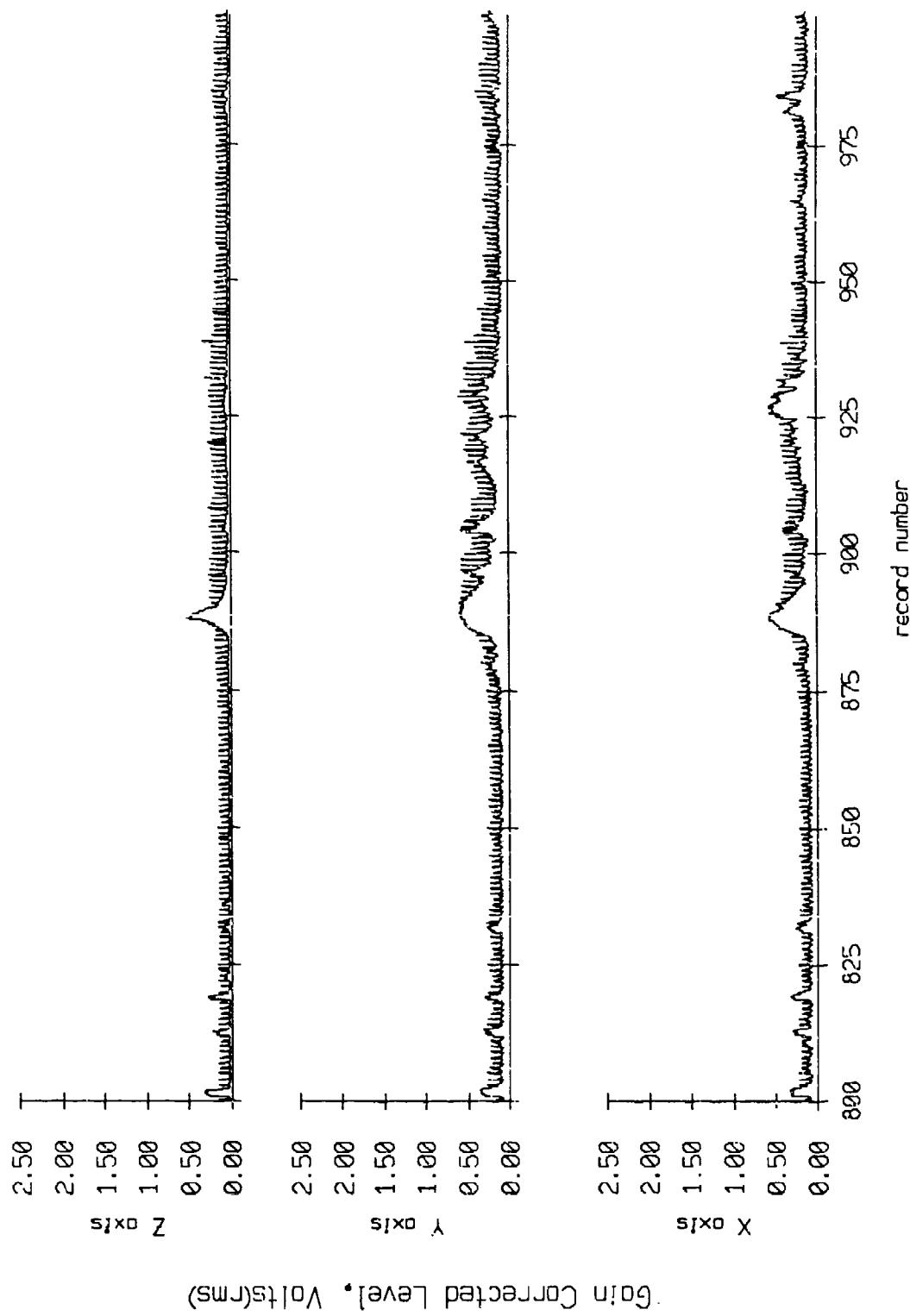


Figure IX.7e

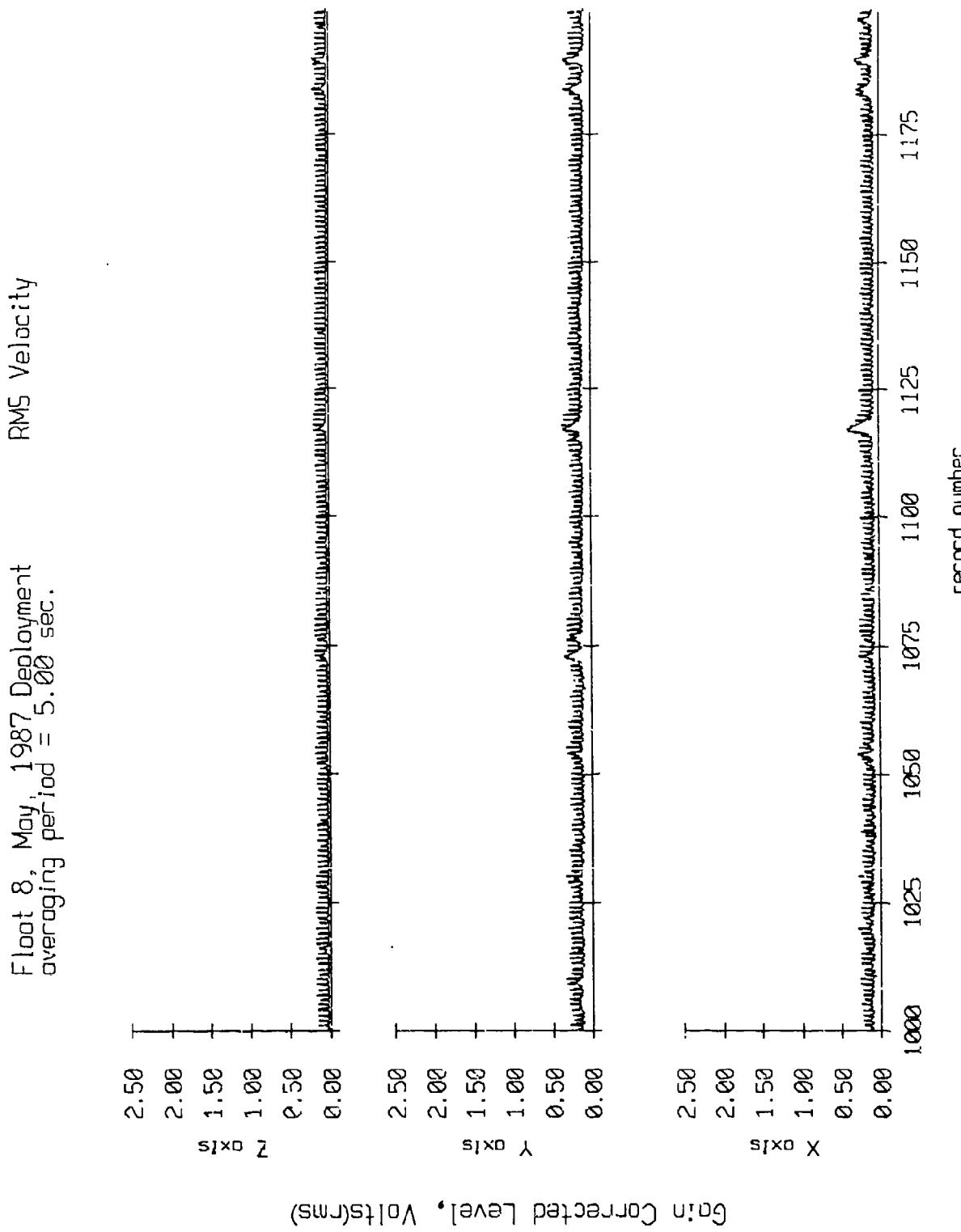


Figure IX.7f

Float 8, May 1987 Deployment
overaging period = 5.00 sec.

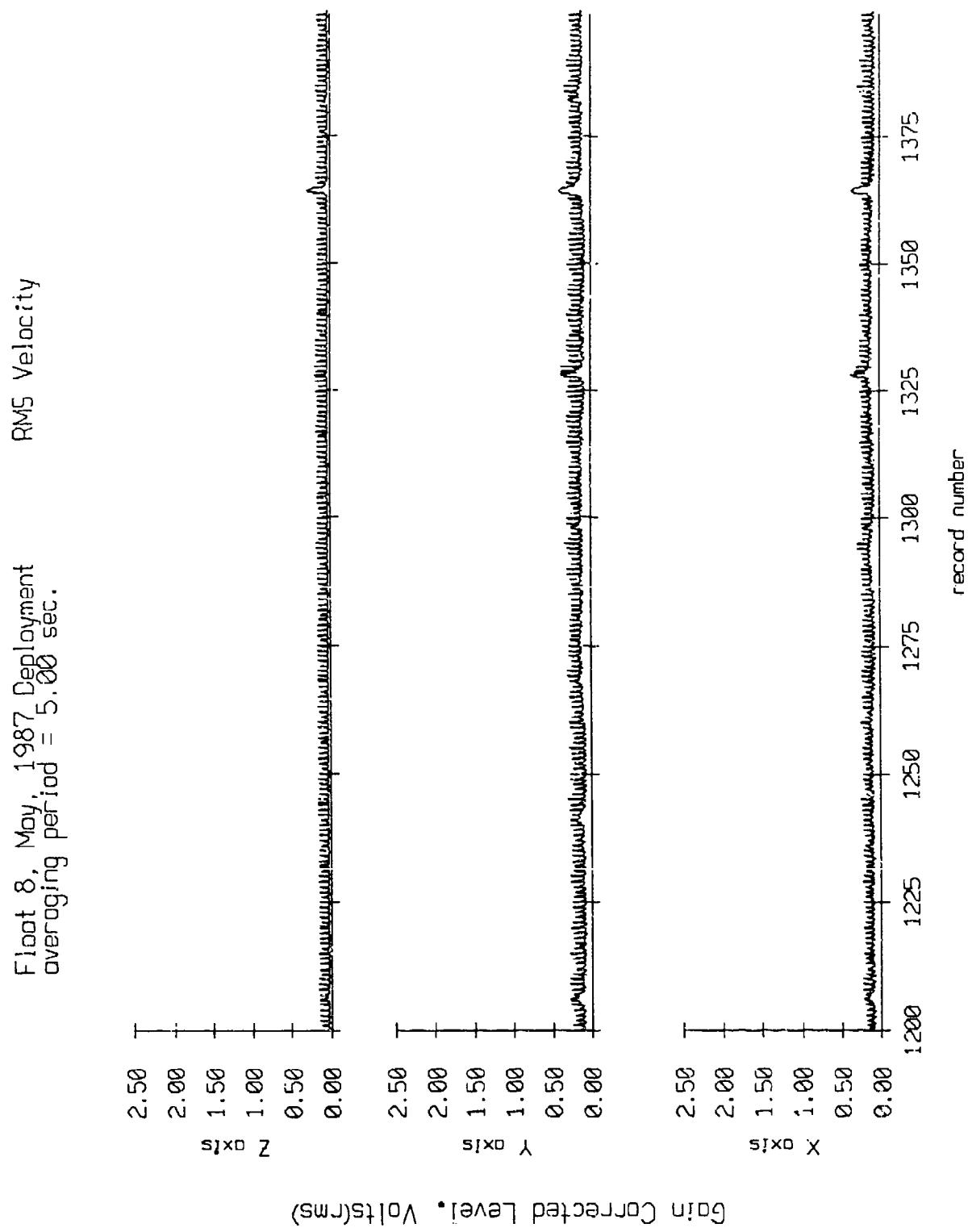


Figure IX.7g

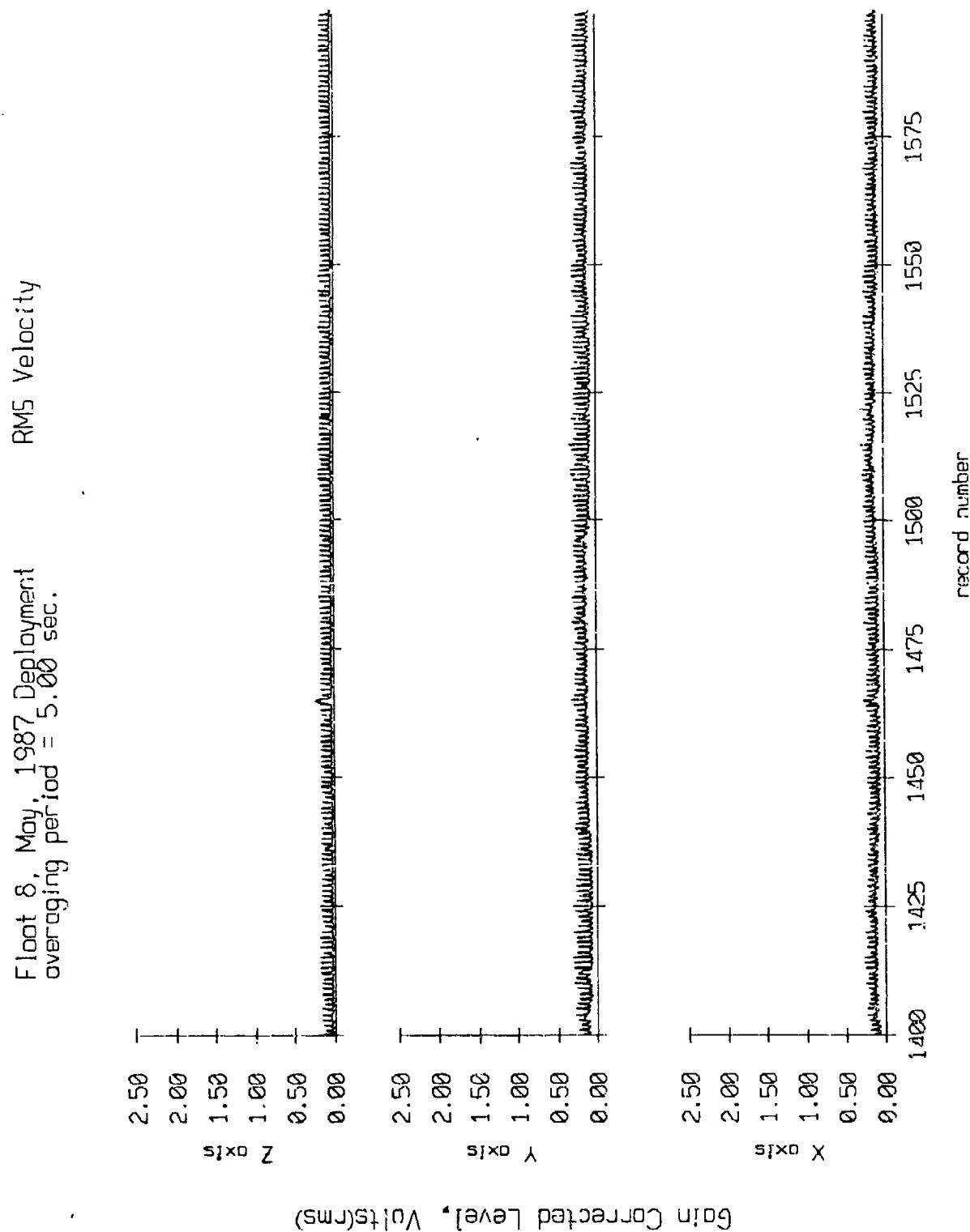


Figure IX.7h

Float 8, May, 1987 Deployment
overaging period = 5.00 sec.

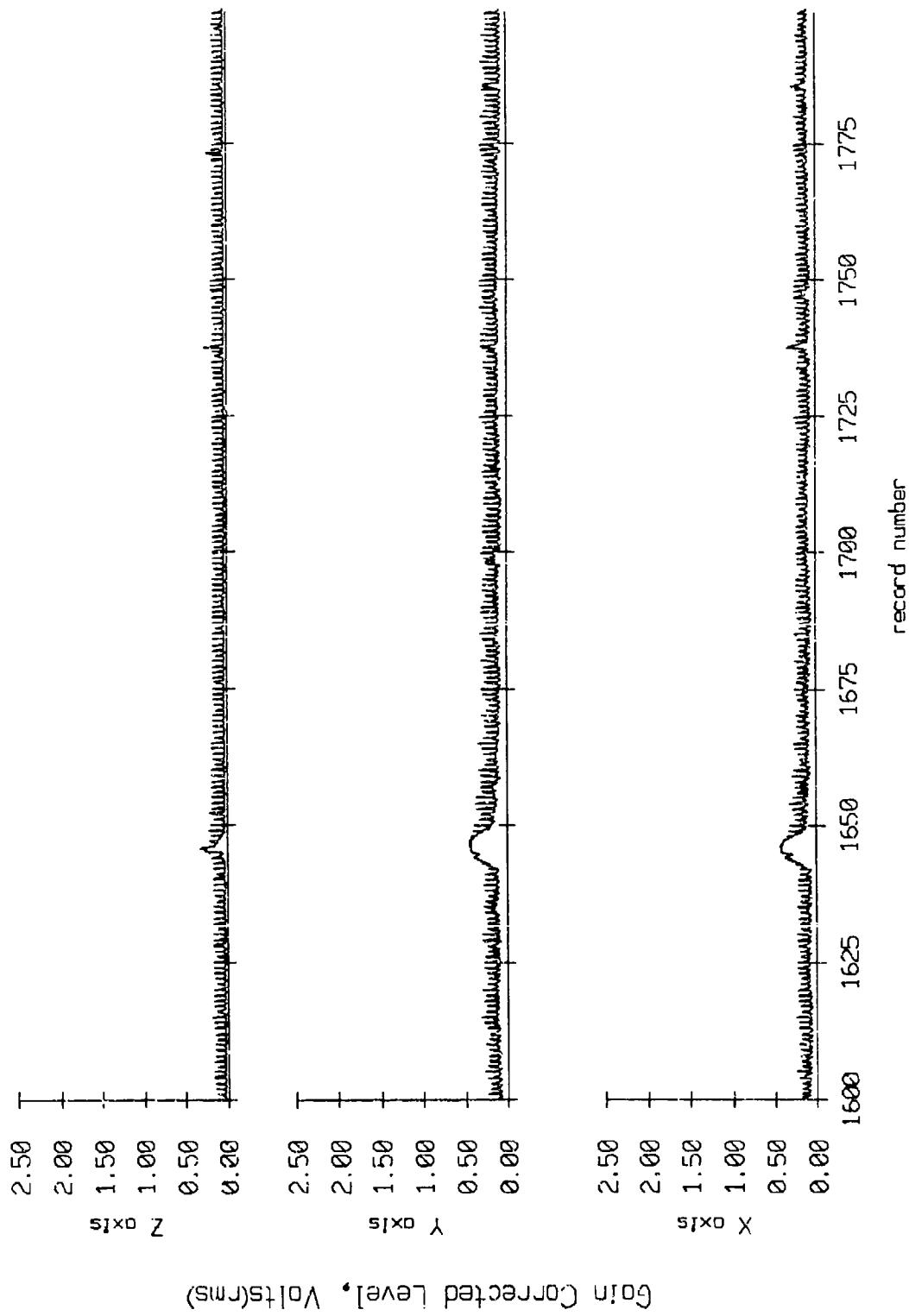


Figure IX.7i

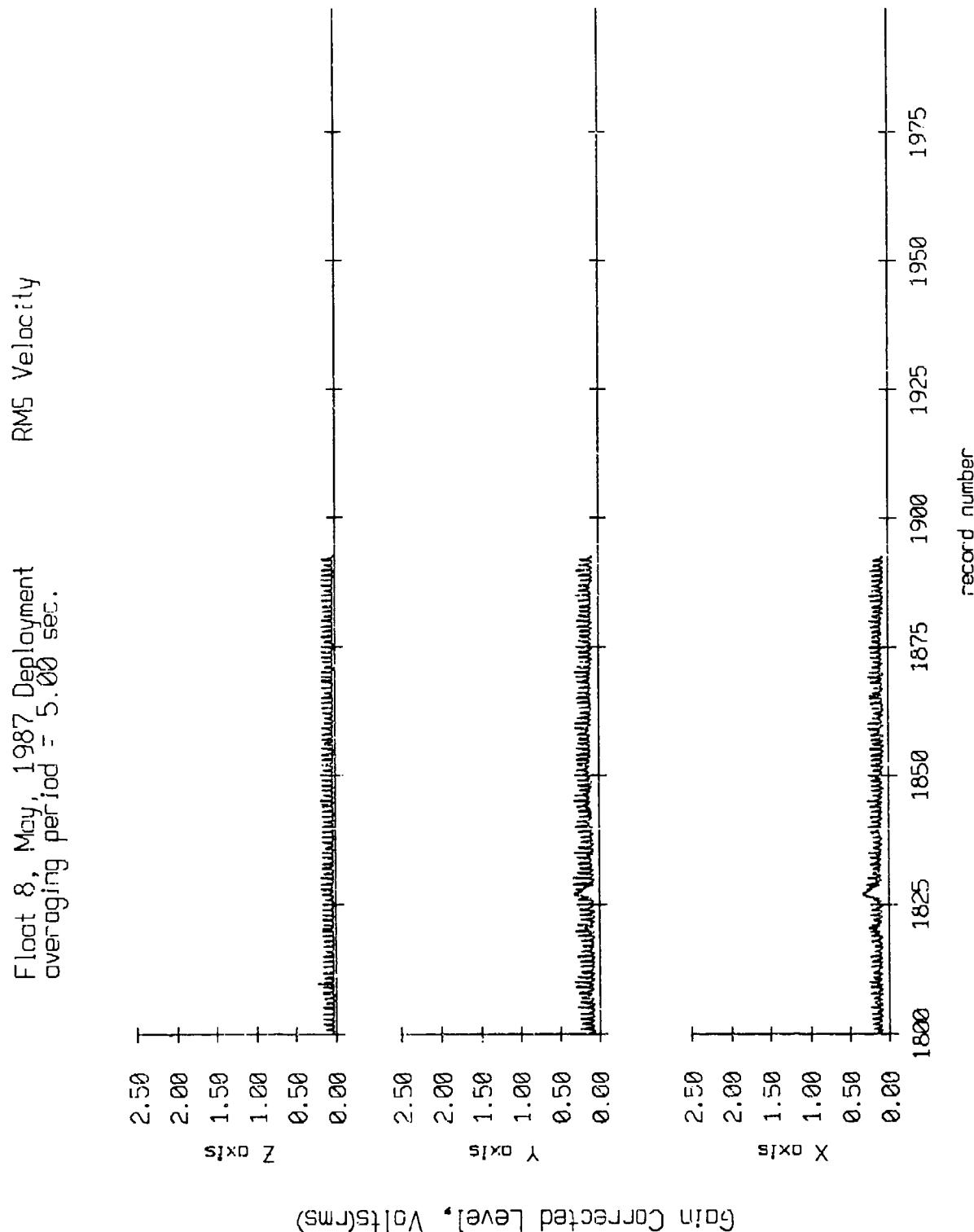
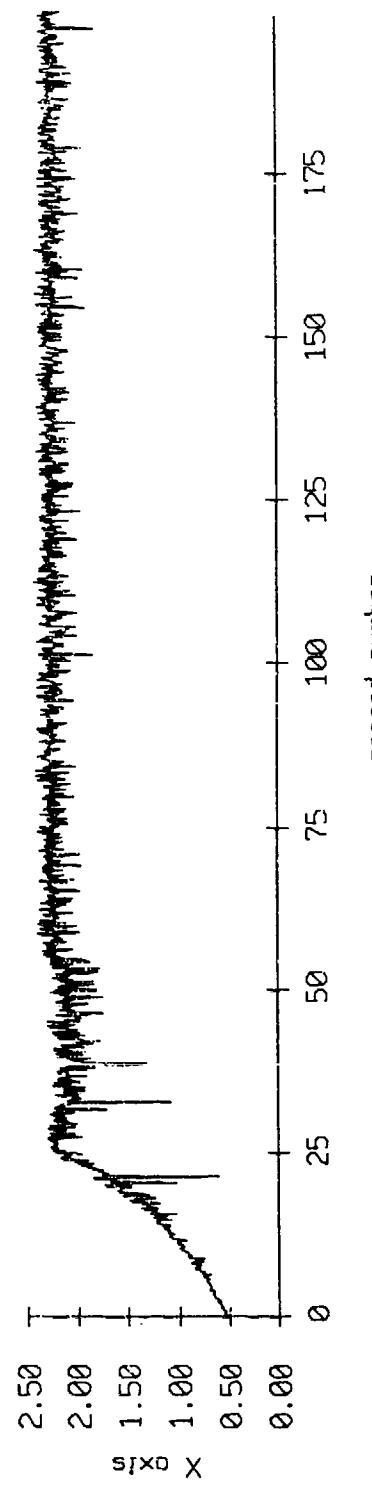
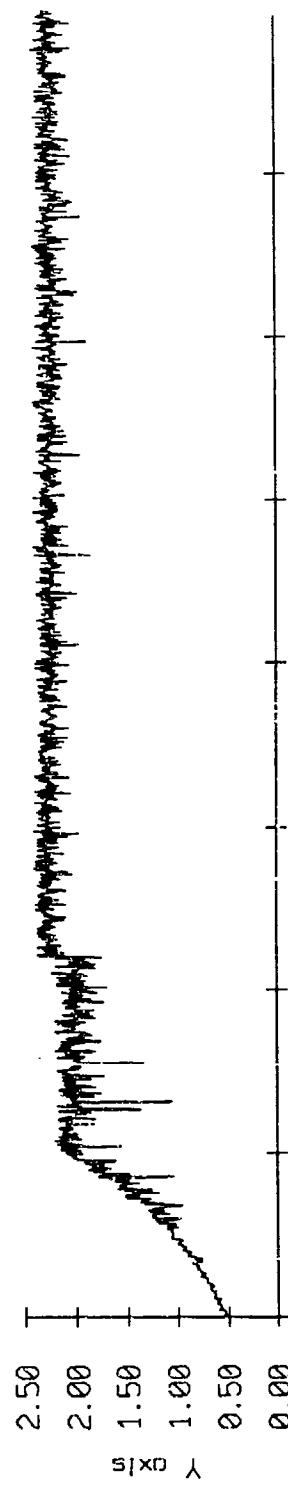
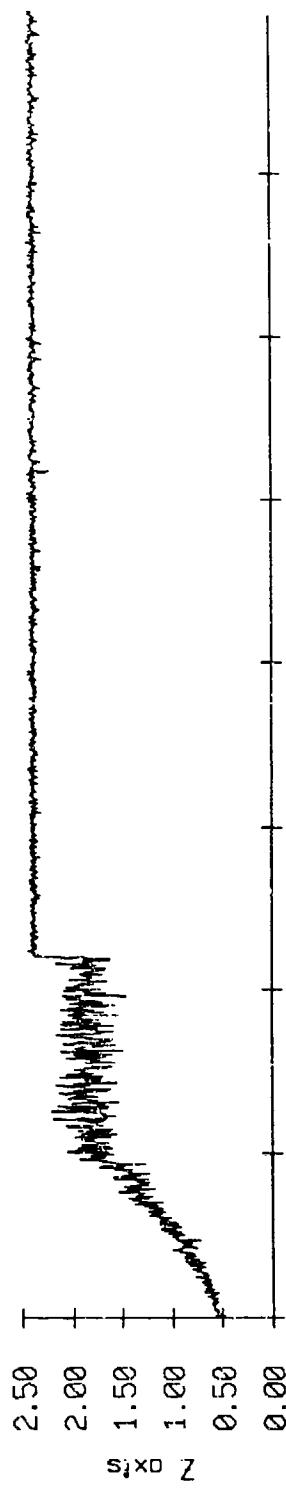


Figure IX.7j

Float 9, Nov. 1987 Deployment
averaging period = 5.00 sec.

RMS Velocity

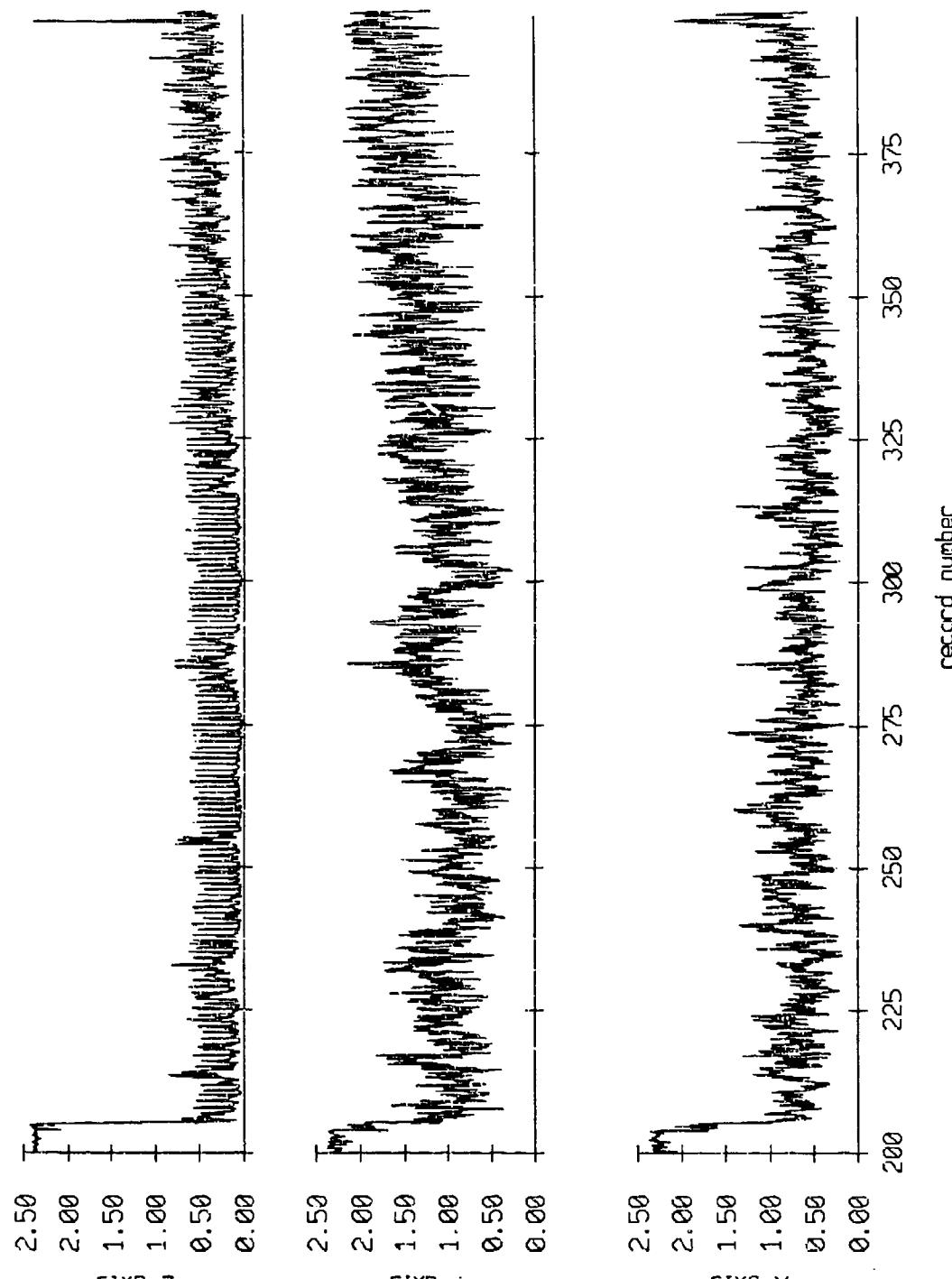


Gain Corrected Level, Volts(RMS)

Figure IX.8a

Fleet 9, May, 1987 Deployment
averaging period = 5.00 sec.

RMS Velocity

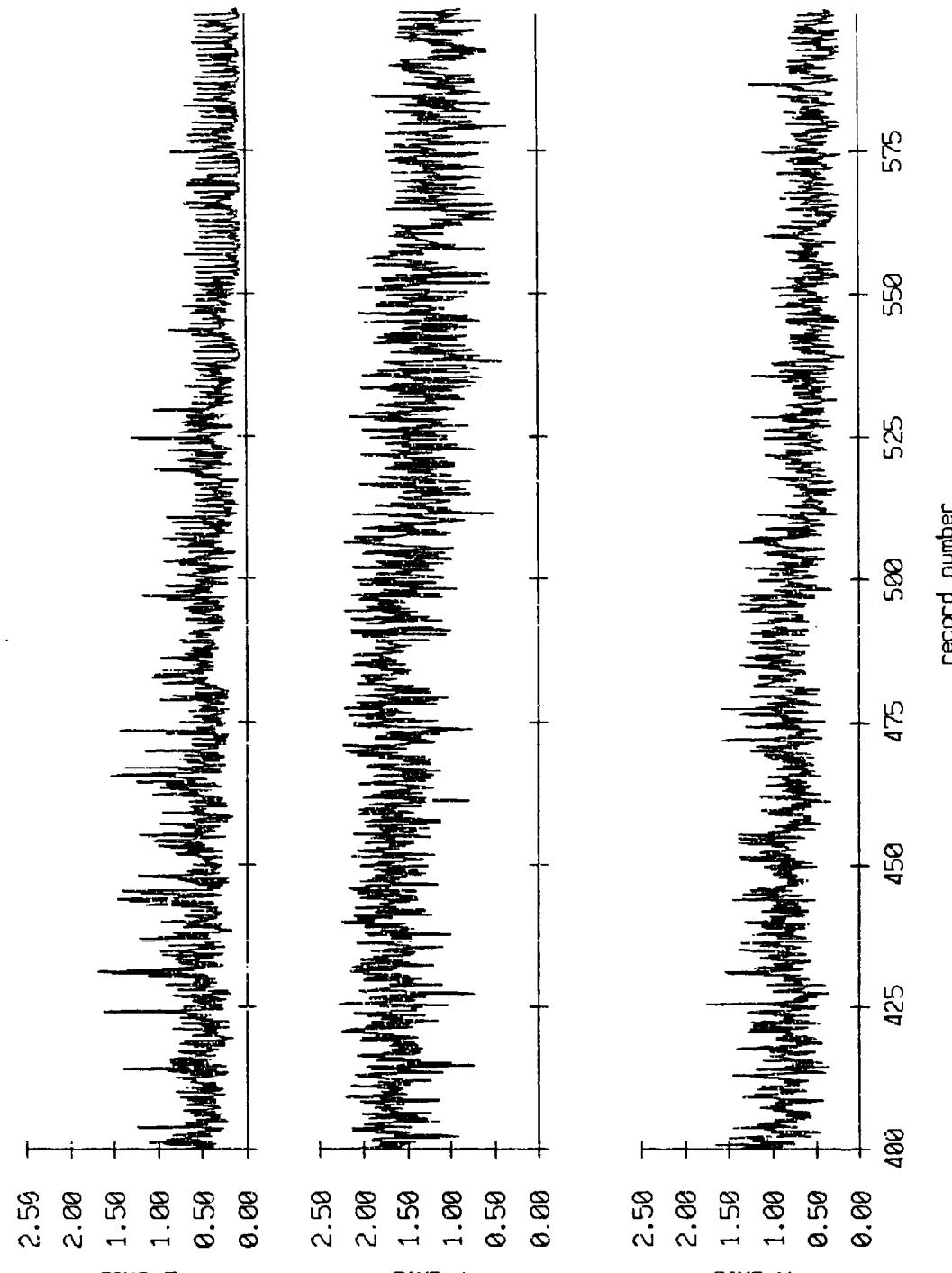


Gain Corrected Level, Volts(RMS)

Figure IX.8b

Float 9, May 1987 Deployment
averaging period = 5.00 sec.

RMS Velocity

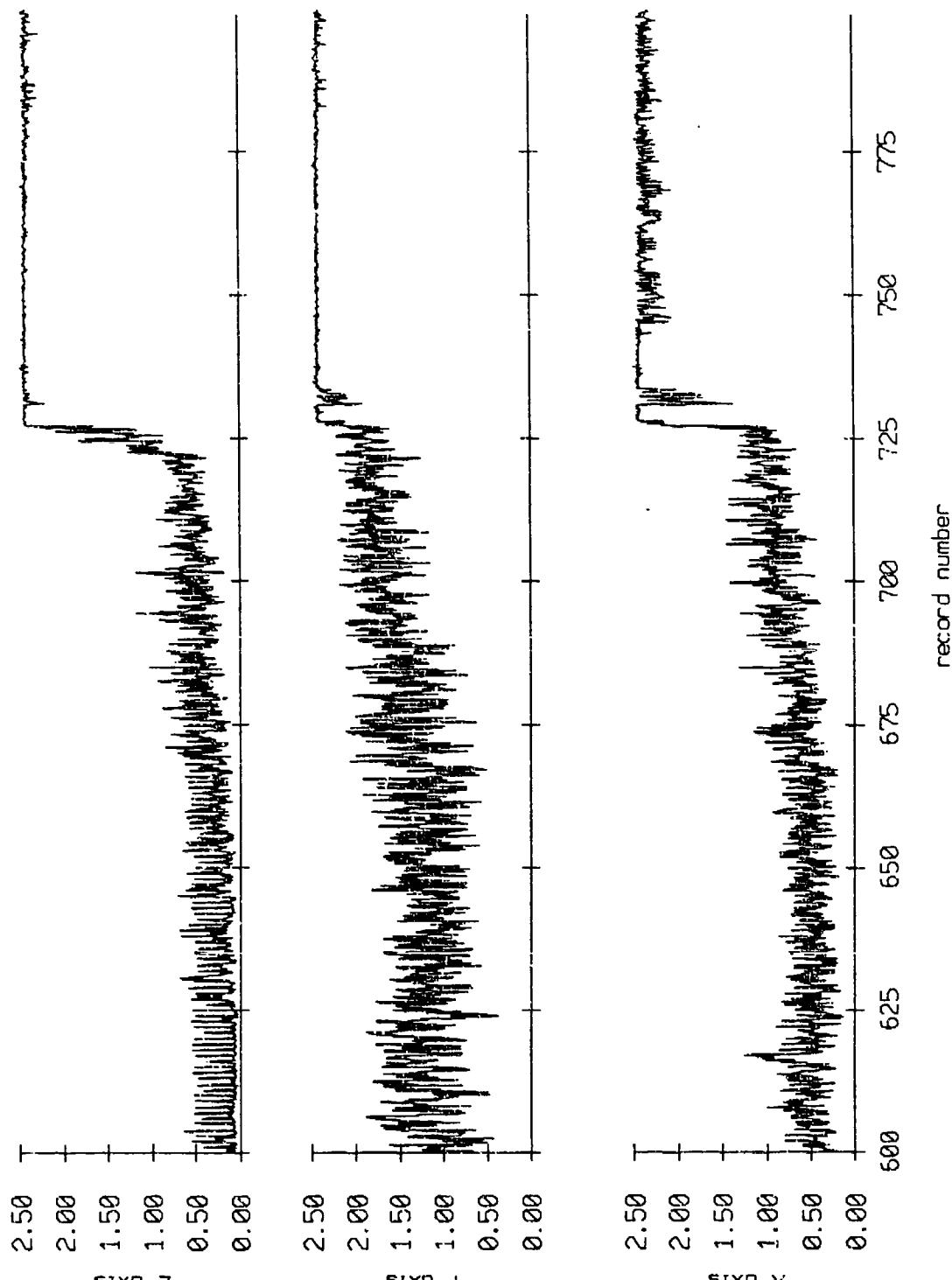


Gain Corrected Level, Volts(RMS)

Figure IX.8c

Float 9, May, 1987 Deployment
overaging period = 5.00 sec.

RMS Velocity



Gain Corrected Level, Volts(RMS)

Figure IX.8d

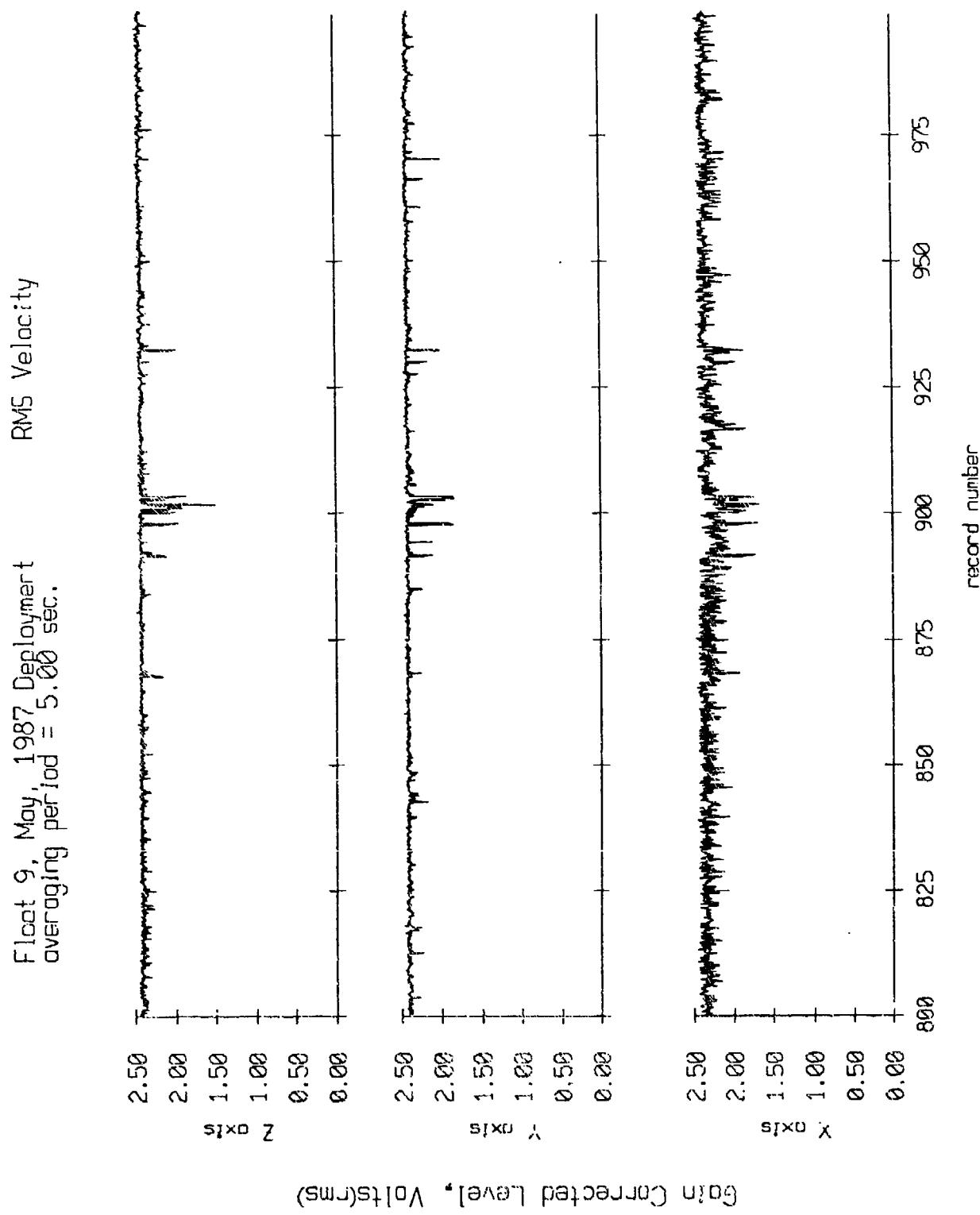


Figure IX.8e

Float 9, May, 1987 Deployment
overaging period = 5.00 sec.

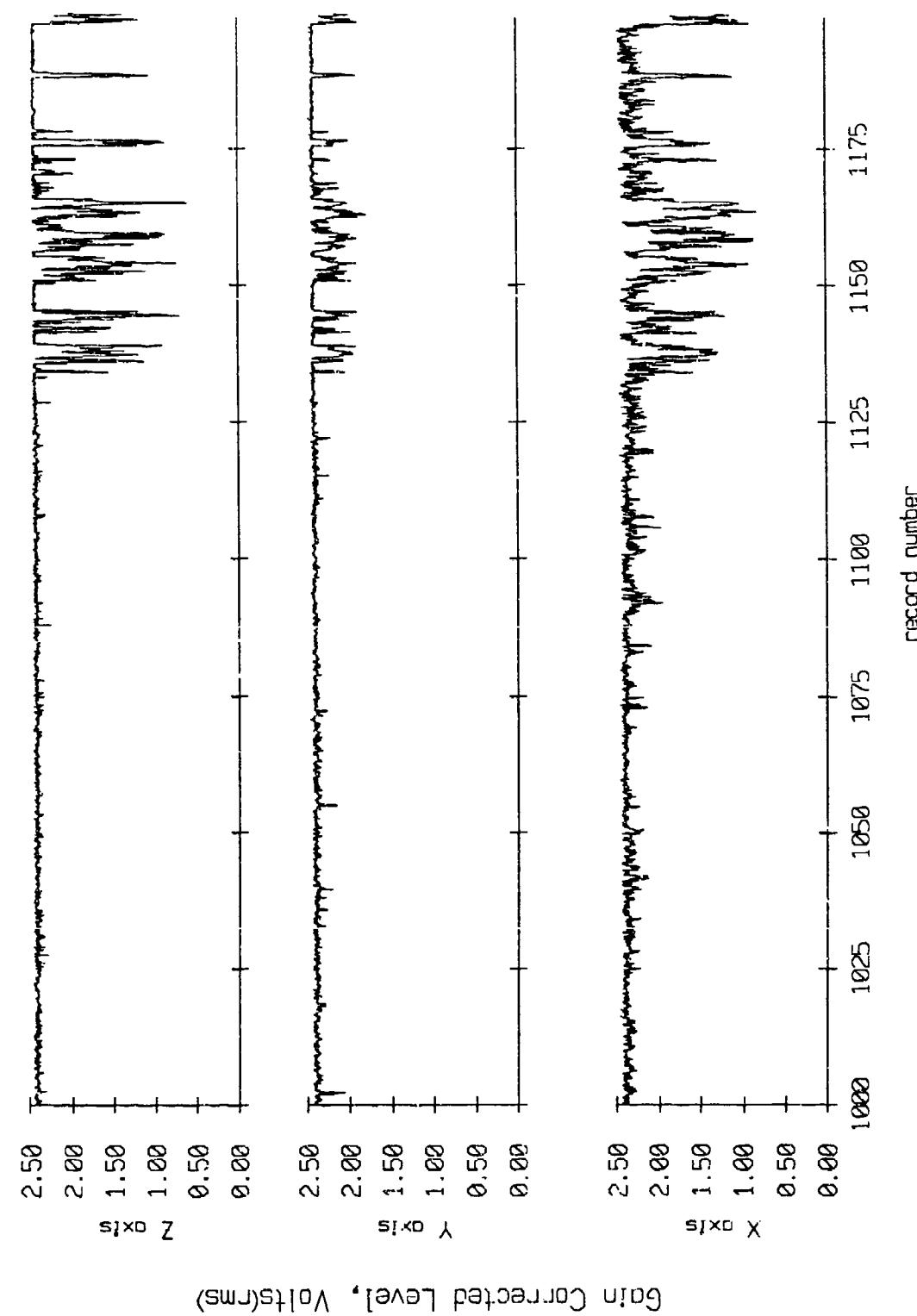
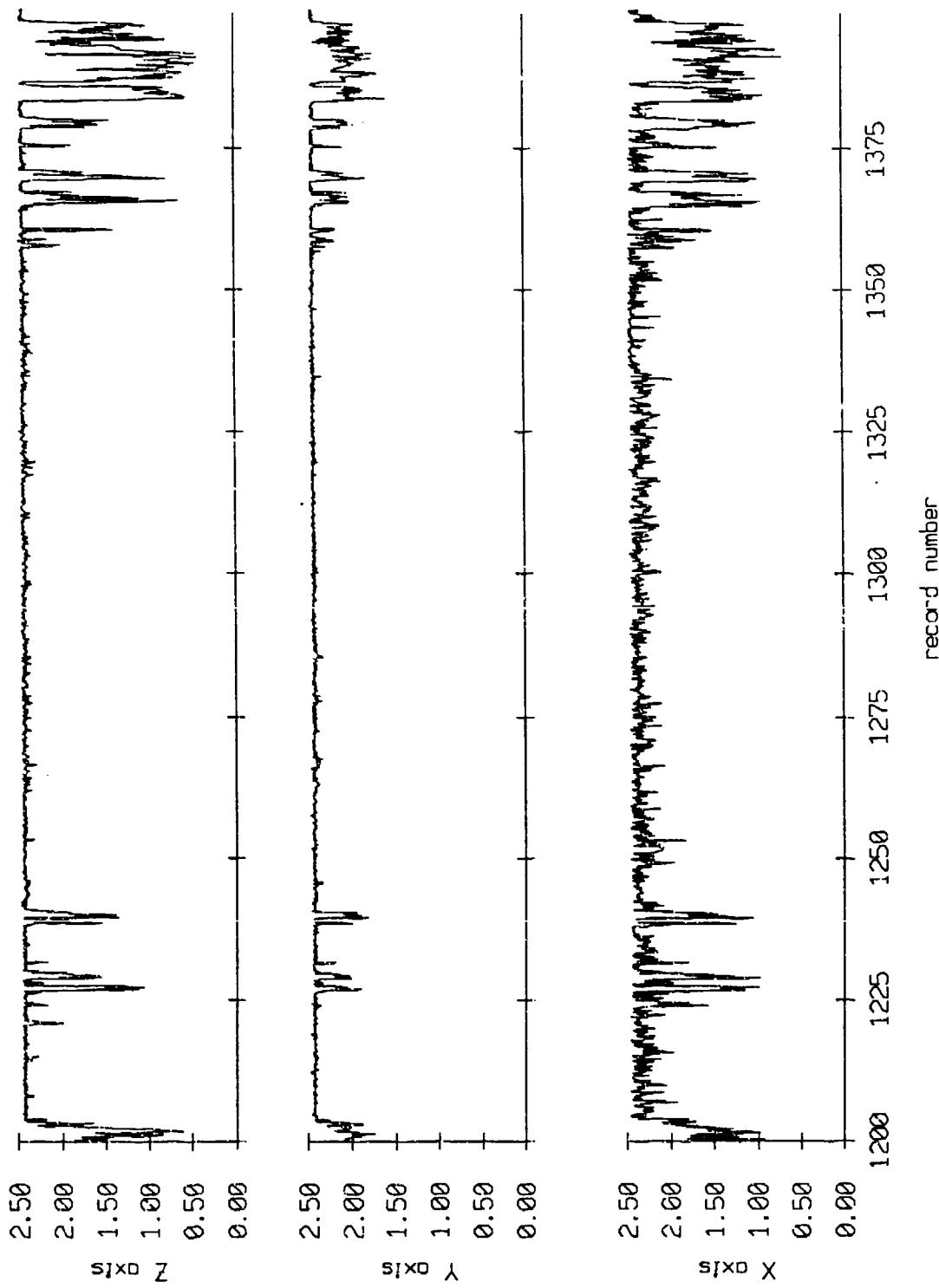


Figure IX.8f

Float 9, May, 1987 Deployment
averaging period = 5.00 sec.

RMS Velocity



Gain Corrected Level, Volts(RMS)

Figure IX.8g

Float 9, May, 1987 Deployment
overaging period = 5.00 sec.

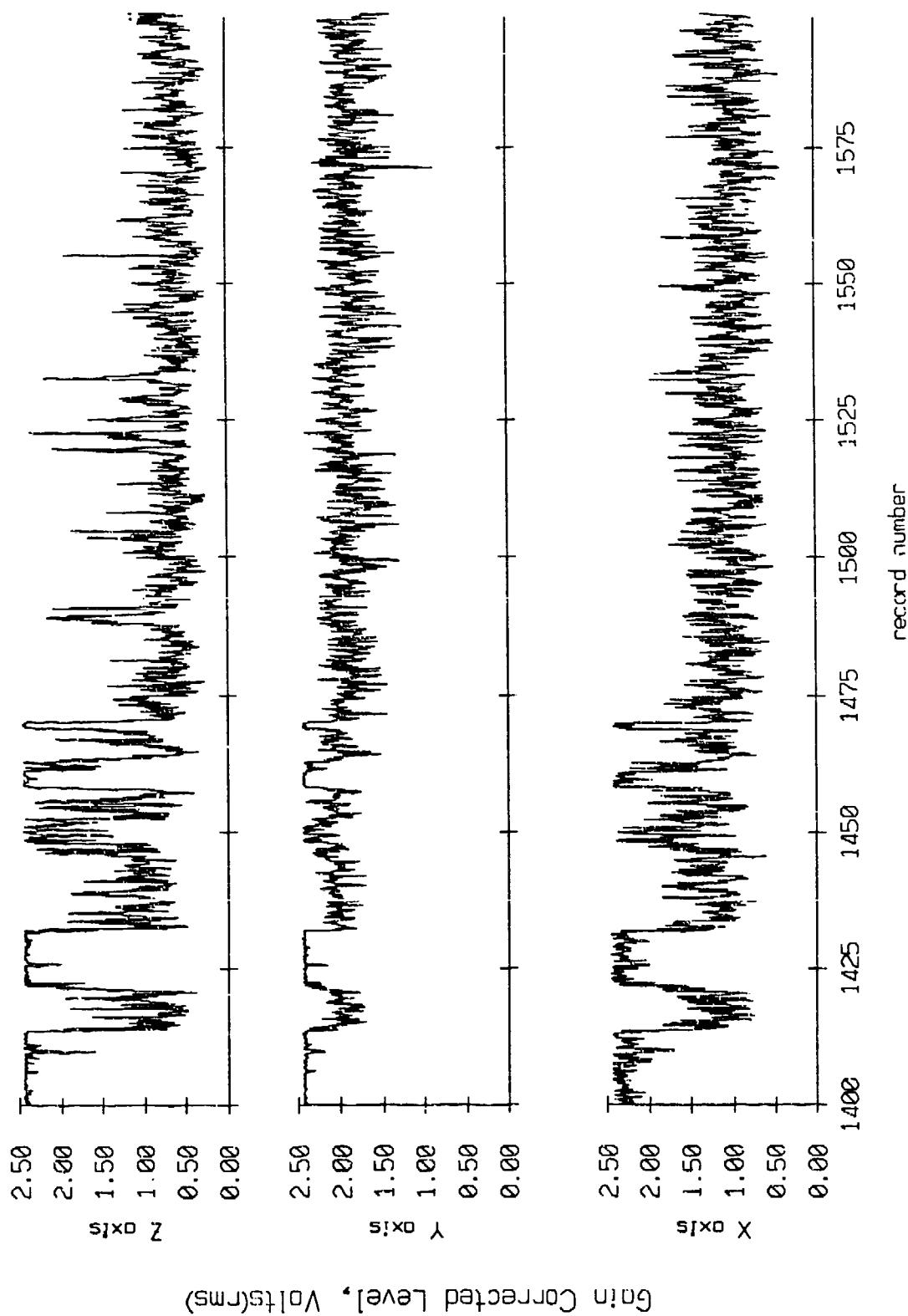


Figure IX.8E

Float 9, May, 1987 Deployment
overgaging period = 5.00 sec.

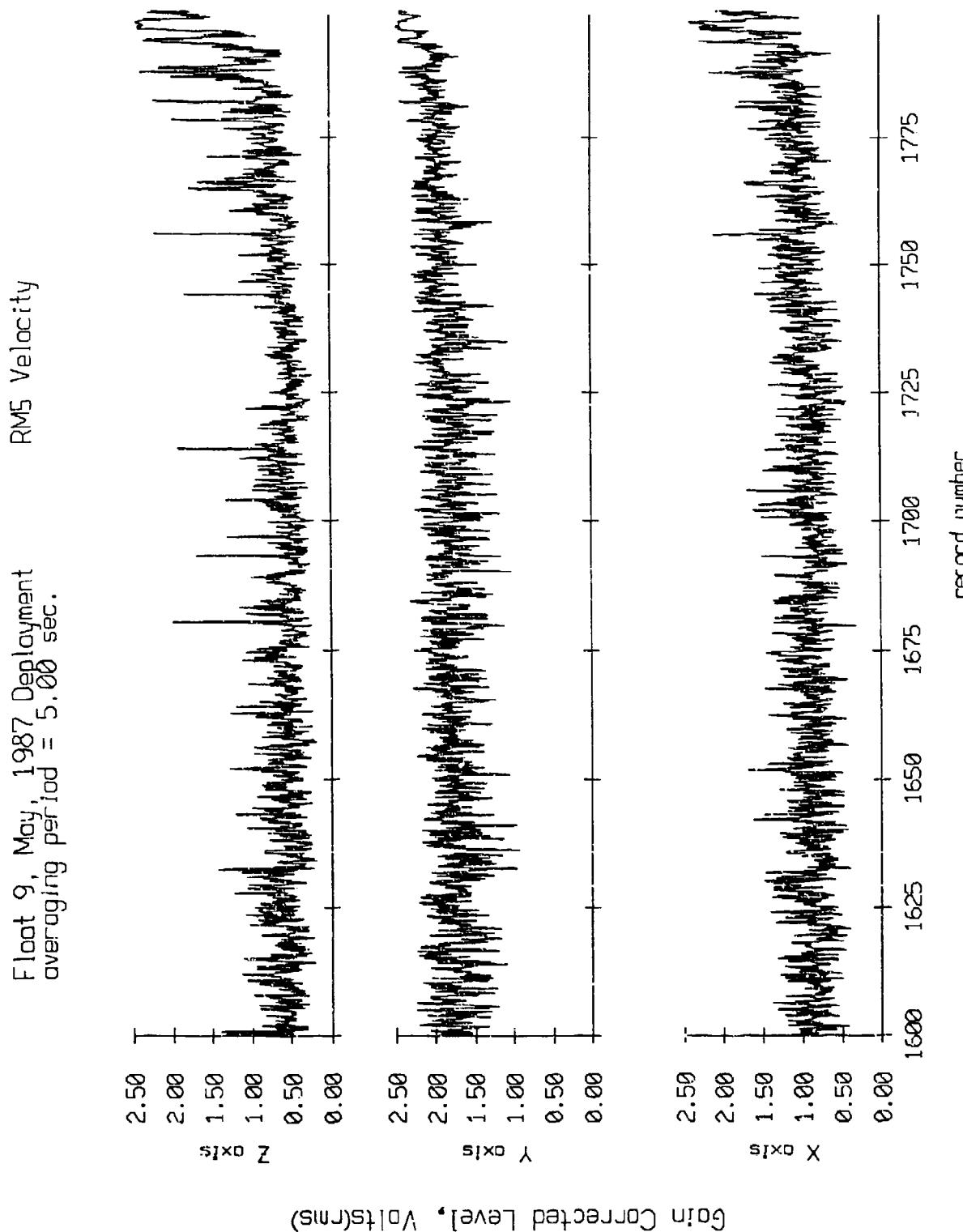


Figure IX.8i

Fleet 9, May, 1987 Deployment
overgoing period = 5.00 sec.

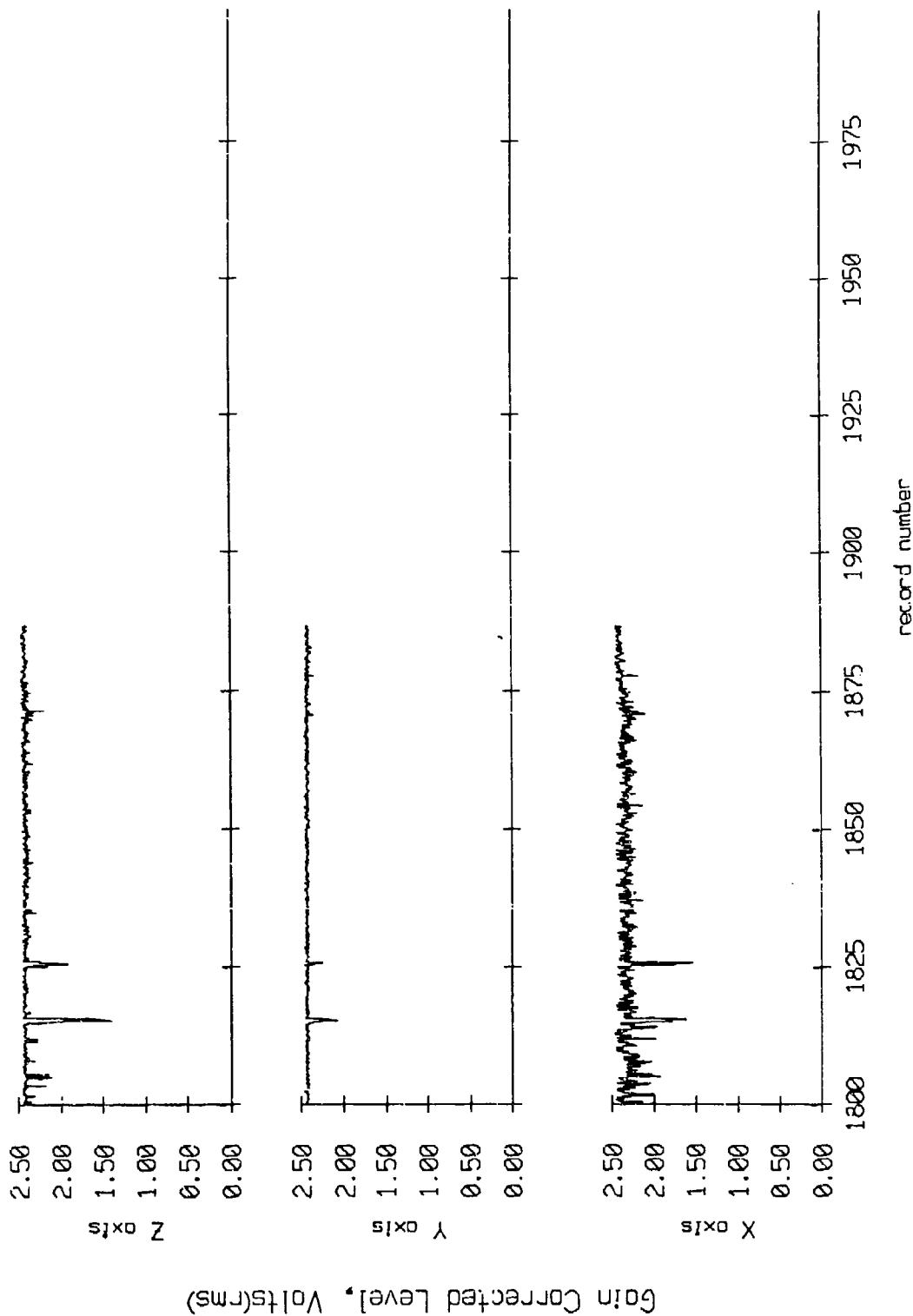


Figure IX.8j

Float 10, May, 1987 Deployment
overaging period = 5.00 sec.

RMS Velocity

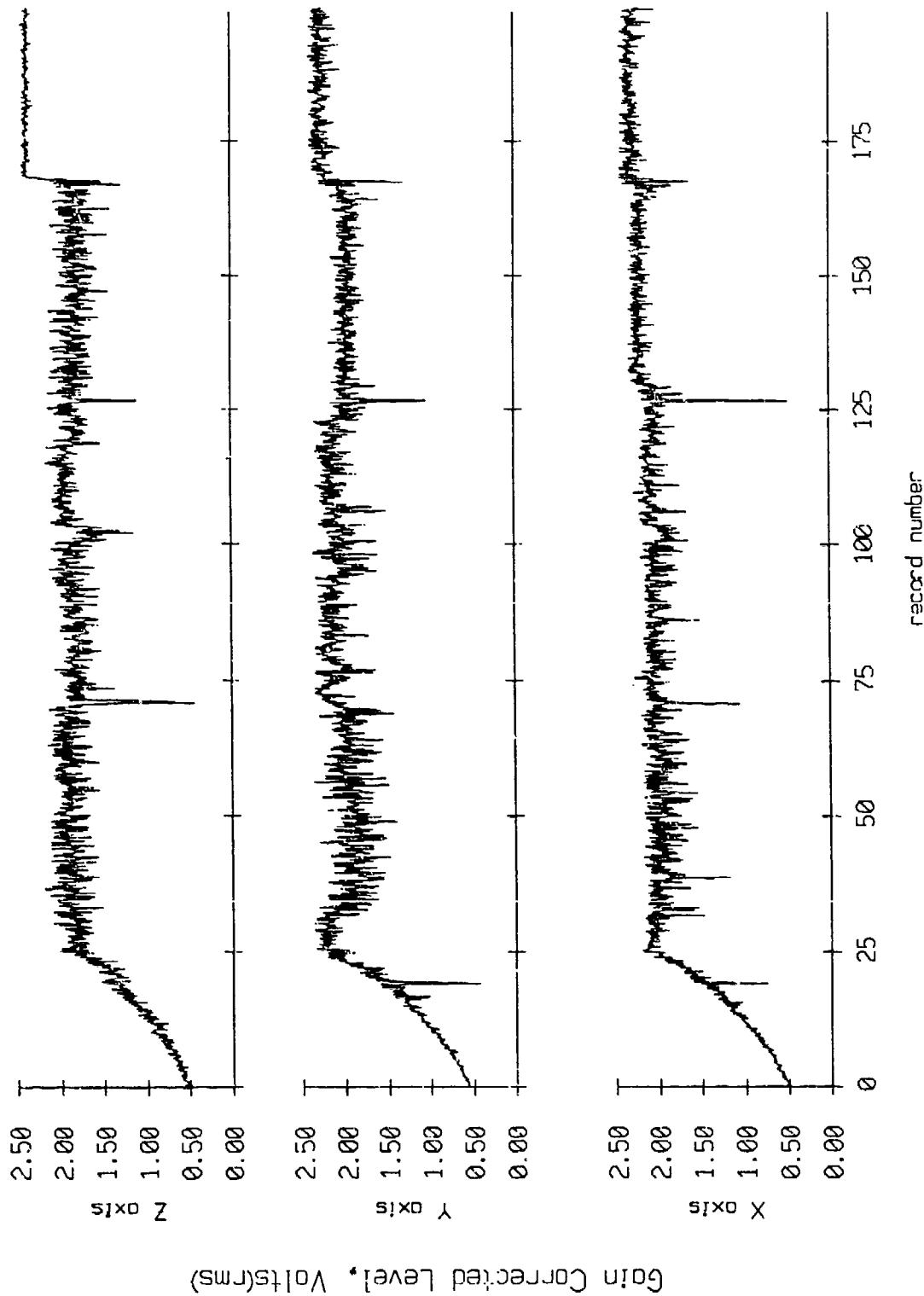
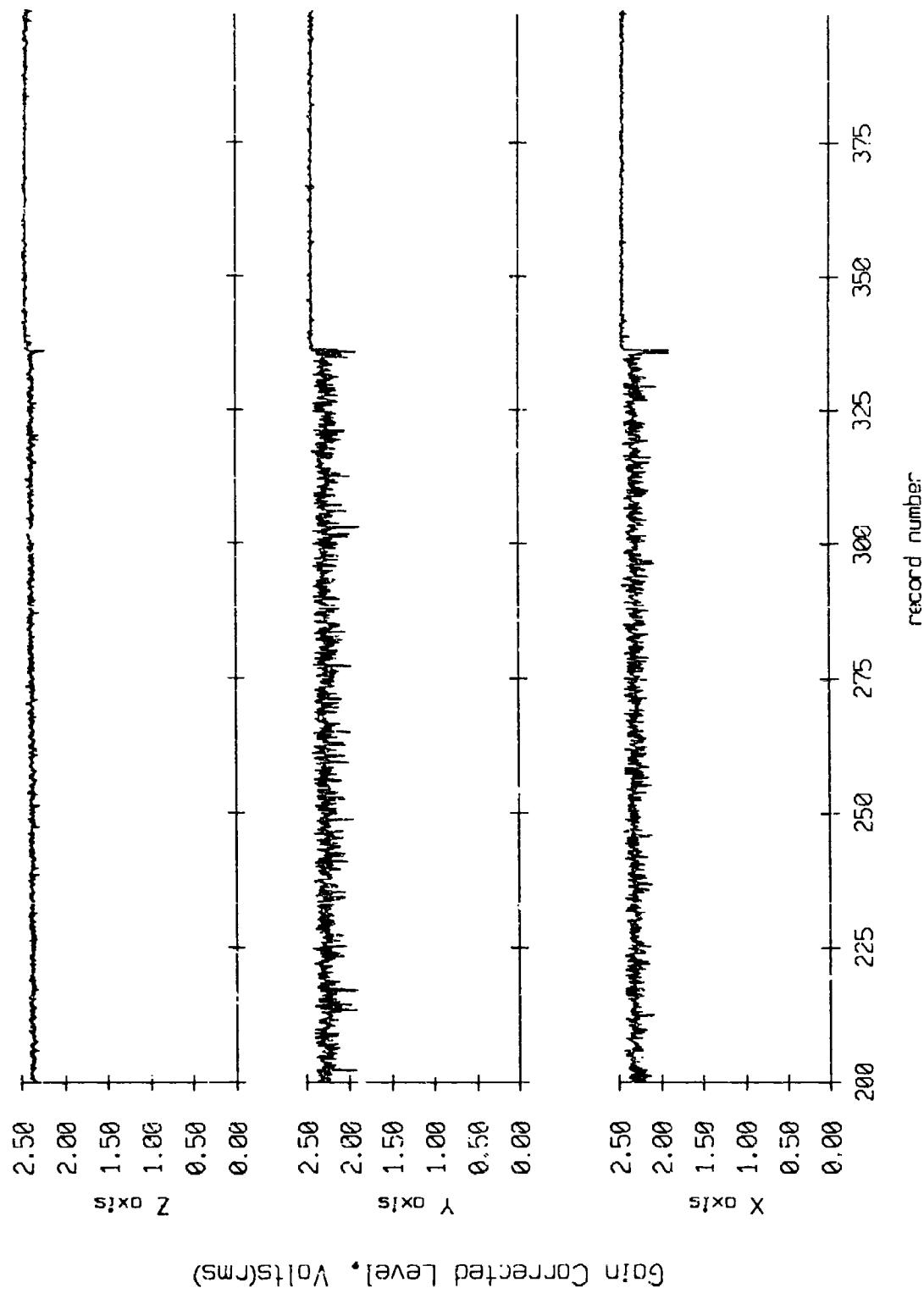


Figure IX.9a

Float 10, May, 1987 Deployment
overgoing period = 5.00 sec.

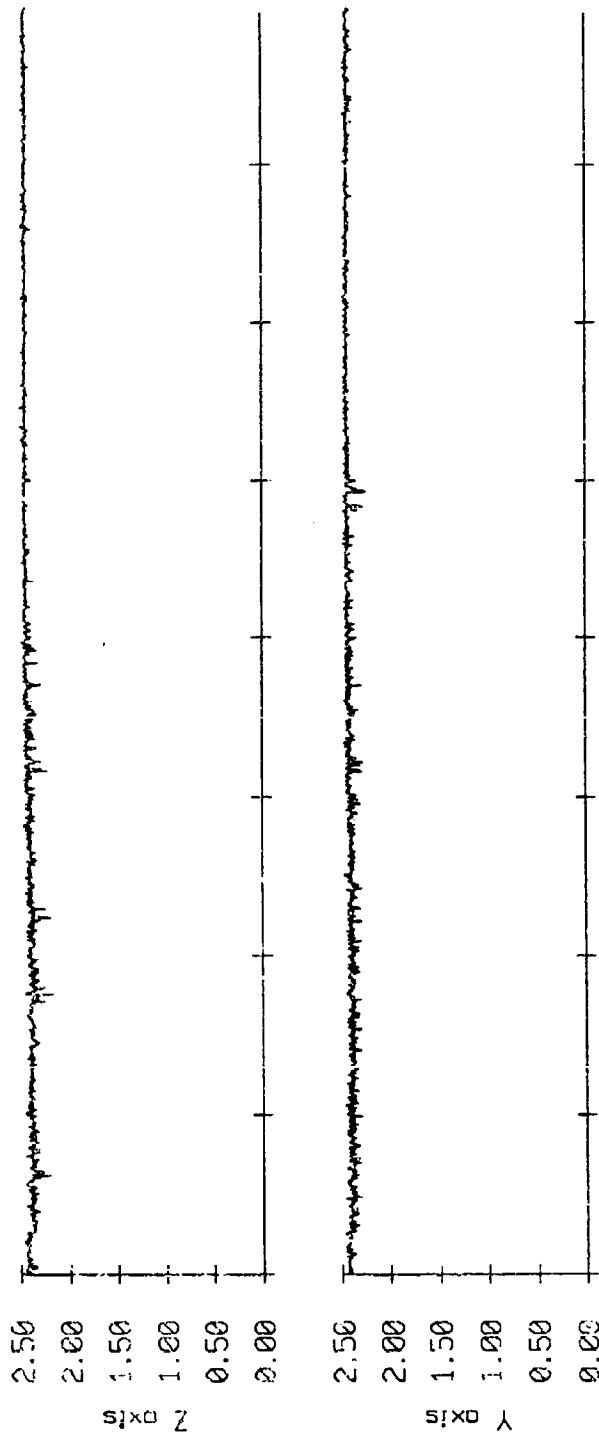


Join Corrected Level, Volts(rms)

Figure IX.9b

Fleet 10, May, 1987 Deployment
averaging period = 5.00 sec.

RMS Velocity



Gain Corrected Level, Volts(rms)

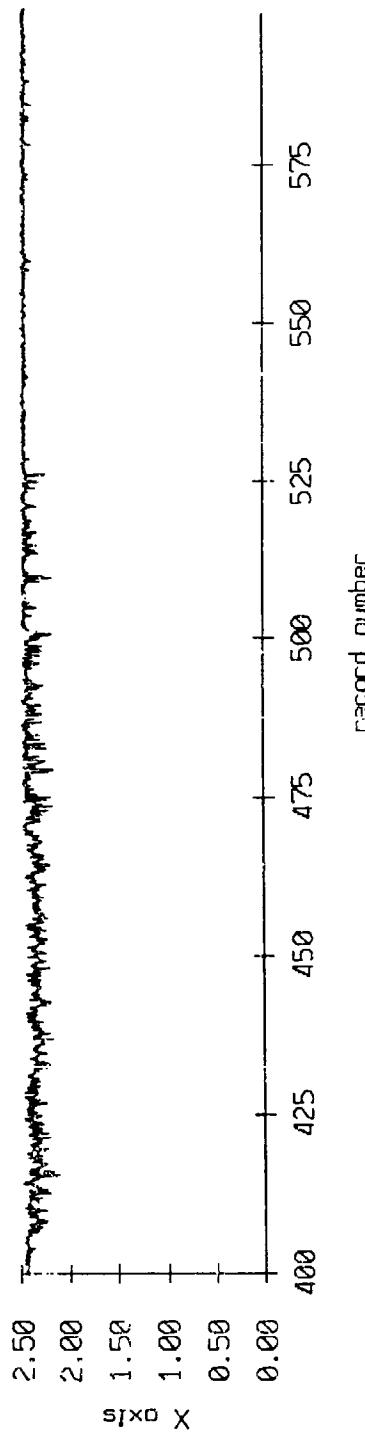


Figure IX.9c

Float 10, Mon, 1987 Deployment
overgning period = 5.00 sec.

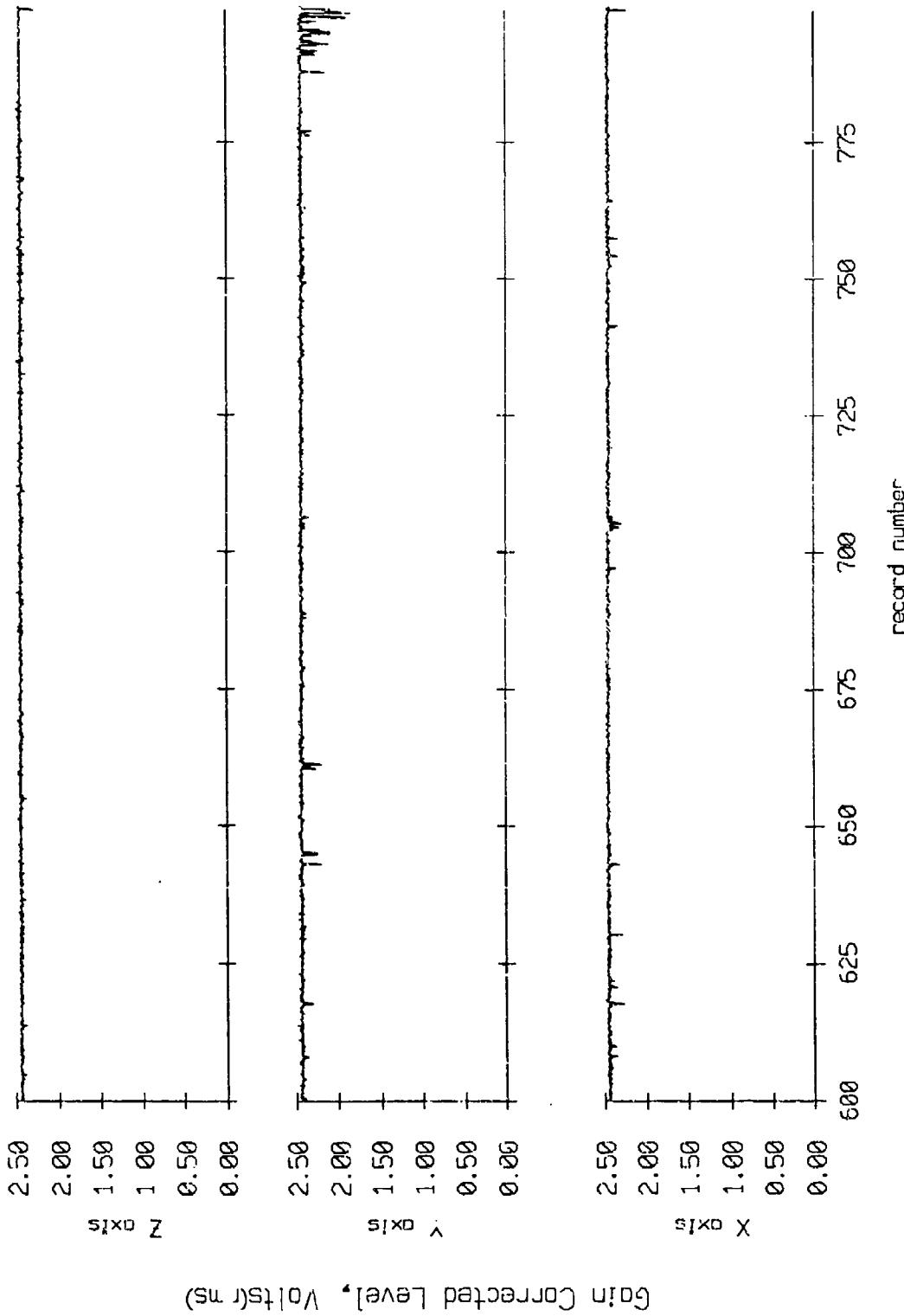


Figure IX.9d

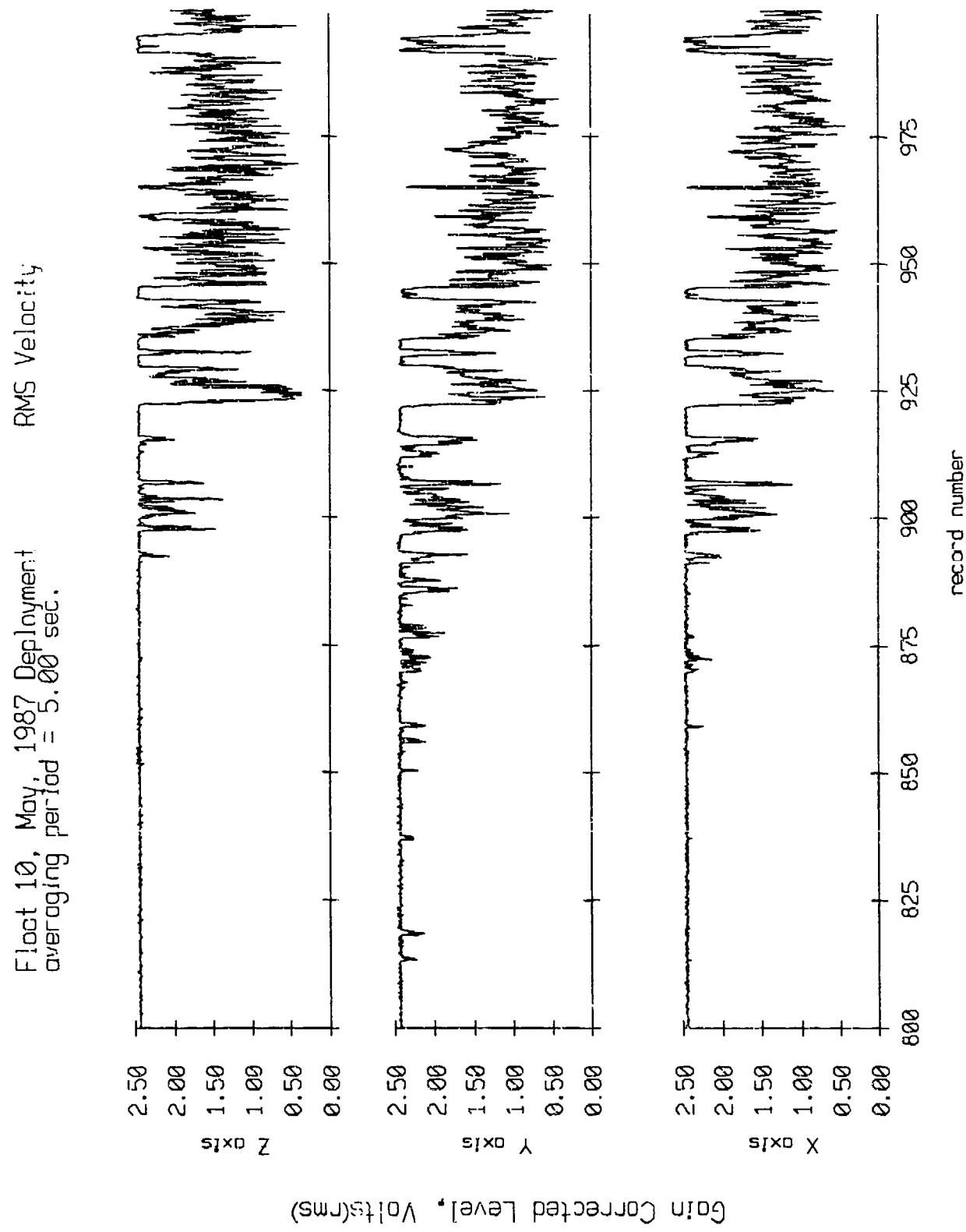


Figure IX.9e

Float 10, May, 1987 Deployment
averaging period = 5.00 sec.

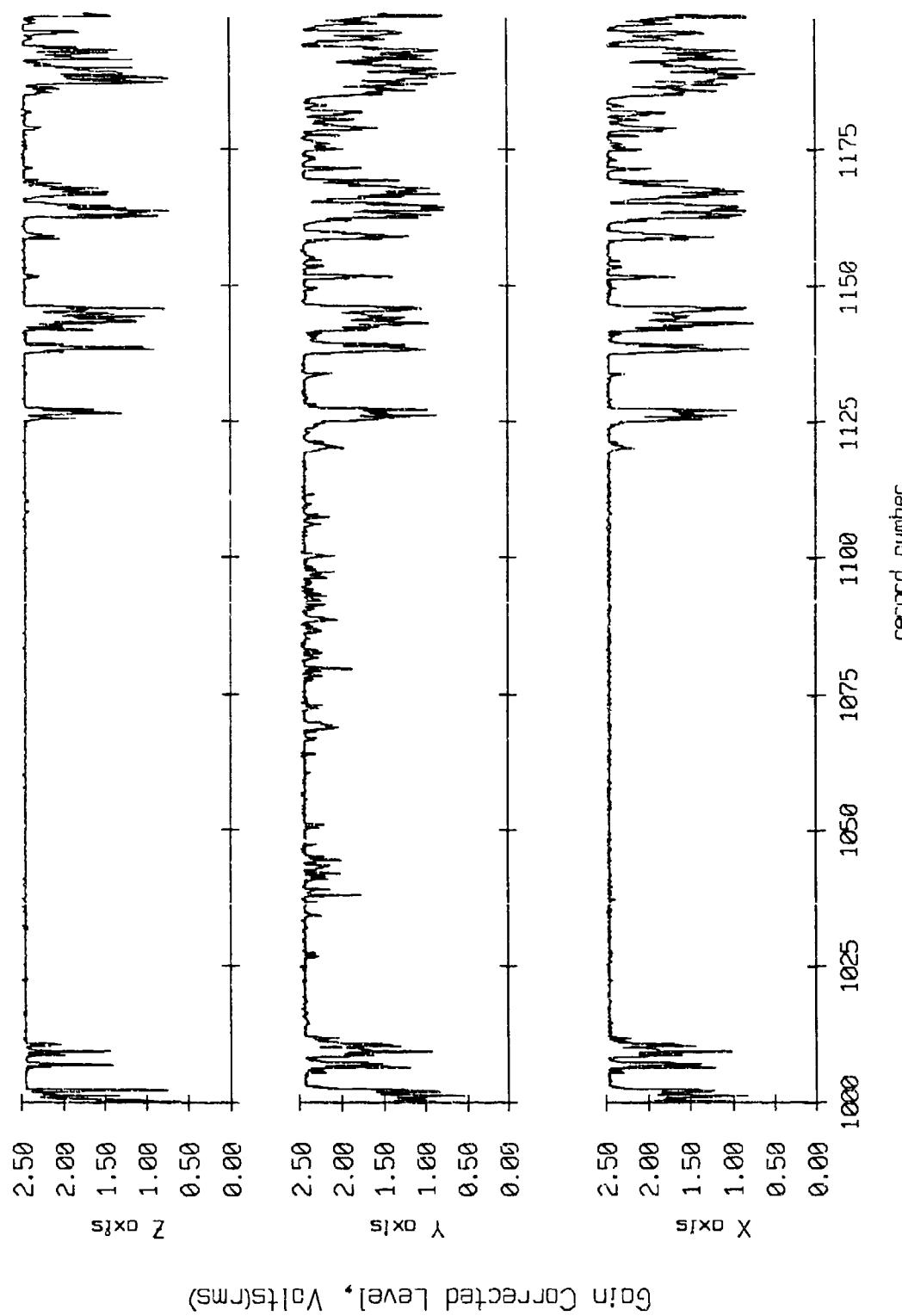


Figure IX.9f

Float 10, May 1987 Deployment
overaging period = 5.00 sec.

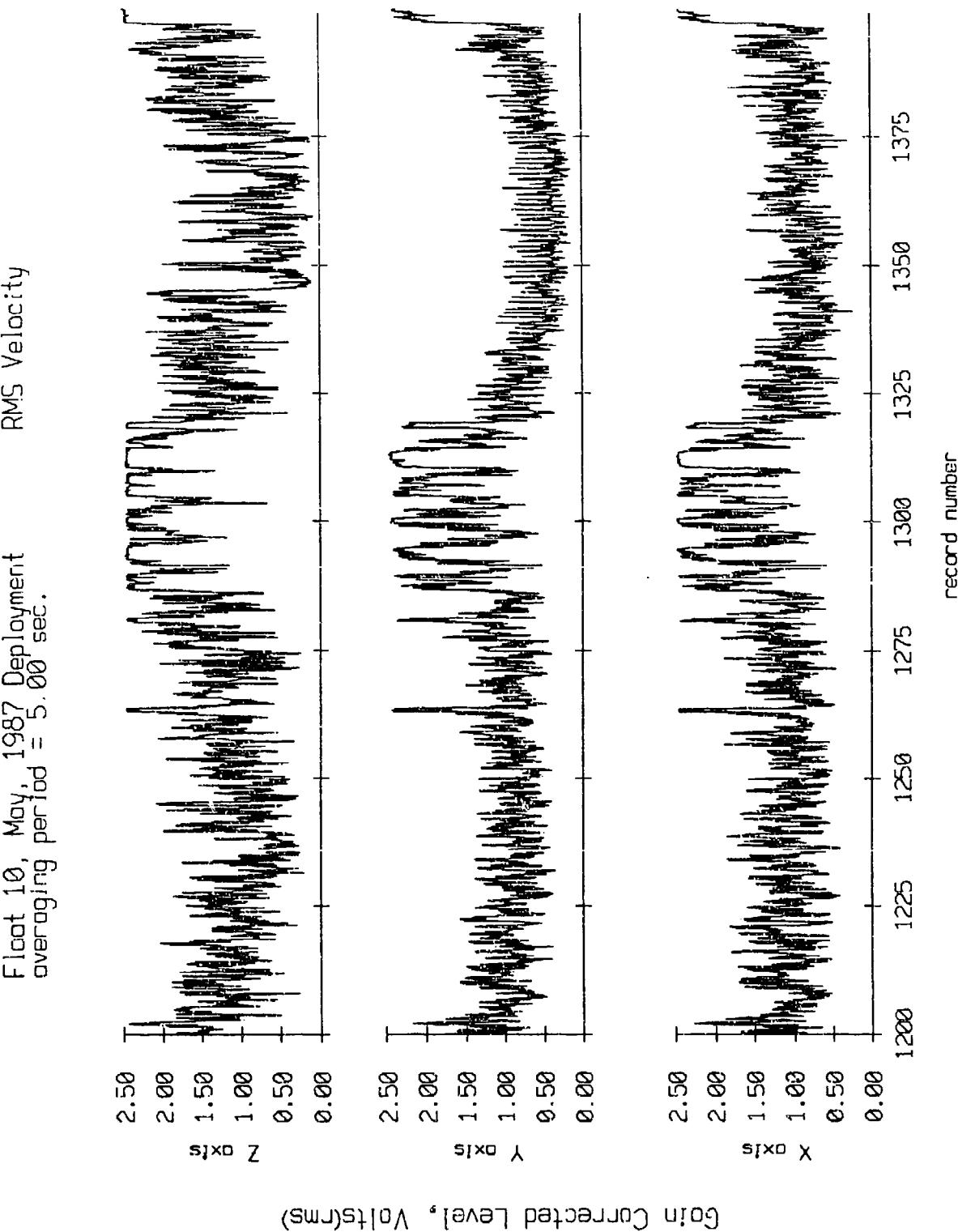


Figure IX.9g

Float 10, May 1987 Sea Trip
Overcycling period = 5.00 sec.

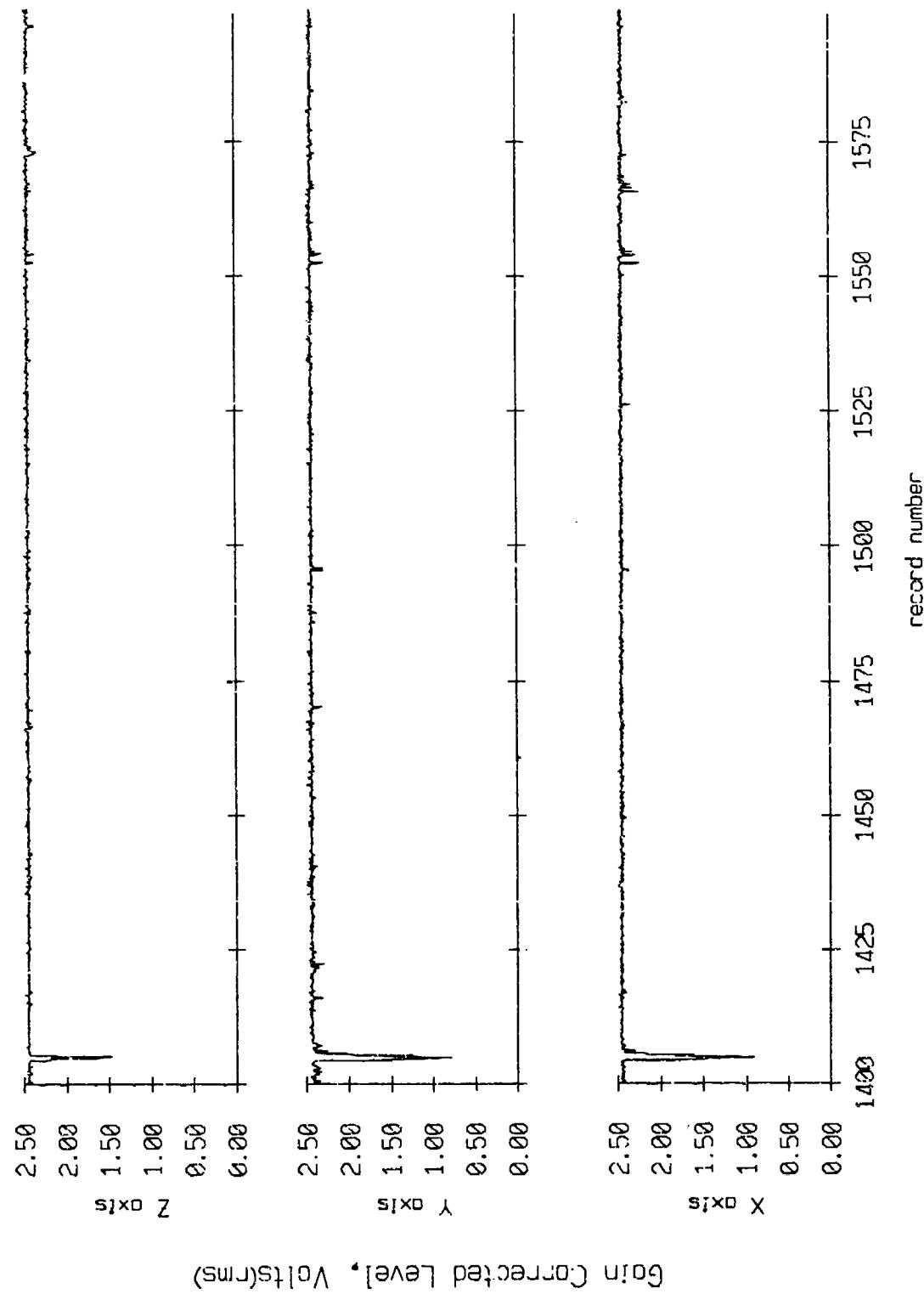
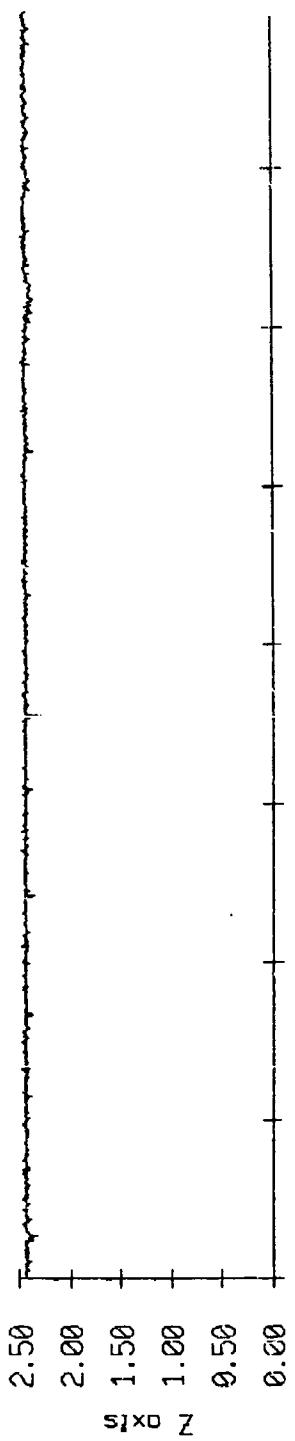


Figure IX.9h

Float 10, May, 1987 Deployment
overgaging period = 5.00 sec.

RMS Velocity



Gain Corrected Level, Volts(rms)

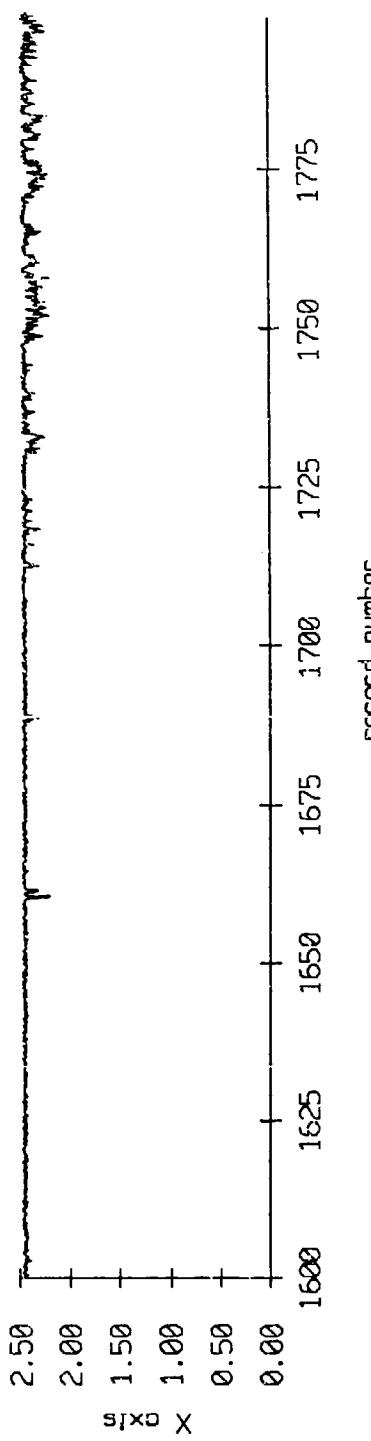


Figure IX.9i

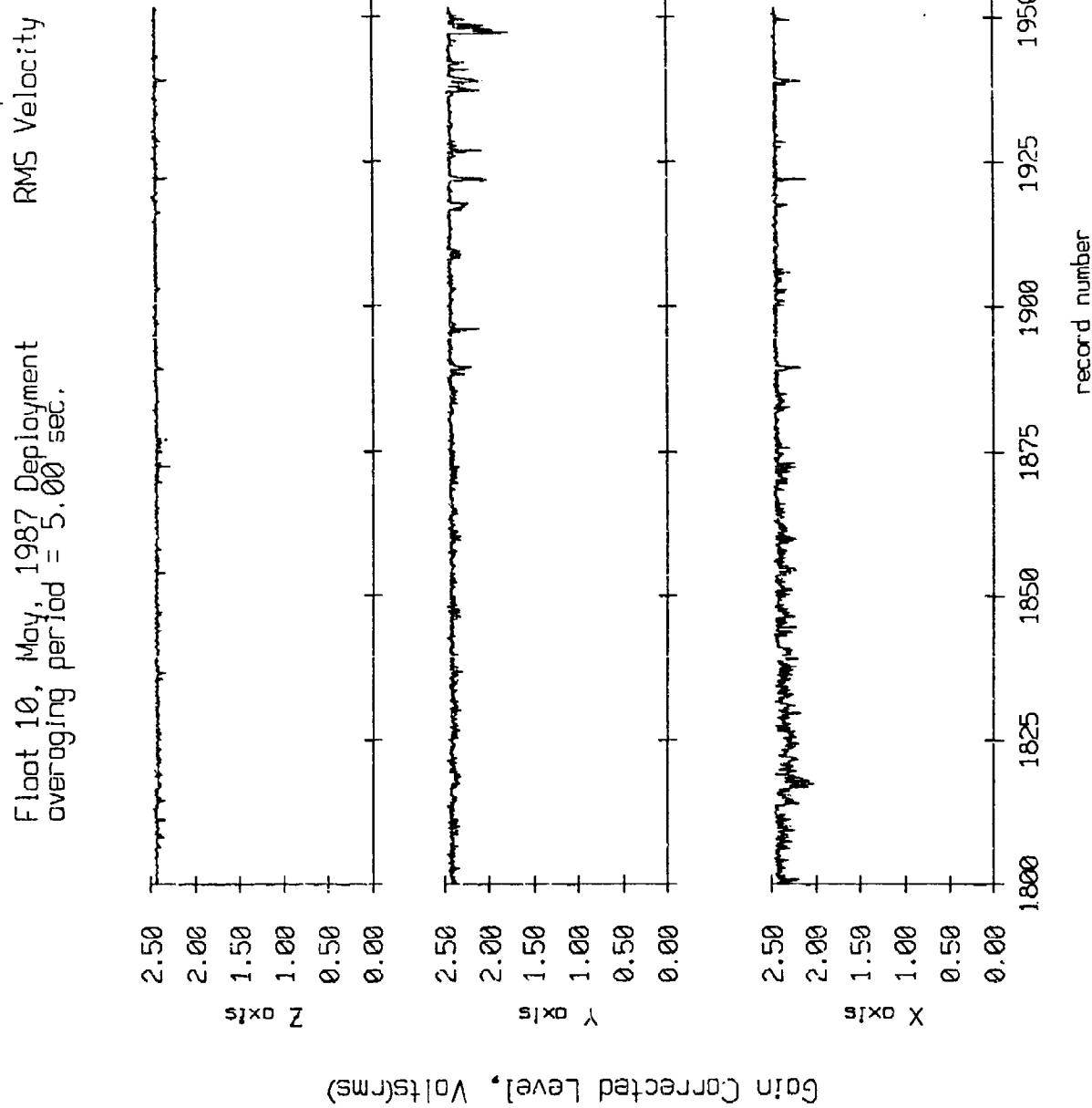
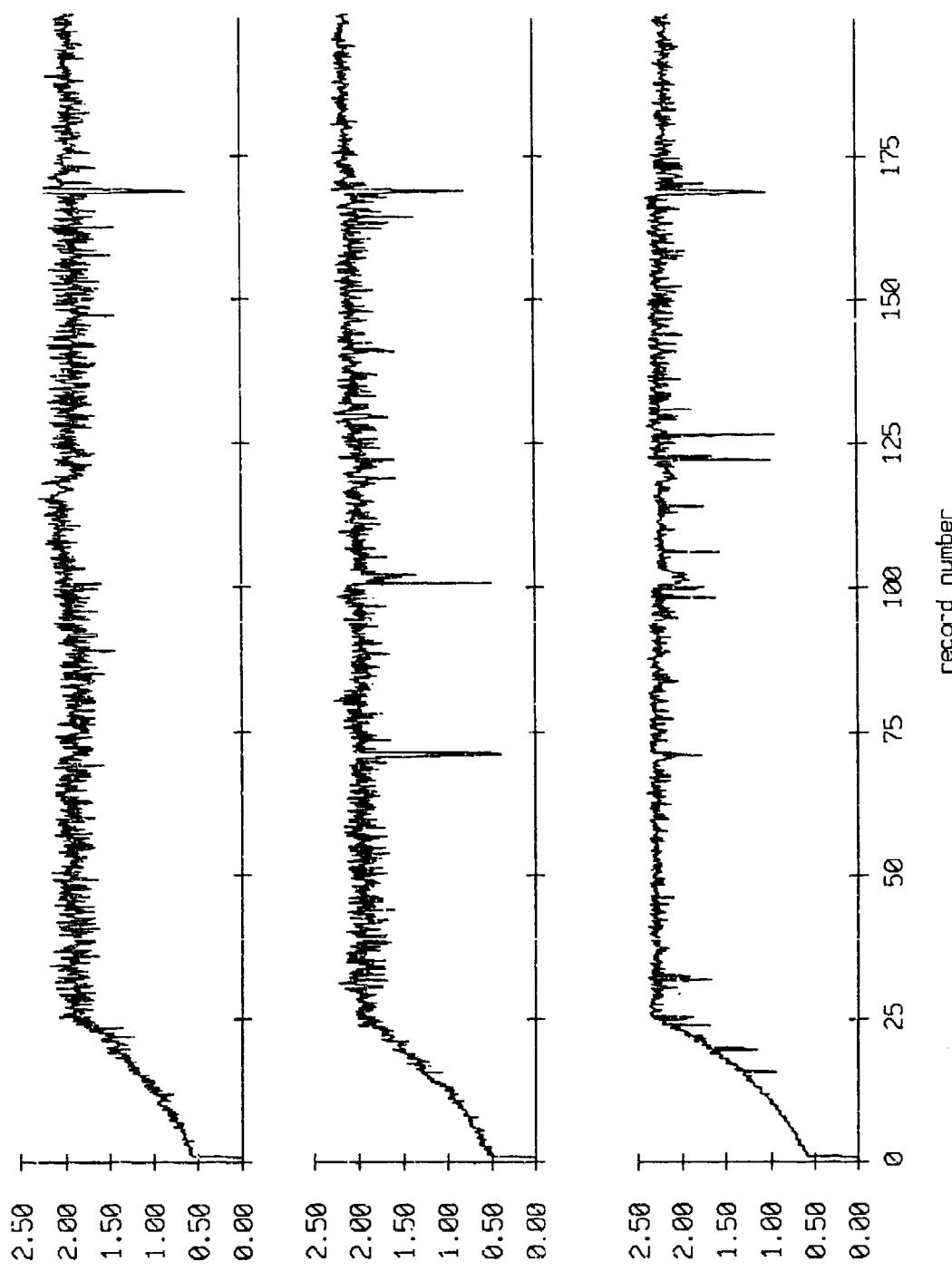


Figure IX.9j

Fleet 11, May, 1987 Deployment
overaging period = 5.00 sec.

RMS Velocity



Gain Corrected Level, Volts(RMS)

Figure IX.10a

Floct 11, May, 1987 Deployment
averaging period = 5.00 sec.

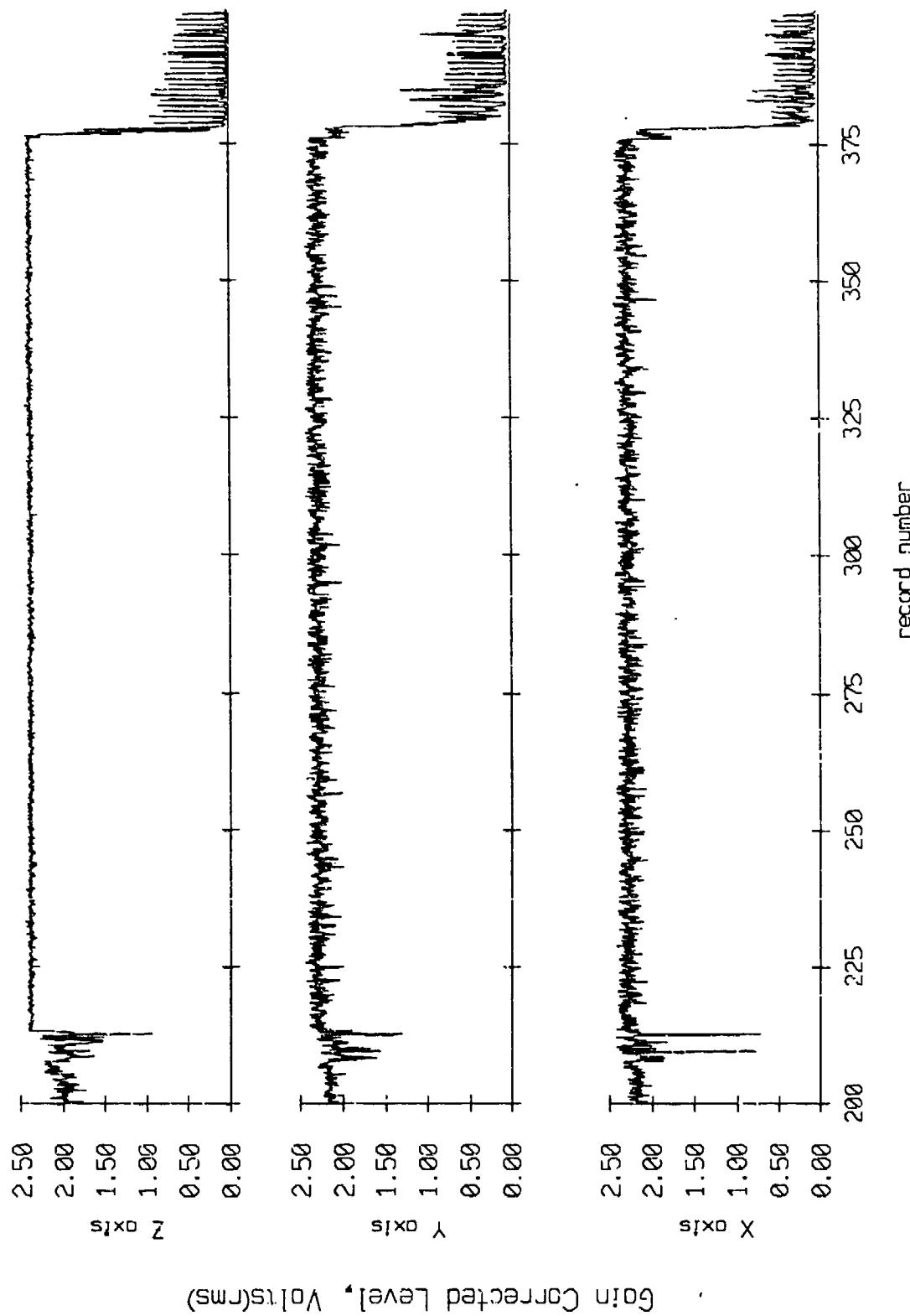


Figure IX.10b

Float 11, May, 1987 Deployment
overaging period = 5.00 sec.

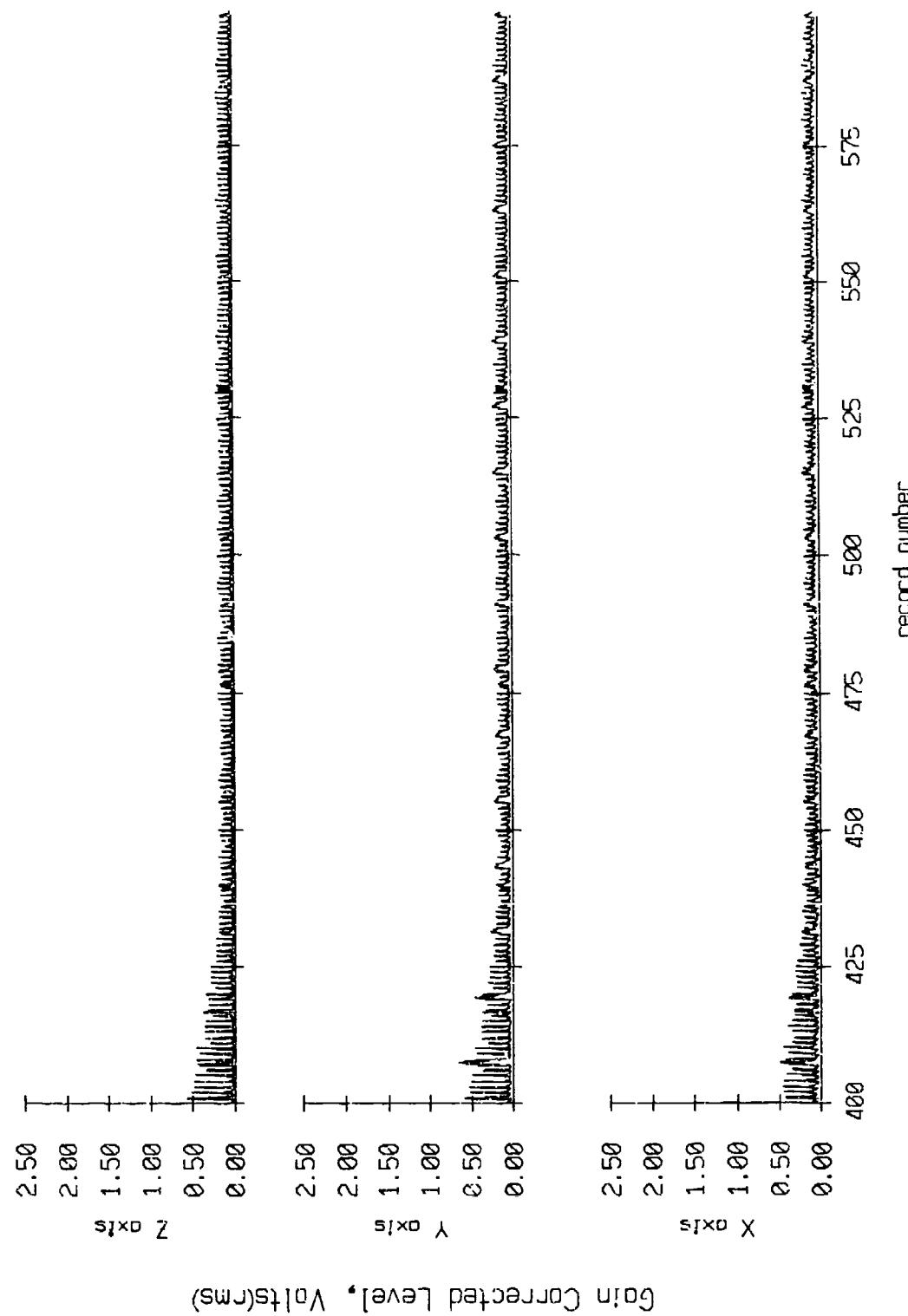


Figure IX.10c

Fleet 11, May, 1987 Deployment
averaging period = 5.00 sec.

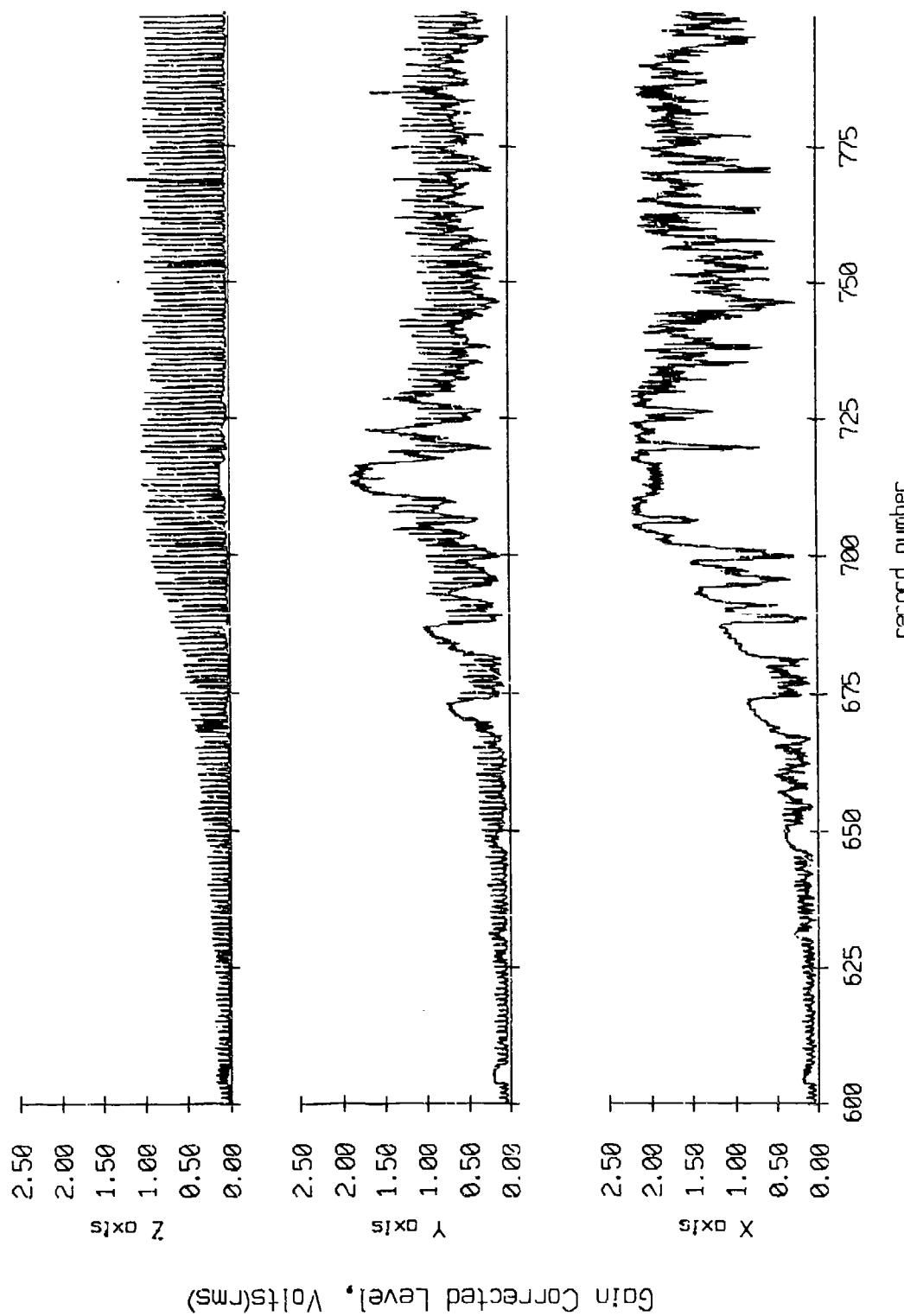


Figure IX.10d

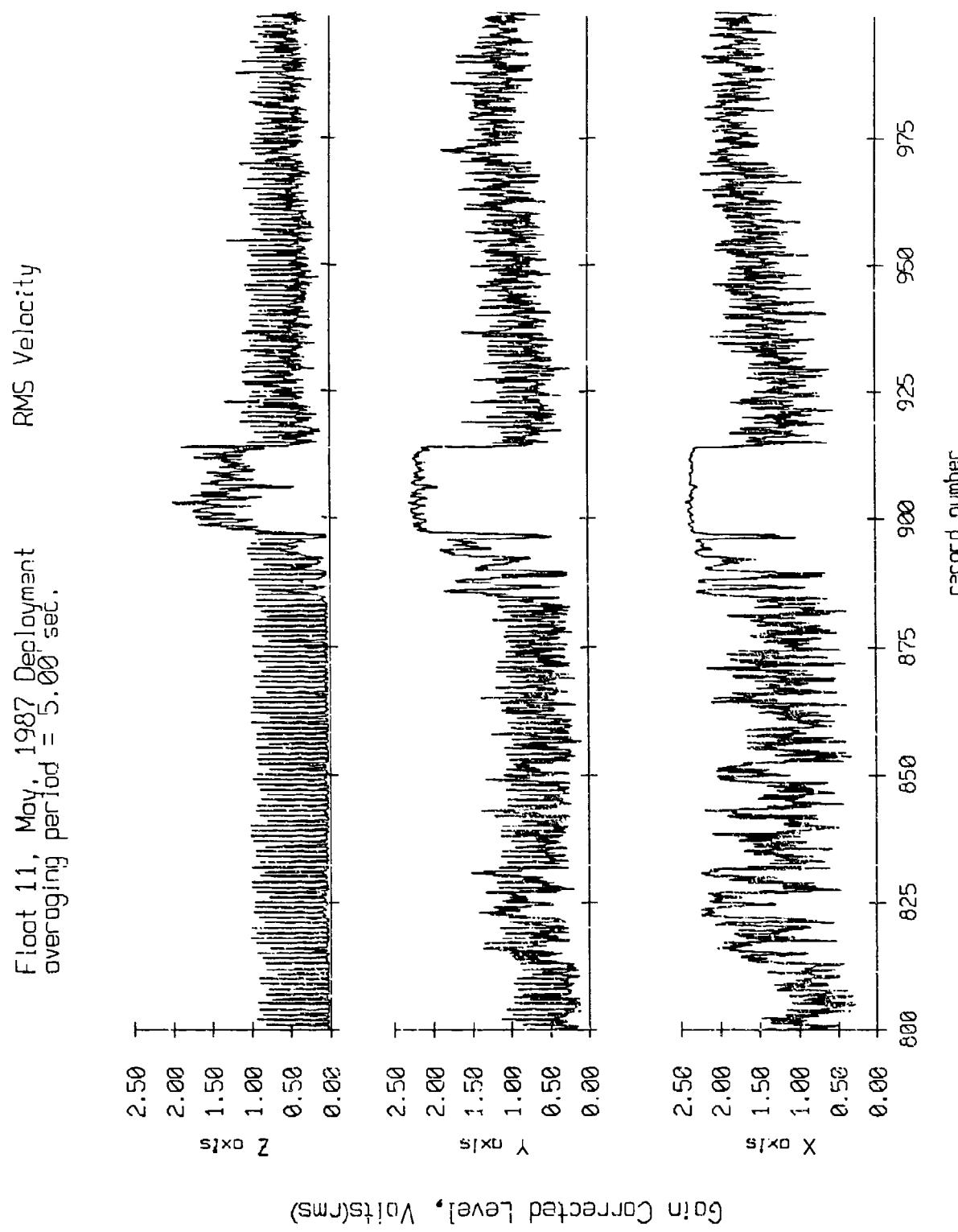


Figure IX.10e

Float 111, May, 1987 Deployment
overgoing period = 5.00 sec.

RMS Velocity

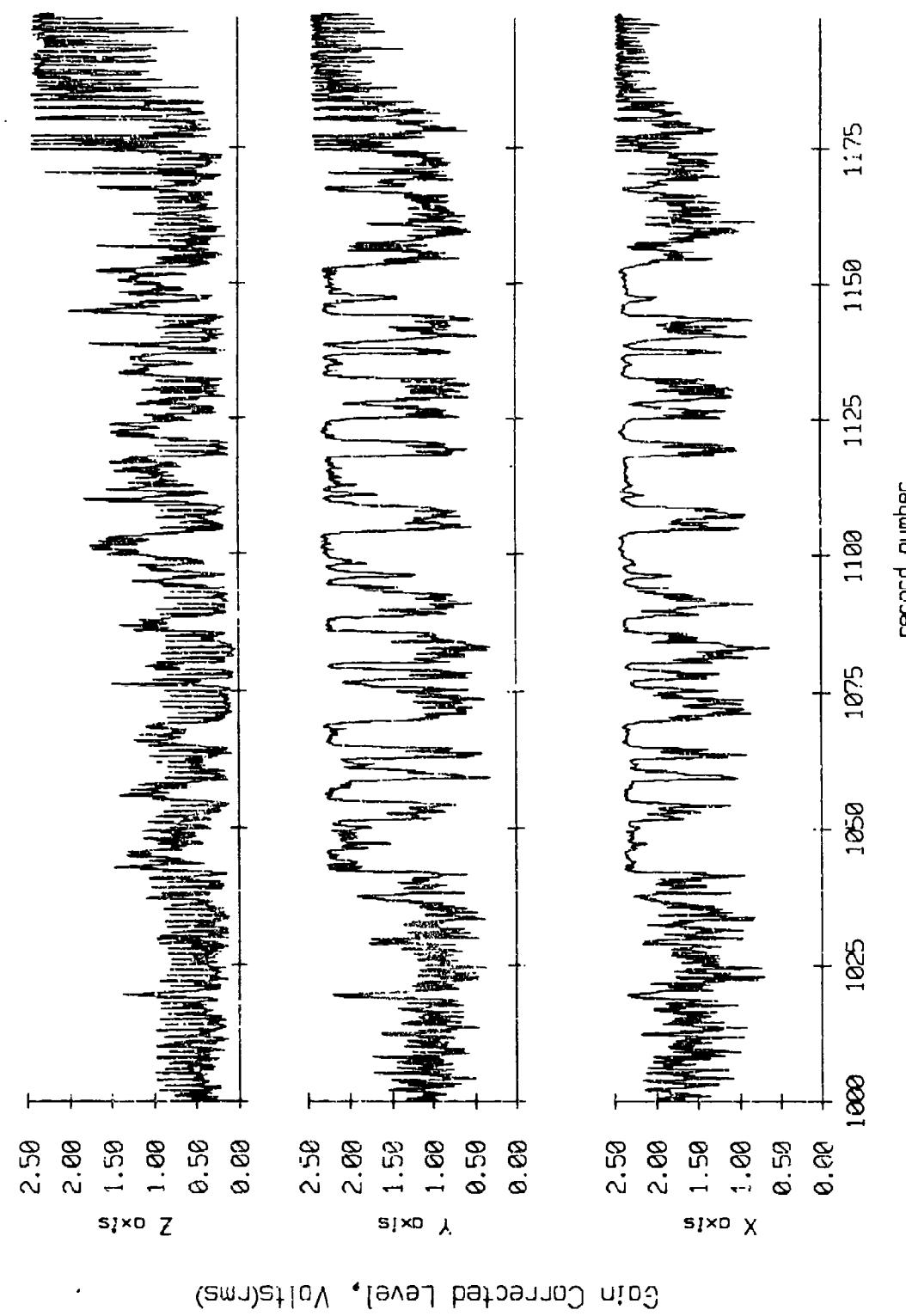


Figure IX.10f

Float 11, May, 1987 Deployment
averaging period = 5.00 sec.

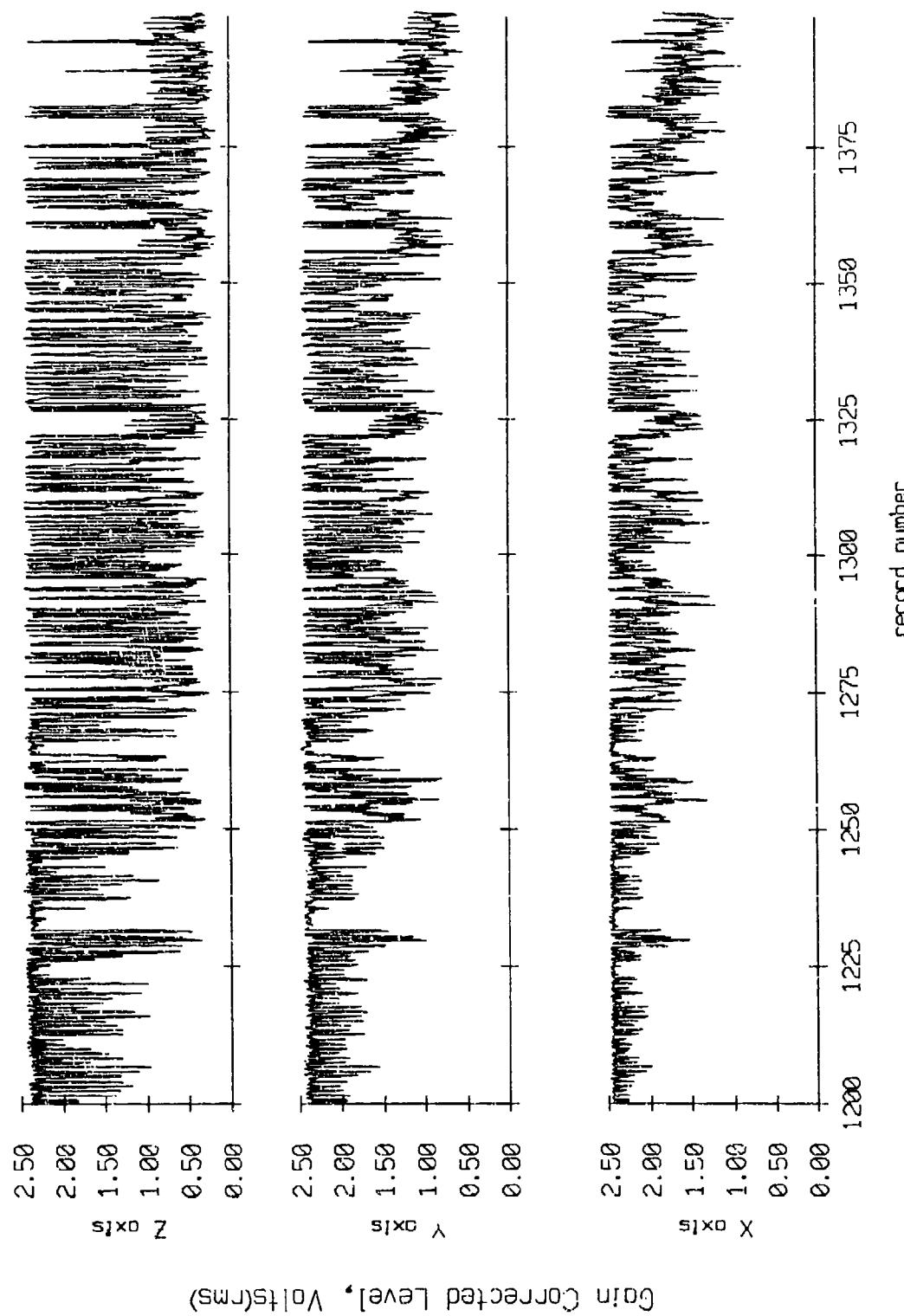


Figure IX.10g

Float 11, May 1987 Deployment
averaging period = 5.00 sec.

RMS velocity

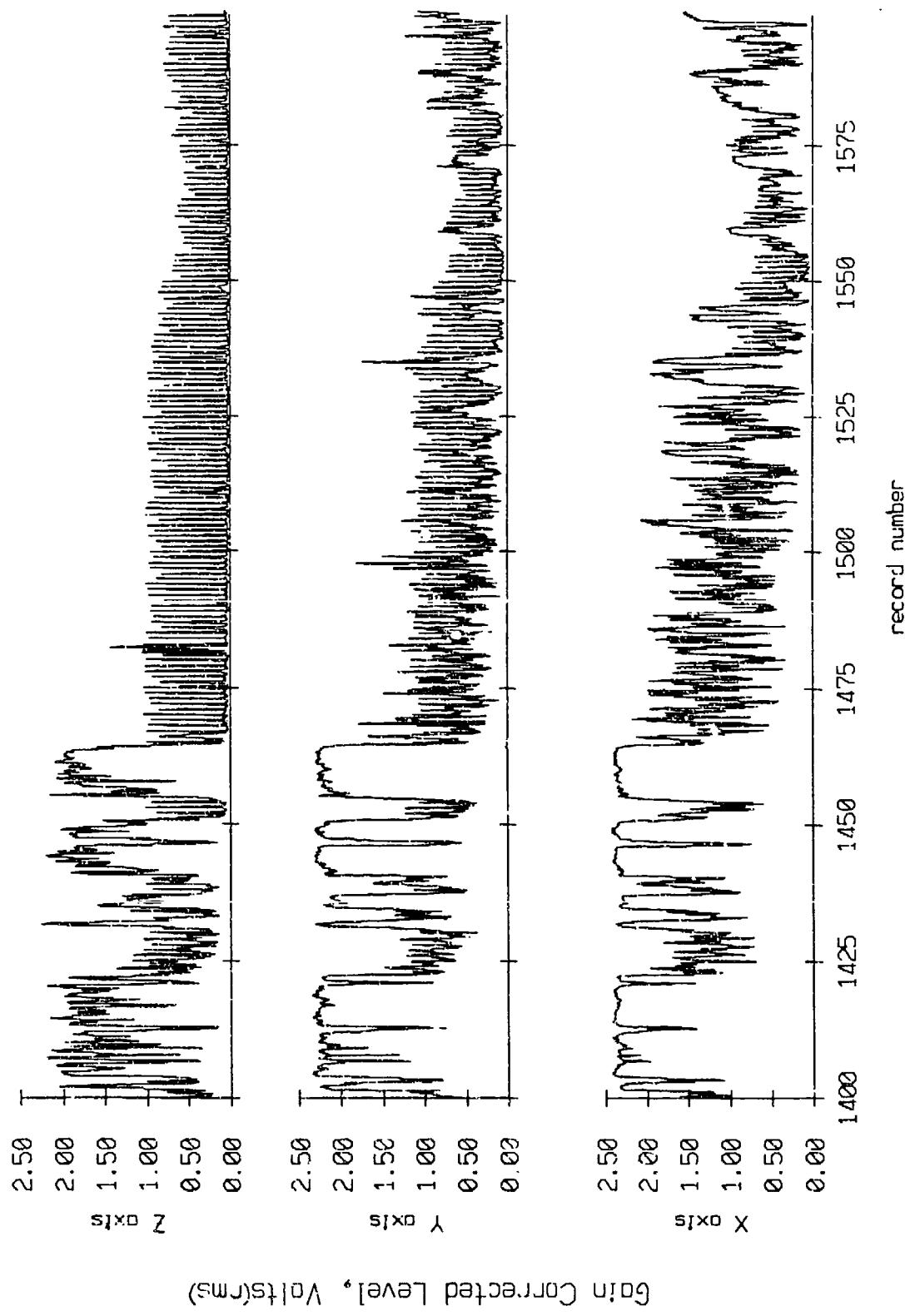
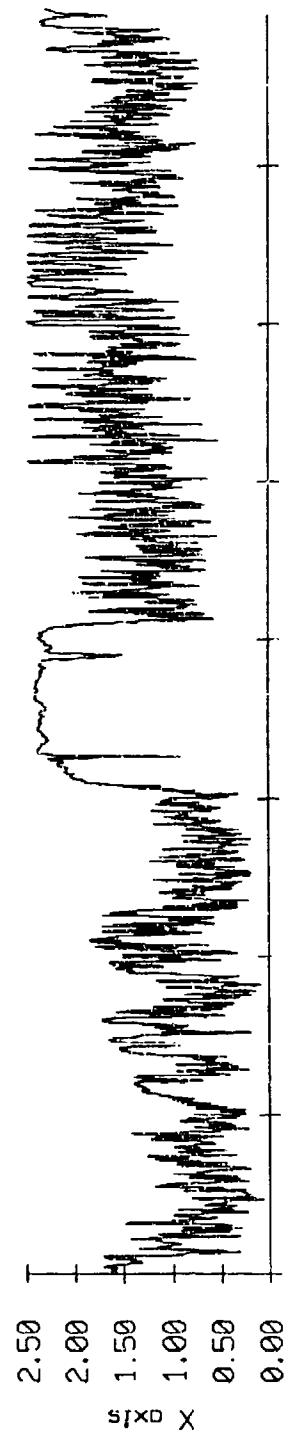
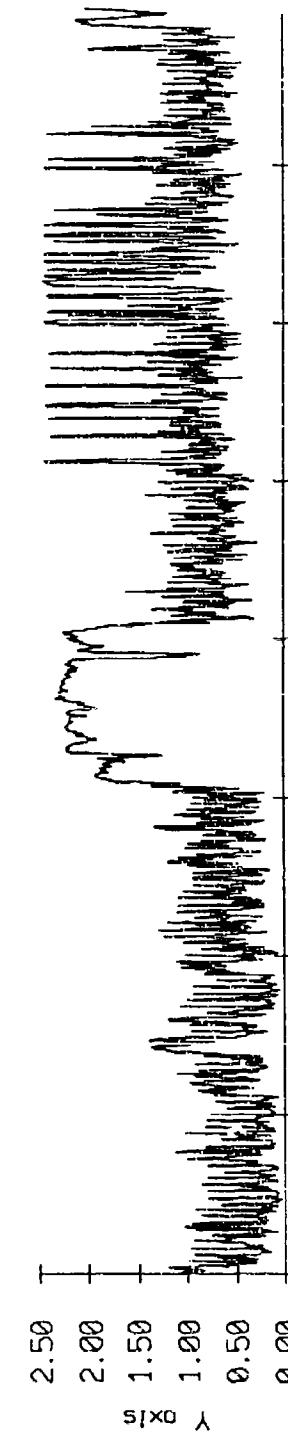
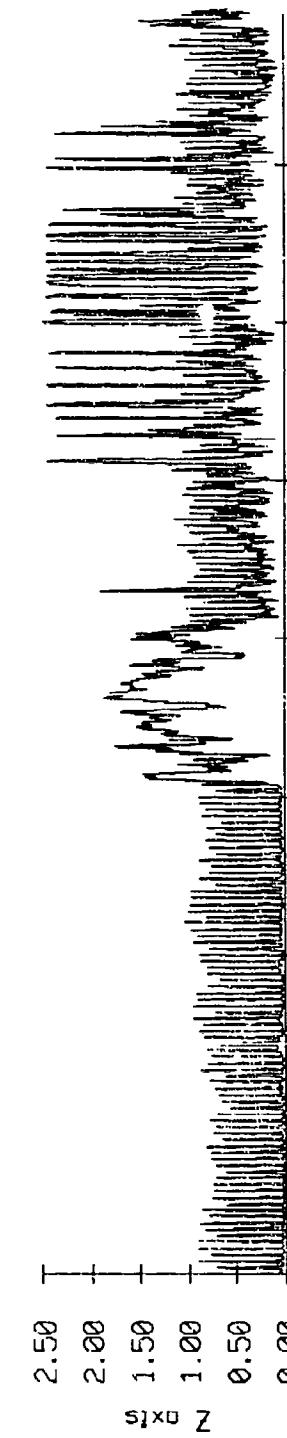


Figure IX.10h

Float 11, May, 1987 Deployment
overaging period = 5.00 sec.

RMS Velocity

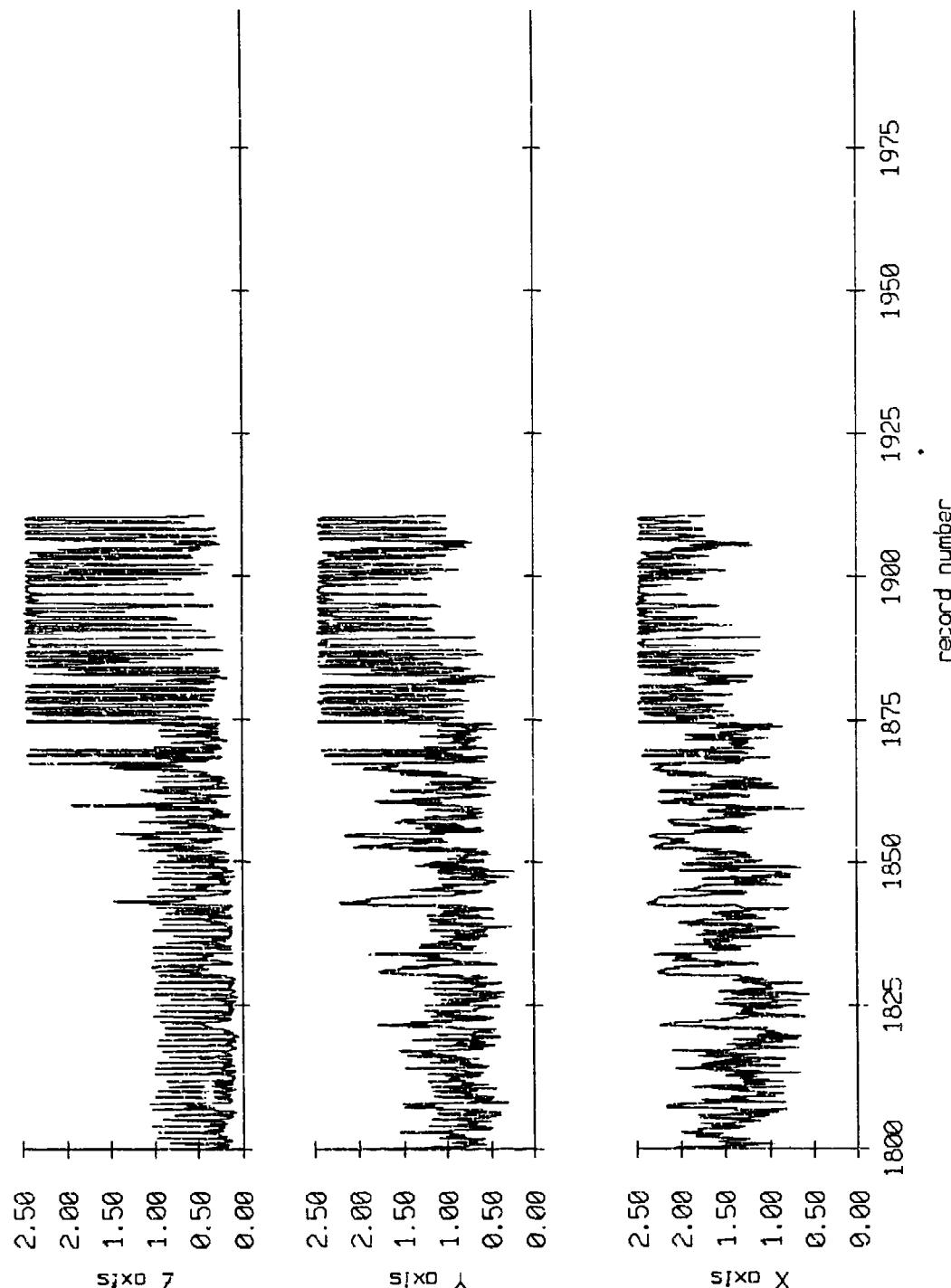


Go in Corrected Level, Volts(RMS)

Figure IX.10i

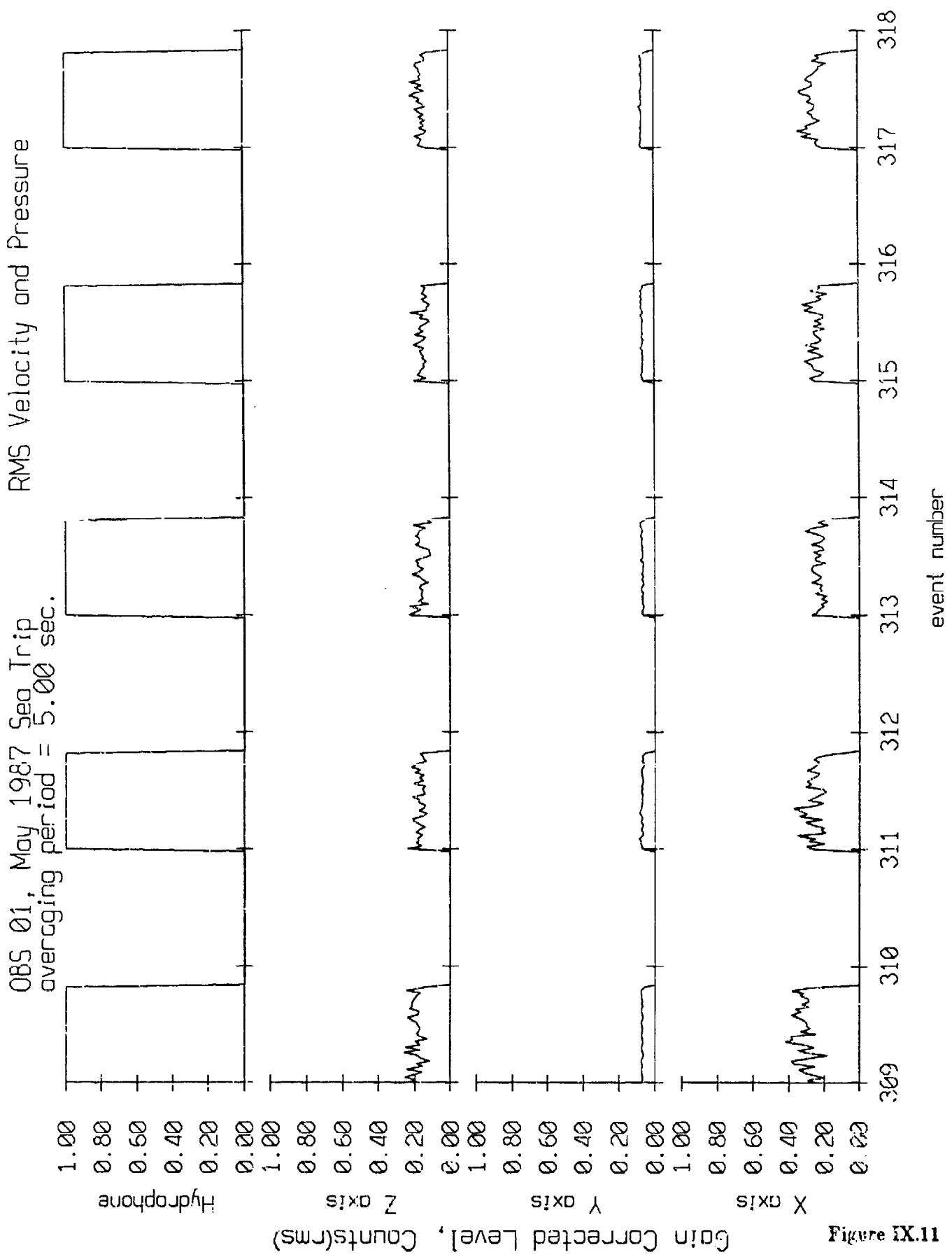
Fleet 11, May, 1987 Deployment
averaging period = 5.00 sec.

RMS Velocity



Gain Corrected Level, Volts(rms)

Figure IX.10j



OBS 02, May 1987 Sea Trip
averaging period = 5.00 sec.

RMS Velocity and Pressure

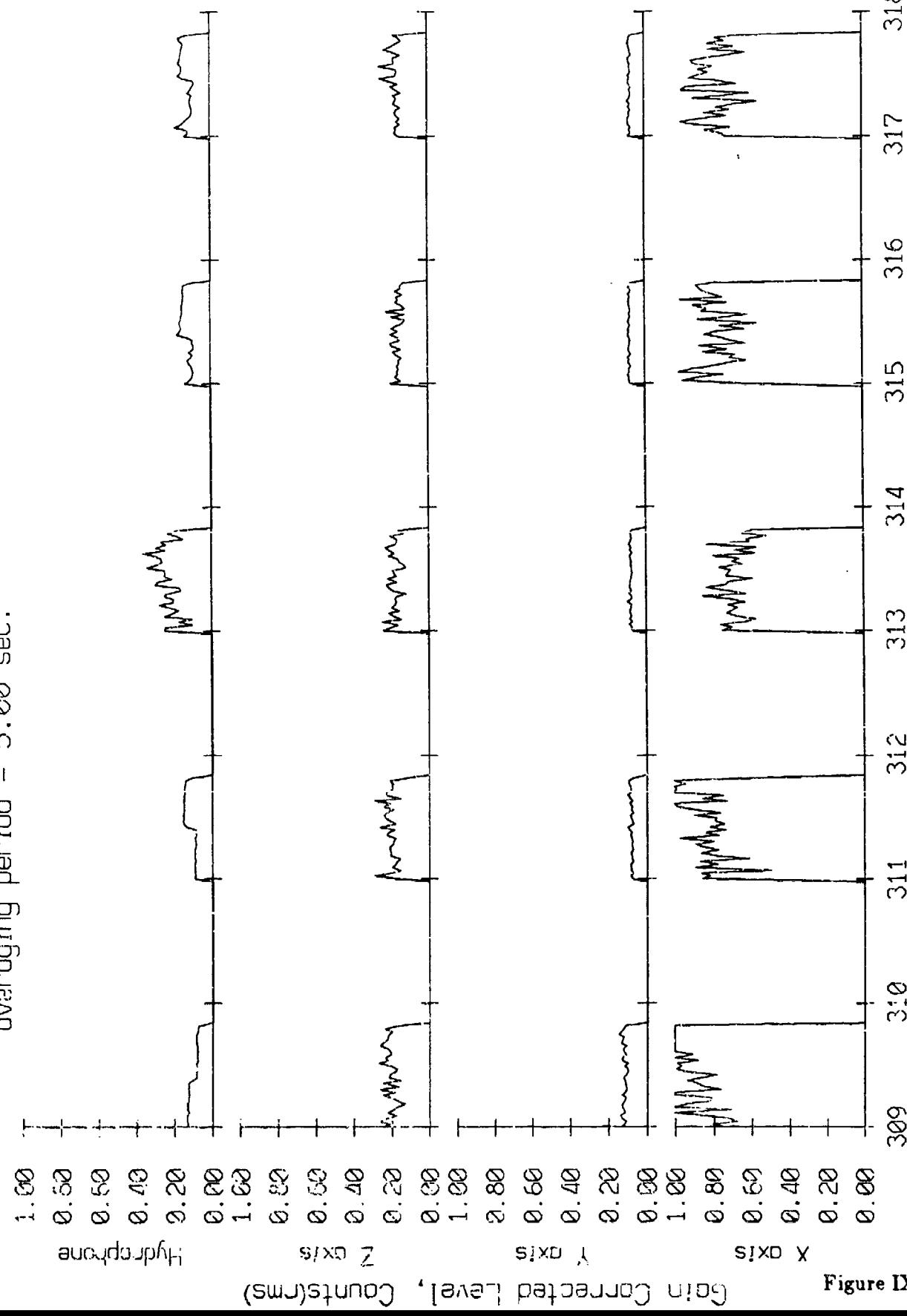


Figure IX.12

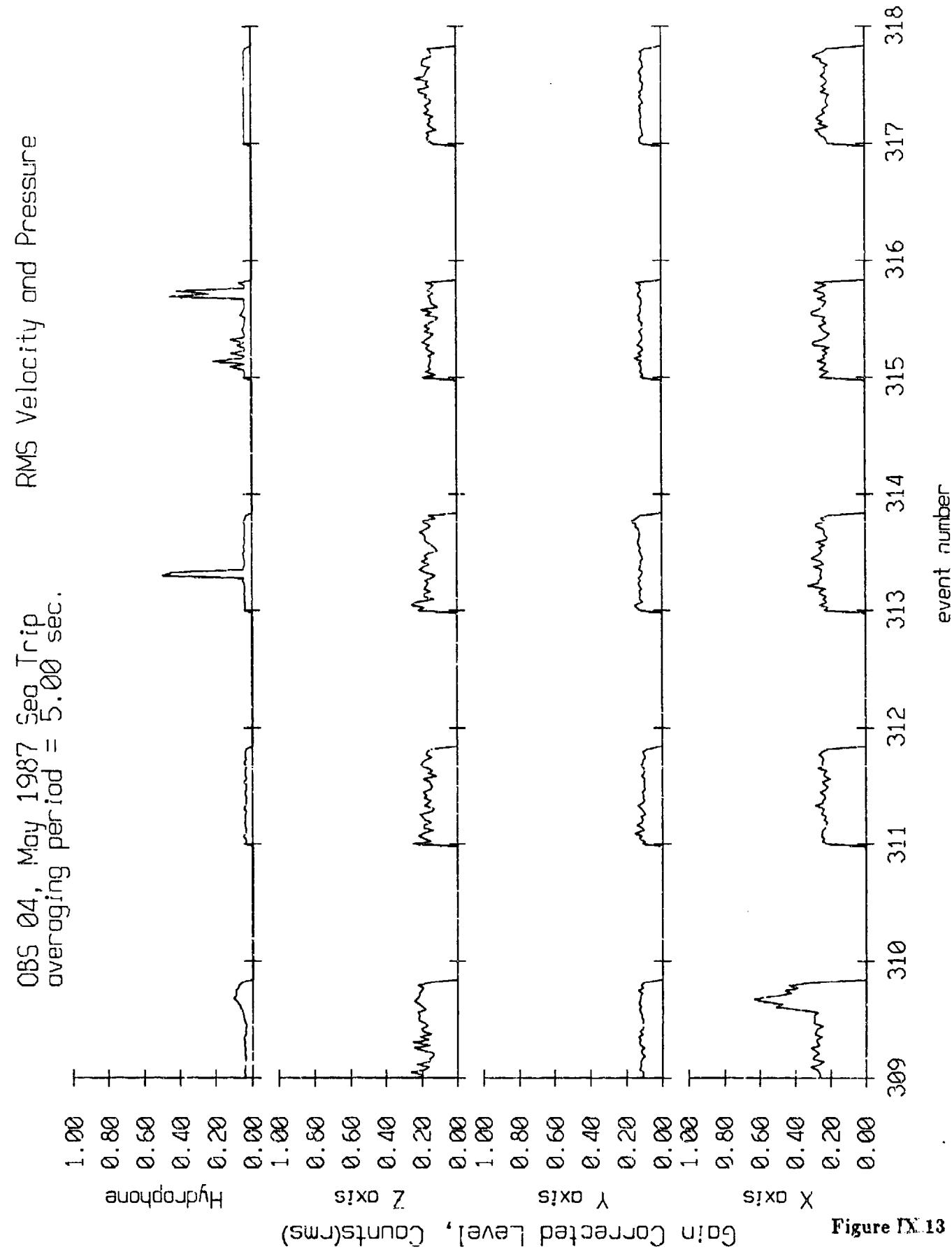
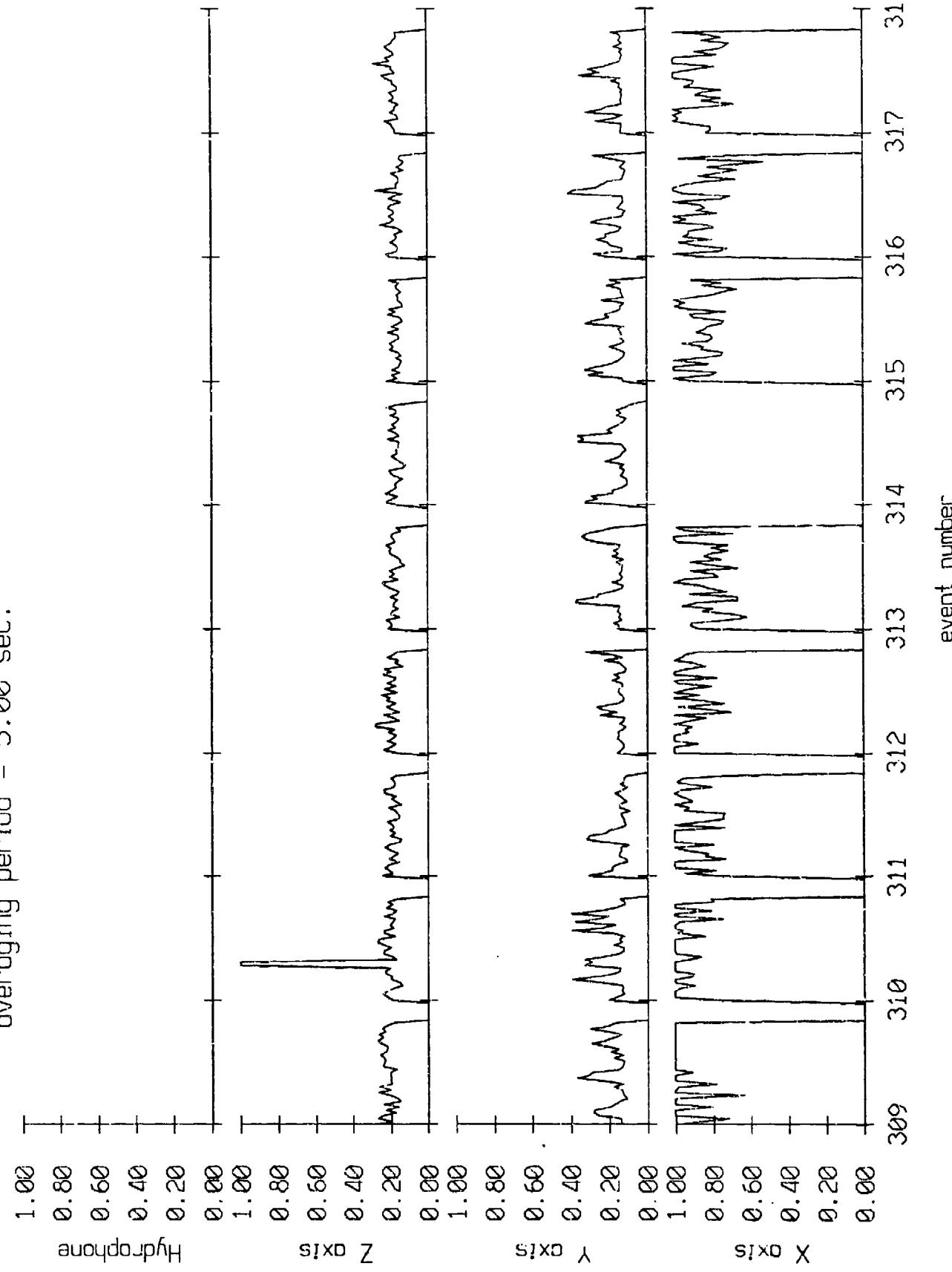


Figure IX.13

OBS 05, May 1987 Sea Trip
overranging period = 5.00 sec.

RMS Velocity and Pressure



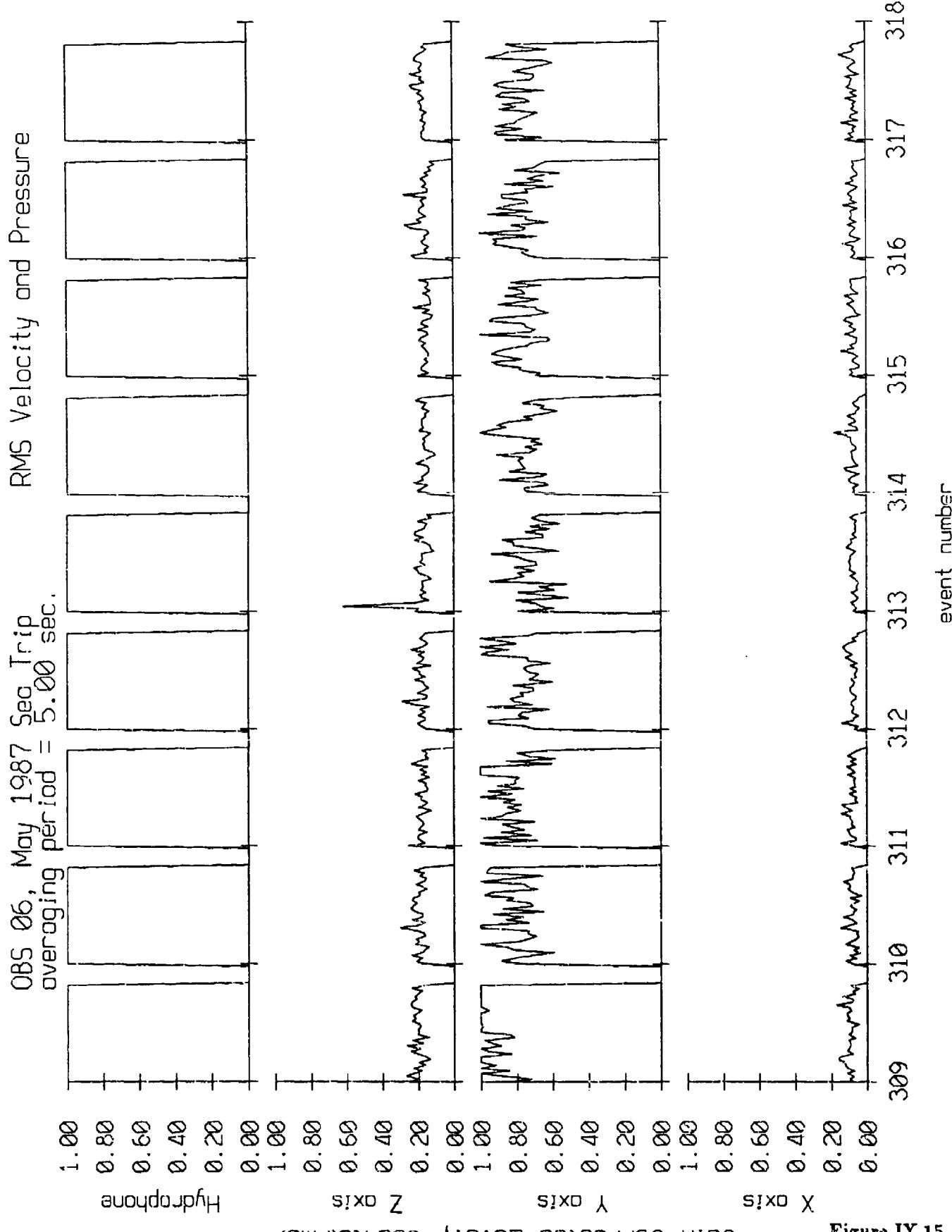
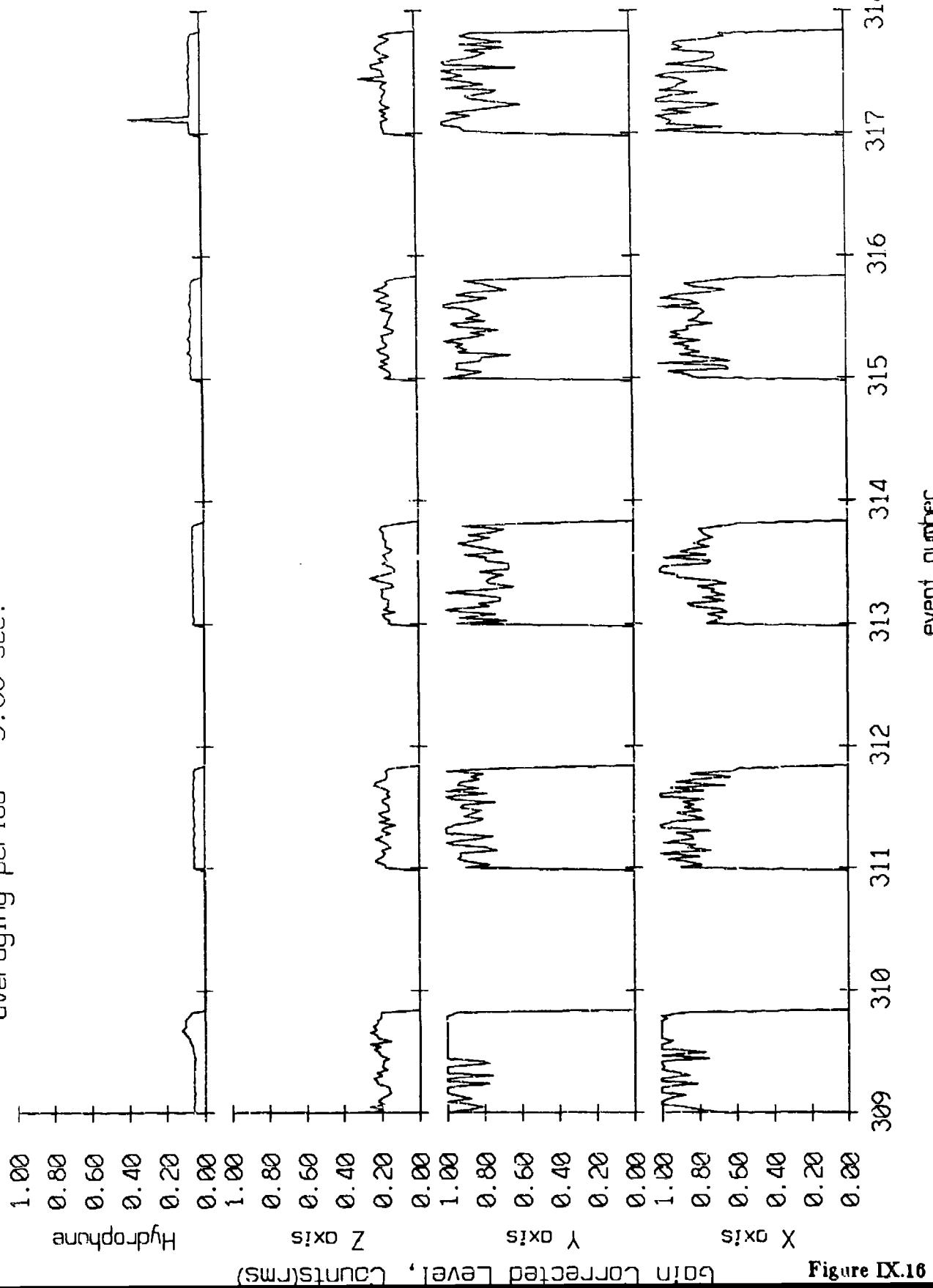


Figure IX.15

OBS 08, May 1987 Sea Trip
averaging period = 5.00 sec.

RMS Velocity and Pressure

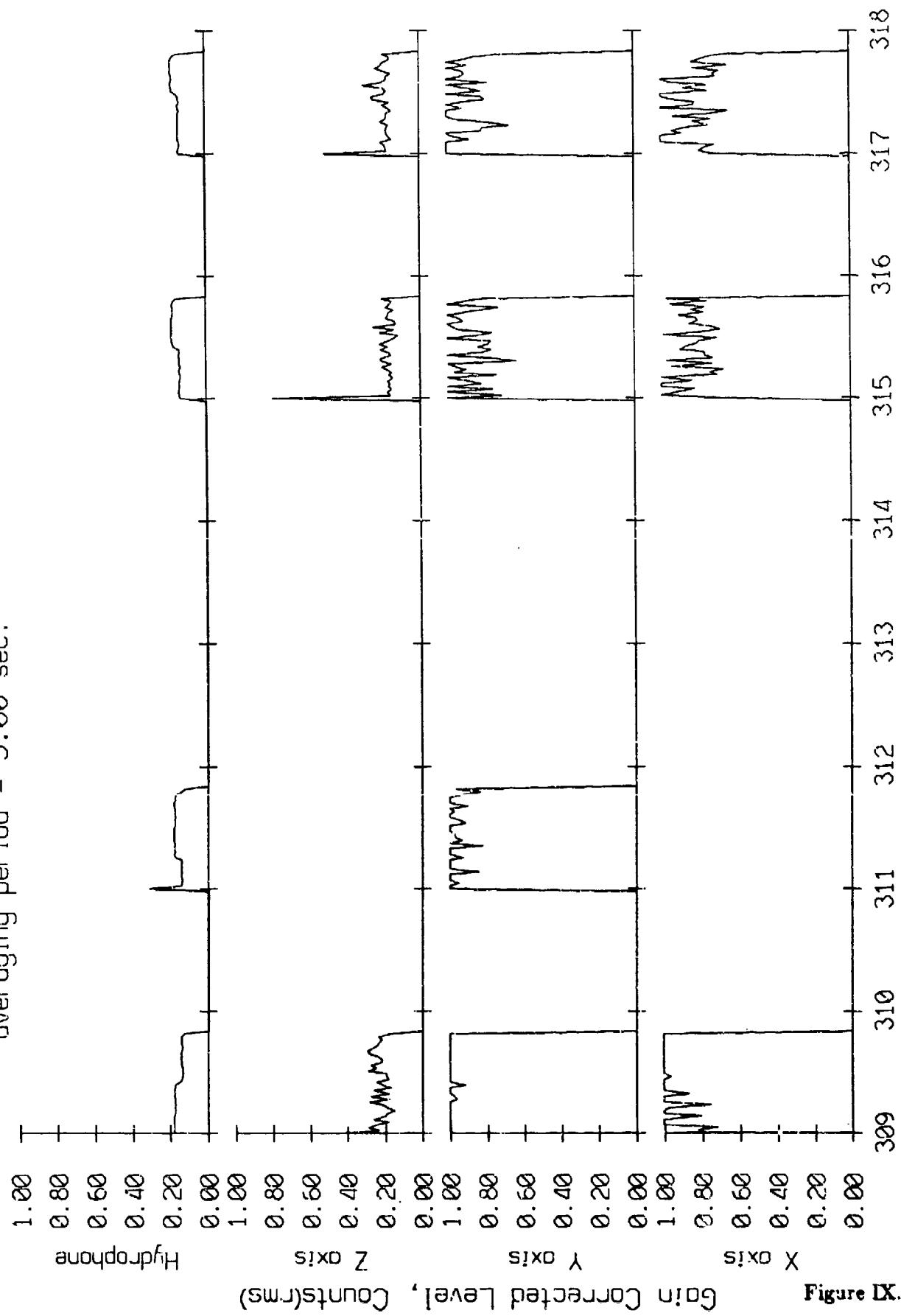


gait uncorrected Level, LDunits(RMS)

Figure IX.16

OBS 12, May 1987 Sea Trip
averaging period = 5.00 sec.

RMS Velocity and Pressure



Gain Corrected Level, Counts(rms)

Figure IX.17

OBS 13, May 1987 Sea Trip
overaging period = 5.00 sec.

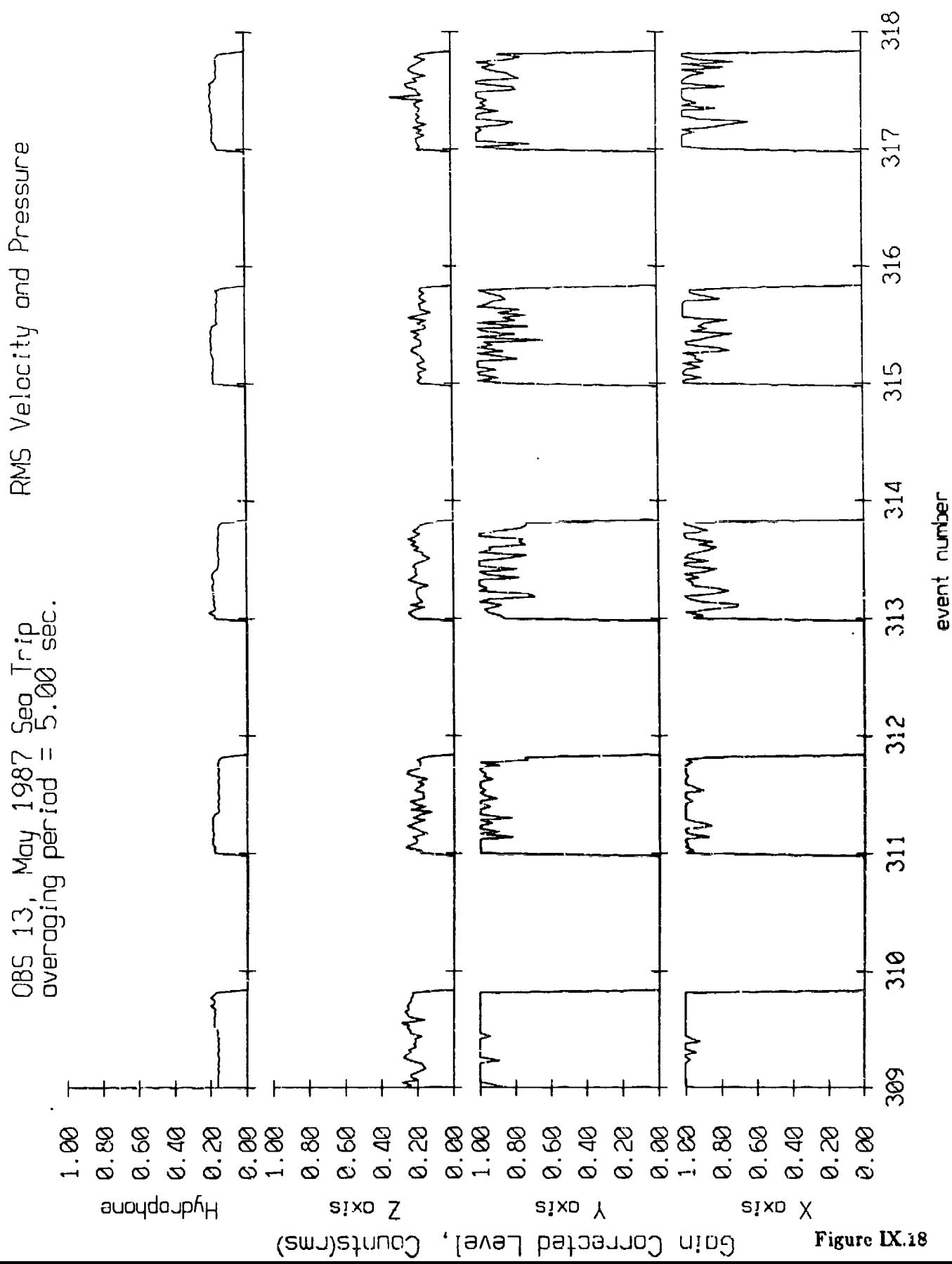


Figure IX.18

OBS 14, May 1937 Sea Trip
averaging period = 5.00 sec.

RMS Velocity and Pressure

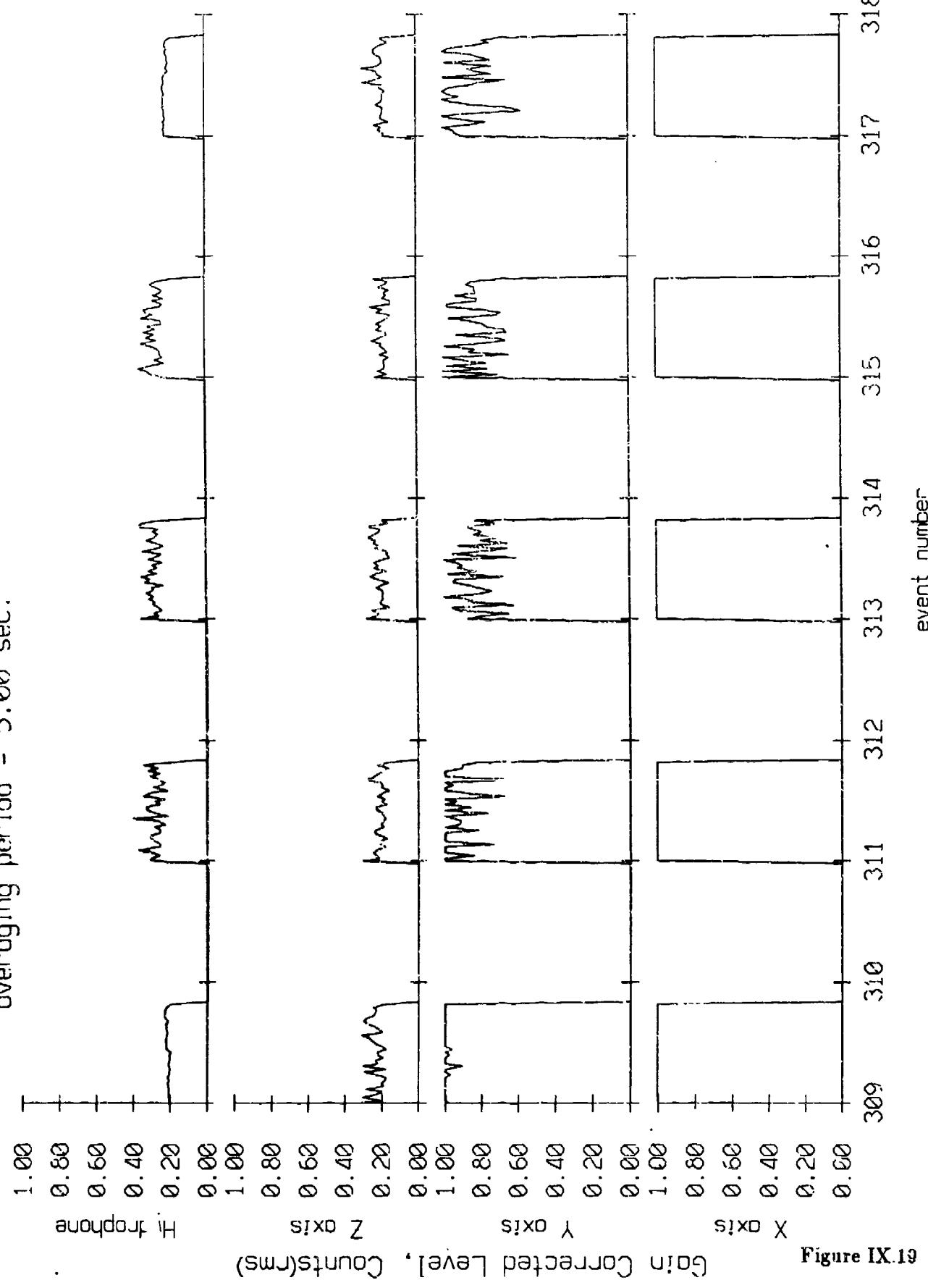


Figure IX.19

Fleet 0, May, 1987 Trip - records 957-968 (x-axis)
vertical axis is approx. -1.0 to 1.0 volts

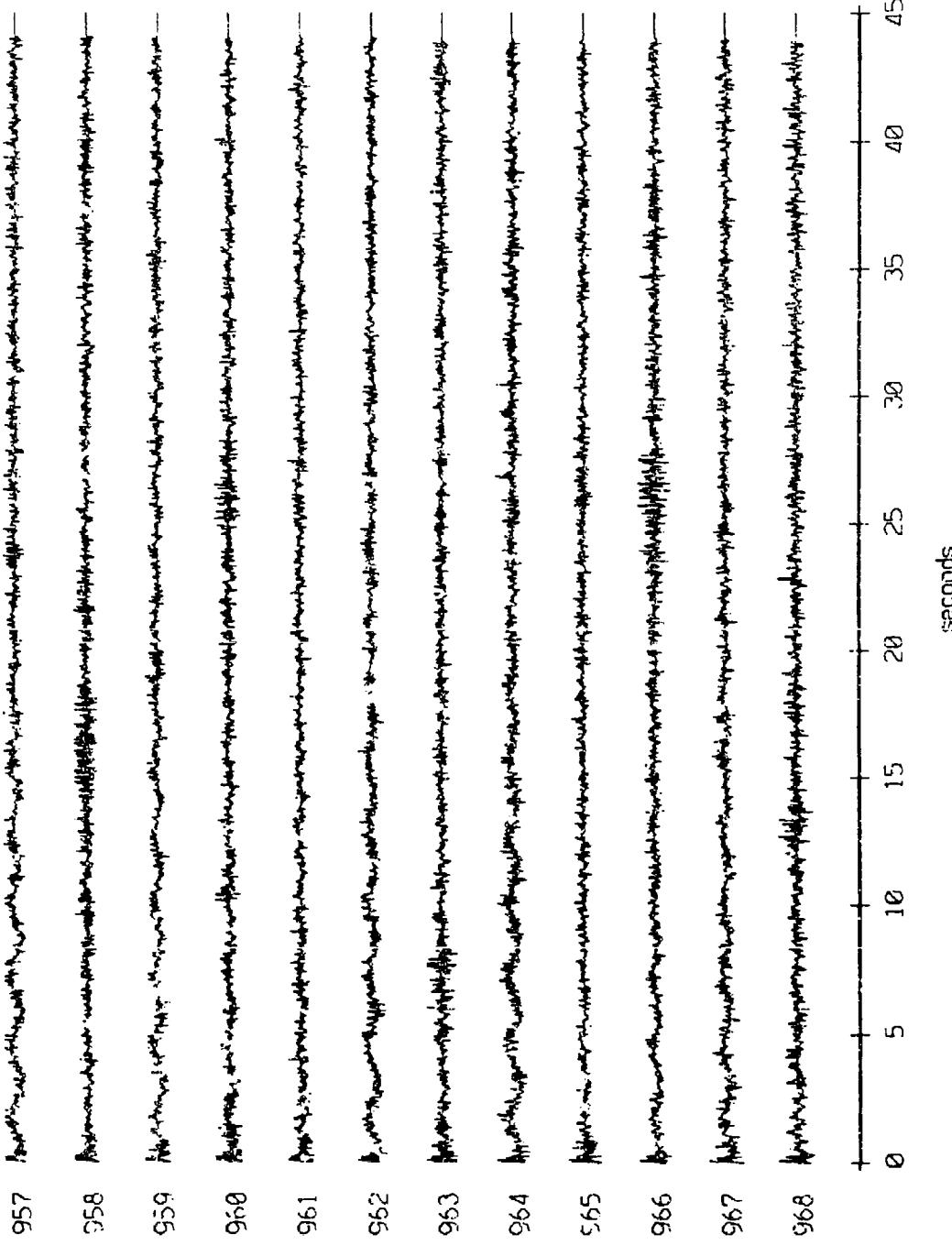


Figure X.1a.i

Float 0, May, 1987 Trip - records 957-968 (y-axis)

vertical axis scale is approx. -1.0 to 1.0 volts

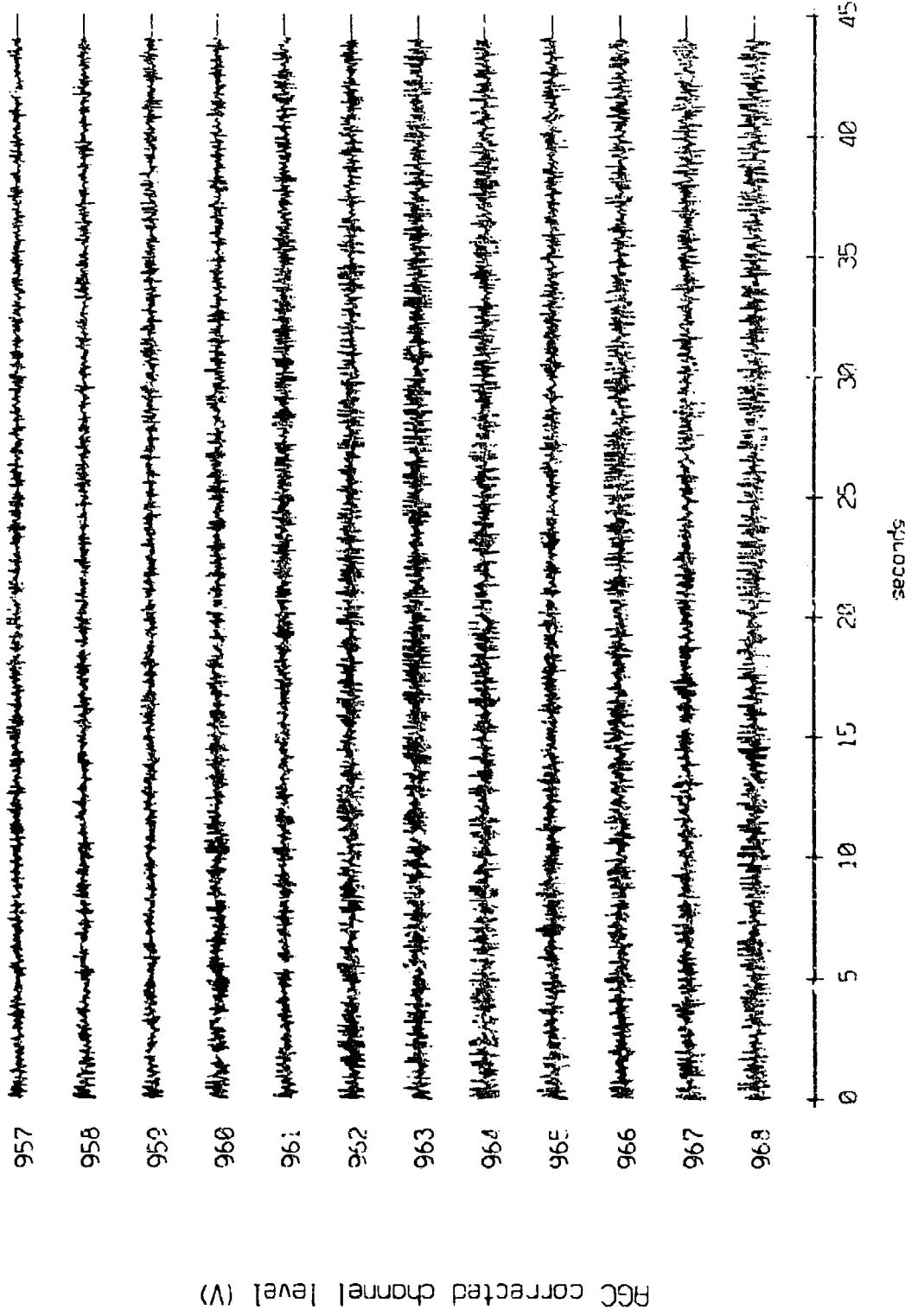


Figure X.1a.j

Fleet 0, May, 1987 Trip - records 957-968 (Z-axis)
vertical axis scale is approx. -1.0 to 1.0 volts

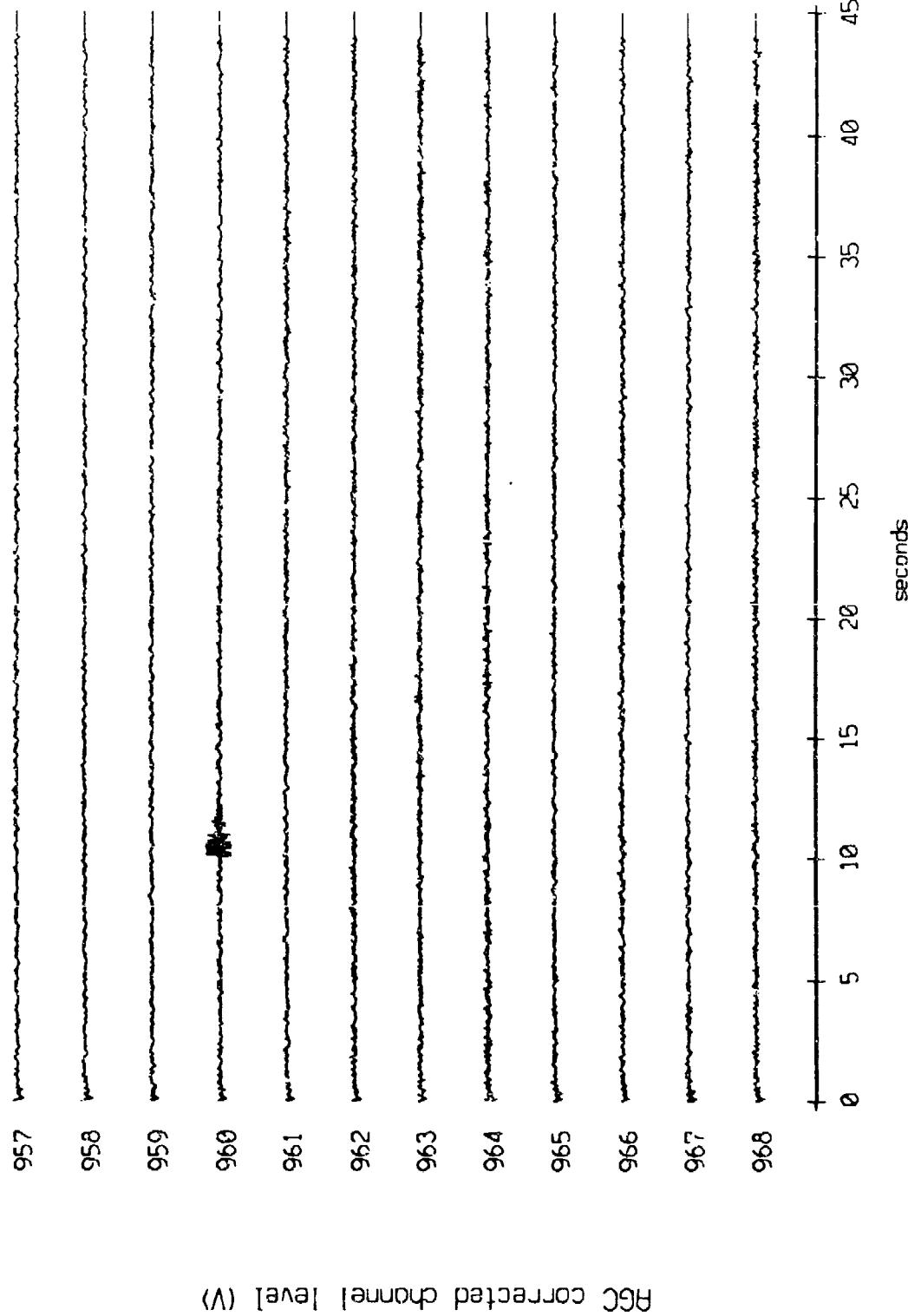
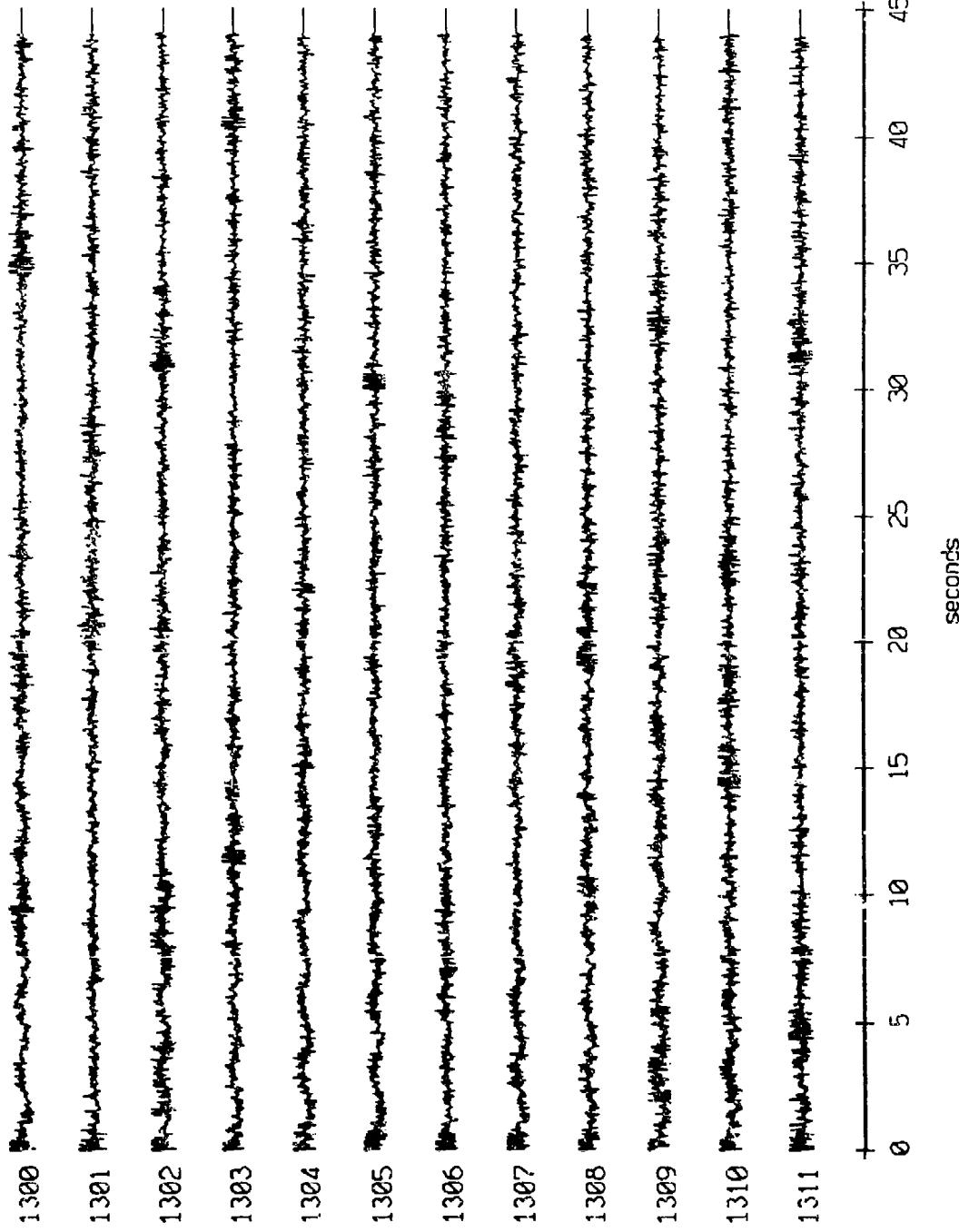


Figure X.1a.k

Float 0, May 1987 Sea Trip - records 1300-1311 (x-axis)
vertical axis scale is approx. -1.0 to 1.0 volts



DGC CORRECTED channel level (V)

Figure X.1b.i

Float 0, May 1987 Sea Trip - records 1300-1311 (y-axis)
vertical axis approx. -1.0 to 1.0 volts

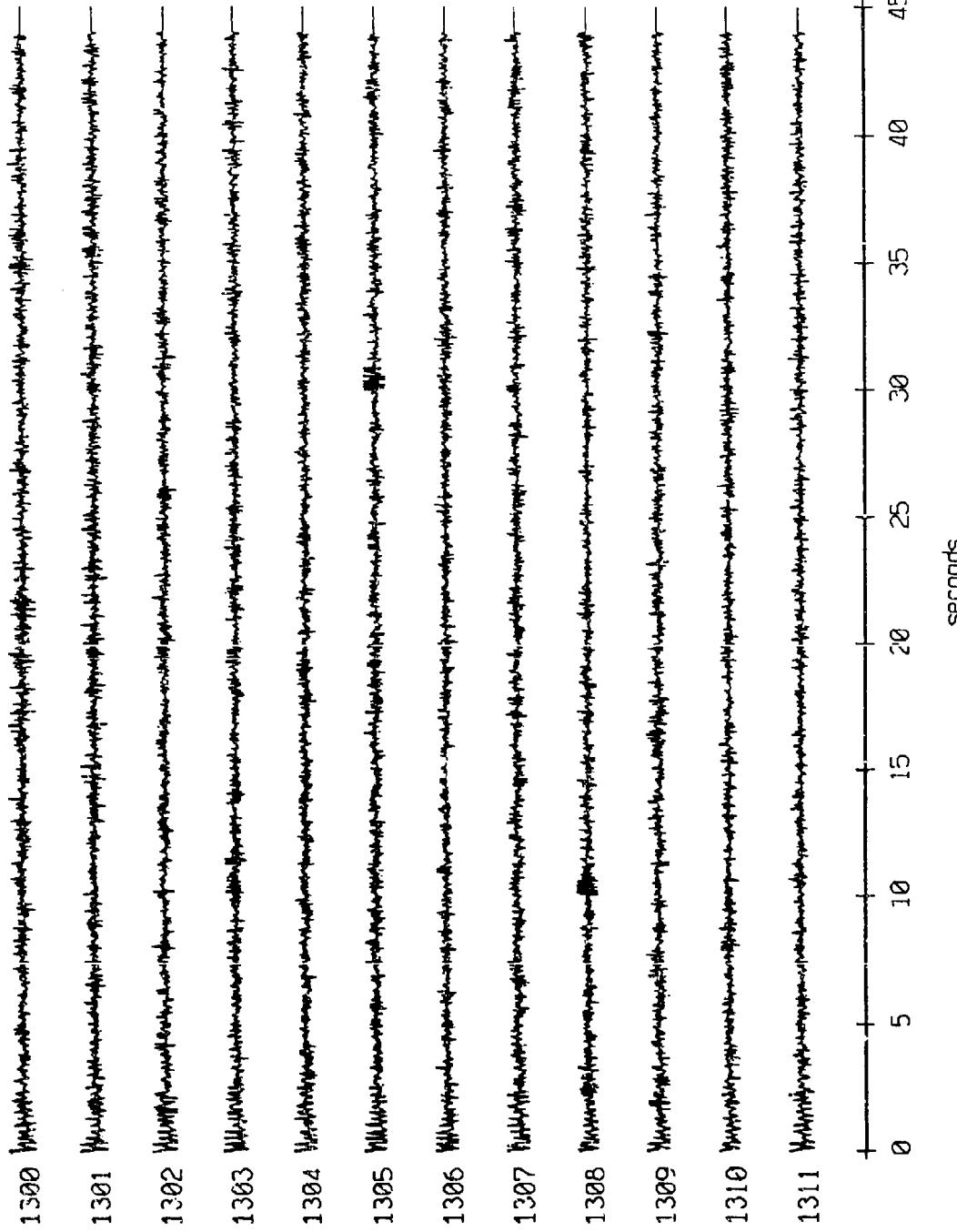
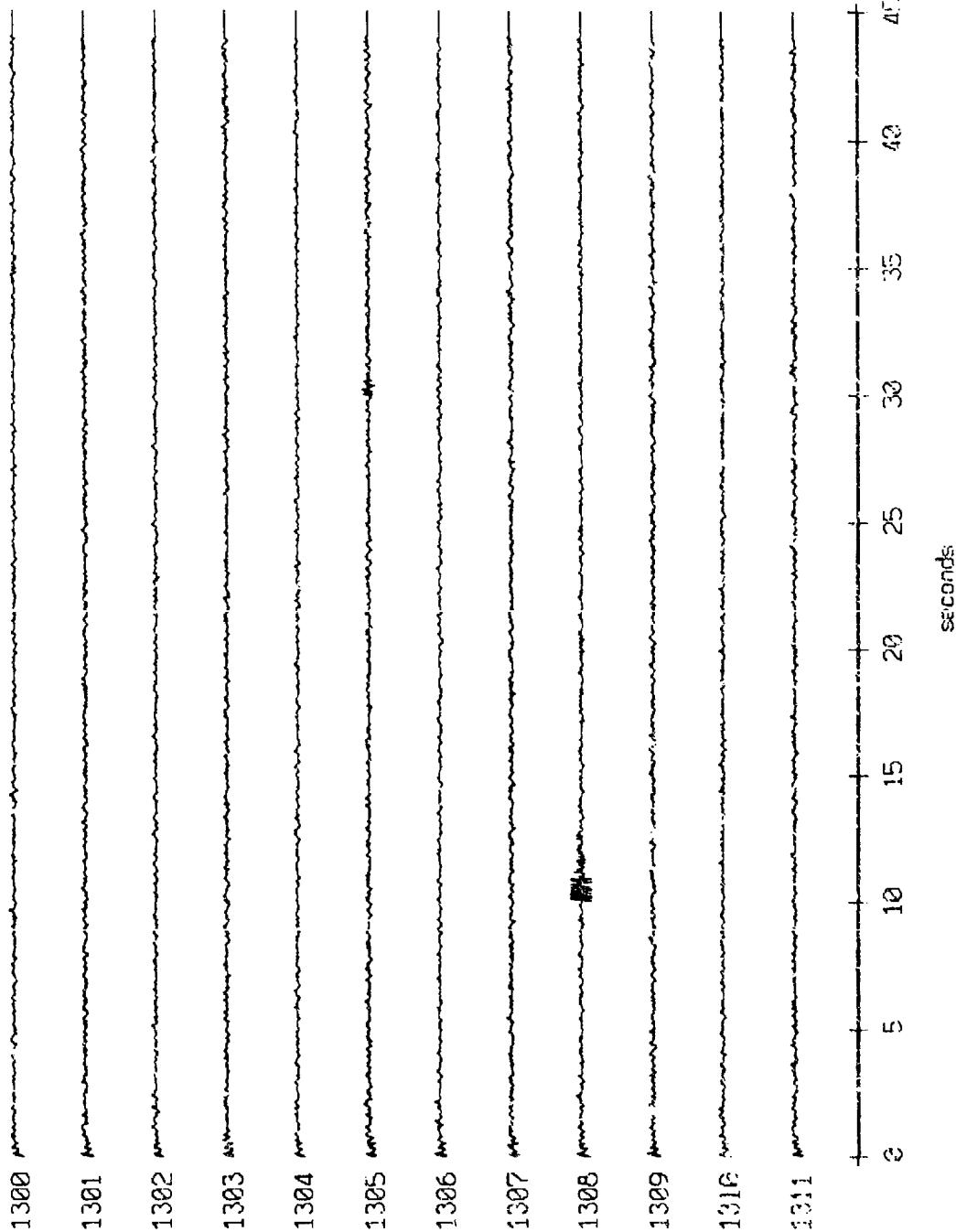


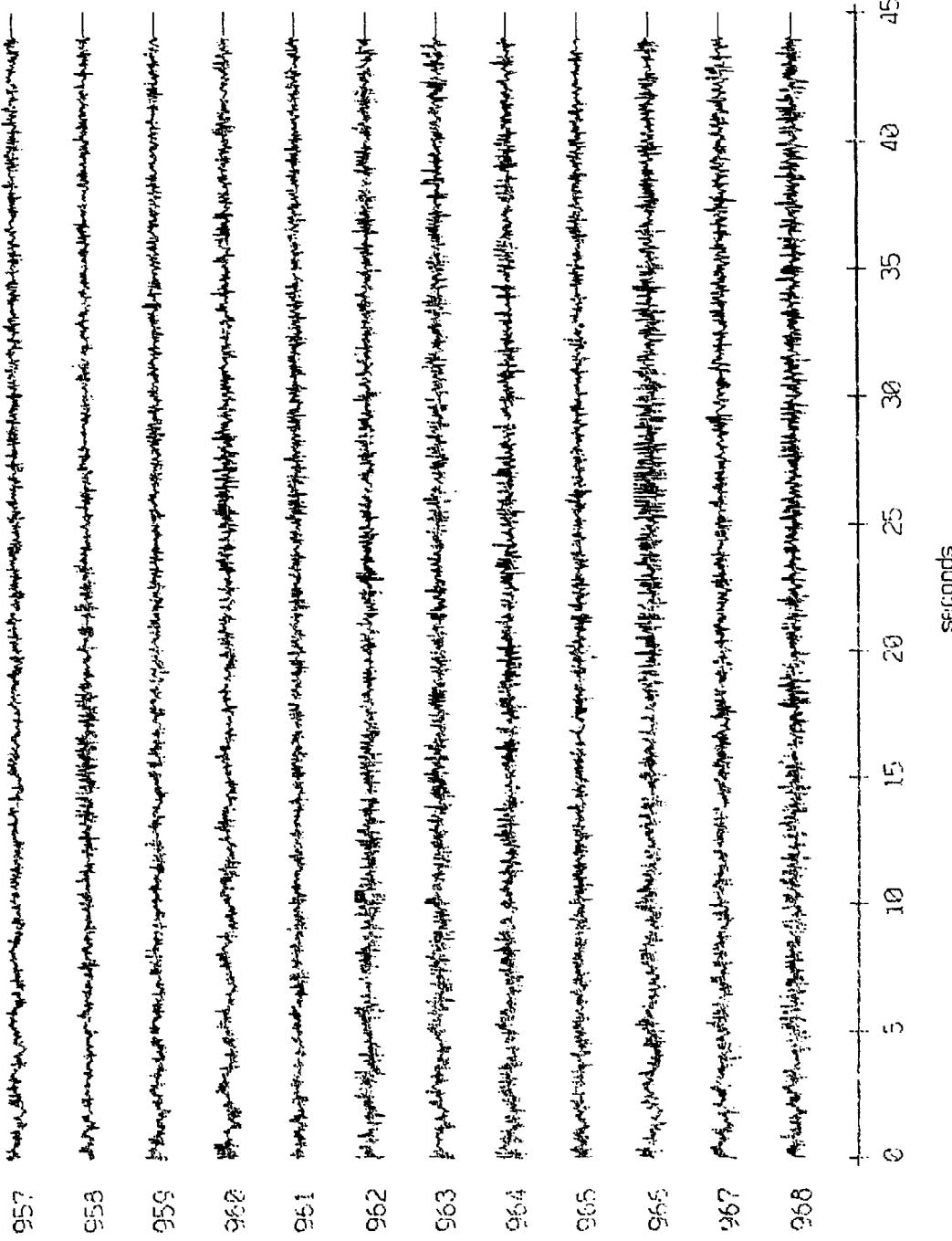
Figure X.1b.j

Flight 0, May 1987 Sea Trip - records 1300-1311 (z-axis)
vertical axis is approx. -1.0 to 1.0 volts



AGC corrected channel level (V)

Fleet 2, May, 1957 Trip - records 957-968 (x-axis)
vertical axis is approx. -1.0 to 1.0 volts



GC corrected channel level (V)

Flight 2, May, 1987 Trip - records 957-968 (Y-axis)
vertical axis scale is approx. -1.0 to 1.0 volts

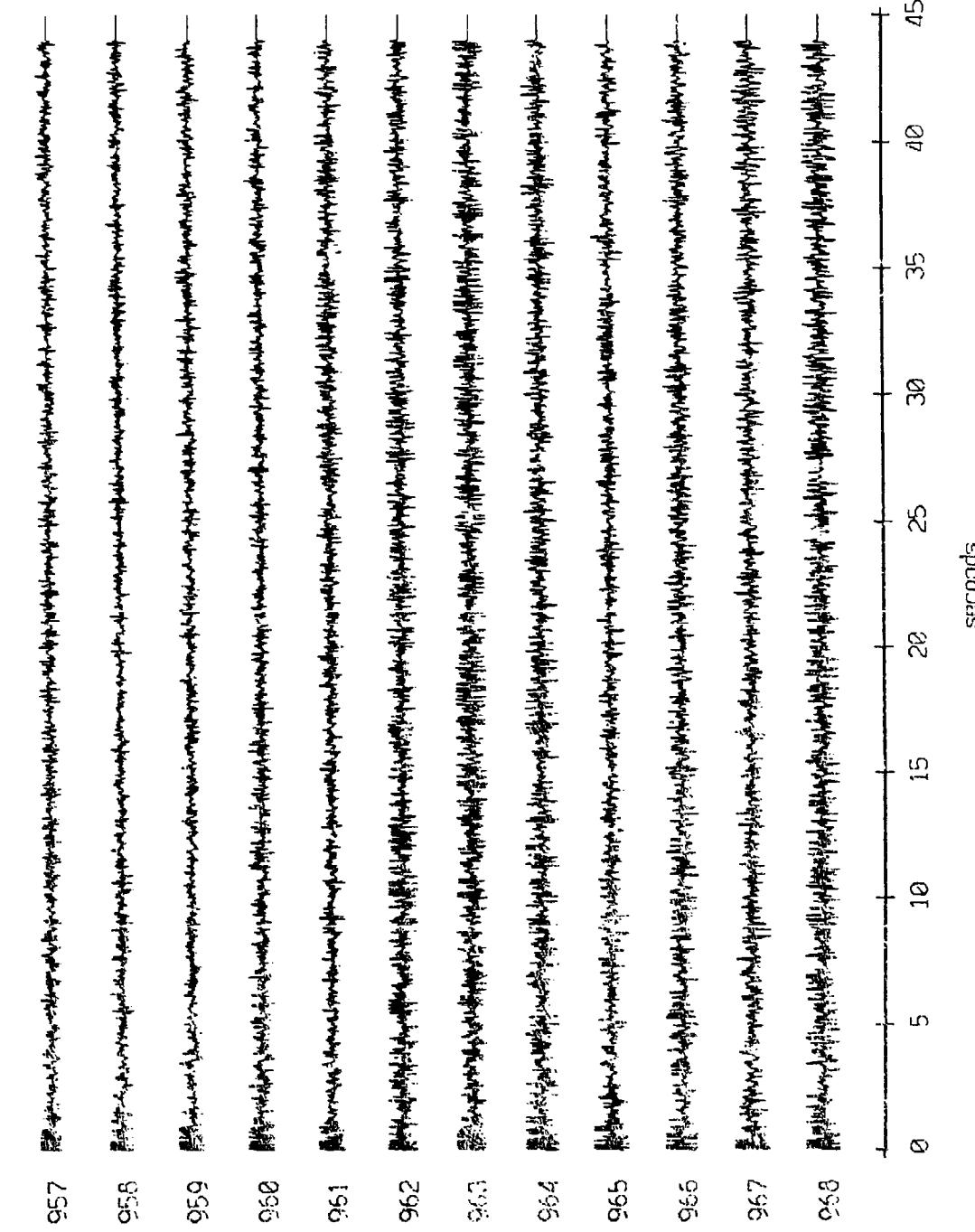


Figure X.2a.j

Float 2, May, 1987 Trip - records 957-968 (Z-axis)
vertical axis scale is approx. 1.0 to 1.0 volts

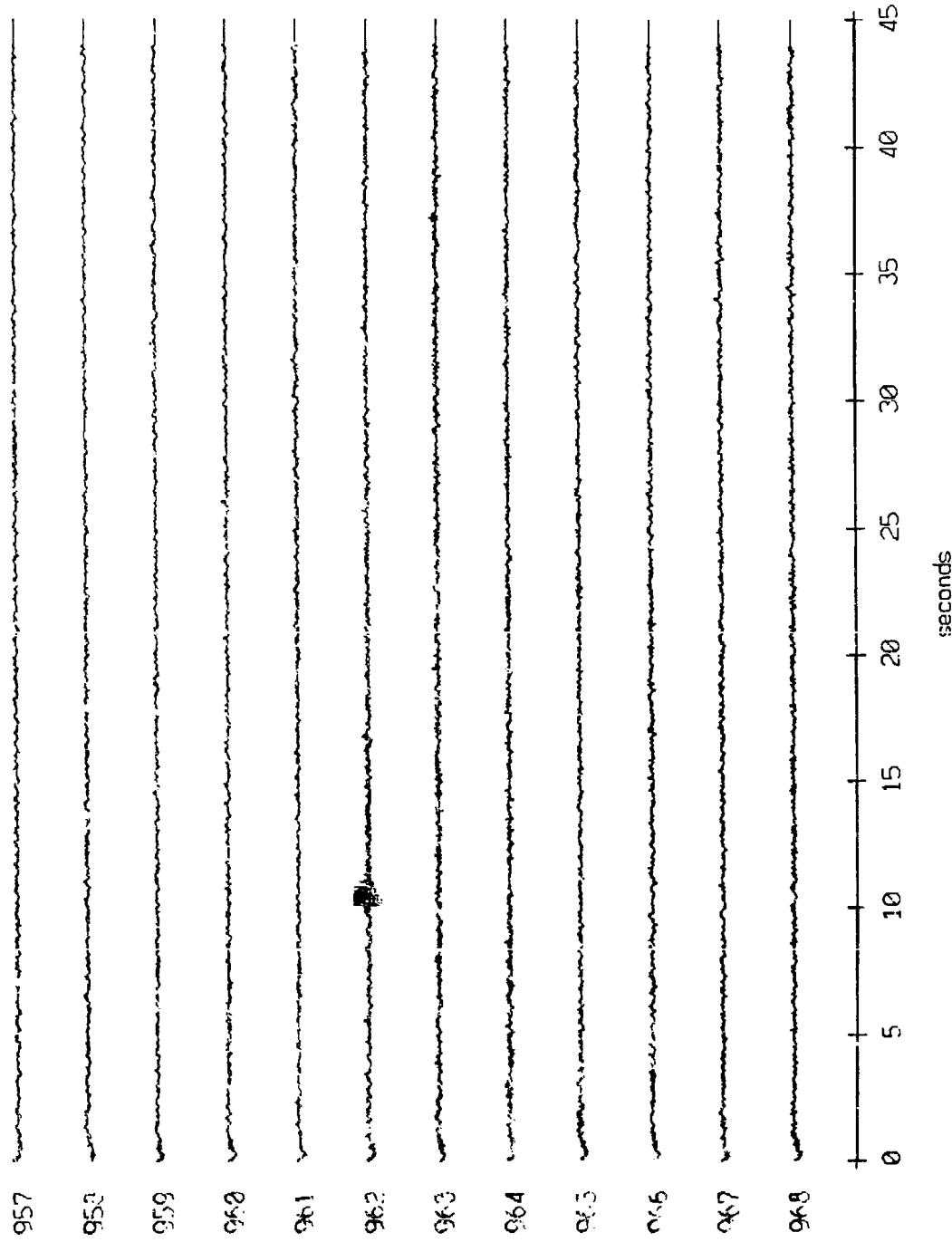
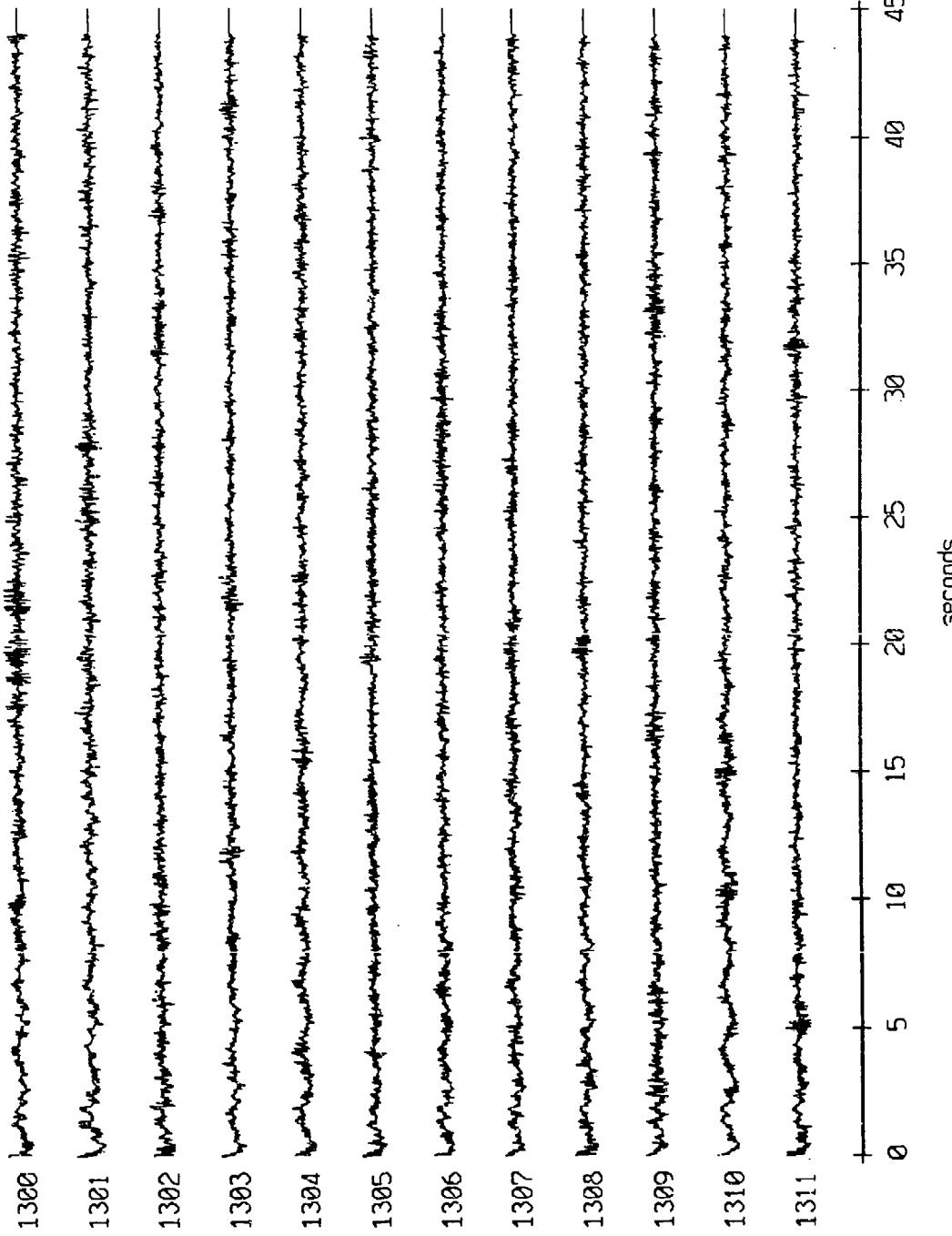


Figure X.2a.k

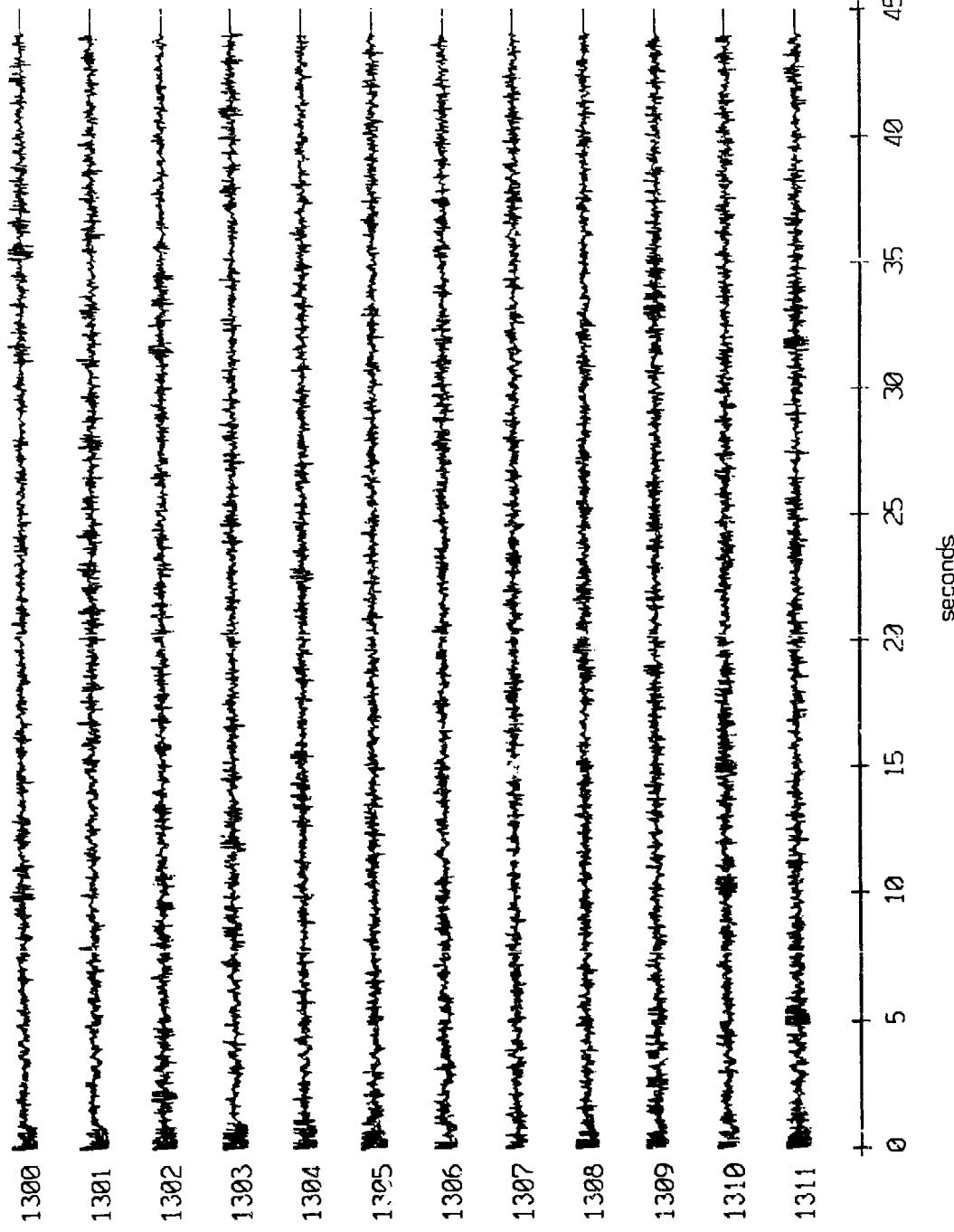
Flood 2, May, 1987 Trip - records 1300-1311 (x-axis)
vertical axis is approx. -1.0 to 1.0 volts



PGC CORRECTED CHANNEL LEVEL (V)

Figure X.2b.i

Float 2, May, 1987 Trip - records 1300-1311 (y-axis)
vertical axis scale is approx. -1.0 to 1.0 volts



AGC corrected chlorine level (V)

Figure X.2b.j

Float 2, May, 1987 Trip - records 1300-1311 (z-axis)
vertical axis scale is approx. -1.0 to 1.0 volts

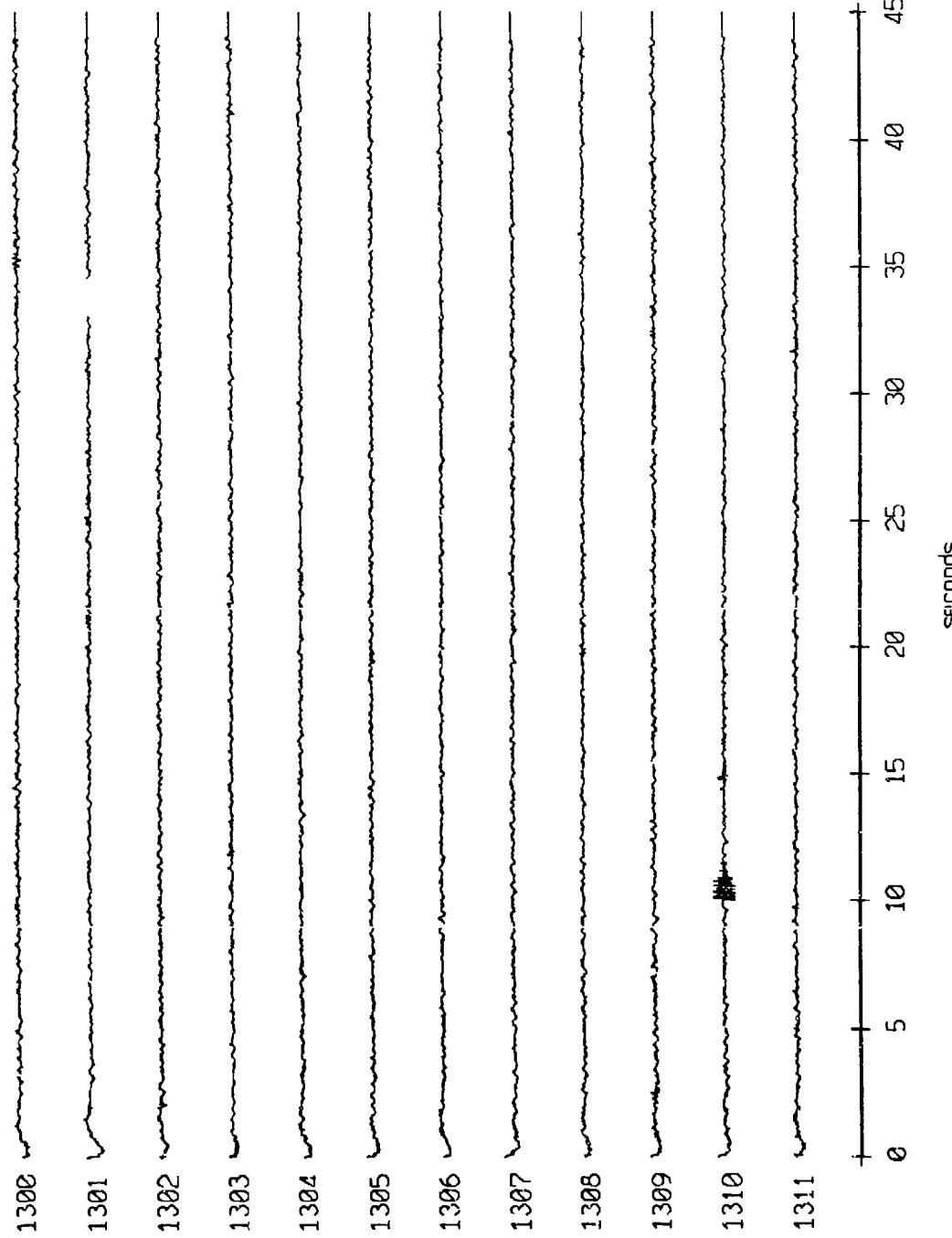


Figure X.2b.k

Flight 3, May, 1987 Trip - records 957-968 (X-axis)
vertical axis scale is approx. -1.0 to 1.0 volts

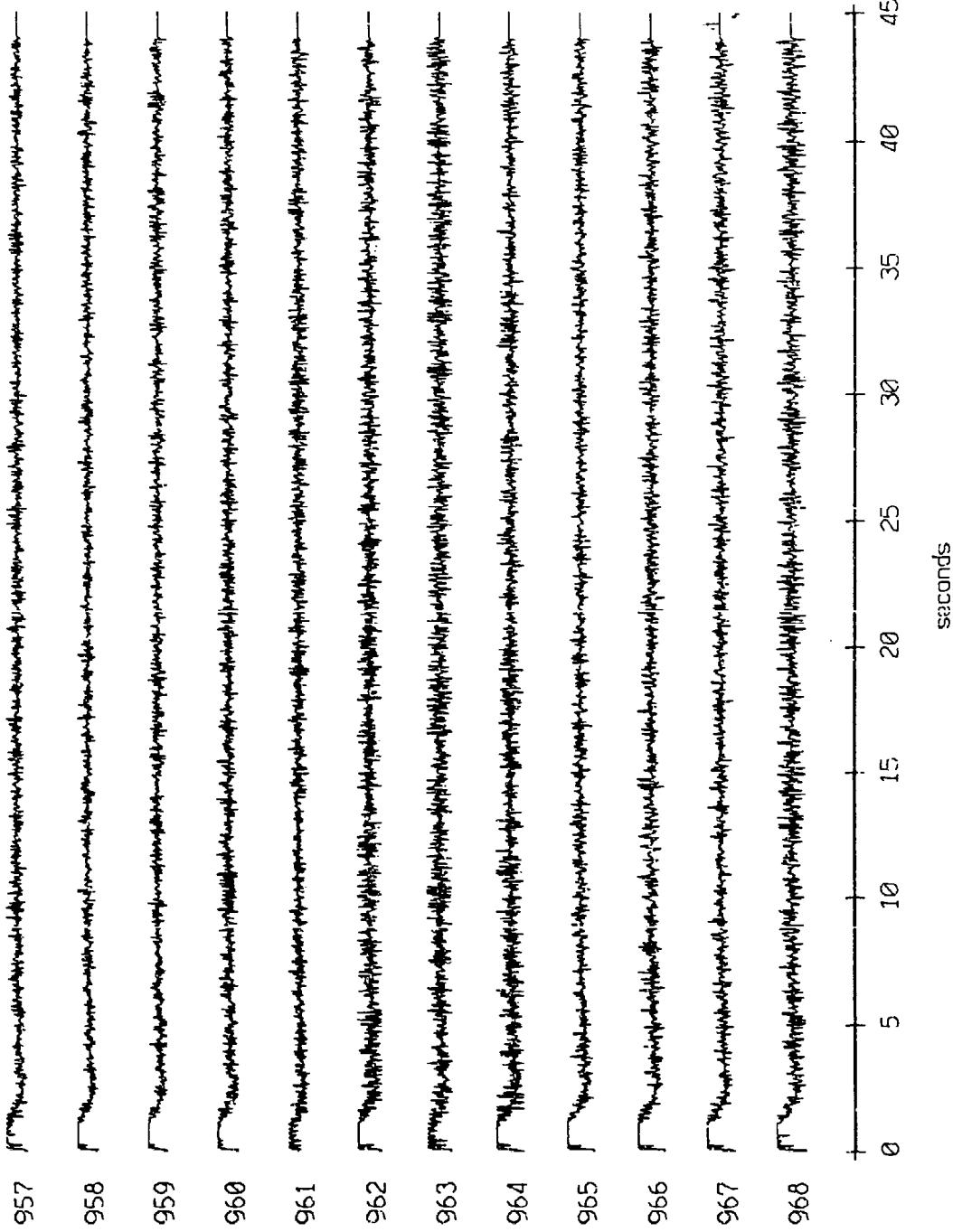


Figure X.3a.i

Flight 3, May, 1987 Trip - records 957-968 (Y-axis is approx. -1.0 to 1.0 volts)

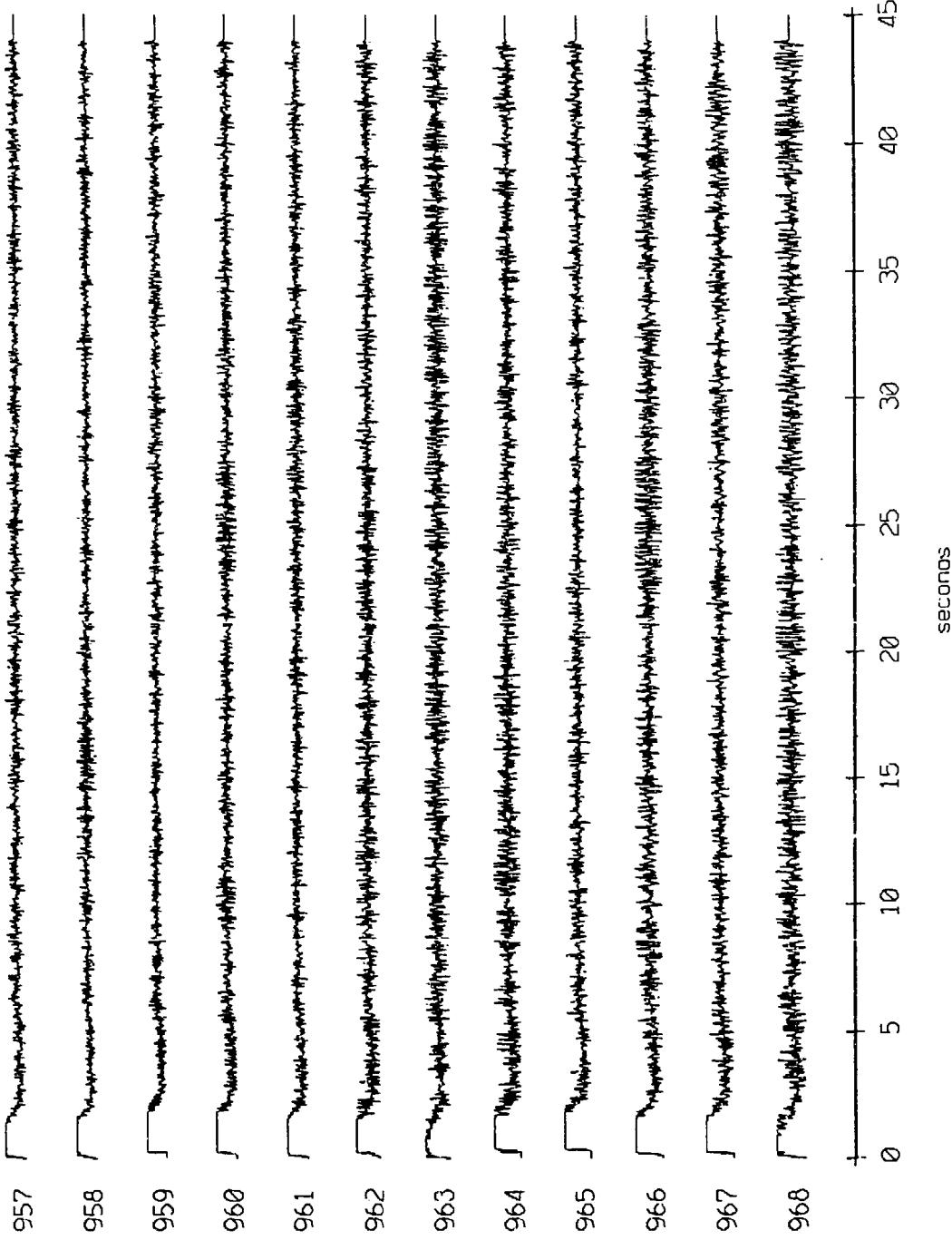


Figure X.3a.j

Flight 3, May, 1987 Trip - records 957-968 (Z-axis)
vertical axis scale is approx. -1.0 to 1.0 volts

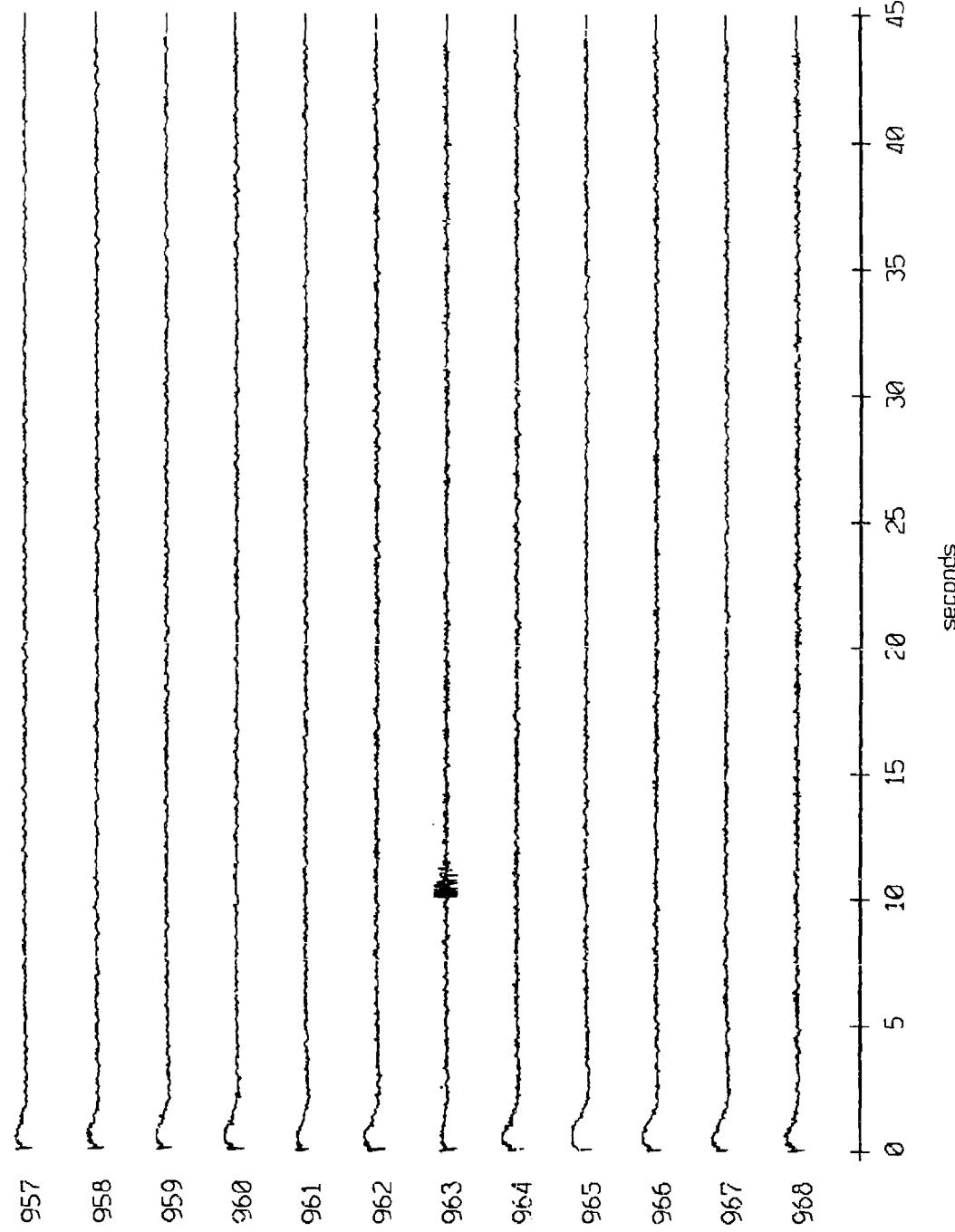


Figure X.3a.k

Float 3, May, 1987 Trip - records 1300-1311 (x-axis)
vertical axis scale is approx. -1.0 to 1.0 volts

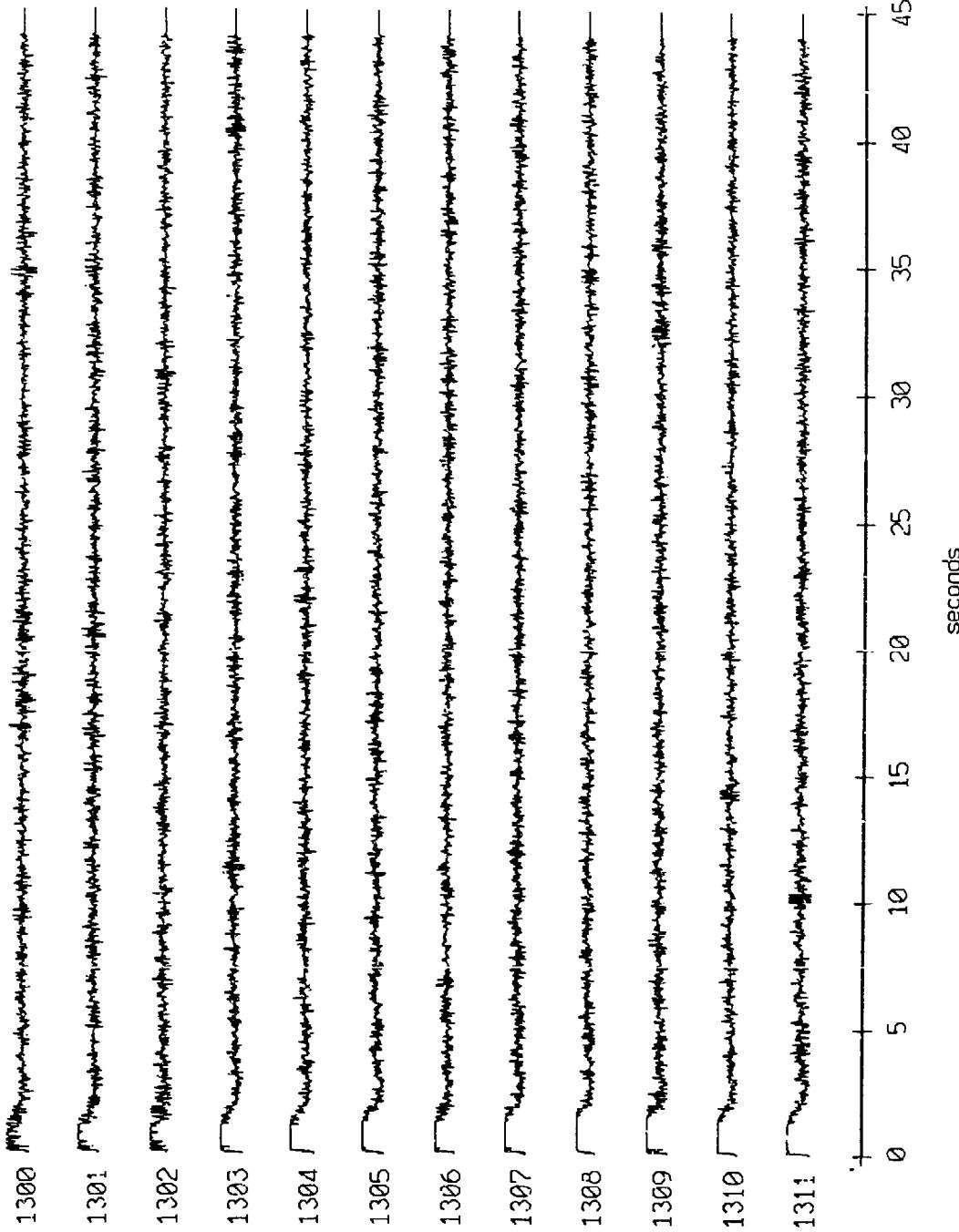
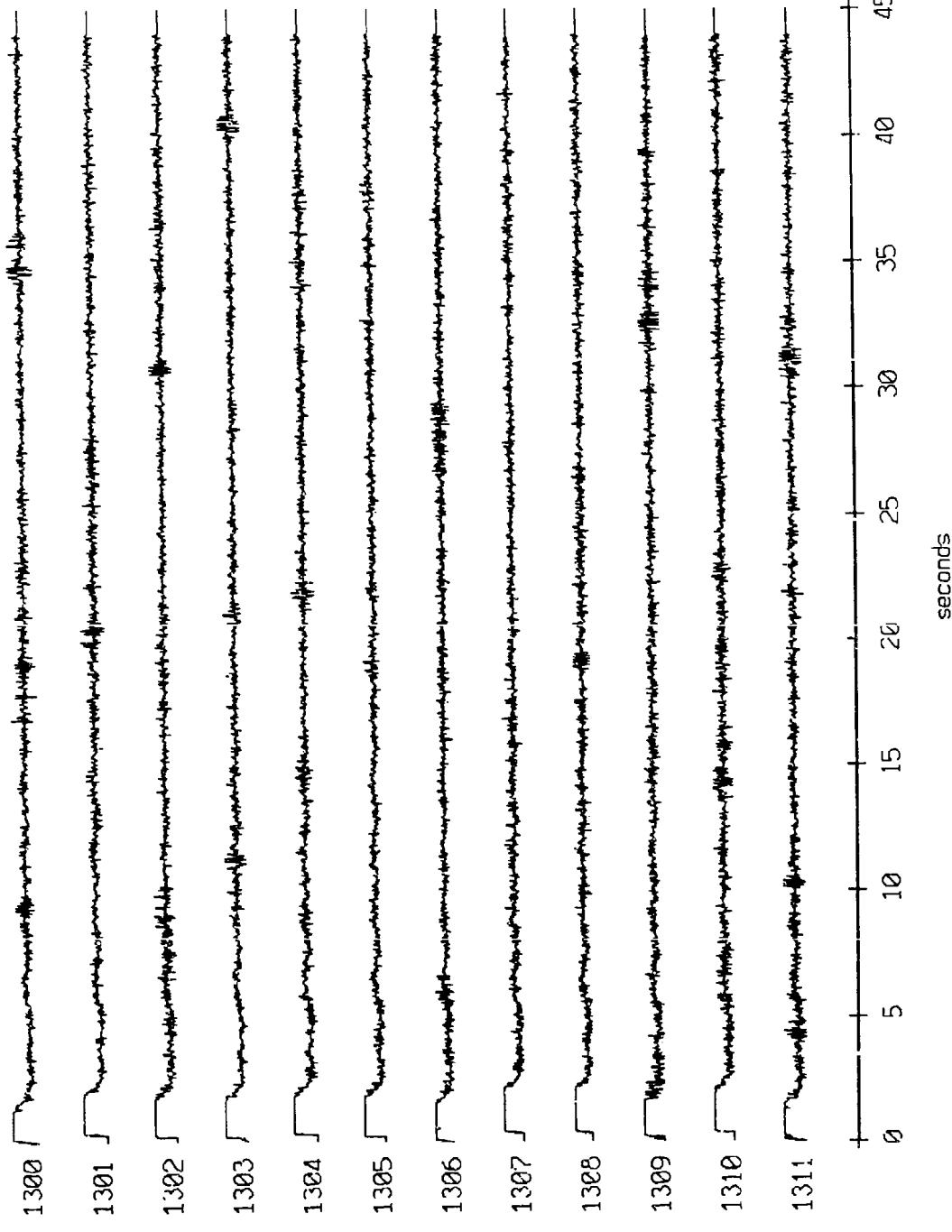


Figure X.3b.i

Float 3, May, 1987 Trip - records 1300-1311 (y-axis)
vertical axis is approx. -1.0 to 1.0 volts



AGC corrected channel level (V)

Figure X.3b.j

Float 3, May, 1987 Trip - records 1300-1311 (Z-axis)
vertical axis is approx. -1.0 to 1.0 volts

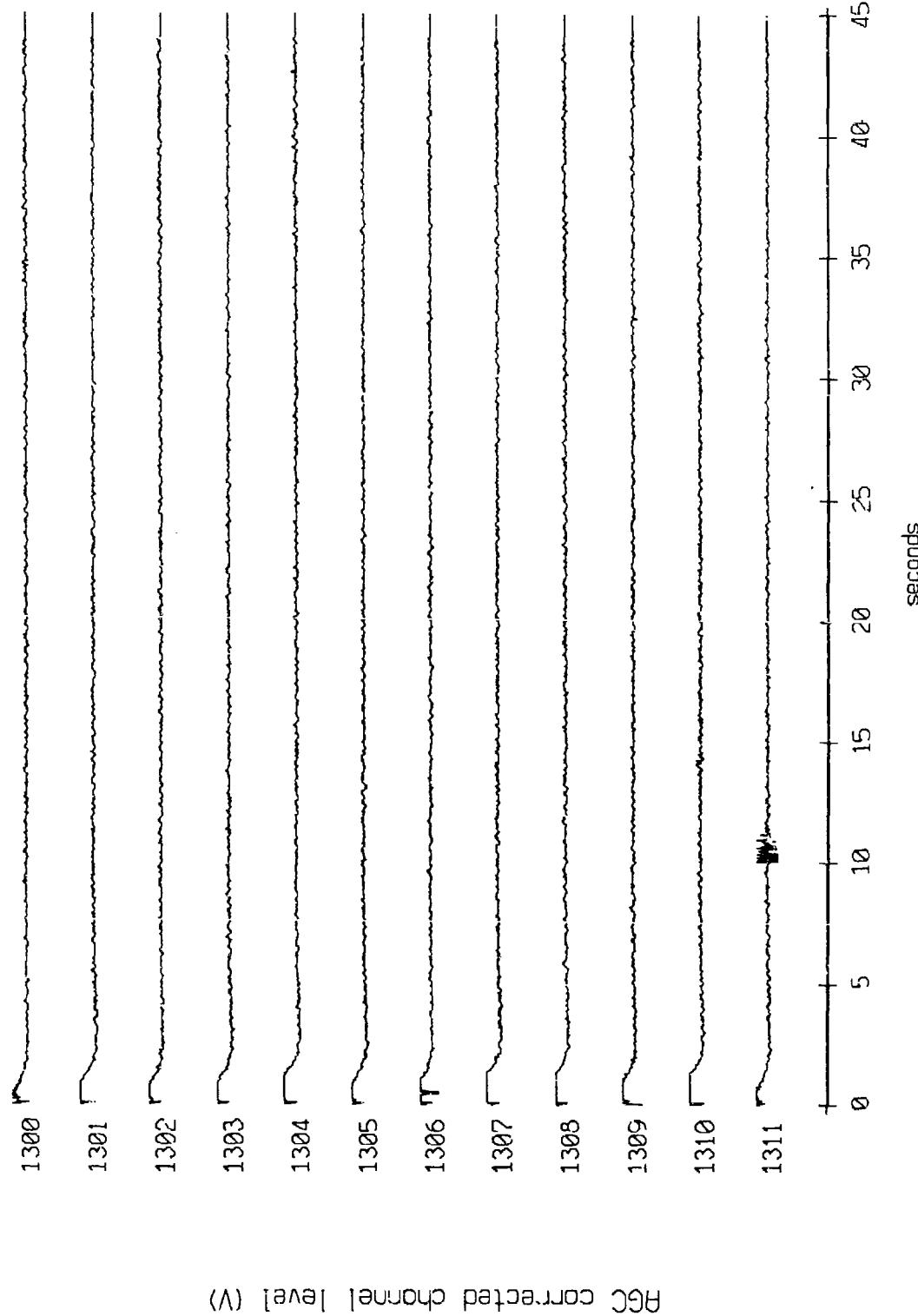


Figure X.3b.k

Float 4, May, 1987 Trip - records 957-968 (x-axis)
vertical axis scale is approx. -1.0 to 1.0 volts

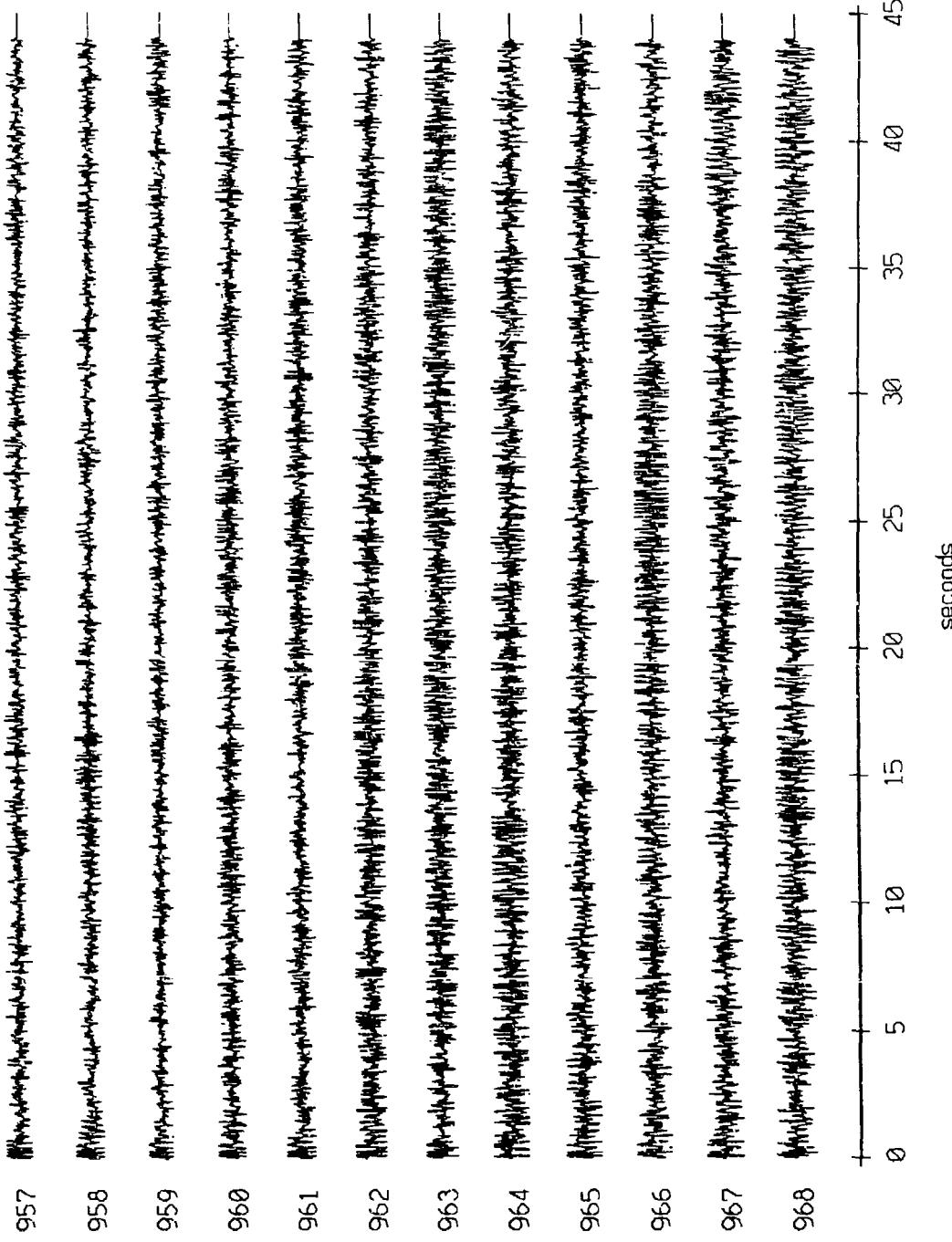


Figure X.4a.i

Float 4, May, 1987 Trip - records 957-968 (Y-axis)
vertical axis is approx. -1.0 to 1.0 volts

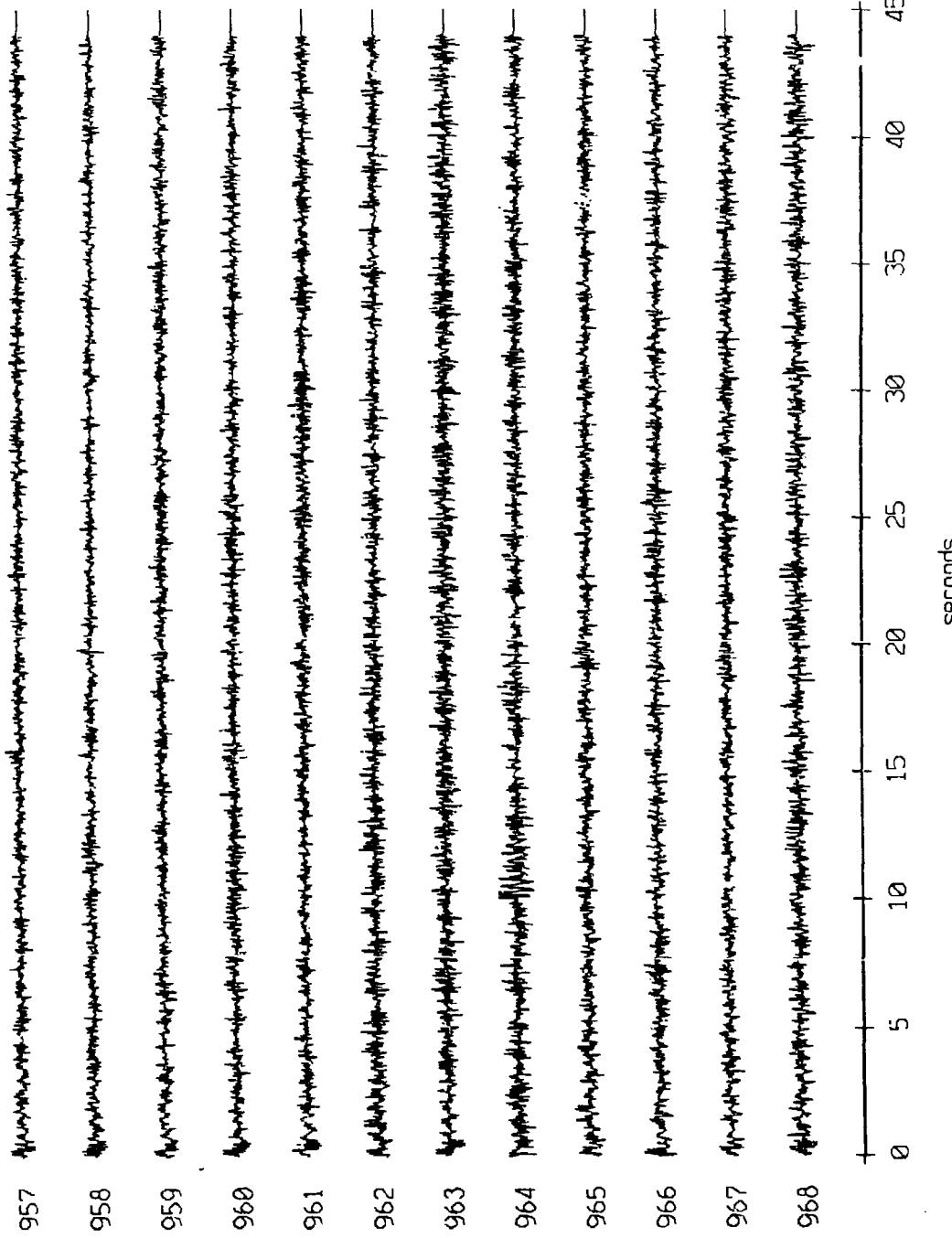


Figure X.4a.j

Float 4, May, 1987 Trip - records 957-968 (z-axis)
vertical axis scale is approx. -1.0 volts

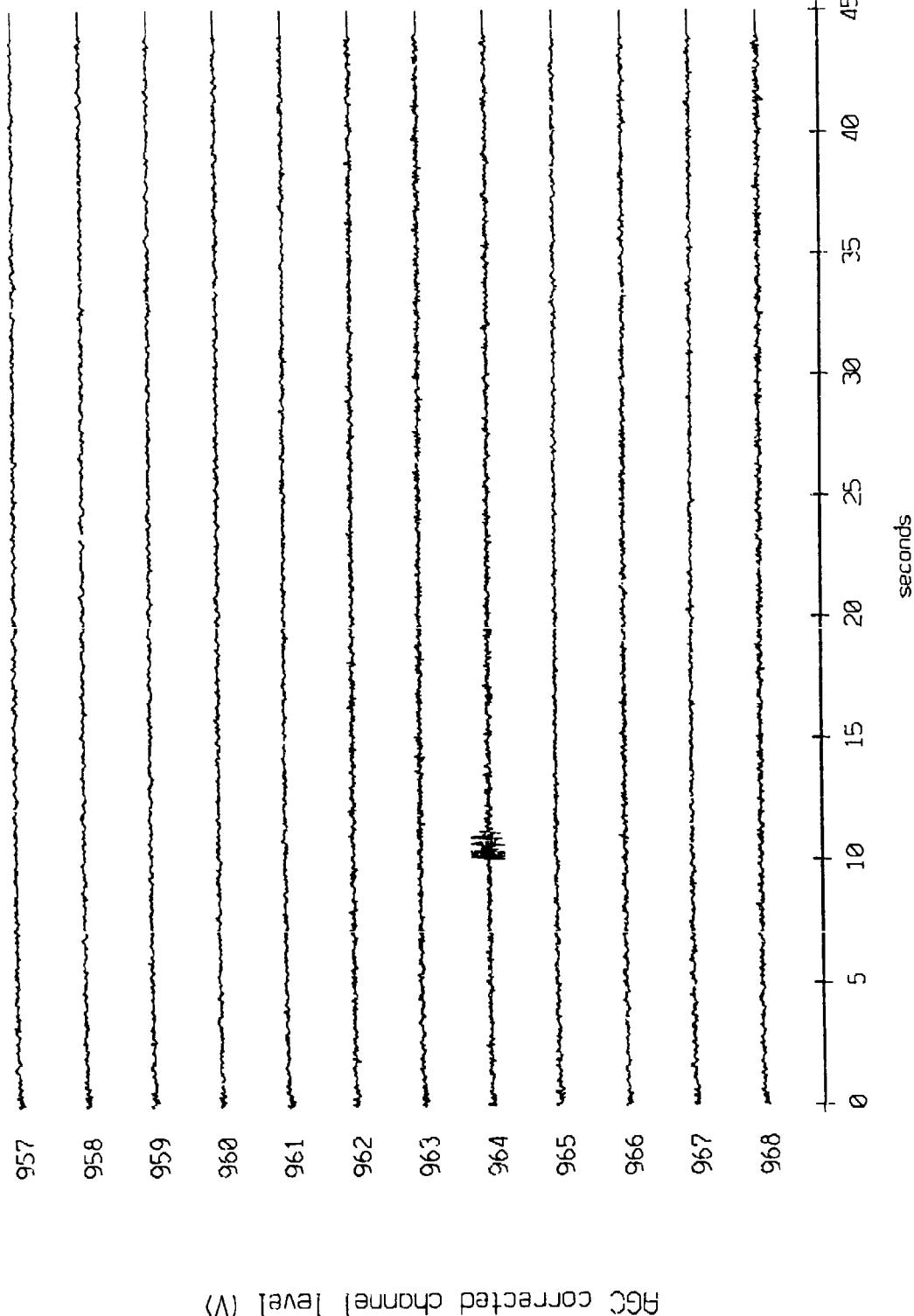
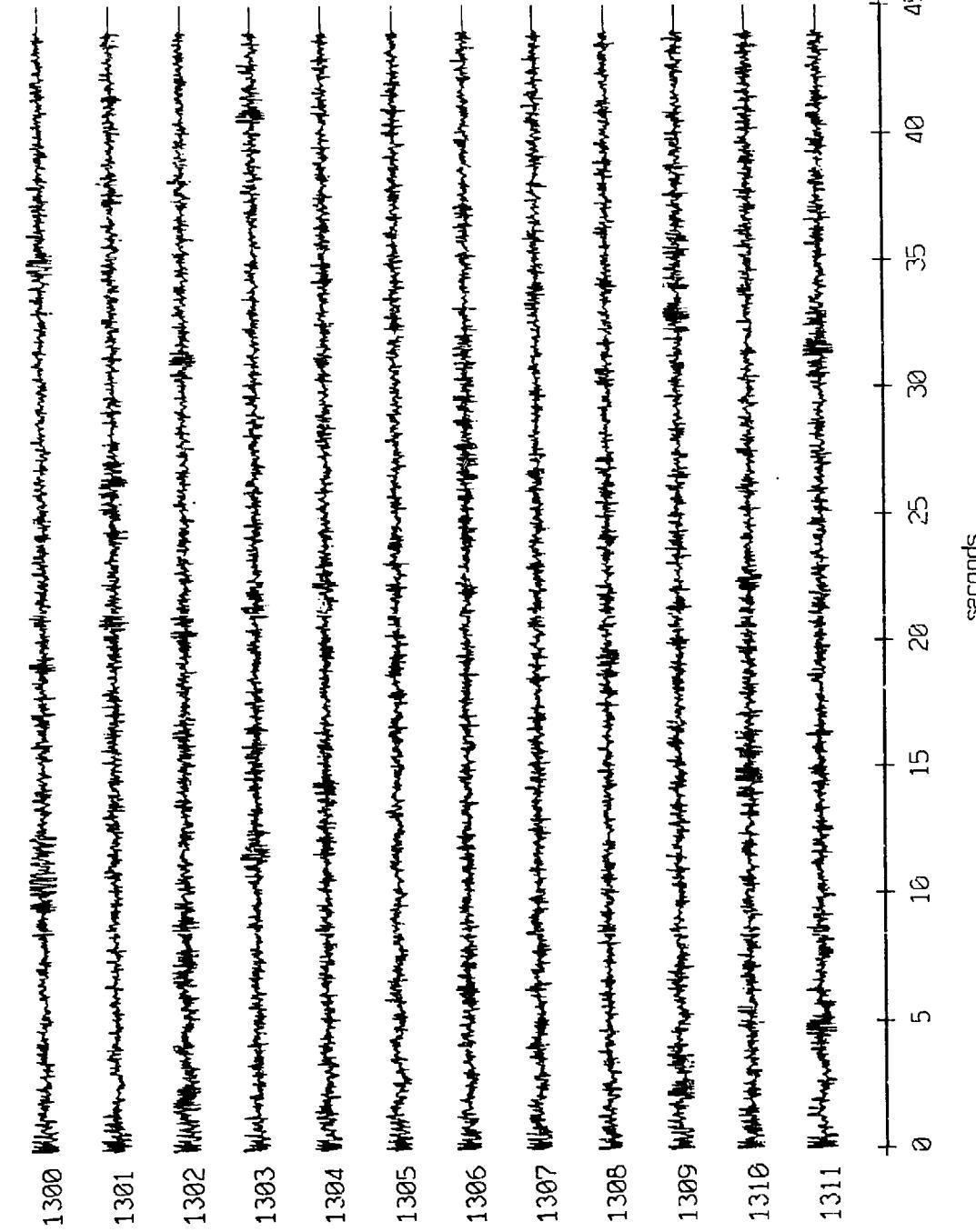


Figure X.4a.k

Float 4, May, 1987 Trip - records 1300-1311 (x-axis)
vertical axis scale is approx. -1.0 to 1.0 volts



RGC corrected channel level (V)

Figure X.4b.i

Flight 4, May, 1987 Trip - records 1300-1311 (y-axis)
vertical axis scale is approx. -1.0 to 1.0 volts

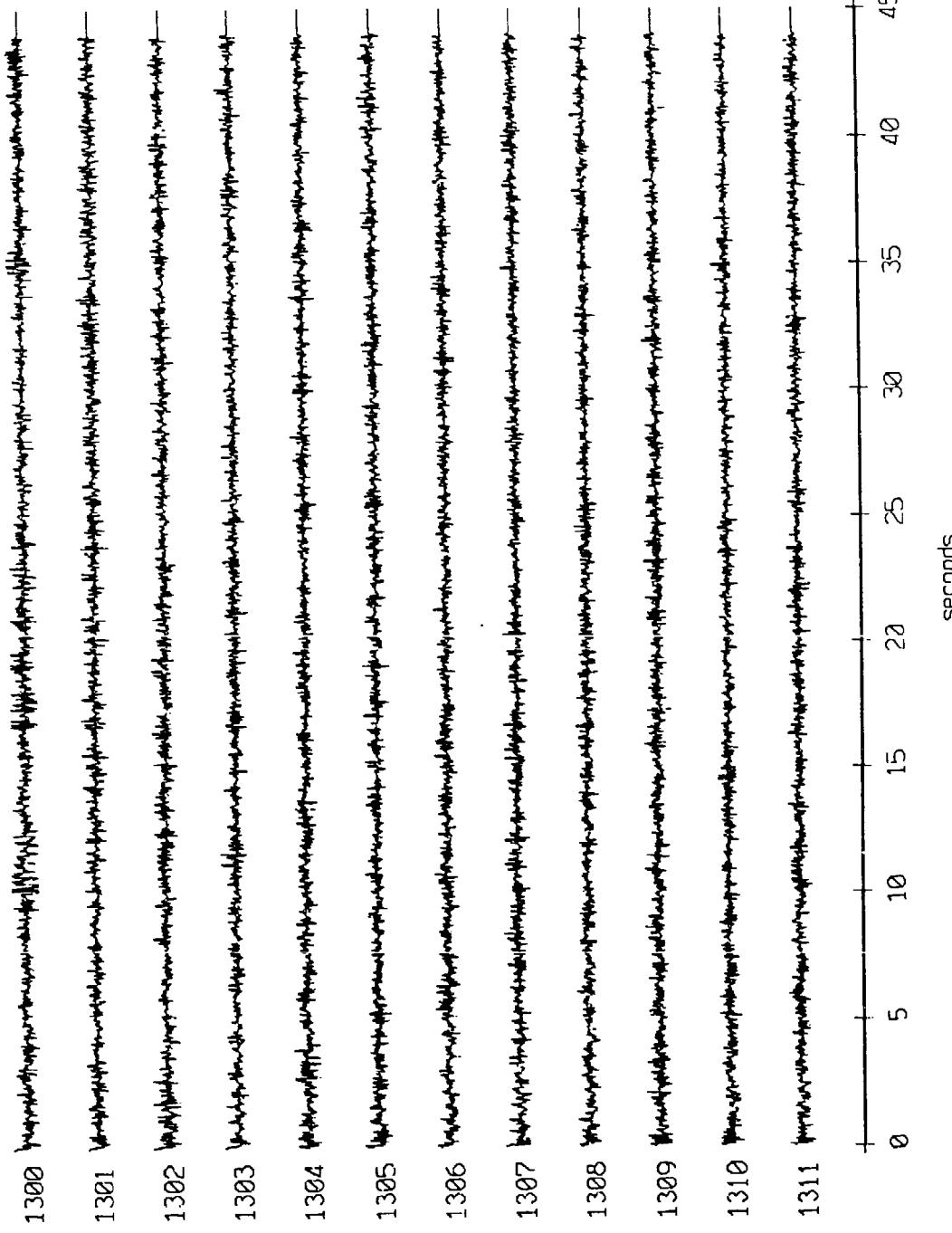
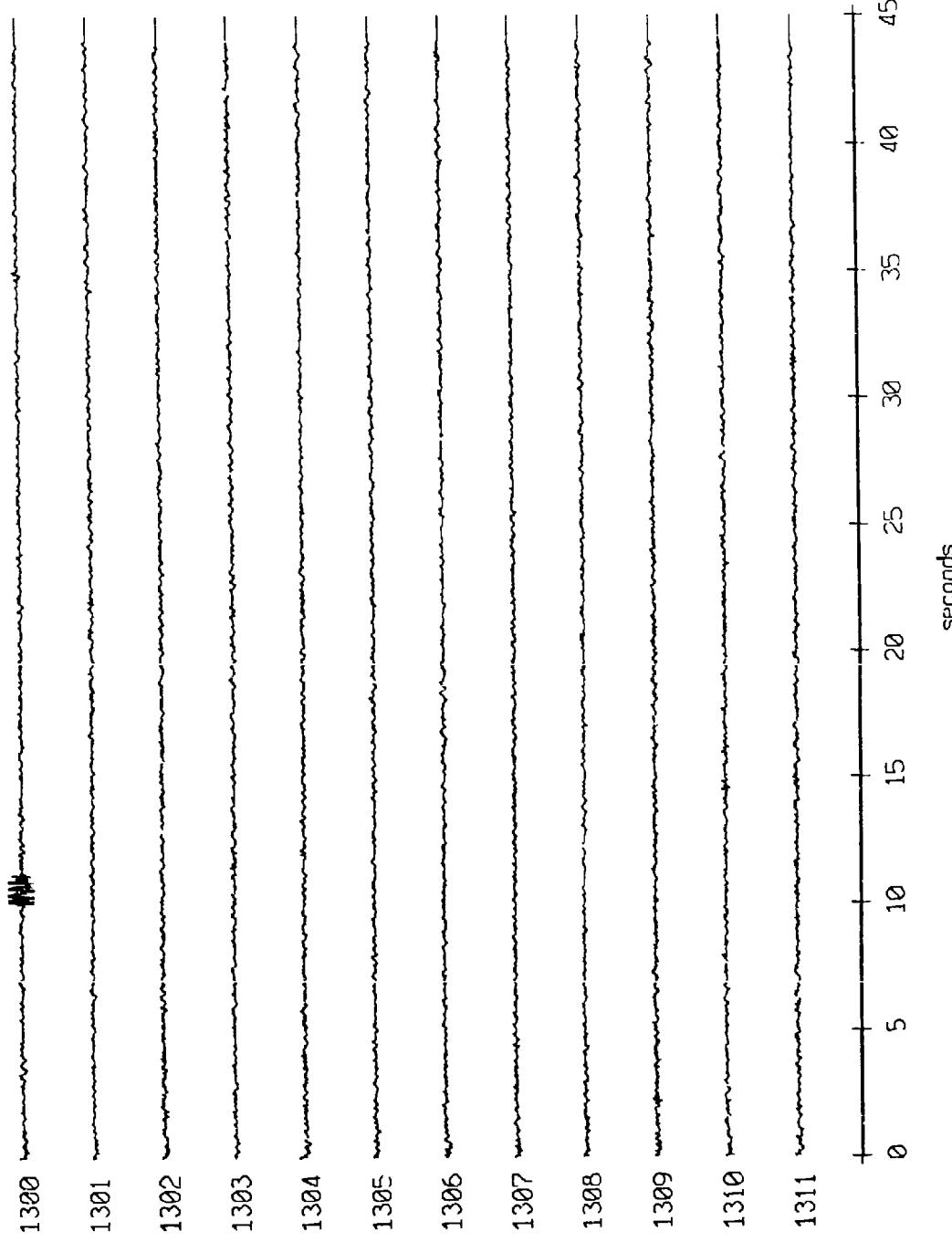


Figure X.4b.j

Float 4, May, 1987 Trip - records 1300-1311 (z-axis)
vertical axis is approx. -1.0 to 1.0 volts



AGC corrected channel level (V)

Figure X.4b.k

Fleet 7, May, 1987 Trip - records 957-968 (x-axis)
vertical axis scale is approx. -1.0 to 1.0 volts

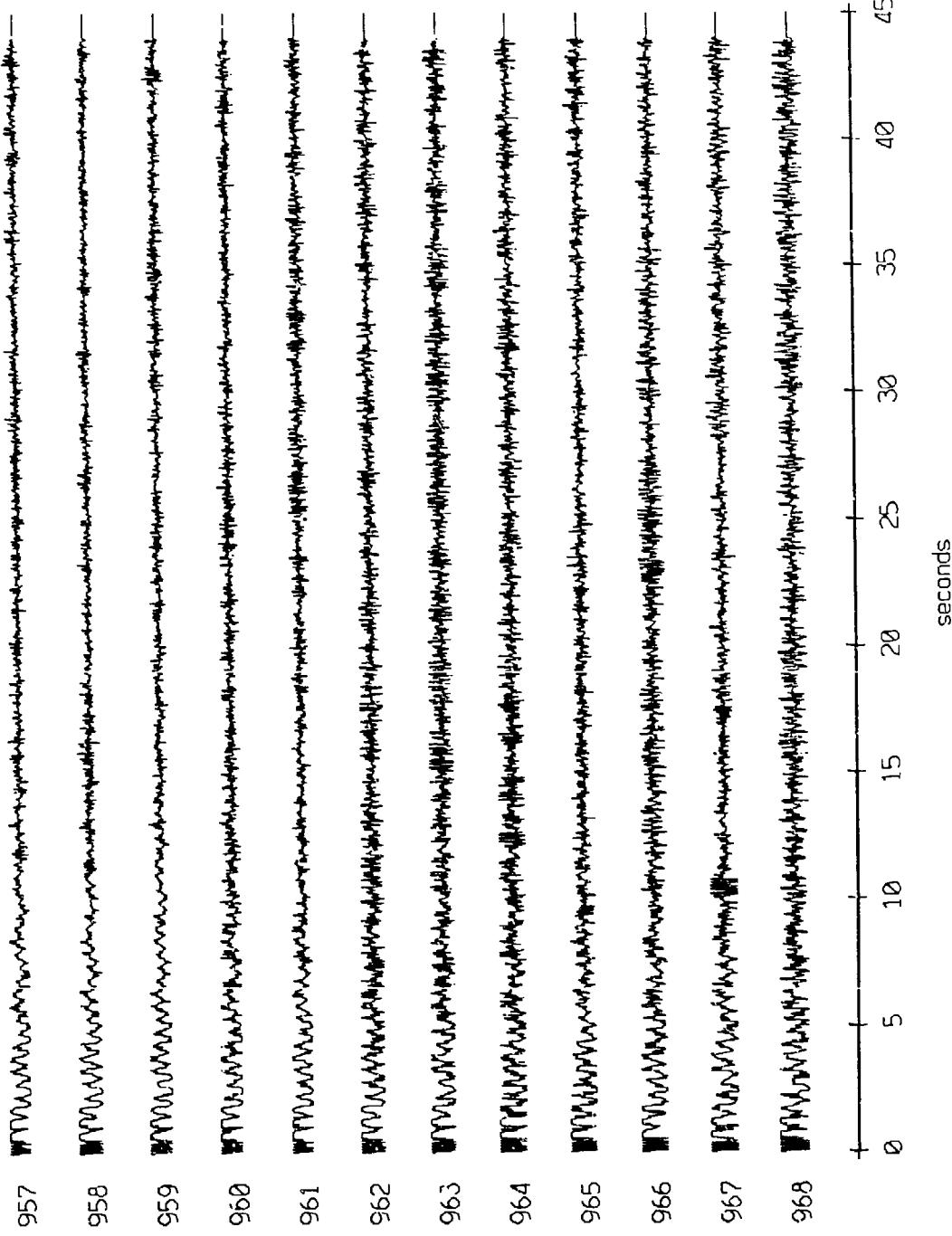


Figure X.5a.i

Fleet 7, May, 1987 Trip - records 957-968 (y-axis)
vertical axis scale is approx. -1.0 to 1.0 volts

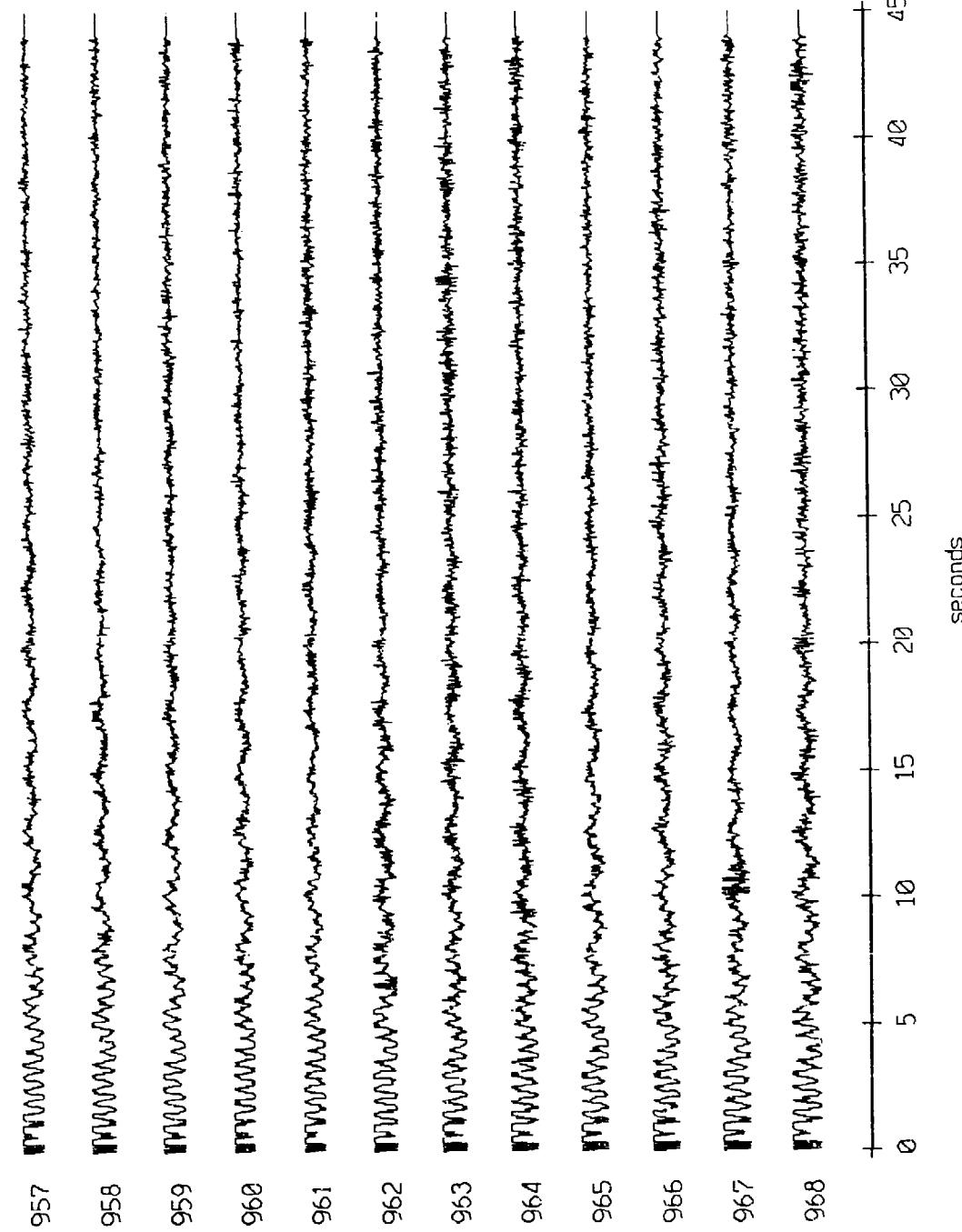


Figure X.5a.j

Flight 7, May, 1987 Trip - Records 957-968 (z-axis)
vertical axis scale is approx. -1.0 to 1.0 volts

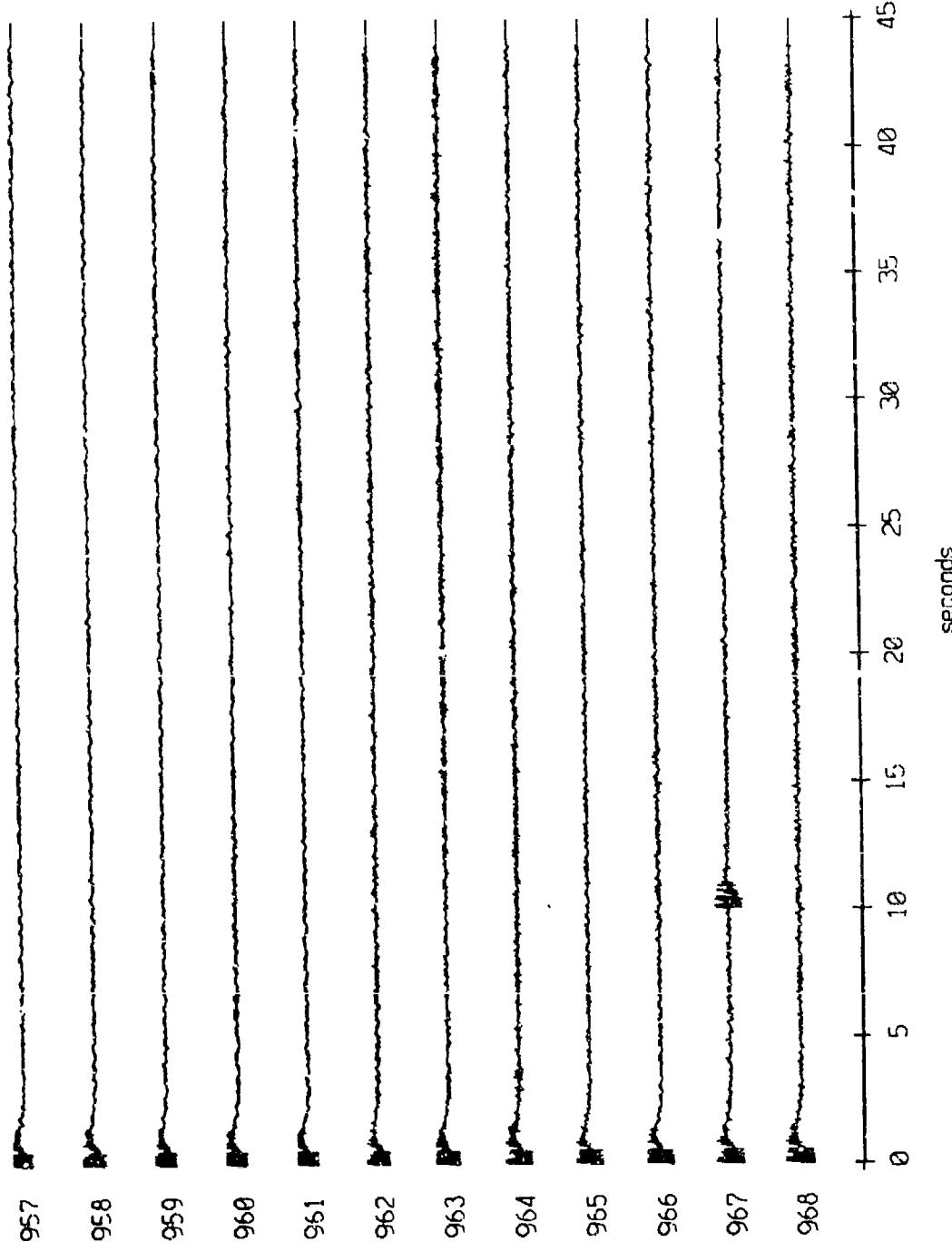


Figure X.5a.k

Flight 7, May, 1987 Trip - records 1300-1311 (X-axis)
vertical axis is approx. -1.0 to 1.0 volts

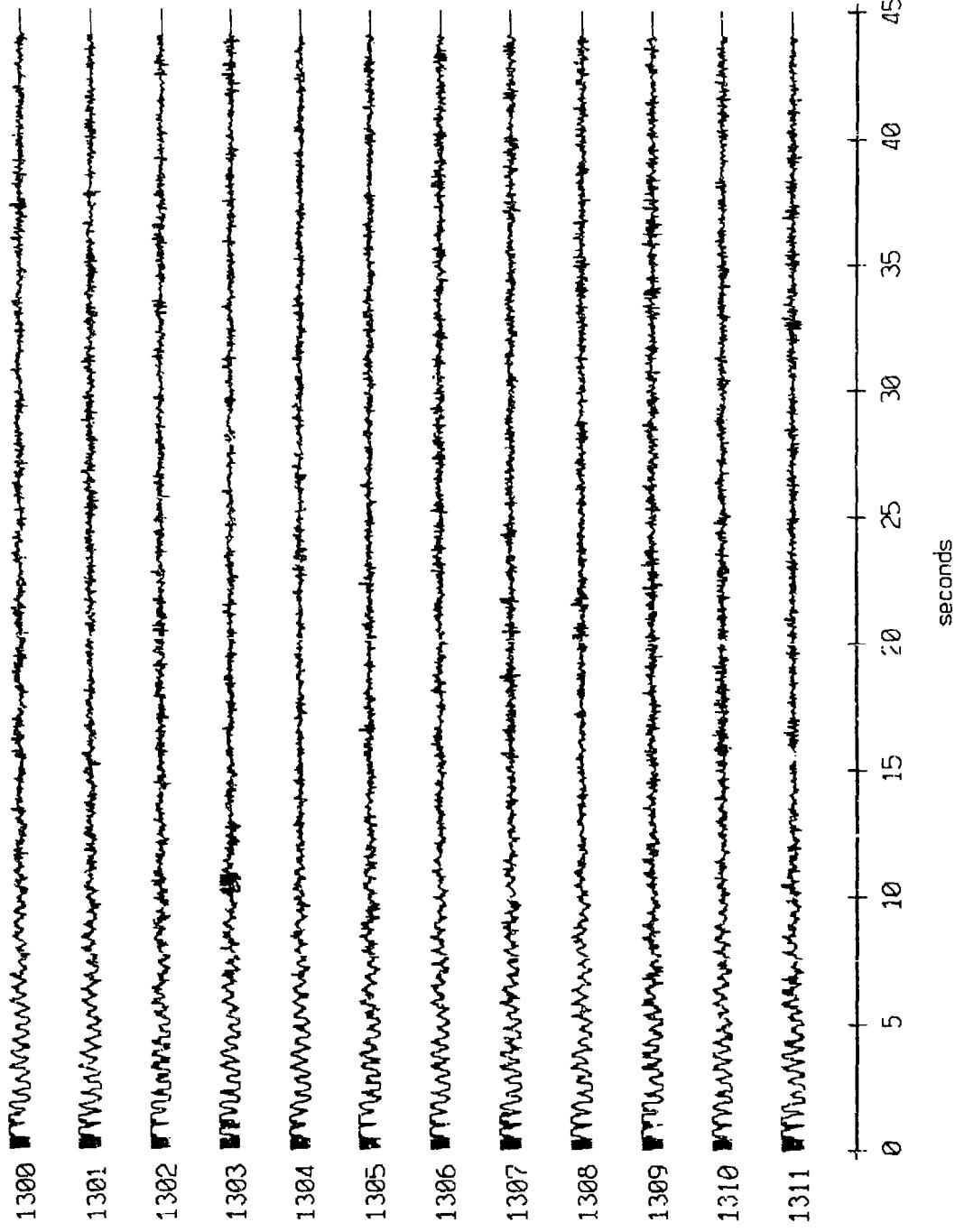


Figure X.5b.i

Flight 7, May, 1987 Trip - records 1300-1311 (y-axis)
vertical axis is approx. -1.0 to 1.0 volts

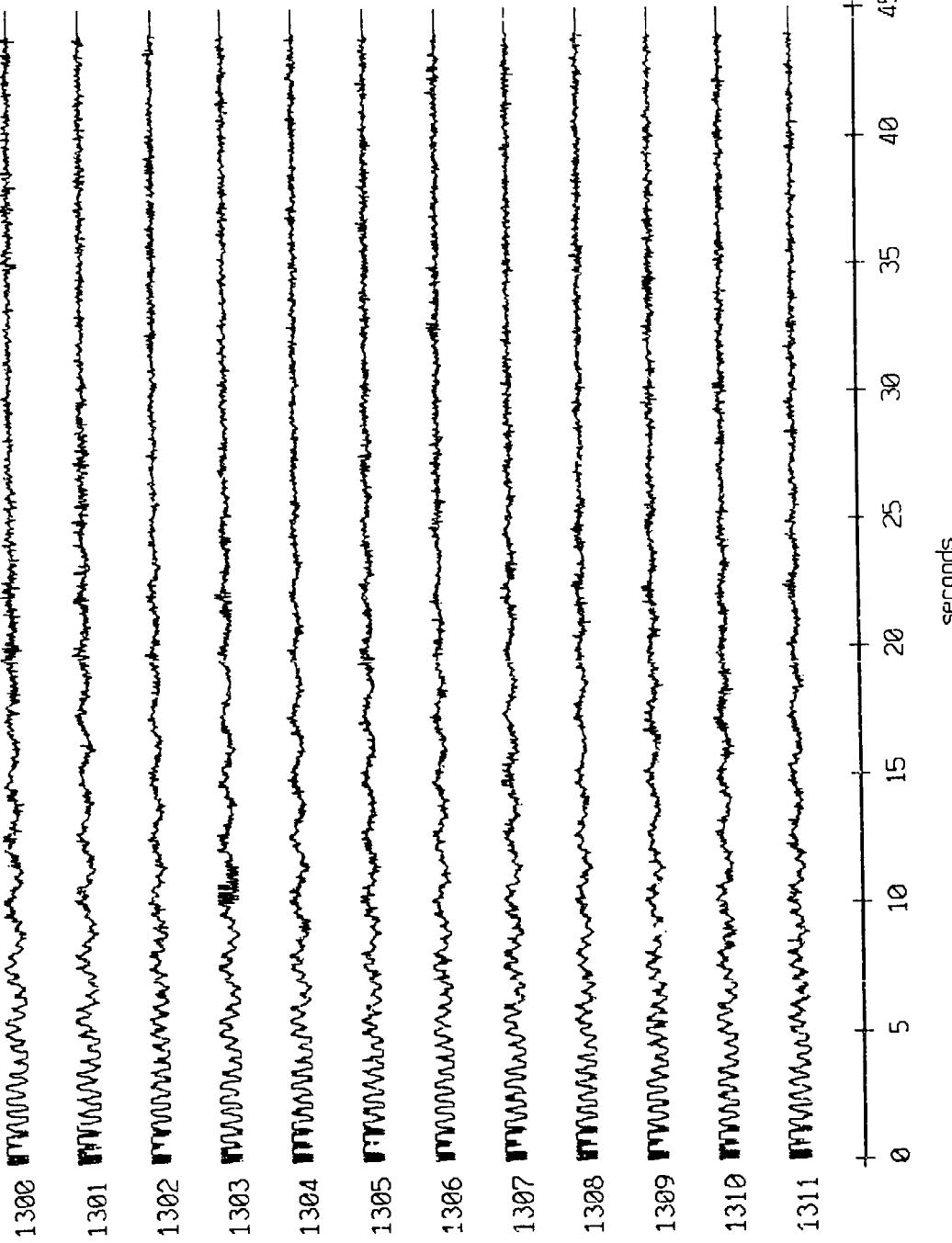


Figure X.5b.j

Float 7, May, 1987 Trip - records 1300-1311 (z-axis)
vertical axis scale is approx. -1.0 to 1.0 volts

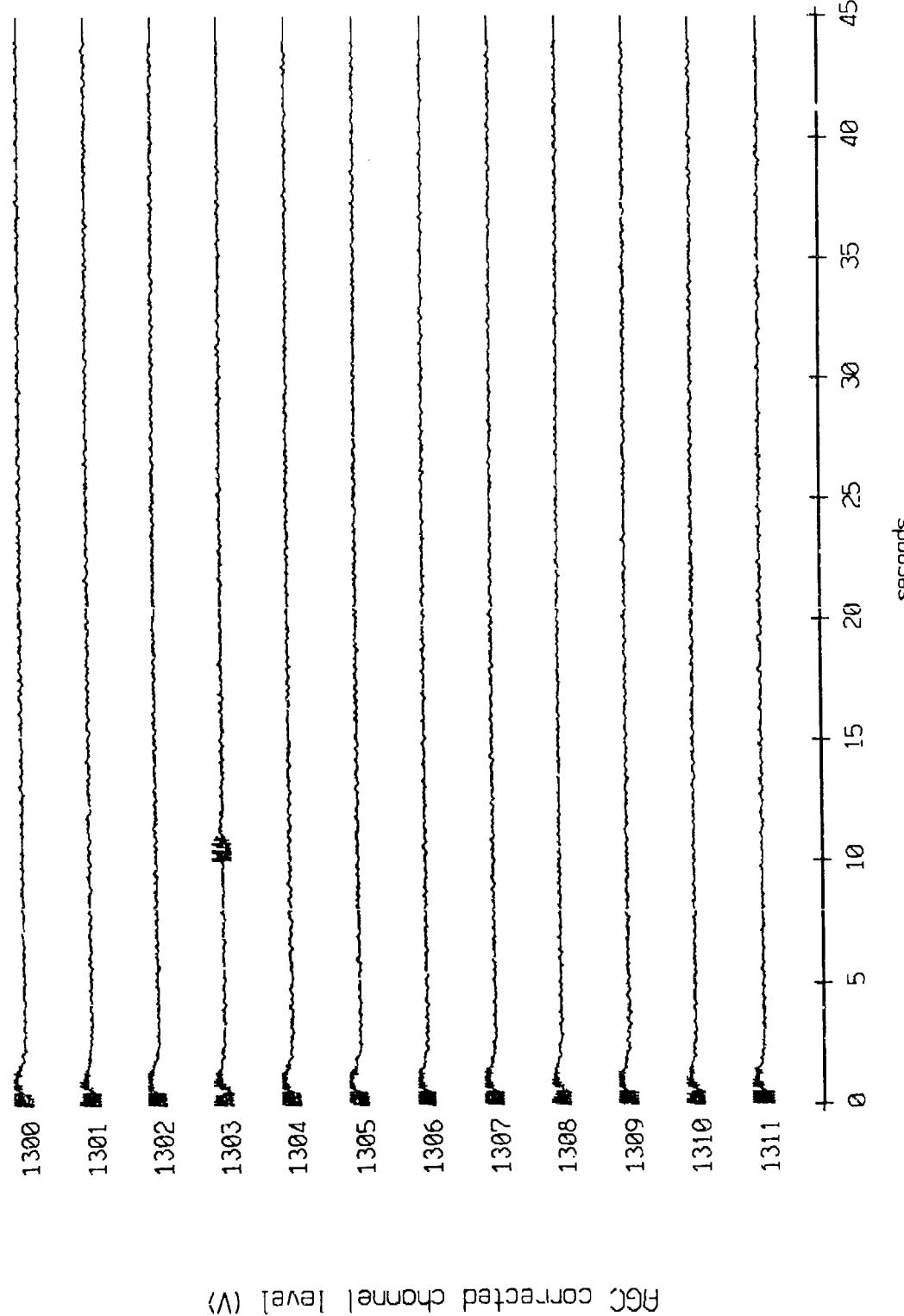
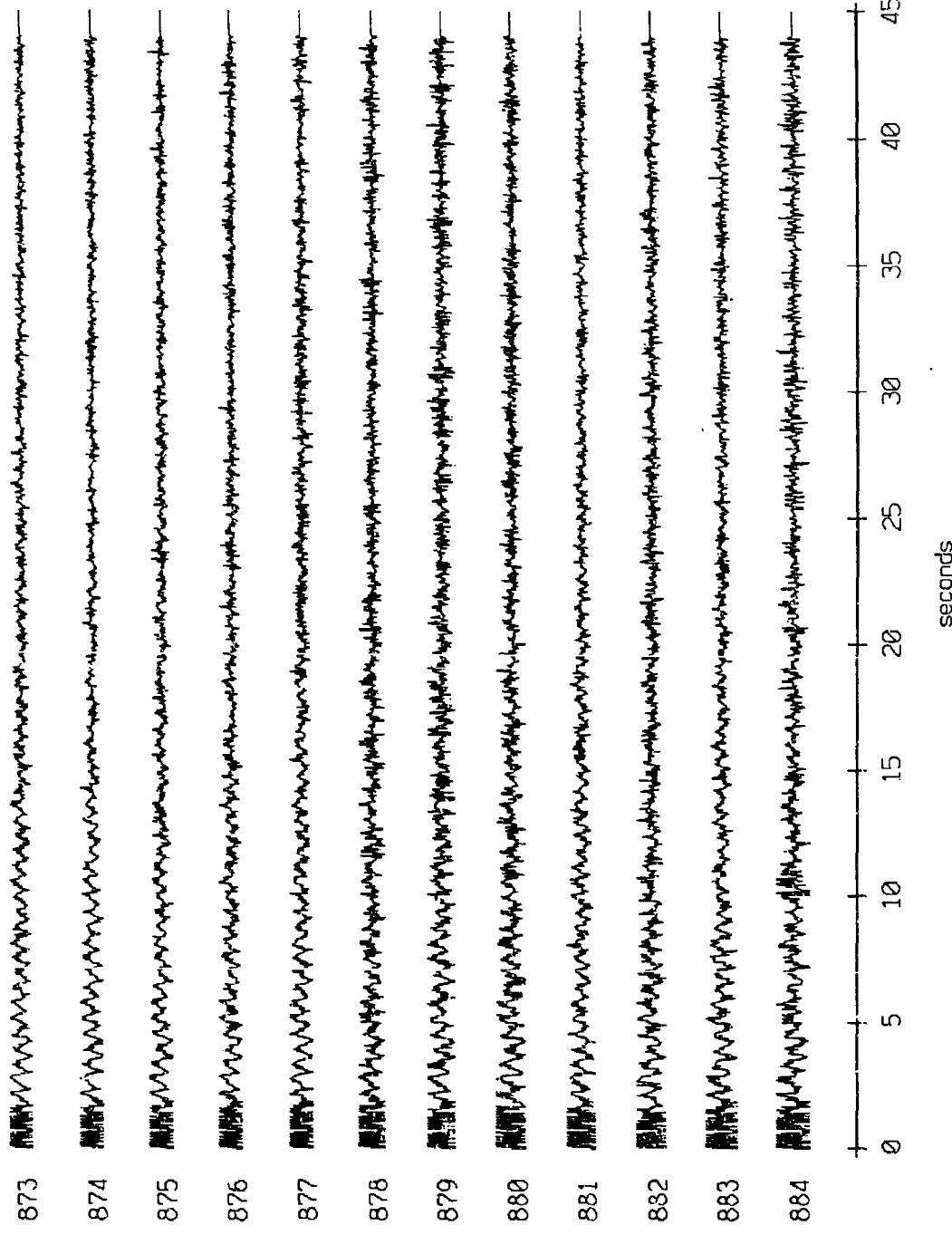


Figure X.5b.k

Float 8, May, 1987 Trip - records 873-884 (X-axis)
vertical axis scale is approx. -1.0 to 1.0 volts



RGC corrected channel [level] (V)

Figure X.6a.i

Float 8, May, 1987 Trip - records 873-884 (Y-axis)
vertical axis scale is approx. -1.0 to 1.0 volts

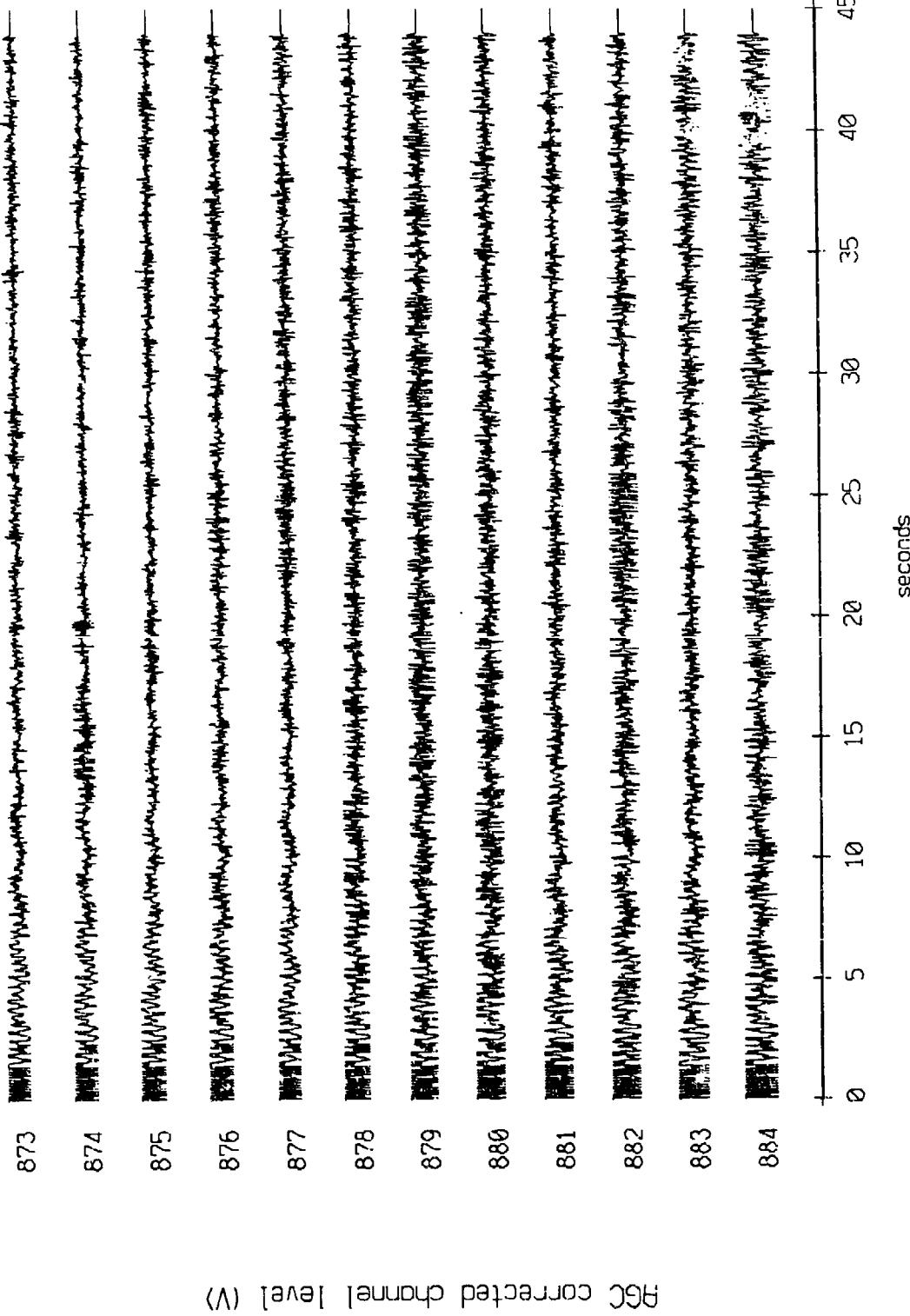


Figure X.6a.j

Float 8, May, 1987 Trip - records 873-884 (Z-axis)
vertical axis is approx. -1.0 to 1.0 volts

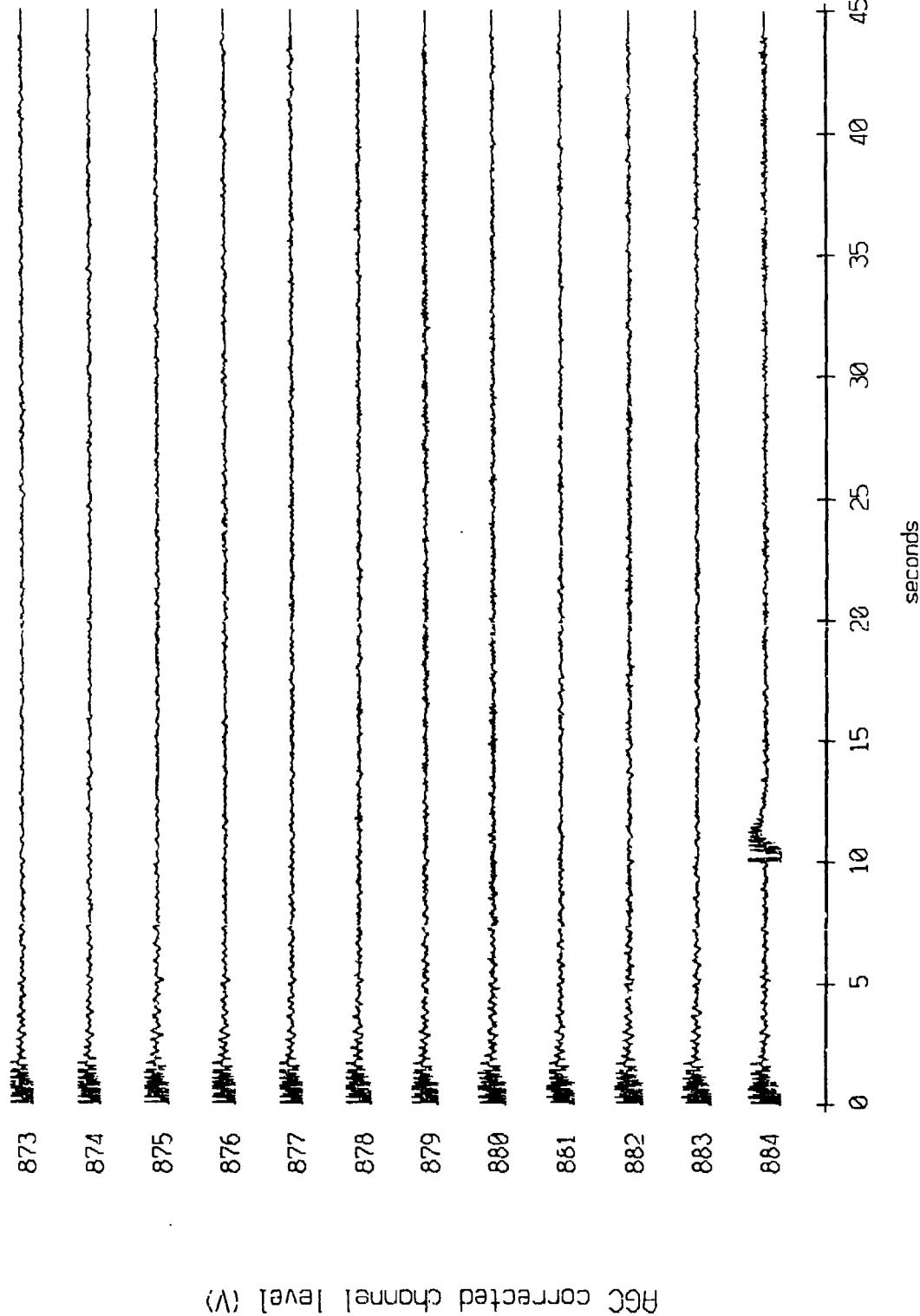


Figure X.6a.k

Fleet 8, May, 1987 Trip - records 1216-1227 (x-ox[is])
Vertical axis is approx. -1.0 to 1.0 volts

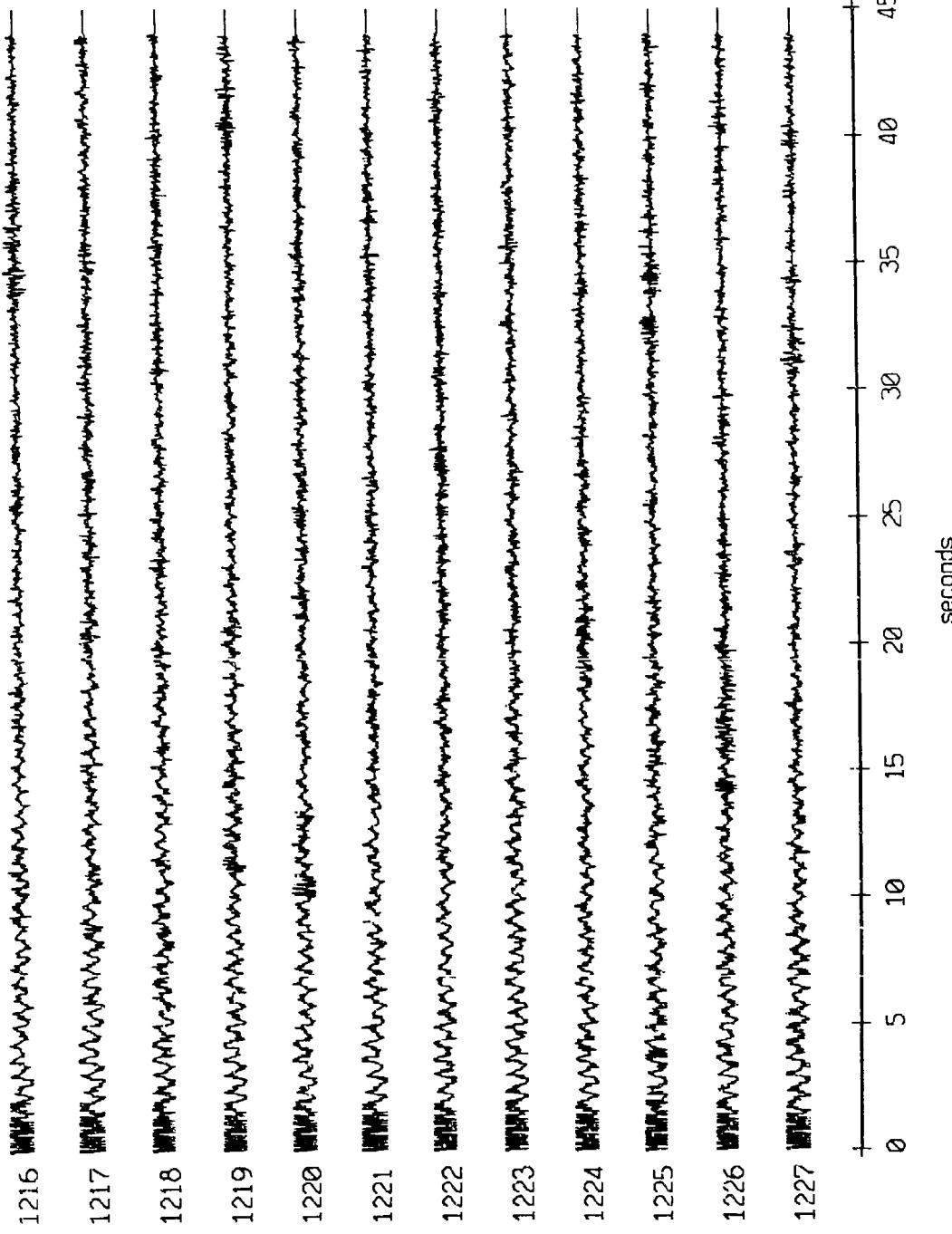


Figure X.6b.i

Float 8, May, 1987 Trip - records 1216-1227 (y-axis)
vertical axis scale is approx. -1.0 to 1.0 volts

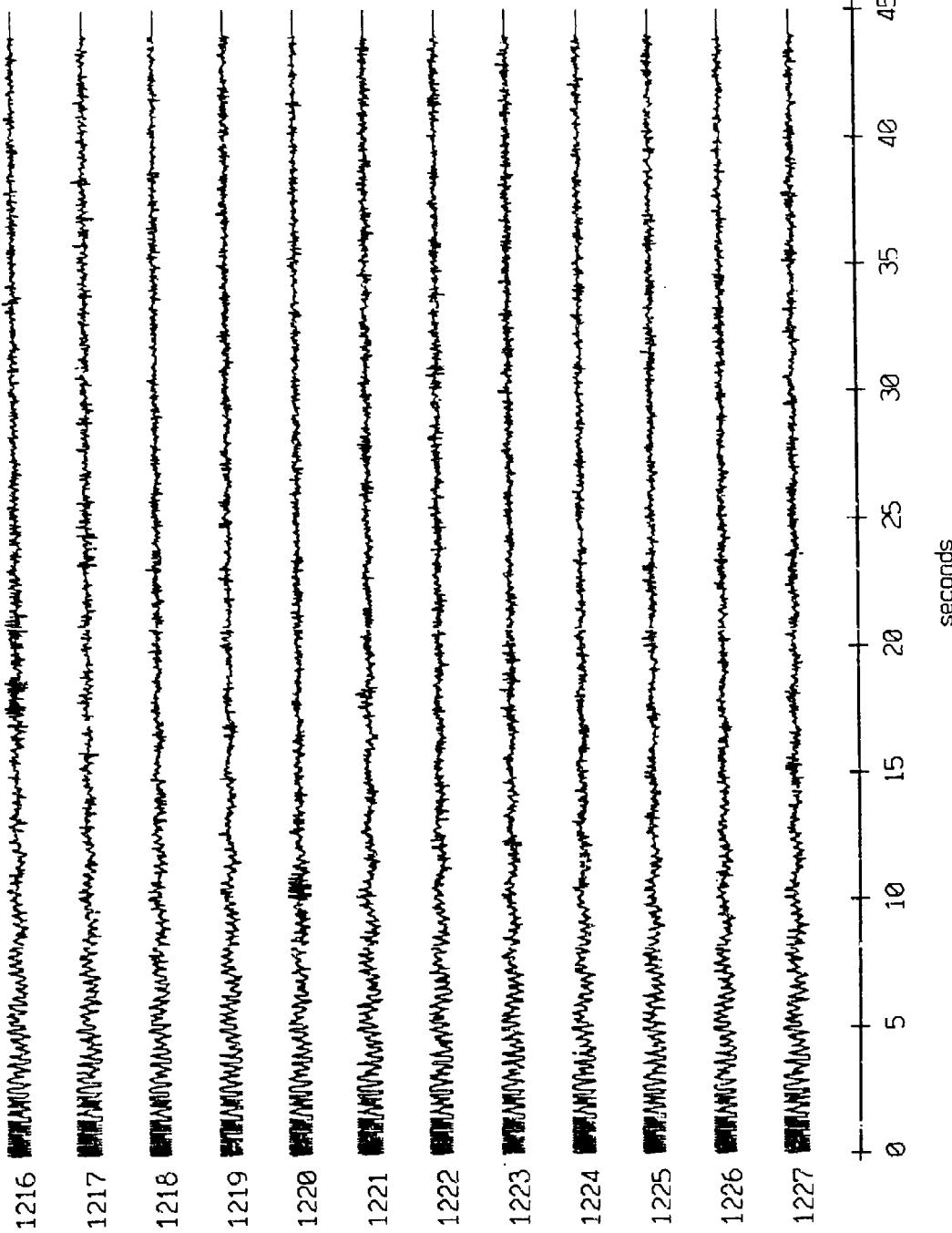


Figure X.6b.j

Fleet 8, May, 1987 Trip - records 1216-1227 (z-axis)
vertical axis scale is approx. -1.0 to 1.0 volts

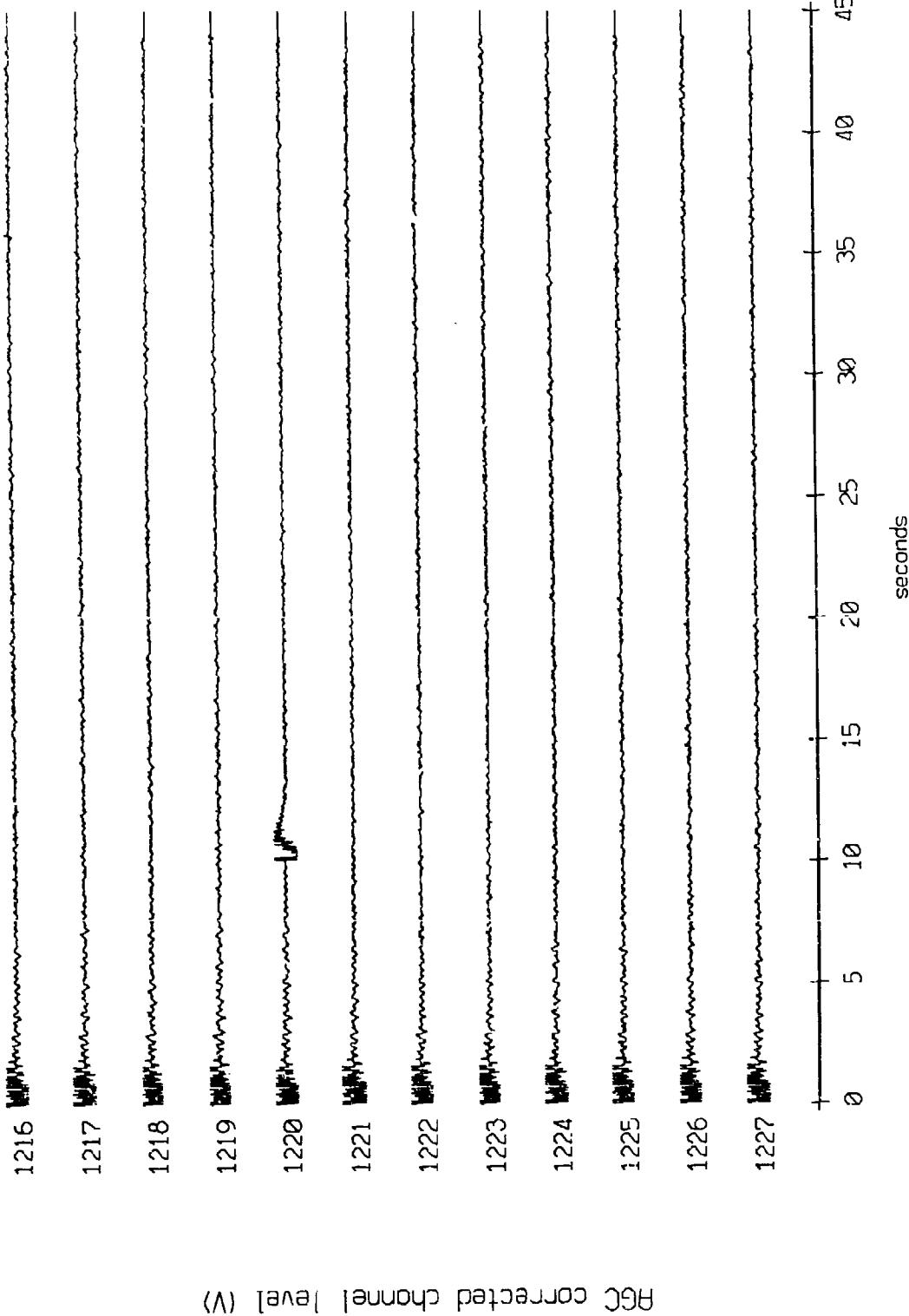


Figure X.6b.k

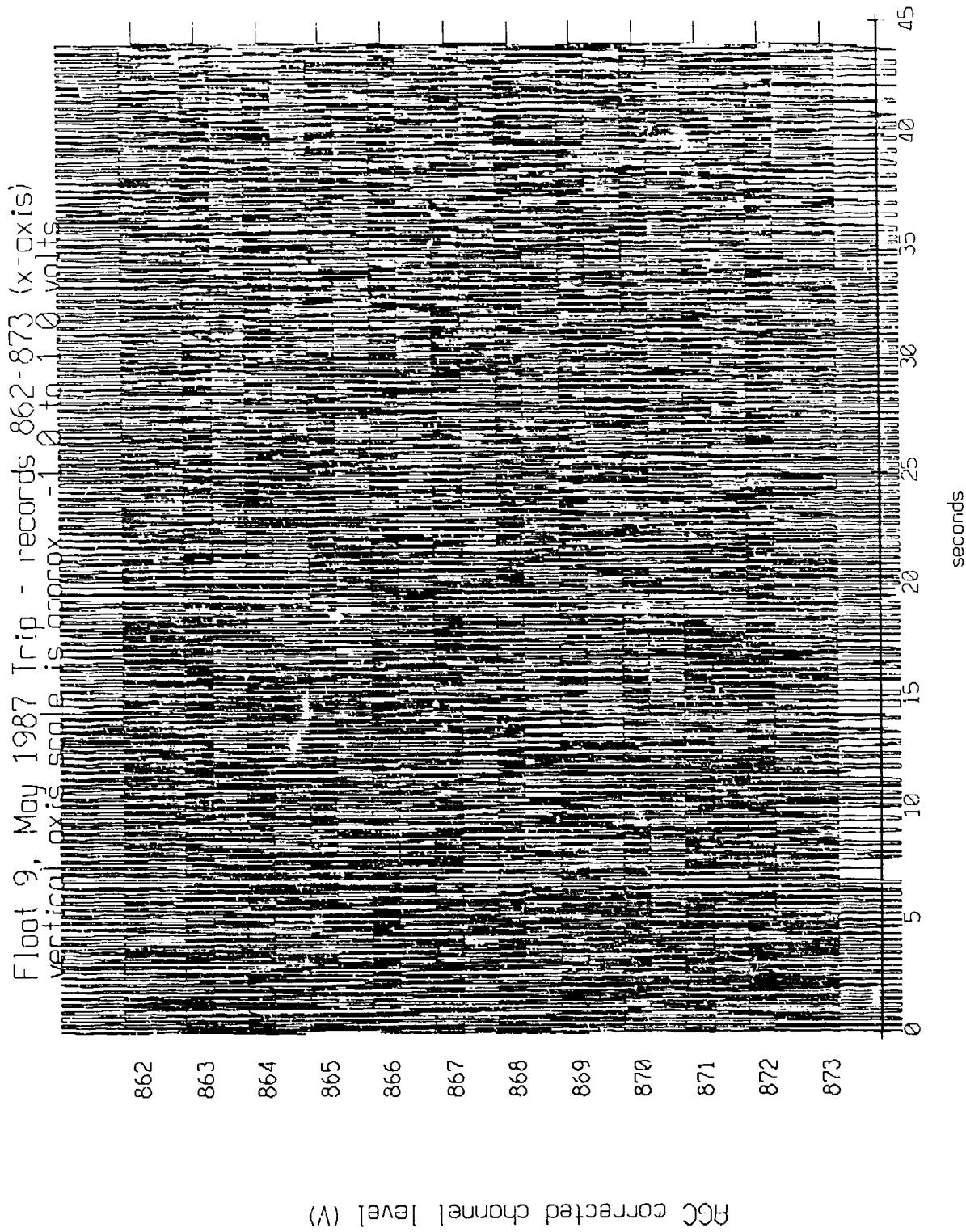


Figure X.7b.i

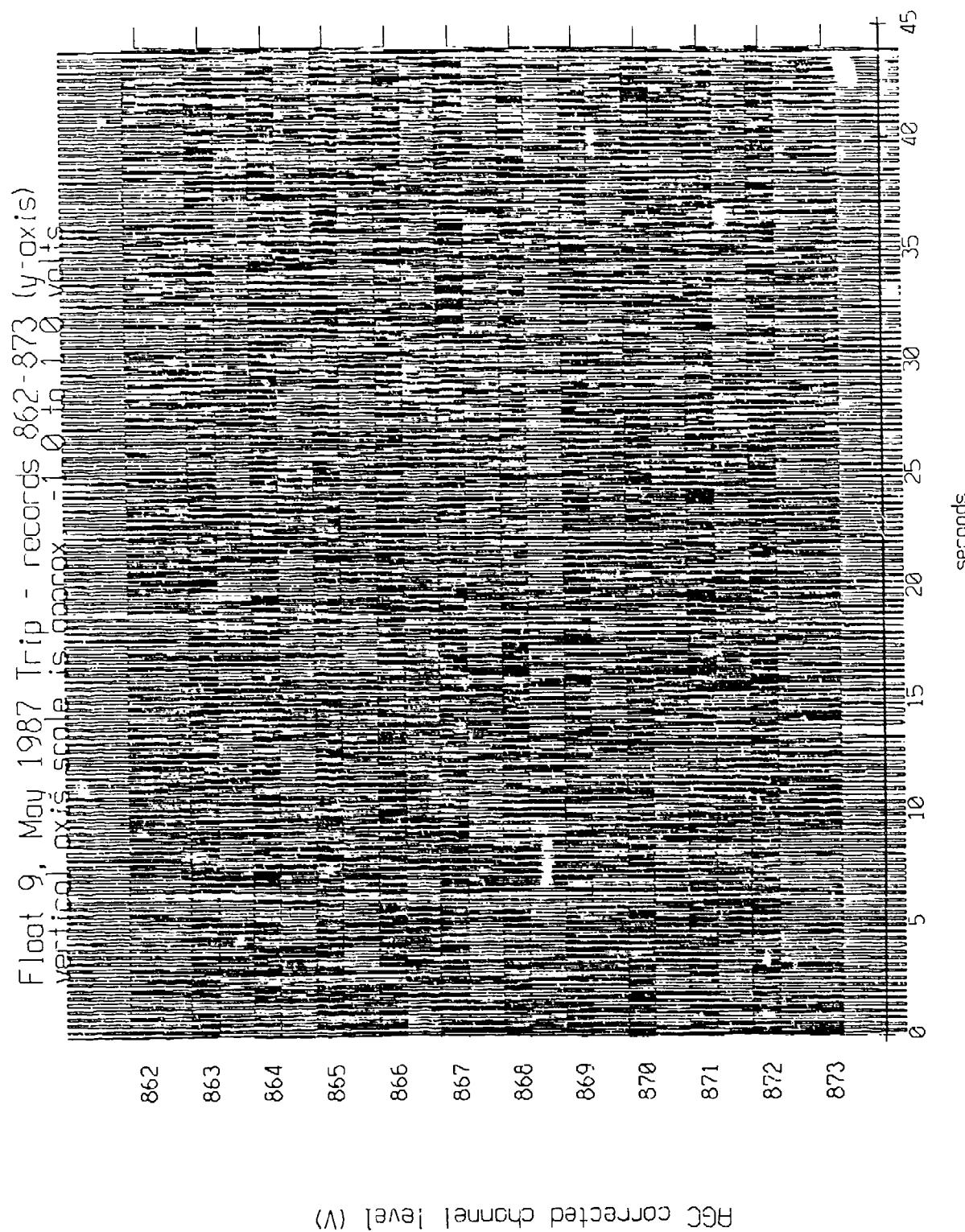


Figure X.7a.j

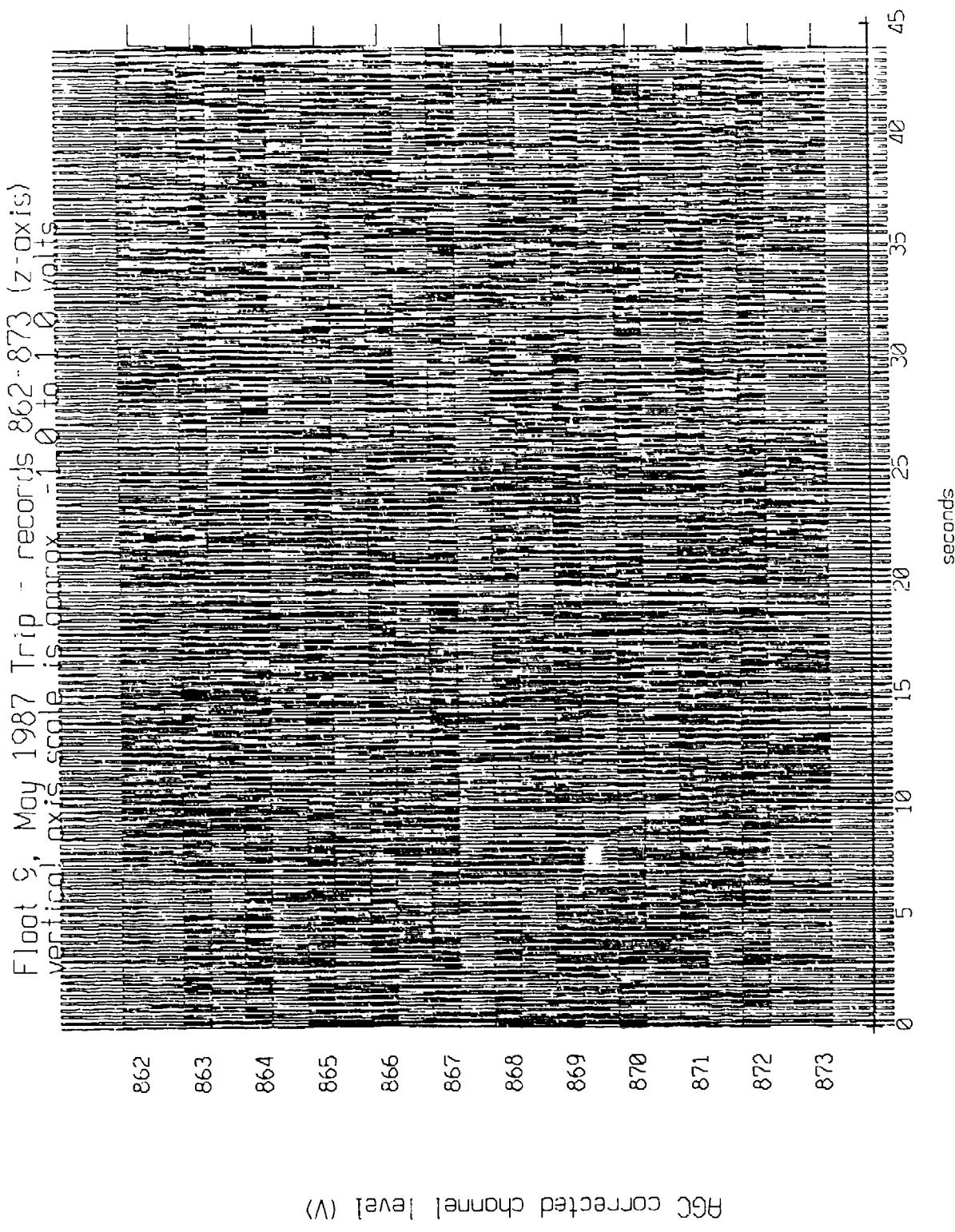


Figure X.7a.k

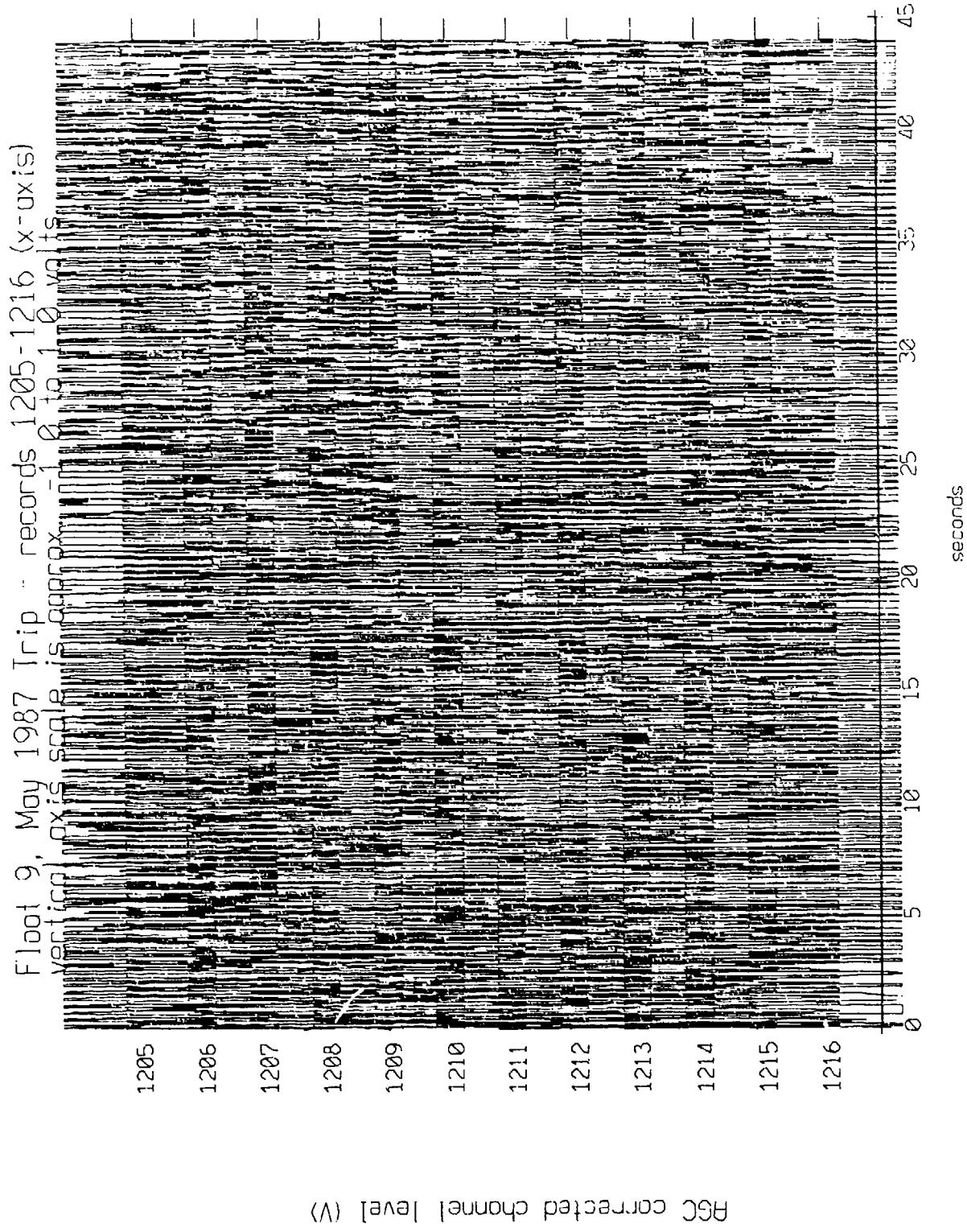
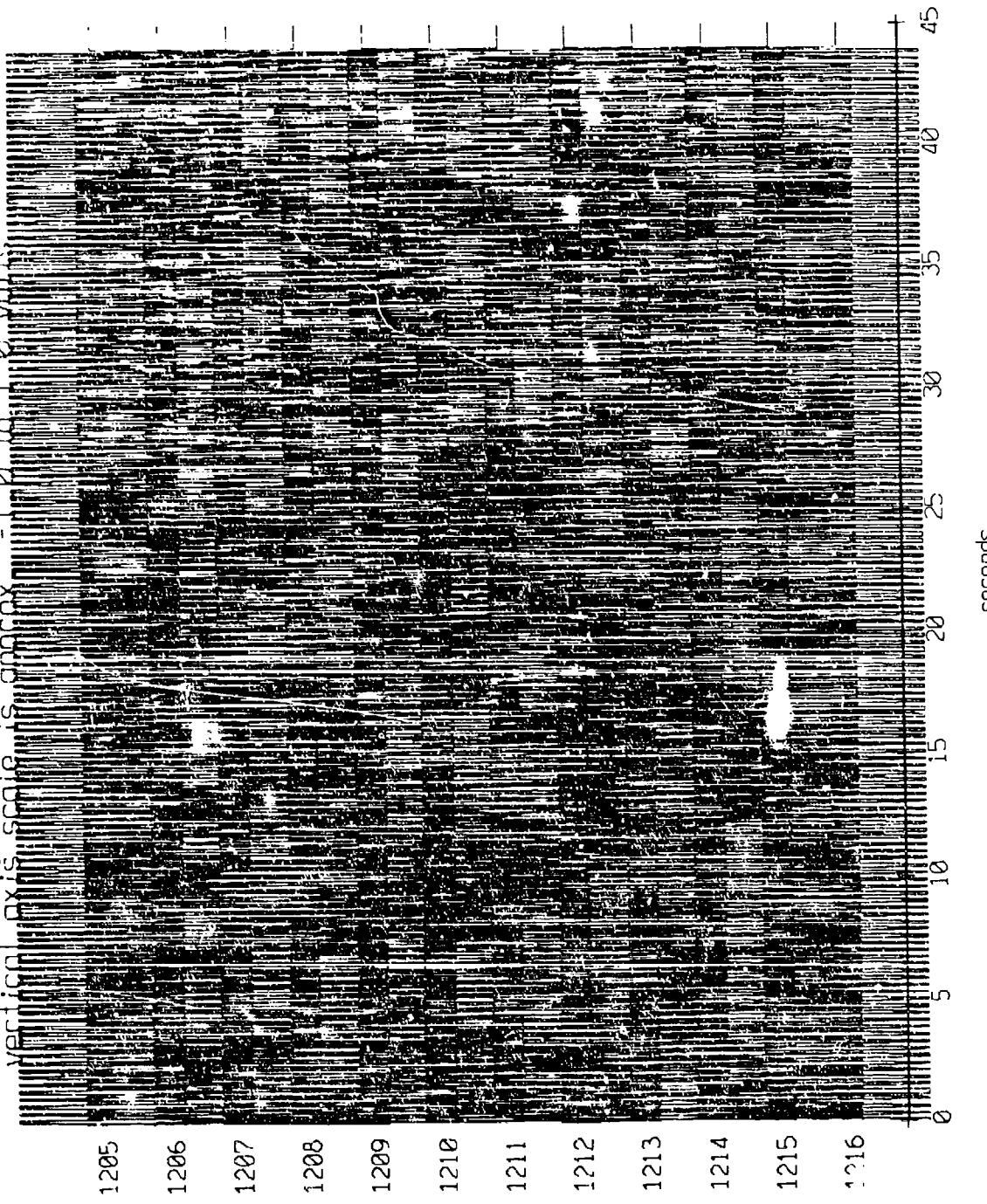


Figure X.7a.i

Flight 9, May 1987 Trip - records 1205-1216 (y axis)



AGC CORRECTED CHANNEL LEVEL (V)

Figure X.7b.j

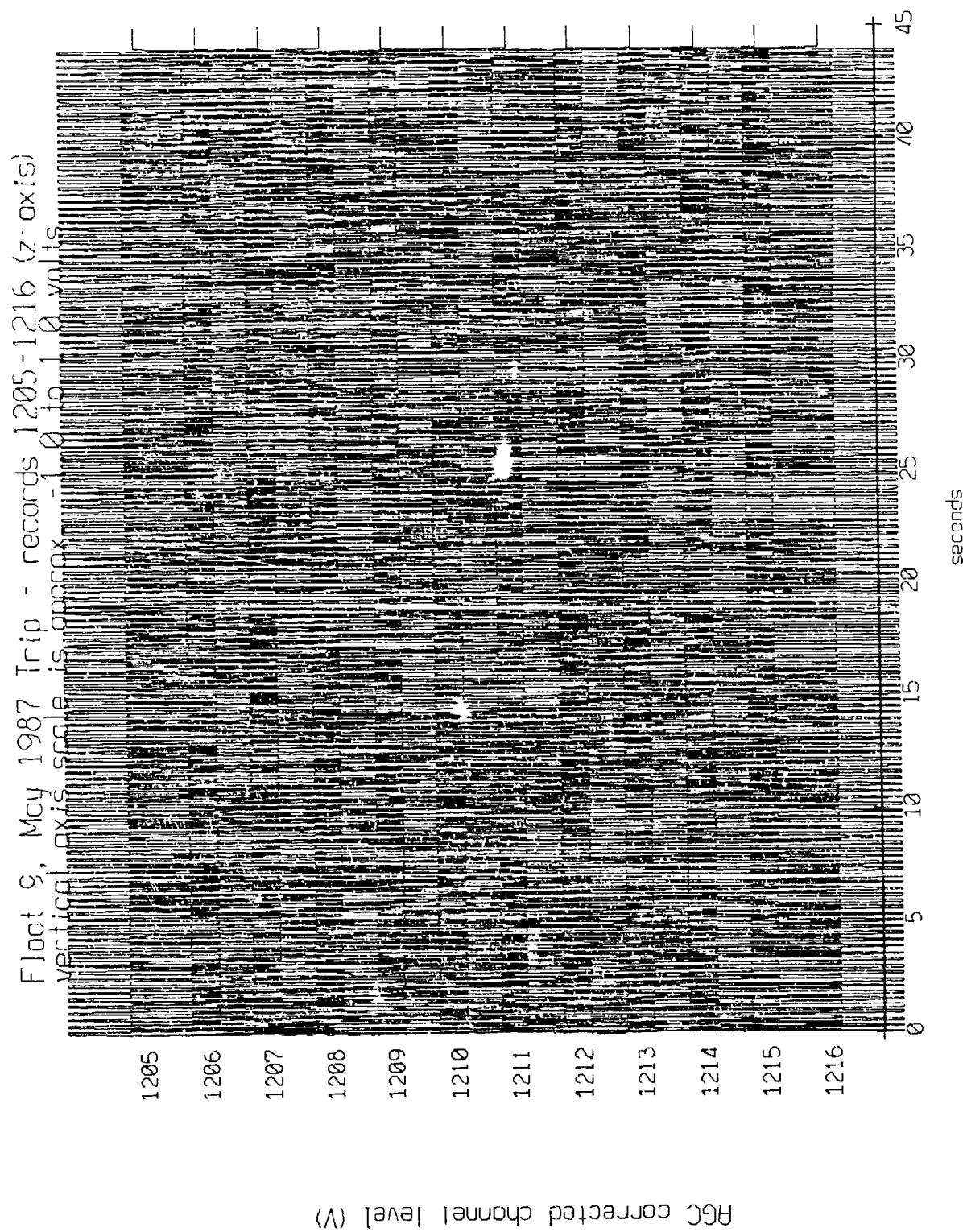


Figure X.7b.k

Float 10 May, 1987 Trip - records 957-968 (x-axis)
vertical axis scale is approx. -1.0 to 1.0 Volts

957 958 959 960 961 962 963 964 965 966 967 968

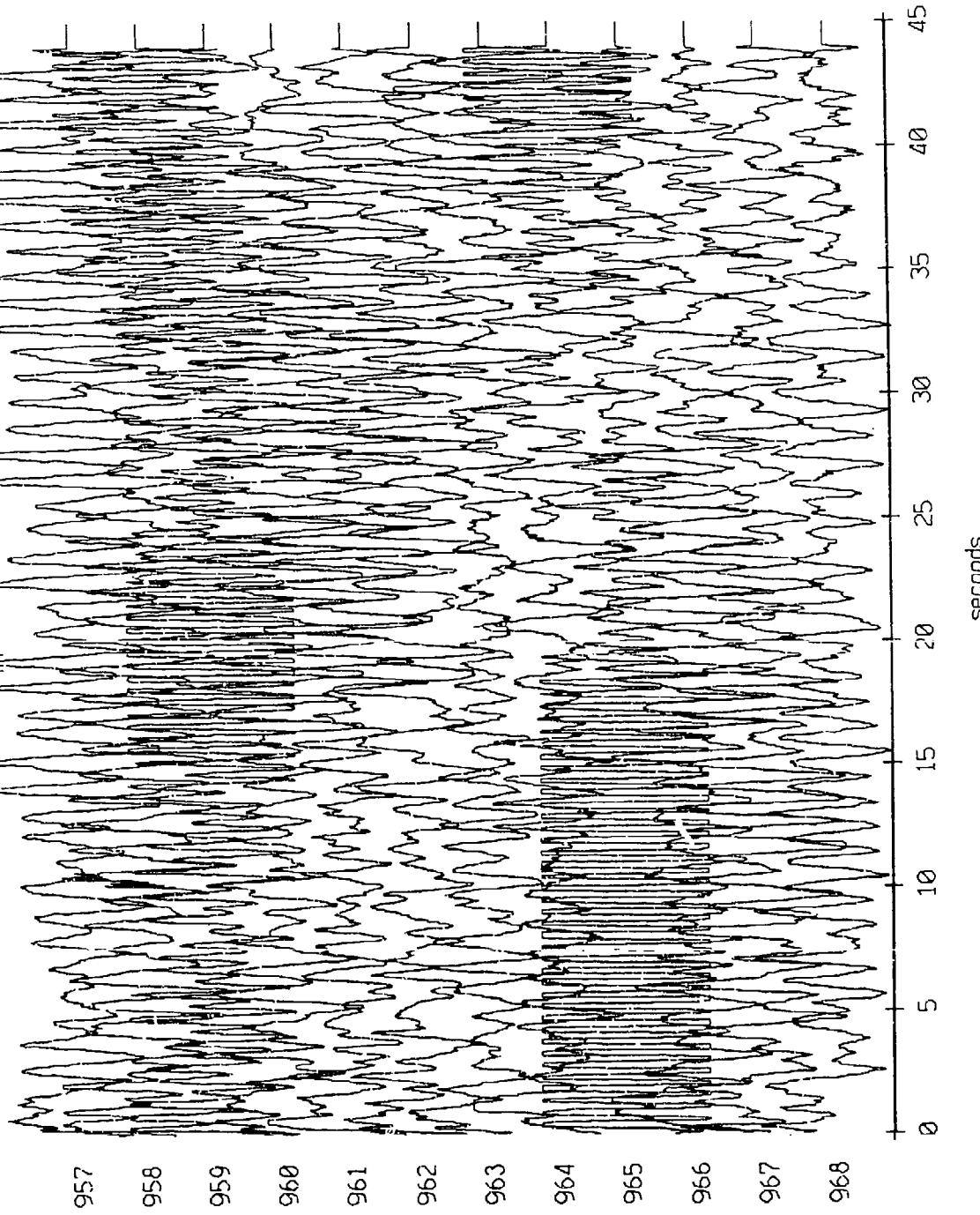
AGC corrected channel level (V)

seconds

45
40
35
30
25
20
15
10
5
0

Figure X.8a.i

Fleet 10, May, 1987 Trip - records 957-968 (y-axis)
vertical axis scale is approx 1.0 to 1.0 volts



AGC corrected channel level (V)

Figure X.8a.j

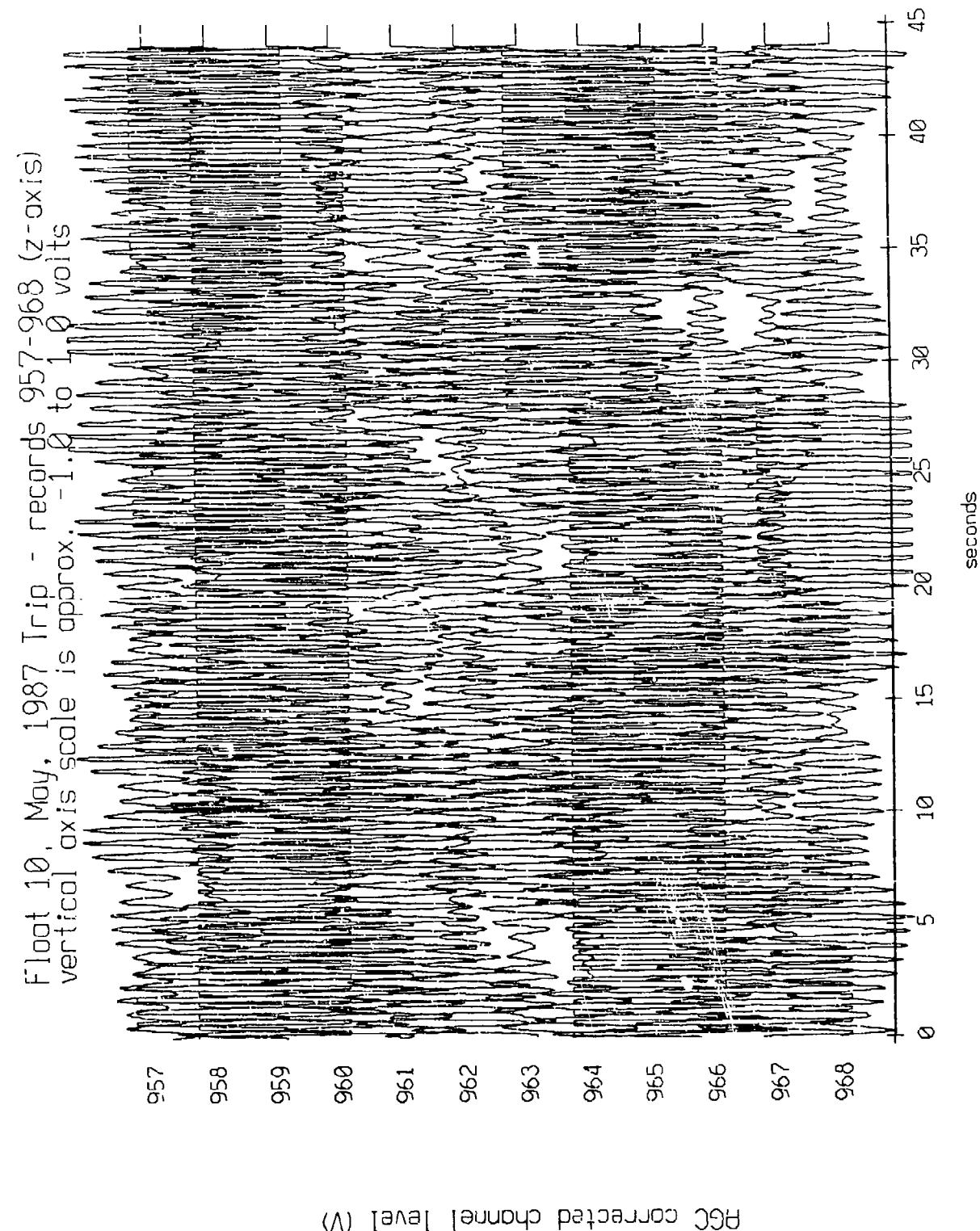


Figure X.8a.k

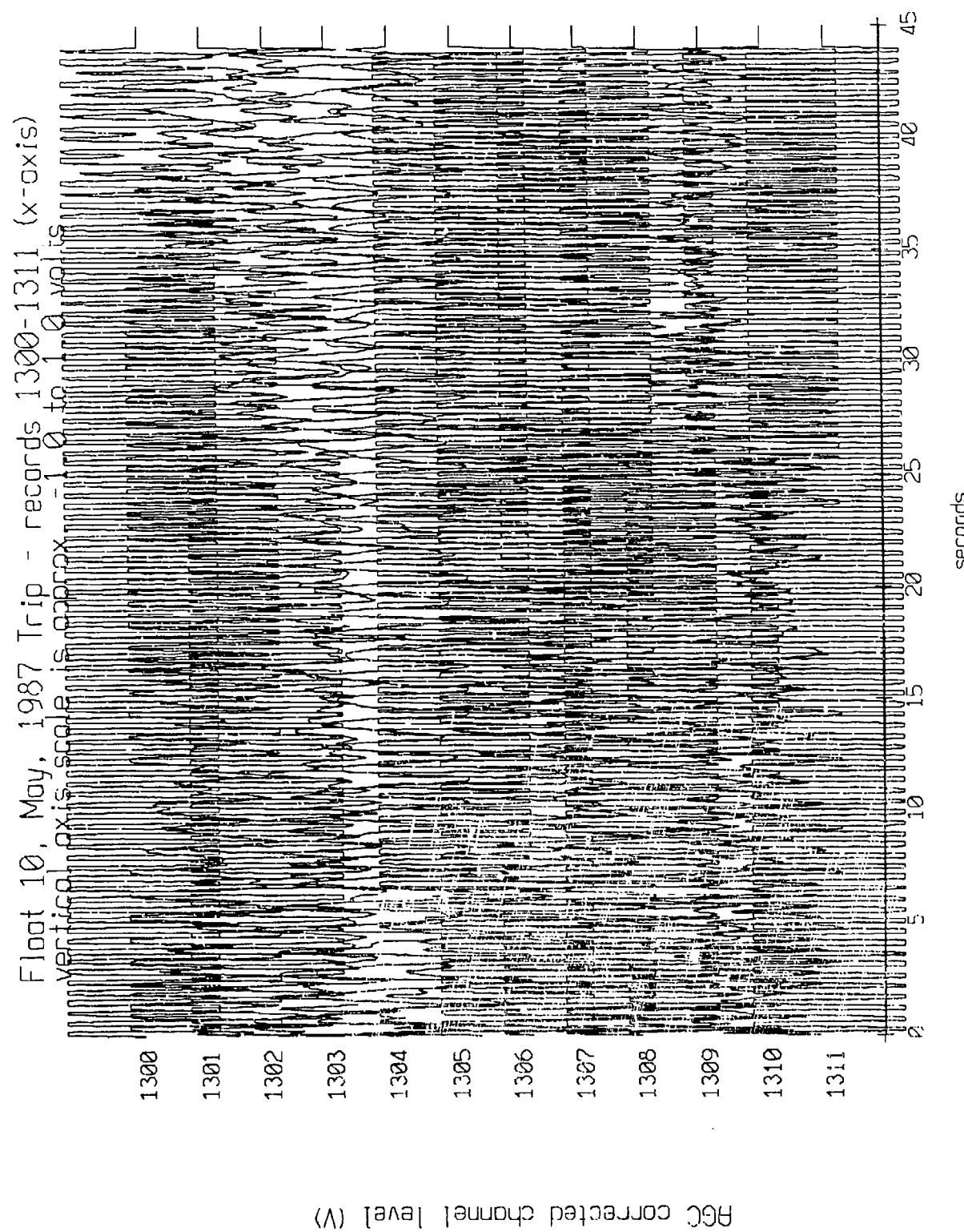


Figure X.8b.i

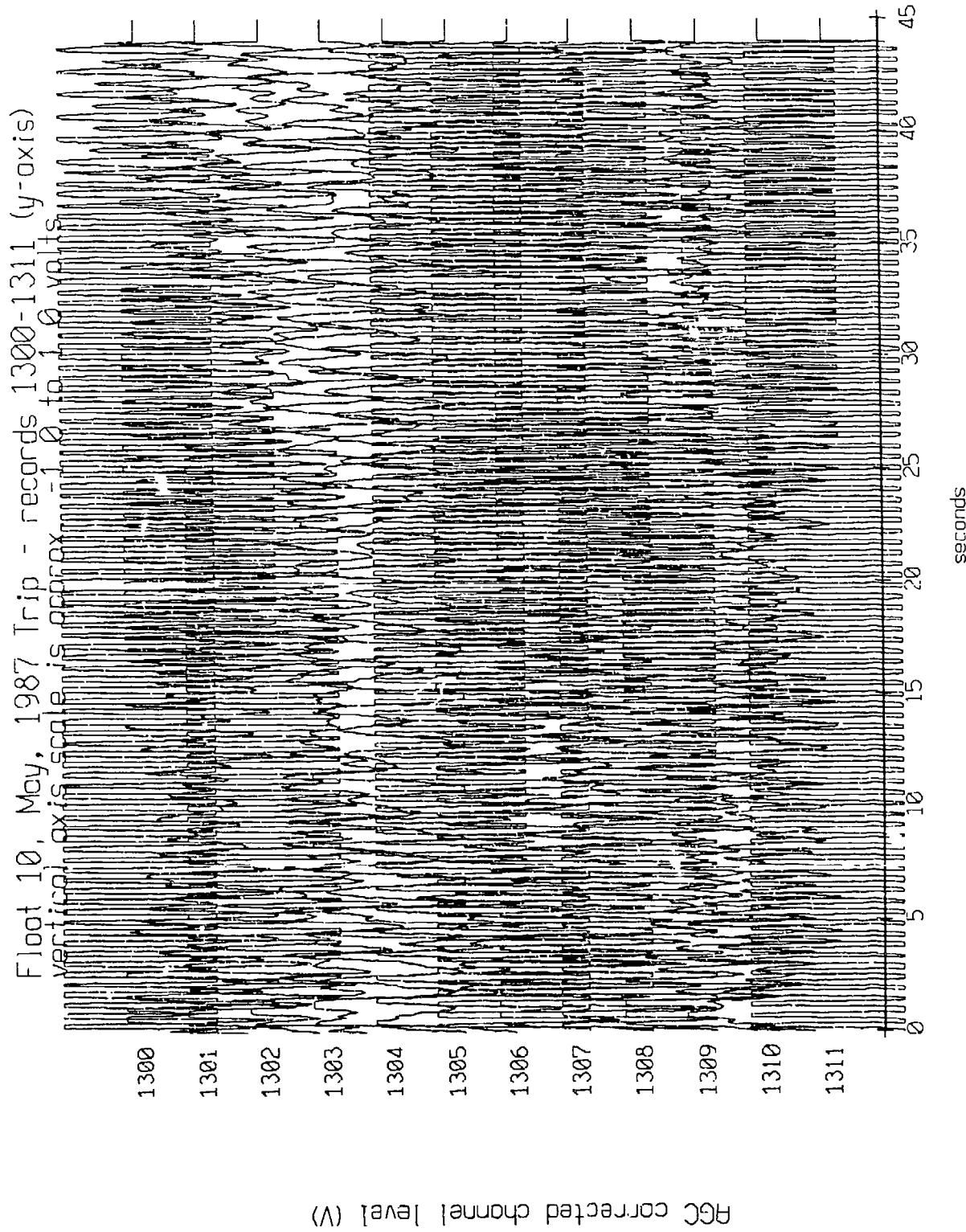
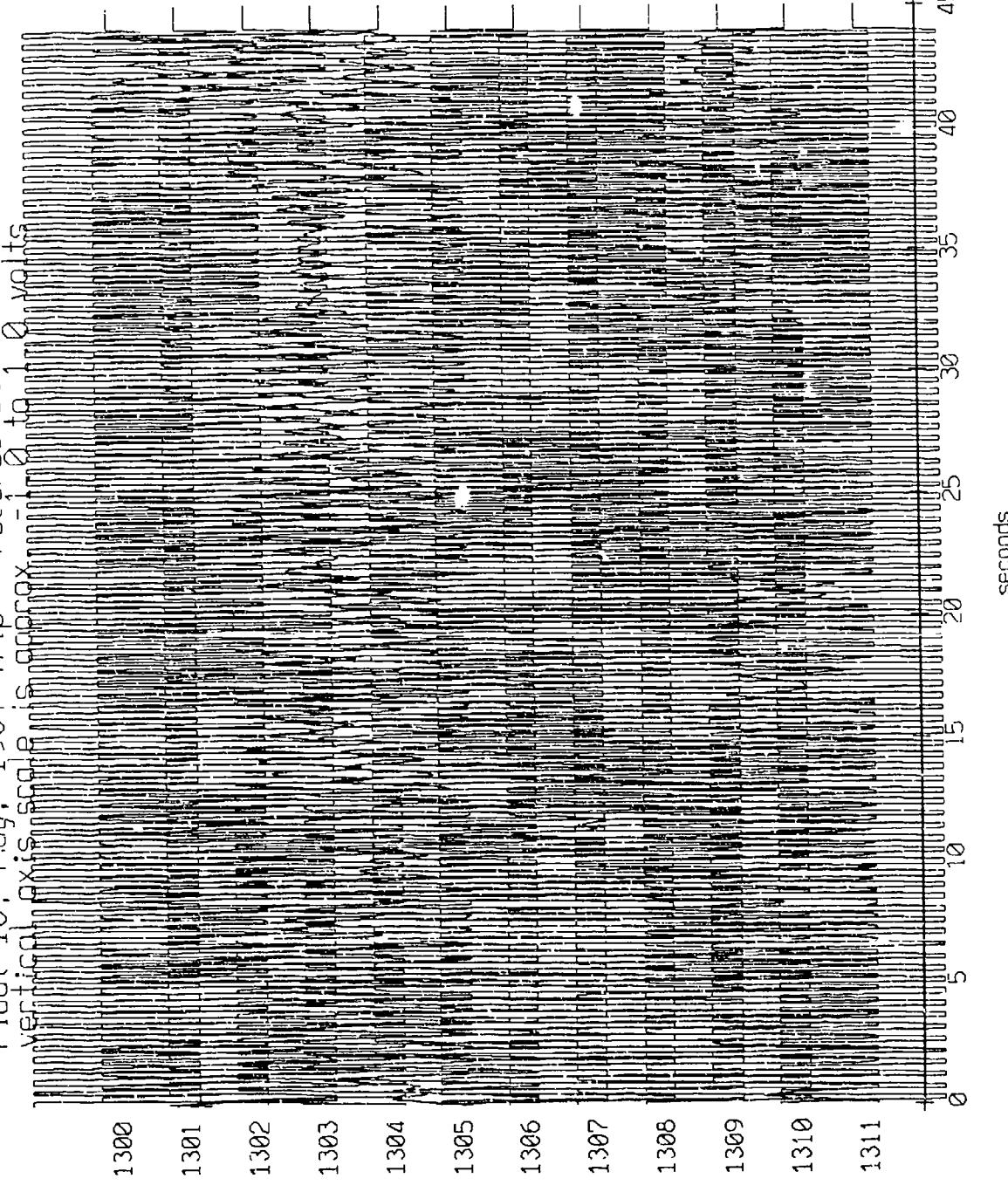


Figure X.8b.j

Float 10, May, 1987 Trip - records 1300-1311 (z-axis)



AGC corrected channel level (V)

Figure X.8b.k

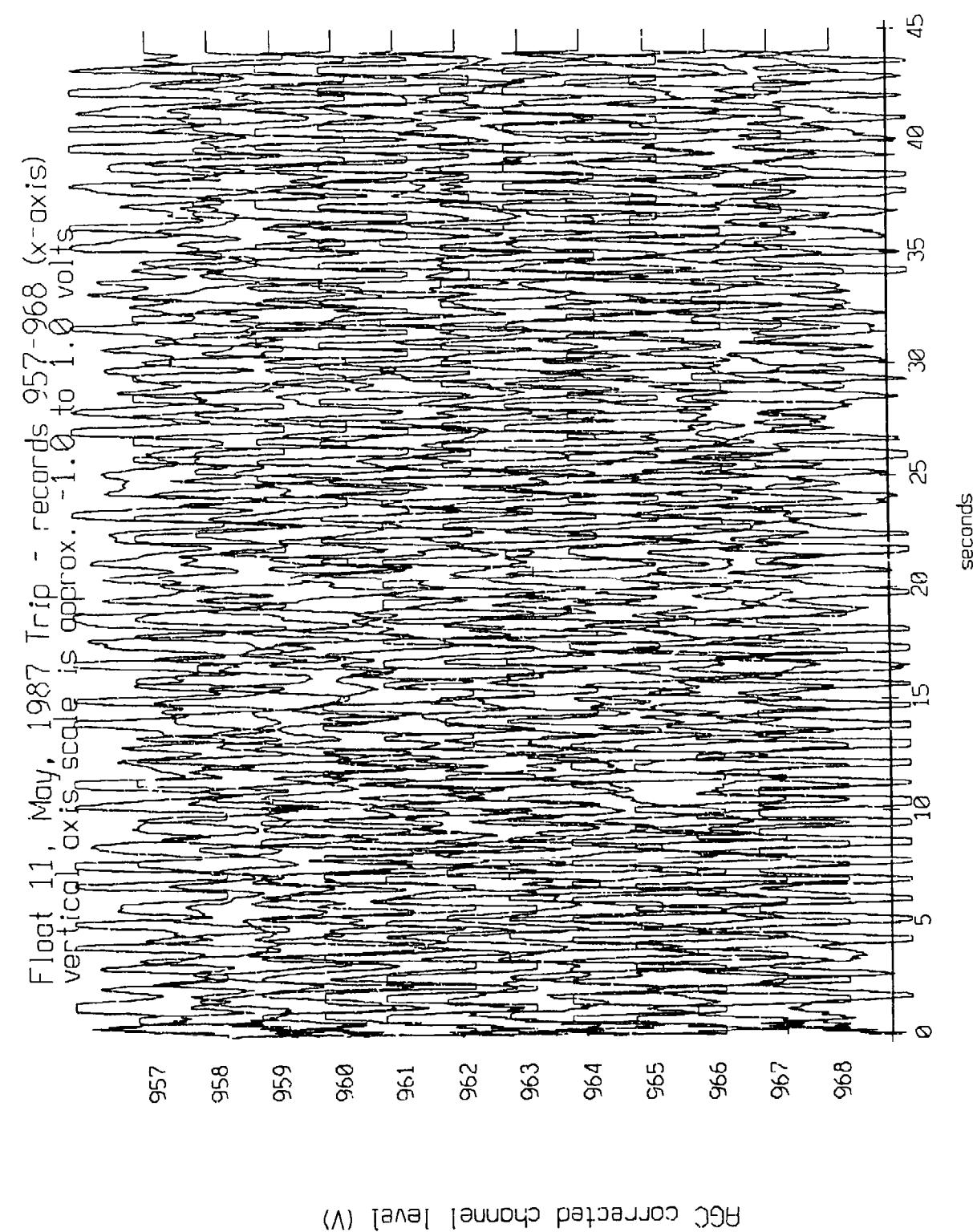
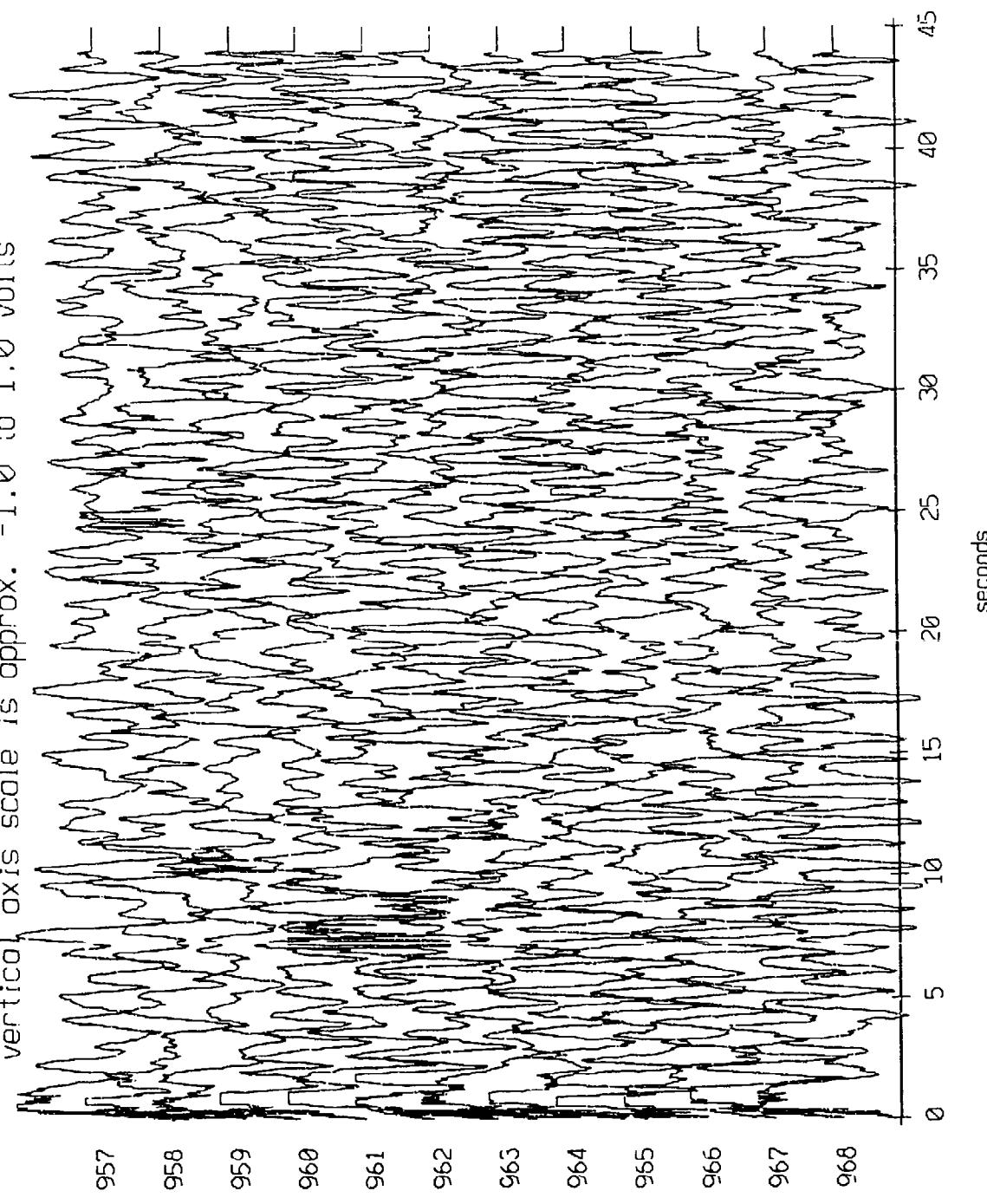


Figure X.9a.i

Fleet 11, May, 1987 Trip - records 957-968 (y-axis
vertical axis scale is approx. -1.0 to 1.0 volts)



AGC corrected channel level (V)

Figure X.9a.j

Flight 11, May, 1987 Trip - records 957-968 (Z-axis)
vertical axis scale is approx. -1.0 to 1.0 volts

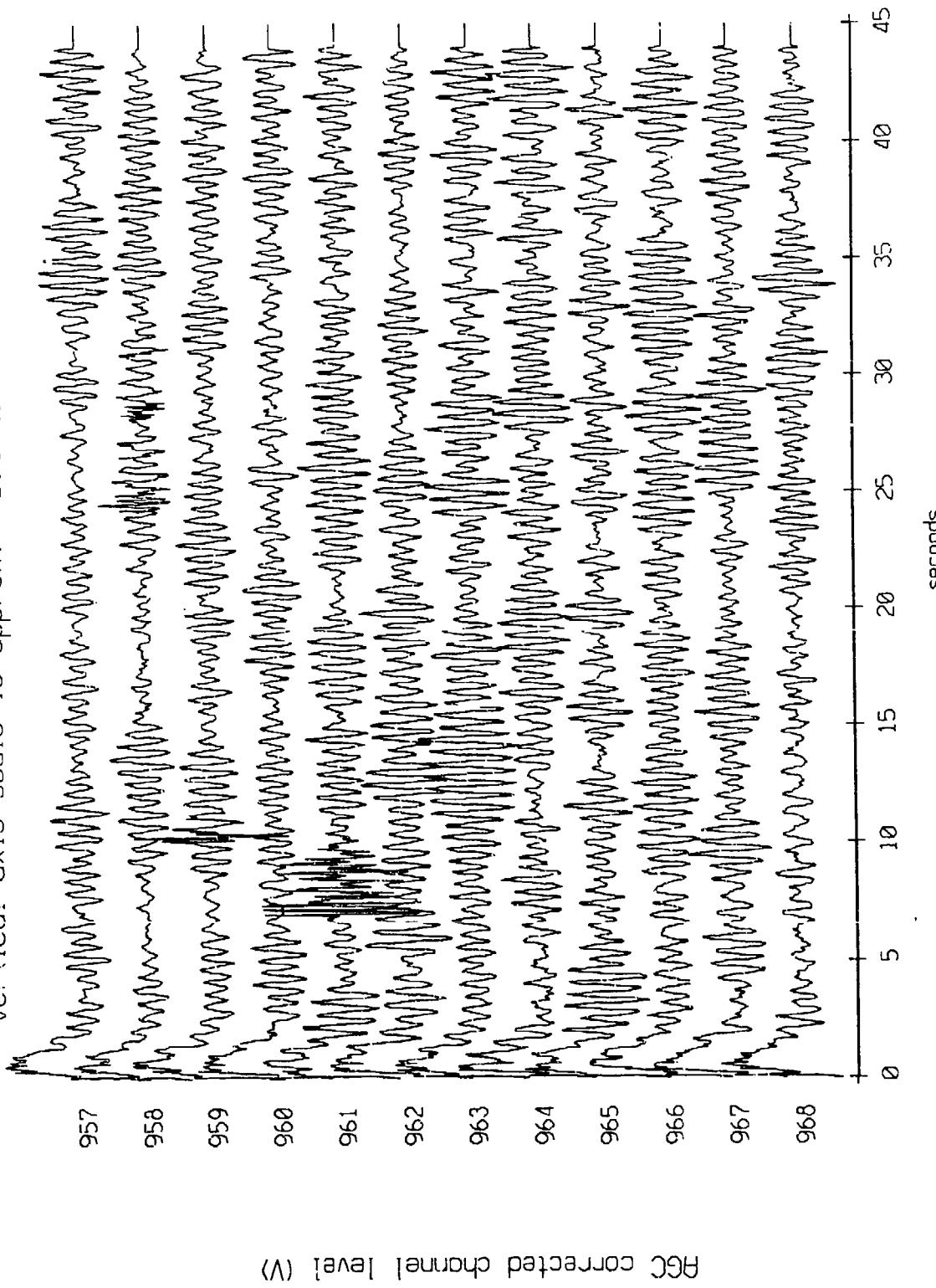


Figure X.9a.k

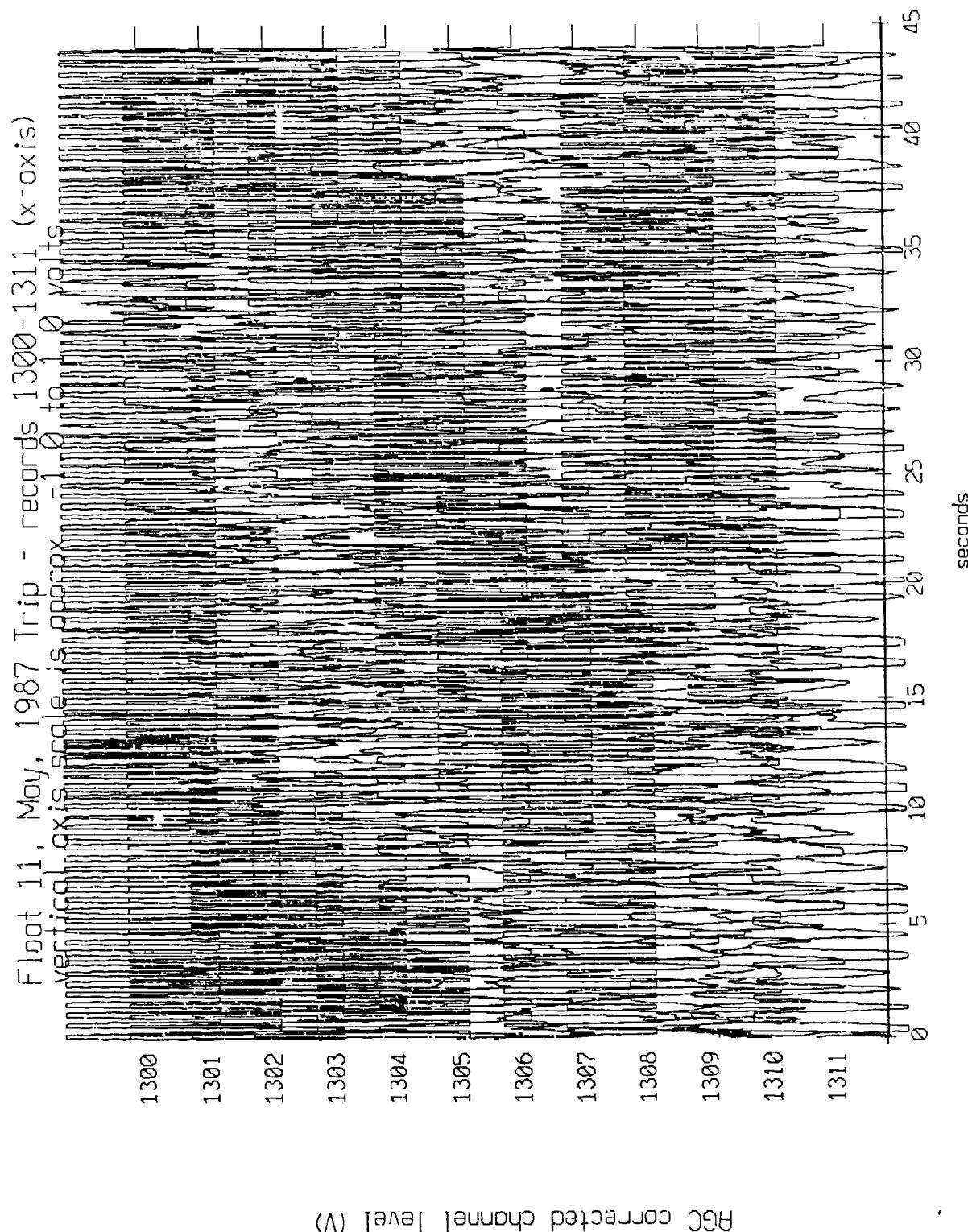


Figure X.9b.i

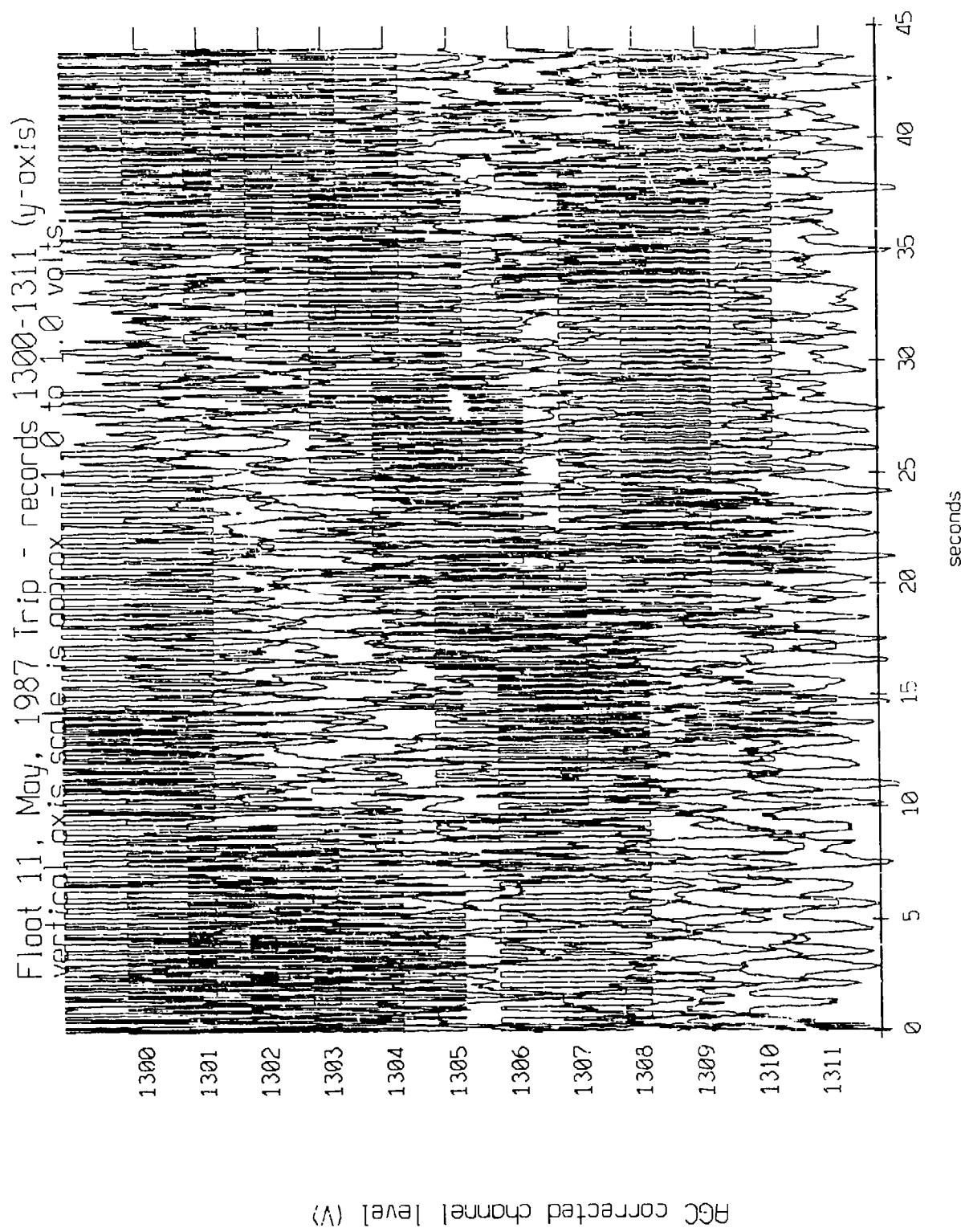


Figure X.9b.j

Float 11, May, 1987 Trip - records 1300-1311 (z axis)

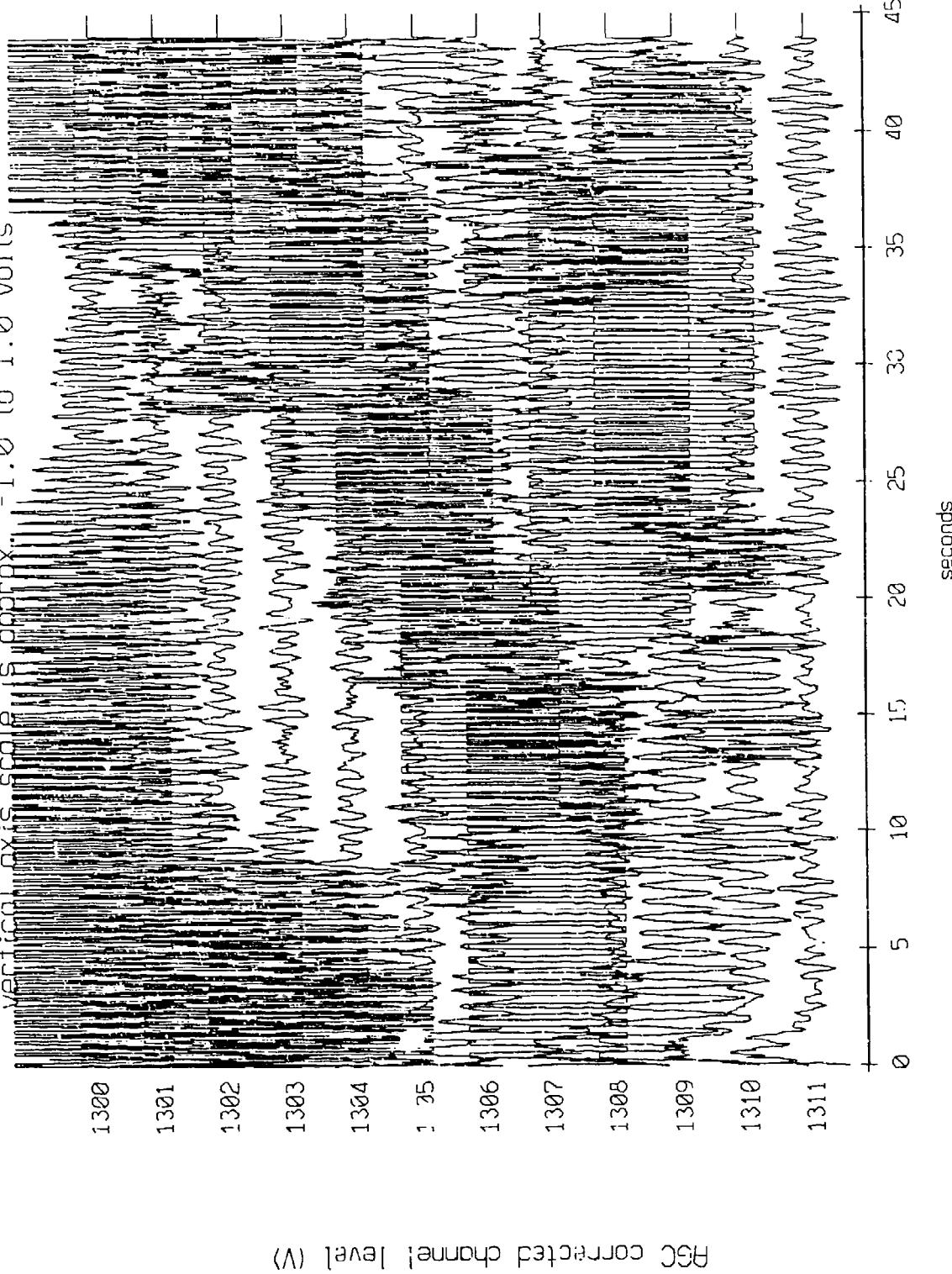


Figure X.9b.k

Flight 11, May, 1987 Trip - records 563-574 (x-axis)
vertical axis scale is approx. -1.0 to 1.0 volts

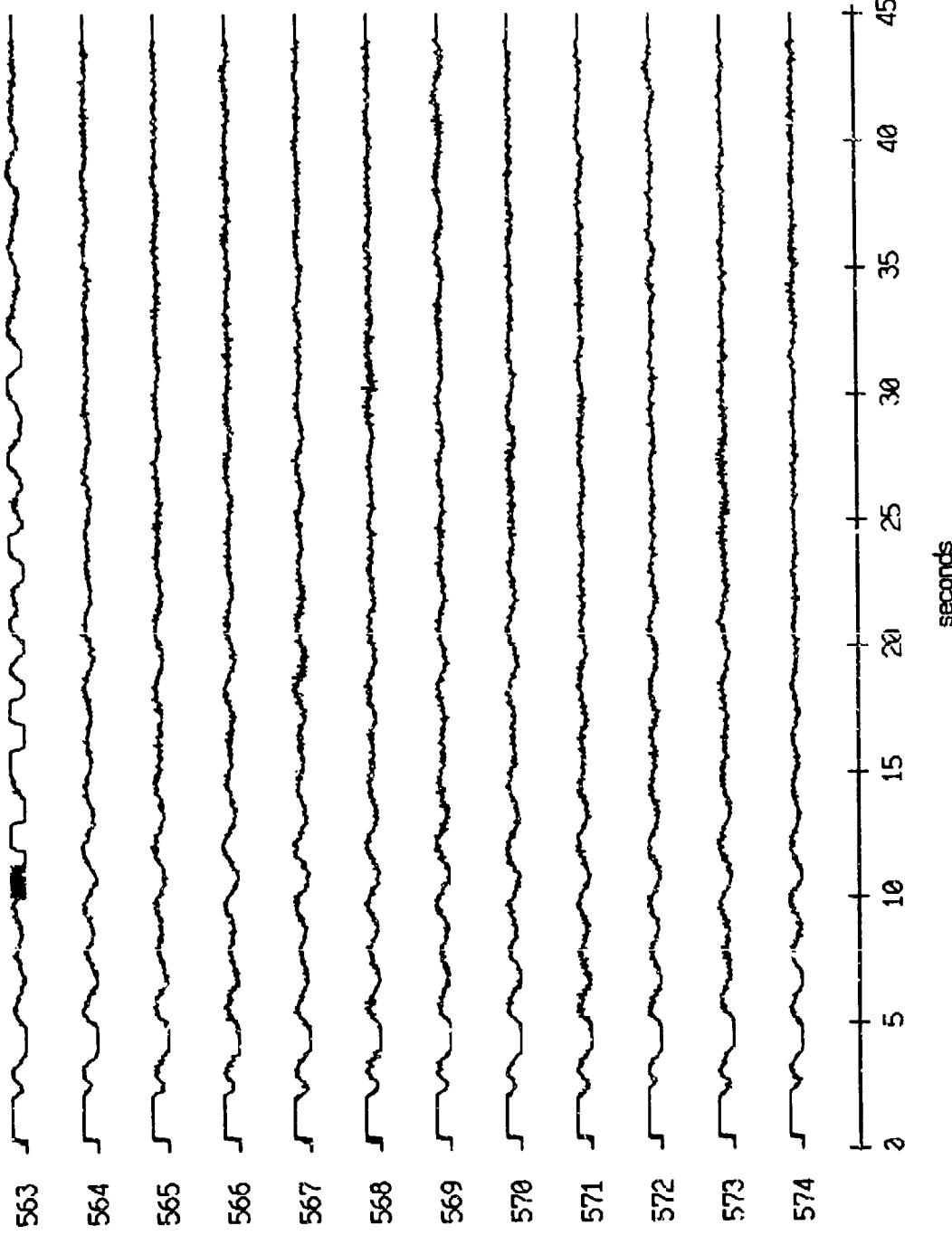
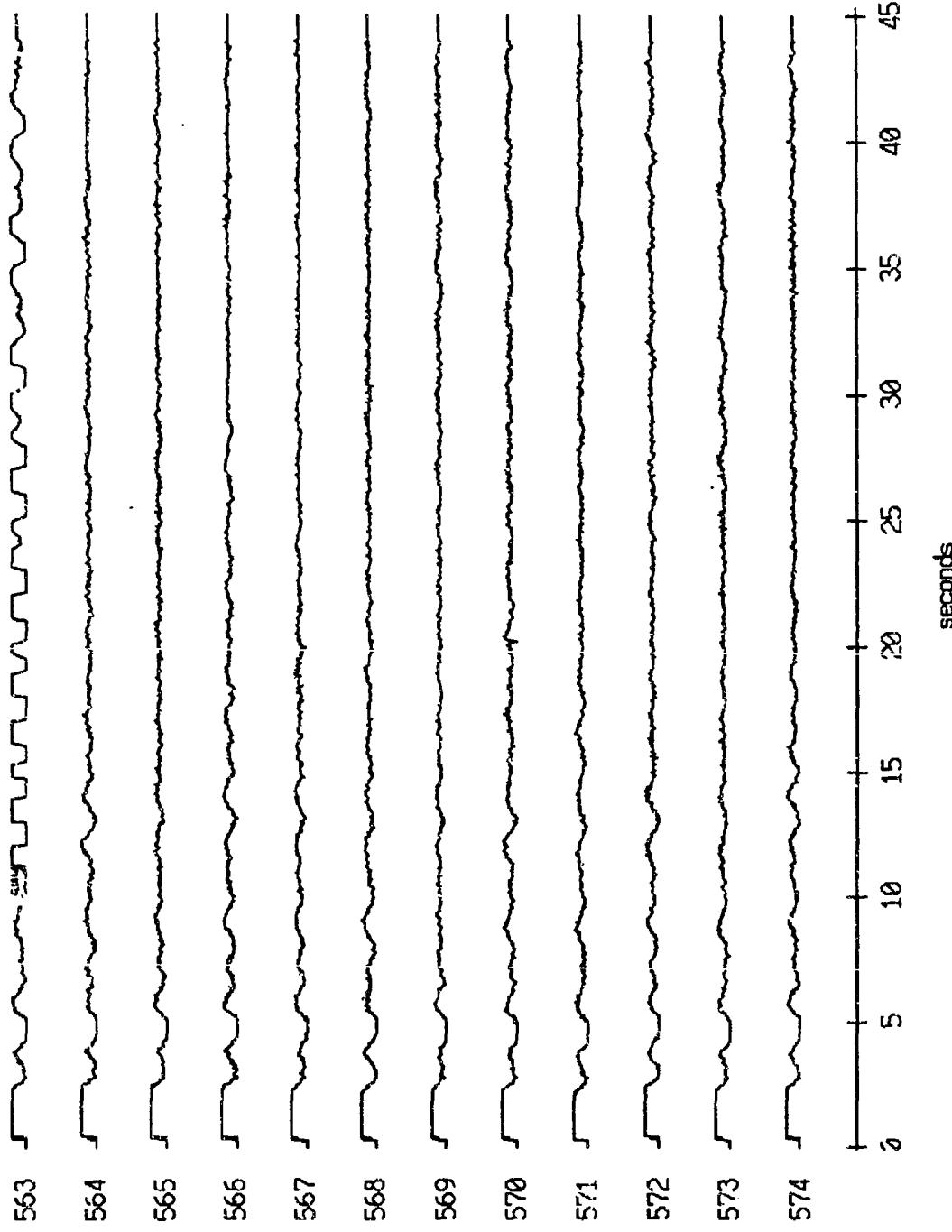


Figure X.9c.i

Flight 11, May, 1987 Trip - records 563-574 (y-axis)
vertical axis scale is approx. -1.0 to 1.0 volts



AGC corrected channel level (V)

Figure X.9c.j

Float 11, May, 1987 Trip - records 563-574 (z-axis)
vertical axis scale is approx. -1.0 to 1.0 volts

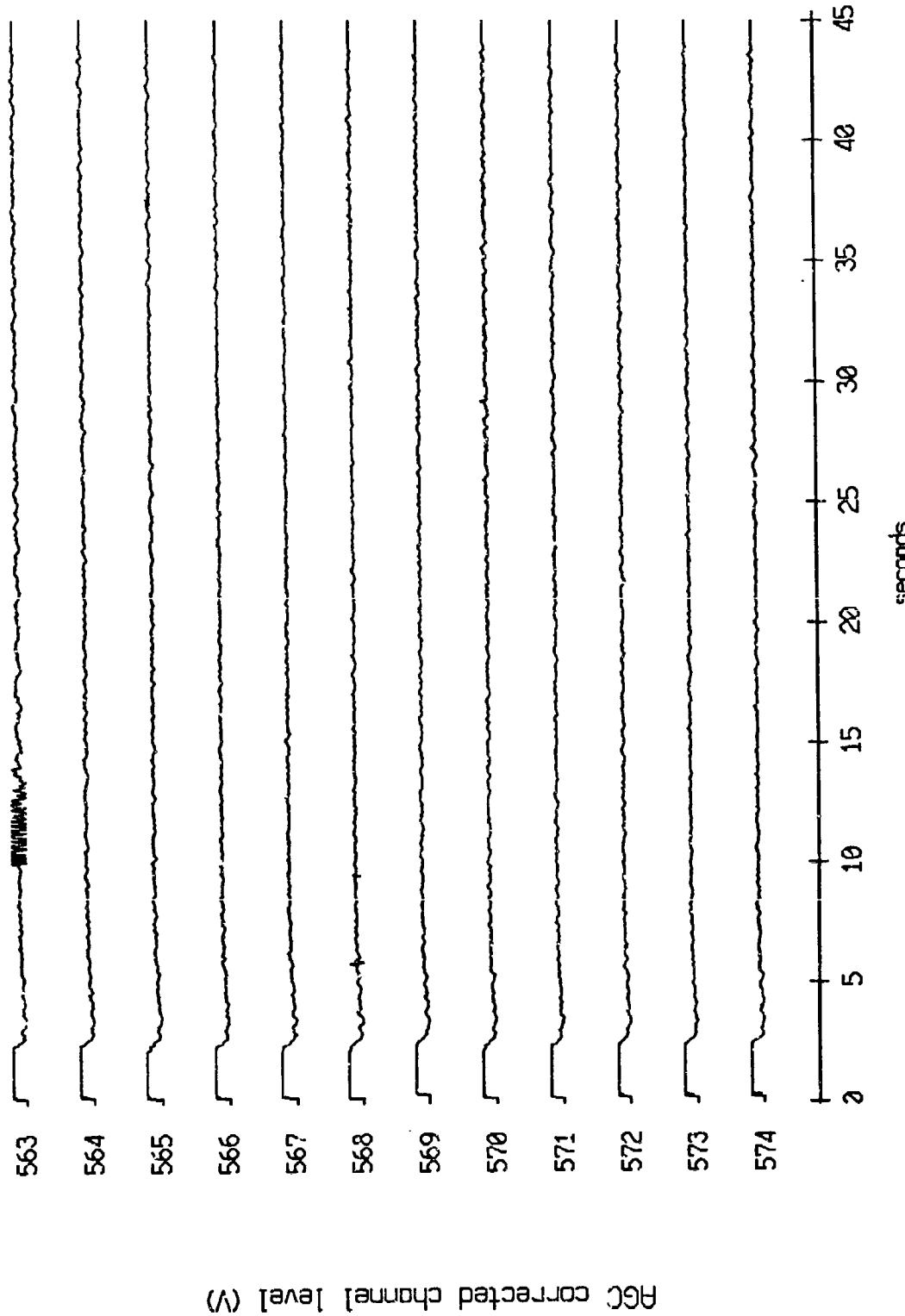
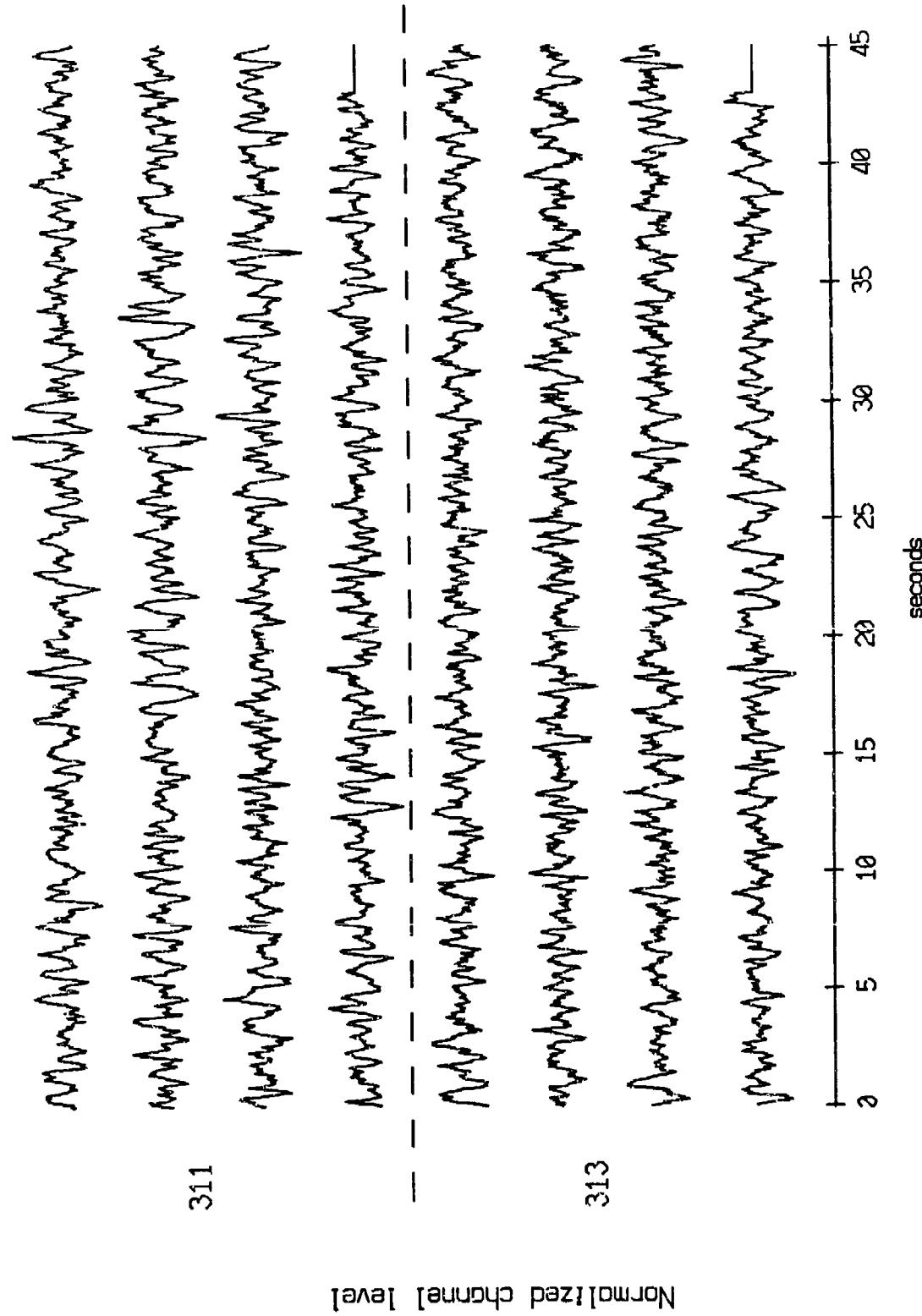


Figure X.9c.k

QES 01, May, 1987 Trip - events 311 and 313 (x-axis)
max gain-corrected amplitude is 1.025565 counts



Normalized channel level

Figure X.10a.i

OBS 01, May, 1987 Trip - events 311 and 313 (y-axis)
max gain-corrected amplitude is 0.341190 counts

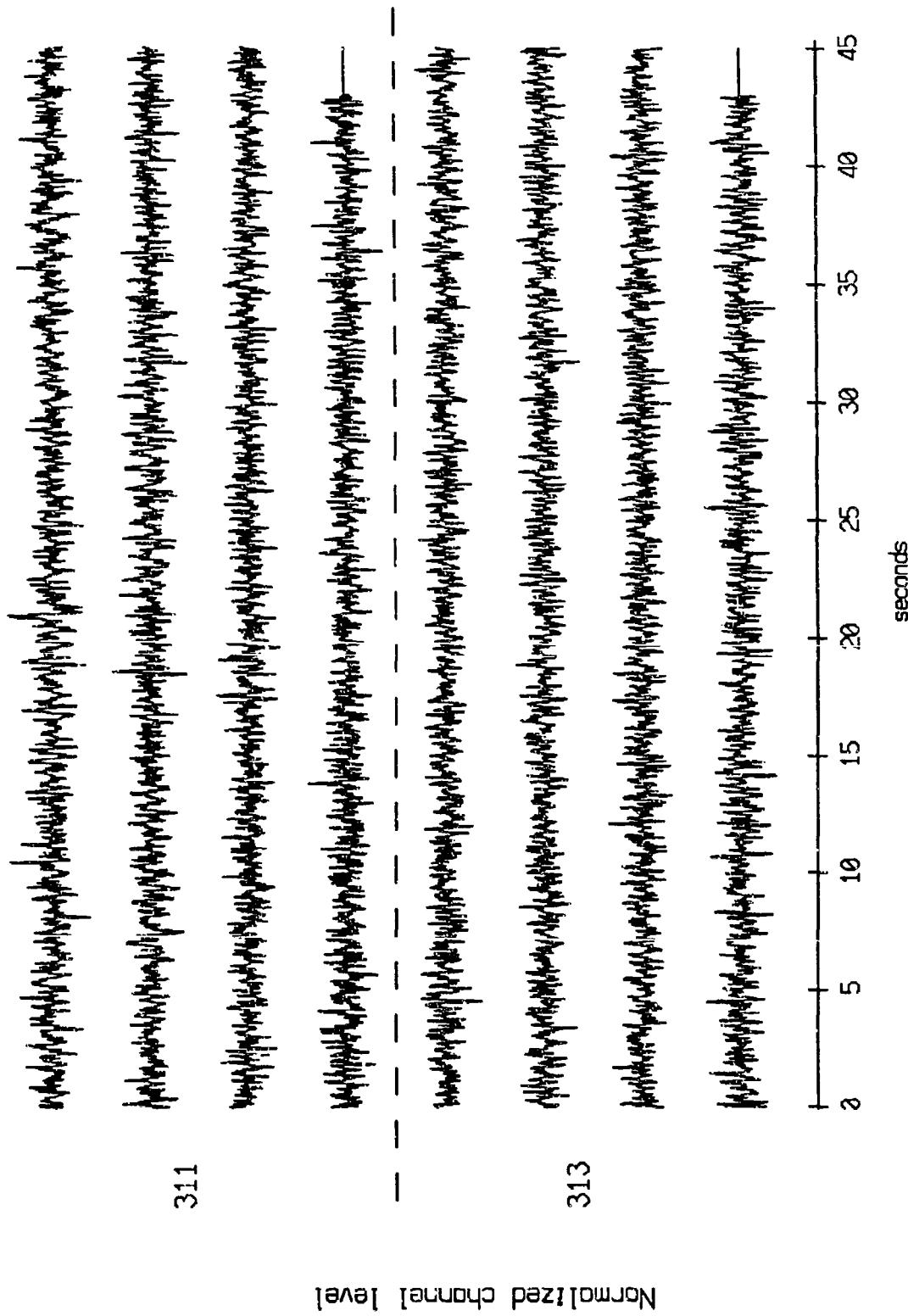
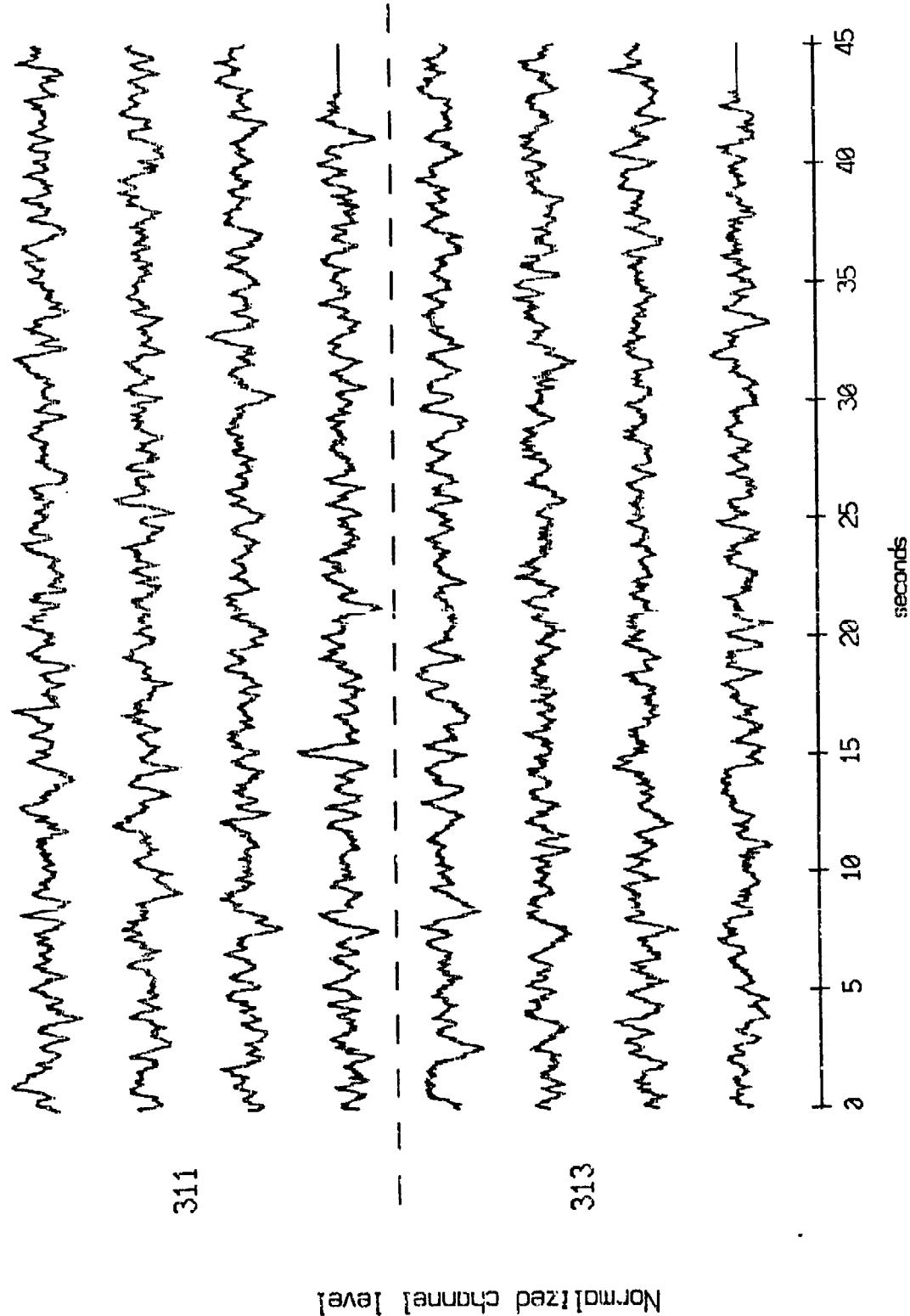


Figure X.10a.j

OBS 01, May, 1987 Trip - events 311 and 313 (z-axis)
max gain-corrected amplitude is 0.788129 counts



Normalized Channel Level

Figure X.10a.k

OBS 01, May, 1987 Trip - events 311 and 313 (pressure)
max gain-corrected amplitude is 206.844 counts

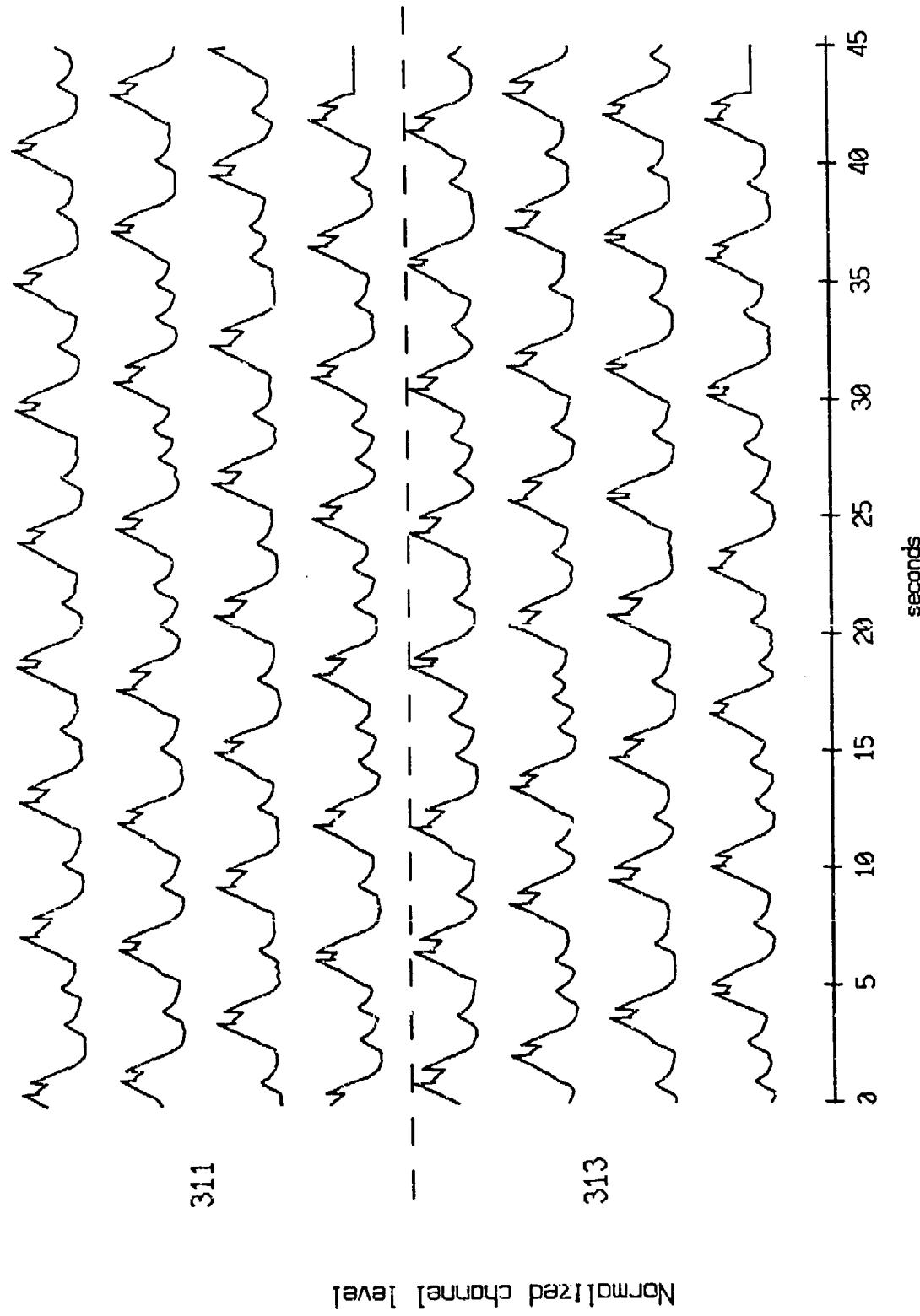
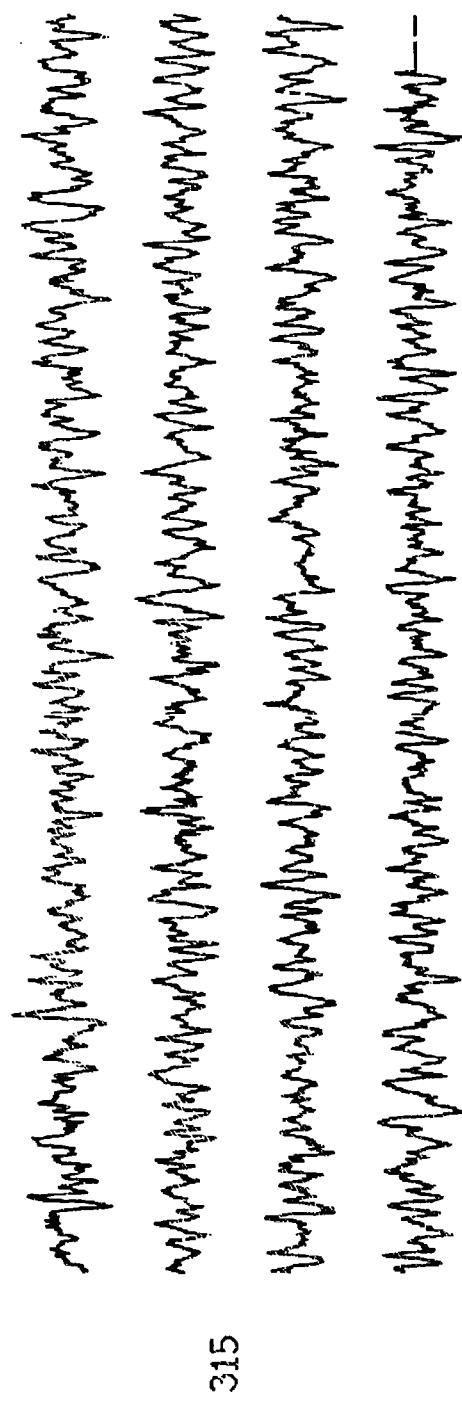


Figure X.10a.l

OBS 01, May, 1987 Trip - event 315 (x axis)
max gain-corrected amplitude is 0.929792 counts



Normalized channel Level

Figure X.10b.i

OBS 01, May, 1987 Trip - event 315 (y^{axis})
max gain-corrected amplitude is 0.311261 counts

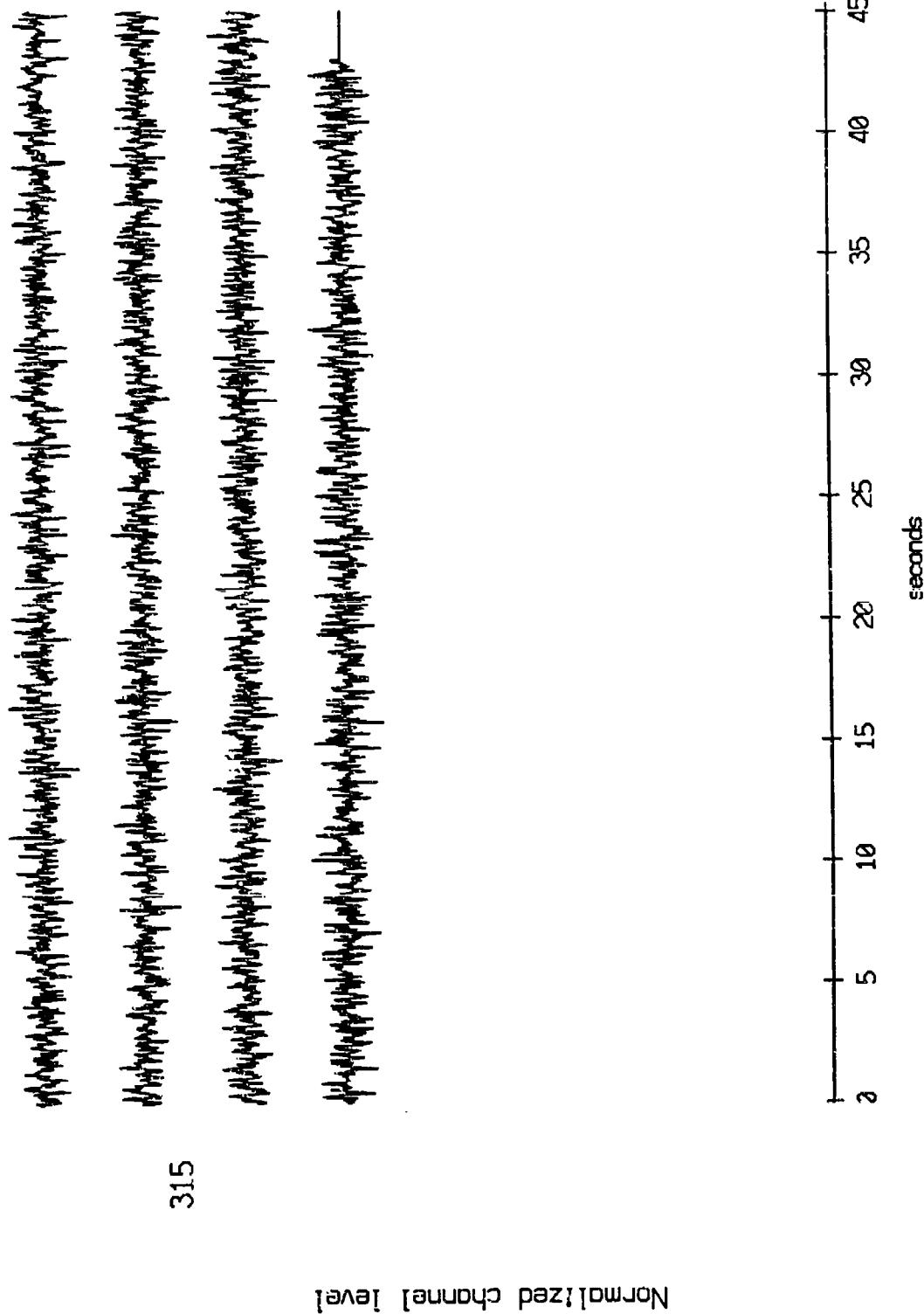


Figure X.10b.j

OBS 01, May, 1987 Trip - event 315 (z axis)
max gain-corrected amplitude is 0.596583 counts

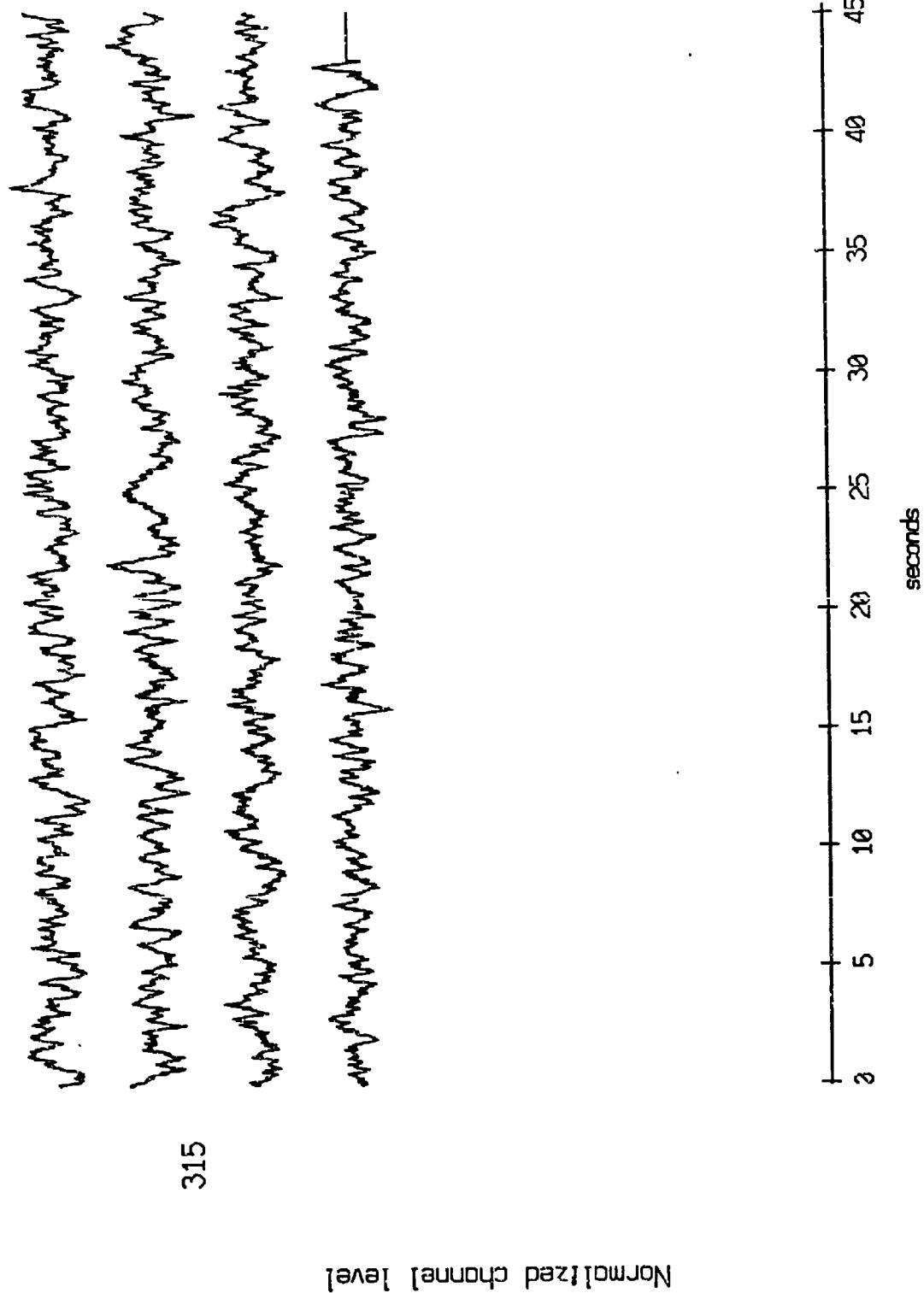
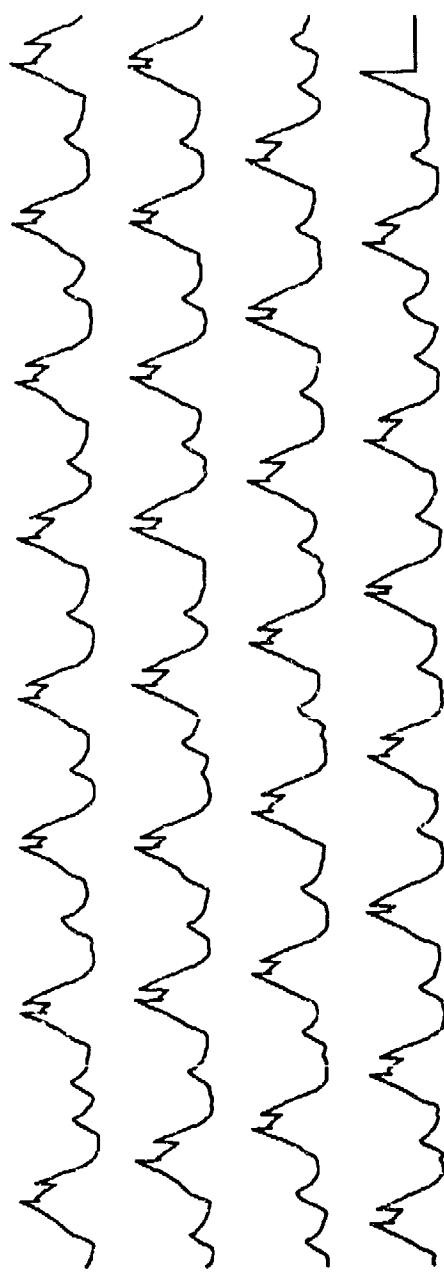


Figure X.10b.k

OBS 01, May, 1987 Trip - event 315 (pressure)
max gain-corrected amplitude is 206.3379 counts



Normalized channel level

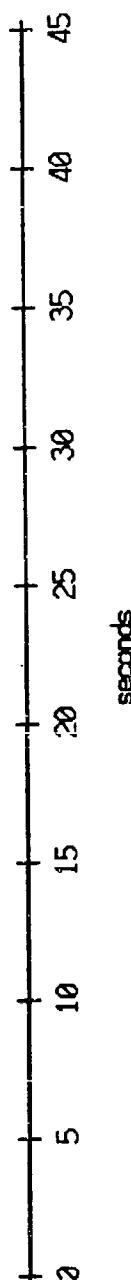


Figure X.10b.1

O3S 02, May, 1987 Trig - events 311 and 313 (x_axis)
max gain-corrected amplitude is 3.358027 counts

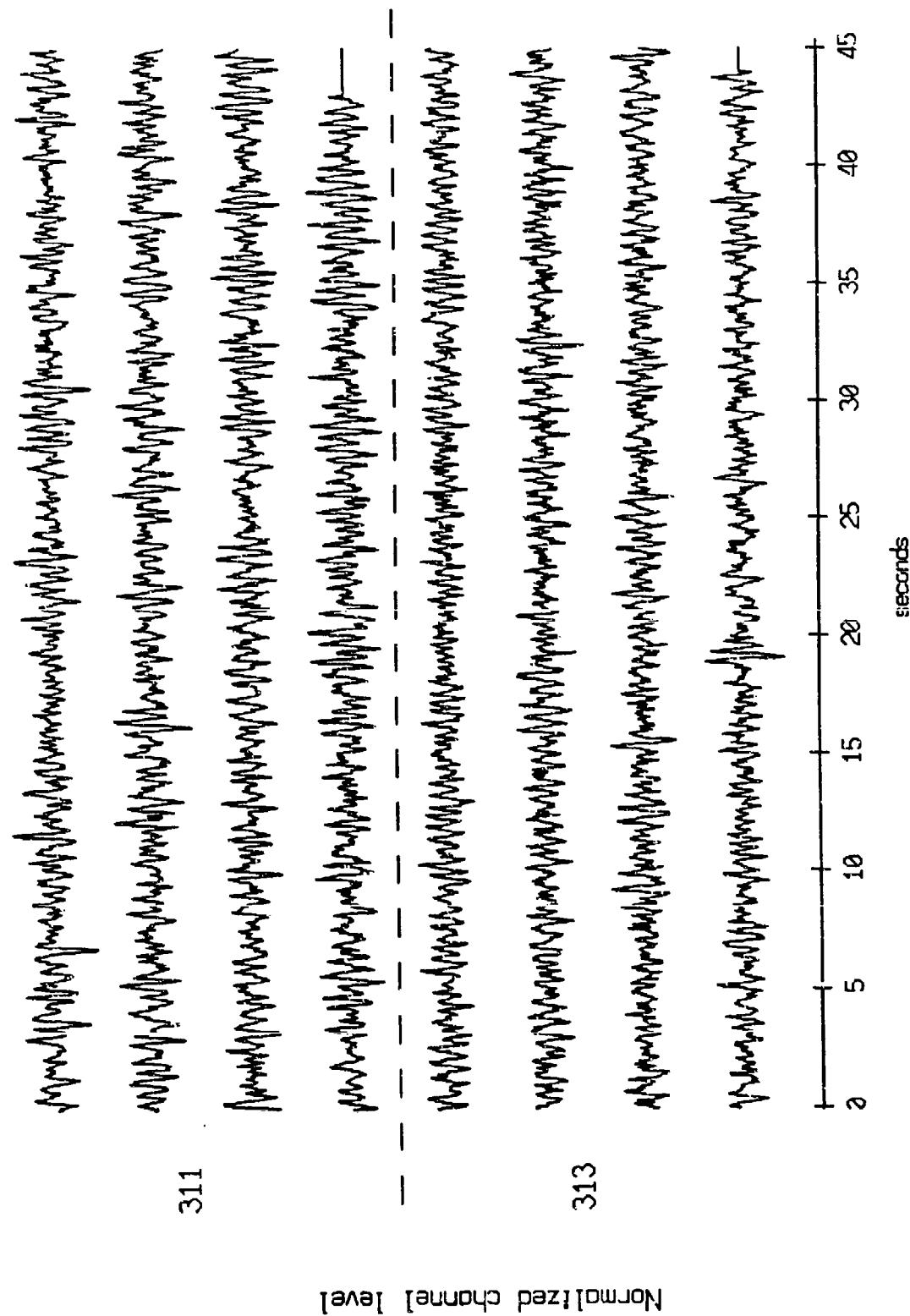


Figure X.11a.i

OBS 02, May, 1987 TriP - events 311 and 313 (y-axis)
max gain-corrected amplitude is 0.359147 counts

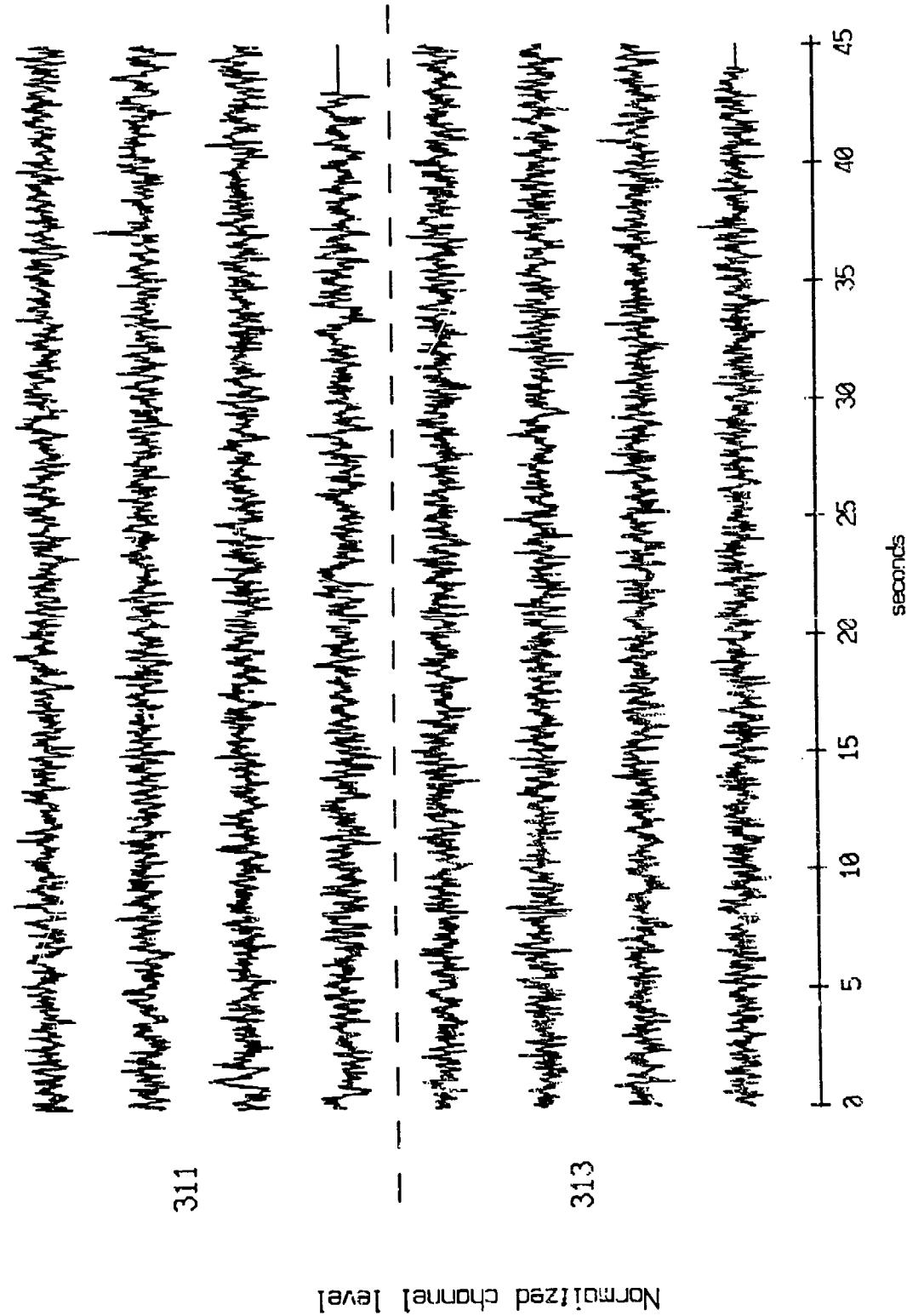
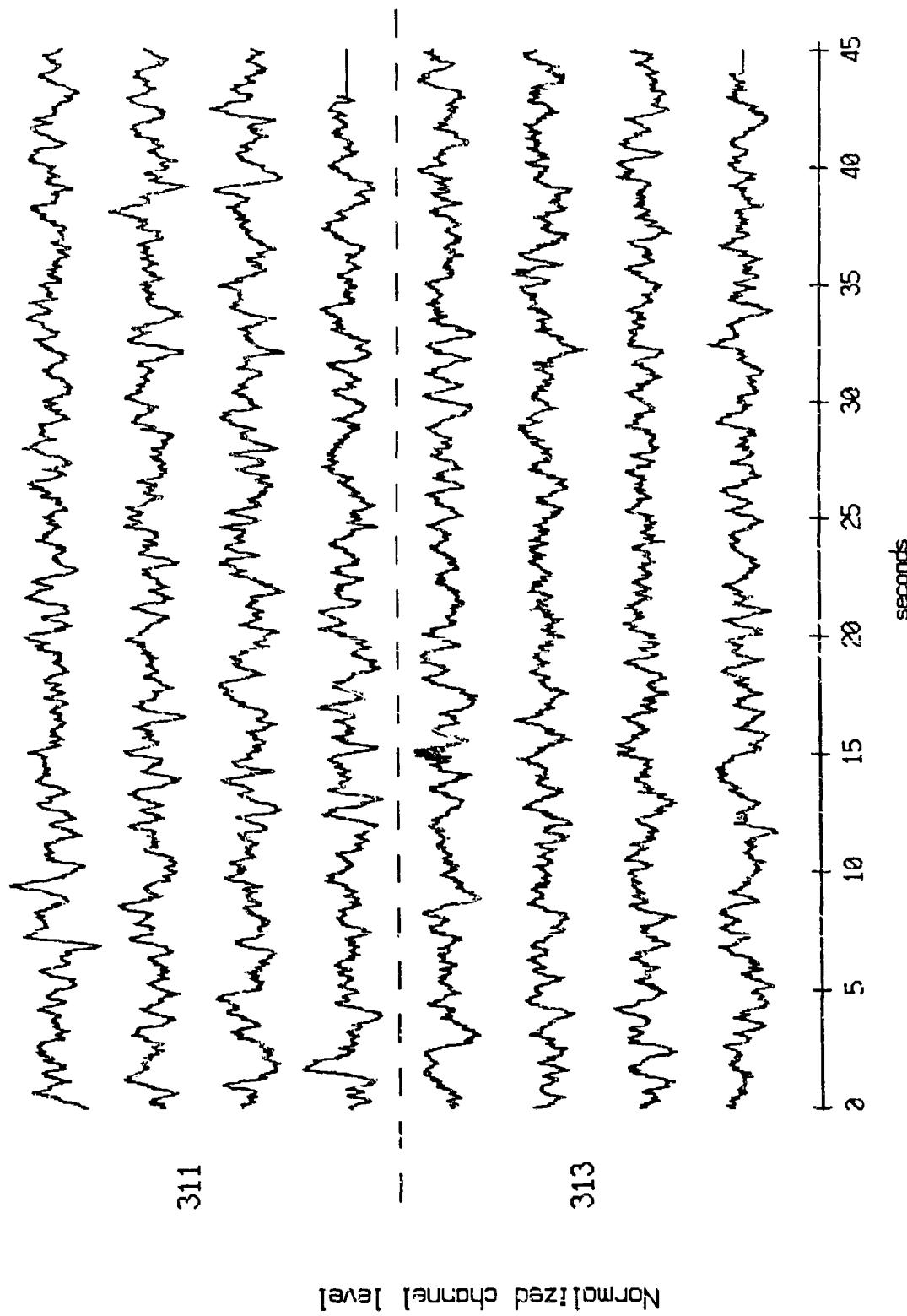


Figure X.11a.j

OBS 02, May, 1987 Trip - events 311 and 313 (z_axis)
max gain-corrected amplitude is 0.792119 counts



Normalized channel level

Figure X.11a.k

OBS 02, May, 1987 Trip - events 311 and 313 (pressure)
max gain-corrected amplitude is 1.731888 counts

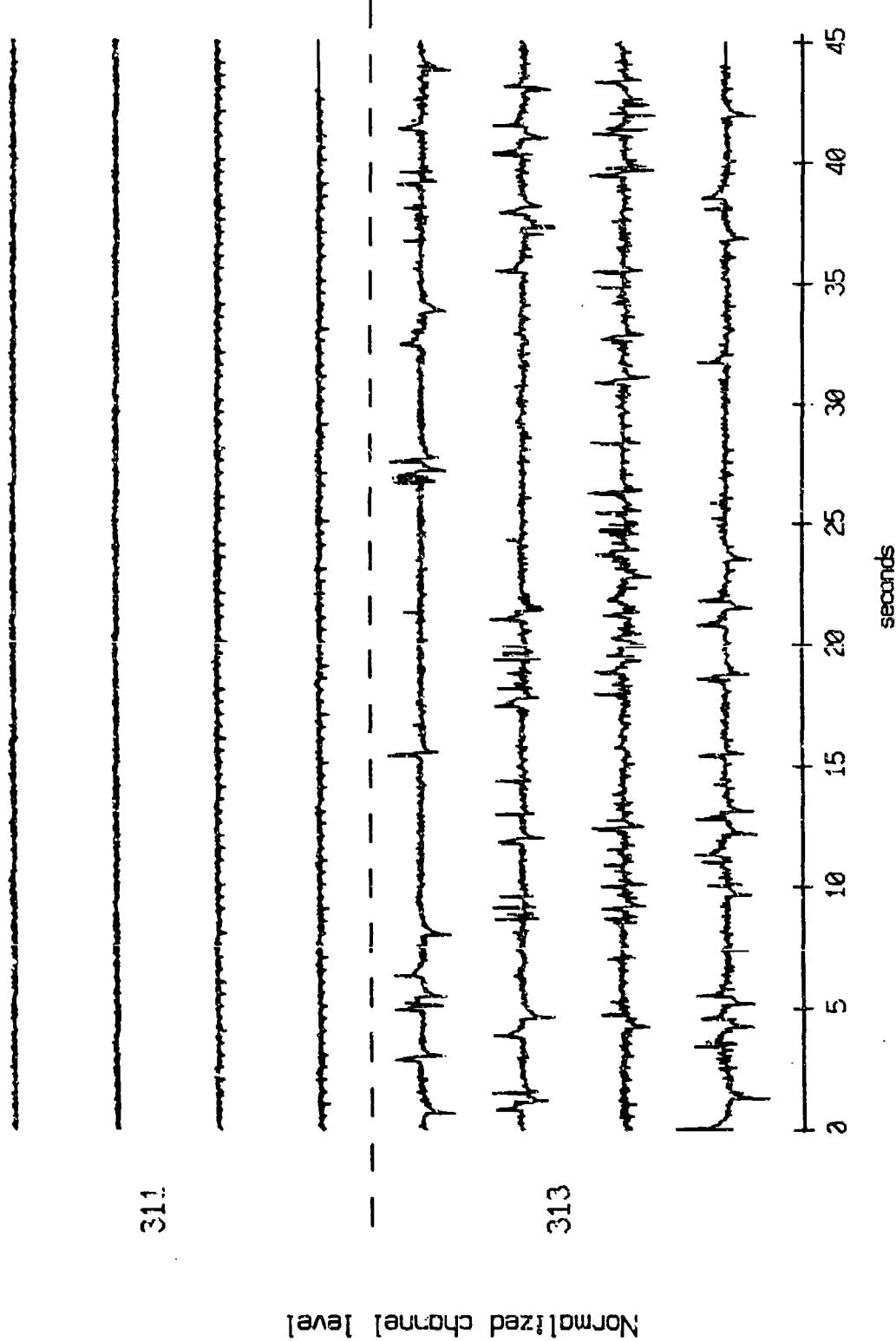
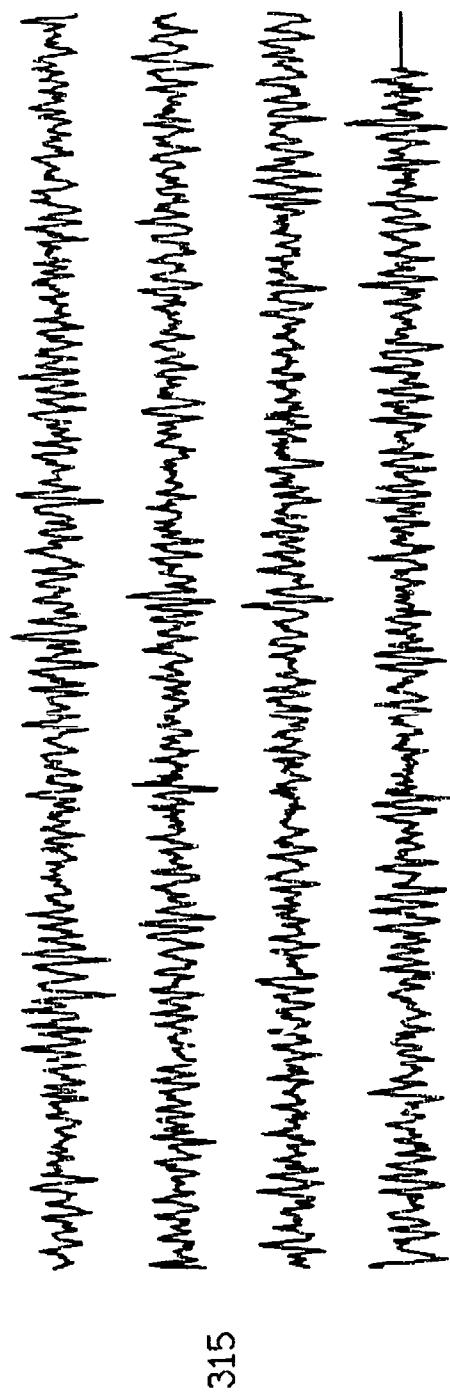


Figure X.11a.l

OBS 02, May, 1987 Trip - event 315 (x axis)
max gain-corrected amplitude is 3.252278 counts



Normalized channel level

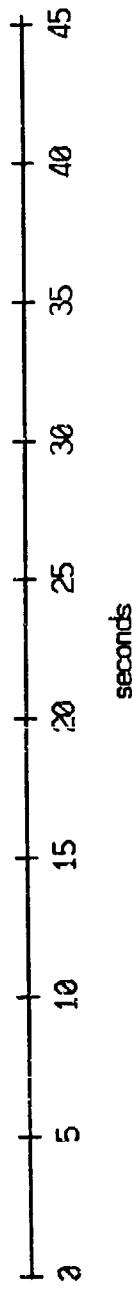
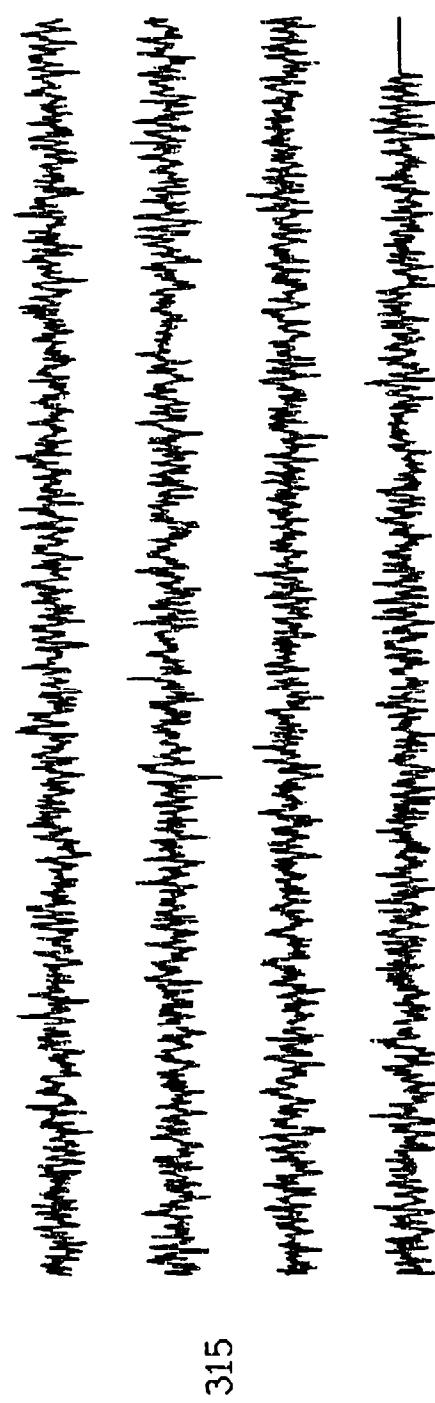


Figure X.11b.i

OBS 02, May, 1987 Trip - event 315 (γ axis)
max gain-corrected amplitude is 0.373114 counts



Normalized channel level

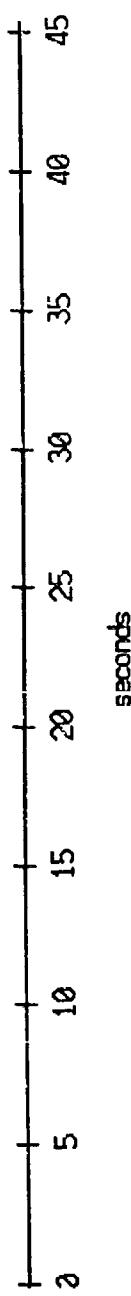


Figure X.11b.j

OBS 02, May, 1987 TRIP - event 315 (Z axis)
max gain-corrected amplitude is 0.598579 counts

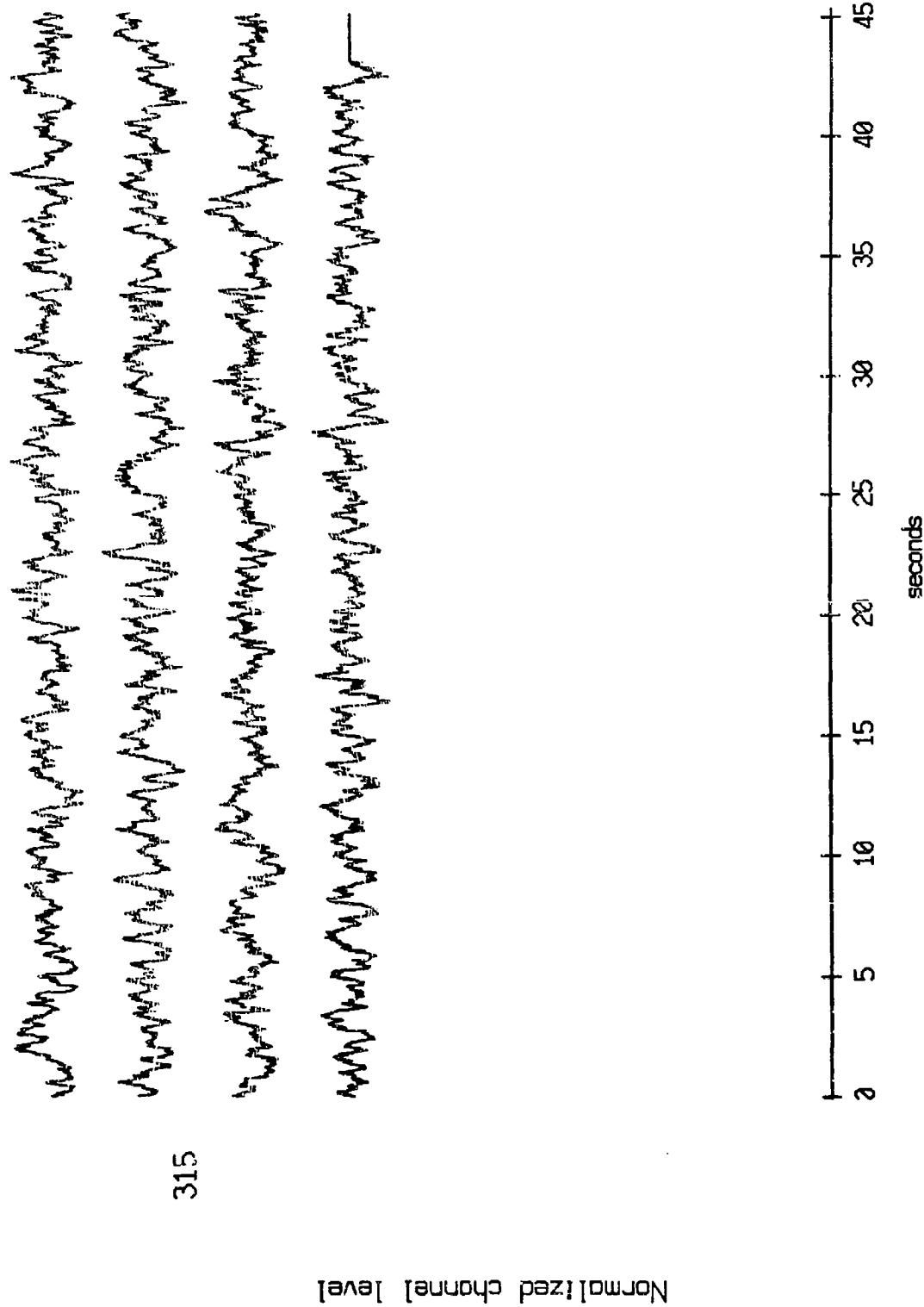
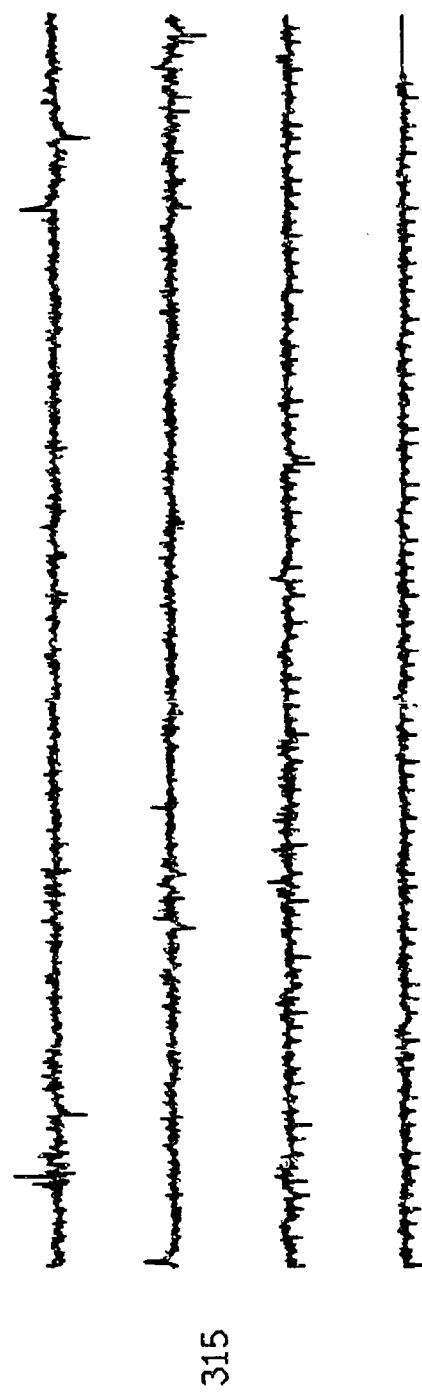


Figure X.11b.k

OBS 02, May, 1987 Trip - event 315 (pressure)
max gain-corrected amplitude is 0.971693 counts



NORMALIZED CHANNEL LEVEL

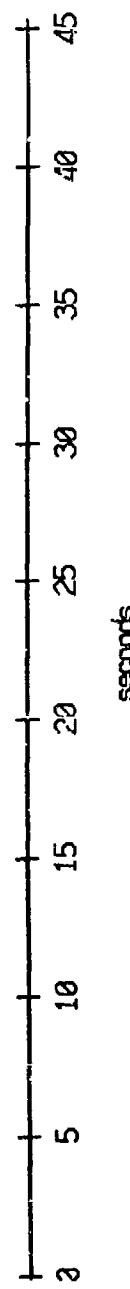


Figure X.11b.l

OBS 04, May, 1987 Trip - events 311 and 313 (x_axis)
max gain-corrected amplitude is 1.081432 counts

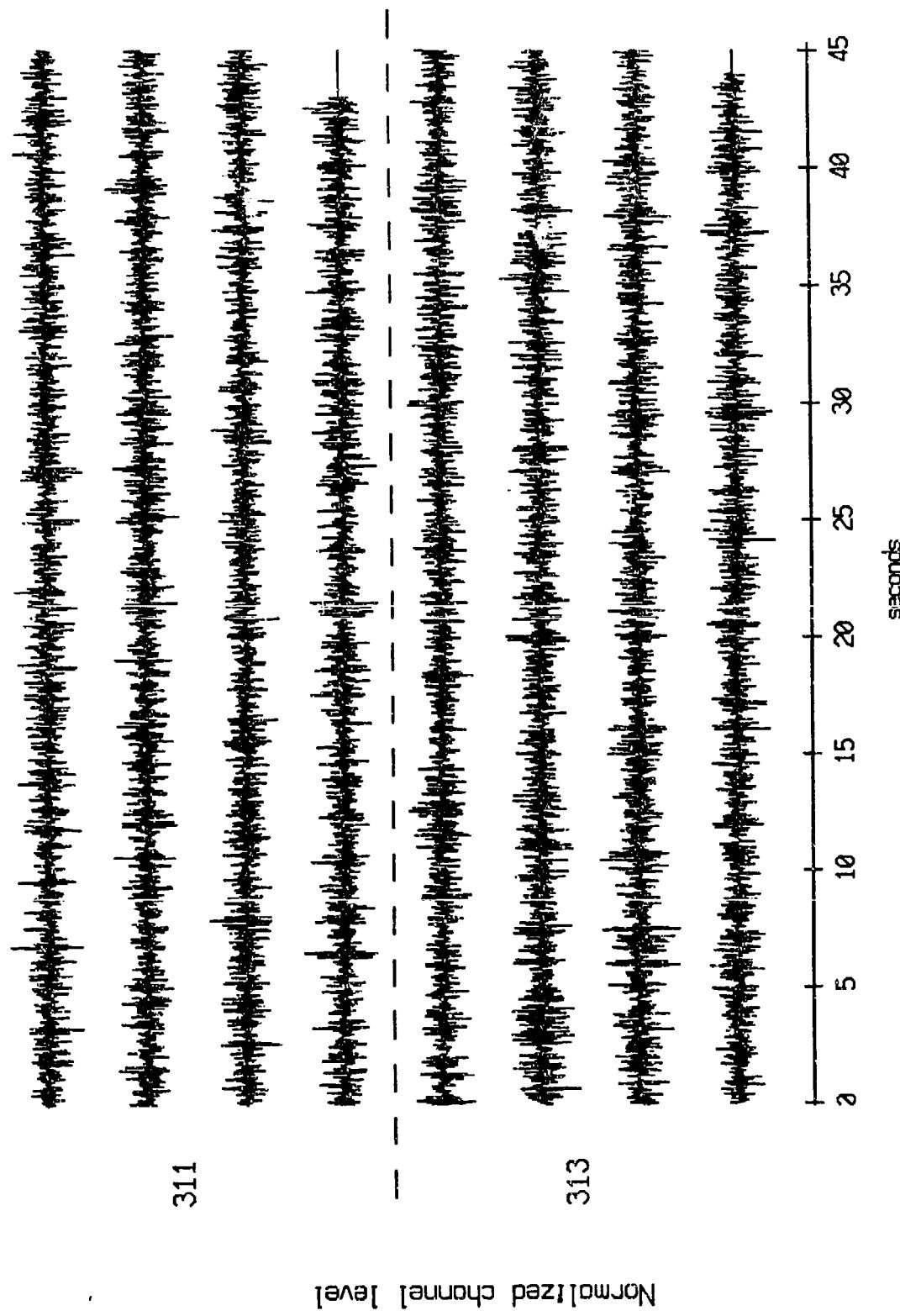


Figure X.12a.i

OBS 04, May, 1987 Trip - events 311 and 313 (y-axis)
max gain-corrected amplitude is 0.504801 counts

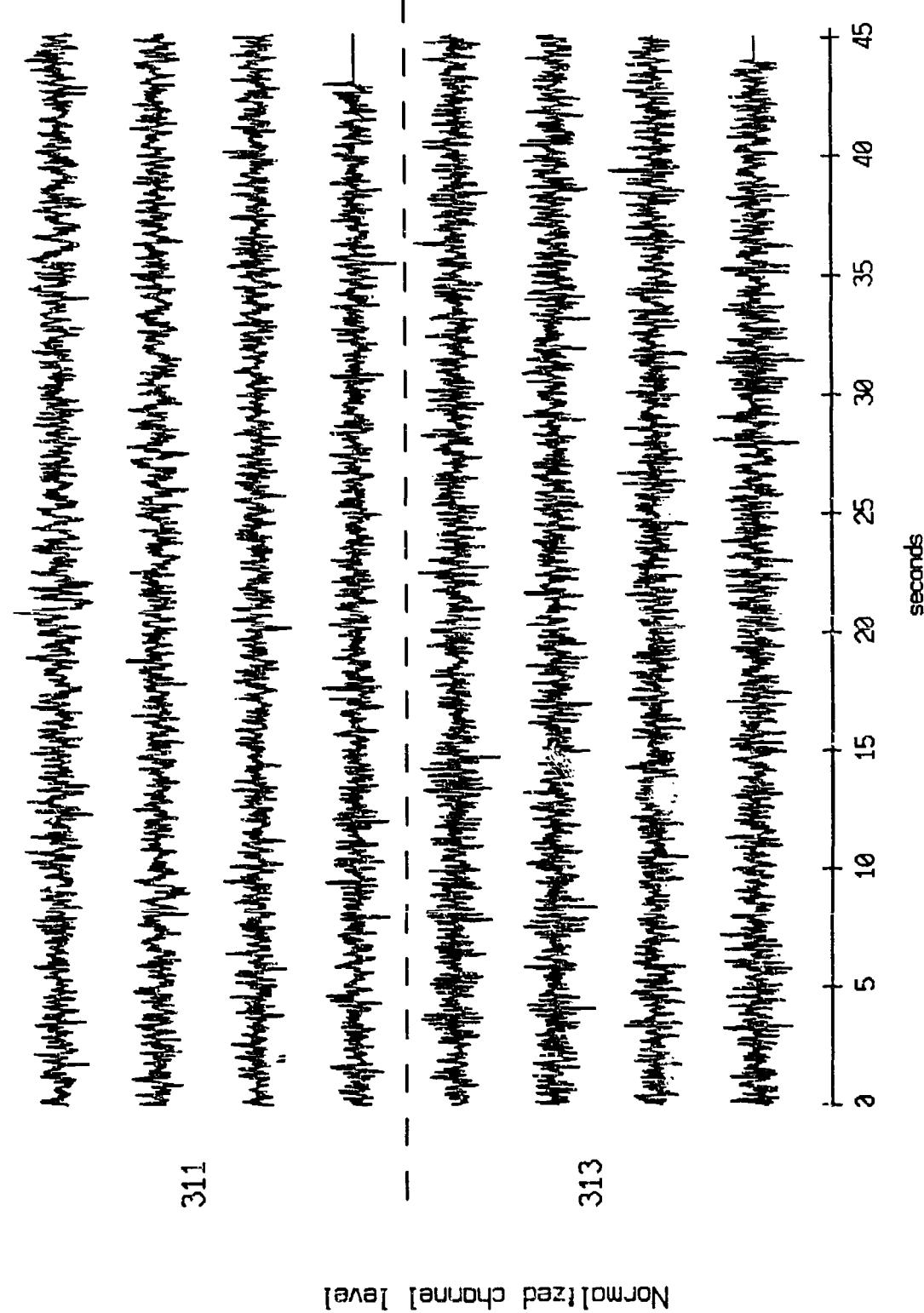
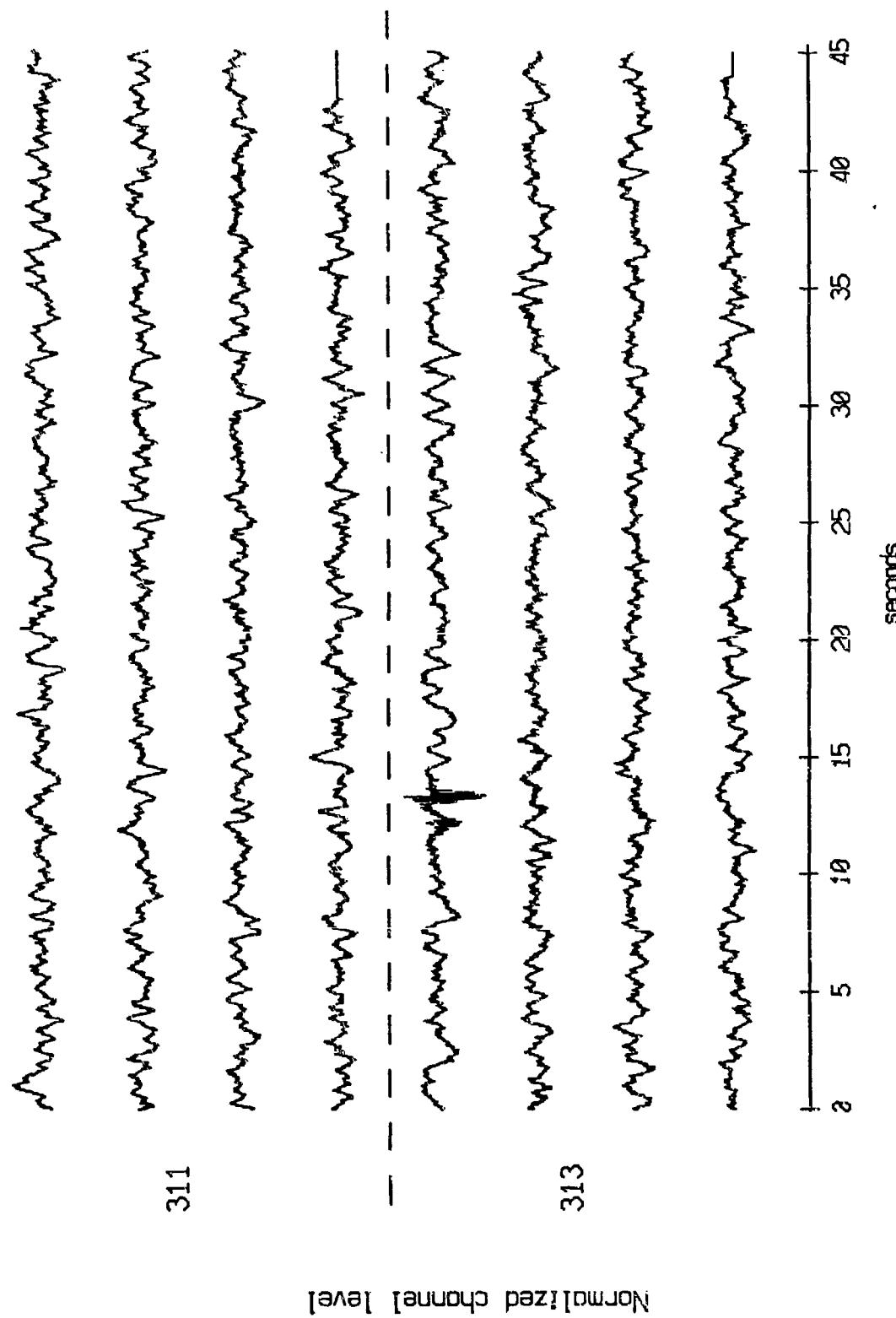


Figure X.12a.j

OBS 04, May, 1987 Trip - events 311 and 313 (z_axis)
max gain-corrected amplitude is 1.165233 counts



Normalized channel level

Figure X.12a.k

OBS 04, May, 1987 Trip - events 311 and 313 (pressure)
max gain-corrected amplitude is 4.086298 counts

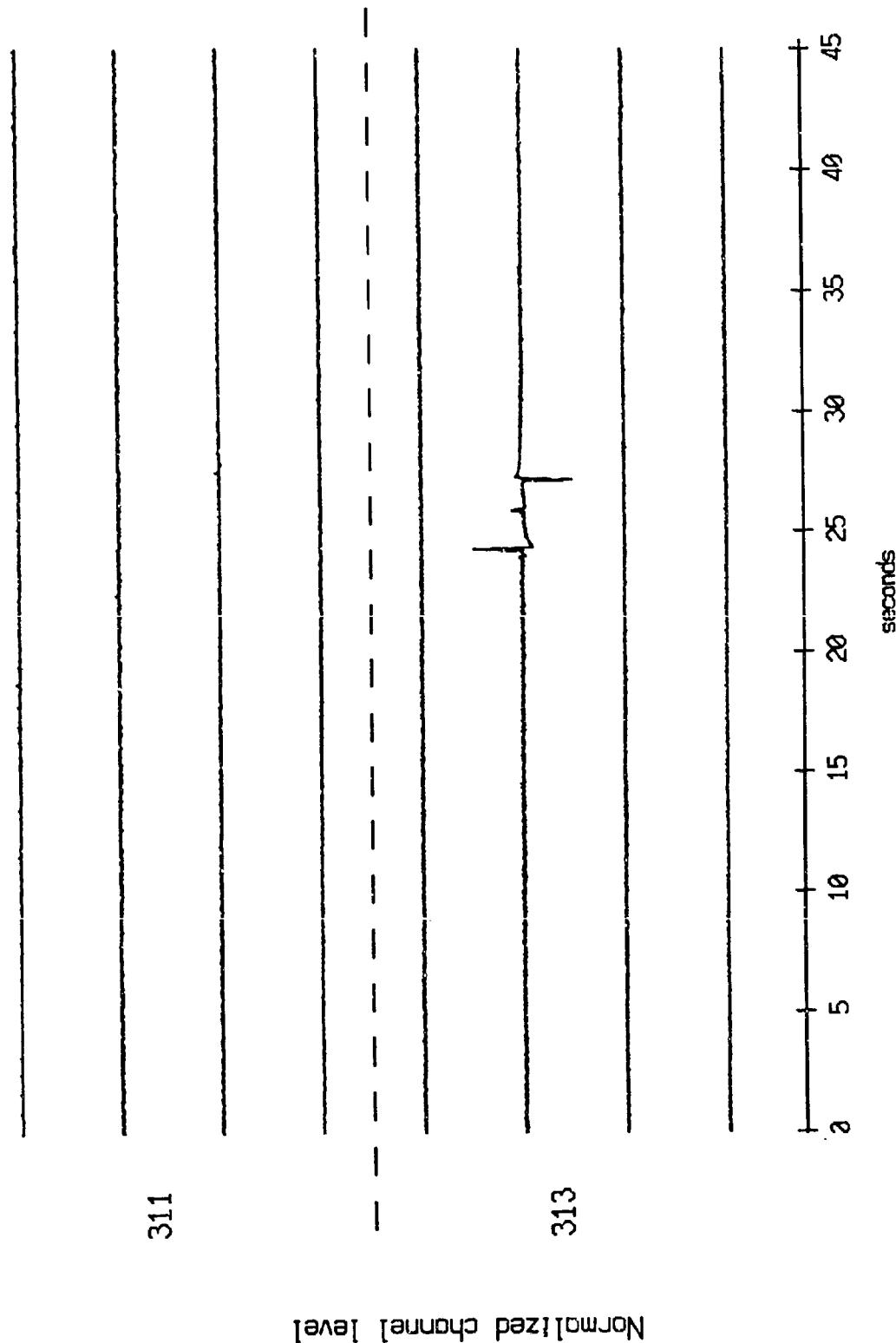


Figure X.12a.1

OBS 04, May, 1987 Trip - event 315 (x axis)
max gain-corrected amplitude is 1.039532 counts

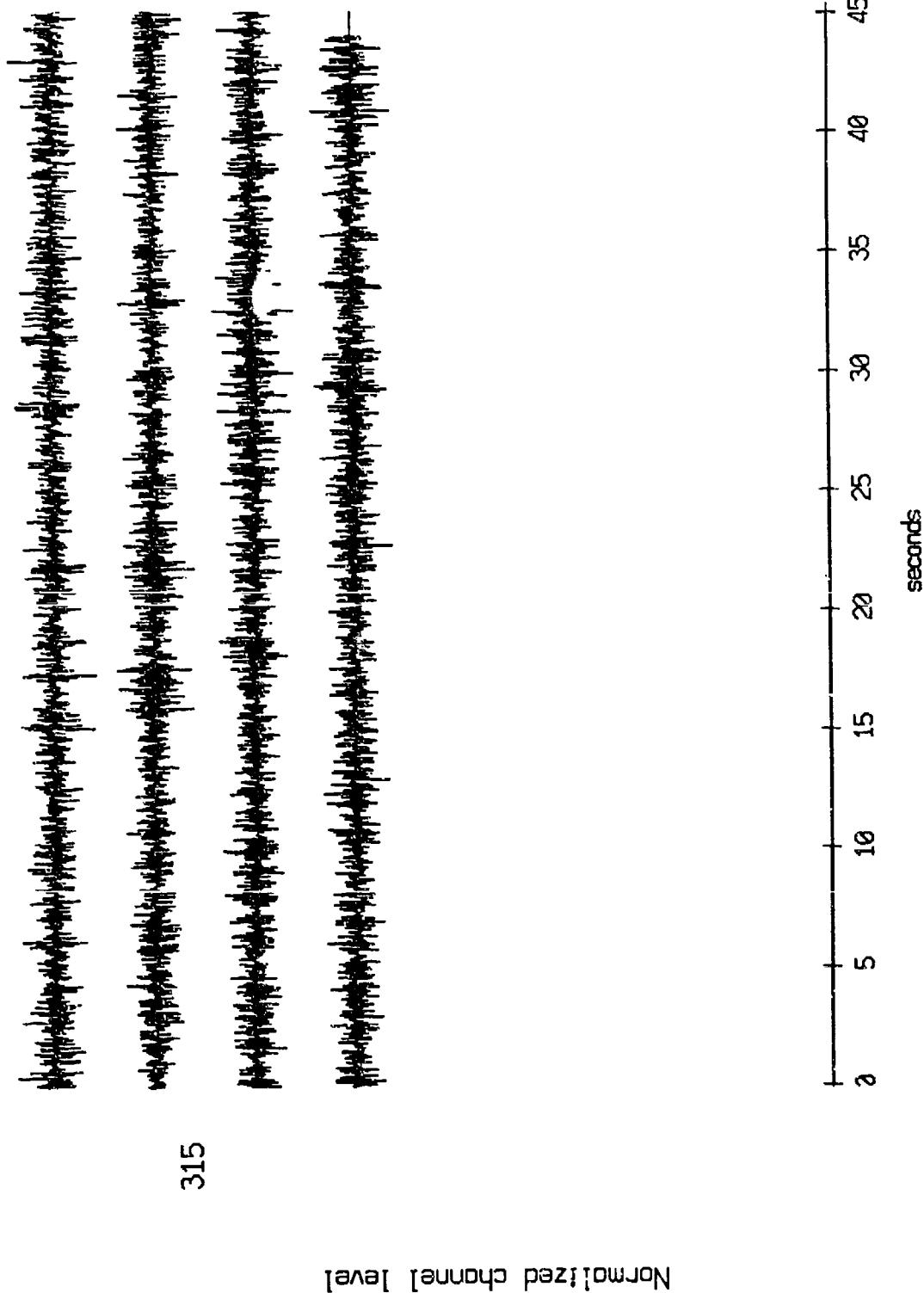
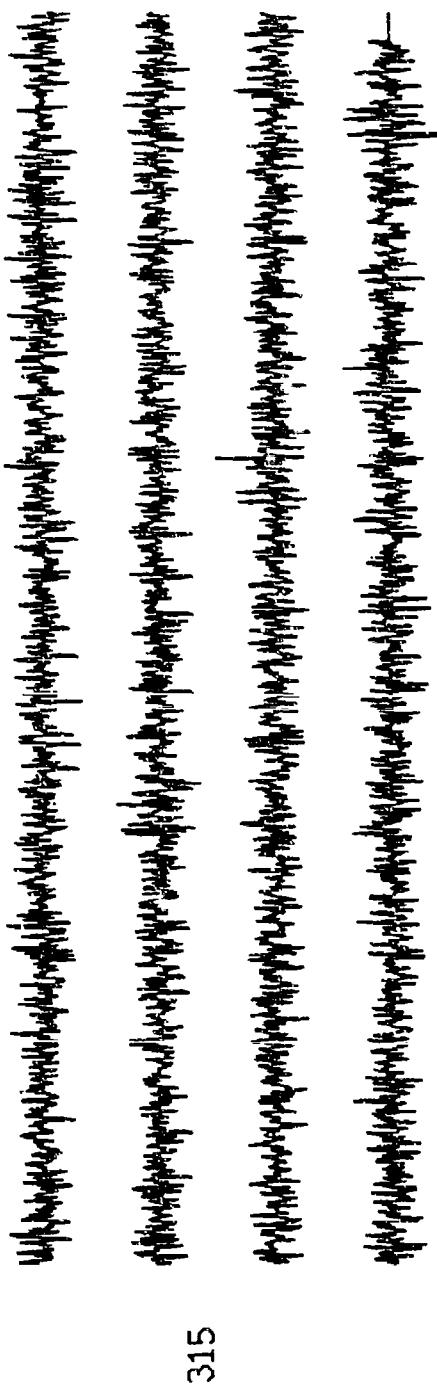


Figure X.12b.i

OBS 04, May, 1987 Trip - event 315 (γ axis)
max gain-corrected amplitude is 0.534730 counts



NORMALIZED CHANNEL LEVEL

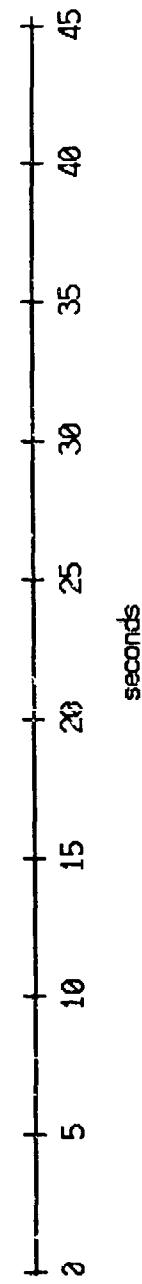


Figure X.12b.j

OBS 04, May, 1987 Trip - event 315 (Z axis)
max gain-corrected amplitude is 0.540716 counts

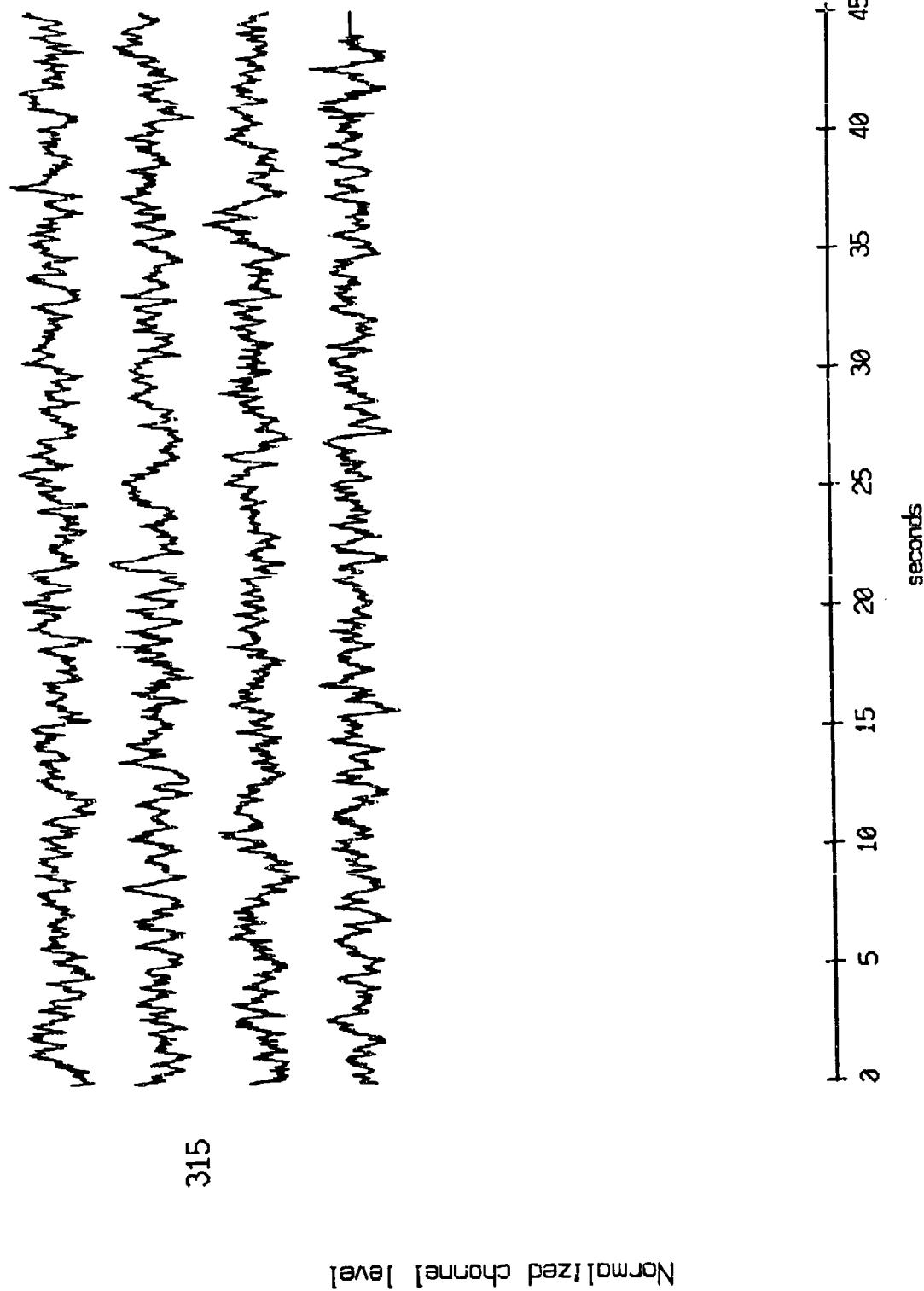


Figure X.12b.k

OBS 04, May, 1987 Trip - event 315 (pressure)
max gain-corrected amplitude is 4.086298 counts

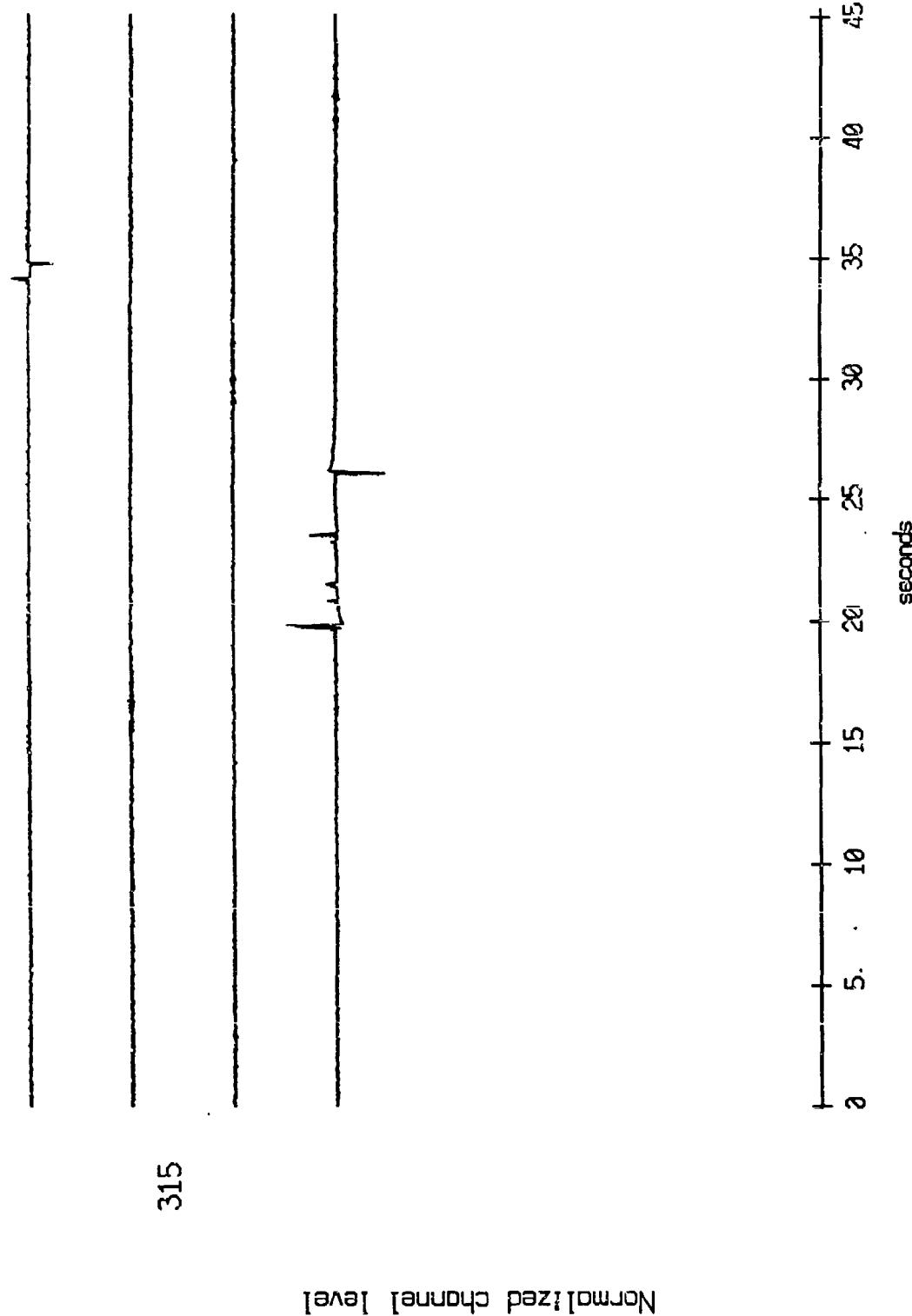
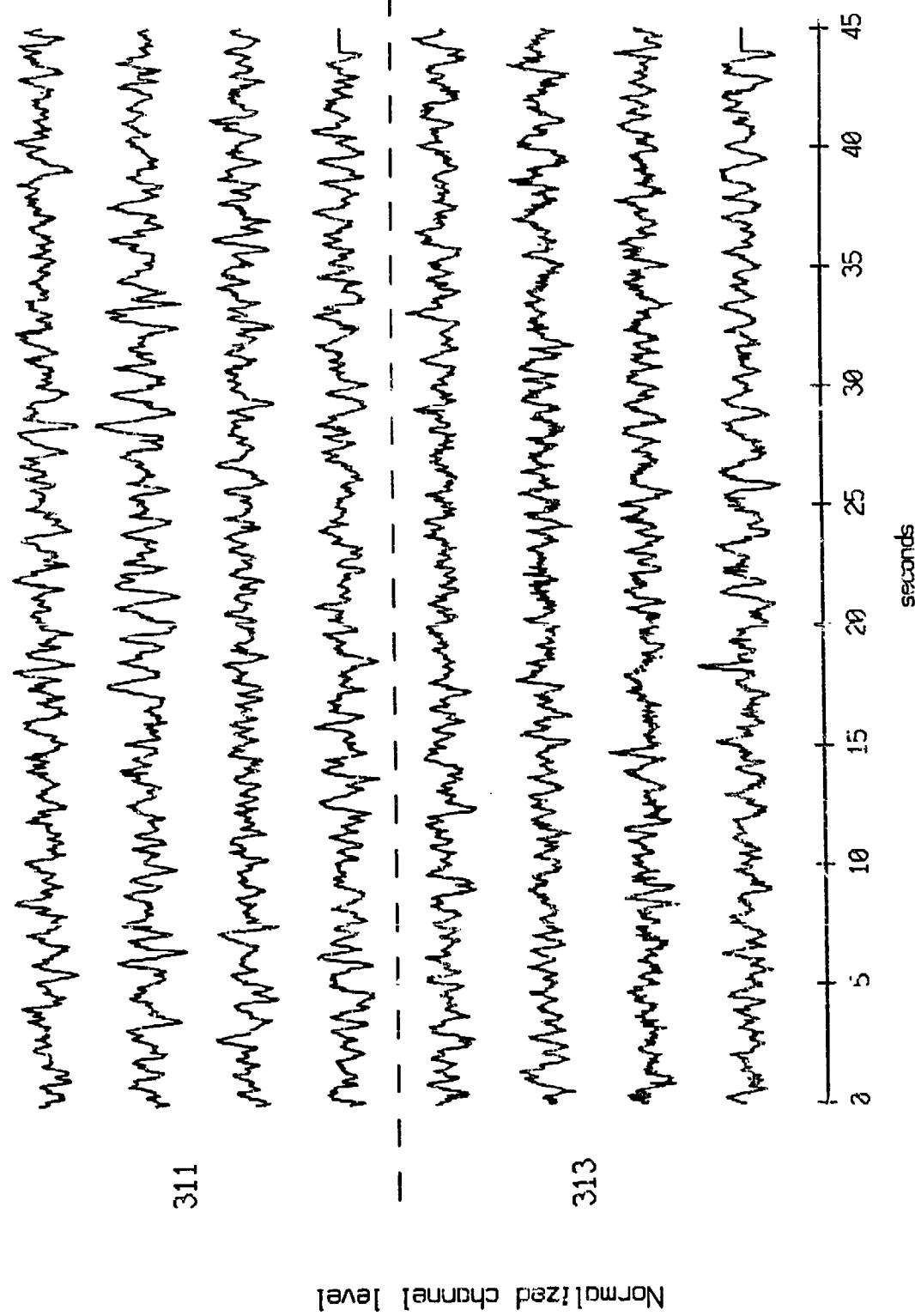


Figure X.12b.l

OBS 05, May, 1987 TriP - events 311 and 313 (x_axis)
max gain-corrected amplitude is 3,968577 counts



Normalized channel level

Figure X.13a.i

085 05, May, 1987 Trip - events 311 and 313 (y-axis)
max gain-selected amplitude is 3.794989 counts

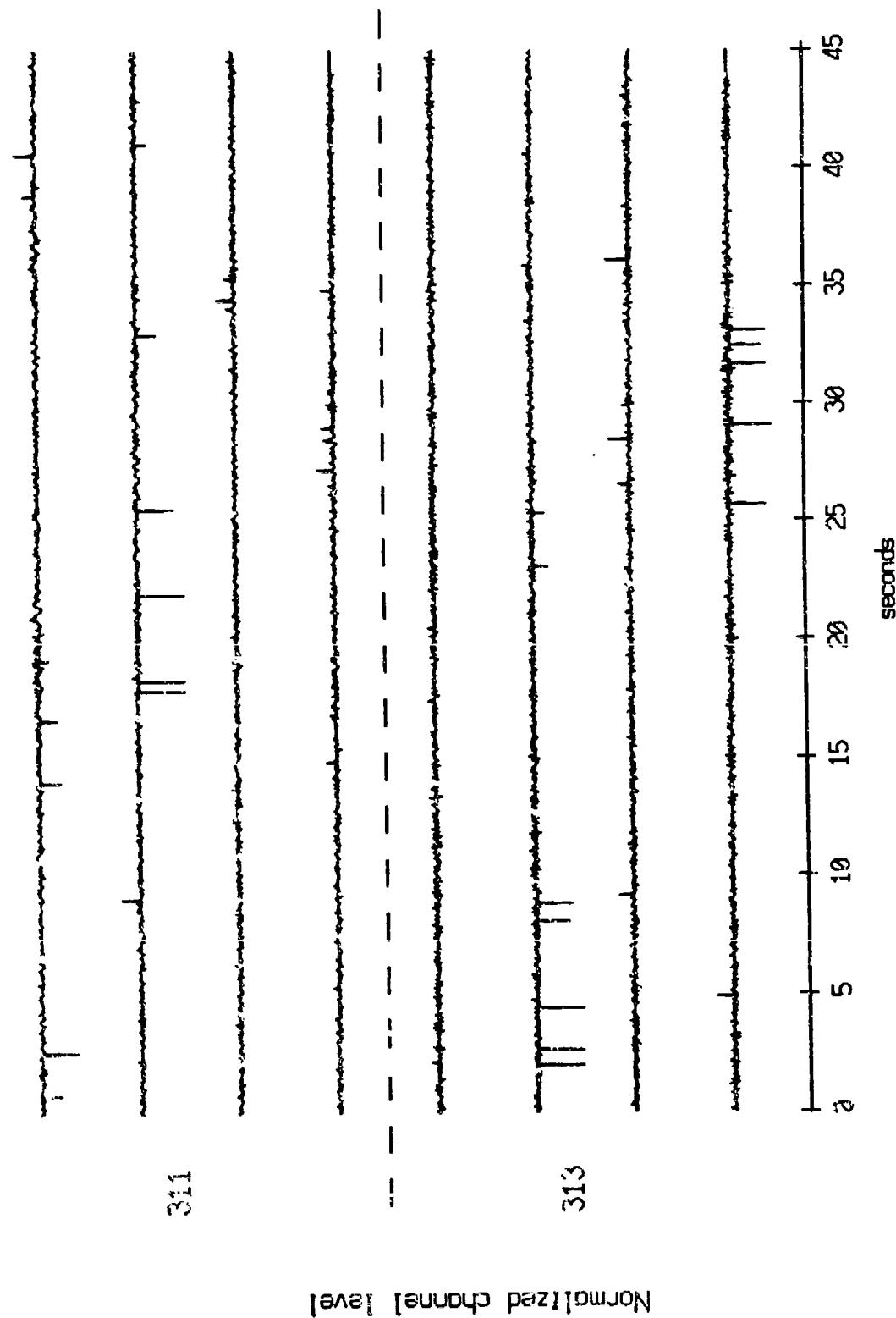


Figure X.13a.j

OBS 05, May, 1987 Trip - events 311 and 313 (z_axis)
max gain-corrected amplitude is 2.563912 counts

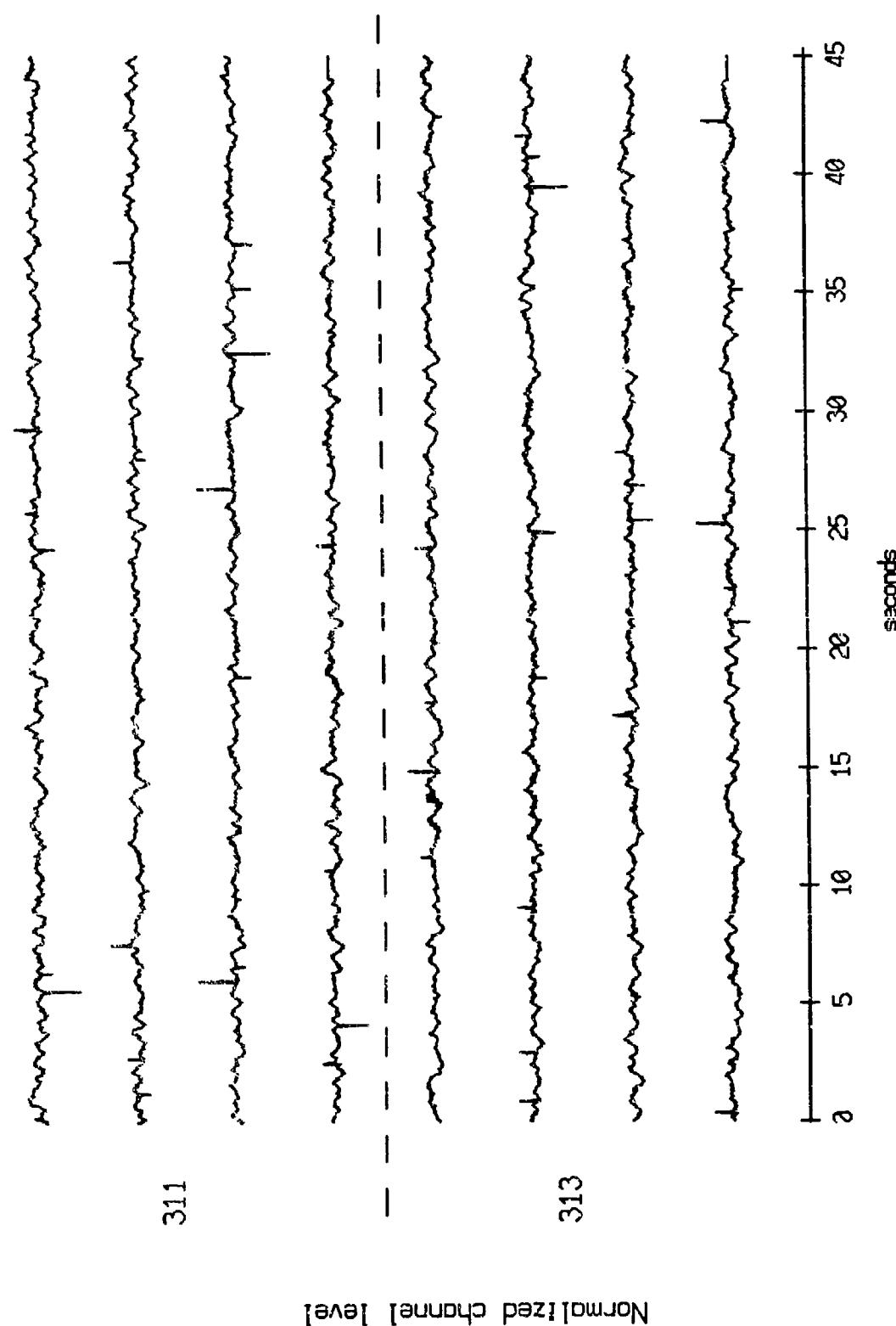
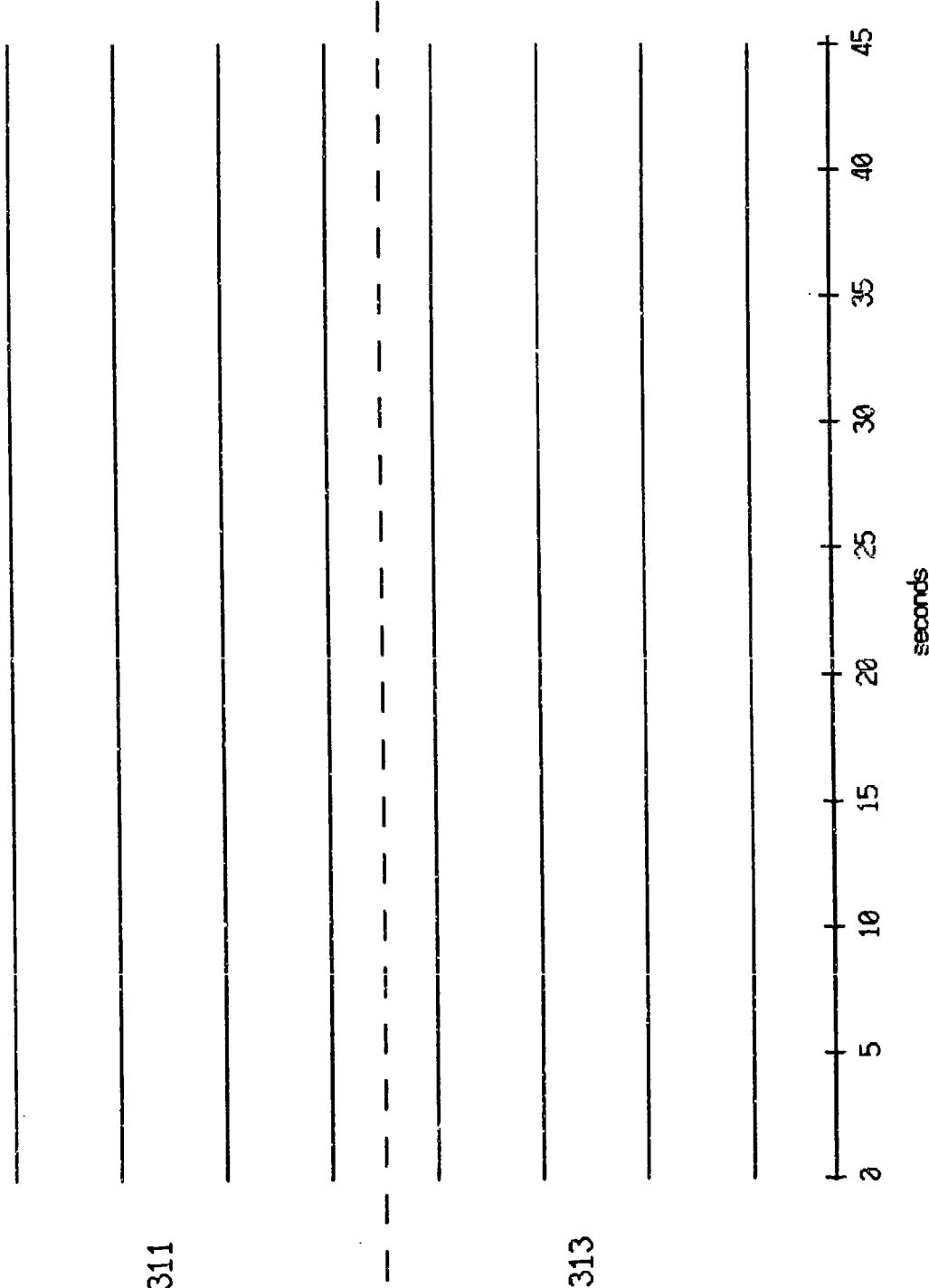


Figure X.13a.k

OBS 05, May, 1987 Trip - events 311 and 313 (pressure)
max gain-corrected amplitude is 0. counts



Normalized channel level

Figure X.13a.1

OBS 05, May, 1987 Trip - events 314 and 315 (x_axis)
max gain-corrected amplitude is 3.298169 counts

314

Normalized channel level

315

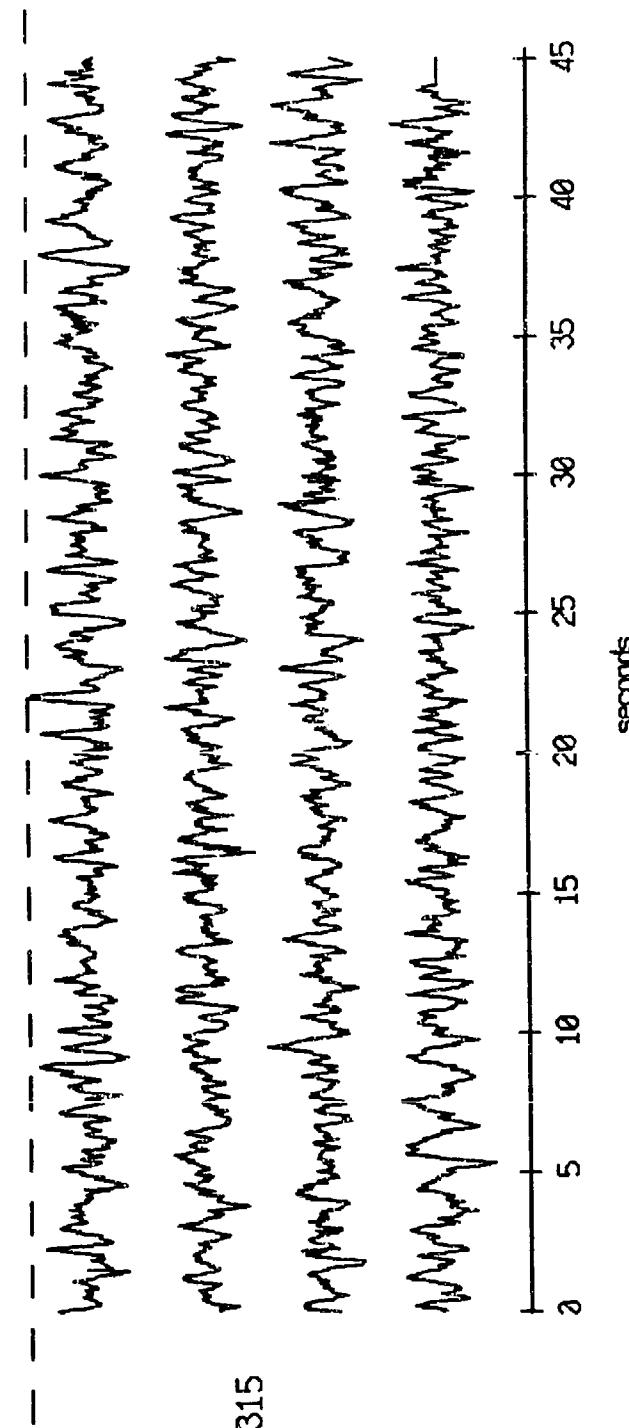
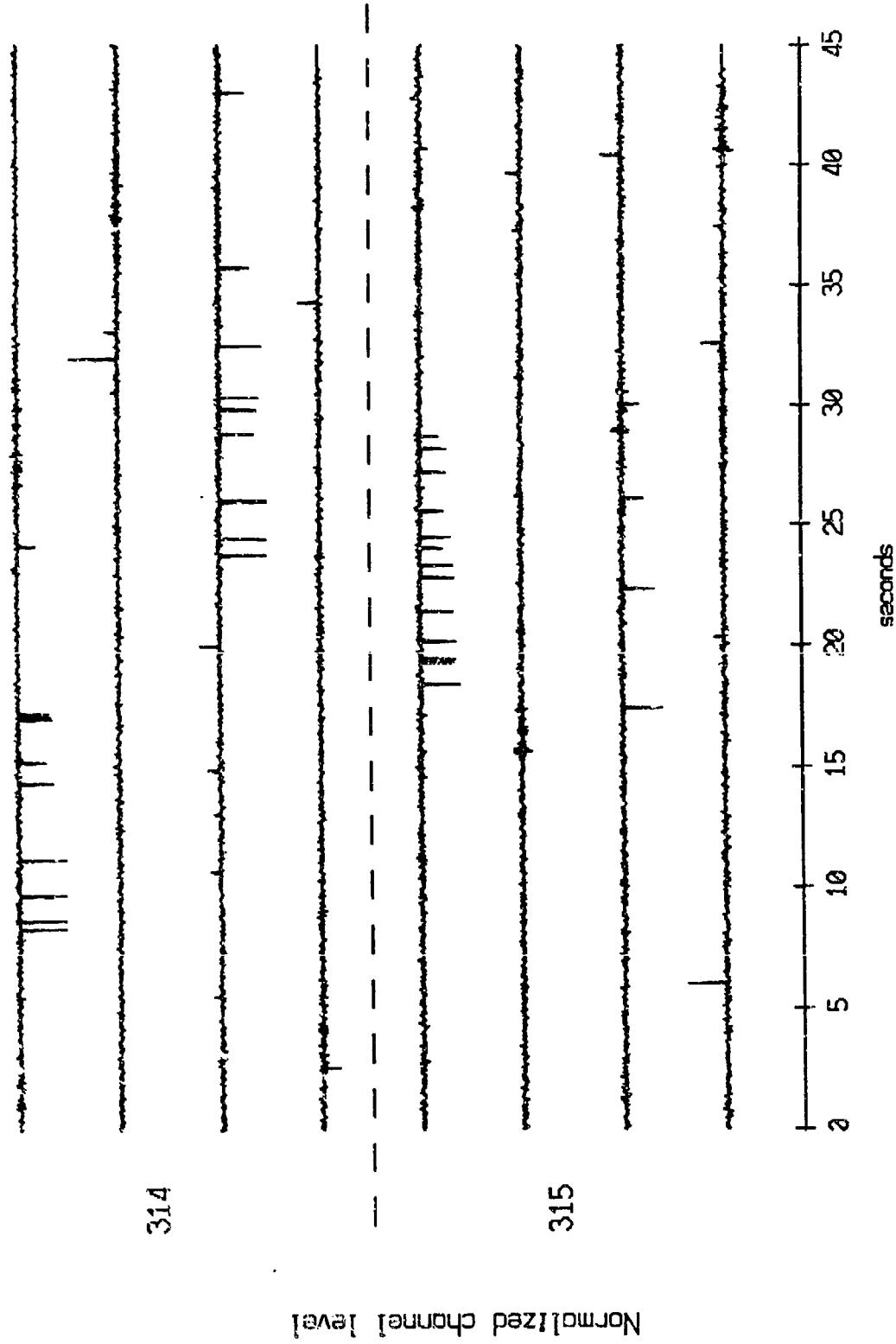


Figure X.13b.i

CBS 05, May, 1987 Trip - events 314 and 315 (y-axis)
Max gain-corrected amplitude is 3.960596 counts



Normalized channel level

Figure X.13b.j

OBS 05, May, 1987 Trip - events 314 and 315 (z_axis)
max gain-corrected amplitude is 2.454173 counts

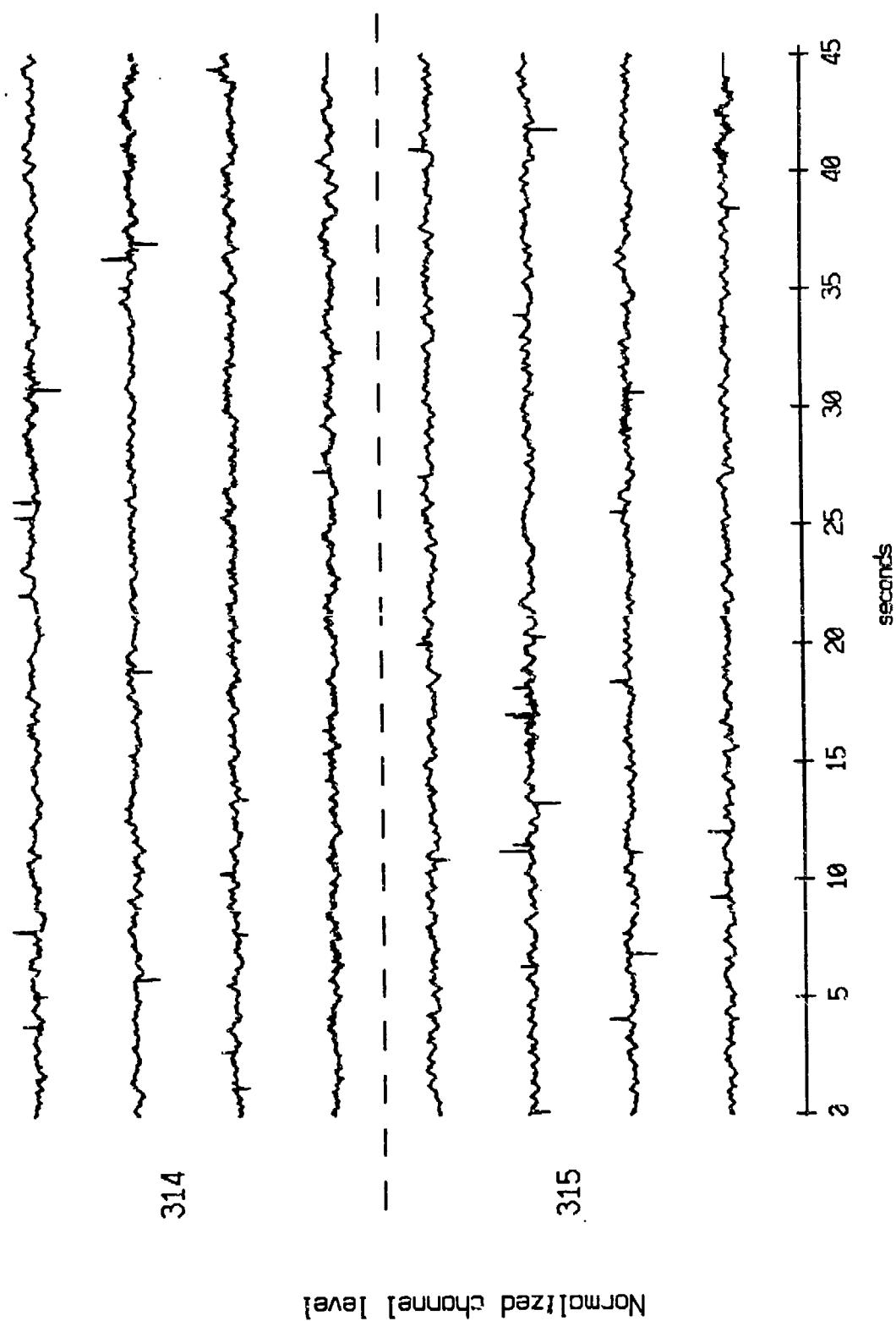


Figure X.13b.k

OBS 05, May, 1987 Trip - events 314 and 315 (pressure)
max gain-corrected amplitude is 0. counts

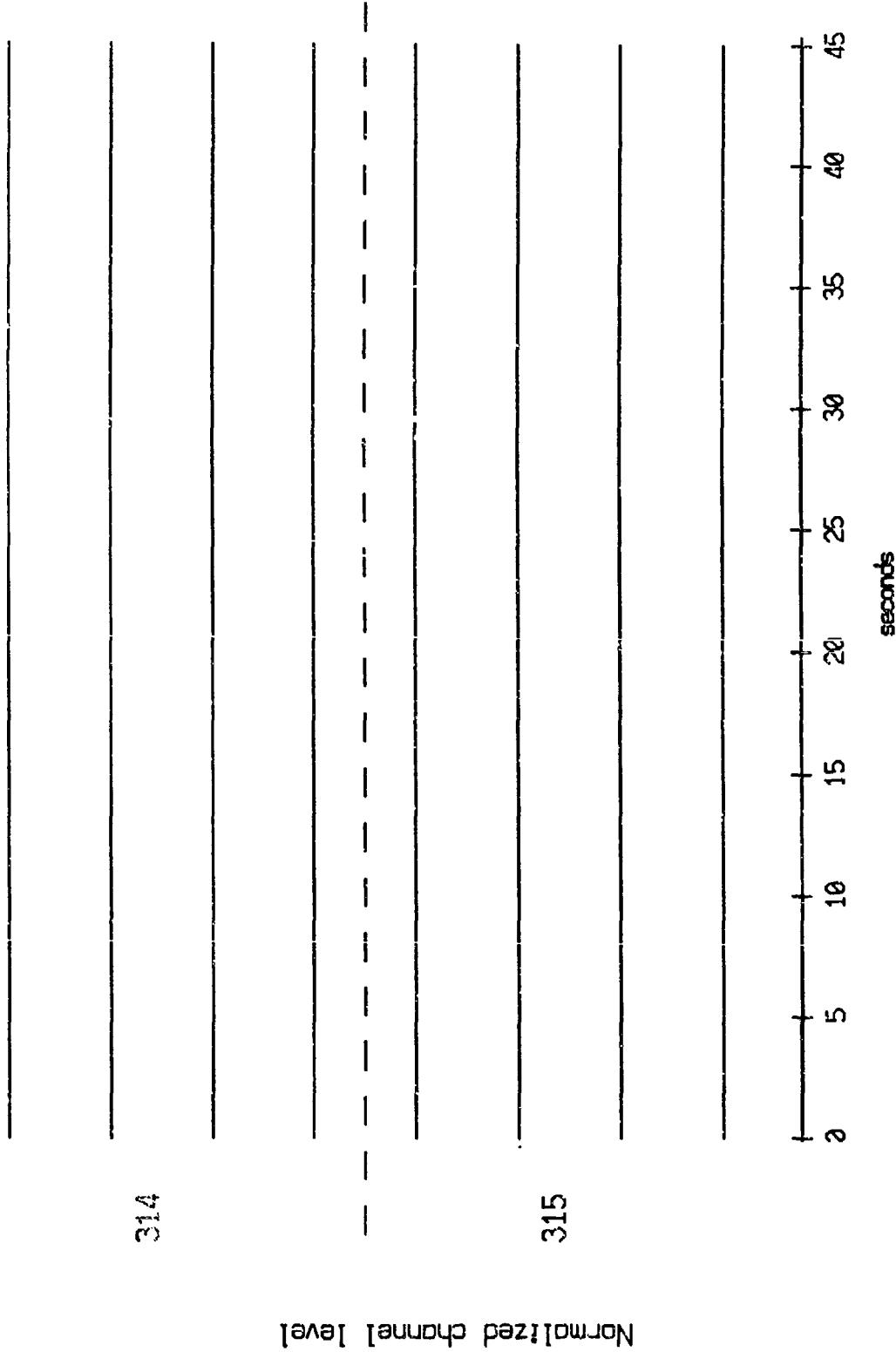
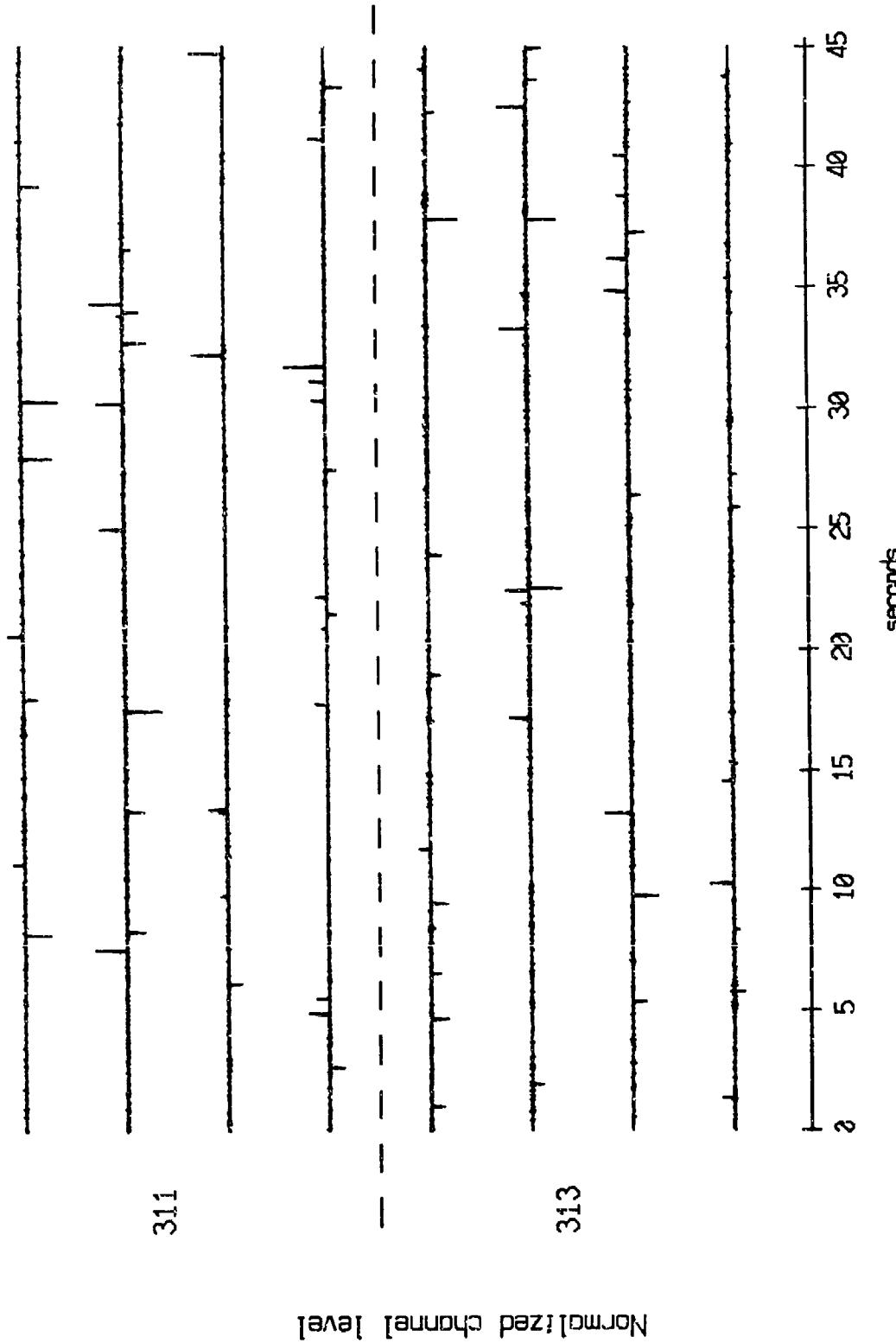


Figure X.13b.1

OBS 06, May, 1987 Trip - events 311 and 313 (x-axis)
max gain-corrected amplitude is 2.418258 counts



Normalized channel level

Figure X.14a.i

OBS 06, May, 1987 Trip - events 311 and 313 (y-axis)
max gain-corrected amplitude is 3.286197 counts

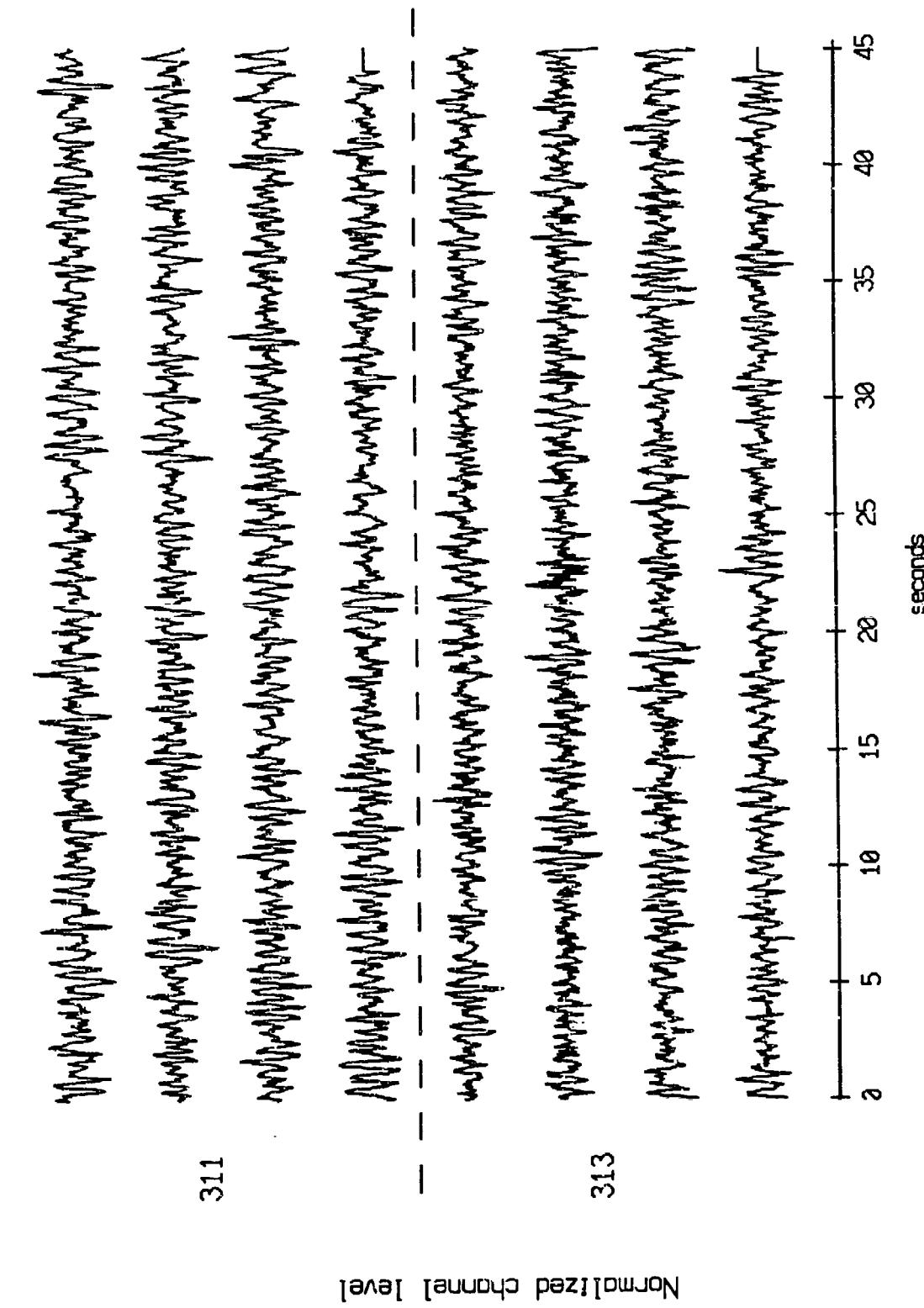


Figure X.14a.j

OBS 06, May, 1987 TriP - events 311 and 313 (z-axis)
max gain-corrected amplitude is 4.088293 counts

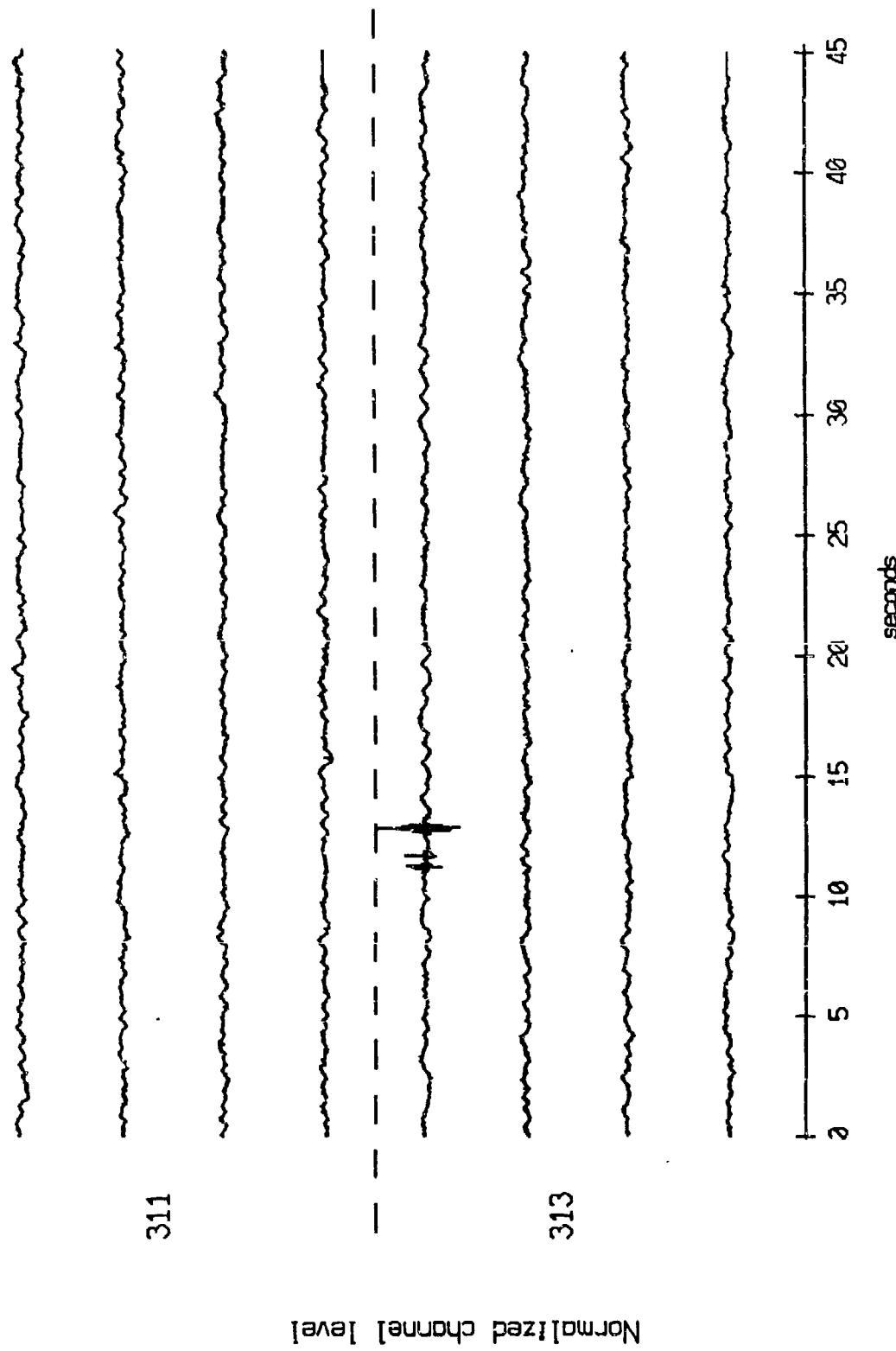


Figure X.14a.k

OBS 06, May, 1987 Trip - events 311 and 313 (pressure)
max gain-corrected amplitude is 39.59172 counts

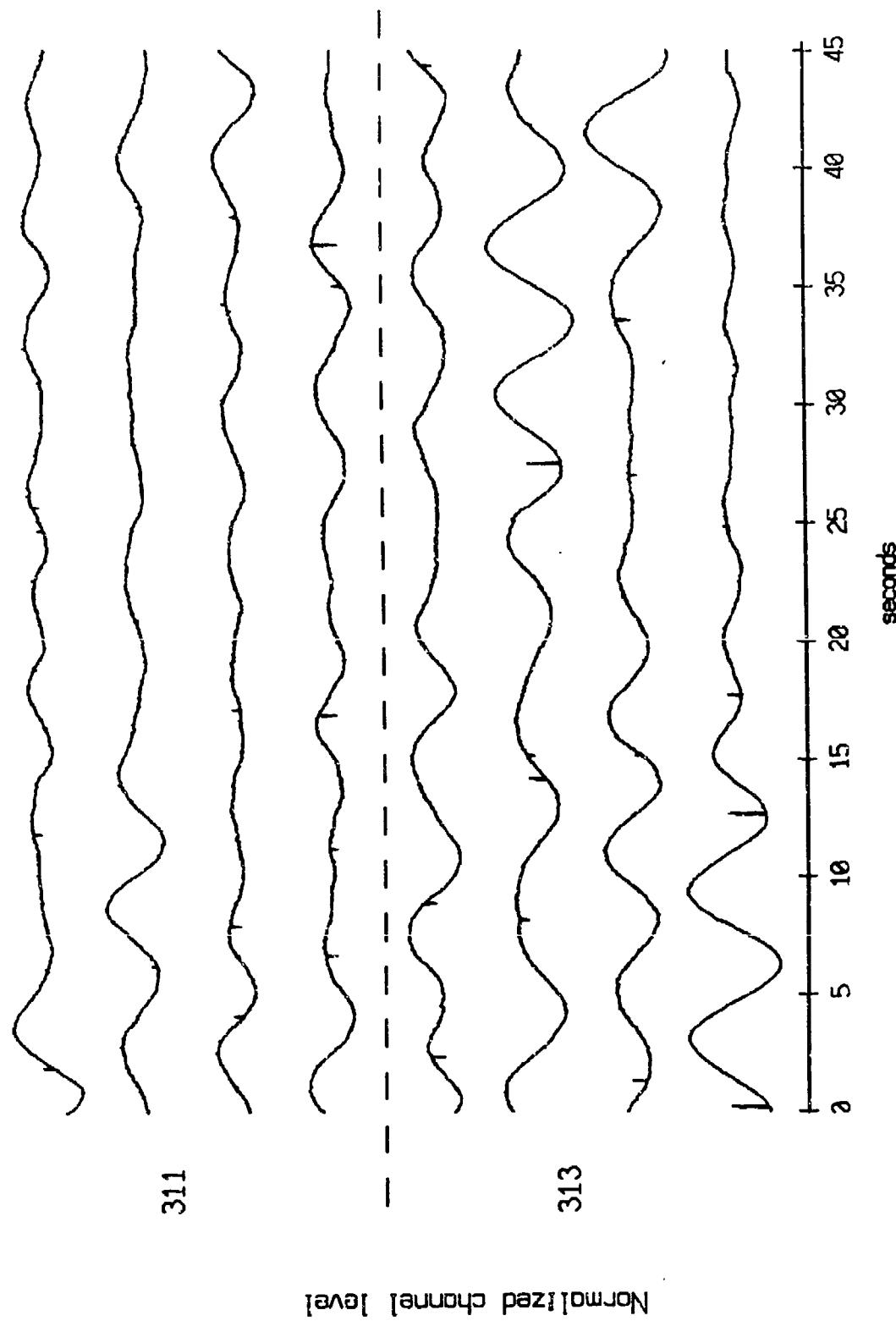


Figure X.14a.l

OBS 06, May, 1987 Trip - events 314 and 315 (x_axis)
max gain-corrected amplitude is 3.32410^7 counts

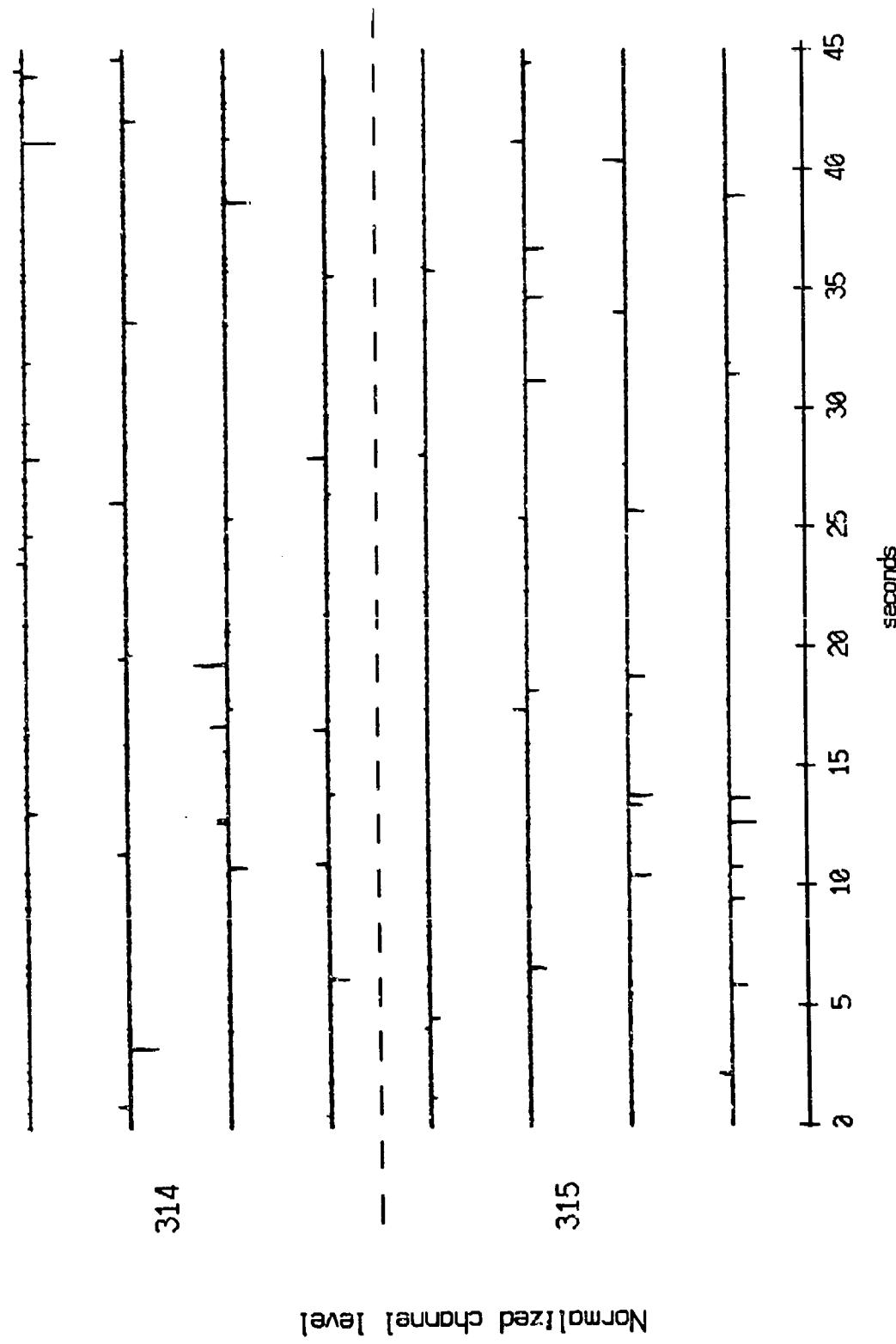


Figure X.14b.i

OBS 06, May, 1987 Trip - events 314 and 315 (y-axis)
max gain-corrected amplitude is 3.725155 counts

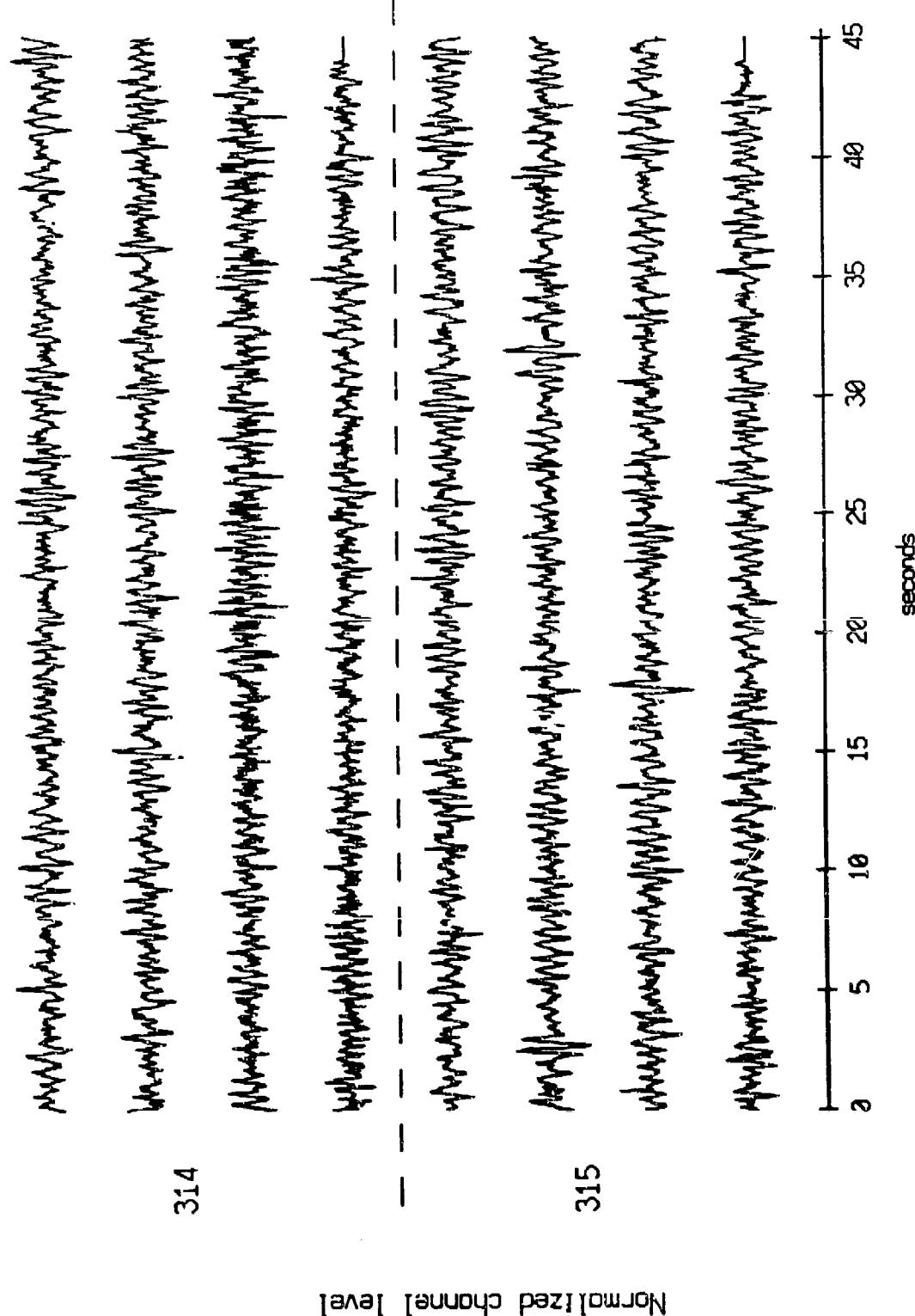


Figure X.14b.j

OBS 06 May, 1987 Trip - events 314 and 315 (z_axis)
max gain-corrected amplitude is 0.610550 counts

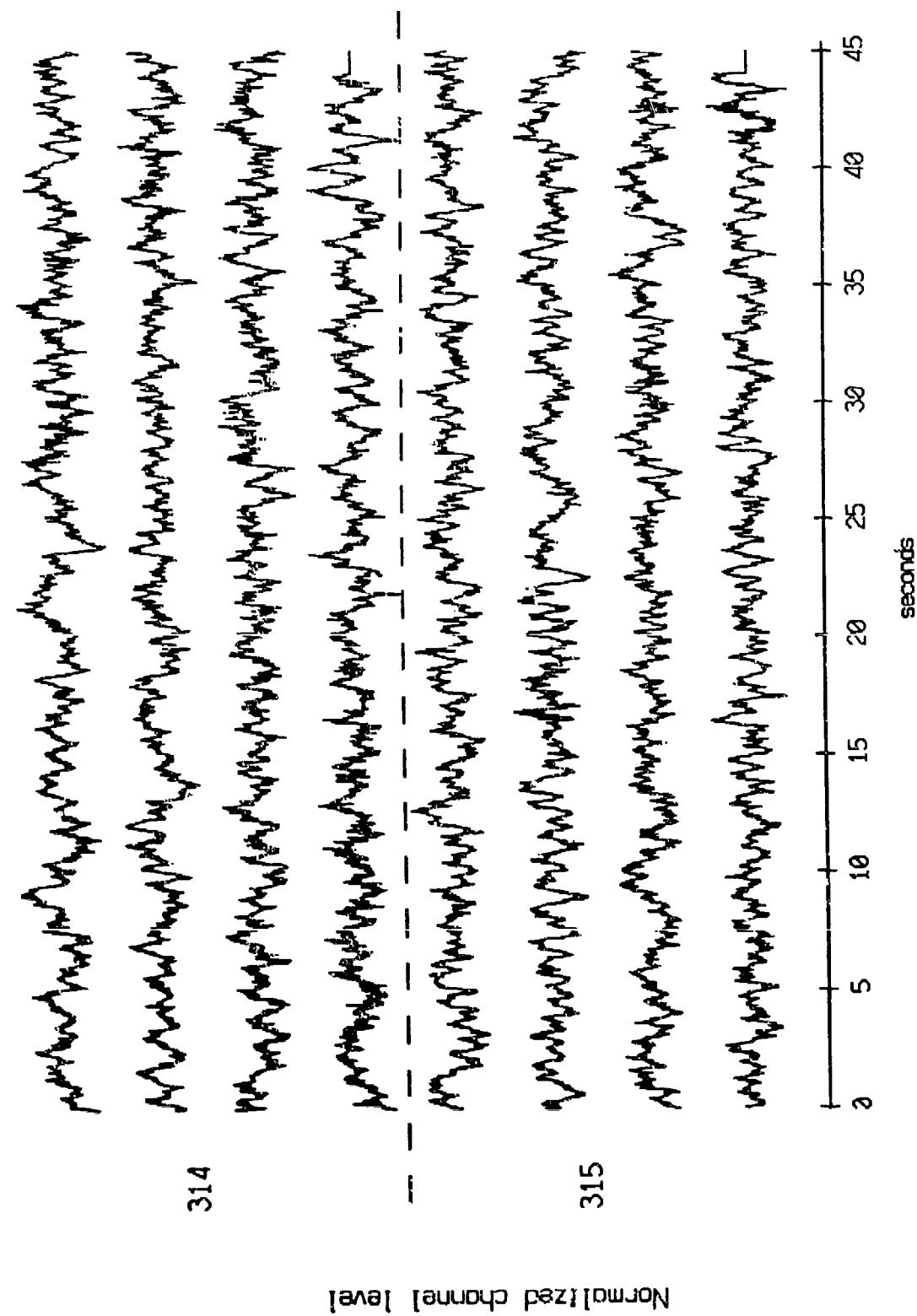


Figure X.14b.k

085 06 May, 1987 Trip - events 314 and 315 (pressure)
max gain-corrected amplitude is 35,03804 counts

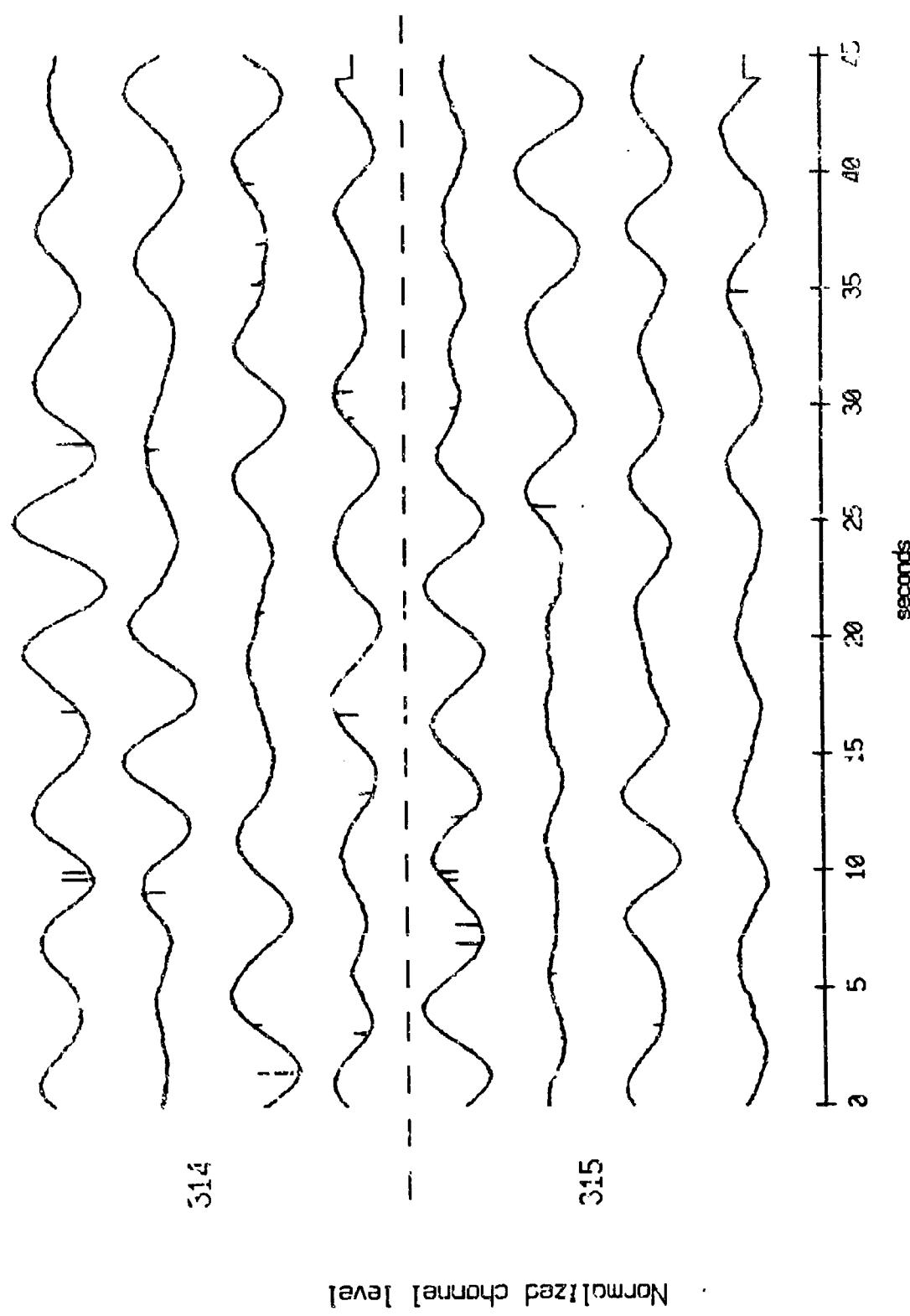


Figure X.14b.l

OBS 08, May, 1987 Trip - events 311 and 313 (x -axis)
max gain-corrected amplitude is 3.300164 counts

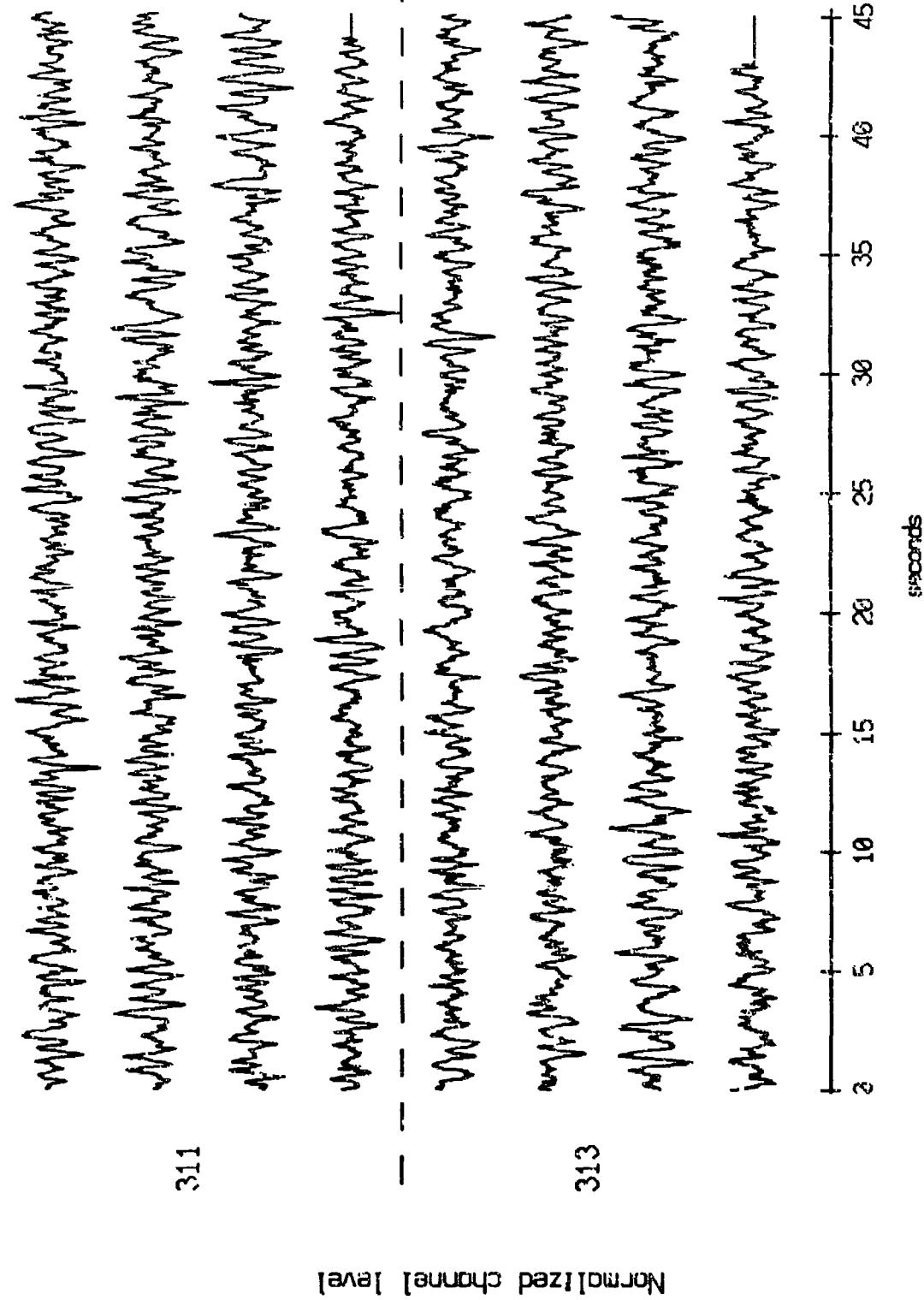


Figure X.15a.i

OBS 08, May, 1987 Trip - events 311 und 313 (y-axis)
max gain-corrected amplitude is .242301 counts

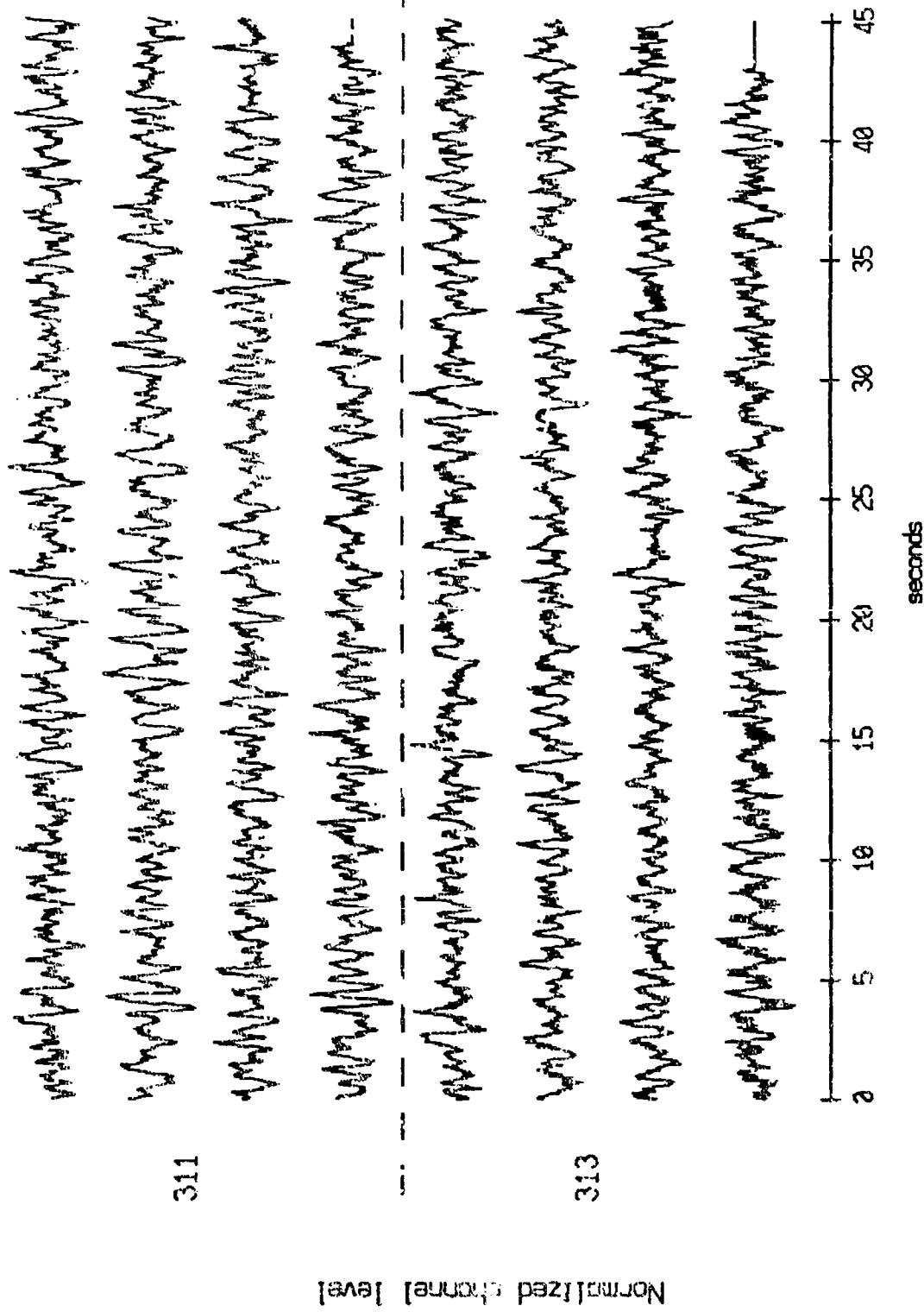


Figure X.15a.j

OBS 08, May, 1987 Trip - events 311 and 313 (z_axis)
max gain-corrected amplitude is 0.808081 counts

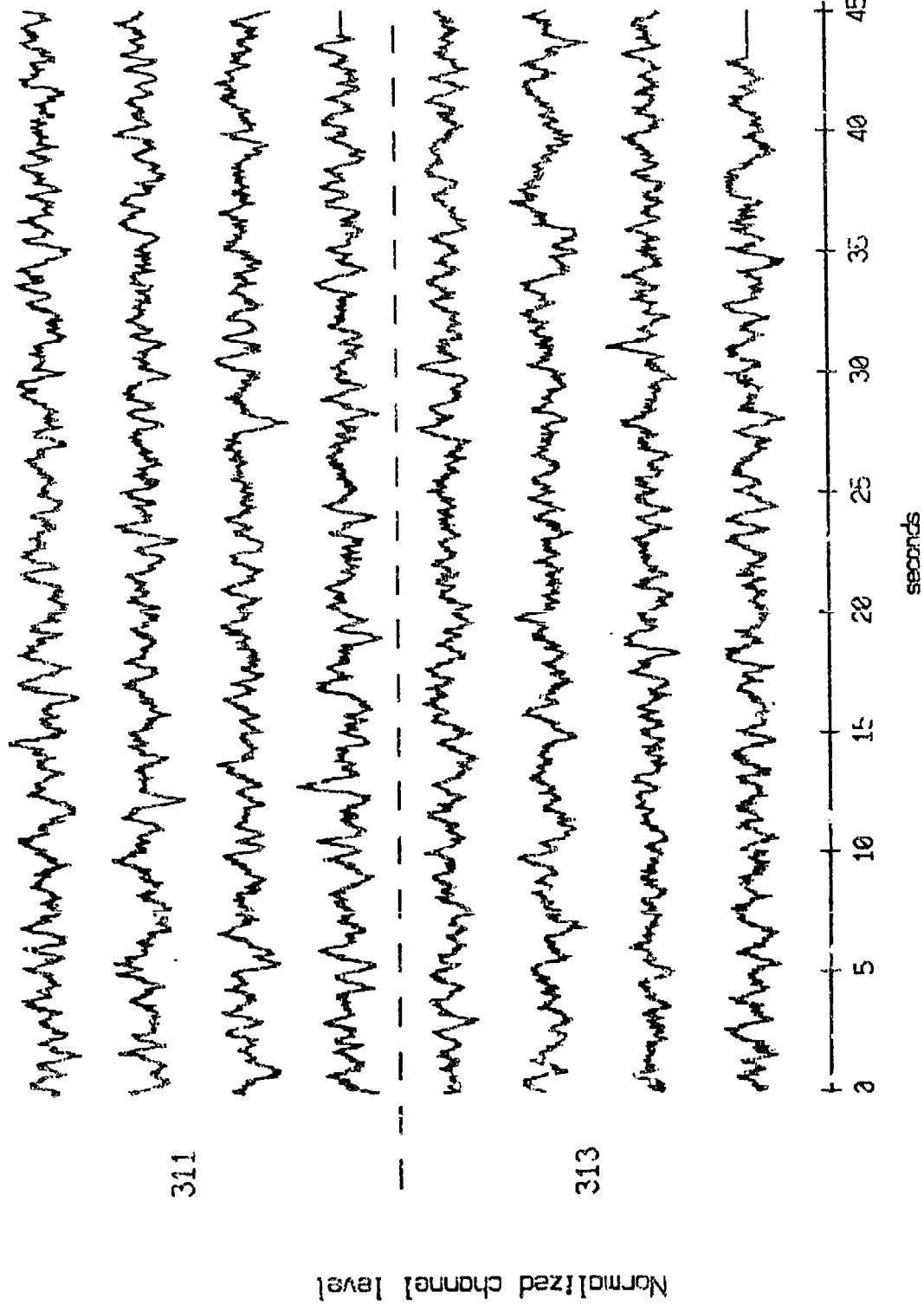
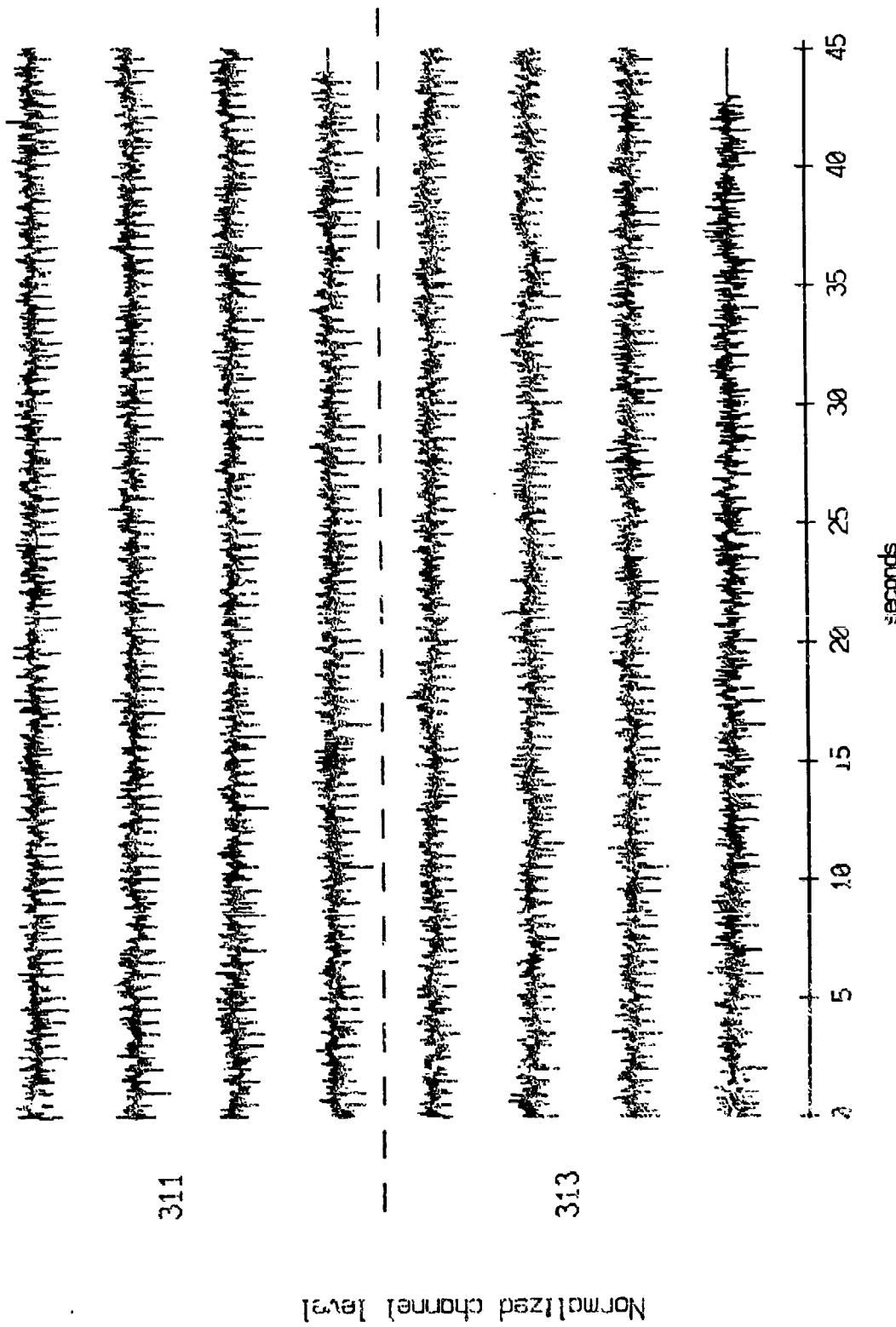


Figure X.15a,k

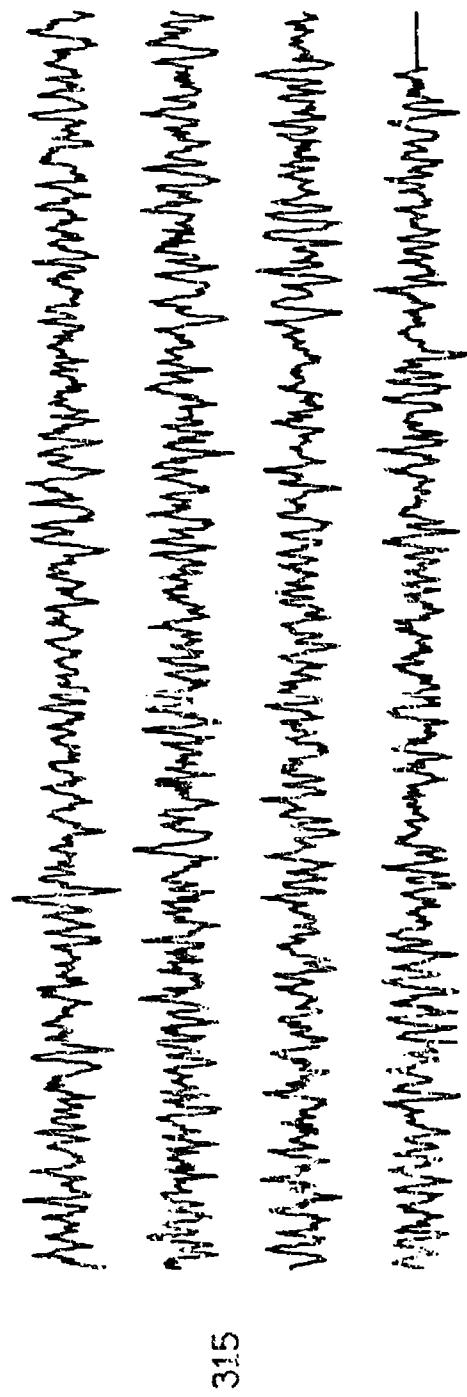
OBS 08, May, 1987 Trip - events 311 and 313 (pressure)
max gain-corrected amplitude is 0.313256 counts



Normalized channel level

Figure X.15a.1

OBS 08, May, 1987 Trip - event 315 (x axis)
mcx gain-corrected amplitude is 3.088666 counts



NORMALIZED CHANNEL LEVEL

Figure X.15c.i

OBS 08, May, 1987 TriP - event 315 (y axis)
max gain-corrected amplitude is 3.20e401 counts

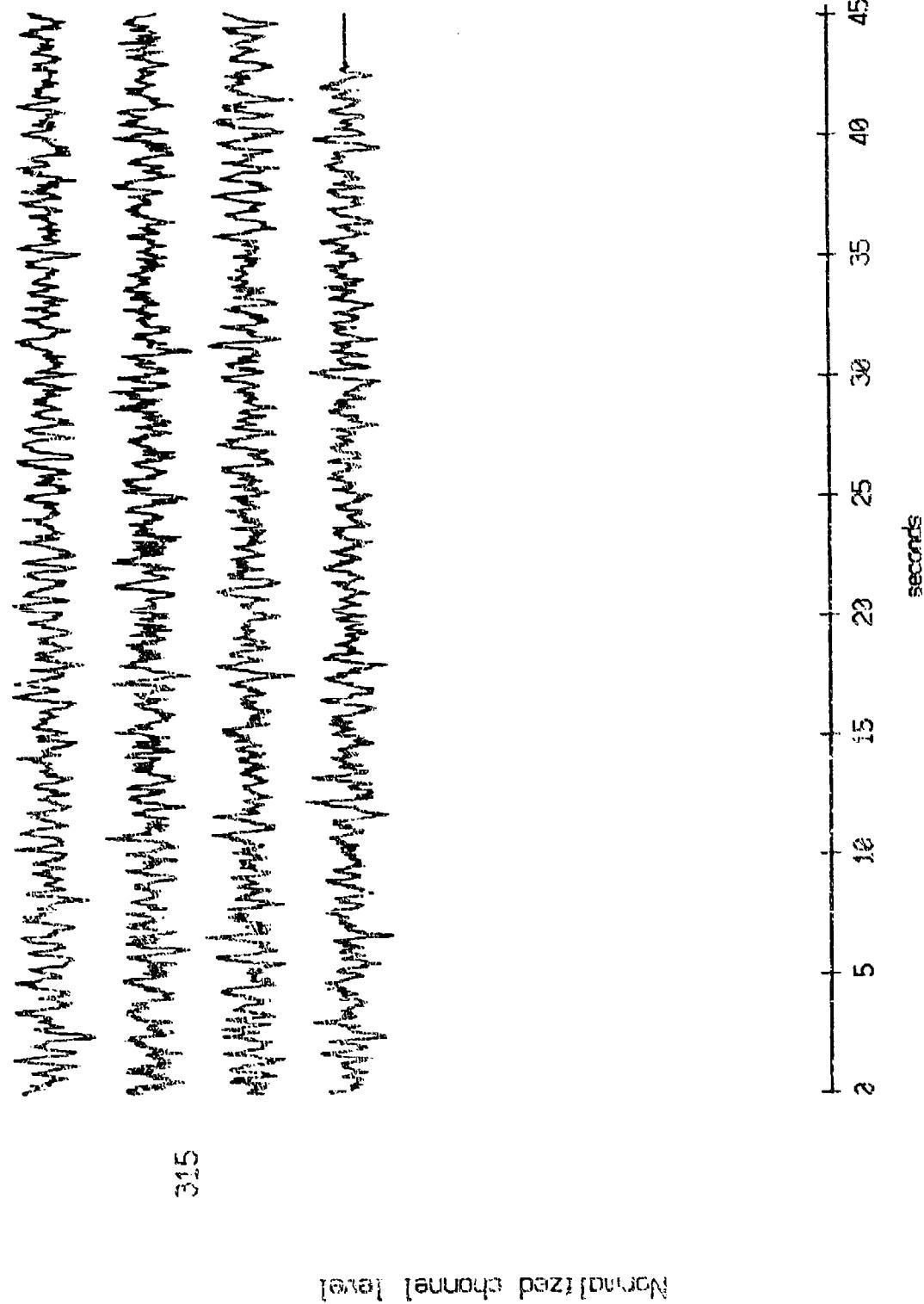
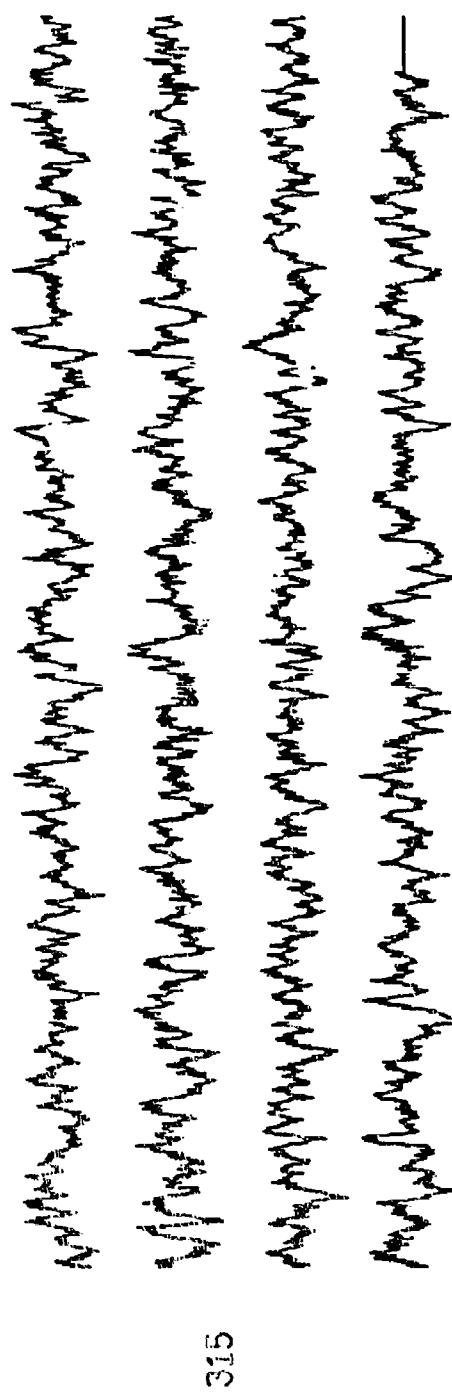


Figure X.15b.j

OBS 08, May, 1987 Trip - event 315 (z axis)
max gain-corrected amplitude is 0.604564 counts



Normalized channel level

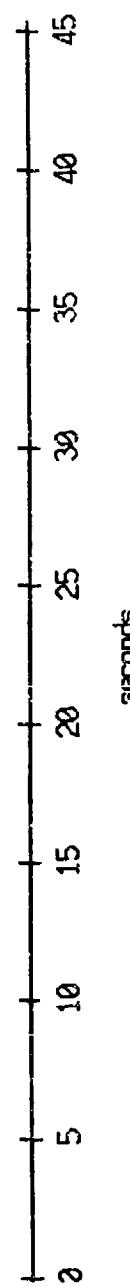


Figure X.15b.k

OBS 08, May, 1987 Trip - event 315 (pressure)
max gain-corrected amplitude is 0.363138 counts

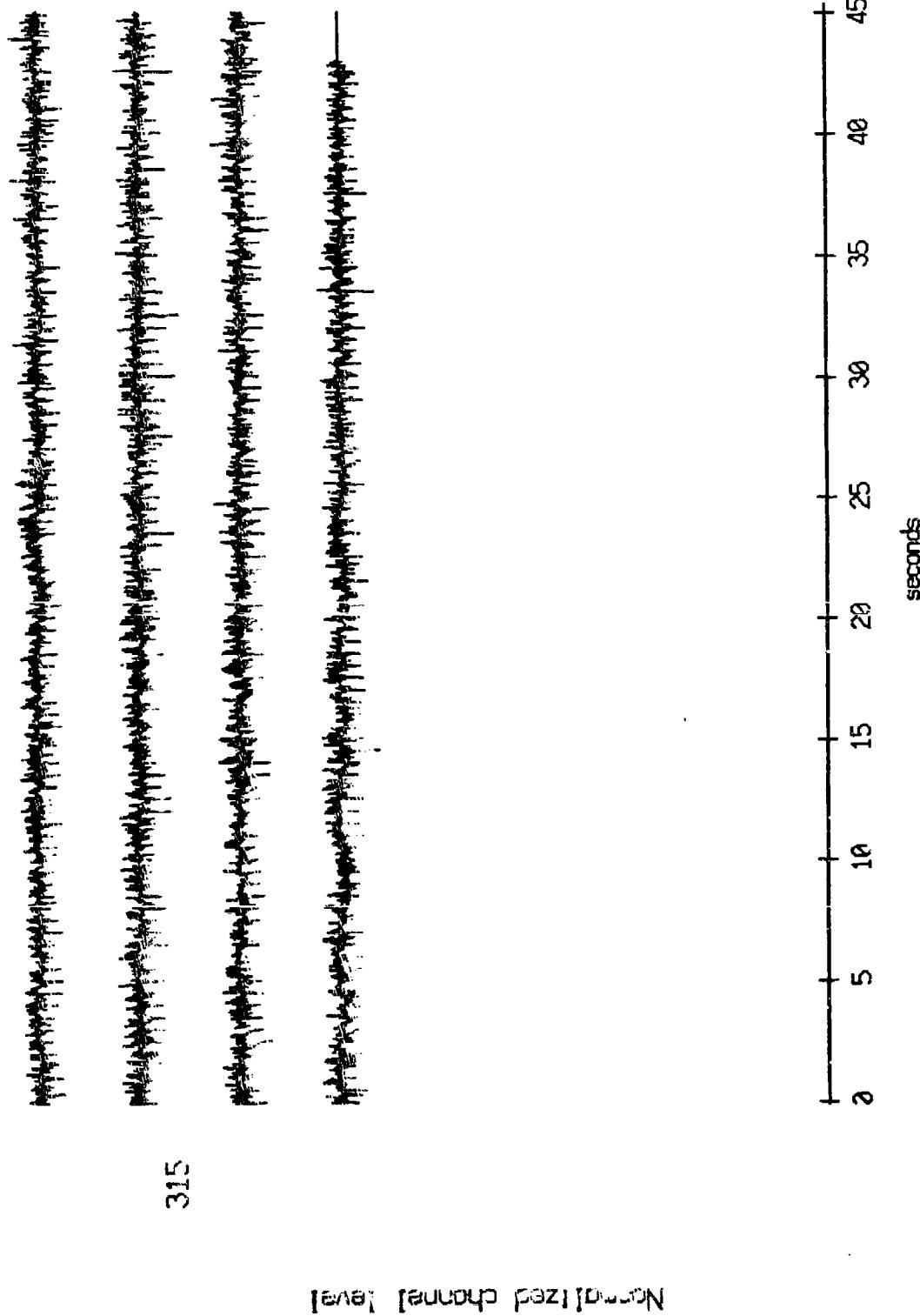
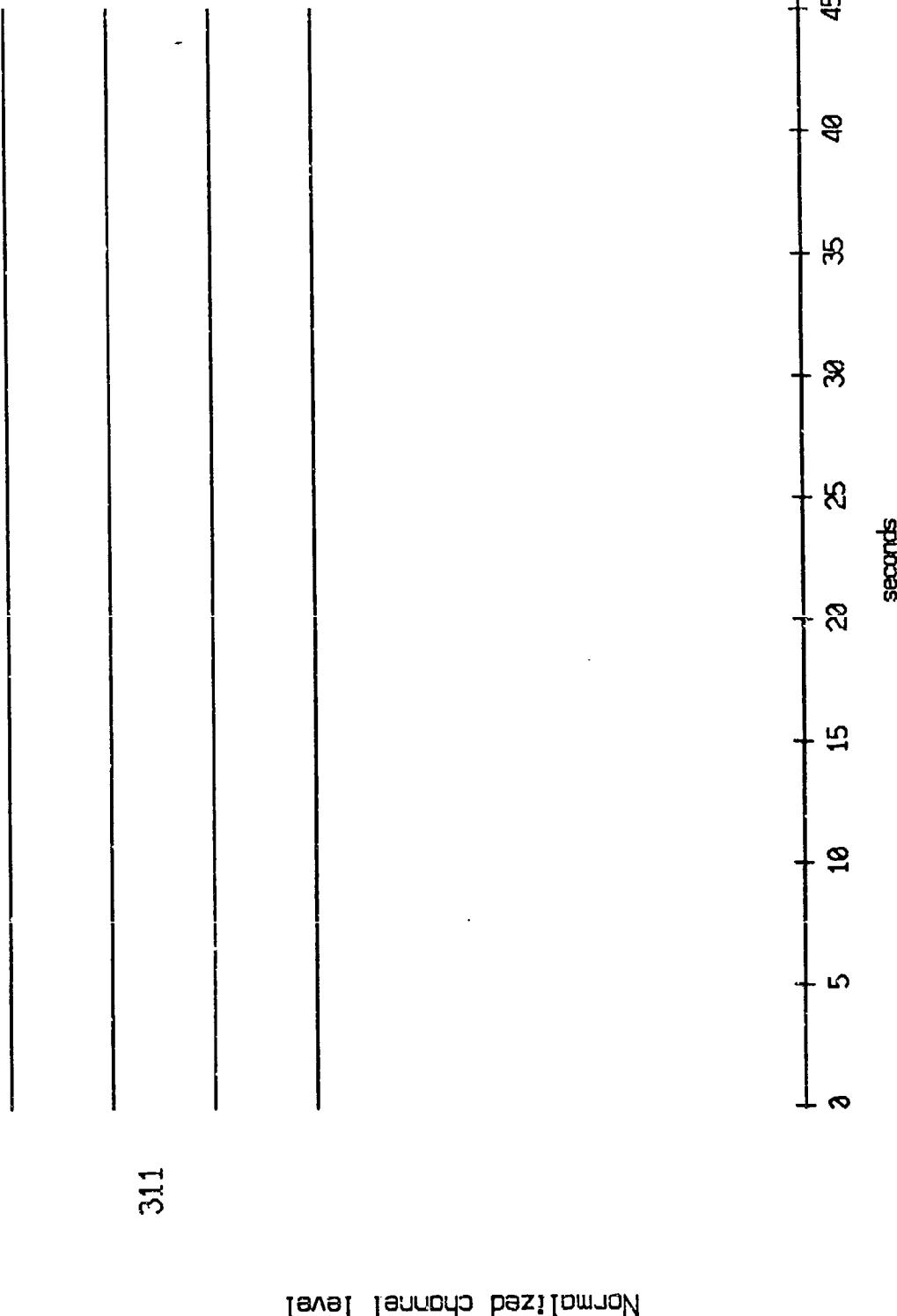


Figure X.15b.1

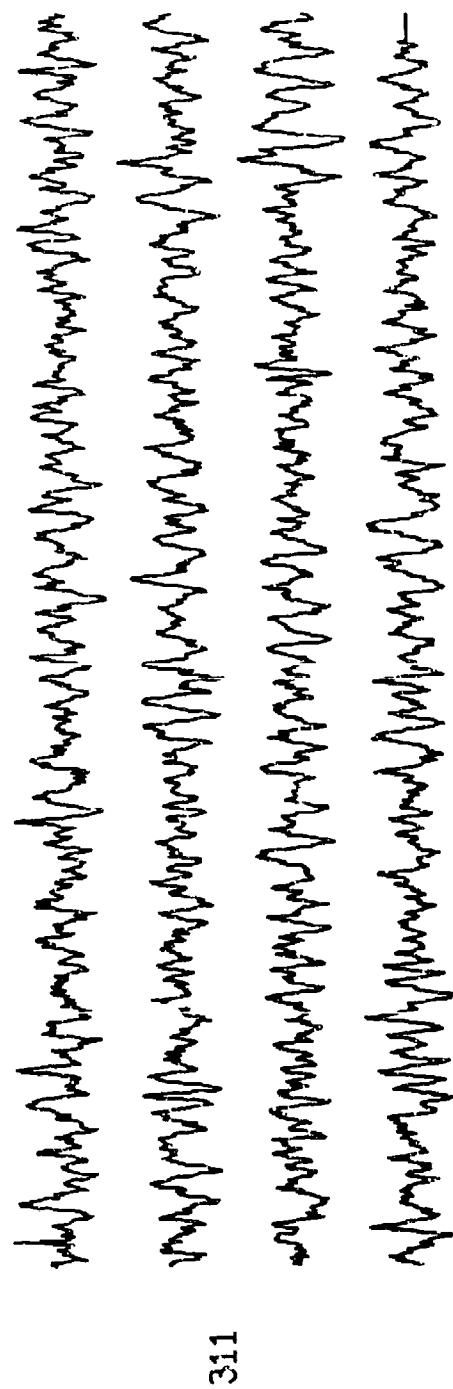
OBS 12, May, 1987 Trip - event 311 (x axis)
max gain-corrected amplitude is 0. counts



Normalized channel level

Figure X.16a.i

OBS 12, May, 1987 Trip - event 311 (Y axis)
max gain-corrected amplitude is 3.964586 counts



Normalized channel level

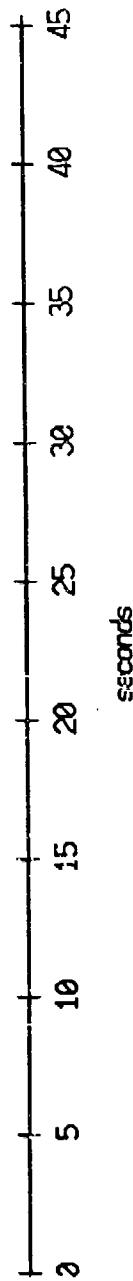


Figure X.16a.j

OBS 12, May, 1987 TriP - event 311 (z axis)
max gain-corrected amplitude is 0. counts

311

Normalized channel level

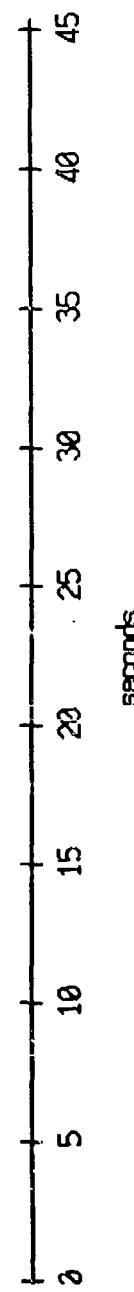


Figure X.16a.k

OBS 12, May, 1987 Trip - event 311 (pressure)
max gain-corrected amplitude is 3.573515 counts

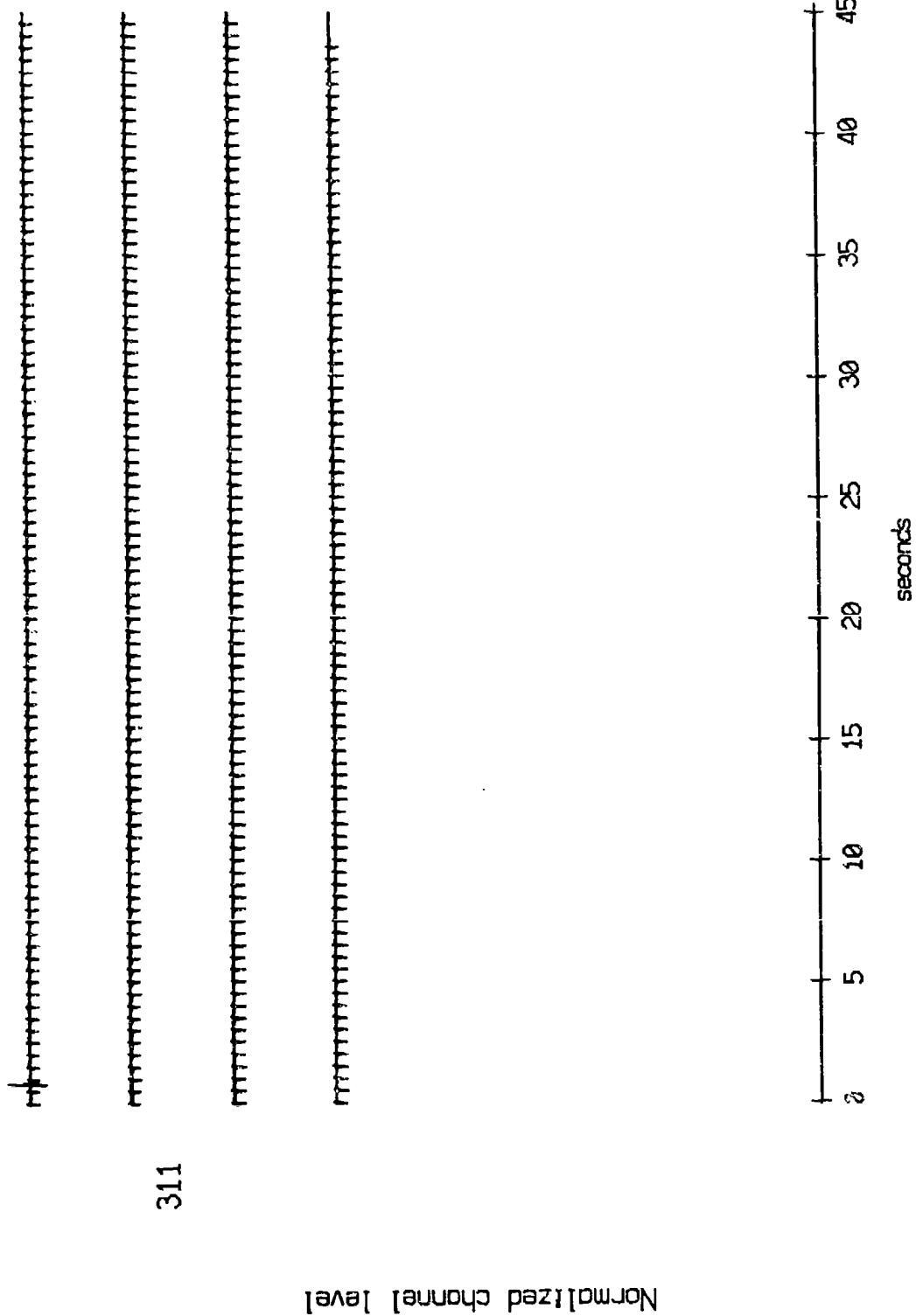
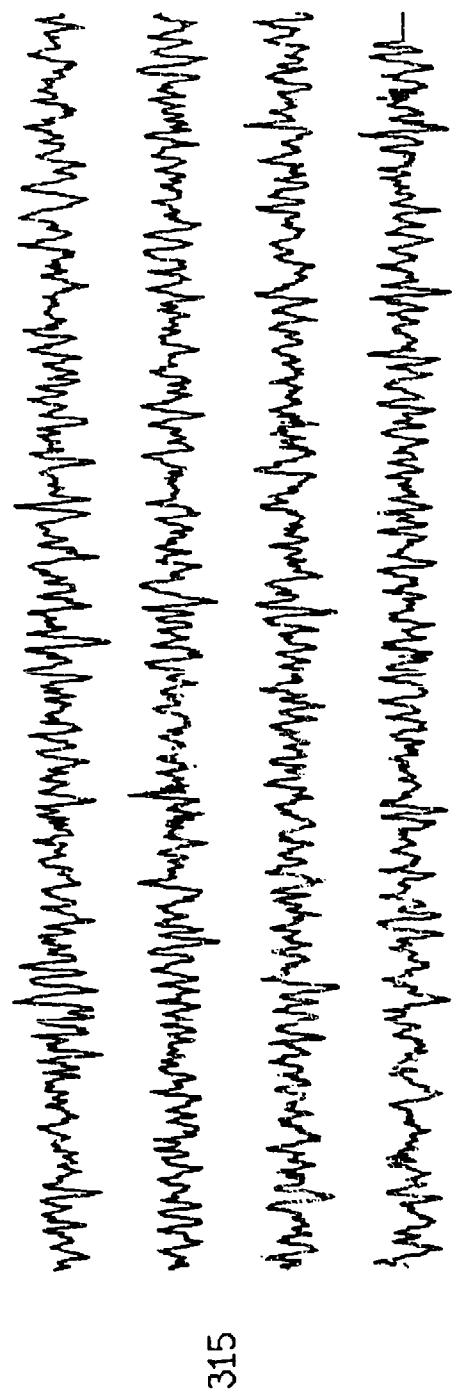


Figure X.16a.1

OBS 12, May, 1987 Trip - event 315 (x axis)
max gain-corrected amplitude is 3.559548 counts



Normalized channel level

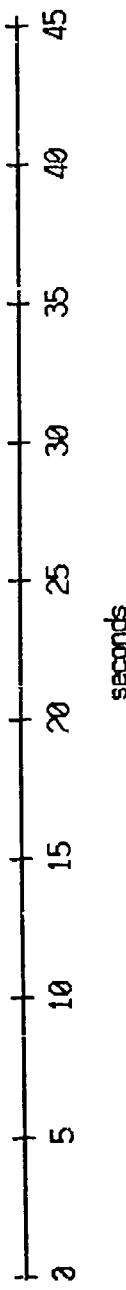


Figure X.16b.i

CBS 12, May, 1987 Trip - event 315 (ν axis)
max gain-corrected amplitude is 3.433846 counts

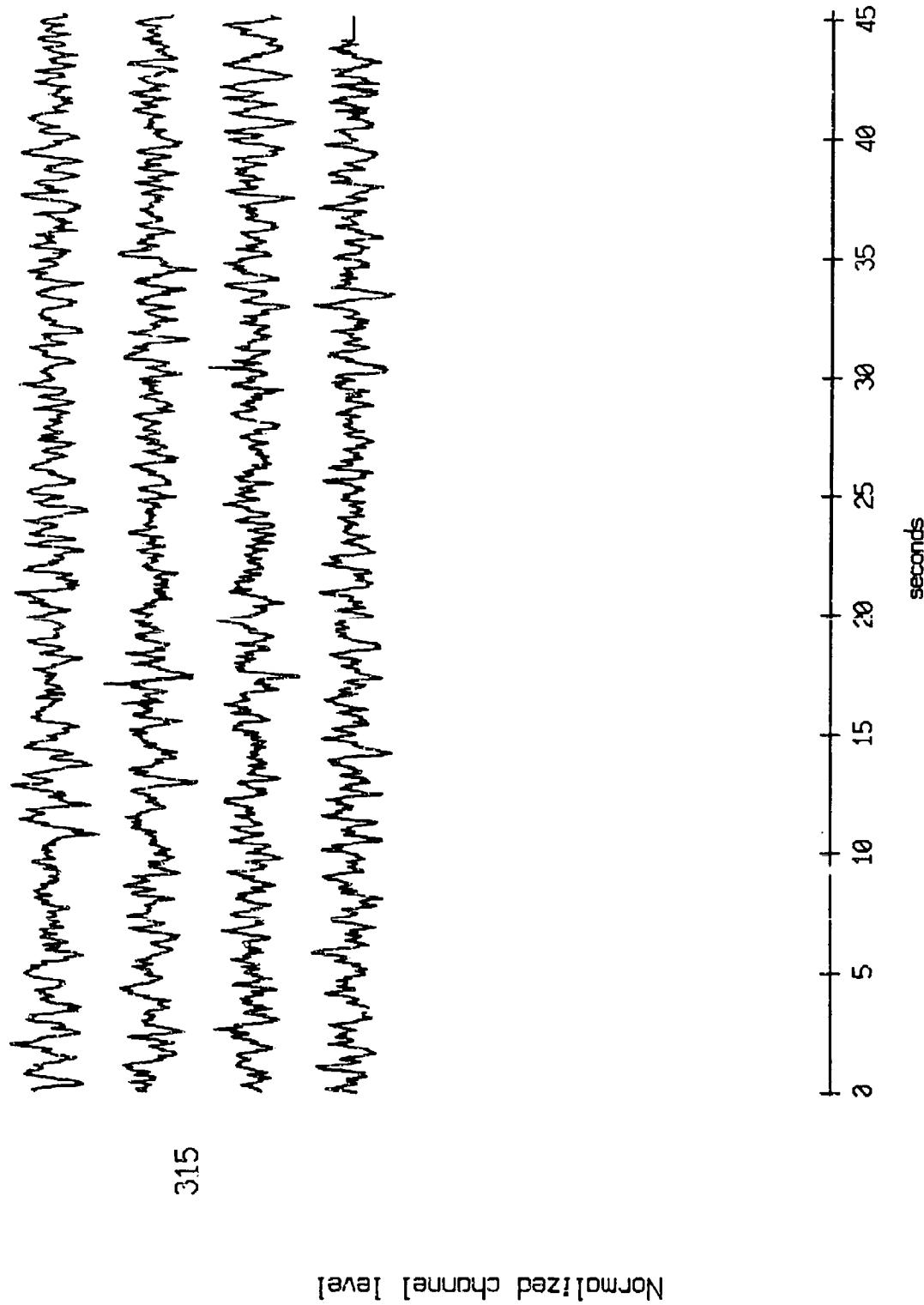


Figure X.16b.j

OBS 12, May, 1987 Trip - event 315 (z axis)
max gain-corrected amplitude is 4.086298 counts

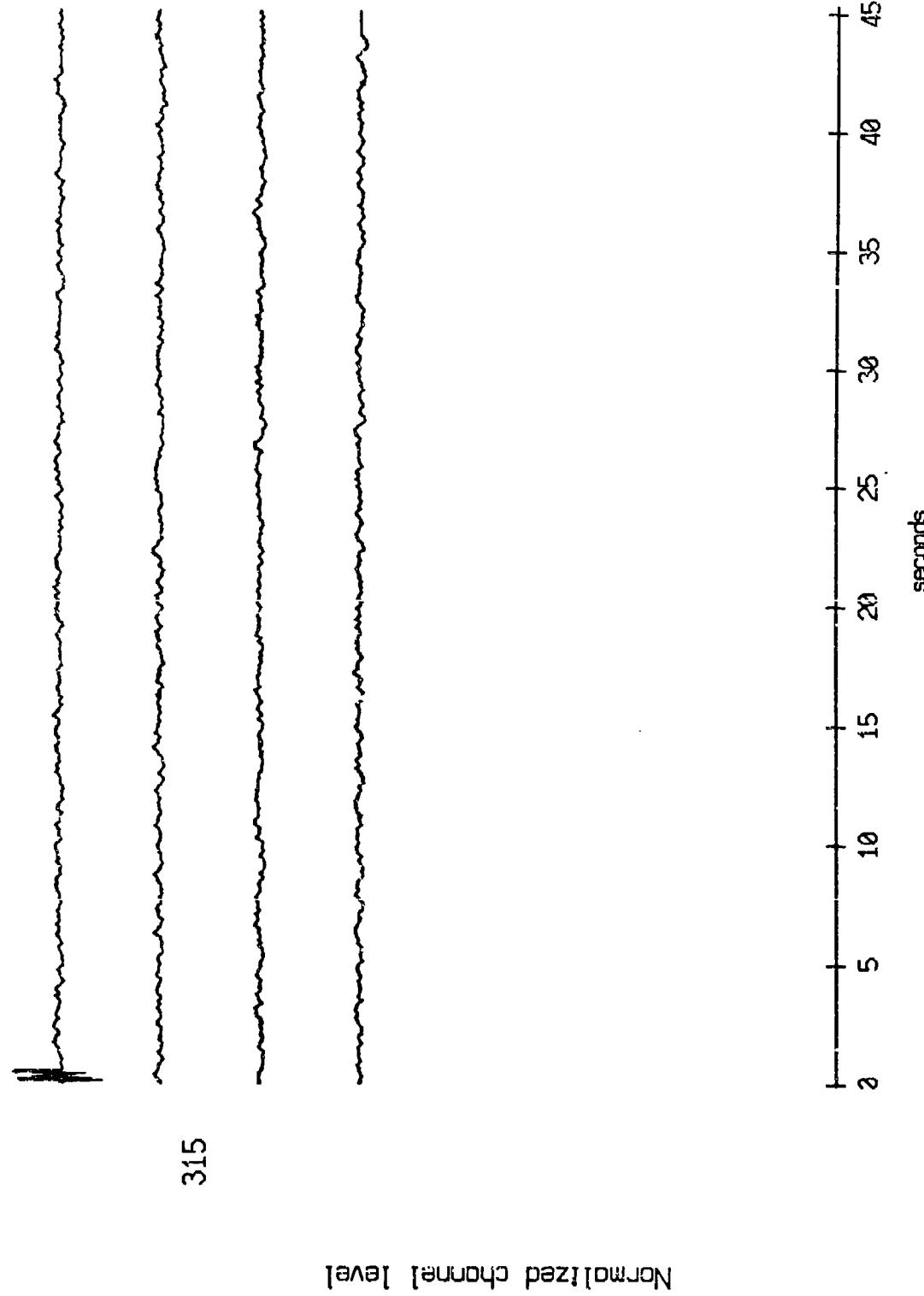


Figure X.16b.k

OBS 12, May, 1987 Trip - event 315 (pressure)
max gain-corrected amplitude is 0.957, 26 counts

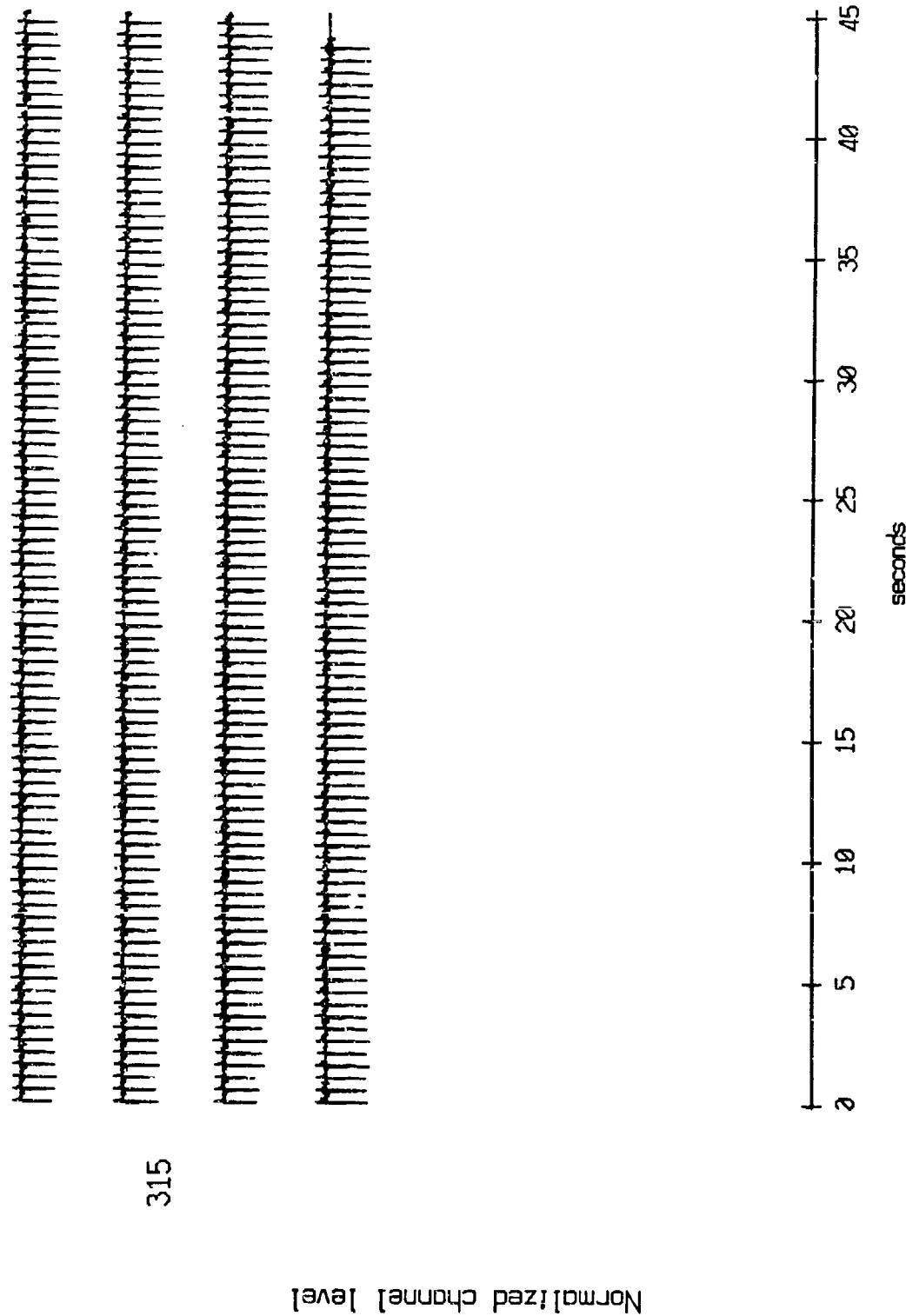


Figure X.16b.1

OBS 13, May, 1987 Trip - events 311 and 313 (x-axis)
max gain-corrected amplitude is 4.084302 counts

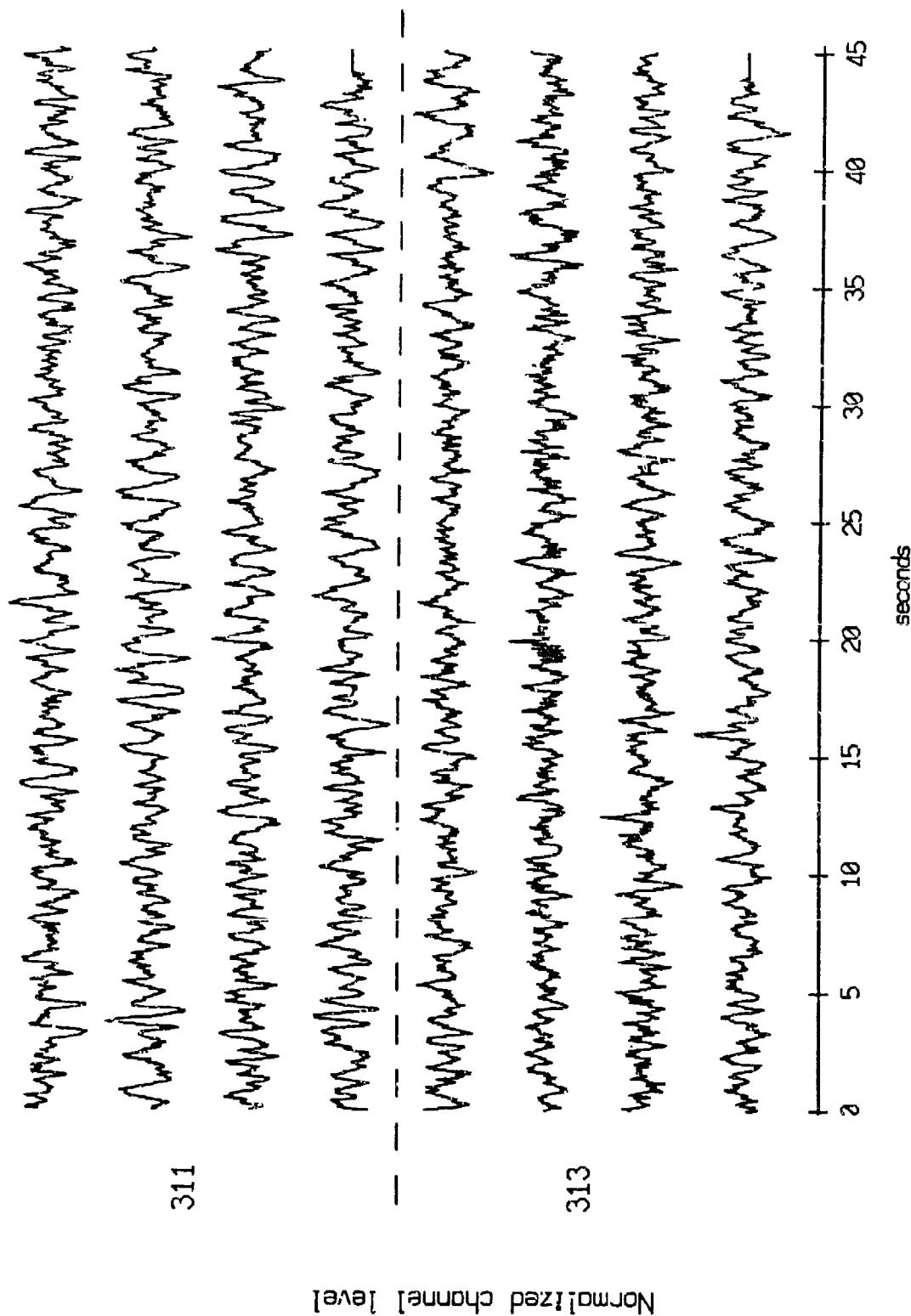
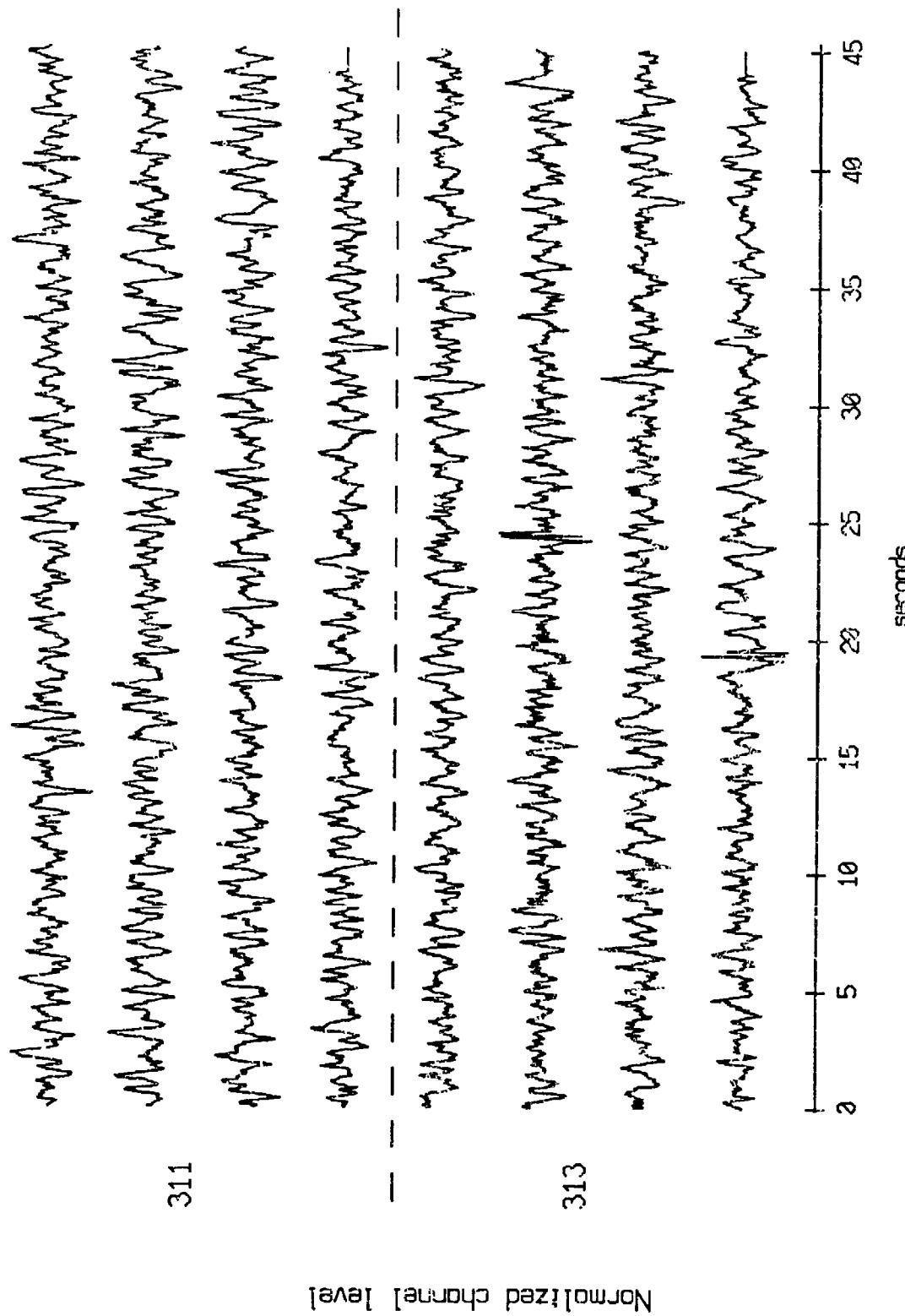


Figure X.17a.i

OBS 13, May, 1987 Trip " events 311 and 313 (y-axis)
max gain-corrected amplitude is 4.086298 counts



Normalized channel level

Figure X.17a.j

OBS 13, May, 1987 TriP - events 311 and 313 (z-axis)
max gain-corrected amplitude is 0.802095 counts

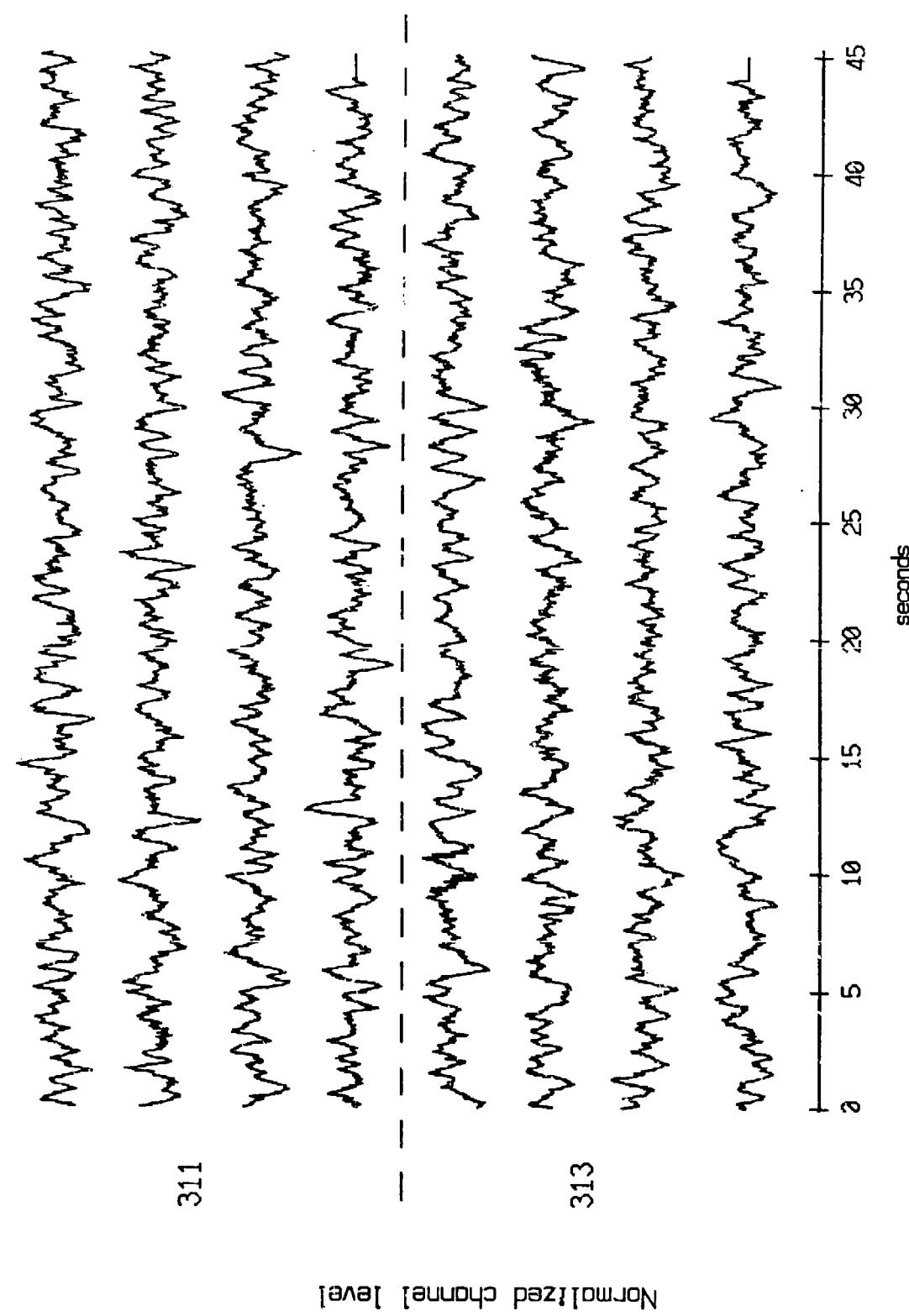


Figure X.17a.k

OBS 13, May, 1987 Trip - events 311 and 313 (pressure)
max gain-corrected amplitude is 2.723533 counts

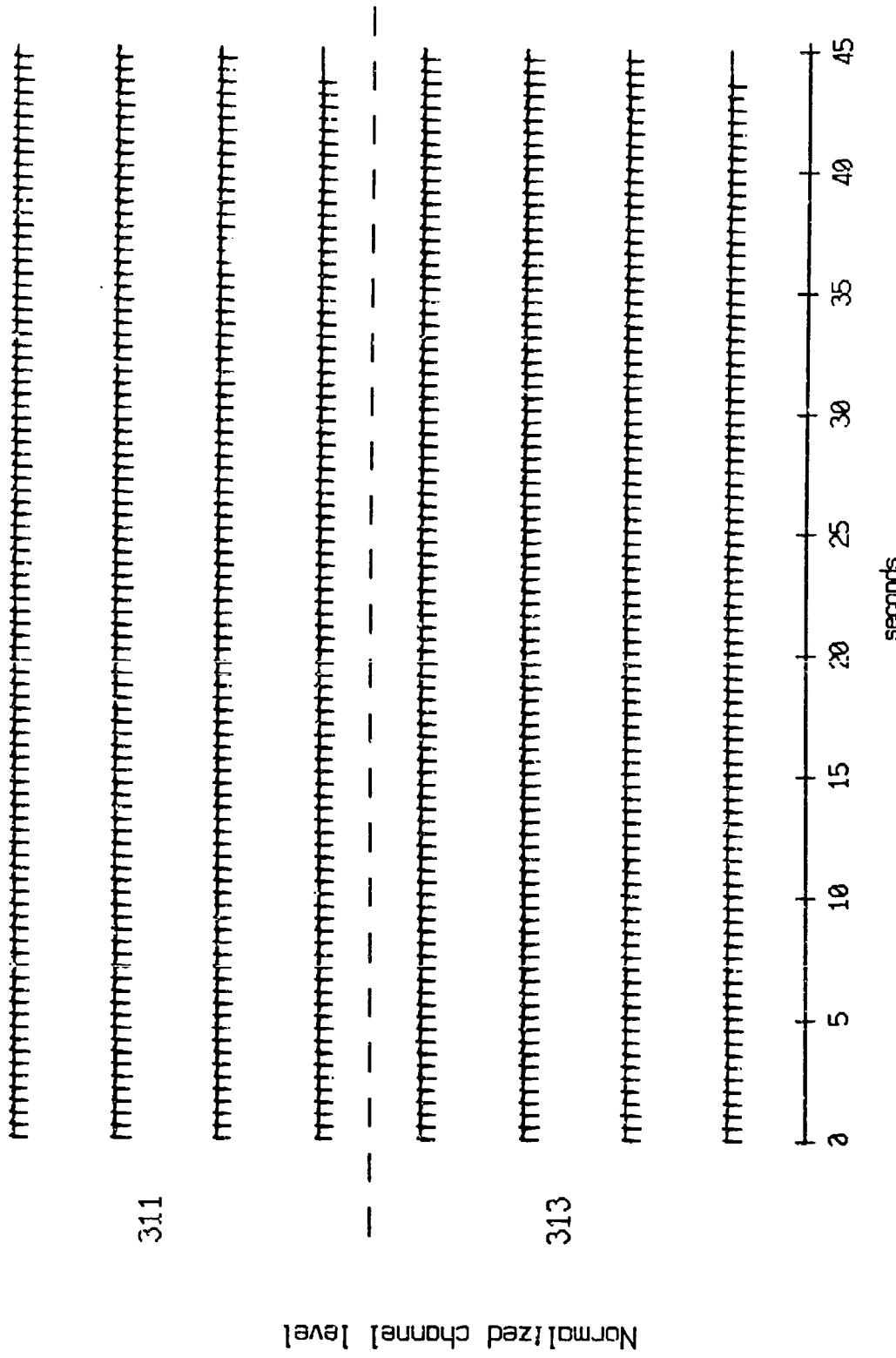


Figure X.17a.l

OBS 13, May, 1987 Trip - event 315 (x axis)
max gain-corrected amplitude is 3.7471×10^3 counts

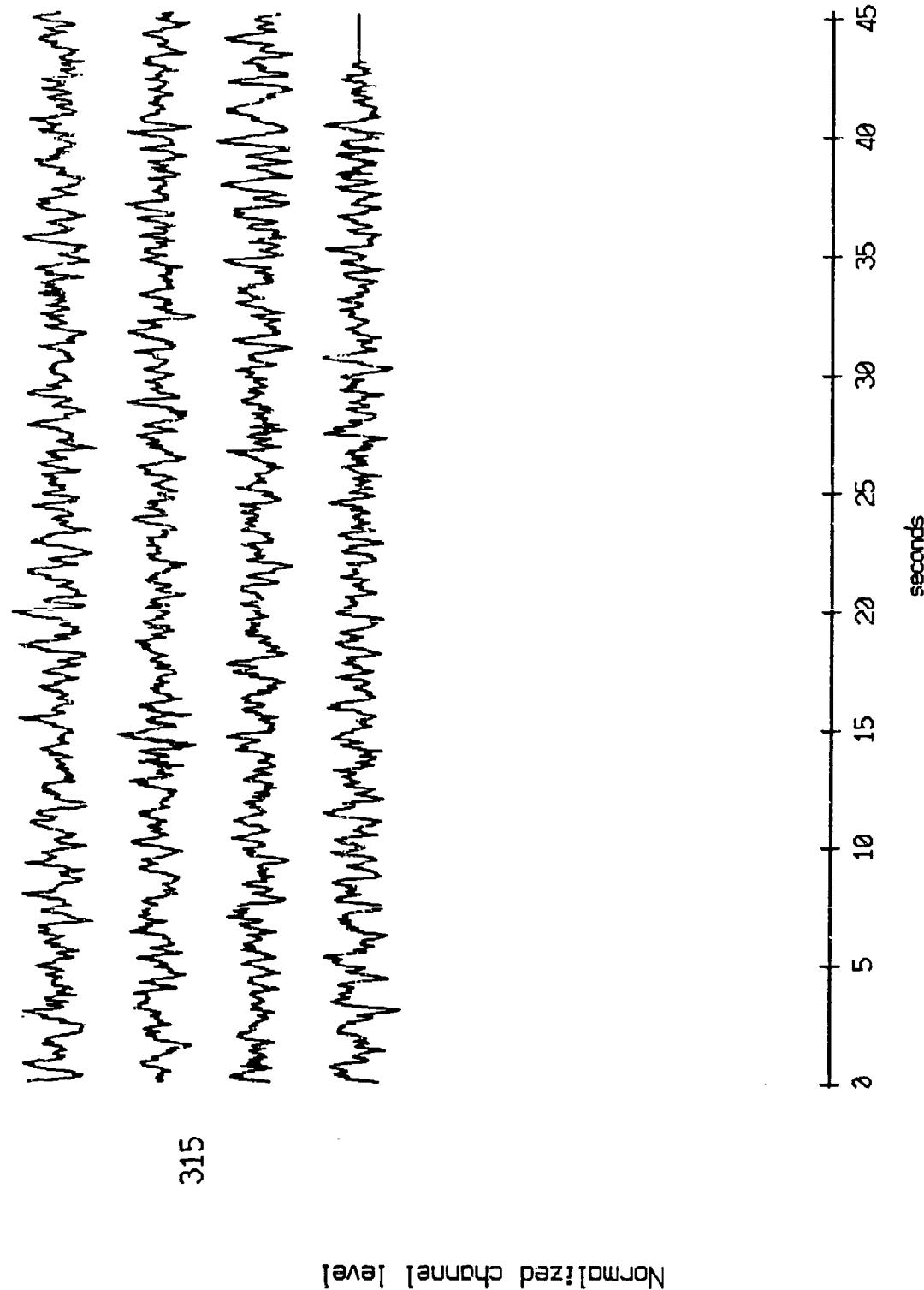
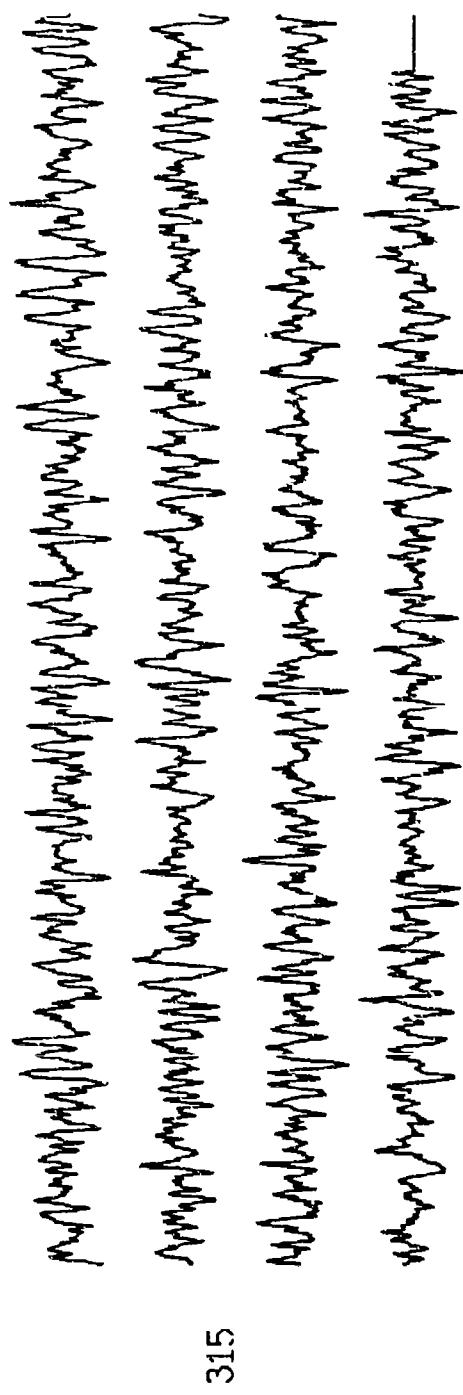


Figure X.17b.i

OBS 13, May, 1987 Trip - event 315 (y^{axis})
max gain-corrected amplitude is 3.216363 counts



Normalized channel level

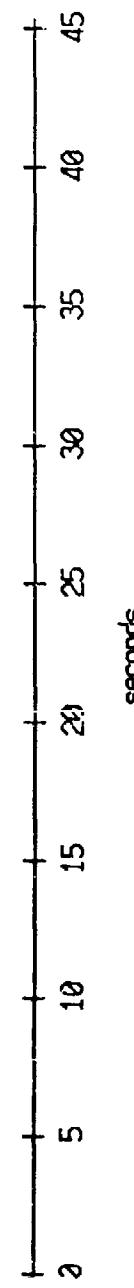
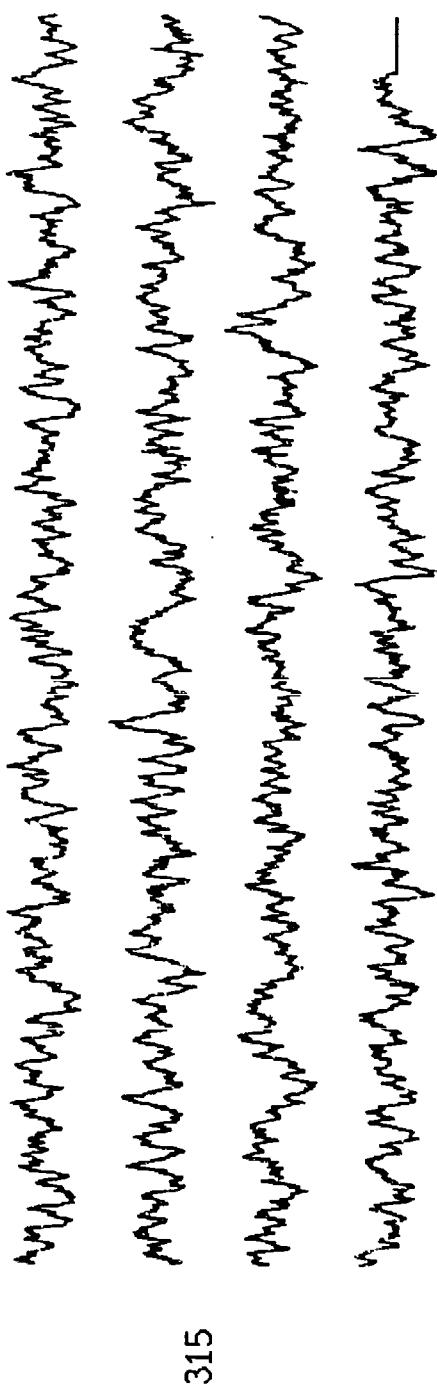


Figure X.17b.j

OBS 13, May, 1987 Trip - event 315 (z axis)
max gain-corrected amplitude is 0.680384 counts



Normalized channel level

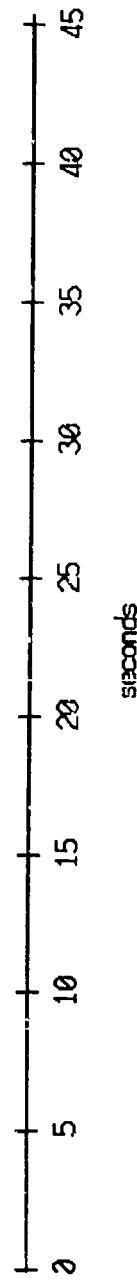
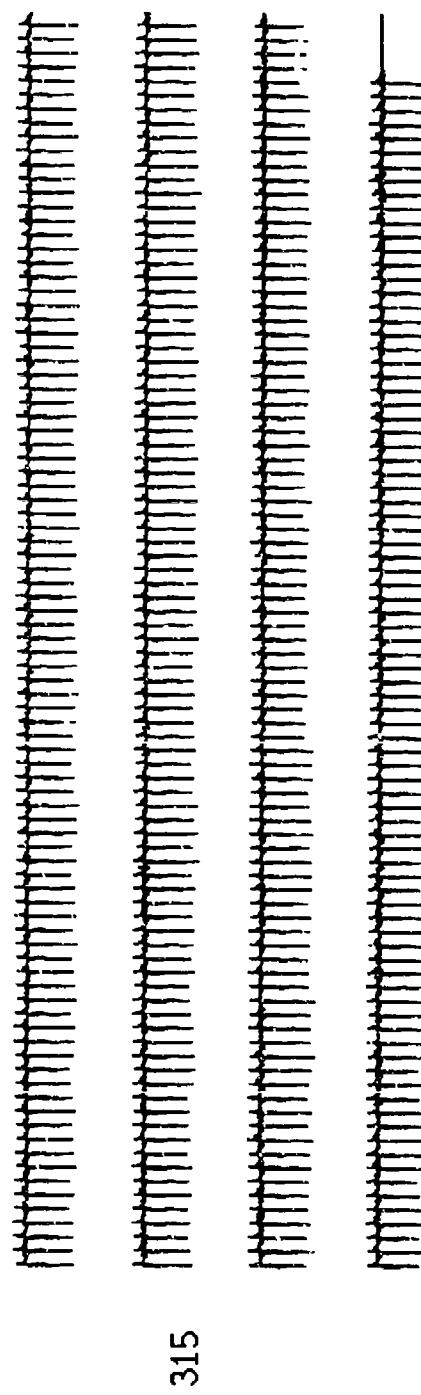


Figure X.17b.k

OBS 13, May, 1987 Trip - event 315 (pressure)
max gain-corrected amplitude is 0.987655 counts



Normalized channel level

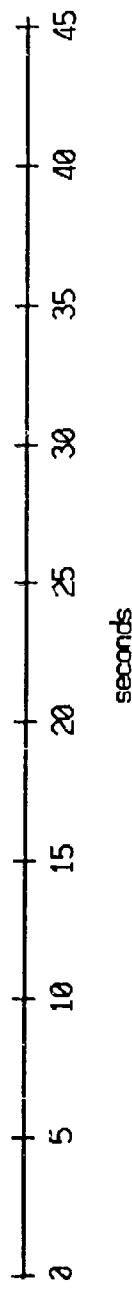


Figure X.17b.1

OBS 14, May, 1987 Trip - events 311 and 313 (x-axis)
max gain-corrected amplitude is 8,145,272 counts

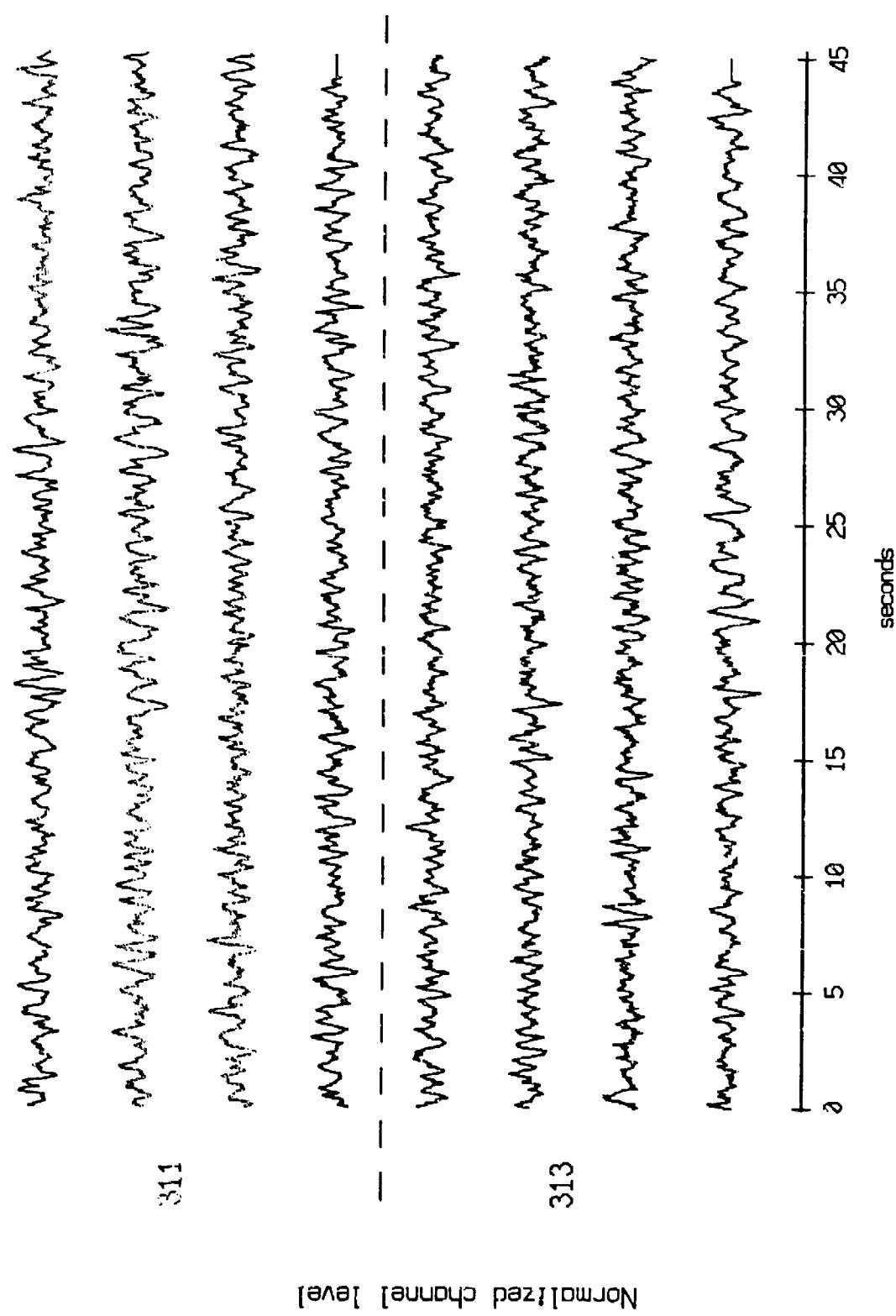


Figure X.18a.i

OBS 14, May, 1987 Trip - events 311 and 313 (y-axis)
max gain-corrected amplitude is 4,082,307 counts

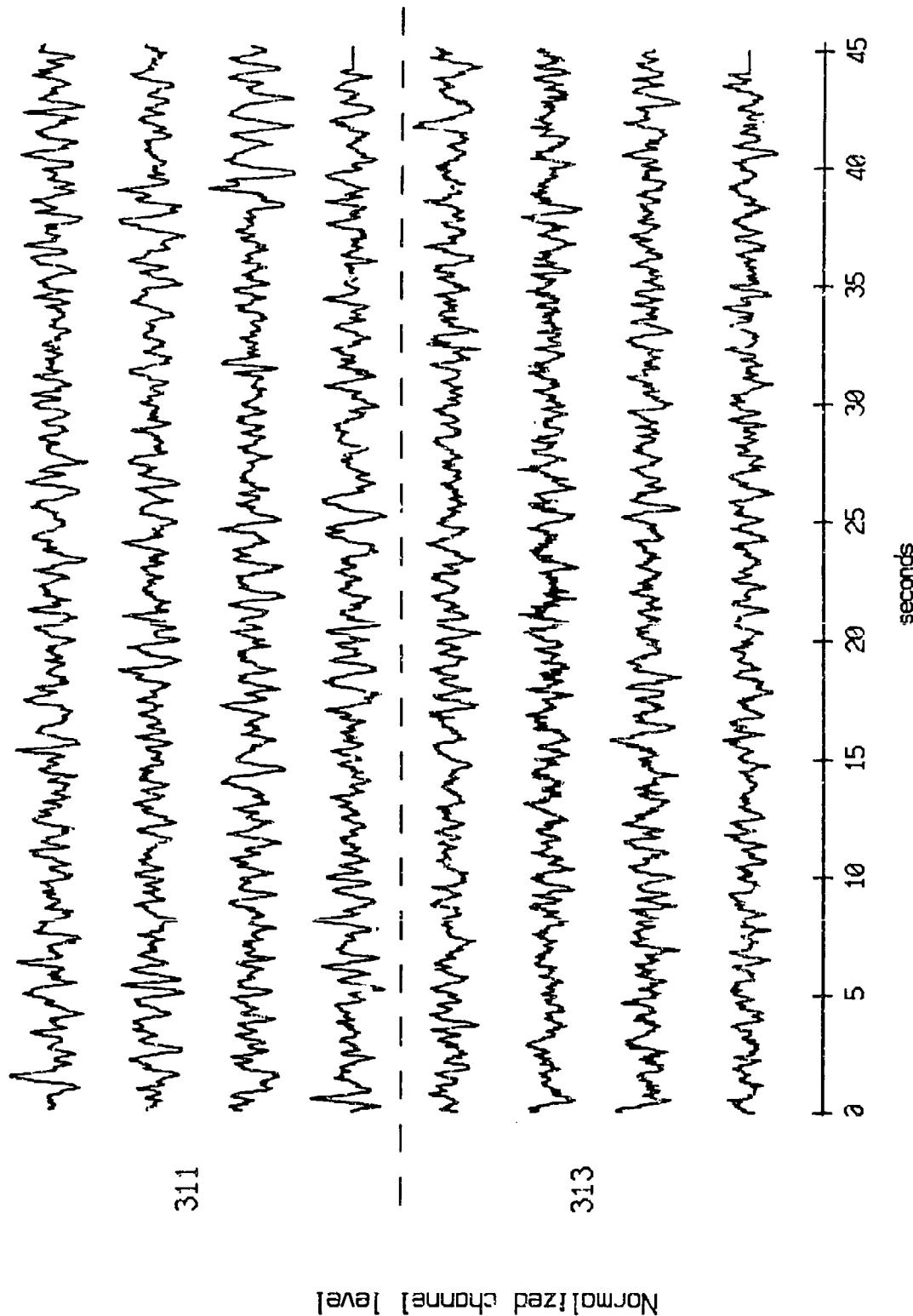


Figure X.18a.j

OBS 14, May, 1987 TriP - events 311 and 313 (z_axis)
max gain-corrected amplitude is 0.861953 counts

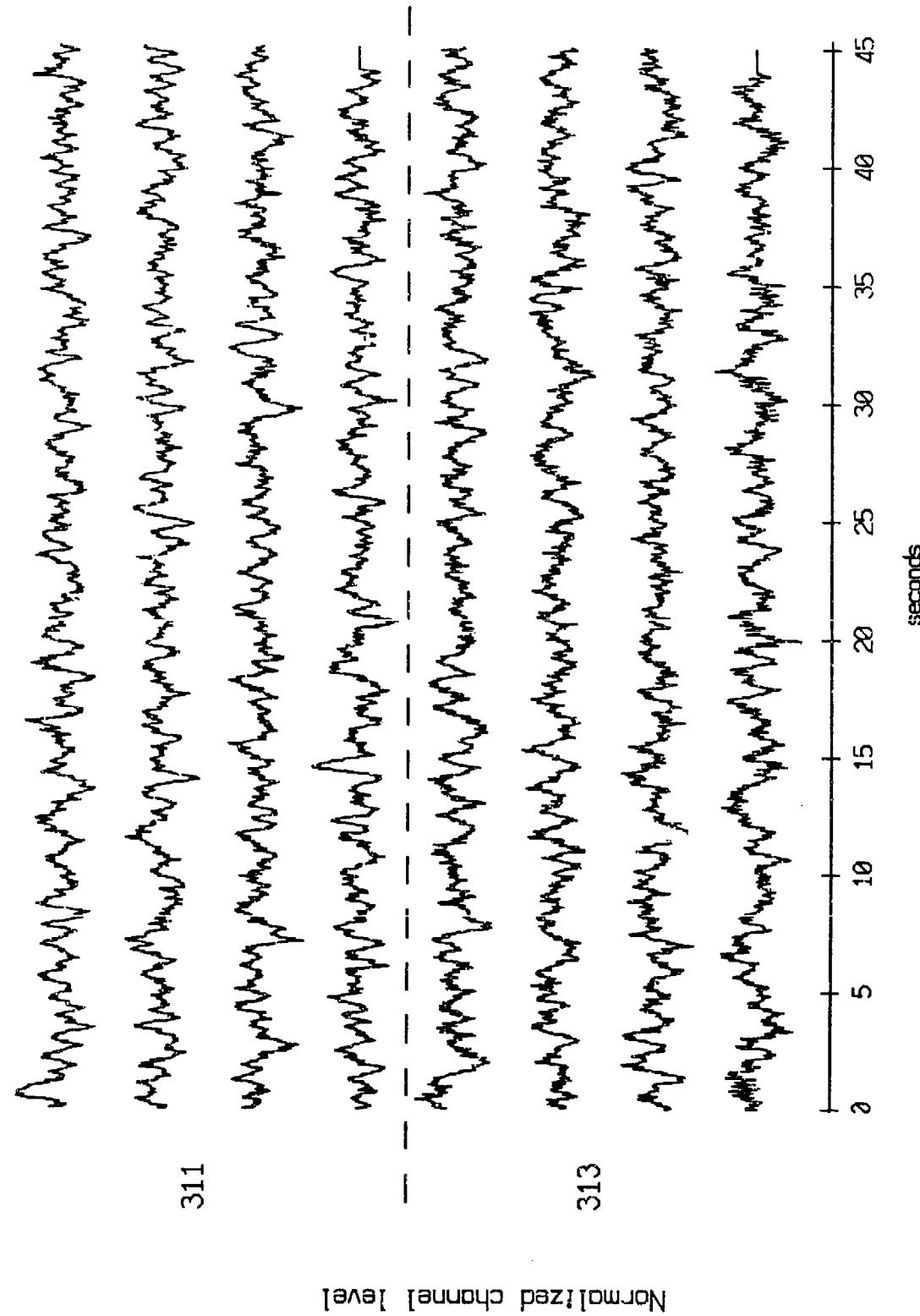


Figure X.18a.k

OBS 14, May, 1987 Trip - events 311 and 313 (pressure)
max gain-corrected amplitude is 4.086298 counts

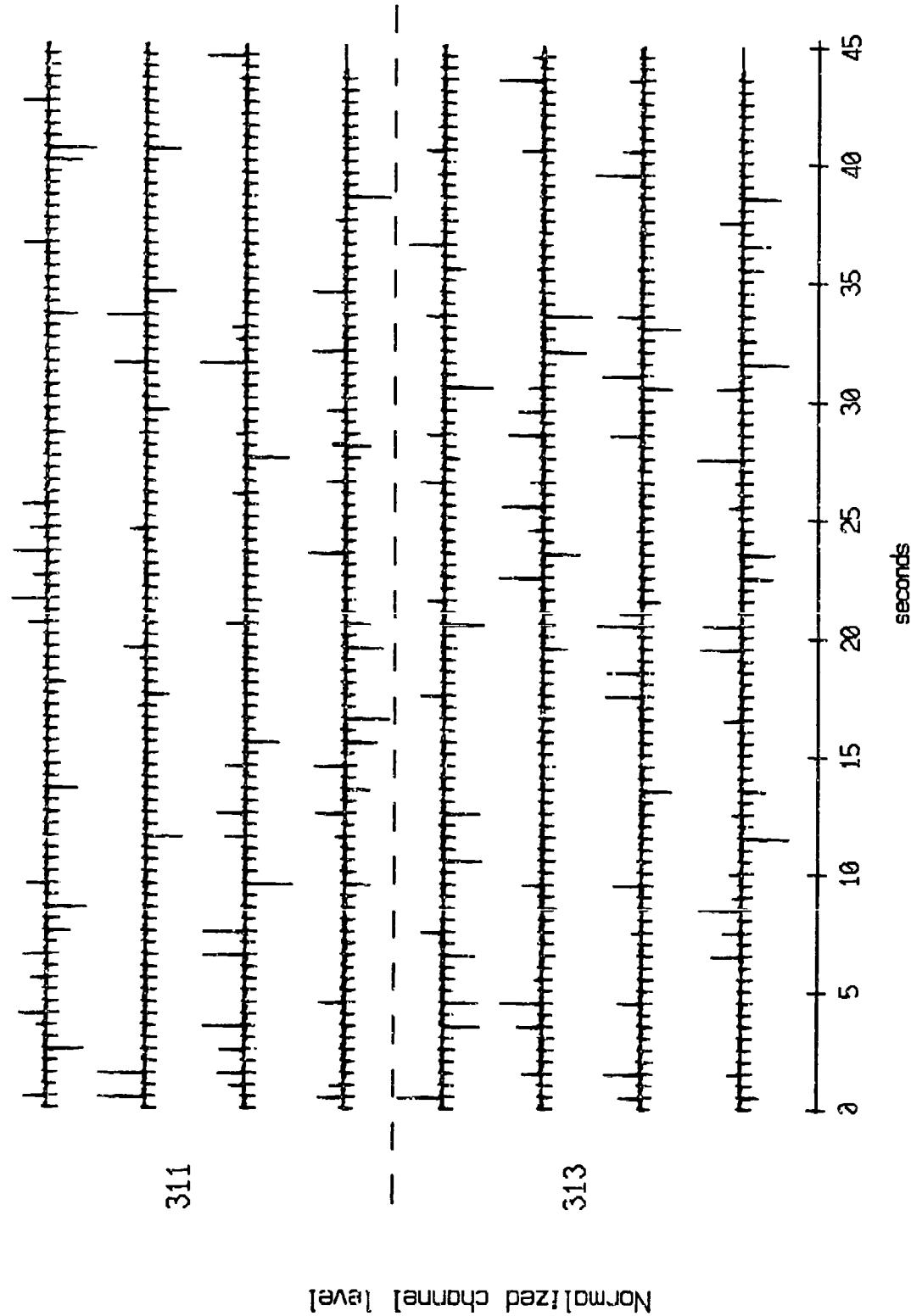


Figure X.18a.1

OBS 14, May, 1987 Trip - event 315 (x^{axis})
max gain-corrected amplitude is 4.090288 counts

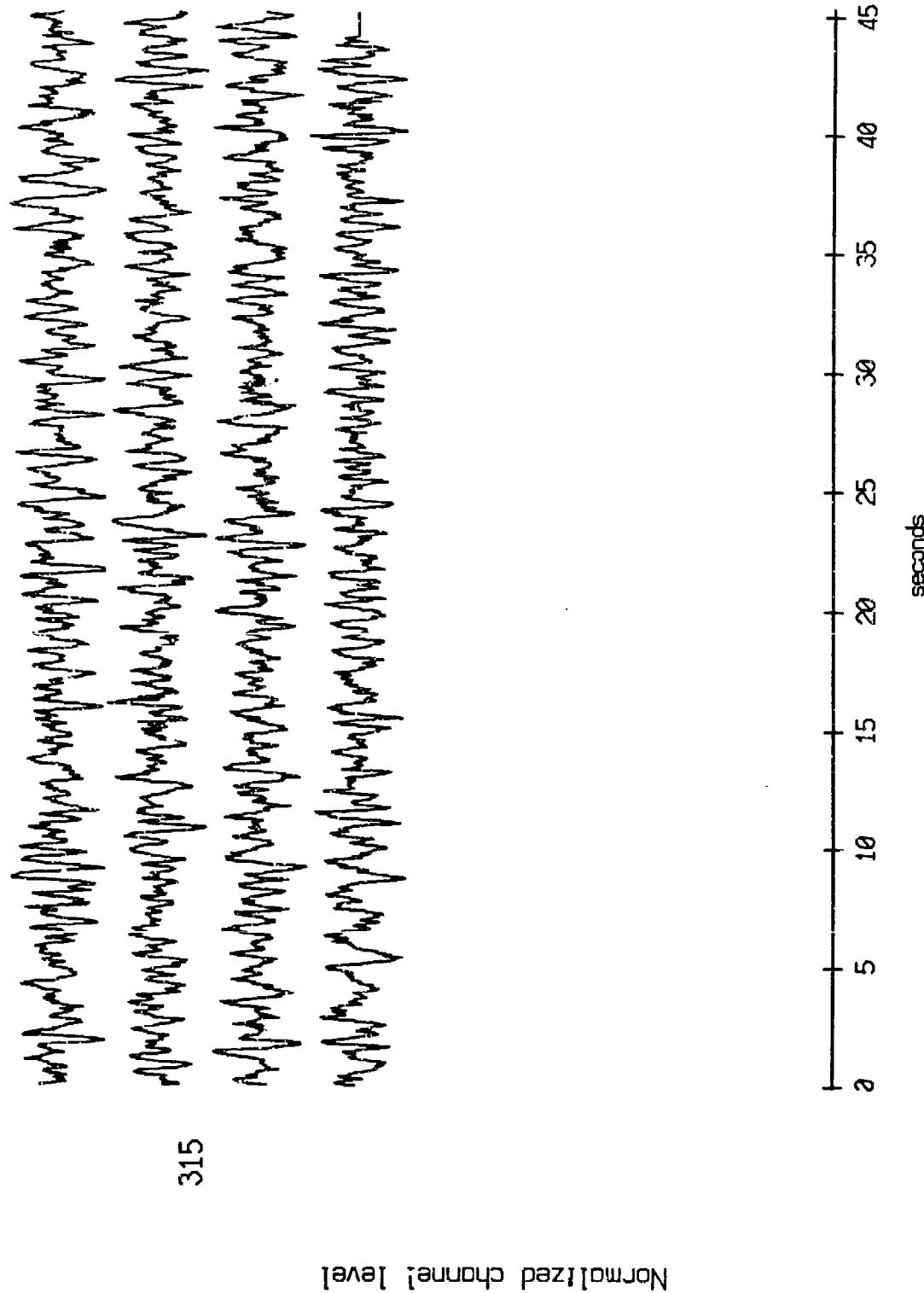


Figure X.18b.i

OBS 14, May, 1987 Trip - event 315 (Y₃ axis)
max gain-corrected amplitude is 3.330053 counts

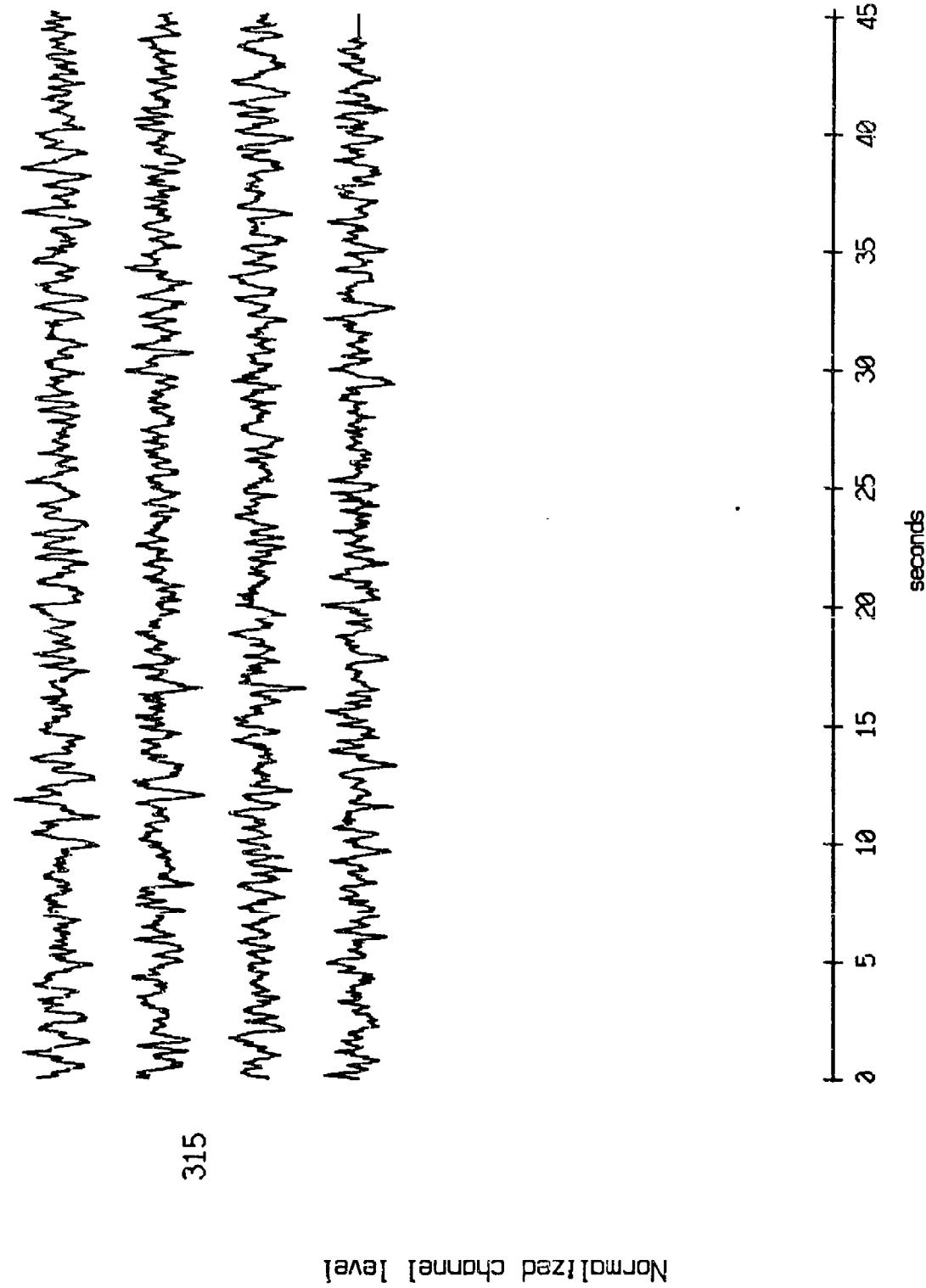
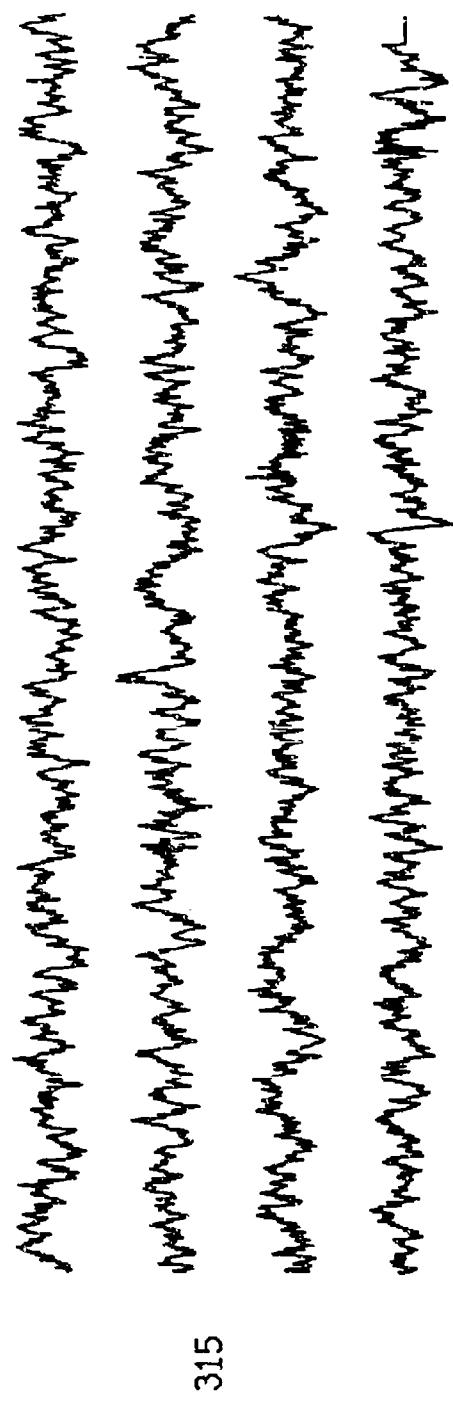


Figure X.18b.j

OBS 14, May, 1987 Trip - event 315 (Z axis)
max gain-corrected amplitude is 0.750219 counts



Normalized channel level

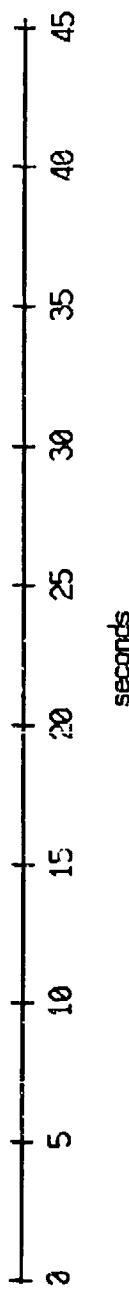


Figure X.18b.k

OBS 14, May, 1987 Trip - event 315 (pressure)
max gain-corrected amplitude is 4.084302 counts

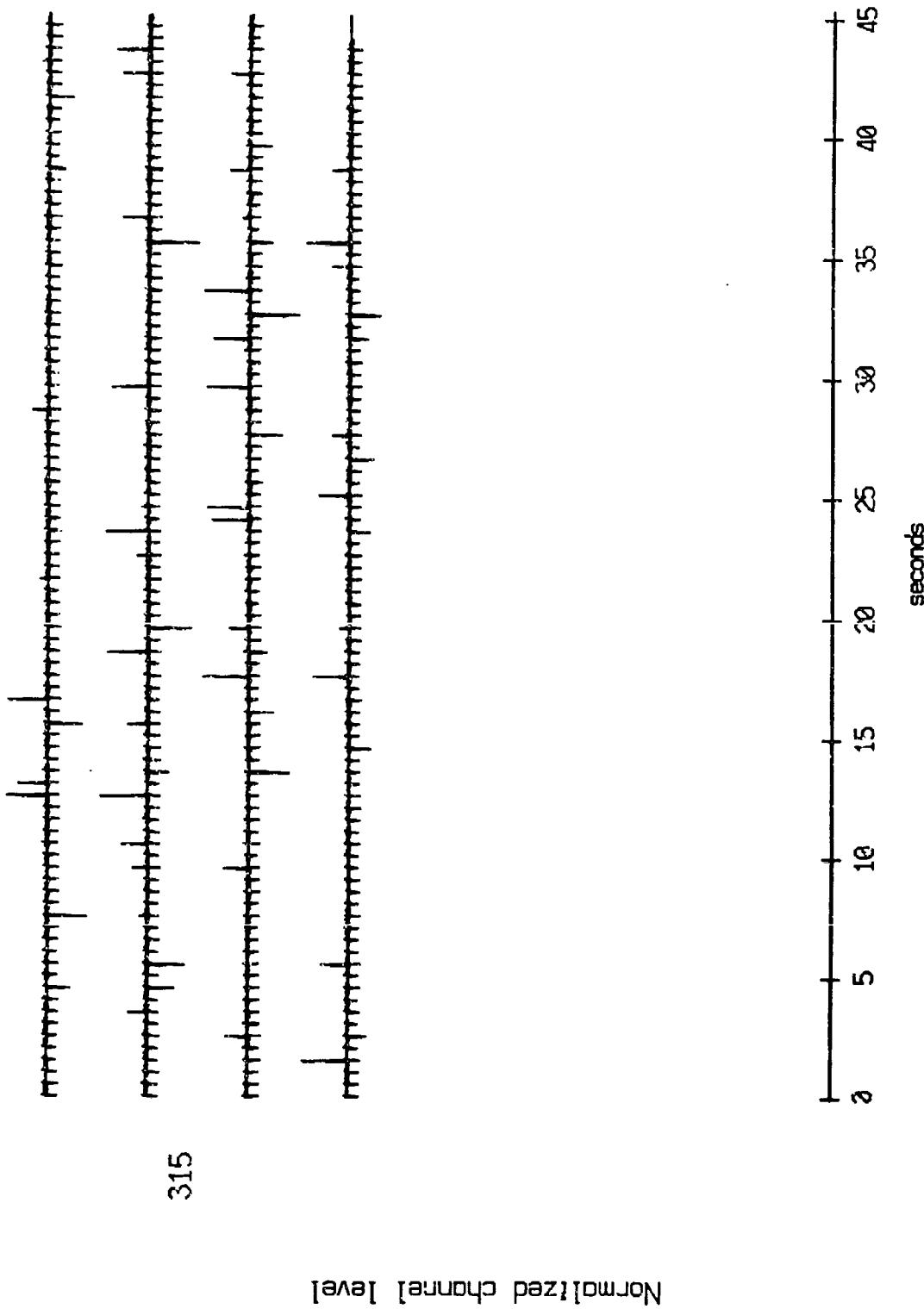


Figure X.18b.1

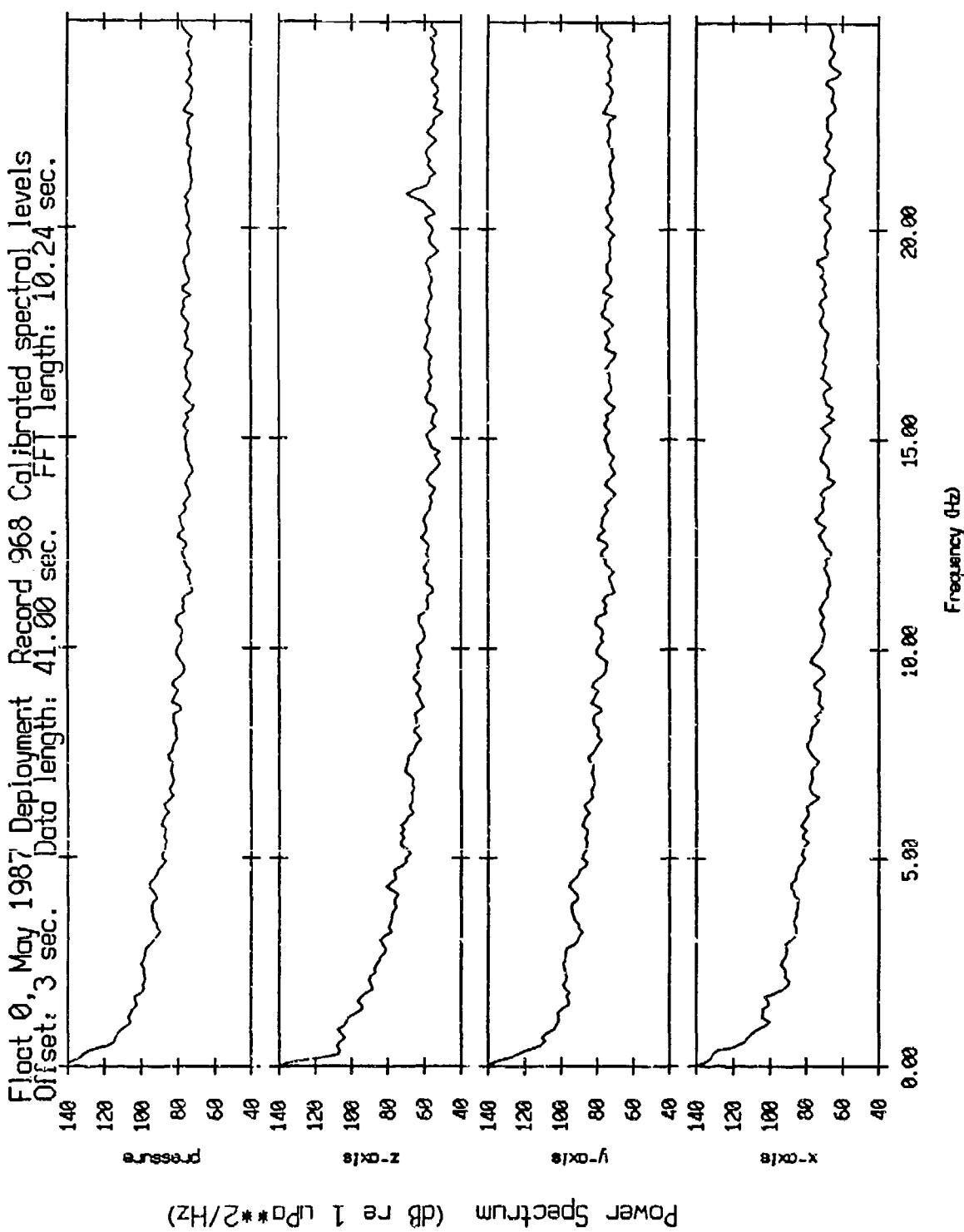


Figure XI.1a

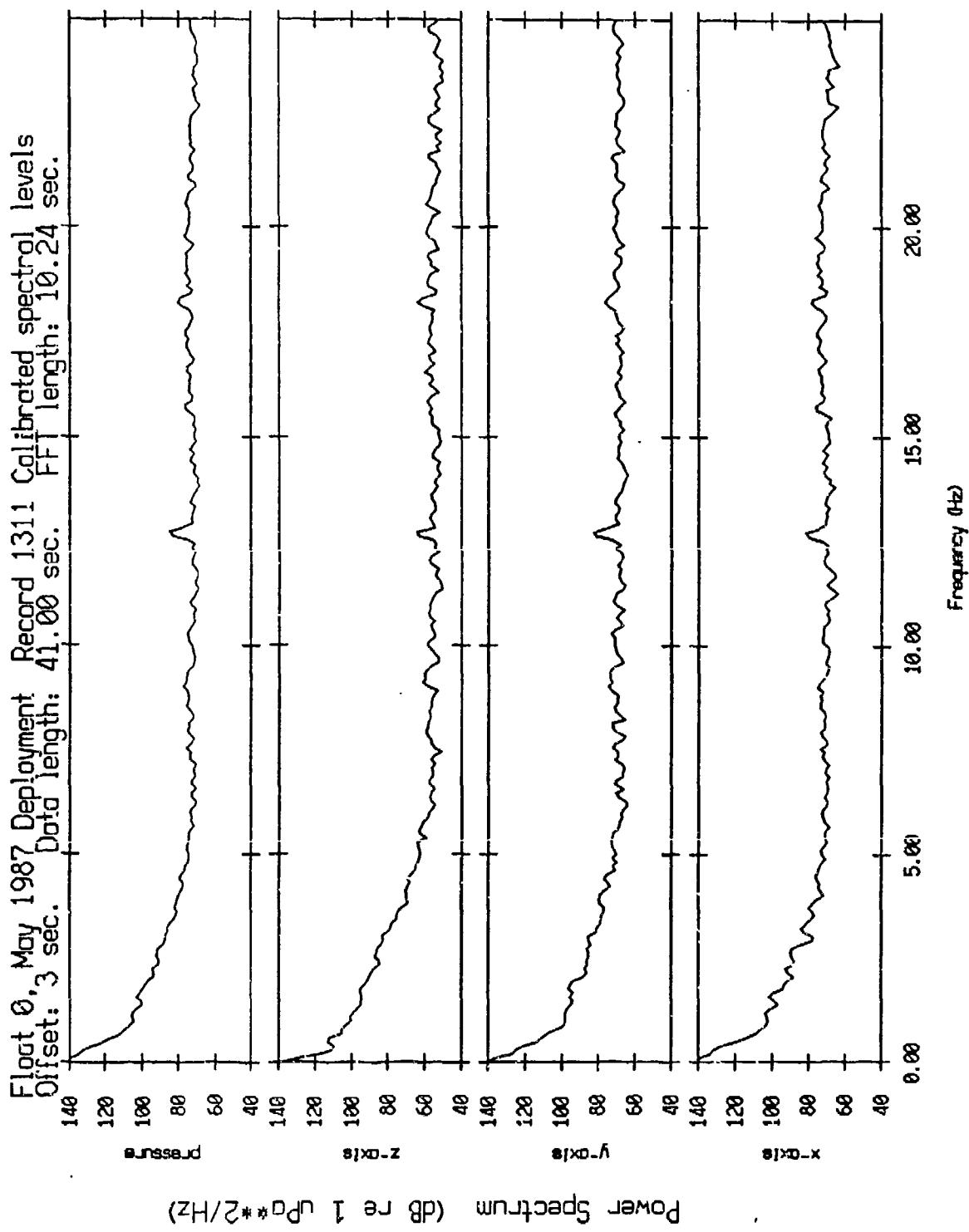


Figure XI.1b

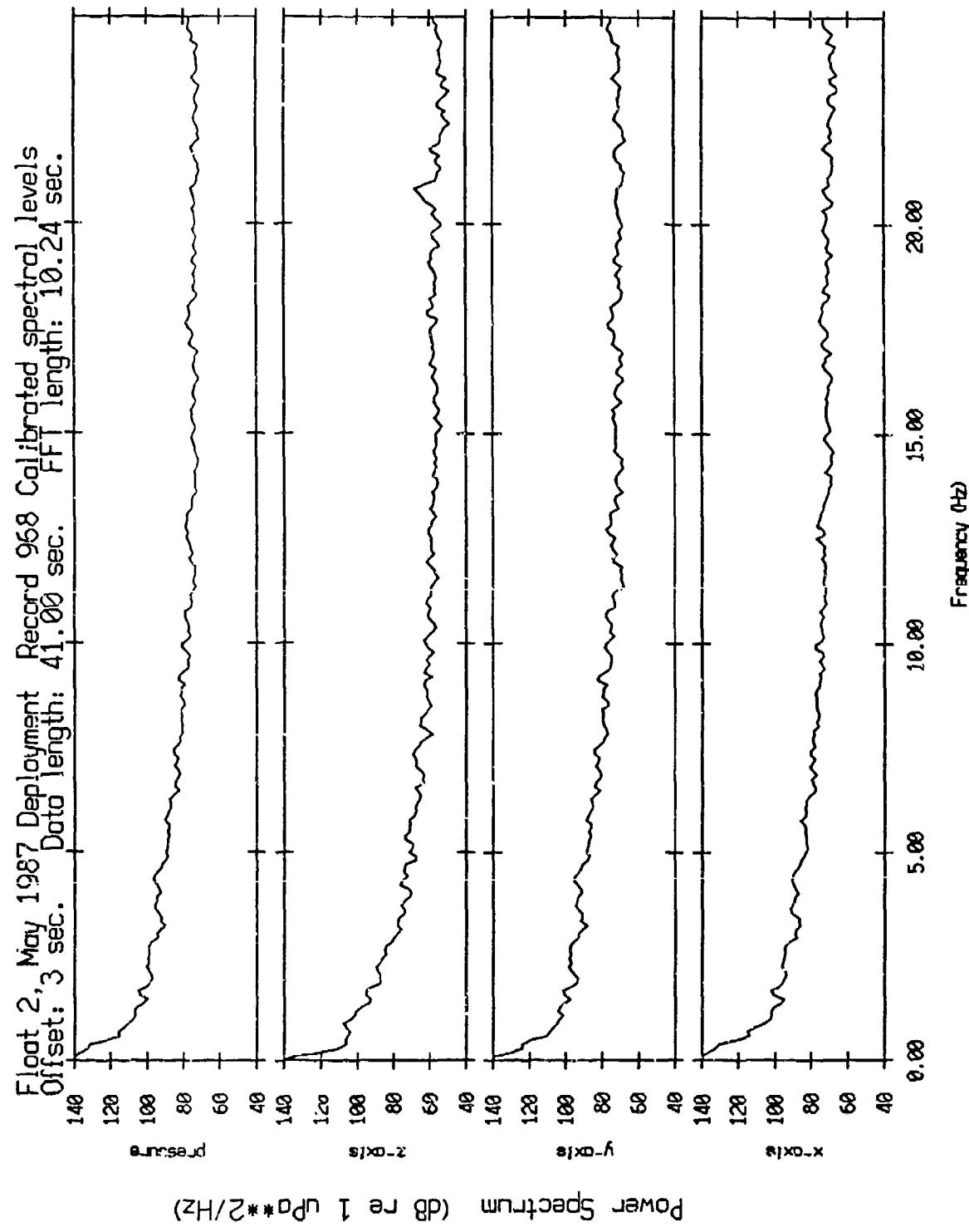


Figure XI.2a

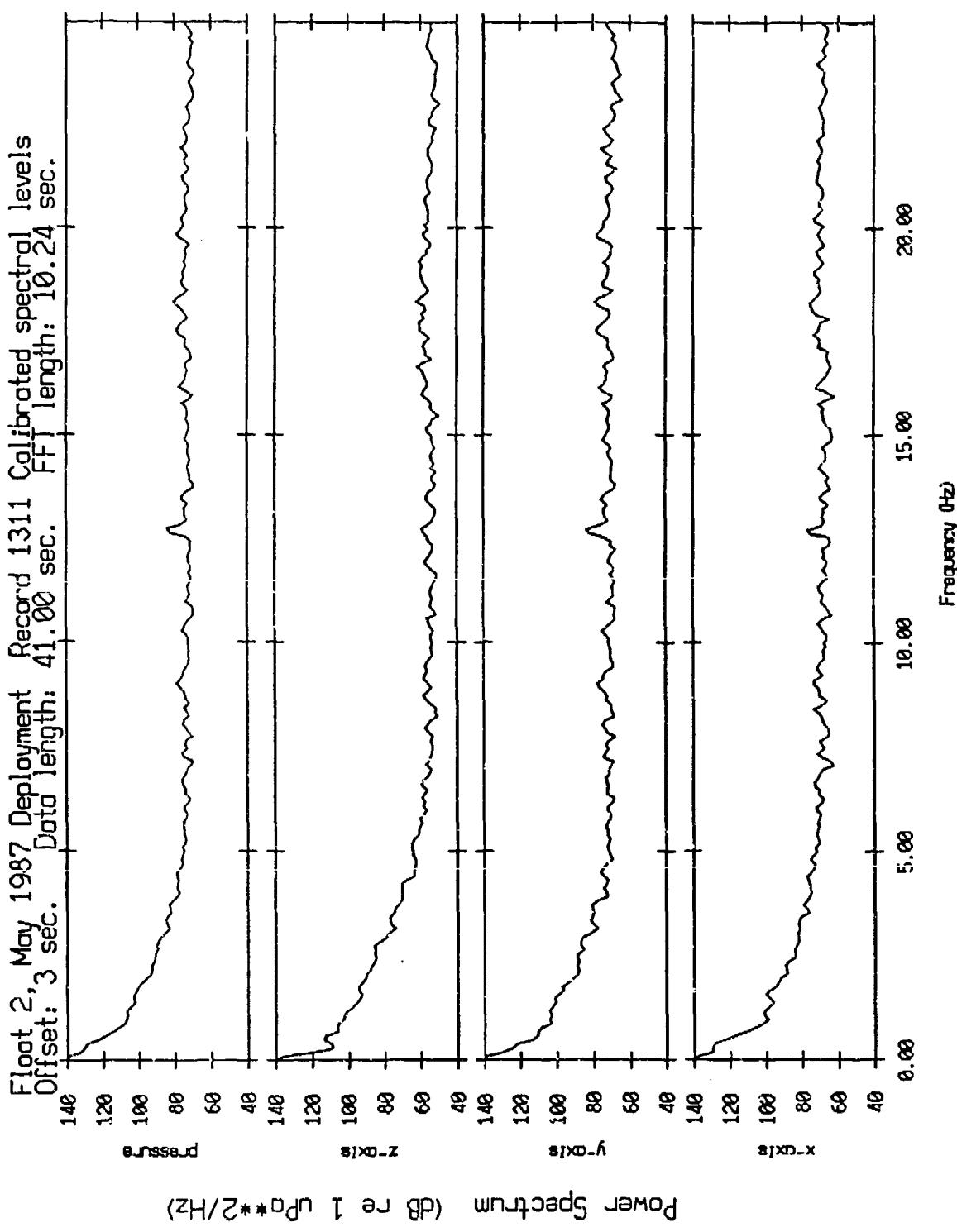


Figure XI.2b

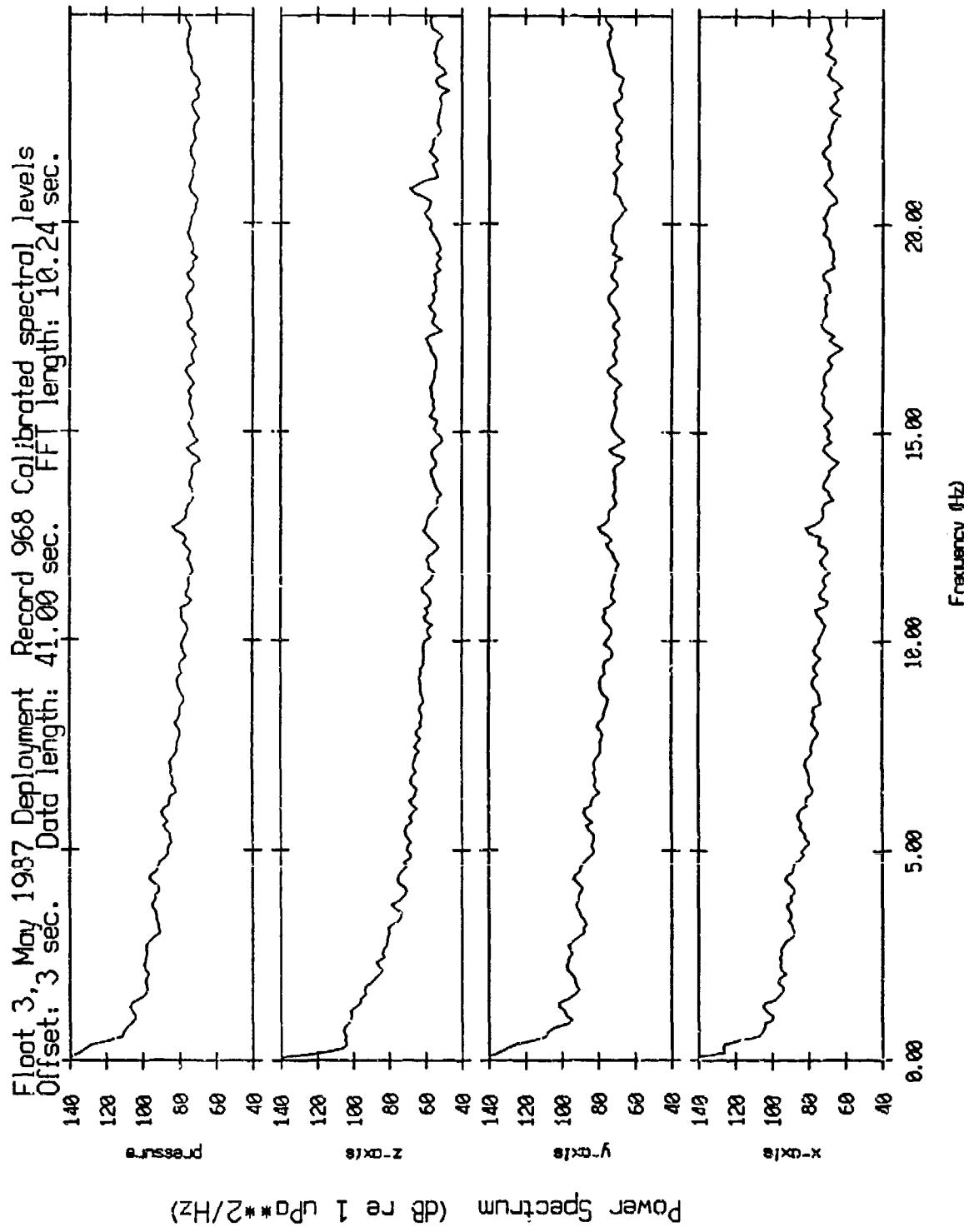


Figure XI.3a

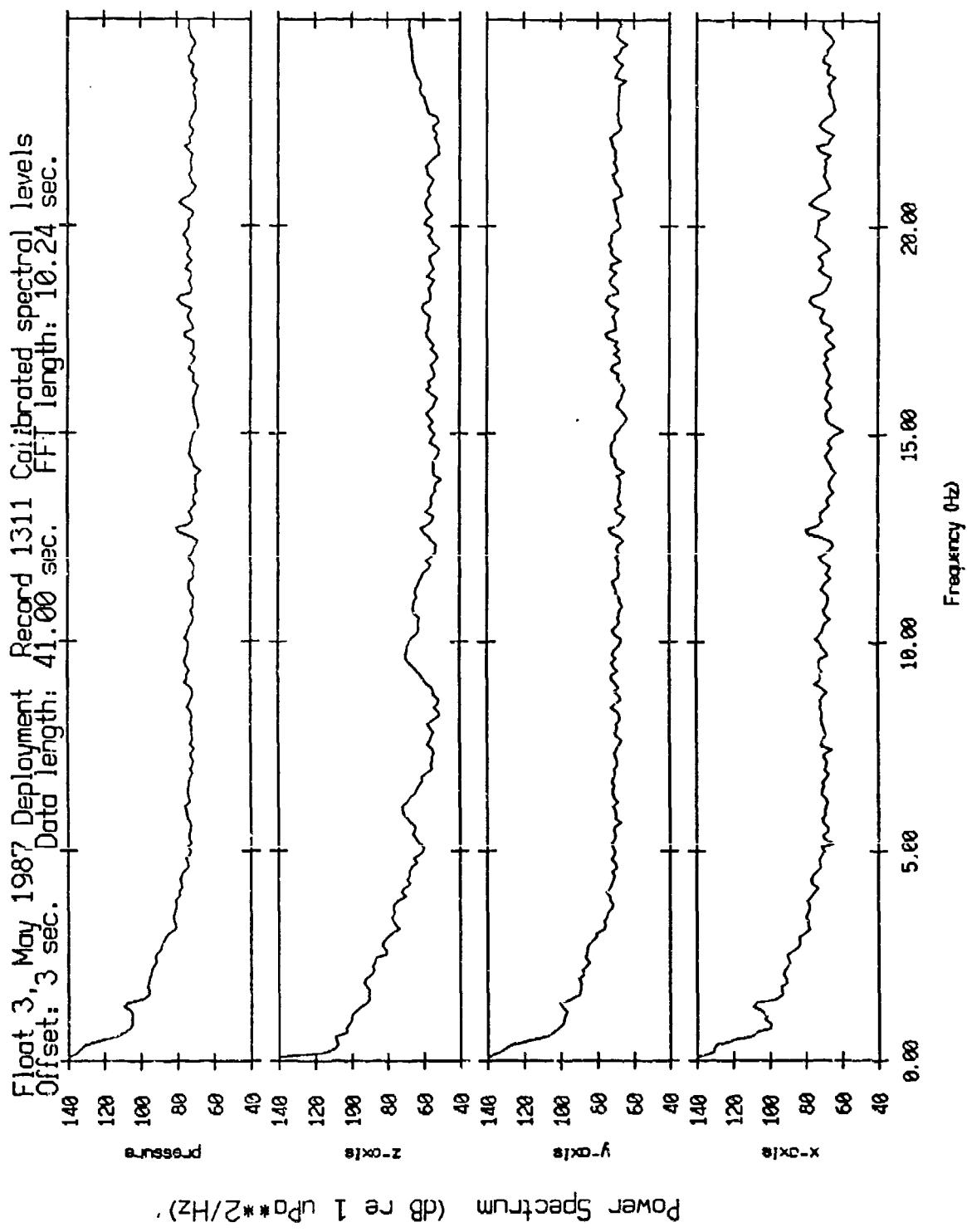


Figure XI.3b

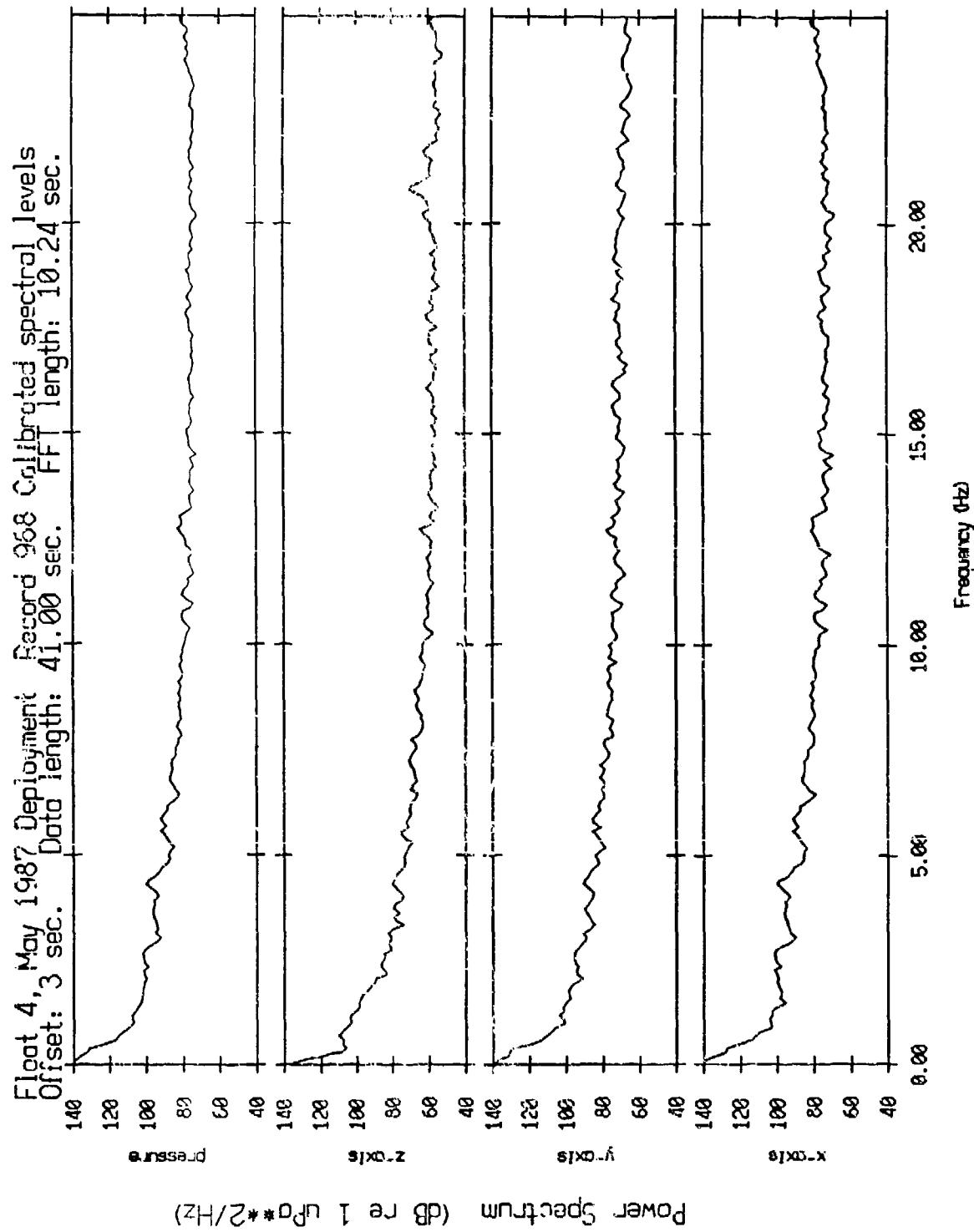


Figure XI.4a

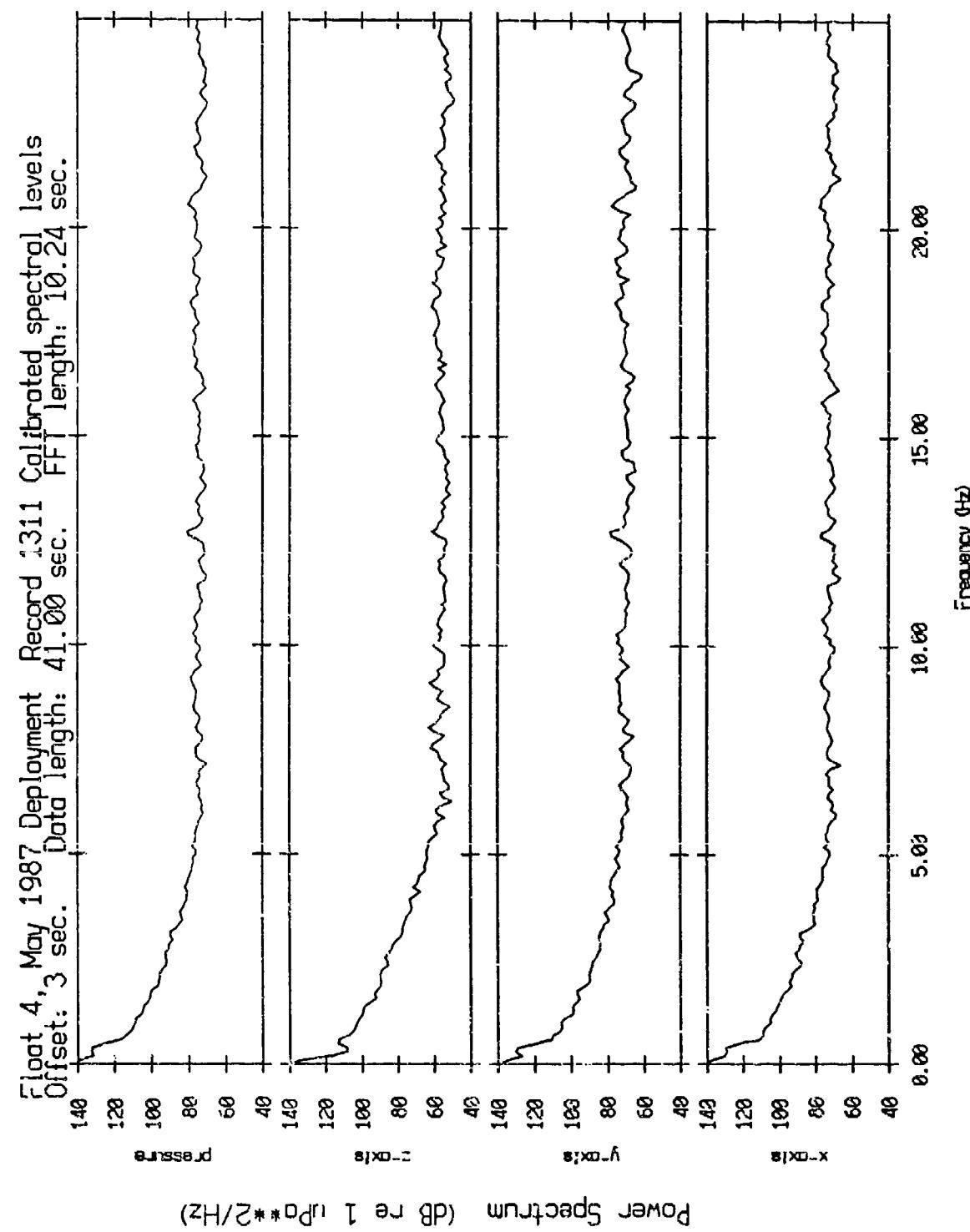


Figure XI.4b

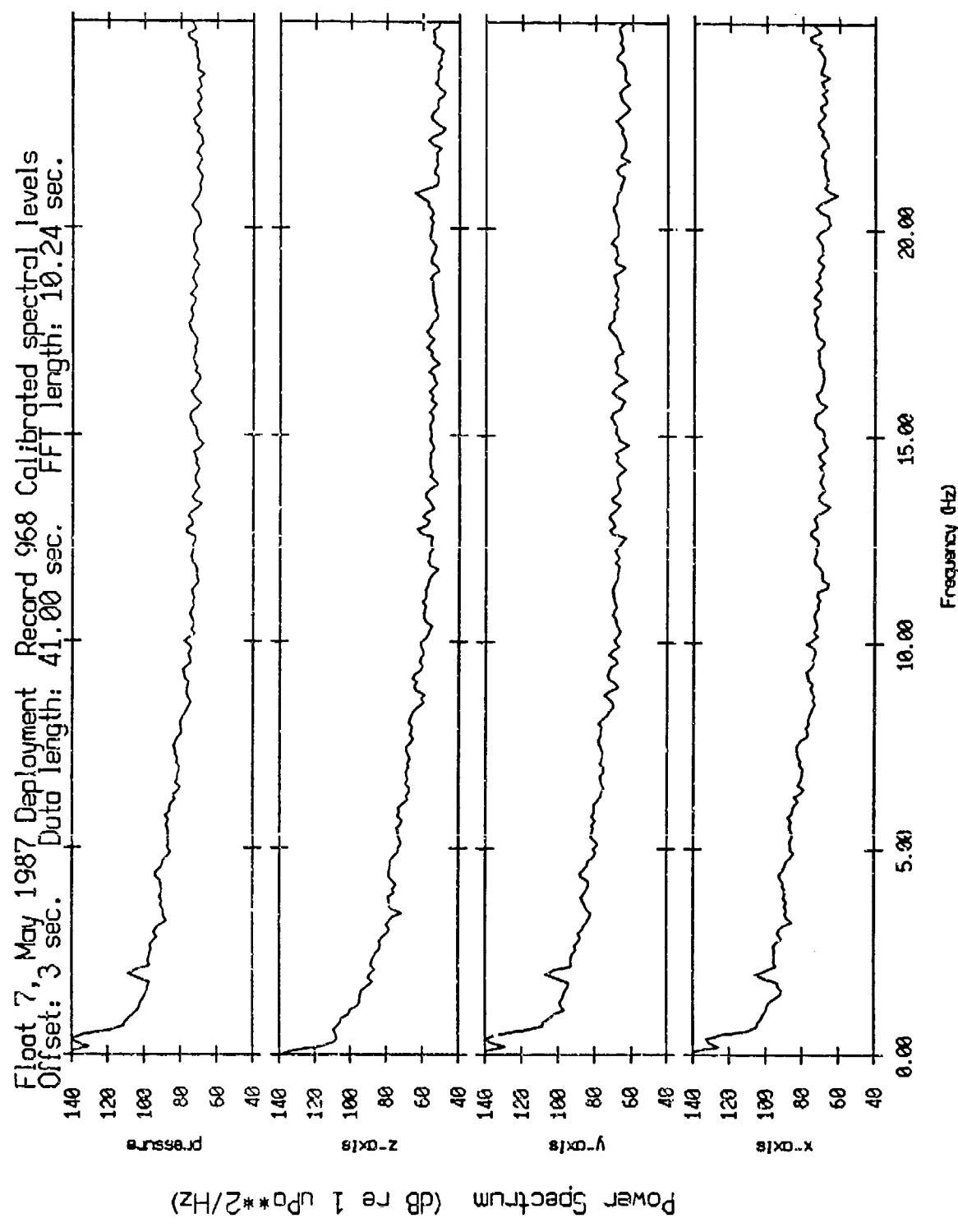


Figure XI.5a

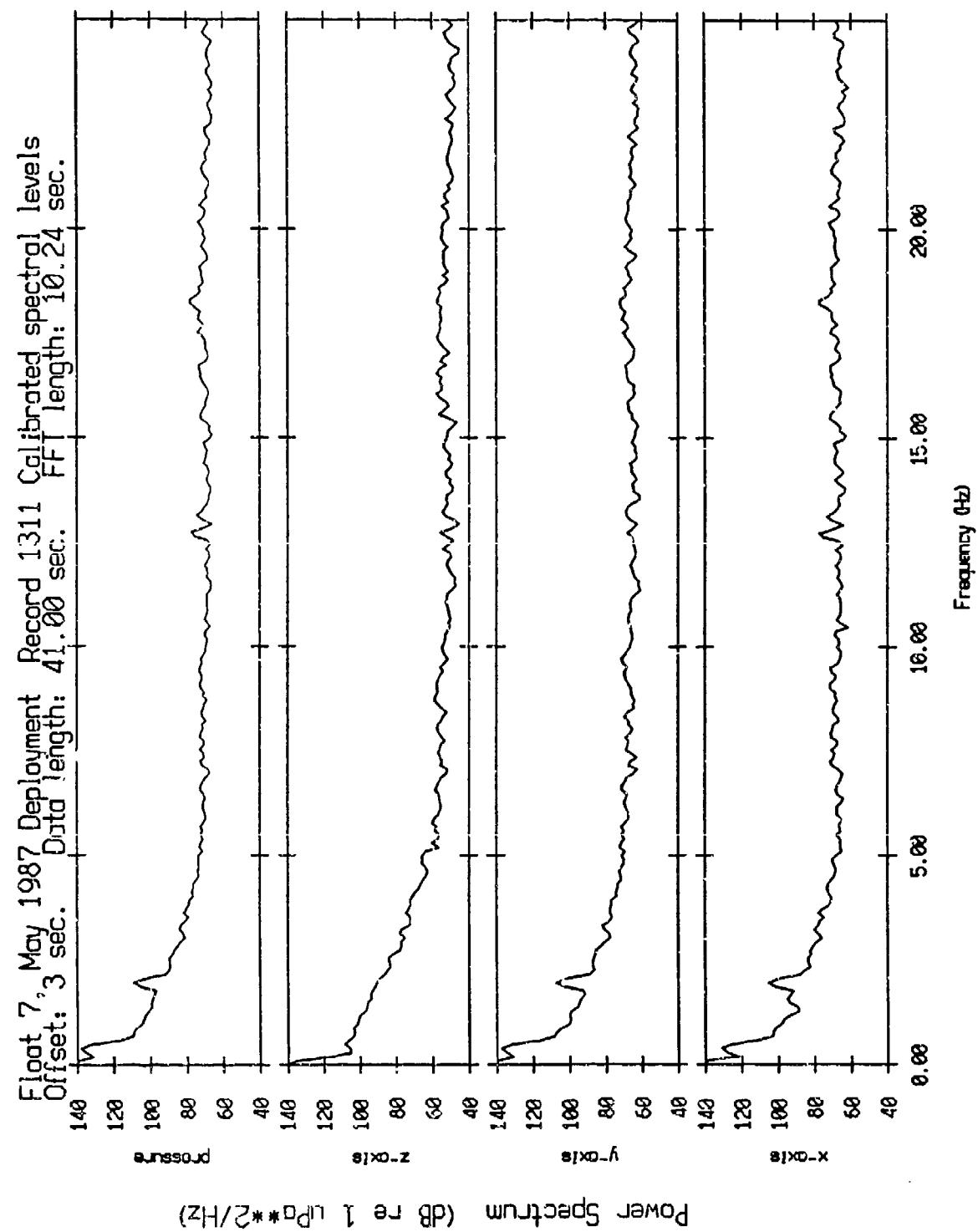


Figure XI.5b

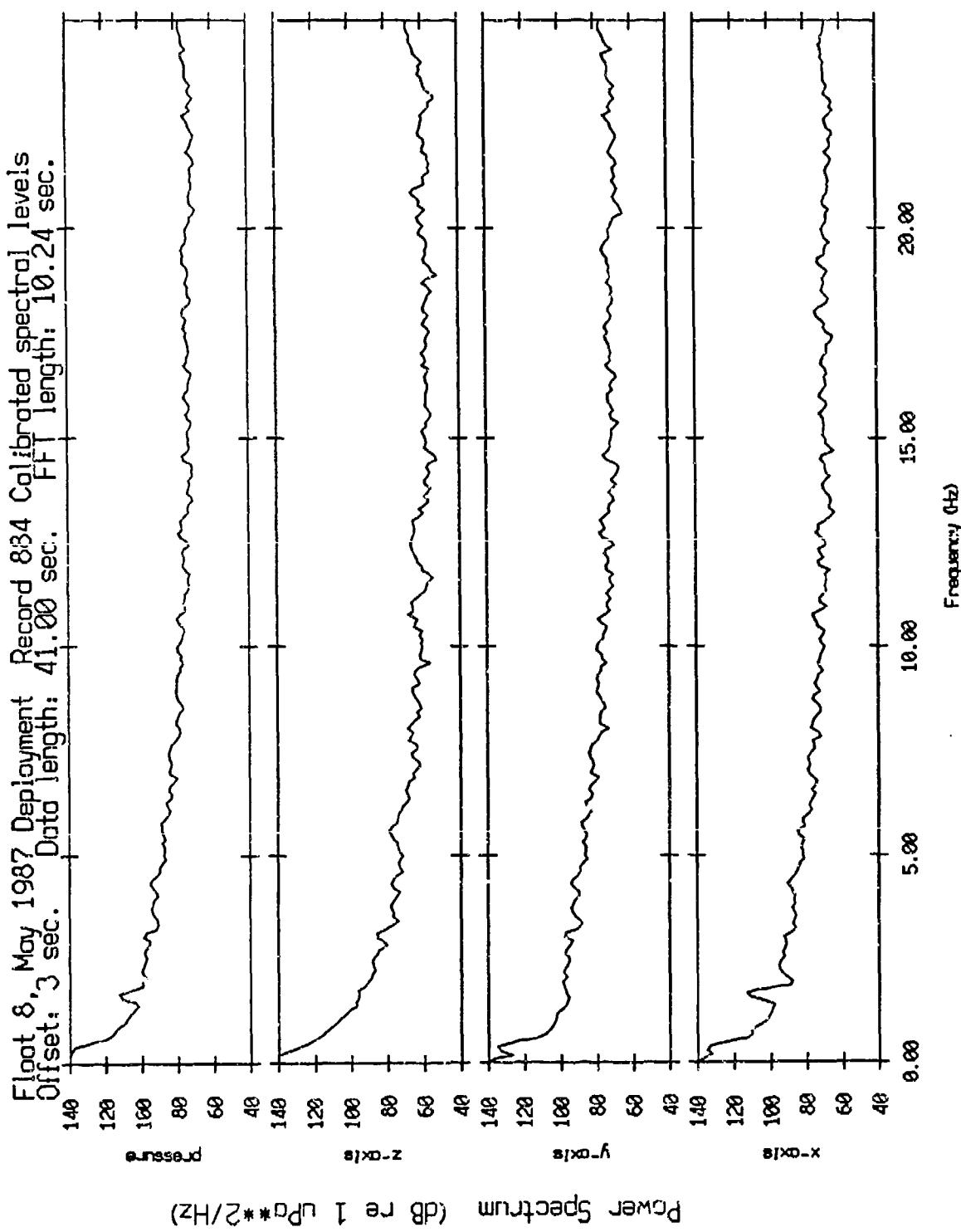


Figure XI.6a

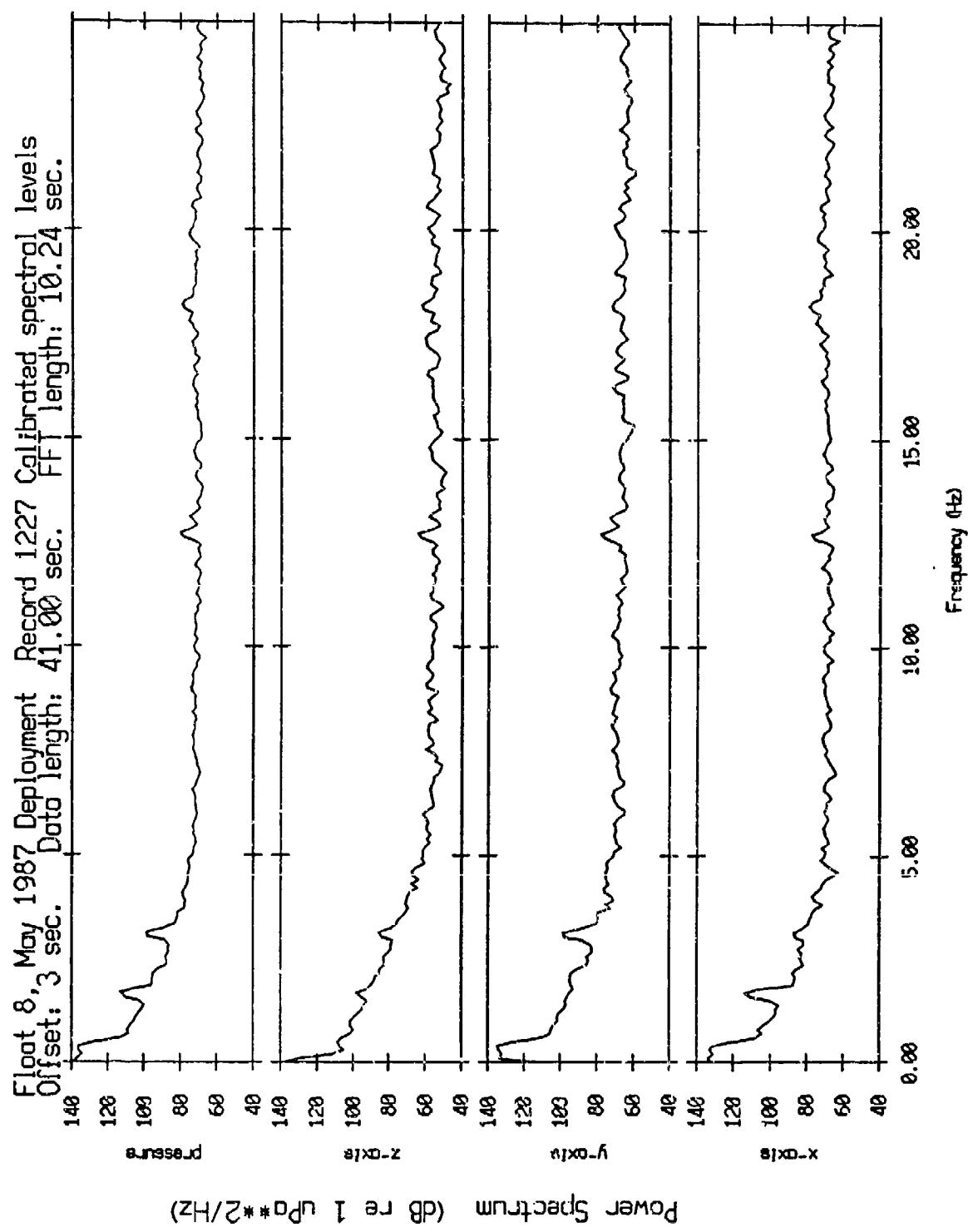


Figure XI.6b

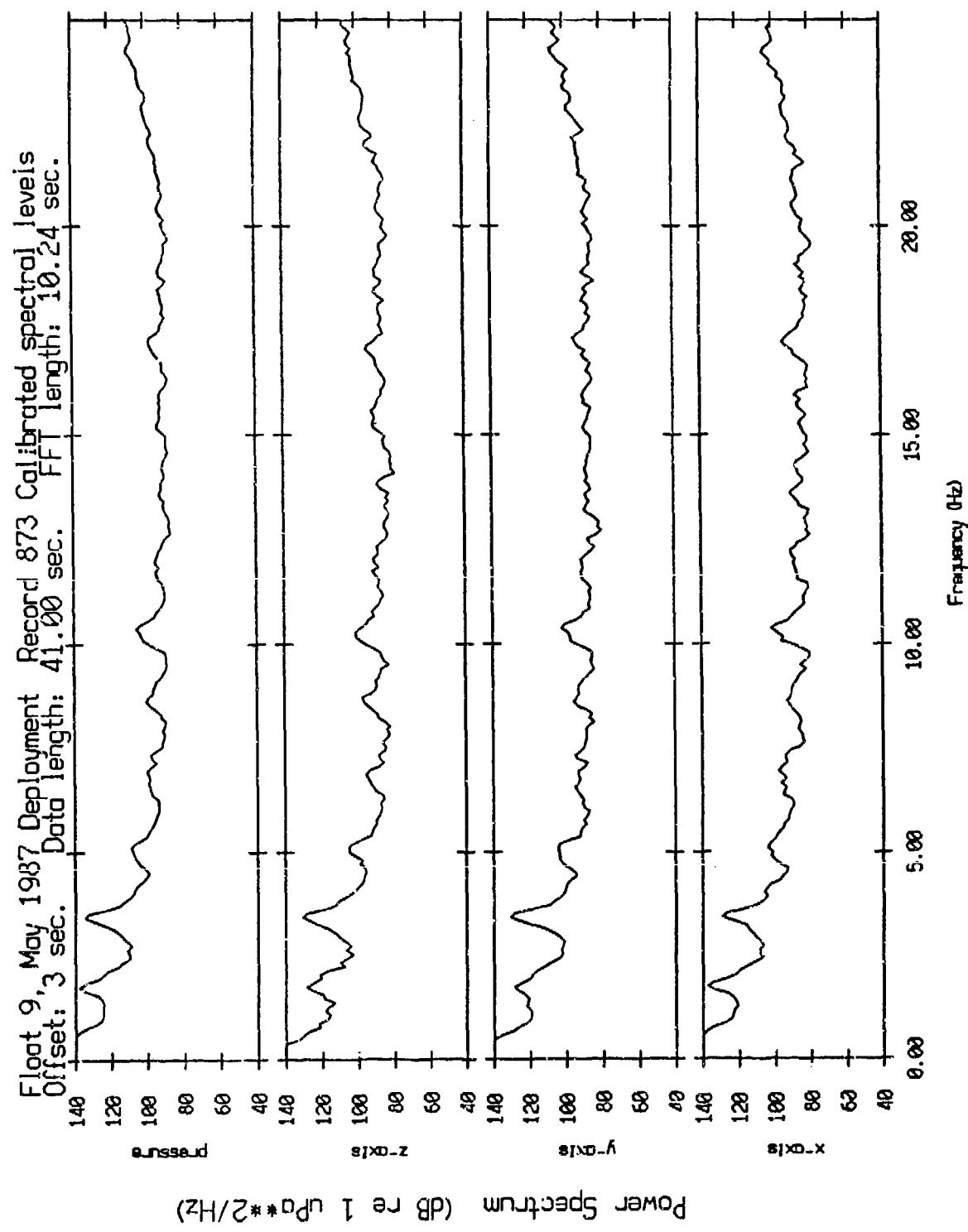


Figure XI.7a

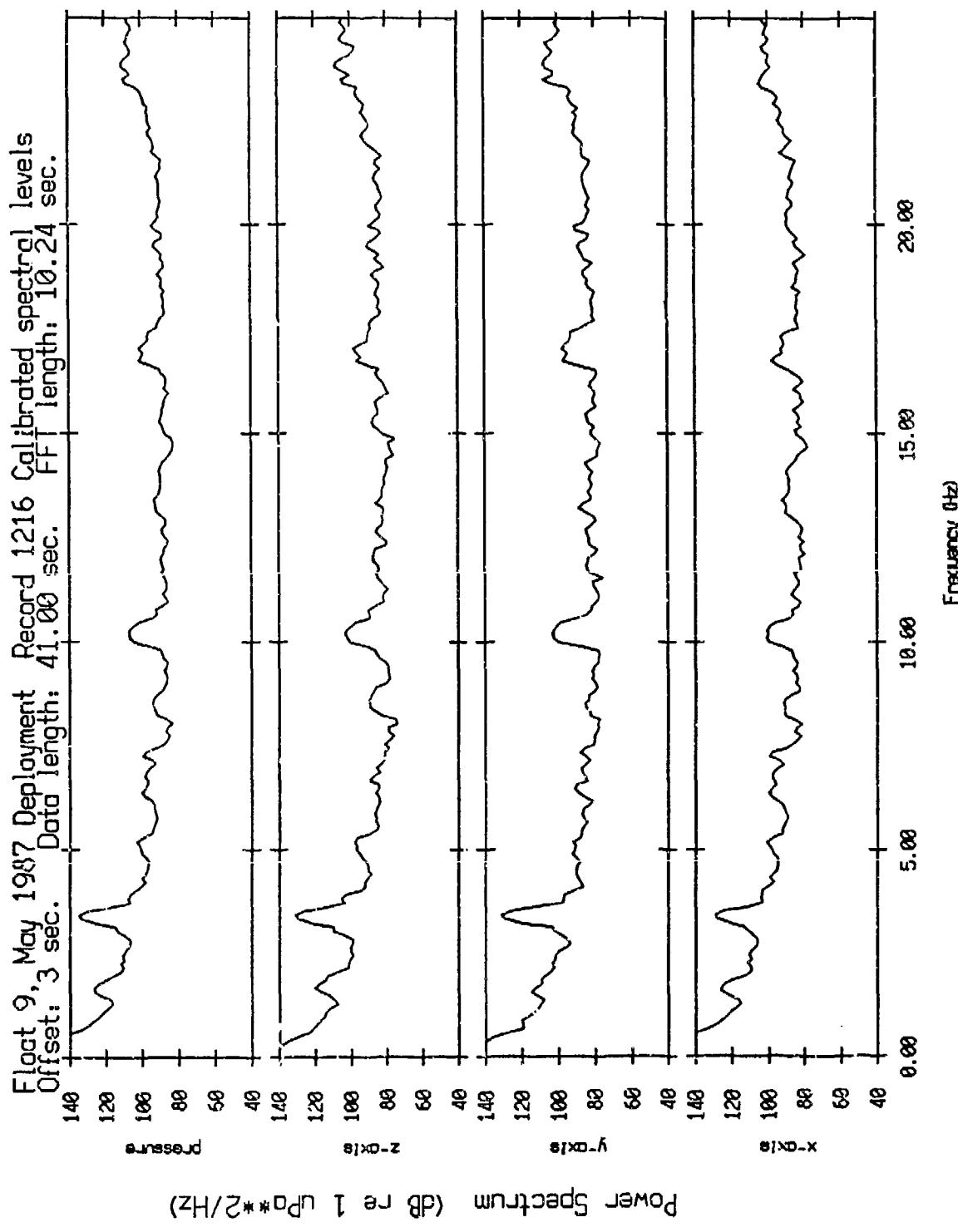


Figure XI.7v

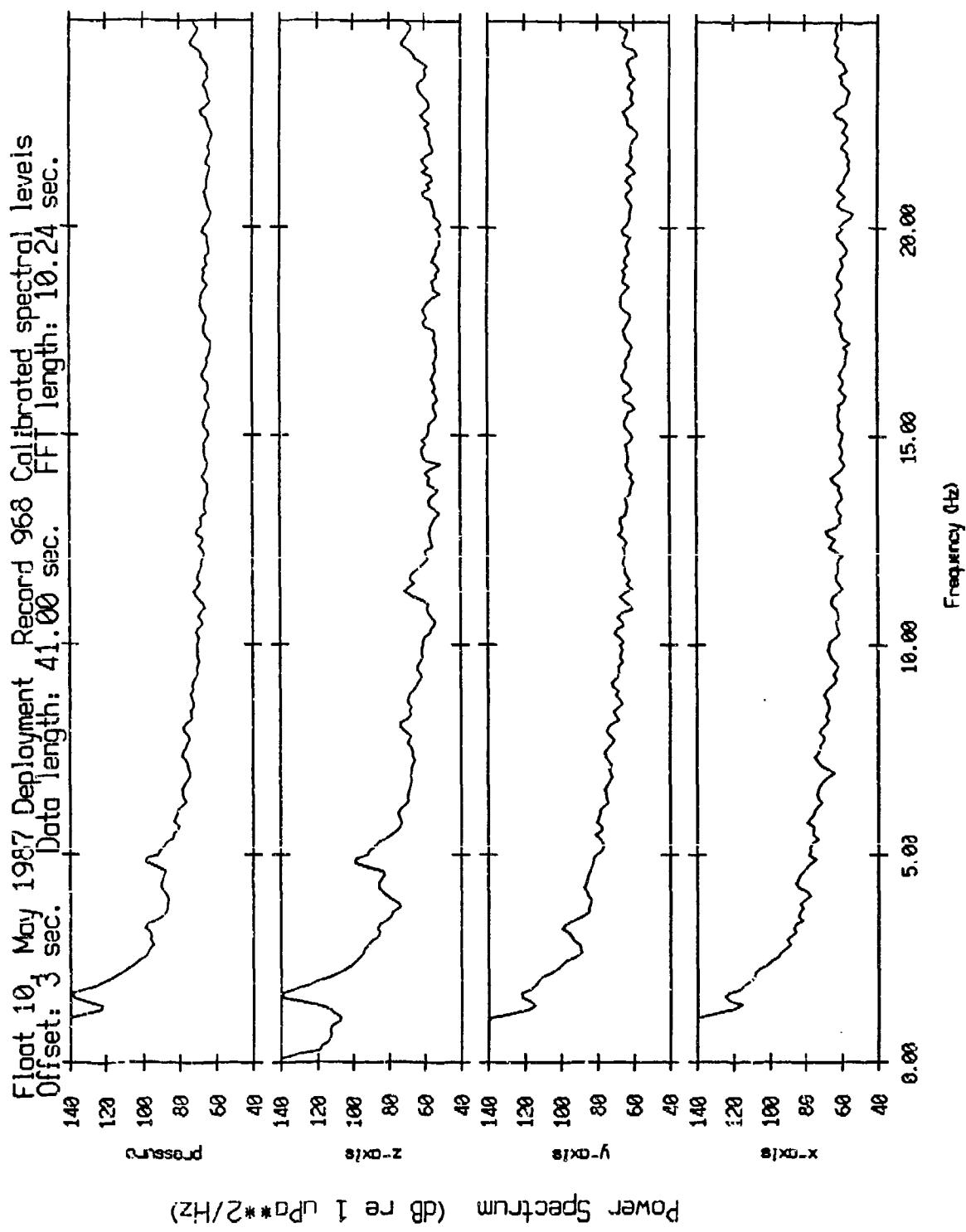


Figure XI.8a

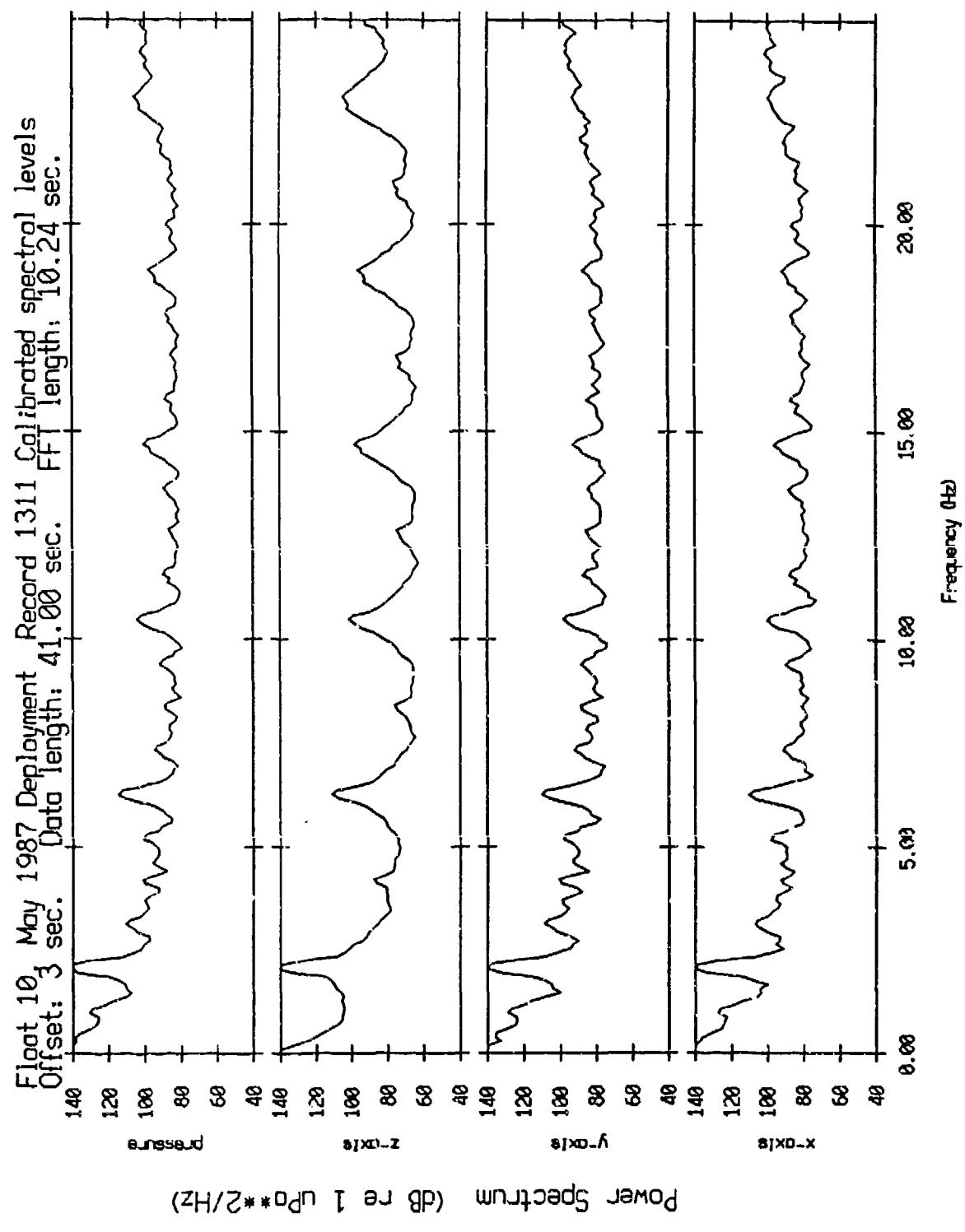


Figure XI.8b

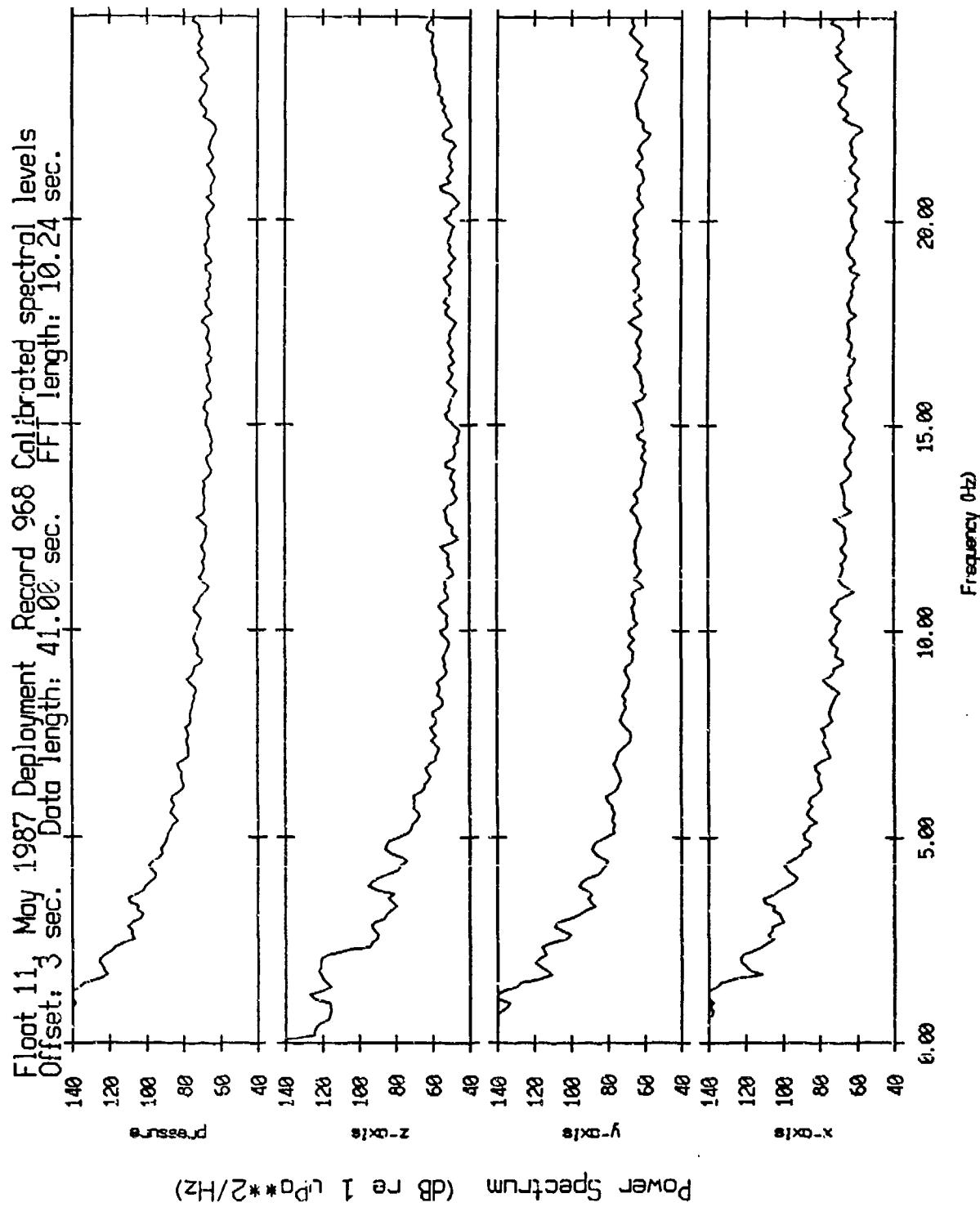


Figure XI.9a

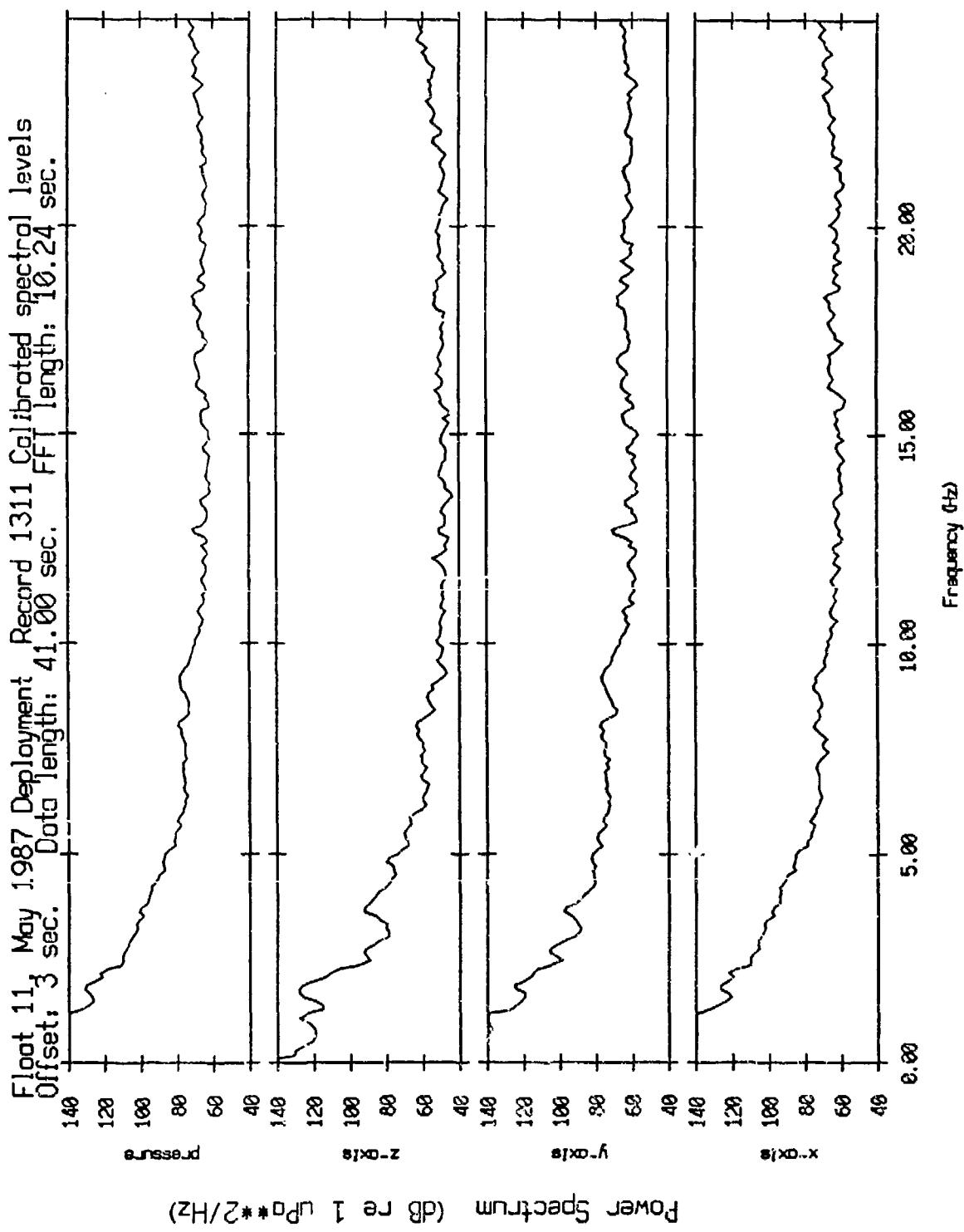


Figure XI.9b

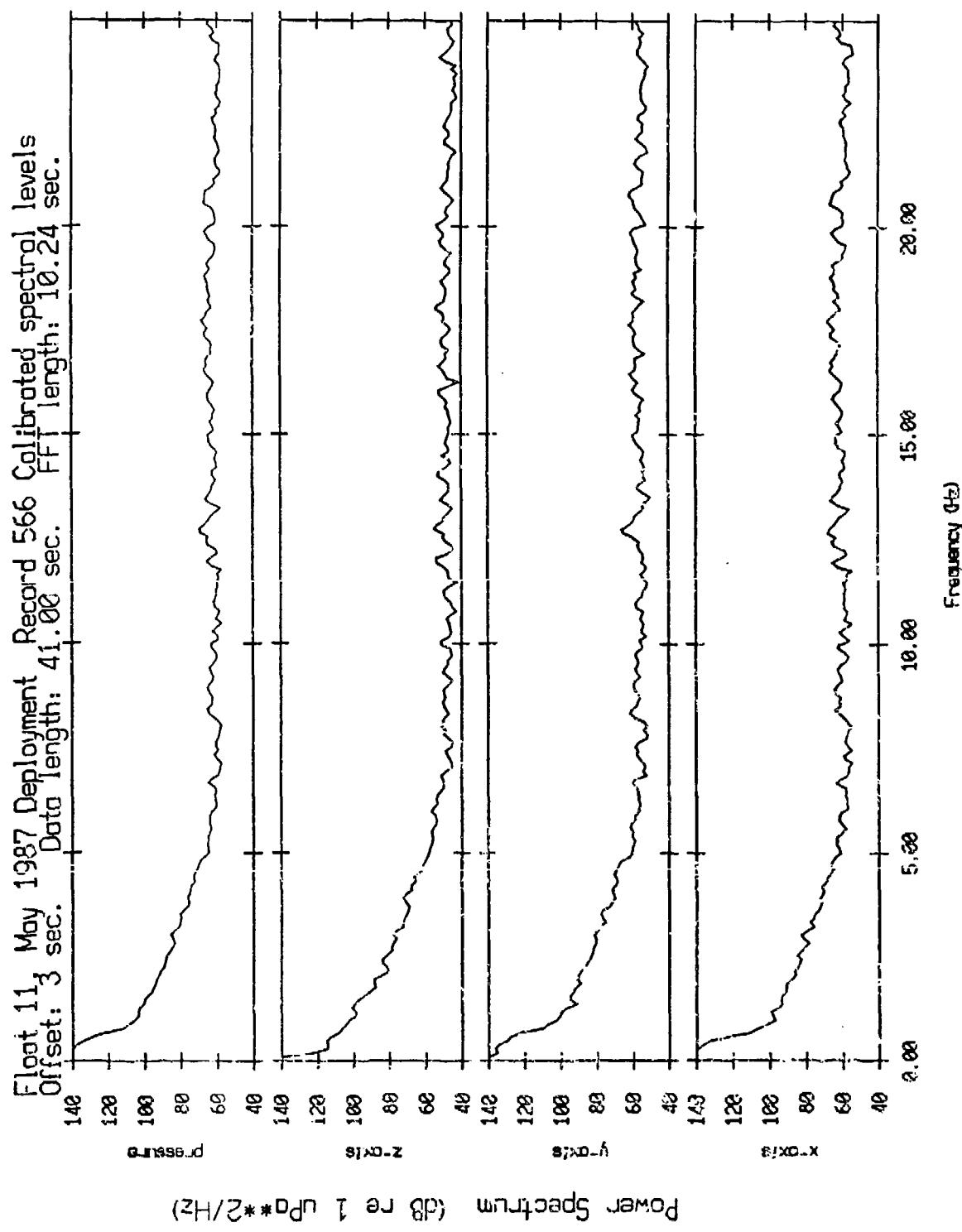


Figure XI.9c

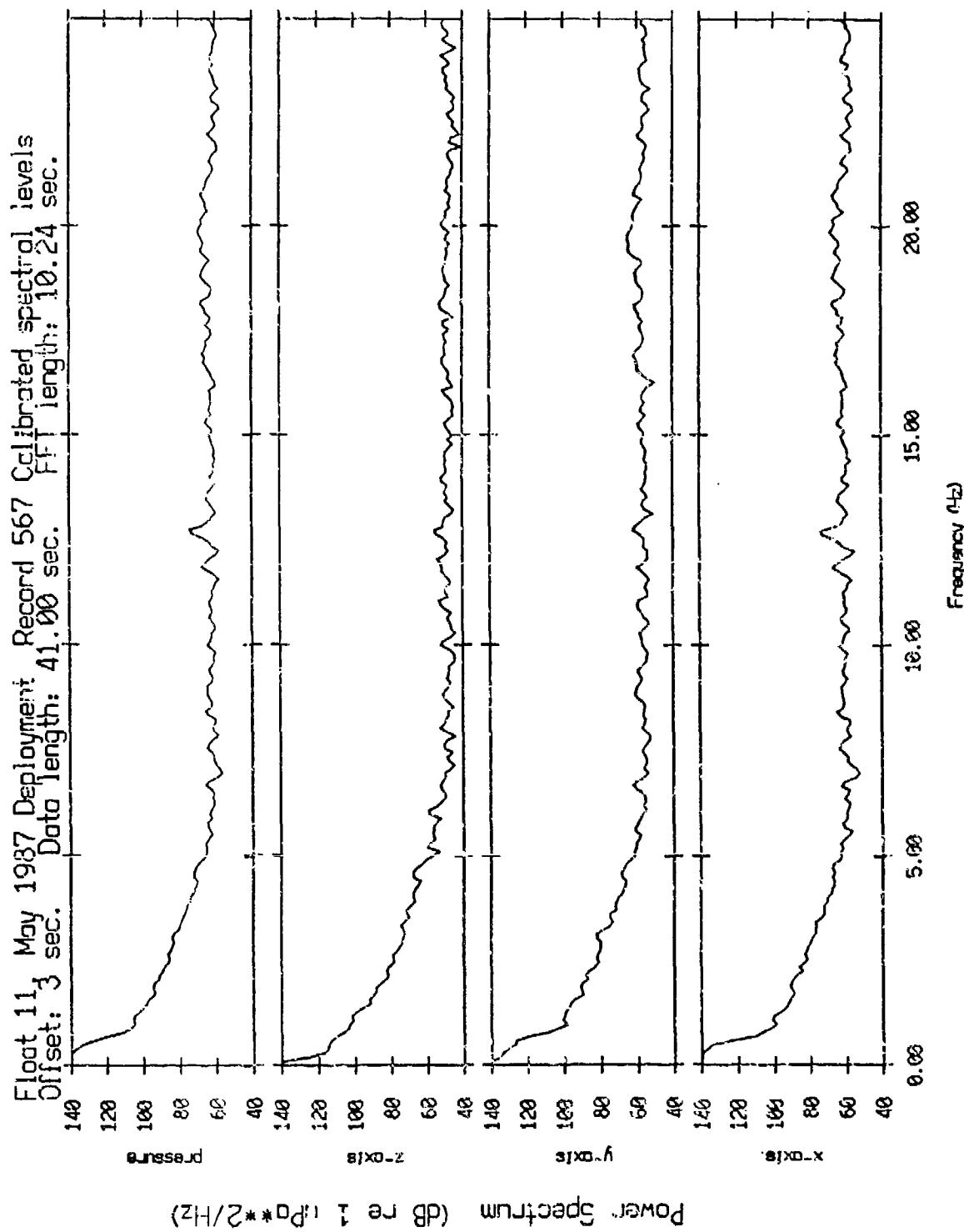


Figure XI.9d

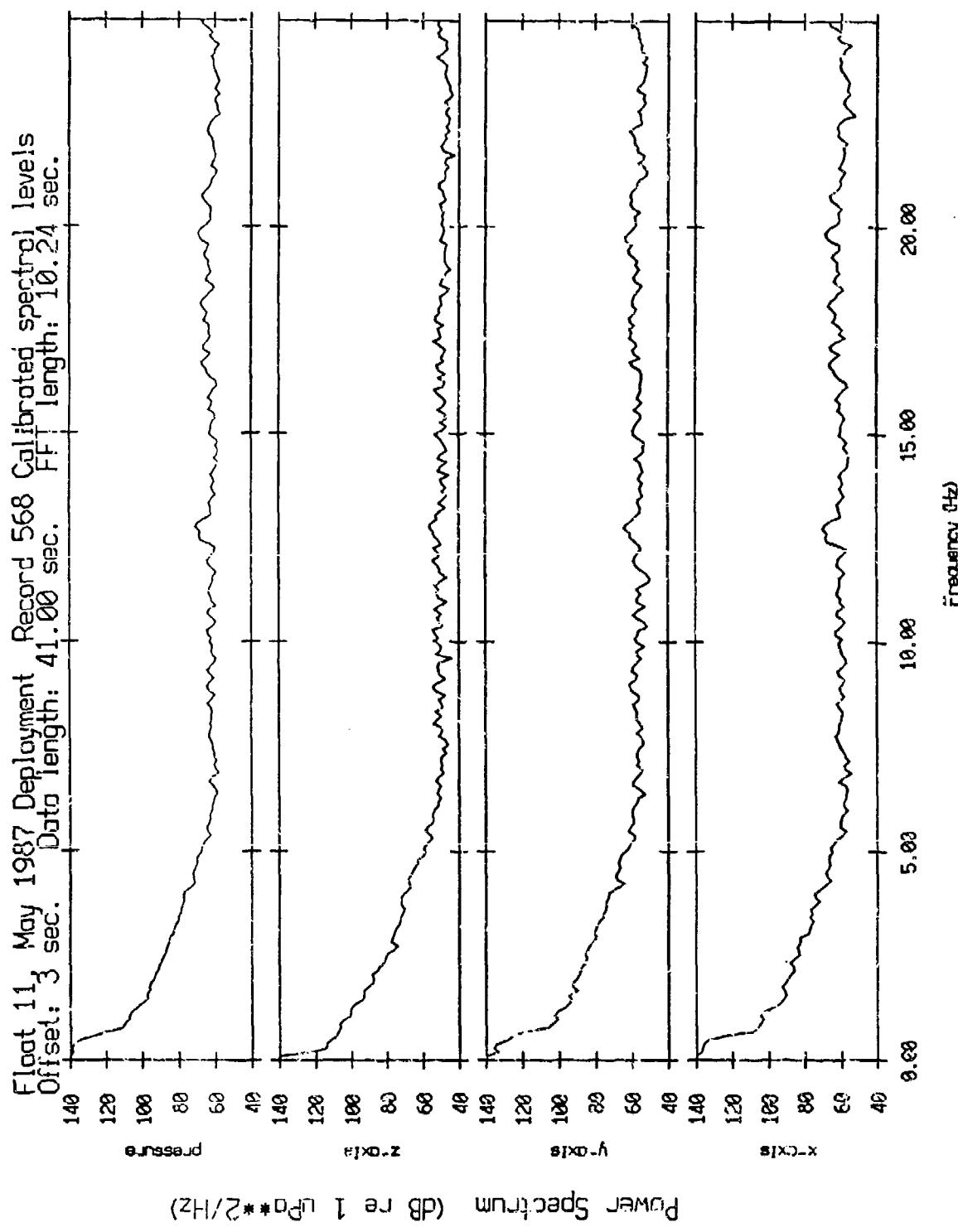


Figure XI.9e

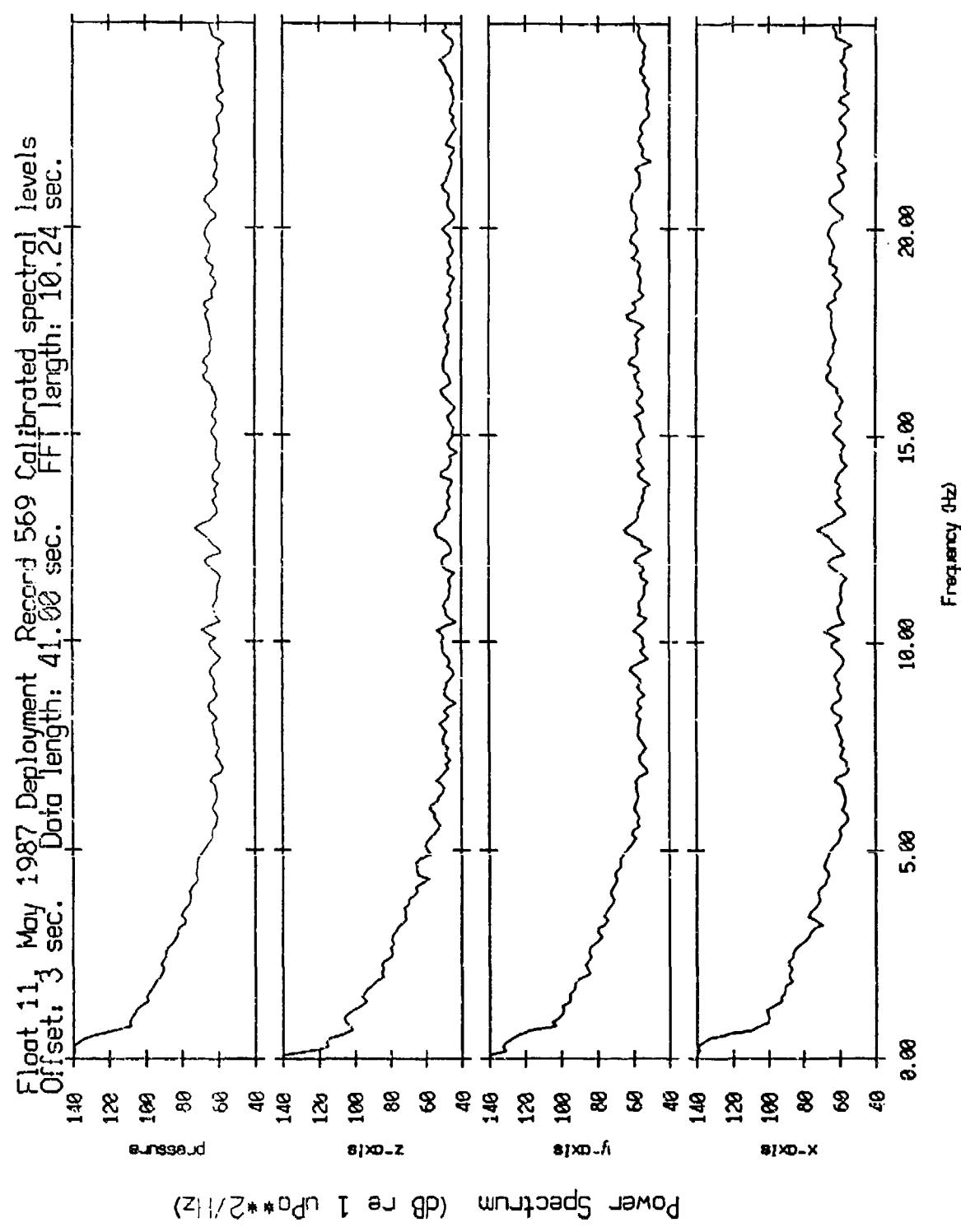


Figure XI.9f

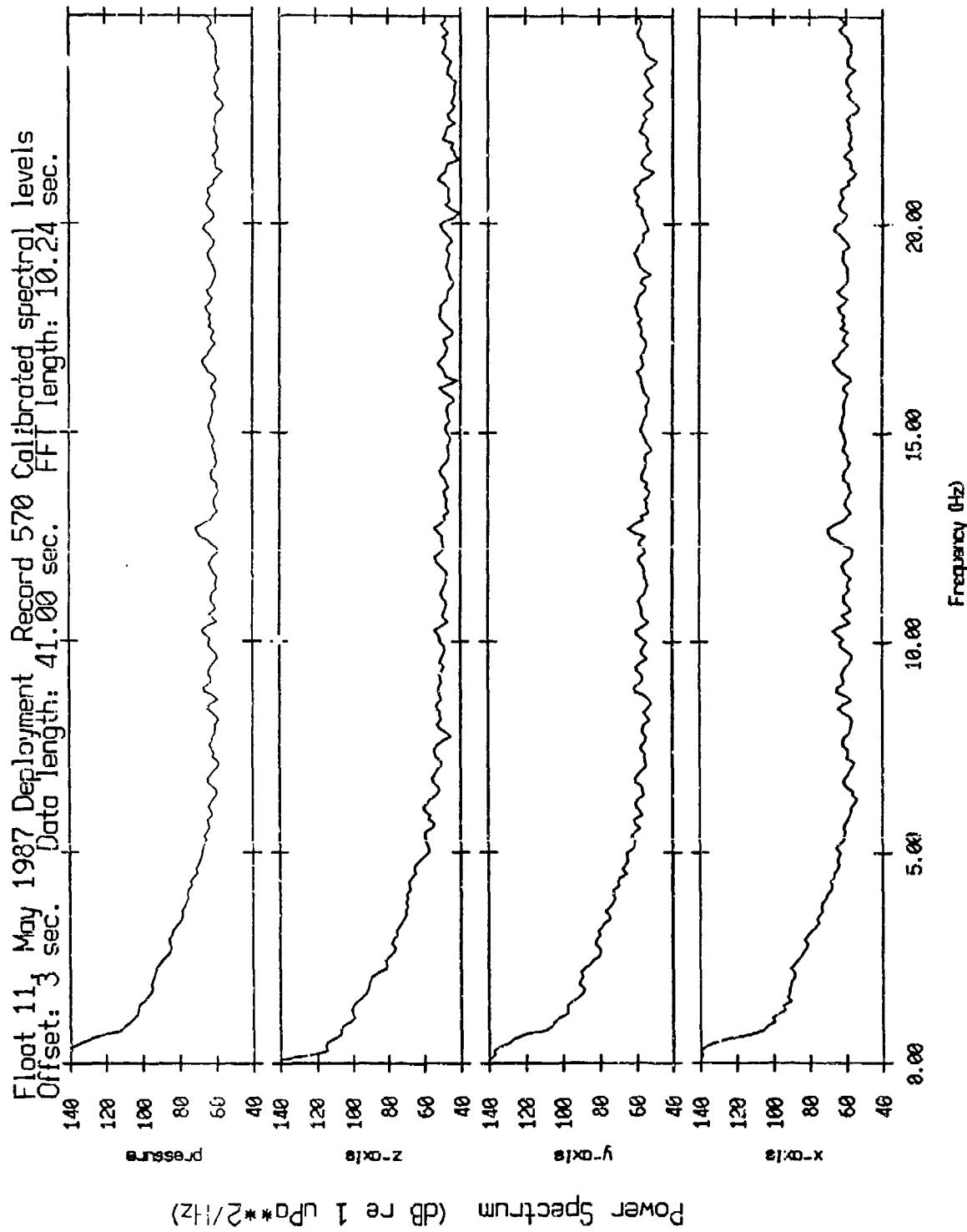


Figure XI.9g

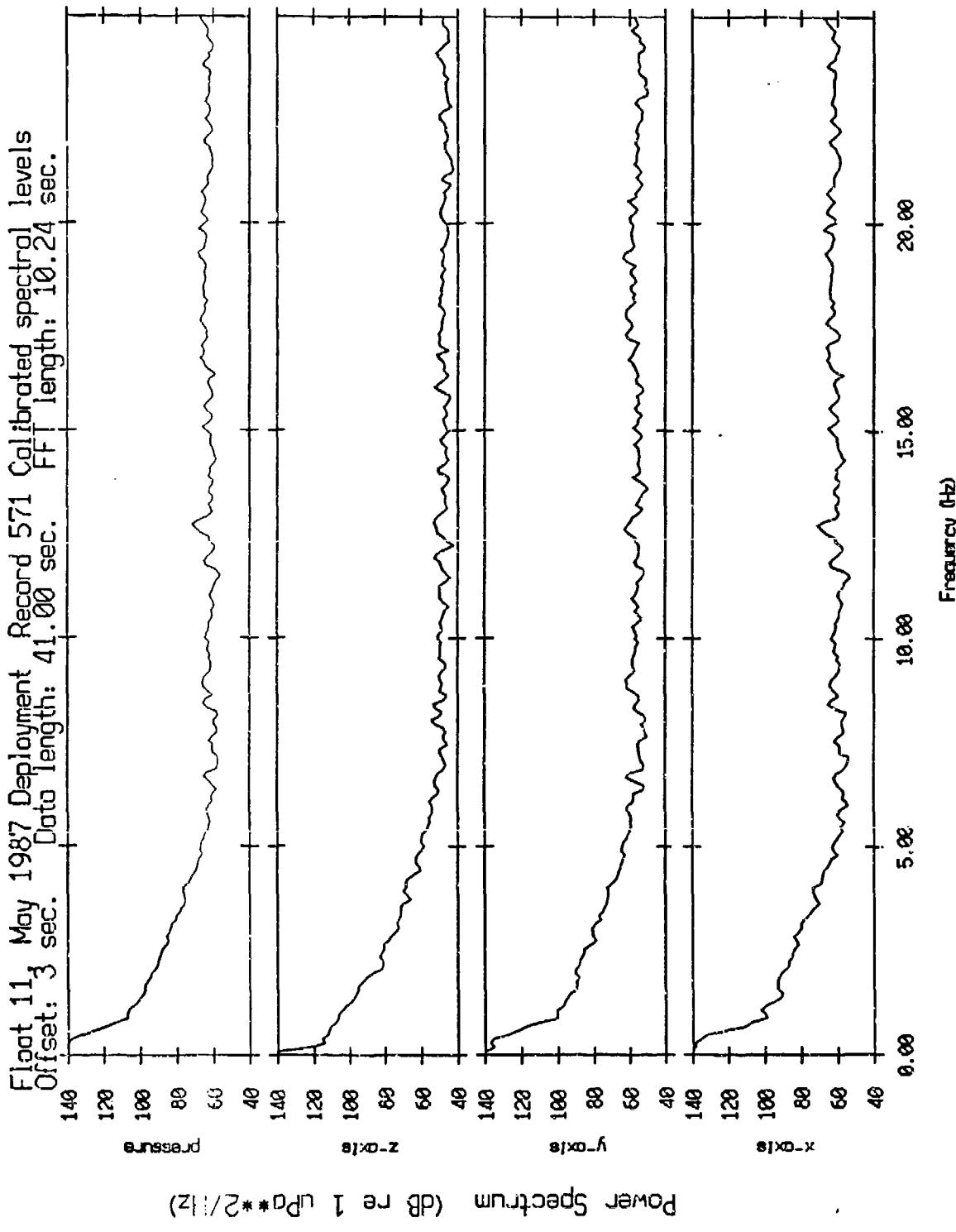


Figure XI.9h

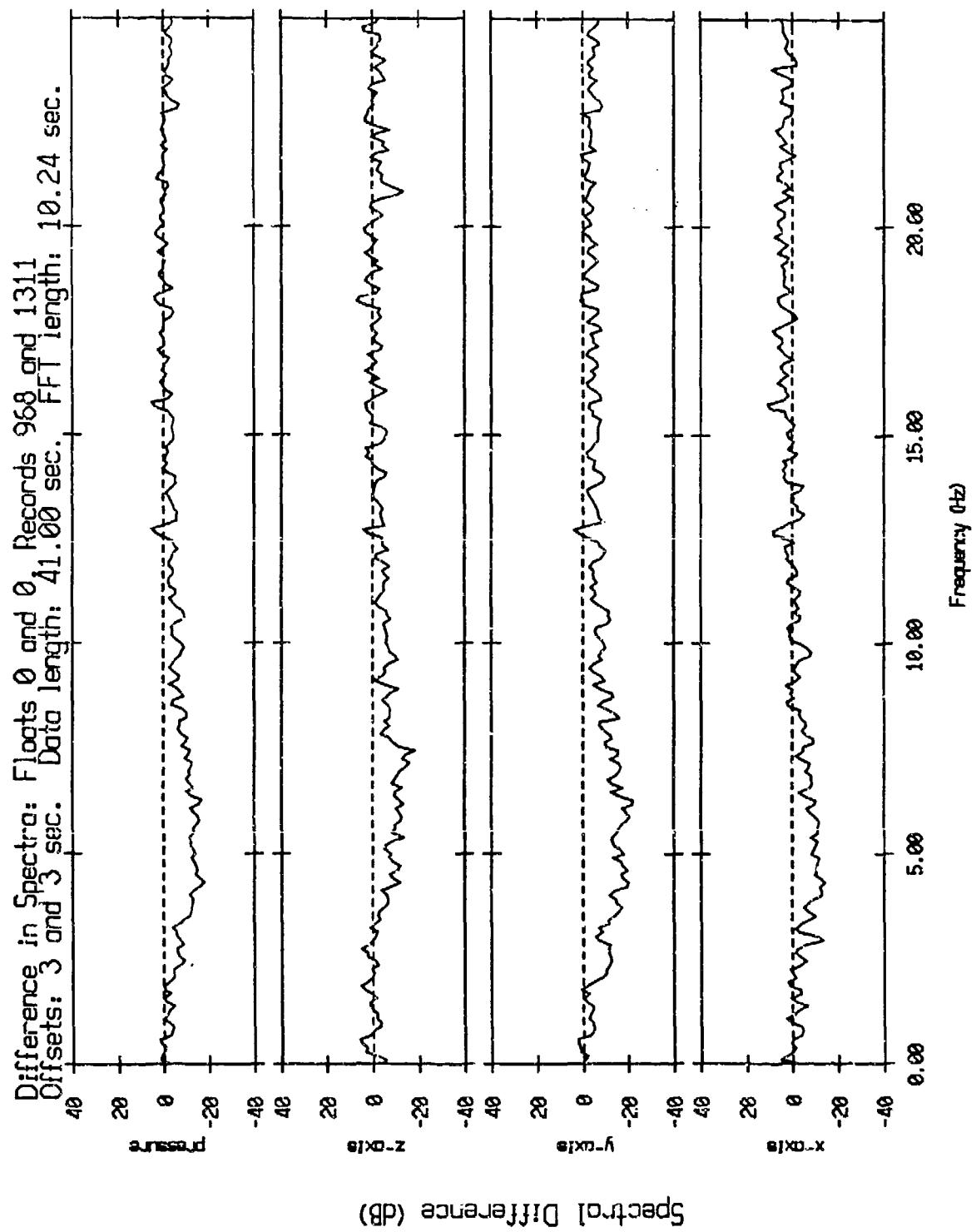


Figure XI.10a

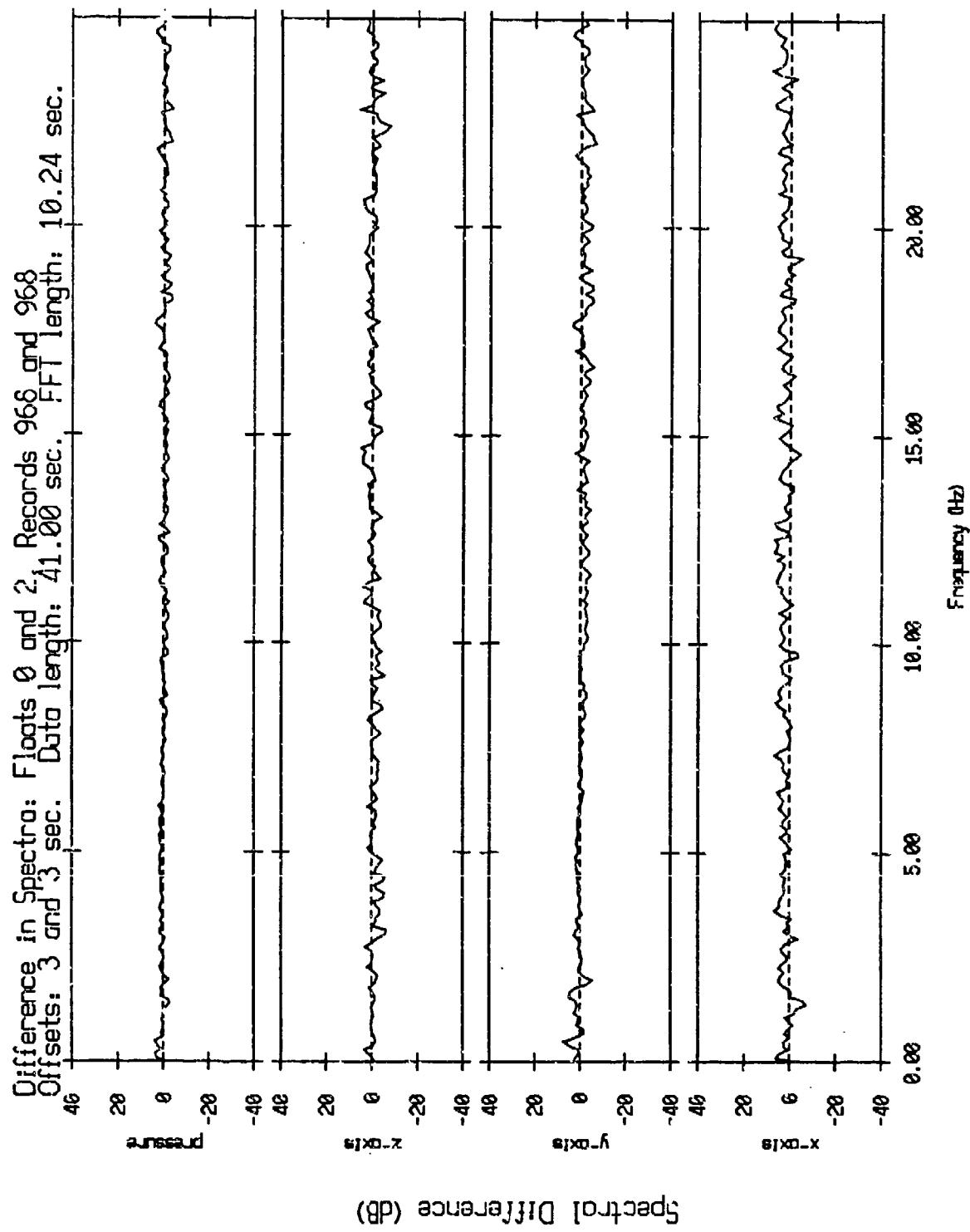


Figure XI.10b

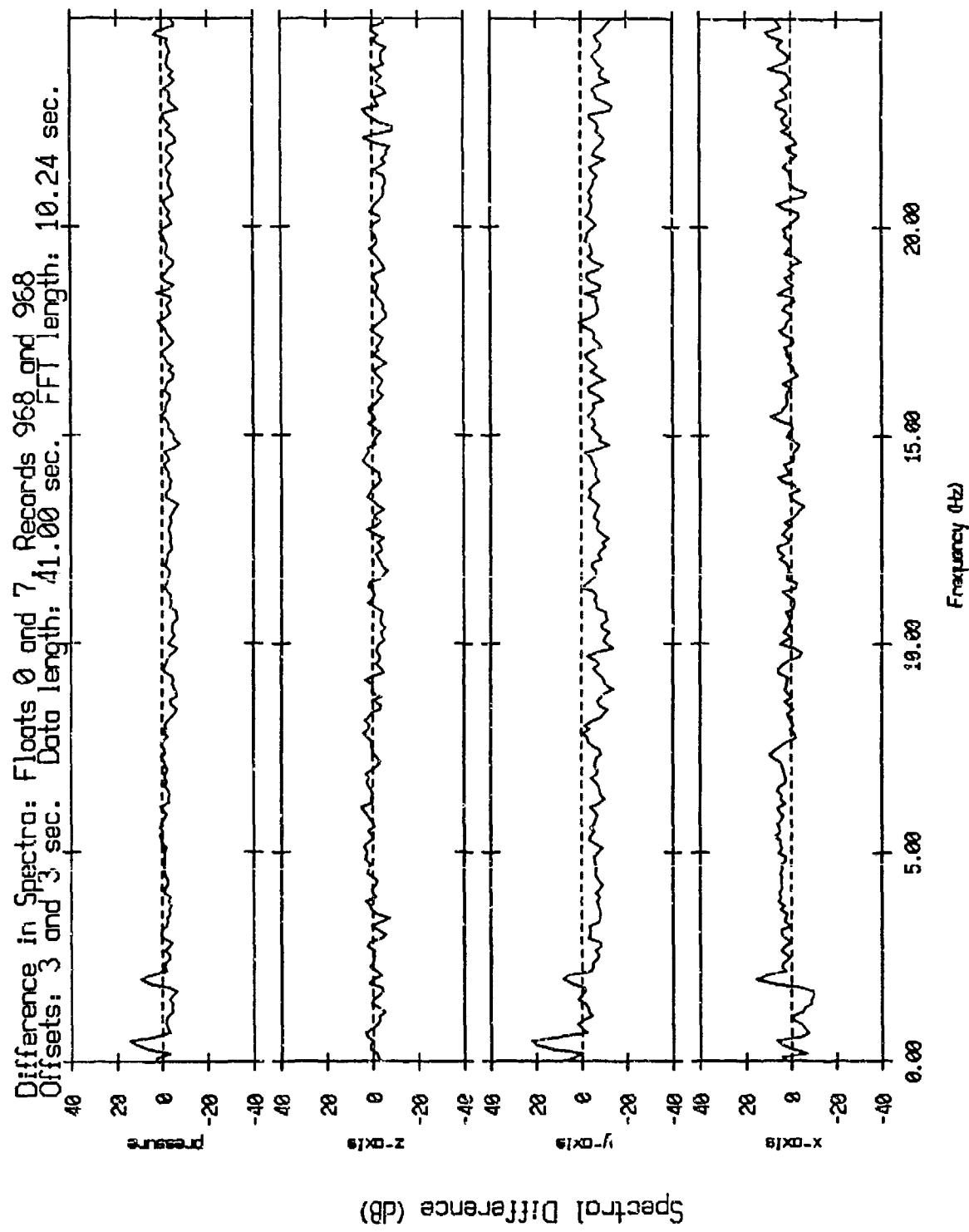


Figure XI.10c

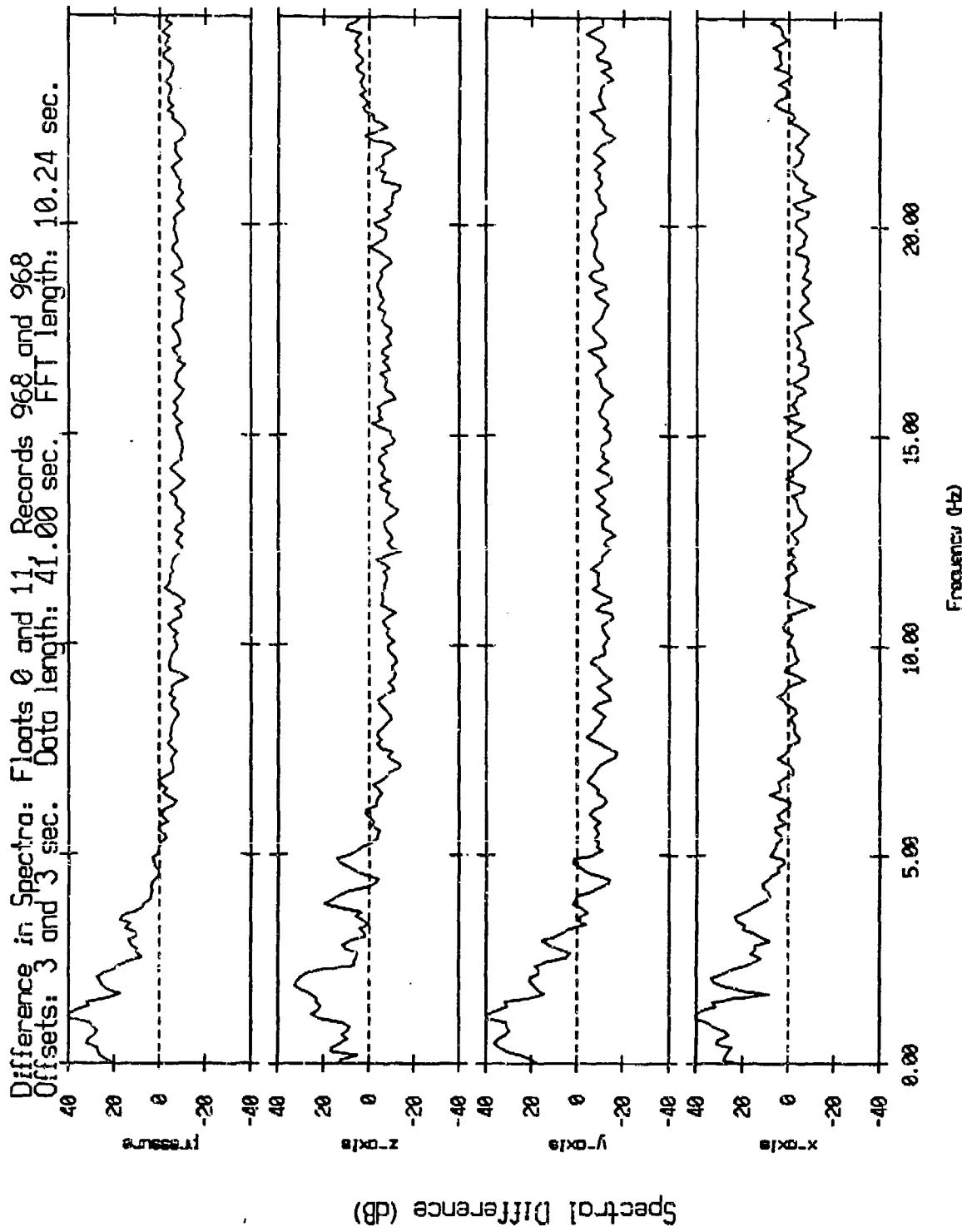


Figure XI.10d

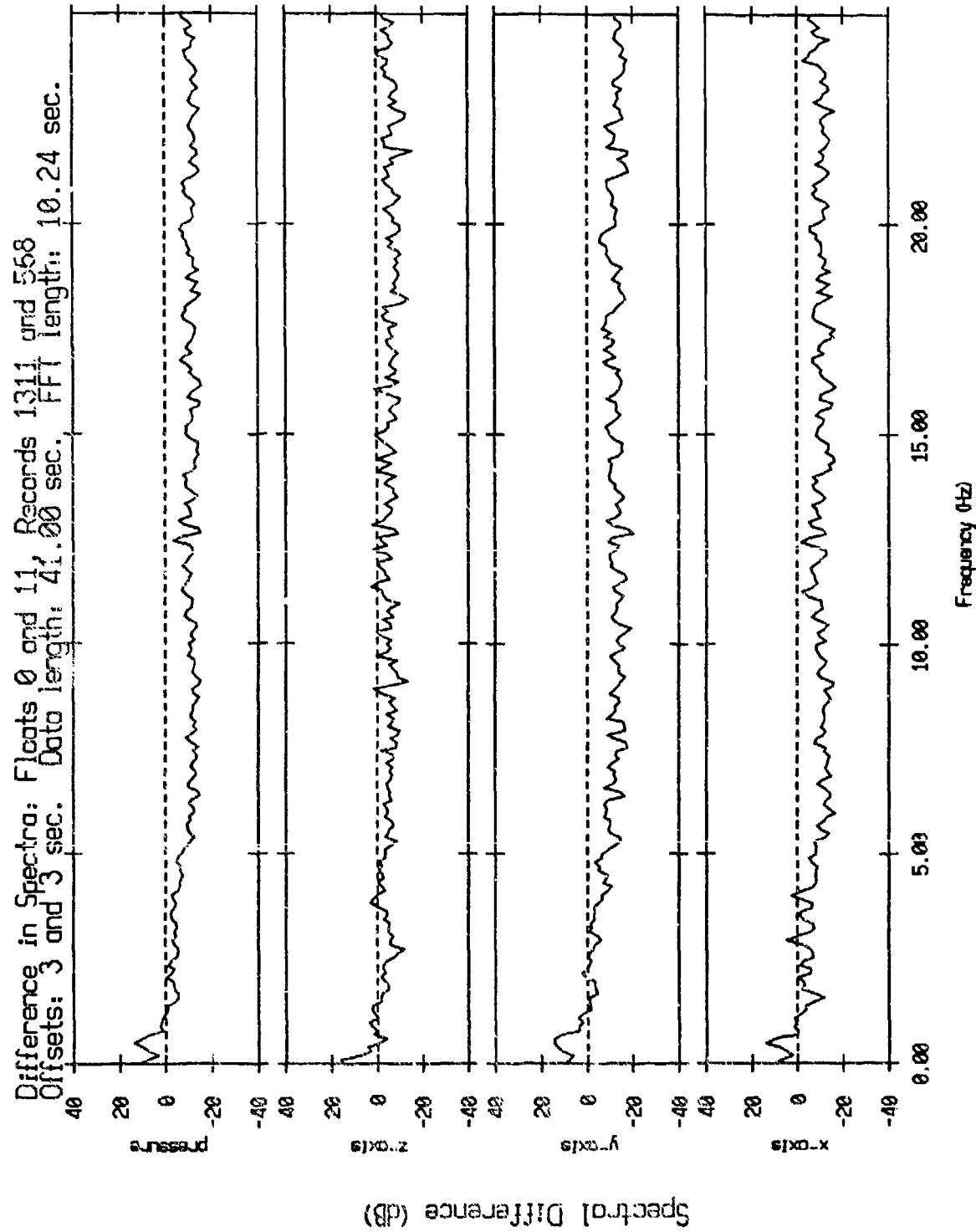


Figure XI.10e

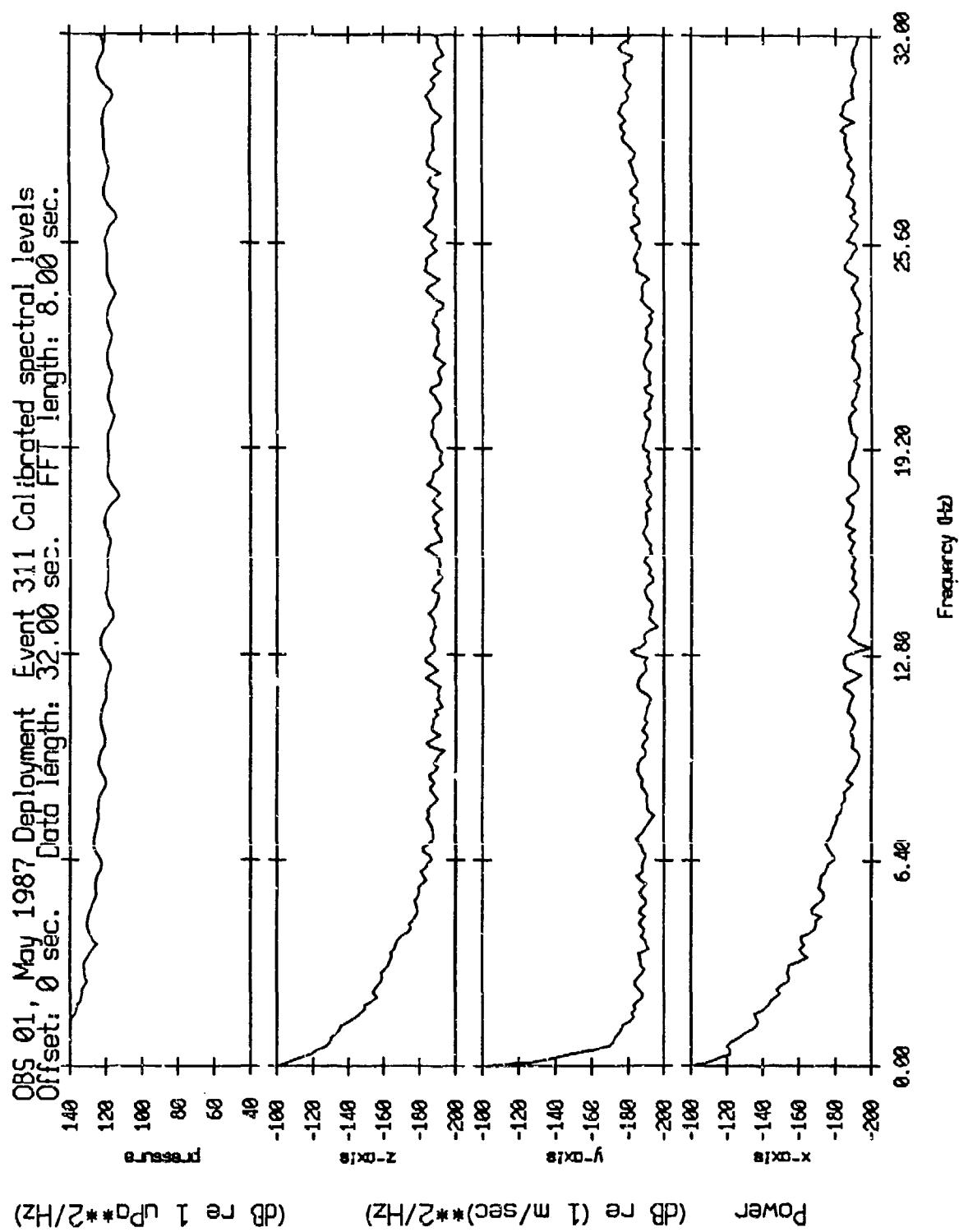


Figure XI.11a

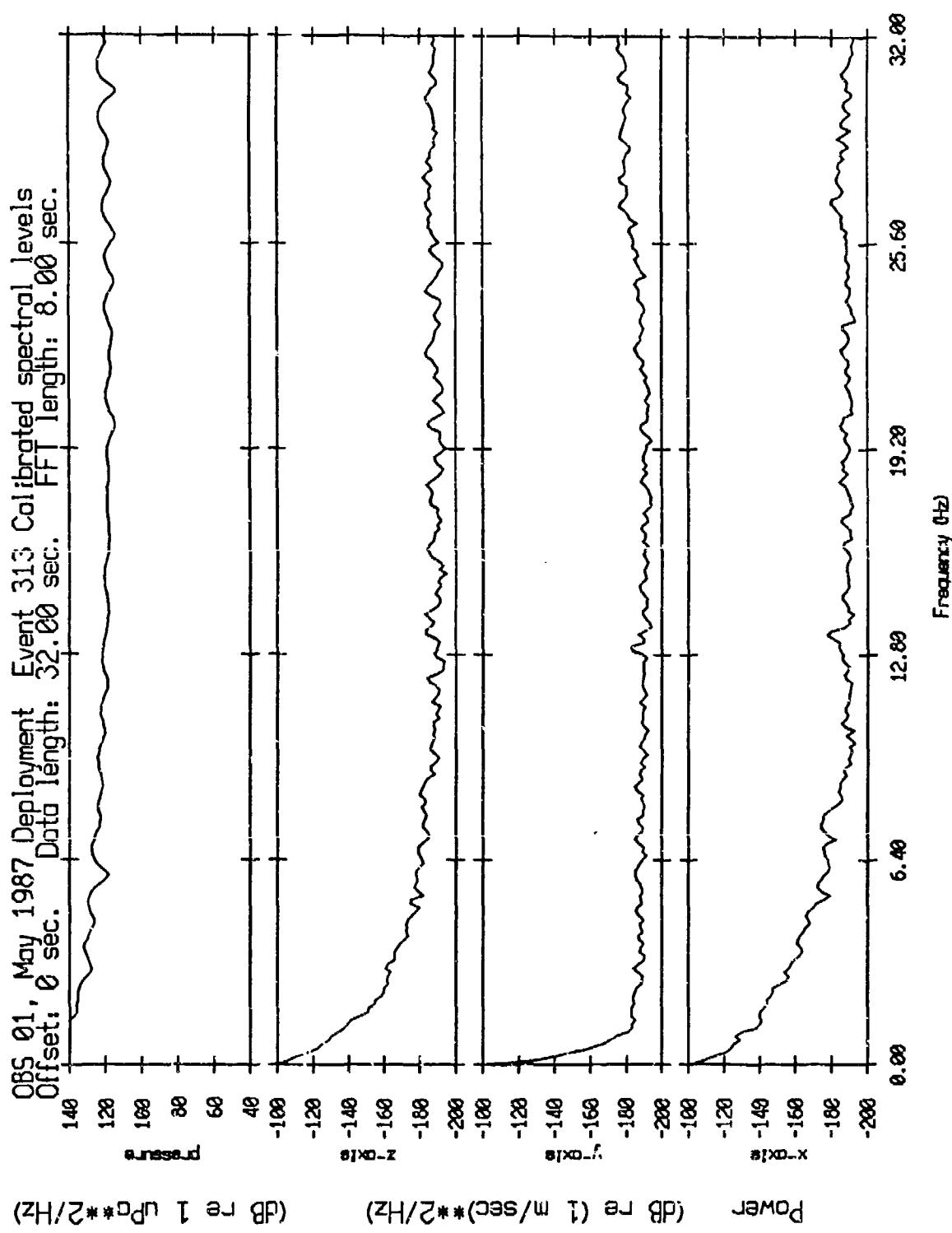


Figure XI.11b

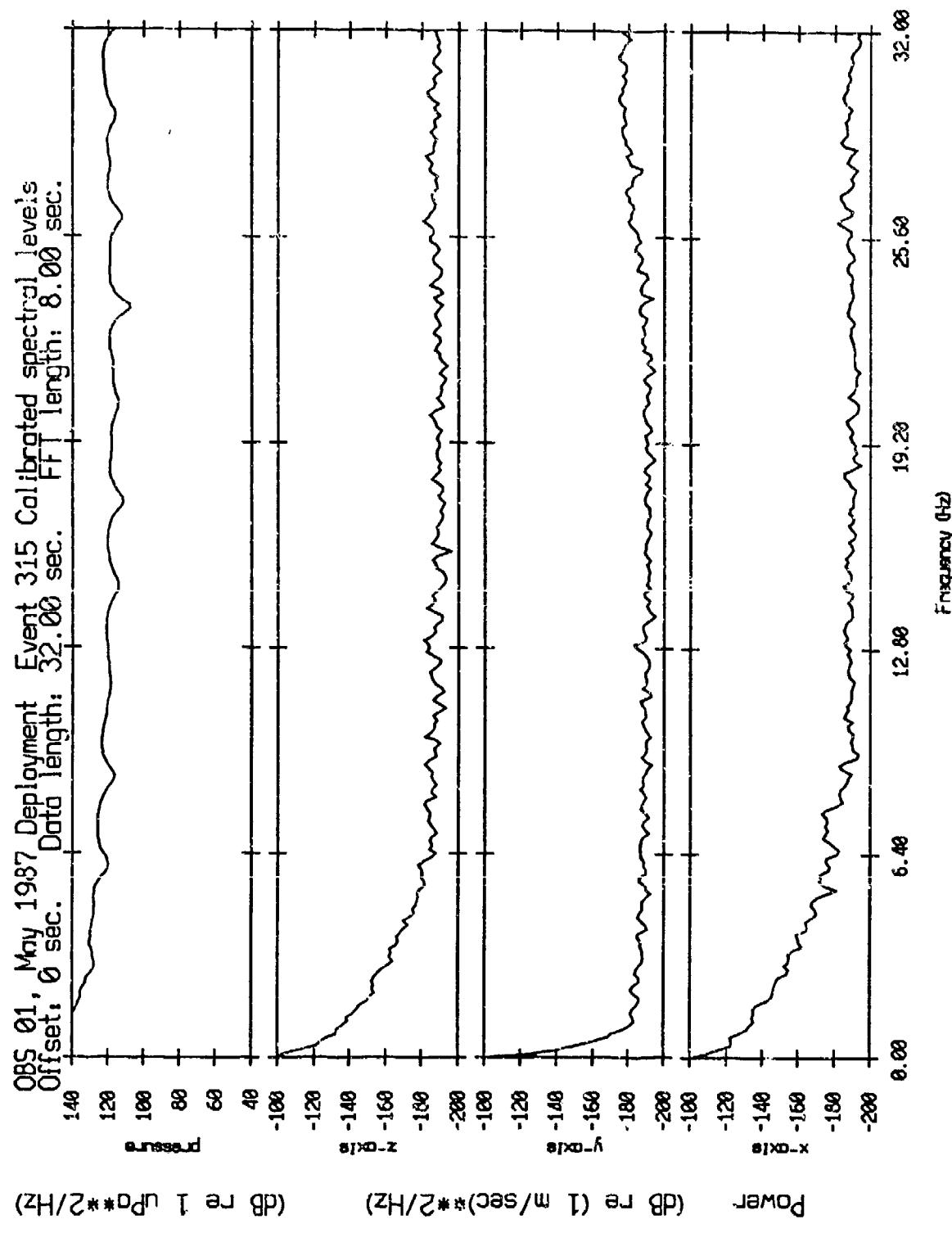


Figure XI.11c

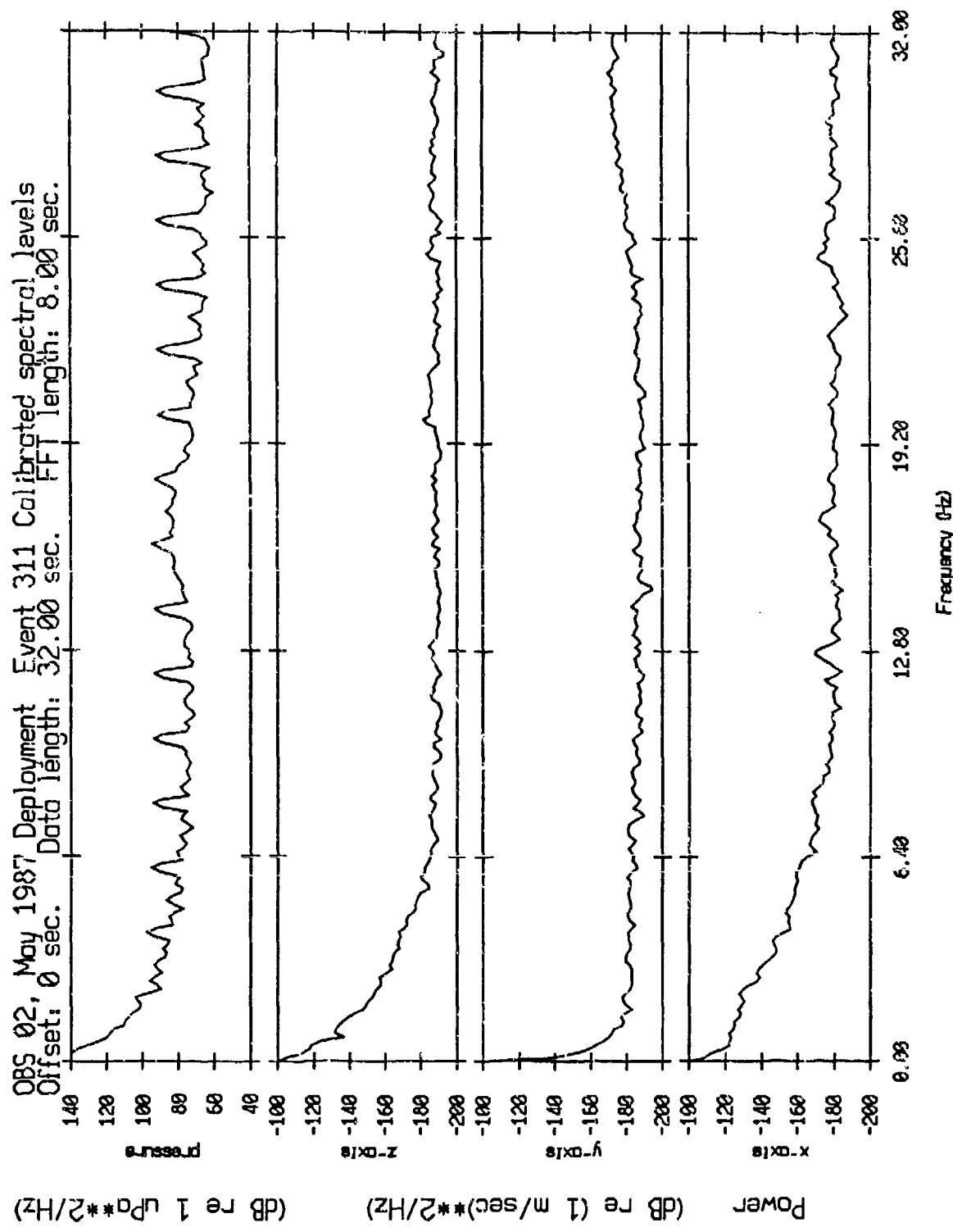


Figure XI.12a

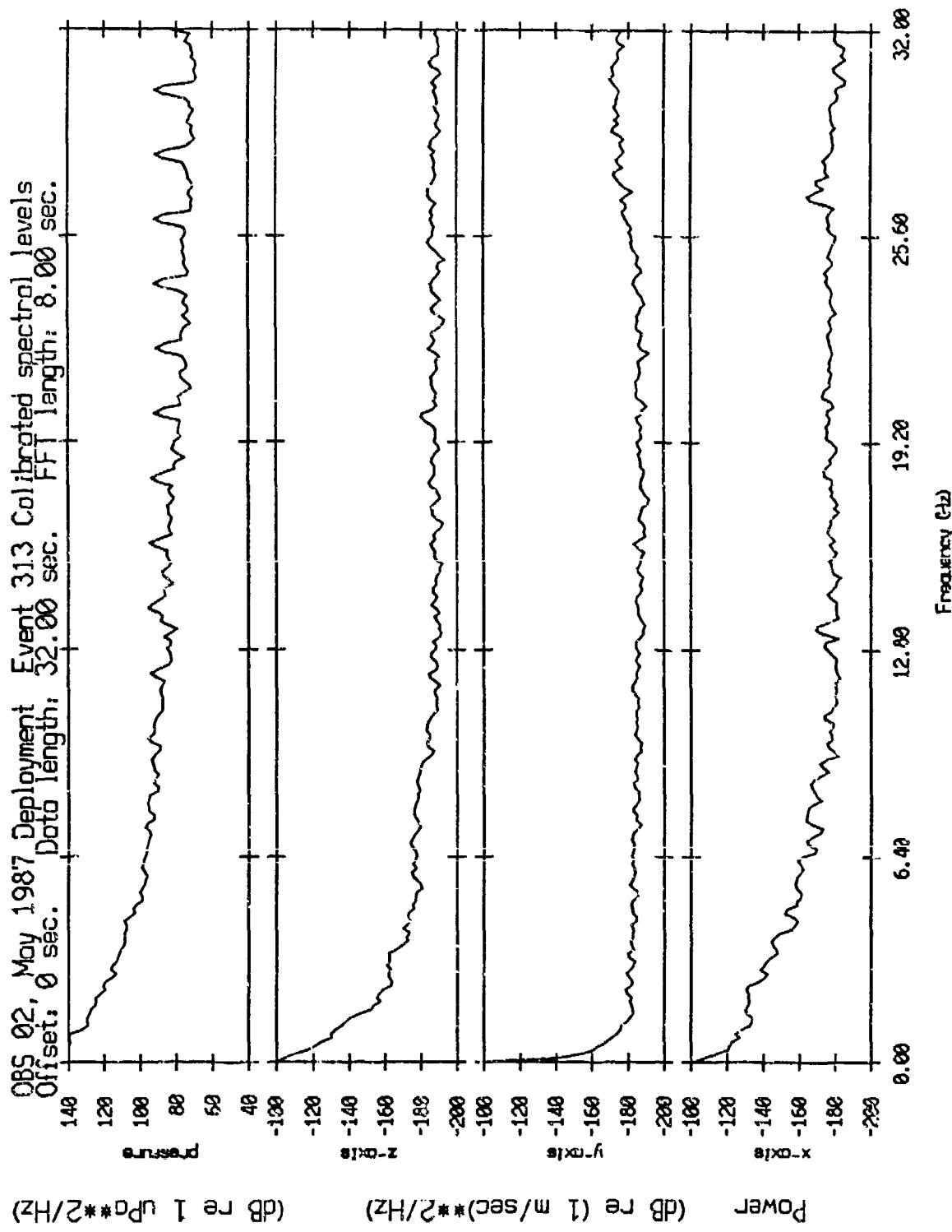


Figure XI.12b

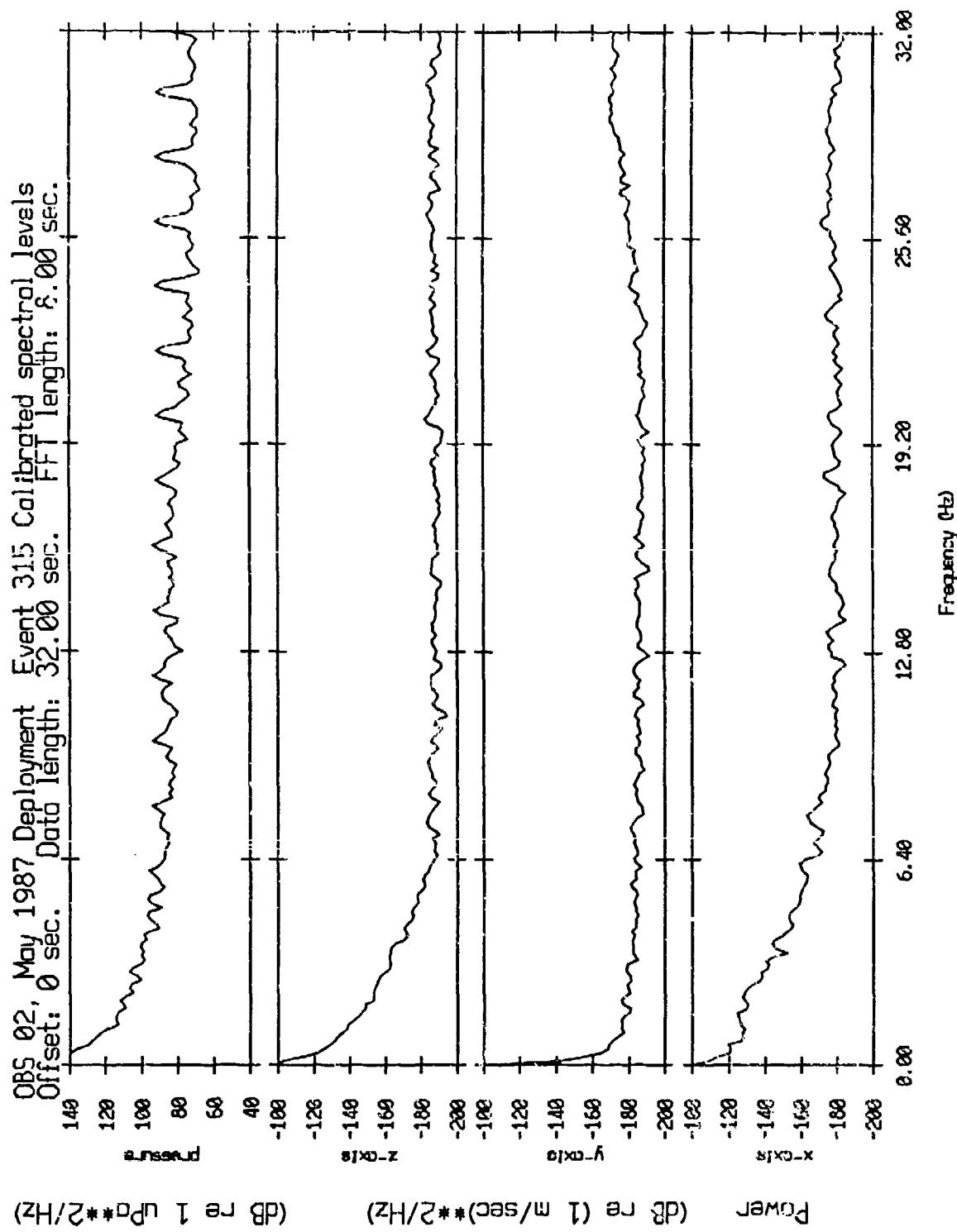


Figure XI.12c

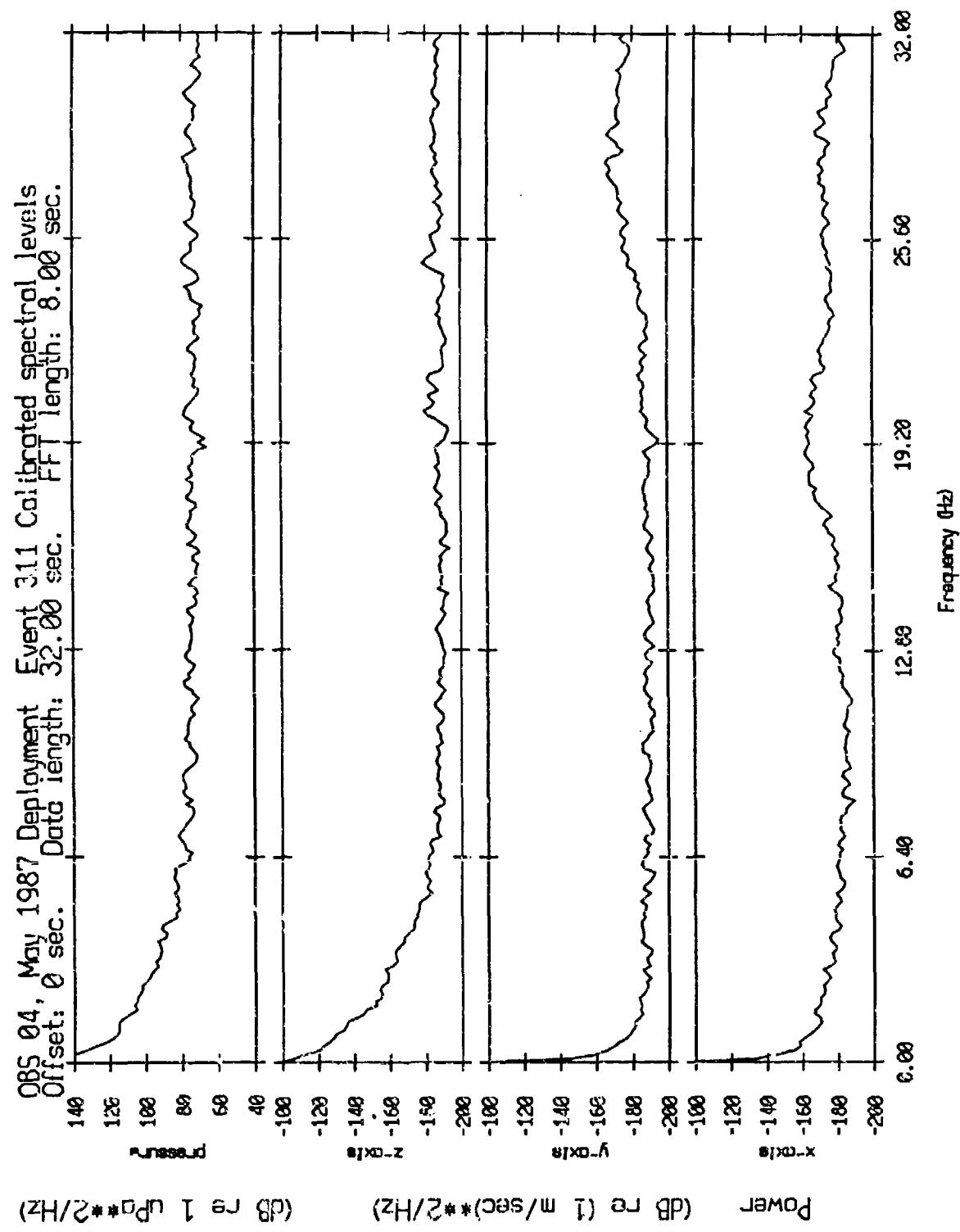


Figure XI.13a

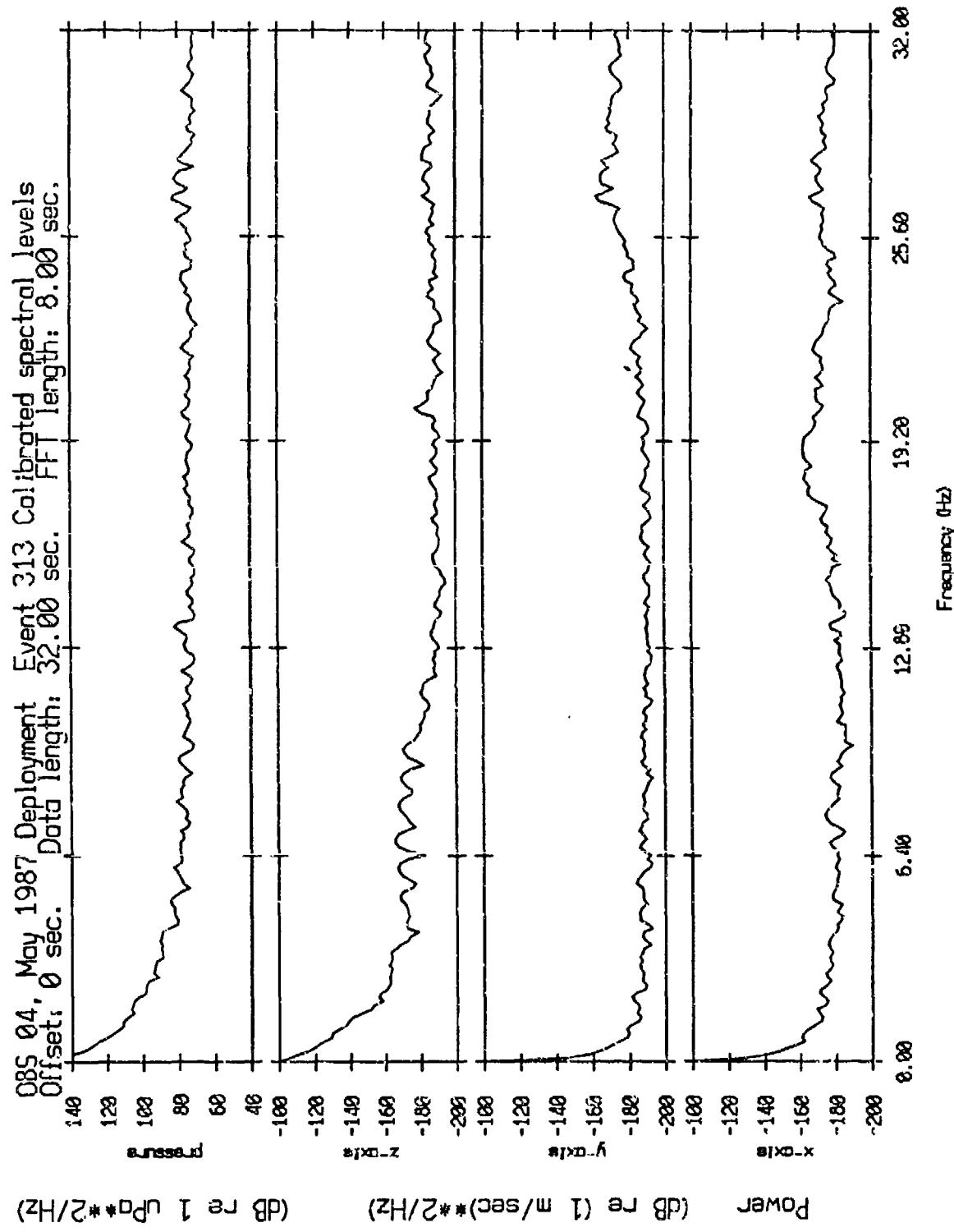


Figure XI.13b

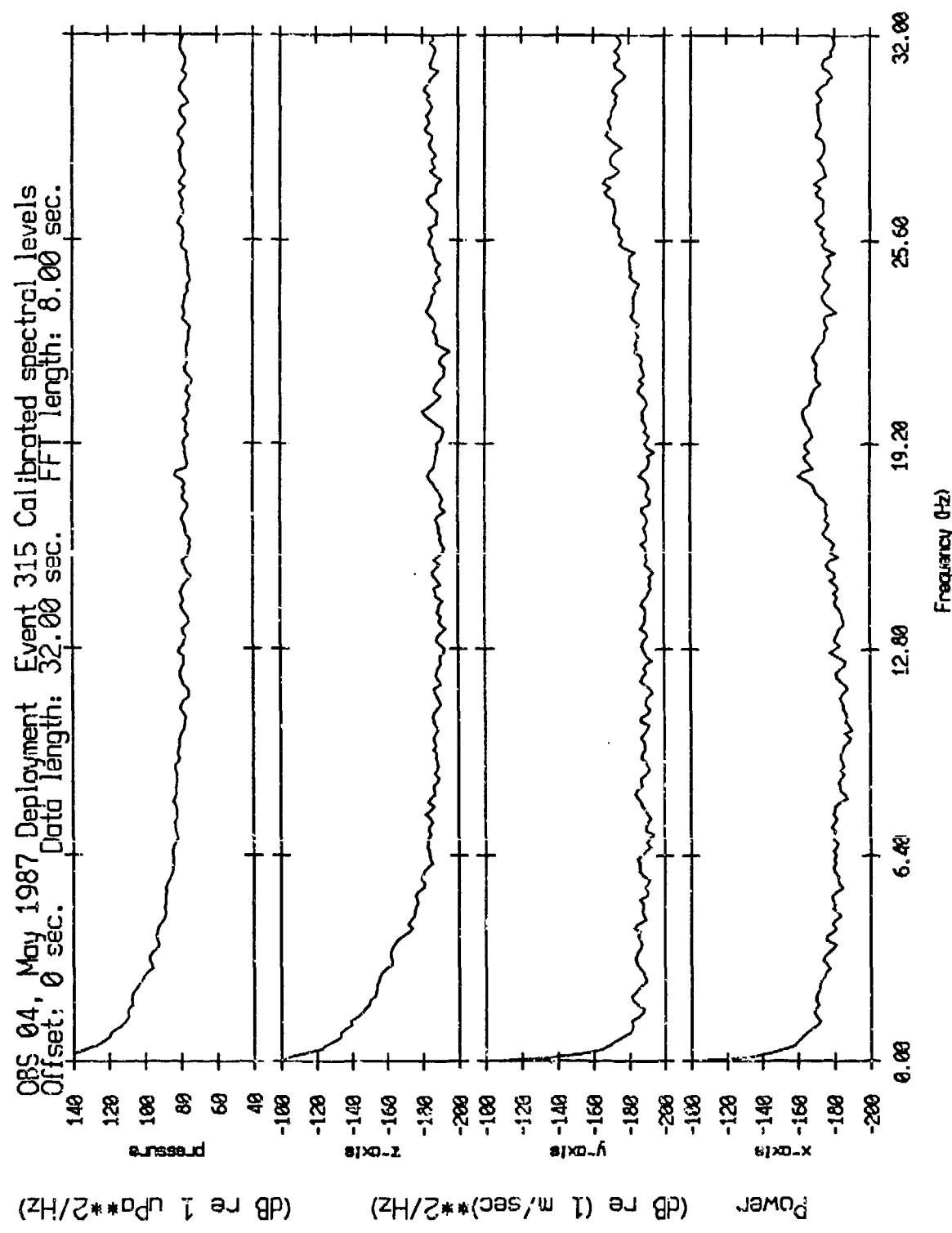


Figure XI.13c

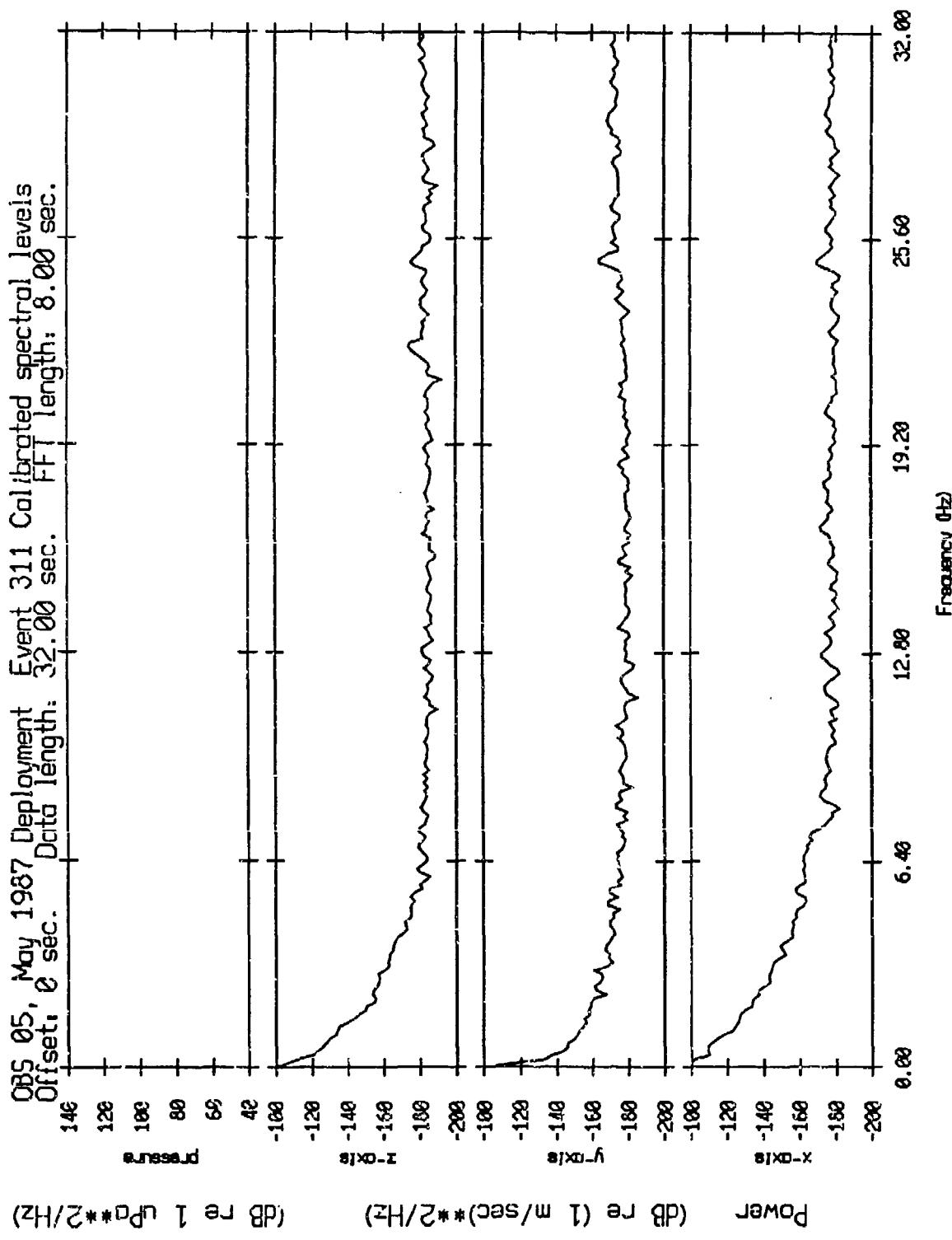


Figure XI.14a

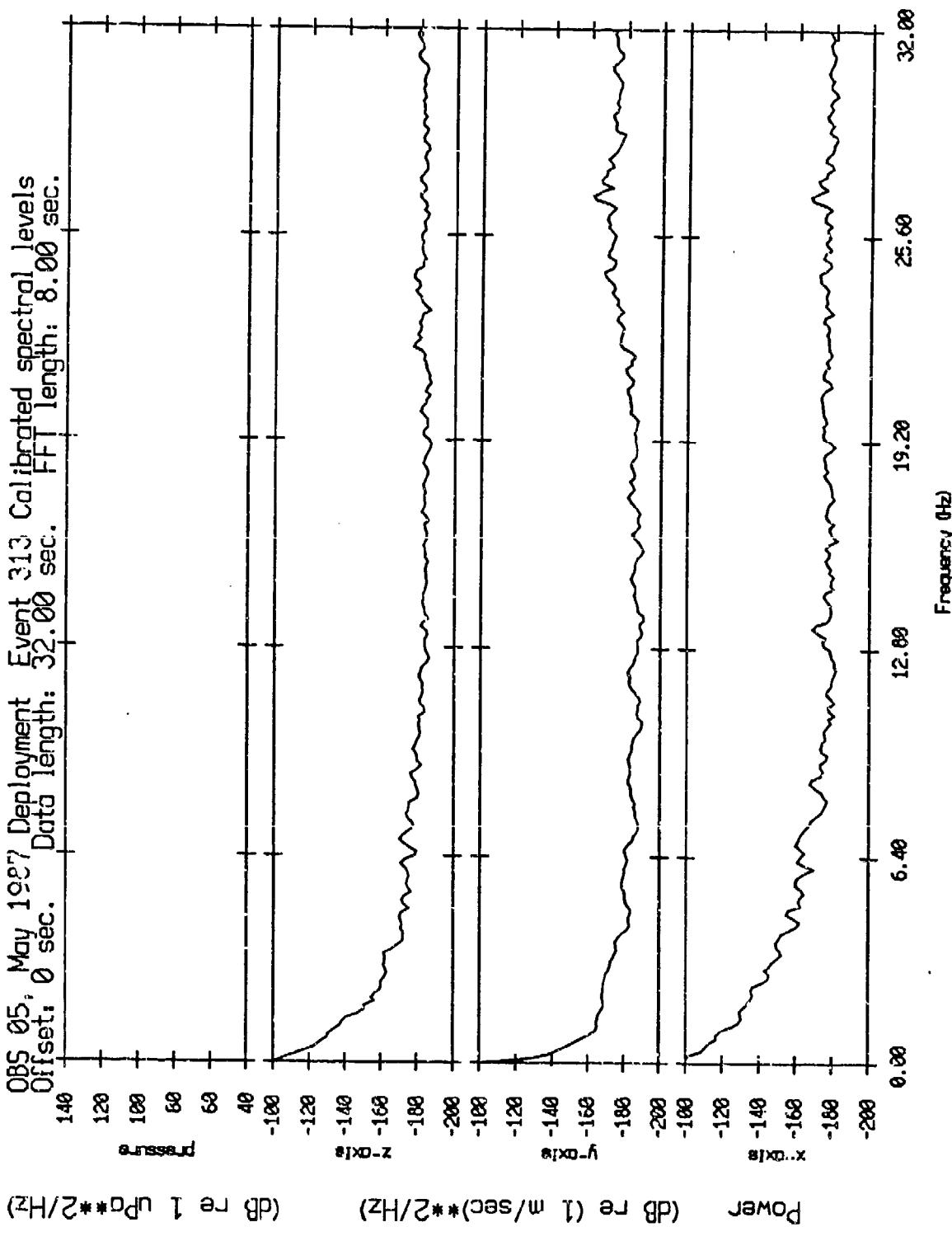


Figure XI.14b

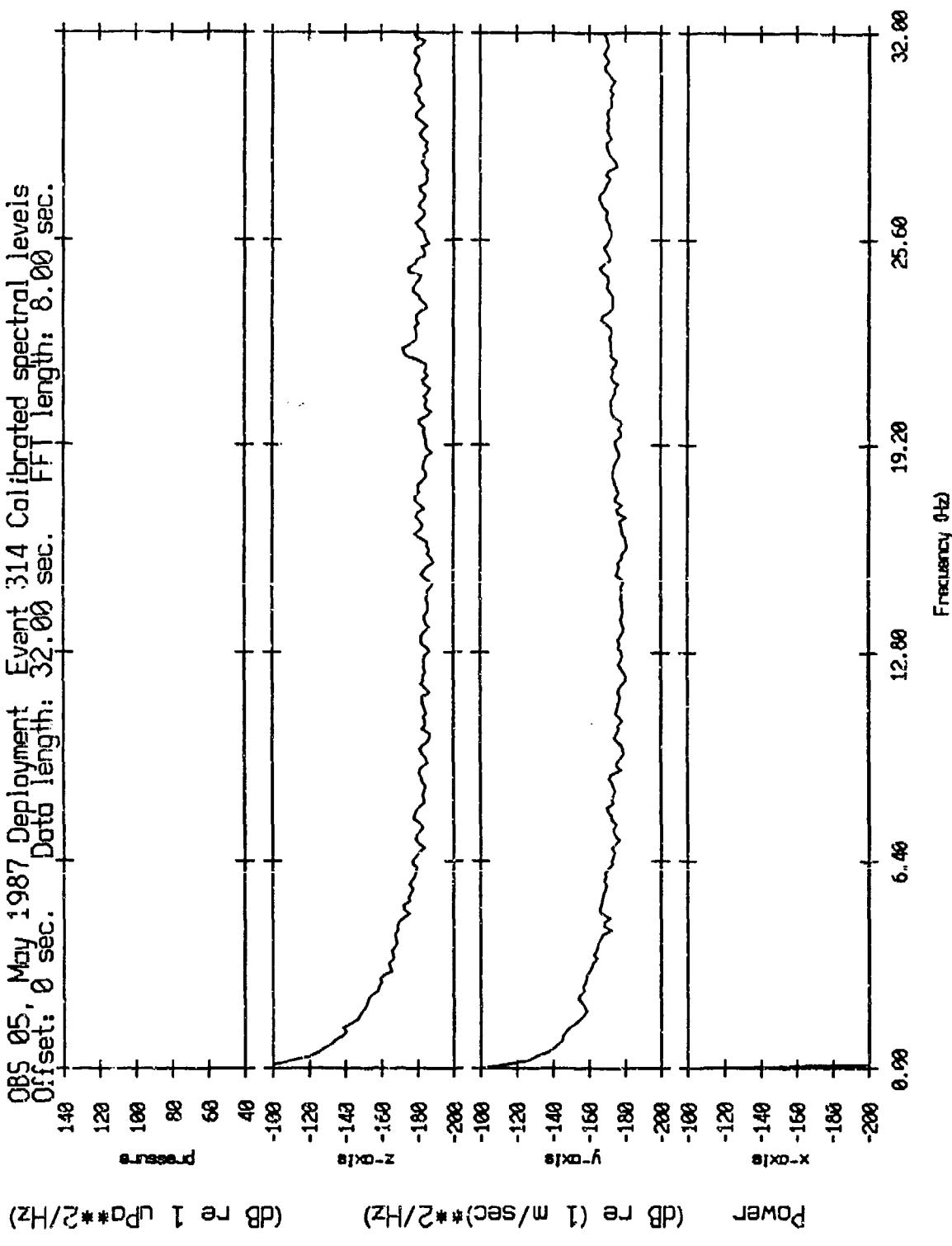


Figure XI.14c

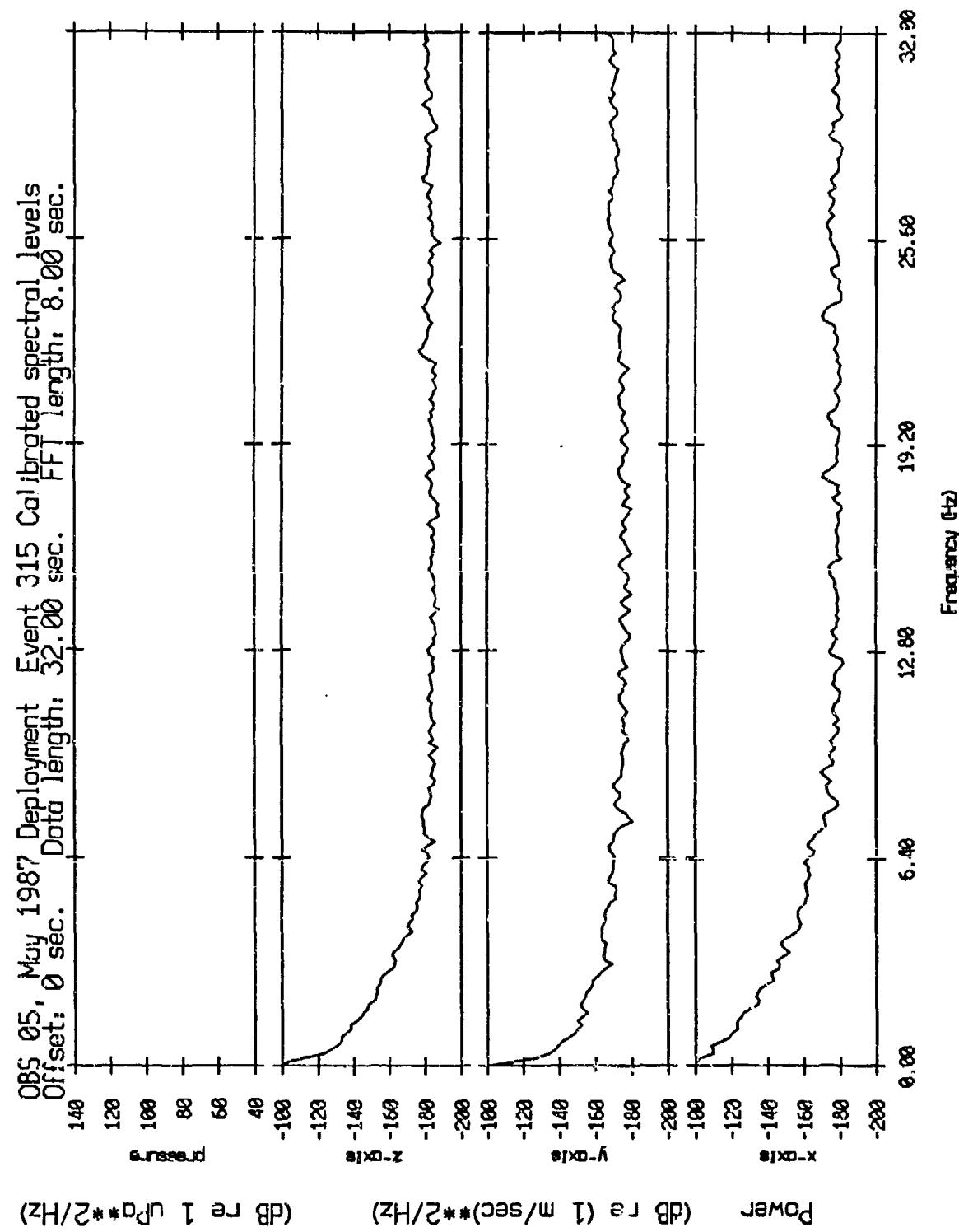


Figure XI.14d

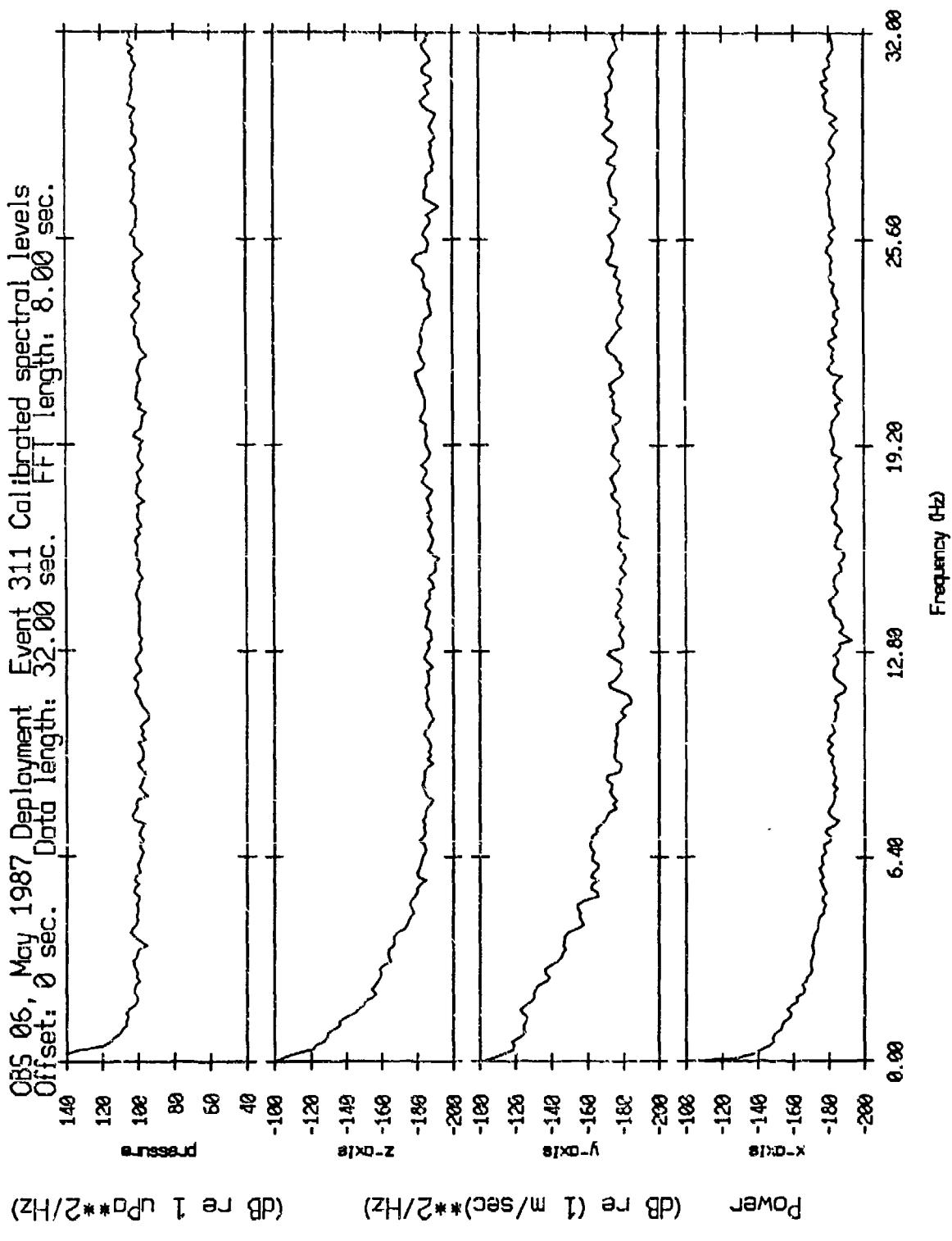


Figure XI.15a

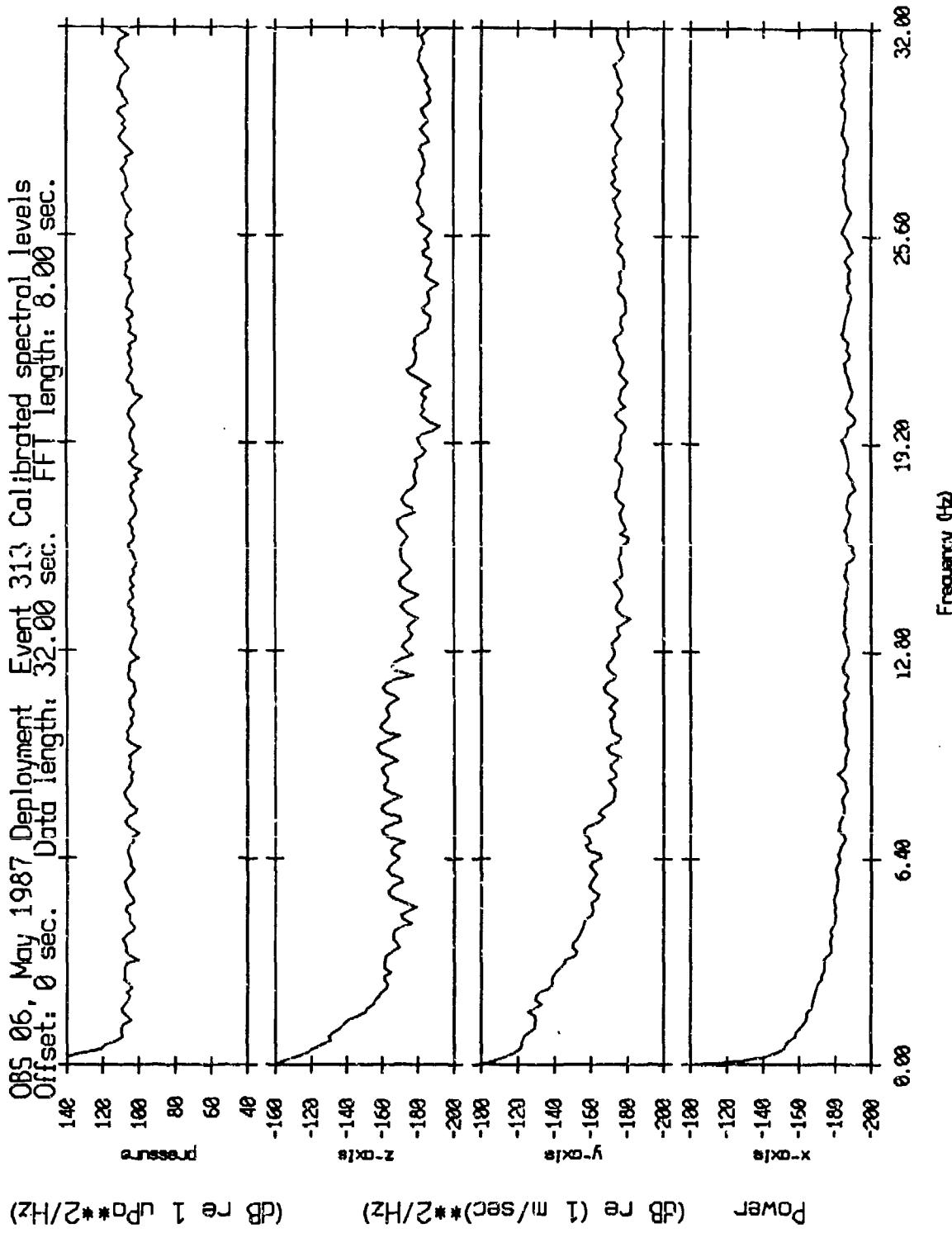


Figure XI.15b

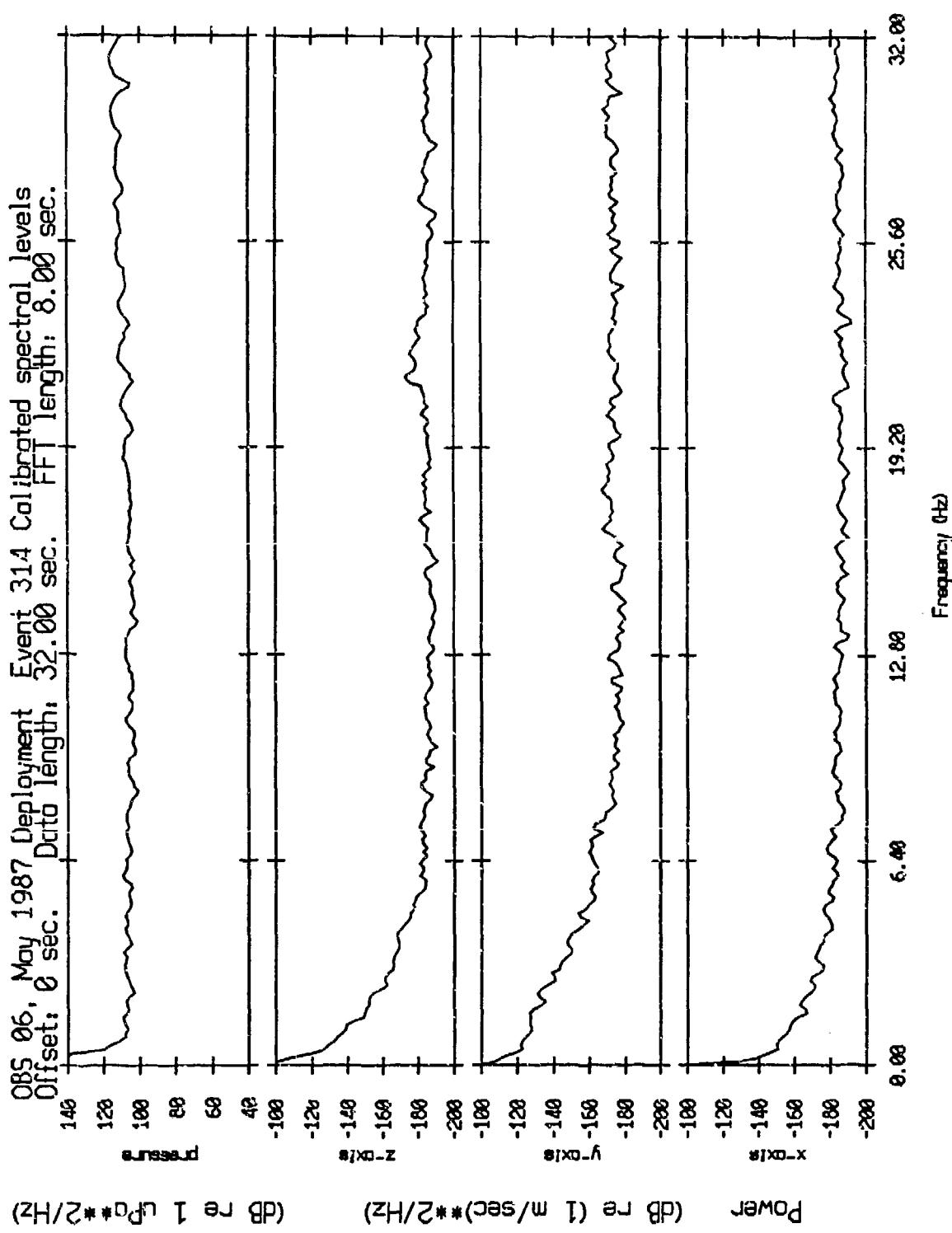


Figure XI.15c

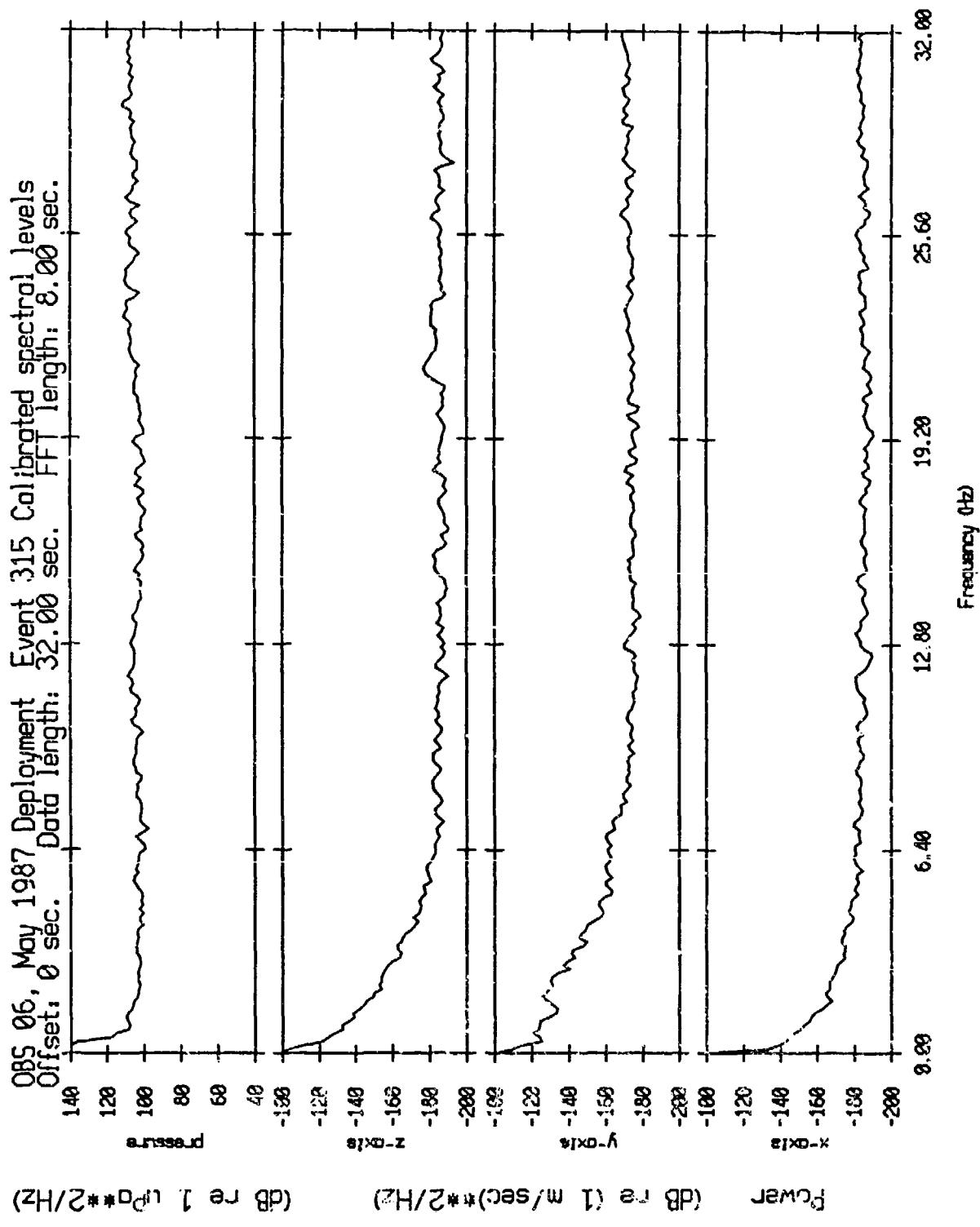


Figure XI.15d

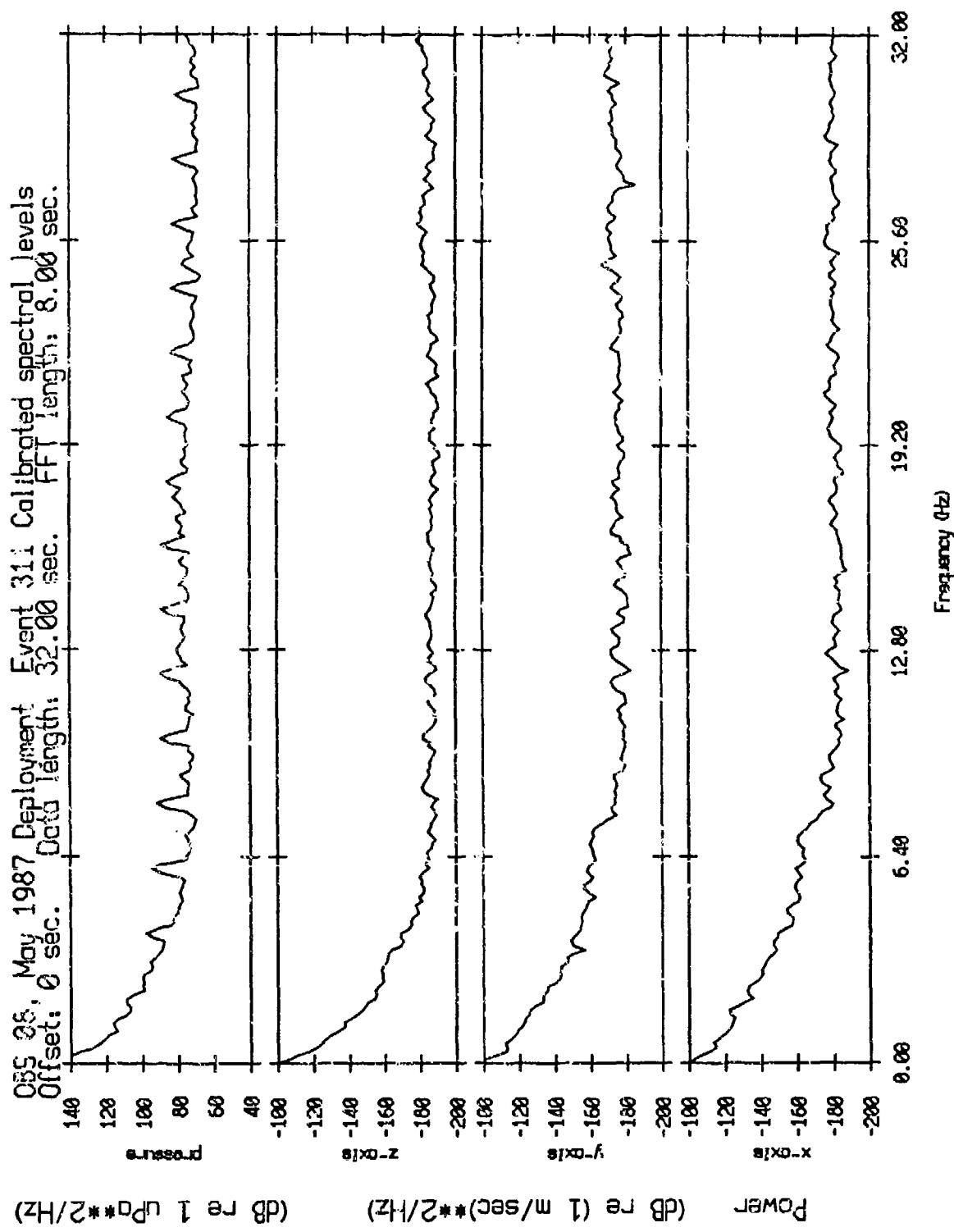


Figure XI.16a

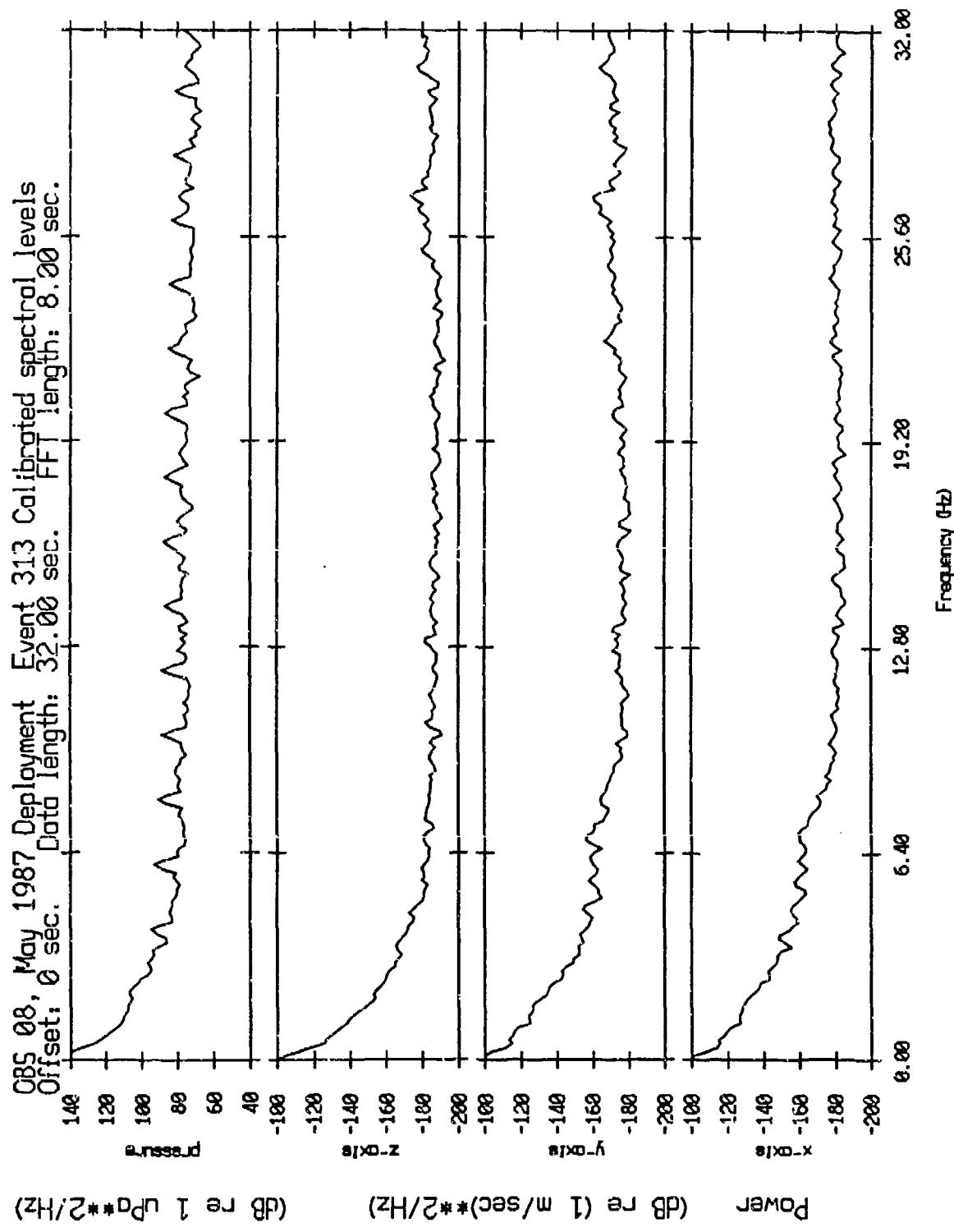


Figure XI.16b

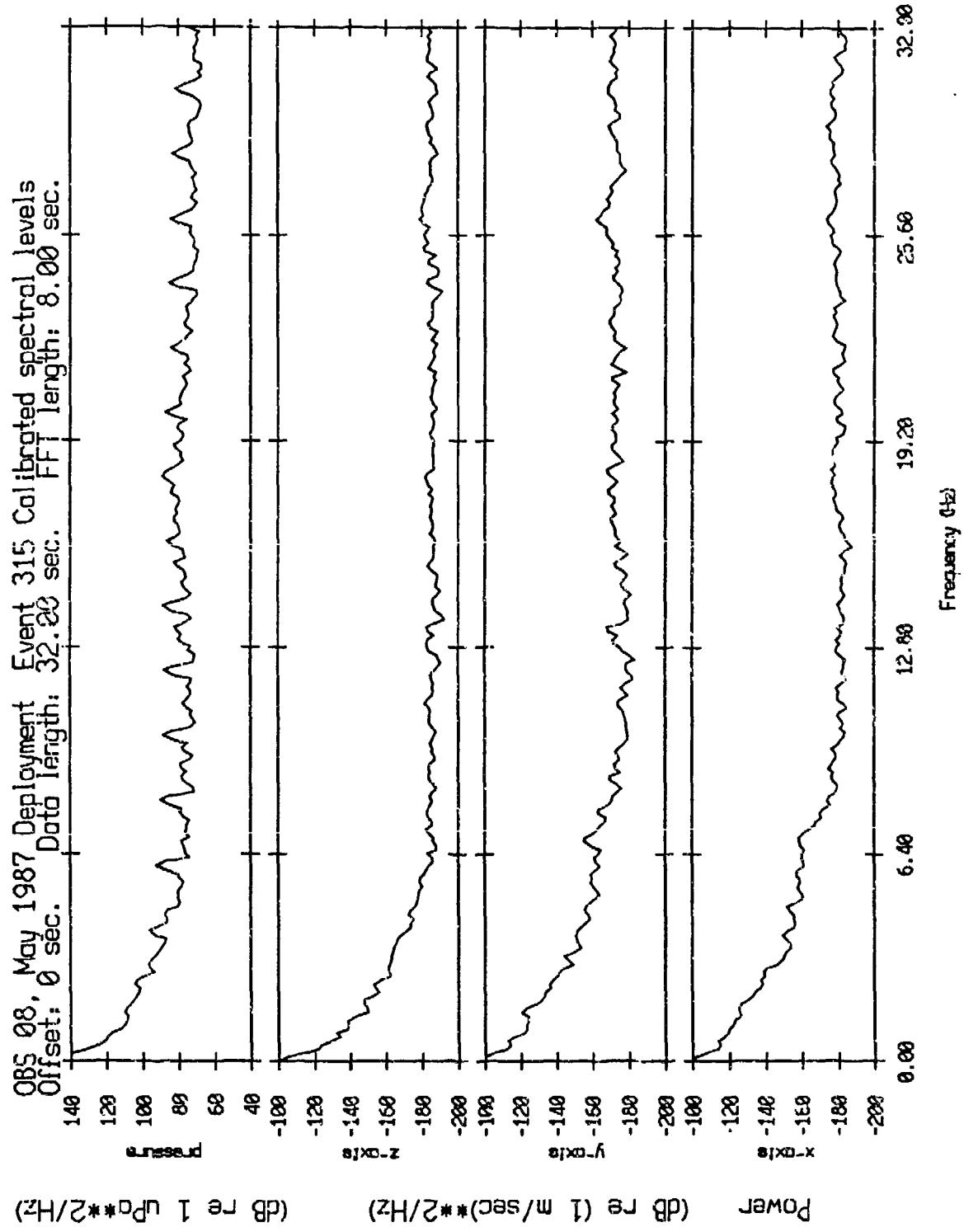


Figure XI.16c

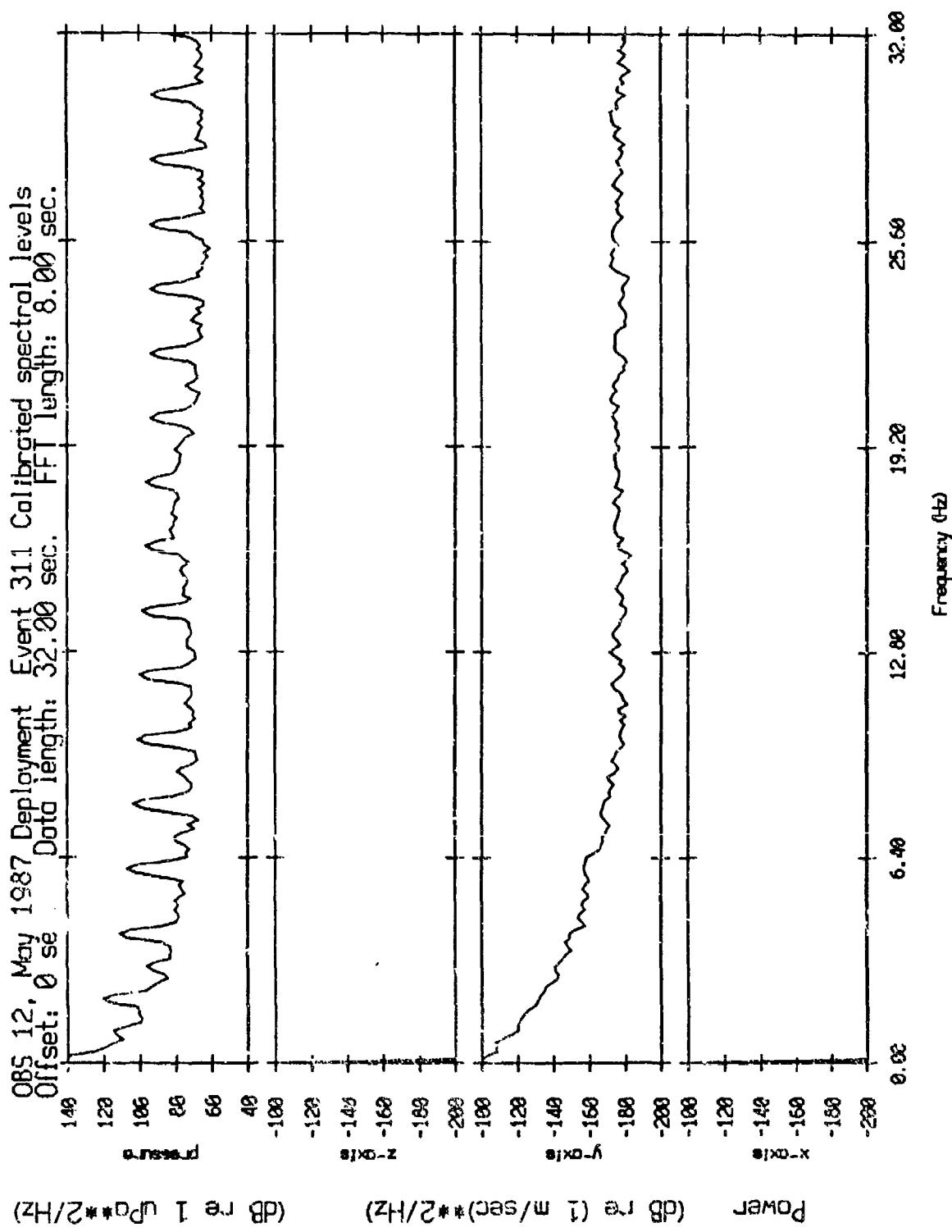


Figure XI.17a

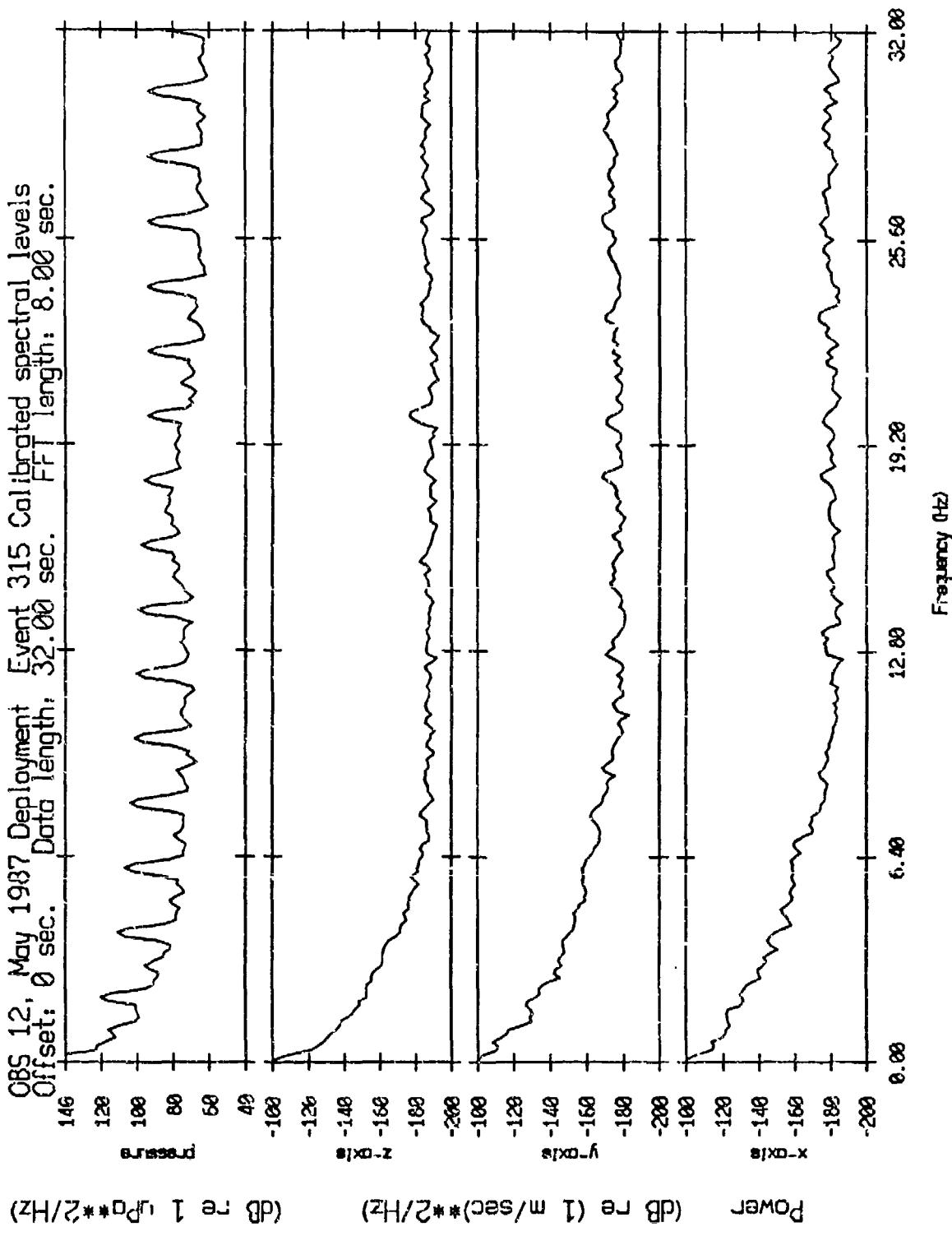


Figure XI.17b

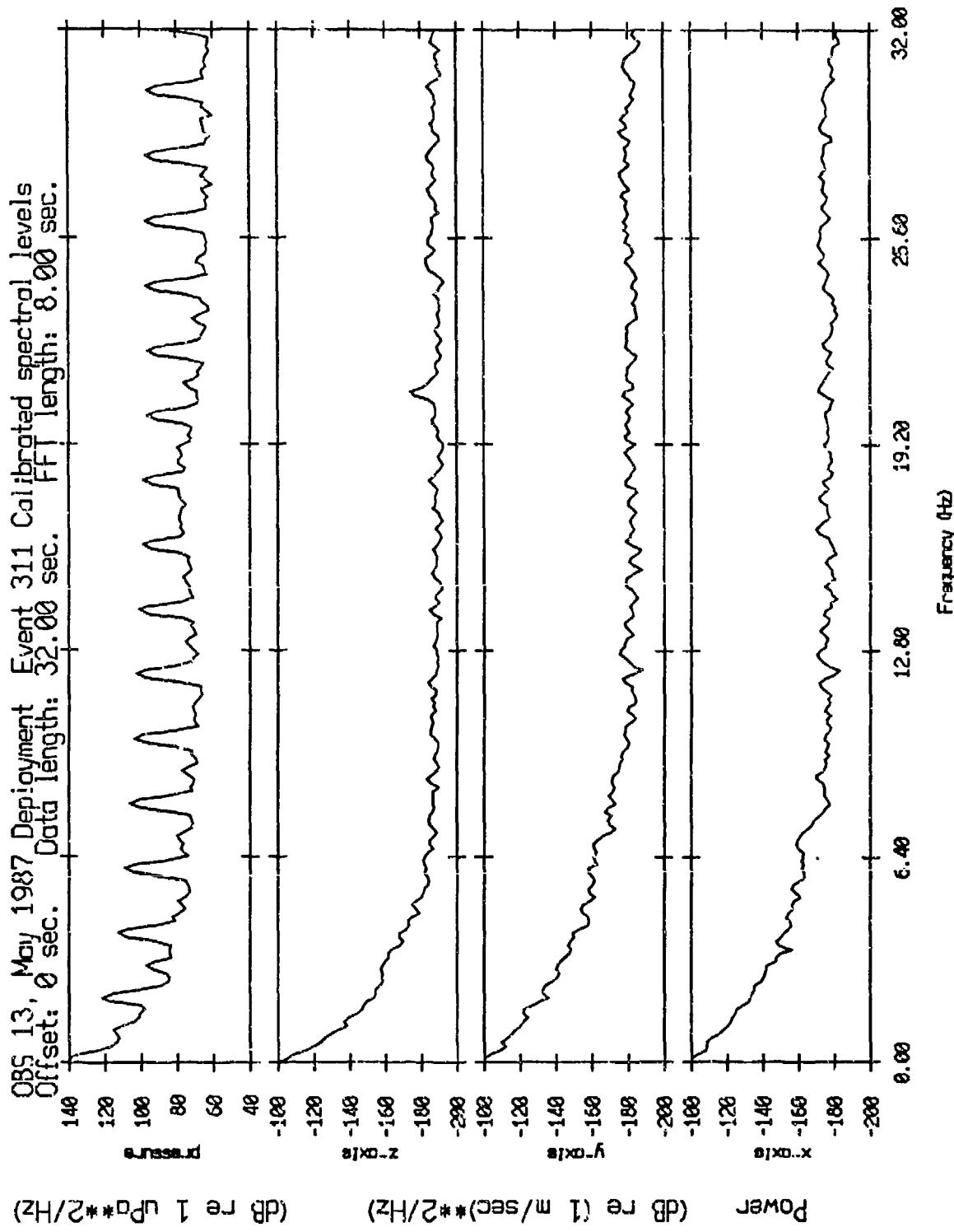


Figure XI.18a

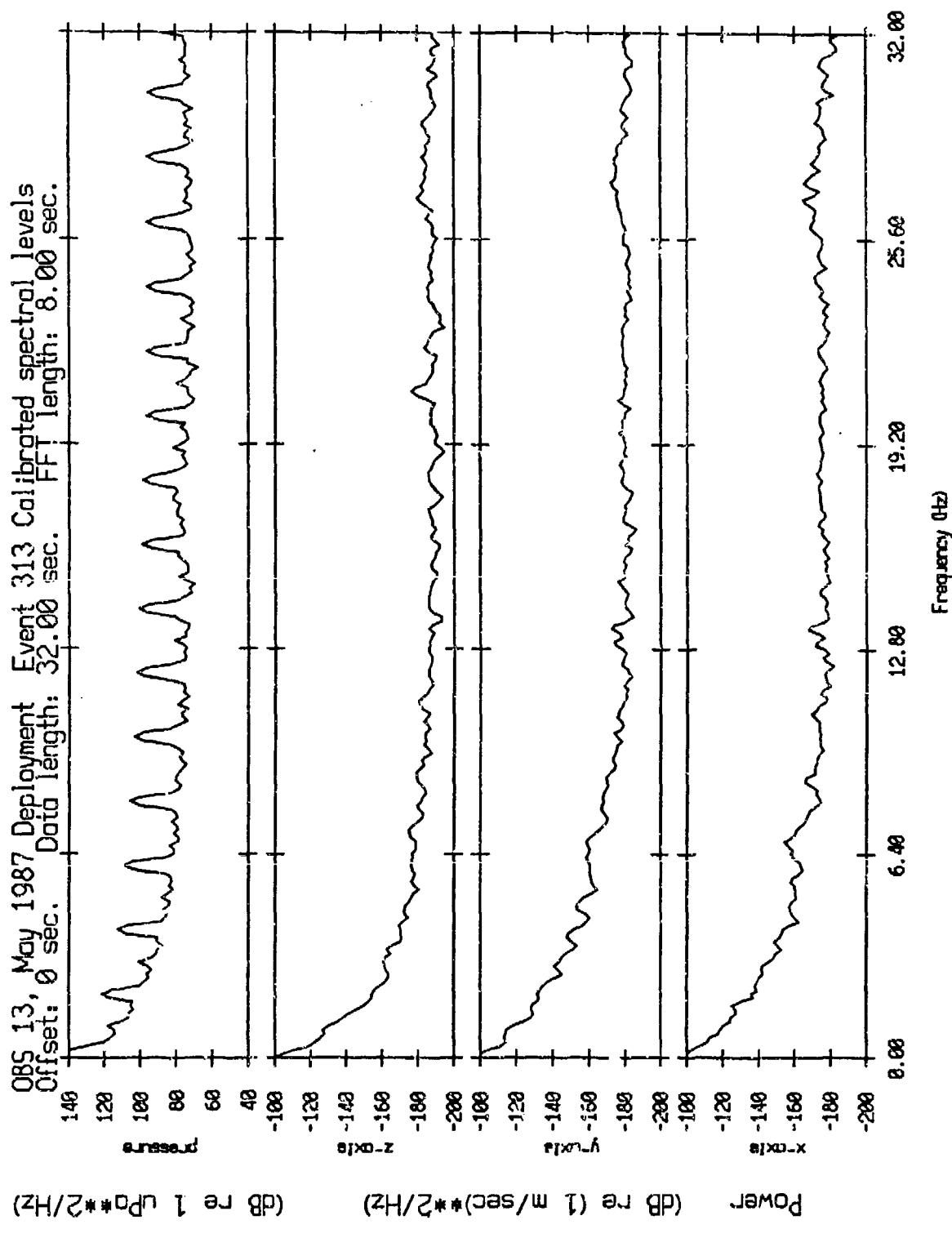


Figure XI.18b

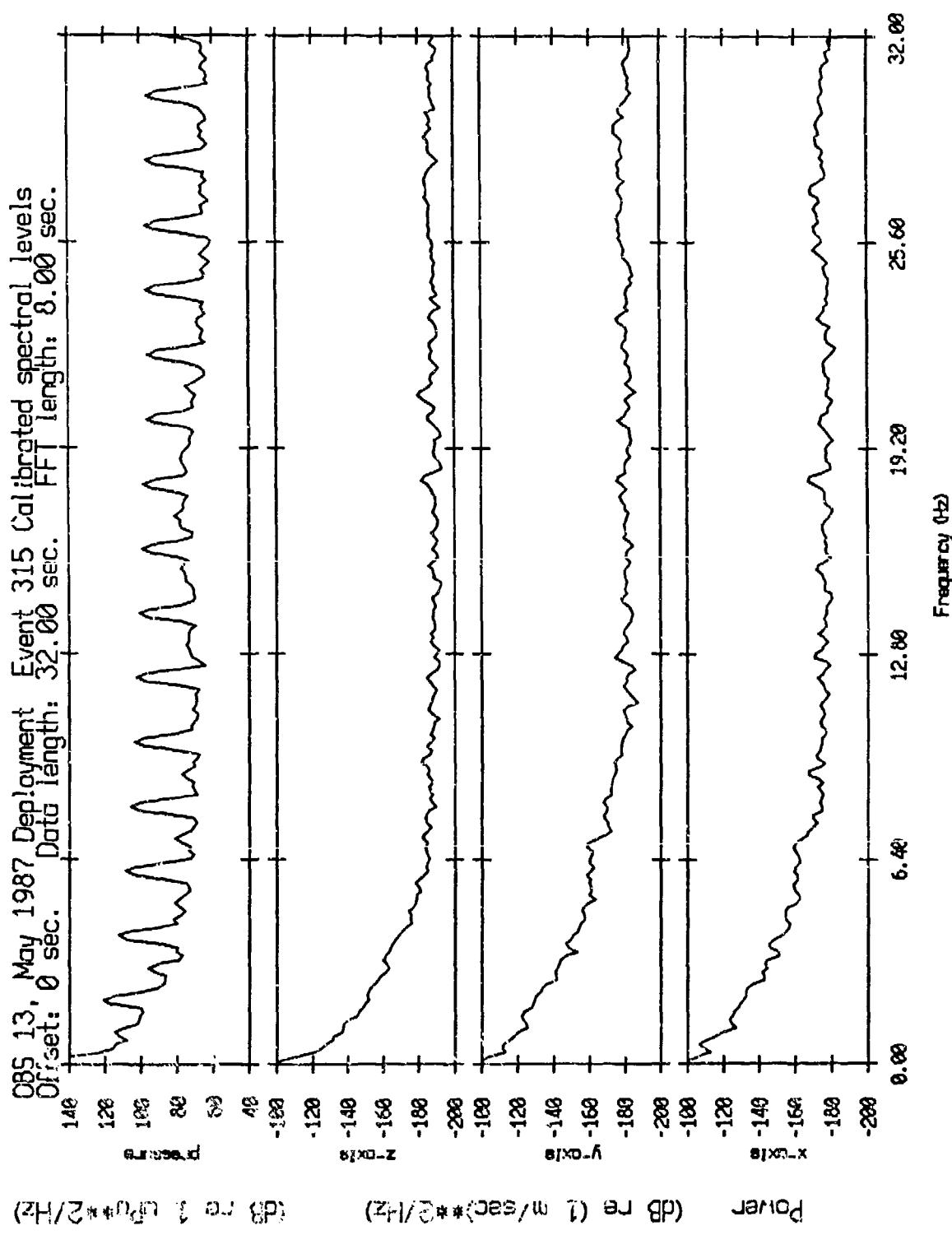


Figure XI.18c

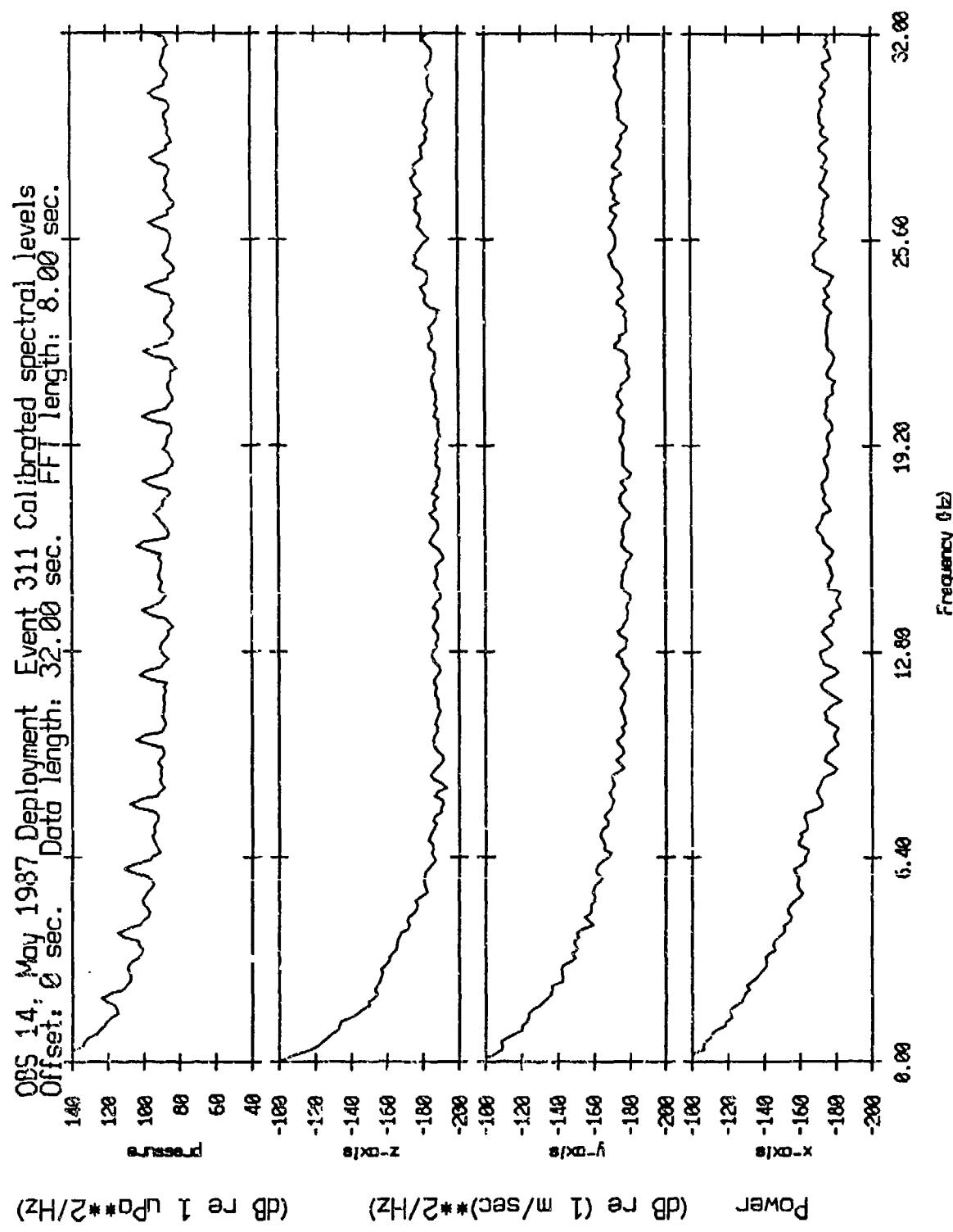


Figure XI.19a

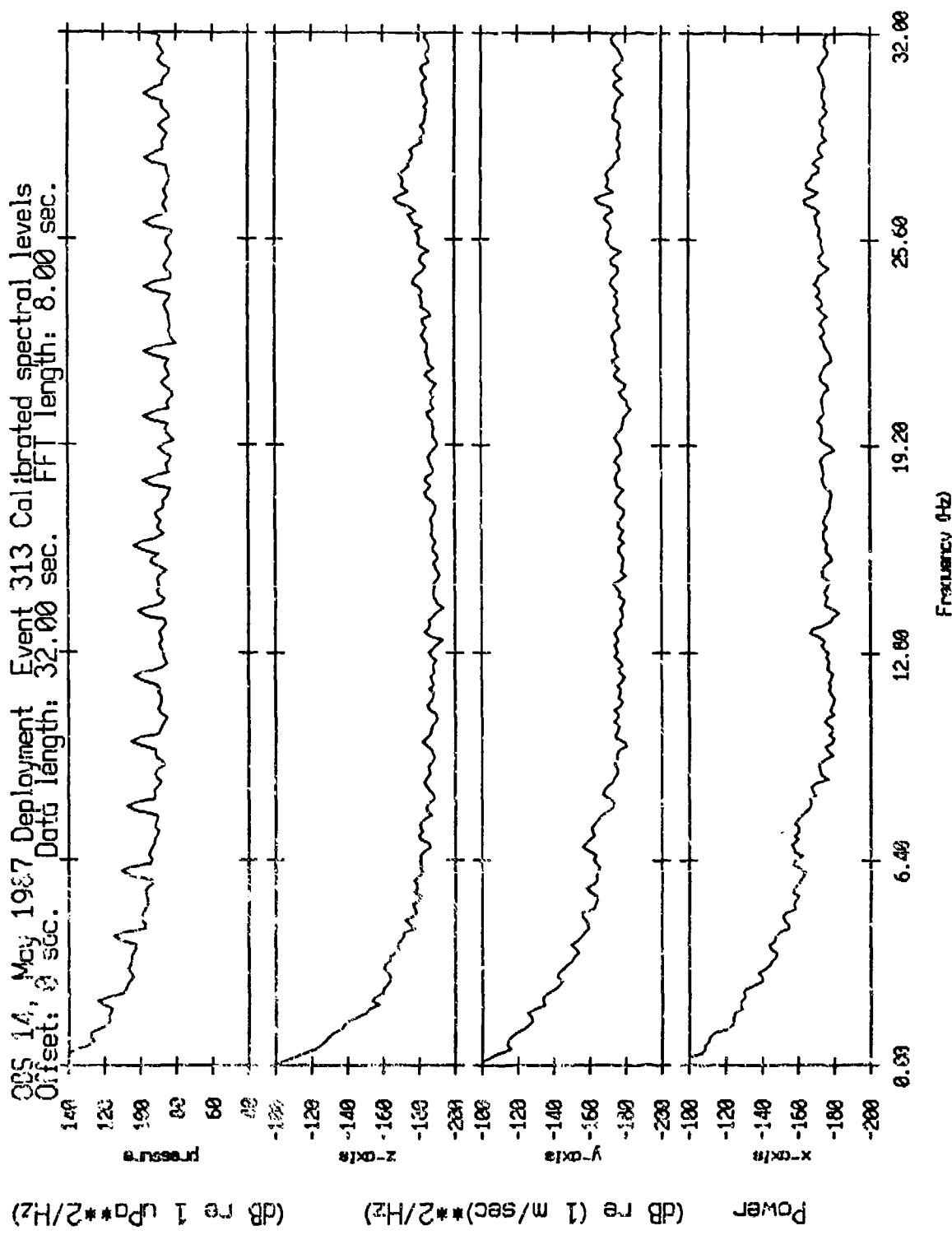


Figure XI.19b

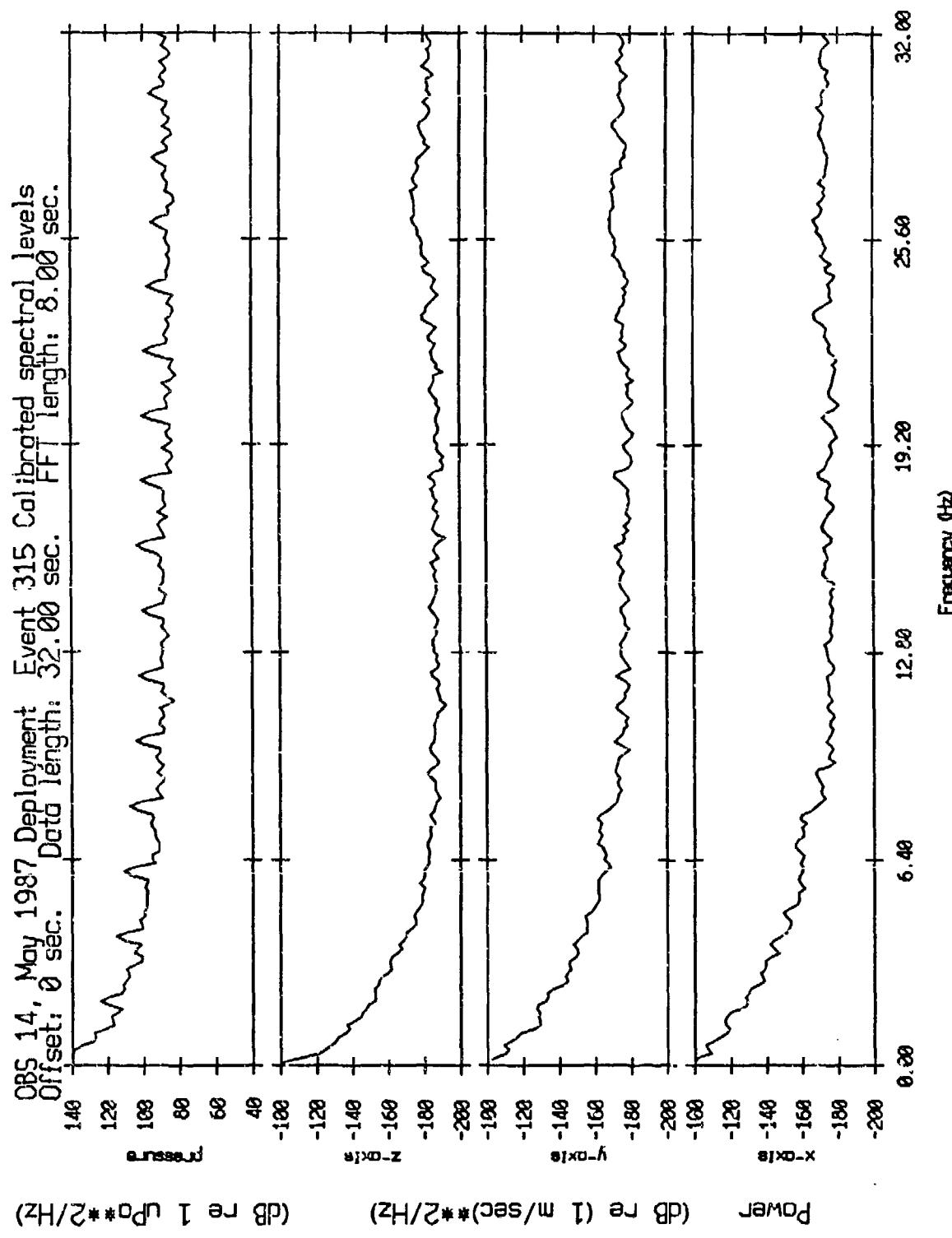


Figure XI.19c

60-11-735 019

REPORT DOCUMENTATION PAGE

1a. REPORT SECURITY CLASSIFICATION UNCLASSIFIED		1b. RESTRICTIVE MARKINGS	
2a. SECURITY CLASSIFICATION AUTHORITY		3. DISTRIBUTION/AVAILABILITY OF REPORT Approved for public release; distribution unlimited.	
2b. DECLASSIFICATION/DOWNGRADING SCHEDULE			
4. PERFORMING ORGANIZATION REPORT NUMBER(S) MPL TECHNICAL MEMORANDUM 402 [MPL-U-15/88]		5. MONITORING ORGANIZATION REPORT NUMBER(S)	
6a. NAME OF PERFORMING ORGANIZATION Marine Physical Laboratory	6b. OFFICE SYMBOL (If applicable) MPL	7a. NAME OF MONITORING ORGANIZATION Office of Naval Research Department of the Navy	
6c. ADDRESS (City, State, and ZIP Code) University of California, San Diego Scripps Institution of Oceanography San Diego, CA 92152	7b. ADDRESS (City, State, and ZIP Code) 800 North Quincy Street Arlington, VA 22217-5000		
8a. NAME OF FUNDING/SPONSORING ORGANIZATION Office of Naval Research	8b. OFFICE SYMBOL (If applicable) ONR	9. PROCUREMENT INSTRUMENT IDENTIFICATION NUMBER N00014-87-K-0010	
8c. ADDRESS (City, State, and ZIP Code) Department of the Navy 800 North Quincy Street Arlington, VA 22217-5000		10. SOURCE OF FUNDING NUMBERS	
		PROGRAM ELEMENT NO.	PROJECT NO.
		TASK NO.	WORK UNIT ACCESSION NO.
11. TITLE (Include Security Classification) Freely Drifting Swallow Float Array: May 1987 Trip Report			
12. PERSONAL AUTHOR(S) G. L. D'Spain, R. L. Culver, W. S. Hodgkiss, and G. L. Edmonds			
13a. TYPE OF REPORT Summary	13b. TIME COVERED FROM _____ TO _____	14. DATE OF REPORT (Year, Month, Day) May 1988	15. PAGE COUNT 457 pgs.
16. SUPPLEMENTARY NOTATION			
17. COSATI CODES		18. SUBJECT TERMS (Continue on reverse if necessary and identify by block number) Swallow floats, ambient ocean noise, ocean bottom seismometers, wind speed measurements	
19. ABSTRACT (Continue on reverse if necessary and identify by block number)			
<p>Representative data collected by the Marine Physical Laboratory's Swallow floats during the 5-6 May, 1987 deployment near 32.5° N, 120.5° W are presented herein. The results include the 8 kHz acoustic localization ping arrival data, the battery voltage, compass heading, and AGC level measurements, and the three-component, VLF particle velocity data. The data set is of extremely high quality and it appears to provide a rich source of information on ambient ocean noise in the 1-20 Hz band.</p> <p>Data from the concurrent deployment of 13 ocean bottom seismometers operated by Dr. L. Dorman's group at Scripps Institution of Oceanography are also presented. These data include the three-component geophone data from the nine properly functioning instruments (instruments 1, 2, 4, 5, 6, 8, 12, 13, and 14), regular OBS hydrophone (OAS model E-2PD) data from instruments 2, 4, 8, 12, 13, and 14, and data from ultra-low frequency hydrophones of the Cox-type design on instruments 1, 5, and 6. A preliminary comparison between the OBS data and the Swallow float geophone data show some common spectral peaks and that calibrated spectral levels are comparable.</p> <p>Finally, to help interpret the acoustic/seismic data collected by the instruments, plots of the position of the research vessel, the Scorpius, are given. Wind speed measurements taken on the Scorpius during the experiment and sound velocity profiles derived from CalCOFI Cruise 8705 hydrographic cast data are presented as well.</p>			
20. DISTRIBUTION/AVAILABILITY OF ABSTRACT <input type="checkbox"/> UNCLASSIFIED/UNLIMITED <input checked="" type="checkbox"/> SAME AS RPT. <input type="checkbox"/> DTIC USERS		21. ABSTRACT SECURITY CLASSIFICATION UNCLASSIFIED	
22a. NAME OF RESPONSIBLE INDIVIDUAL W. S. Hodgkiss		22b. TELEPHONE (Include Area Code) (619) 534-1798	22c. OFFICE SYMBOL MPT